DEVELOPMENT OF A STEM CELL-BASED TISSUE ENGINEERED VASCULAR GRAFT

by

Lorenzo Soletti

Master of Science, Politecnico di Milano, 2002

Submitted to the Graduate Faculty of

The Swanson School of Engineering in partial fulfillment

of the requirements for the degree of

Doctor of Philosophy

University of Pittsburgh

2008

UNIVERSITY OF PITTSBURGH

SWANSON SCHOOL OF ENGINEERING

This dissertation was presented

by

Lorenzo Soletti

It was defended on

September 8th, 2008

and approved by

Dr. William R. Wagner, Professor, Surgery and Bioengineering

Dr. Johnny Huard, Professor, Orthopaedic Surgery, Molecular Genetics, Biochemistry, Bioengineering, and Pathology

Dr. Bradley Keller, Professor, Pediatrics, School of Medicine

Dissertation Director: Dr. David A. Vorp, Associate Professor, Surgery and Bioengineering

DEVELOPMENT OF A STEM CELL-BASED TISSUE ENGINEERED VASCULAR GRAFT

Lorenzo Soletti, Ph.D.

University of Pittsburgh, 2008

Limited autologous vascular graft availability and poor patency rates of synthetic grafts for small-diameter revascularization (*e.g.*, coronary artery bypass, peripheral bypass, arteriovenous graft for hemodyalisis access, *etc.*) remain a concern in the surgical community. A tissue engineering vascular graft (TEVG), including suitable cell source, scaffold, seeding, and culture methods can potentially solve these limitations. Muscle-derived stem cells (MDSCs) are multipotent cells, with long-term proliferation and self-renewal capabilities, which represent a valid candidate for vascular tissue engineering applications due to their plasticity/heterogeneity. The poly(ester urethane) urea (PEUU) is also an attractive potential candidate for use as a TEVG due to its elasticity and tunable mechanical and degradation properties. We hypothesized that a novel scaffold optimally seeded with stem cells, acutely cultured and stimulated *in vitro*, and ultimately implanted *in vivo* will remodel into a functional vascular tissue.

To test this hypothesis, we developed an innovative, multidisciplinary framework to fabricate and culture a TEVG in a timeframe compatible with clinical practice. In this approach, MDSCs were incorporated into a newly-designed and characterized PEUU-based scaffold via a novel seeding device, which was tested quantitatively for cell seeding uniformity and viability. The seeded TEVGs were acutely cultured in dynamic conditions and assessed for cell phenotype, proliferation, and spreading. The conduits were then implanted systemically in a small and a

large animal model and assessed, at different time points, for patency rate, remodeling, and cellular engraftment and phenotype.

The seeding technology demonstrated a rapid, efficient, reproducible, and quantitatively uniform seeding without affecting cell viability. The PEUU scaffold that was developed is suitable for arterial applications, exhibiting appropriate strength, compliance, and suture retention properties. The dynamic culture resulted in cell proliferation and spreading within the 3D scaffold environment. Rat preclinical studies suggested a role of the seeded MDSCs in the maintenance of patency and in the remodeling of the TEVG toward a native-like structure. Pig studies were inconclusive due to a poor pre-implantation cell density.

Future work should address this and other issues encountered during the large animal study, and should test longer time points in both models. Finally, this approach might benefit from a more readily available cell source such as the bone marrow.

TABLE OF CONTENTS

LIST OF TABLES

LIST OF FIGURES

PREFACE

This work represents the result of five years of research endeavour in the stimulating collaborative environment of the McGowan Institute for Regenerative Medicine at the University of Pittsburgh. During these years, I had the fortune of meeting a number of people that have either been instrumental for my scientific, professional, and personal growth, or that have been supporting me through their work, thoughts, and sympathy. I would like to dedicate this work to these people as a sincere recognition for the collective effort made to make this ambitious project happen, and as a personal sign of gratitude for helping me appreciate the multifaceted value of this life journey more than its destination.

In particular, I would like to start acknowledging (in alphabetical order) the co-authors of this dissertation work, which have led to a number of published or soon-to-be published peer-reviewed publications in international journals. Each of them has played a critical role in providing expertise for the very multidisciplinary aspects of this project: Bridget M. Deasy, PhD, Mohammed S. El-Kurdi, PhD, Burhan Gharaibeh, PhD, Jianjun Guan, PhD, Nav Yash Gupta, MD, Yi Hong, PhD, Johnny Huard PhD, Timothy M. Maul, PhD, Brian Morelli, BS, Alejandro Nieponice, MD, John J. Stankus, PhD, David A. Vorp, PhD, and William R. Wagner, PhD. Among these, I would like to dedicate a special mention and thank you to Dr. Nieponice with whom I have shared a great deal of the responsibilities of this work, and that has been through the years a close collaborator, mentor, and friend.

I would like to thank my advisor Dr. Vorp, for the number of opportunities given to me in these years, and for the scientific freedom and exposure that allowed me to explore and develop many of the solutions described in this work, as well as to collaborate in additional, unrelated work.

I would like to thank the remaining members of my PhD committee: Dr. Huard, Dr. Wagner, and Dr. Keller for their feedback and advice, instrumental for identifying a number of relevant project and career objectives.

I acknowledge here the source of funding that allowed to sustain "the burn rate" of this project: NIH R01 HL069368-01A1 to Drs. Wagner and Vorp, AHA 0525585U to Dr. Nieponice.

I dedicate a very special note to the Chair of the Bioengineering Department, Professor Harvey S. Borovetz, who has provided an invaluable "paternalistic" academic and personal support through these years, and to his close colleagues Lynette K. Spataro and Joan L. Williamson who have scrupulously taken care of all my academic administrative matters in a very professional and friendly way.

The Vascular Research Laboratory team (past and present) has played another important role in this work for sharing the same "boat" while navigating in different weather conditions; for giving precious technical advice, and for lending pairs of hands when needed. Thank you all: Doug W. Chew, Elena Di Martino, PhD, Donna J. Haworth, Jessica L. LoSurdo, Sanket N. Patel, Diana M. Gaitan, Anton Xavier, Roberta F. Melick, Scott J.S. VanEpps, PhD, Deborah A. Cleary, Melissa A. Morgan, Joseph E. Muthu, Wei He, PhD. In particular, Doug Chew for being one of those individuals always available to solve a problem or to share thoughts and laughter, thank you.

Many people within the McGowan Institute have been supporting my cause providing technical, administrative, or logistical help. I wish to mention and acknowledge them here: Jennifer Debarr, Dan McKeel, William J. Federspiel, PhD, Ann M. Steward-Akers, PhD, John Murphy, Sandra S. Hall, Gillian L. McShane, Kate Lewis, Lauren Kokai, Buffie J. Kerstetter, Joseph M. Hanke, and Michael J. Firda.

During these years, I had the pleasure of mentoring and being assisted by a number of people who performed critical work to retrieve and quantify large volumes of data necessary for this dissertation. Thank you guys: Brian C. Morelli, Garret A. Viglione, Robert J. Toth, Randy Christner, Jennifer Bacior.

I have also received great technical help from collaborators from the Rangos Research Center and from the Center for Biological Imaging: Jessica Tebbets, Joseph M. Feduska, Kazuro L. Fujimoto, MD, Marc Rubin, and Jonathan Franks. Thank you.

A number of individuals have inspired the business-related aspects of this work as well as my understanding of the field instrumental for my career: Alexander P. Ducruet, PhD, Paul J. Petrovich, Amy E. Brunetto, Harold T. Safferstein, PhD, Larry Miller, David S. Smith, David W. Wagner, Mark J. Gartner, PhD, Babs Carryer, and Alessandro Biglioli.

My friends have shared with me the highs and lows of these years and provided their personal support in many different ways: Daniel S. Shrager, Vinod K. Sharma, Pietro Bajona, Alessandro Acquisti, Stefano Gridelli, Cristiano Spadaccio, George Engelmayr, Mohammed El-Kurdi, Edward El-Saad, Fabrizio Fazzi, Michelangelo DiGiuseppe, Virginio Salvi, Armando Cioffi, and Roberto Musi.

I would like to conclude this section dedicating the most special and visceral gratitude to my family. I had the fortune of having loving and caring parents, who contributed making me

the person I am: Dad, Giuseppe Maria (Bepi) is one of the smartest, opinionated and informed people I know. He infused in me a sense of infinite curiousity toward the phenomenological world and the love and importance of reading and studying. Mom, Barbara, with her immense sensibility and tolerance showed me the value of compassion toward life and human conditions and the ephemerality of competition. My sister, Laura was instrumental in giving me a realistic view on life keeping things "in perspective".

Finally, my beloved Teya, the love of my life, thank you from my heart for all your support and for teaching me that Virgil's quote "*Omnia vincit amor*" was not only a literary exercise...

1.0 INTRODUCTION

Cardiovascular disease is the leading cause of mortality in the United States [1] and in Europe [2]. Coronary artery disease, in particular, accounts for approximately 50% of the total mortality [1, 2]. Other conditions such as peripheral artery disease and end stage renal disease are associated with overwhelming mortality, morbidity, and costs [3, 4]. These three pathologies have in common the therapeutic need for surgical revascularization or vascular access which is usually accomplished via vascular bypass utilizing autologous portions of the vasculature (**Figure 1.1**). Synthetic biodurable grafts have been successfully used to bypass large caliber high-flow blood vessels, but have invariably failed when used to reconstruct small-caliber arteries [5]. The lack of a suitable vascular graft material coupled with the tremendous need for a viable vascular substitute has stimulated many attempts to make small-diameter (ID < 5 mm) tissue engineered vascular grafts (TEVGs). This can be accomplished by incorporating cells or other biological components (*e.g.*, growth factors, cytokines, *etc*.) in a variety of bioerodable tubular scaffolds or by just providing acellular, temporary conduits to allow natural vascular remodeling events to take place [6]. Although some of the previous approaches have shown promising results, most of them have exhibited mechanical, functional, or practical inadequacies hampering their clinical translation.

This introductory chapter reviews the clinical significance of the need for alternative vascular substitutes, important structural and functional features of native arteries, and a

comprehensive literature review describing previous attempts in the development of TEVGs. In this way, the reader will be provided with a better understanding of the problem and the solutions proposed in this work.

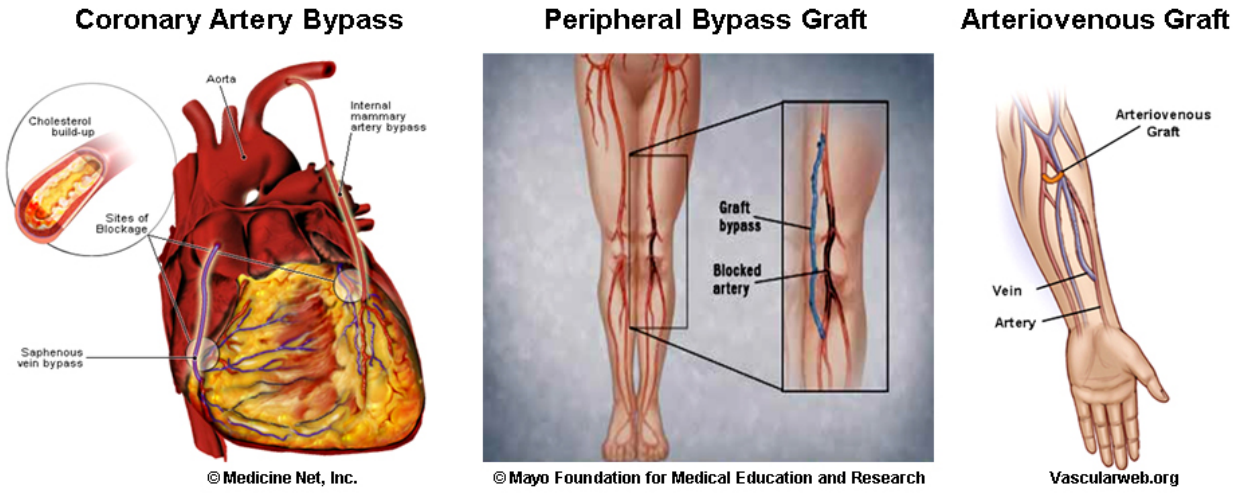

Figure 1.1 Clinical need for TEVGs. The figure shows the most common uses of small-diameter vascular grafts in the clinic. **Left:** During coronary artery bypass procedures small autologous vessels (usually saphenous vein and the ITA) are used to bypass stenoses or obstructions in different locations of the coronary tree. The bypass grafts are anastomosed proximally to the ascending aorta, and distally, downstream of the coronary obstructions. When using the ITA (gold standard for single bypass), a redirection of the artery is performed with a single distal anastomosis downstream of the coronary obstruction. **Center:** During lower limbs revascularization procedures, long segments of veins (usually saphenous vein), are used to bypass segments of obstructed arteries in the leg. Two end-to-side anastomoses are performed. **Right:** Patients with end-stage kidney failure require repeated access to high-flow vascular conduits for hemodialysis. In many cases a vascular graft is implanted to create an arteriovenous connection allowing arterial flow withdraw in a subcutaneous (venous) location.

1.1 CLINICAL SIGNIFICANCE

In the United States approximately 600,000 surgical procedures are performed yearly to bypass coronary or peripheral arteries (**Figure 1.1**) [1, 3] affected by common pathologies such as atherosclerosis or deteriorated by diabetes complications. In particular, coronary artery bypass represents the most common operation and relies mostly on the use of patient's saphenous veins or distal redirection of the internal thoracic artery (ITA). Over 30% of the patients bypassed with venous portions fail to reach a 10-12 year period free of re-operations or percutaneous transluminal angioplasty [7]. Further, the use of more effective arterial segments such as ITA, radial artery, or gastroepiploic artery is limited by their size, availability, and/or co-morbidities related to the loss of functional arterial segments. Synthetic grafts such as expanded polytetrafluoroethylene (ePTFE AKA Goretex®) and polyethylene terephthalate (PET AKA Dacron®) have invariantly failed in these small caliber applications due to thrombosis, intimal hyperplasia, or calcification [8].

The prevalence of patients receiving hemodialysis is approximately 340,000 in the U.S. [4]. Hemodialysis requires consistent and repeated access to the systemic circulation and adequate blood flow rate to enable a dialysis membrane to achieve complete blood detoxification in a reasonable amount of time. The most effective dialysis access configuration is currently the one represented by the native radial artery to cephalic vein fistula (**Figure 1.1**). However, 77% of the patients in the U.S. rely on access constituted either by a synthetic PTFE graft [9] or chronic catheters [10]. All of these currently-used vascular access solutions are prone to stenosis, chronic inflammation, and infections [5, 11]. Therefore, development of a successful TEVG could have significant clinical implications.

Another critical area of possible application for TEVGs is the one related to traumatic injuries from accidents or from the battlefield, including those deriving from severe lacerations, blunt trauma, explosion, or gunshots. These injuries often involve damage or loss of consistent portions of tissues including major arteries or veins, and necessitating conduit replacement [12, 13]. Larger blood vessels may be replaced or bypassed with synthetic vascular grafts to reestablish blood supply in a reconstructed tissue portion. However, these synthetic options are, again, not suitable for small diameter blood vessels, including those of the extremities (*e.g.*, tibial artery, radial artery, *etc*.). The graft of choice is often the saphenous vein for lower limb injuries [14].

The cost of cardiovascular diseases and stroke is estimated to be $403.1 billion per year in the U.S., according to the American Heart Association and the National Heart, Lung, and Blood Institute (NHLBI) [1]. Therefore, a large margin exists for the development of new technologies aimed to reduce costs while improving outcomes. The development of a rapidly available TEVG, able to mechanically and functionally mimic the native vasculature and to self-repair in the case of damage would alleviate the overwhelming need of healthy artery substitutes associated with cardiovascular disease, hemodialysis treatment, or traumatic vascular injuries.

1.2 ARTERIAL ANATOMY AND PHYSIOLOGY

Arteries are biological conduits carrying the blood from the heart to the tissues via a hierarchical branching system spanning in size from the large arteries (internal diameter (ID) ~ 2-3 cm) to the capillaries (ID ~ 8-10 μm) and in function from elastic arteries to mass exchange vessels [15]. The arterial wall is a complex biological structure made of three different concentric layers

namely, the *tunica intima*, *media*, and *adventitia* (**Figure 1.2**). Each layer has its own specific features, but also its own peculiar mechanical, structural, and functional role. Usually, depending on the caliber of the artery and its location in the arterial branching system, structural and functional differences exist among homologous layers. In general, the *tunica intima* consists of the endothelium, a single epithelial layer of interconnected (with gap junctions) endothelial cells (ECs) firmly adhered onto a thin collagenous (type IV) layer called basal lamina. The endothelium is responsible for a variety of vascular functions including hemostasis, regulation of vasoactivity, angiogenesis, secretion of cytokines, and selective control of mass transport across the arterial wall [16].

The *tunica media* is a thick, multilaminar layer including smooth muscle cells (SMCs) oriented circumferentially to the blood vessel centerline and several concentric fenestrated elastic laminas providing mechanical energy storage and allowing for transmural mass transport. SMCs are embedded in an extracellular matrix (ECM) made of collagen (mostly, type III), proteoglycans, glycosamino-glycans (GAGs), and elastin. The medial layer provides mechanical support to the artery to withstand the wall stresses deriving from arterial pressure, but also to properly reflect via elastic recoil the pressure waveforms generated by the heart contractions [17]. The *tunica media* is innervated and vascularized by vasa-vasorum, and is responsible for the vasoactivity (vasoconstriction and vasodilation) of the arterial wall.

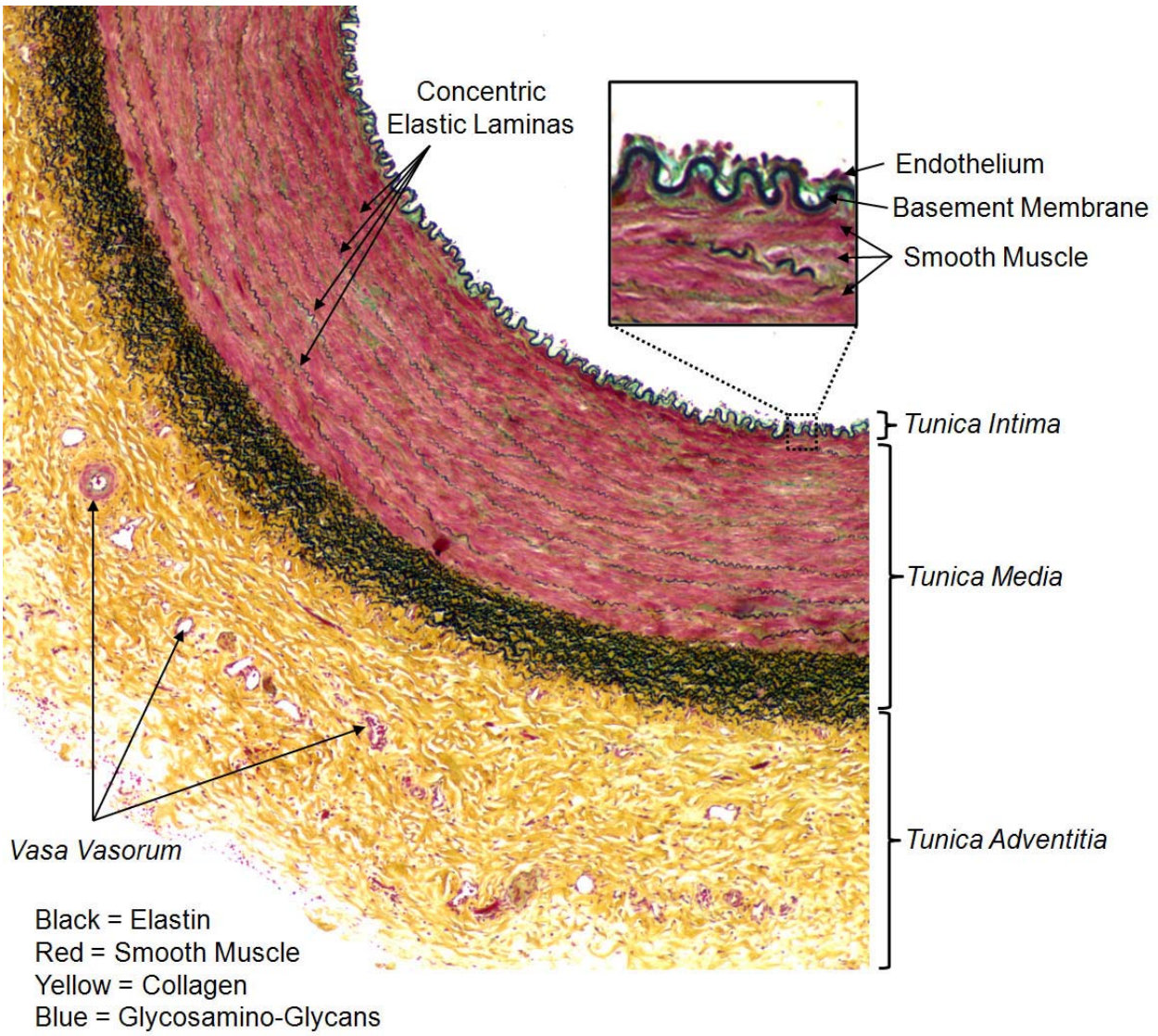

Figure 1.2 Anatomy of a pig carotid artery visualized via Movat's Pentachrome stain. The three different layers of a native artery are indicated. Innermost, the *tunica intima* is in contact with the blood and consists of endothelial cells tightly attached to each other and to an underlying collagenous *basal lamina* (or basement membrane). In an intermediate position, the *tunica media* provides most of the structural support for the artery and consists of smooth muscle cells embedded in a matrix made of concentric laminas of collagen and elastin. Outermost, the *tunica adventitia* provides external structural support and attachment to surrounding tissues and is made of collagen and fibroblasts.

SMCs are compacted and interconnected (*e.g.*, via gap junctions) in smooth muscle fibers wrapping around the artery, and have the necessary protein machinery to generate fiber contractions. Coordinated contractions or relaxations of smooth muscle fibers cause variations in caliber of the artery as a response to biochemical stimuli [15].

Finally, the *tunica adventitia* is a vascularized fibrous layer wrapping the other two layers of the artery, providing mechanical support and anchorage to perivascular and surrounding tissues or organs. Fibroblasts, pericytes, microvascular endothelial cells, and mast cells are the main cellular components of the adventitial layer [16]. These cell types are mainly responsible for the synthesis of ECM and for the vascular response to injury.

Arteries have the important function of storing mechanical energy during pulse wave propagation (systole) and returning it during diastole in the form of elastic recoil. This property is known as the Winkessel effect and allows for the maintenance of blood flow through downstream arteries also during diastole. The mechanical properties of an artery, in particular the compliance – defined as intraluminal variation in volume due to variations in pressure (dV/dP) – influence the propagation of the mechanical pulse wave. Therefore, the mechanical properties of the arterial wall influence the hemodynamics within it. In some pathological vascular conditions causing changes in mechanical properties, the resulting variations in hemodynamics have been associated with endothelial dysfunctions leading the increased risk of atherosclerosis [18]. Sudden local variations in compliance, for example, due to the coupling of the arterial wall with a highly stiffer vascular graft, have been related to intimal hyperplasia [19, 20]. This phenomenon is commonly called “compliance mismatch”.

Another critical function of the arterial tree is the regulation of the blood pressure through vasoactivity. The mechanisms of blood pressure regulation are multiple and their explanation is

beyond the scope of the current dissertation. However, one of those mechanisms involves the response of the arterial tissue to biochemical stimuli inducing contractions or relaxation of the smooth muscle fibers as previously described. Changes in arterial caliber result in variations in vascular resistance causing pressure and flow modulations [17].

1.3 TEVG APPROACHES

Although the term "Tissue Engineering" was first proposed by Y.C. Fung, a pioneer in the fields of biomechanics and bioengineering in 1985 [21], and its concepts were formally elaborated in the late 1980s by Joseph Vacanti and Robert Langer [22], it was Eugene Bell that in the late 1970's first explored the possibility of culturing cells within biological matrices for the purpose of tissue regeneration [23]. A definition for tissue engineering provided by Robert Nerem in the early 1990s was: "(tissue engineering is) the use of living cells, together with extracellular components, either natural or synthetic, in the development of implantable parts or devices for the restoration or replacement of function" [24]. The extracellular component (or scaffold) provides a temporary architecture on which seeded cells can organize and develop into the desired tissue prior to implantation with concurrent ECM deposition. During the formation, deposition, and organization of the newly generated ECM, the scaffold is degraded and hopefully metabolized, eventually leaving behind a functional tissue. Ideally, the scaffold should not persist once the cells have produced their own matrix [25]. The classic paradigm of tissue engineering is based on five different steps. The first consist of harvesting and isolating cells either from an autologous, allogeneic, or xenogeneic source. The second is the culturing and expansion of cells to the desired cell number. In the third step the cells obtained are seeded into

or onto a scaffold. The resulting construct is subsequently cultivated and stimulated *in vitro* during the fourth step. The final step is the implantation (**Figure 1.3**).

There is a difference that must be underlined between tissue engineering approaches that entail a cellular component and those that rely on guided tissue regeneration *in vivo* without previous cell seeding. These approaches use acellular matrices that are repopulated by the host organism after implantation.

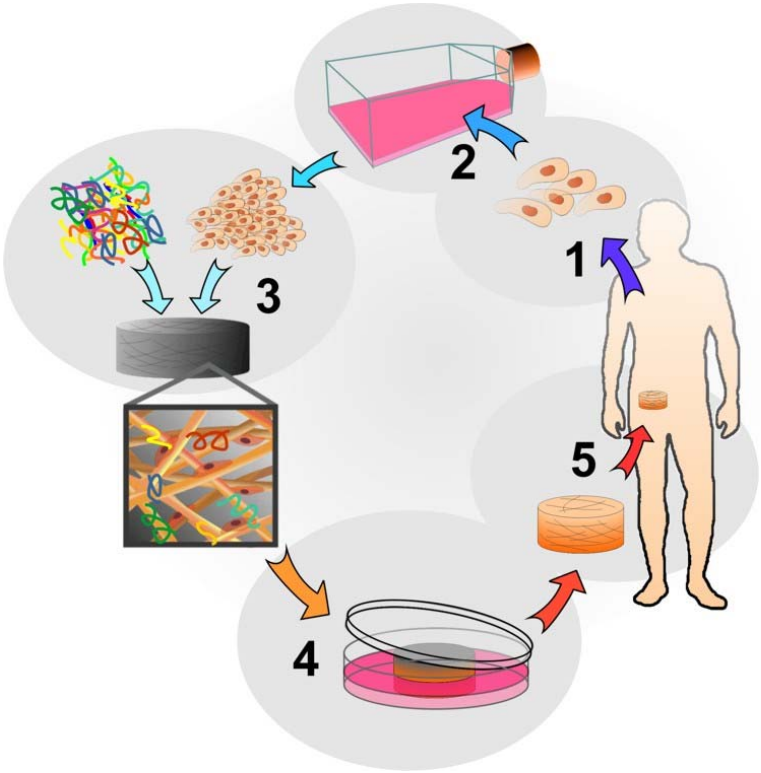

Figure 1.3 Tissue engineering paradigm. The pictorial represents the classic tissue engineering pipeline in which the cells are initially harvested and isolated from the patient (1), cultured and expanded *in vitro* (2), and then seeded into or onto temporary matrices or scaffolds (3). The seeded scaffolds are cultured into bioreactors for a variable amount of time (4), and then are finally implanted into the patient to restore and replace functional or structural tissues.

Over the last three decades, several approaches have been attempted to incorporate "biological" components and functionality into tubular conduits to overcome the limitations of the existing biodurable, small-diameter vascular grafts. Early attempts toward this end were pioneered by Zilla *et al.* and consisted of luminal surface seeding of ECs onto existing synthetic graft materials such as Goretex® or Dacron®, or surface modifications to promote EC adhesion *in vivo* [26]. The rationale behind this approach was to reduce graft thrombogenicity and to extend graft patency by means of an internal lining of ECs. These approaches lead to several clinical trials; however, several drawbacks limited their success. In particular, the lack of the graft mechanical compliance due to the intrinsic stiffness of the materials, the absence of a capillary support system of the formed neointimal tissue, and the loss of cellular contents over time [27]. In general, the absence of biodegradation of synthetic materials might hinder the normal tissue remodeling response, thus becoming a physical barrier to long-term outcomes and a source of infection and calcification [28].

The first approach to develop a fully biological vascular conduit made of cells and ECM was described by Weinberg *et al.* who reported a tissue-like tube consisting of three layers composed, respectively, of allogeneic ECs, smooth muscle cells (SMCs), and fibroblasts [29]. However, in order to withstand physiologic arterial pressures, these constructs required additional support sleeves made of Dacron®, thus jeopardizing the benefits derived from the completely biological nature of the constructs. L'Heureux *et al.* described a novel technique using sheets made of cells embedded into their own ECM coaxially wrapped around a mandrel [30, 31]. This technique allowed for the creation of an allogeneic collagen-based construct with suitable mechanical properties. More recently, this group has been pursuing the same approach using skin fibrosblasts [32]. However, this approach might be limited in its clinical and

commercial feasibility due to the extensive culture periods necessary to fabricate the TEVGs (6-9 months). Campbell *et al.* proposed the use of *in vivo* natural remodeling processes to generate cellularized matrix tubes around a tube implanted in the peritoneal or pleural cavities [33]. The tubes were mechanically sound but were composed essentially of myofibroblasts, limiting the functional properties of the constructs and requiring a dedicated surgical procedure for the harvesting of the TEVGs. Nerem *et al.* extensively investigated the effect of mechanical stimulations applied to vascular cells *in vitro* [34], and postulated the critical role of biomechanics in vascular TE [35]. Niklason *et al.* pioneered the integration of cells into porous, synthetic tubular scaffolds and the effect of several biochemical factors in the *in vitro* culture of TEVGs [36, 37]. Shin'oka *et al*. proposed the use of a porous biodegradable scaffold seeded in the surgical setup with autologous bone marrow-derived cells and implanted with no intermediate tissue culture [38, 39].

1.4 SCAFFOLDS FOR TEVGS

One of the heaviest areas of investigation in vascular tissue engineering is the development of an optimal tubular scaffold to foster cell adhesion, integration, remodeling, and functionality, as well as to provide the necessary mechanical integrity over an extended period of time to withstand physiologic pressures and flows [40]. The scaffold should also possess mechanical properties similar to native vasculature. High material stiffness, for example, has been implicated in failure due to "compliance mismatch". This condition can further lead to myointimal hyperplasia and consequent graft failure. Moreover, the scaffold should not possess significant plastic behavior when exposed to physiological ranges of stress and strain since this

can lead to aneurysm formation. The fundamental difference between a traditional vascular graft and a TEVG based on scaffolds is the biodegradation of the scaffold material of construction. TEVGs thus depend on the capacity of donor- and host-derived cells to secrete and remodel ECM into a native-like structure in tandem with scaffold resorption.

The materials used as scaffolds for vascular tissue engineering applications have varied, ranging from biodegradable synthetic polymers to natural biopolymers or decellularized native tissue. Additionally, surface modification of these materials is an expanding research field aimed at modulating cell-material interaction acting upon the surface chemistry. Each of these approaches has its pros and cons and the tissue engineering community has not found a consensus in defining the most promising approach to pursue. Summarized below are some examples of previously investigated classes of scaffolds or surface modifications.

1.4.1 Biodegradable synthetic materials

Synthetic materials have the advantage of being highly tunable and reproducible in their mechanical and structural properties as well as in their degradation kinetics. The synthesis of the polymer and the processing and manufacturing into scaffolds are, in fact, completely performed under controllable conditions. Changing the molecular weight or the concentration of the polymer or altering its backbone with other chemistries affects the physical and mechanical properties of the scaffold. Generally, higher molecular weights or concentration results in an increase in stiffness and strength and in a subsequent reduction of the degradation rate [41]. Also a physical blend of the material with other polymers, or a chemical modification of the polymer backbone with other monomer species can affect the mechanical properties and degradation behavior. The resulting blend or copolymer will have some properties of the newly

introduced species depending on the mixture ratio used [42]. The processing of the polymer is another variable influencing the properties of the scaffold. In particular, the processing technique defines the scaffold geometry, and its structural and microstructural features. Different processing will result in different textures spanning from a dense to a spongy-like or fibrous microstructure. The microstructure of the scaffold will influence not only the physical, mechanical and degradation properties of the scaffold [43] but also its affinity for cell adhesion and motility [44]. Porosity and pore connectivity can be obtained and controlled via specific processing such as salt leaching, thermally induced phase separation (TIPS), and microfabrication technology. Fibers, meshes, and felts can be generated by other processing including 3D fiber deposition, and electrospinning (ES).

Common synthetic biodegradable biomaterials used for fabricating a TEVG are the aliphatic polyesters. Examples of this class of material are the poly-L-lactic acid (PLLA), polyglycolic acid (PGA), polycaprolactone (PCA), and their related copolymers [45, 46]. These materials have shown supra-physiologic stiffness levels and lack of biocompatibility of their degradation products, thereby limiting their applications in cardiovascular applications [47]. Their high stiffness has been related to compliance mismatch, while the local acidic environment generated by the degradation bioproducts of this class of polymers has been shown to cause an adverse inflammatory response [48, 49]. Polyhydroxyalkanoates (PHAs) are bacterial-derived biopolyesters produced by fermentation of sugars or lipids. The material has high elasticity and mechanical strength and, depending upon its composition, may be modulated to desired material properties, ranging from stiff and strong to flexible and ductile. A copolymer PHA-PGA scaffold has been fabricated to increase the elasticity and prevent the observed aneurysm formation in simple PGA tubular grafts [50].

Biodegradable polyurethanes represent attractive potential candidates for use in TEVG scaffold fabrication due to their elasticity and tunable mechanical and degradation properties. In particular, a class of biodegradable, elastomeric poly(ester urethane)urea (PEUU) polymer has been shown to be cytocompatible, yield non-toxic degradation products, and to be processable into scaffolds via different techniques [51, 52]. A TIPS process has been used to produce highly porous scaffolds [53]. This process has been shown to yield a microstructural milieu capable of promoting efficient cell integration, cell attachment, and diffusion of nutrients allowing for culture *in vitro* [54, 55]. ES is a different processing technique, which can yield nanofibrous PEUU with similar architectural and mechanical properties to those of native collagenous ECM [56, 57]. It was demonstrated that by varying the rotational speed of the target onto which the PEUU was deposited, that the degree of structural anisotropy and associated mechanical properties could be reproducibly controlled and mathematically modeled [56]. More recently, the challenge of evenly distributing cells throughout the thickness of these relatively tight porous ES scaffolds has been largely overcome by a novel process in which cells and PEUU are co-deposited, termed "cellular microintegration" [57, 58]. Collectively, the flexibilities of PEUU chemistry and processing techniques provide a plethora of permutations from which to choose and combine in designing a new scaffold for vascular tissue engineering applications.

1.4.2 Natural biopolymers or decellularized native tissue

Natural polymers provide a better environment for cell growth and have a reduced inflammatory response following *in vivo* degradation. Within this category, three different approaches can be identified: fashioning of materials derived from natural matrix into a tubular construct [59-62],

formation of a tubular construct from decellularized ECM materials [63], or use of intact, decellularized blood vessels [64].

Tubular constructs fabricated from molded matrix/cell suspensions undergo cell-mediated compaction via cellular attachment to the gel matrix and its cell-mediated contraction resulting in water release from the gel within days of gelation. This phenomenon typically confers improved mechanical properties due to increased material density and structural organization, and can induce cell alignment in the presence of physical constraints such as a rigid mandrel within the tube. However, biological hydrogel-based matrices are often limited by reduced mechanical properties and poor reproducibility [60, 65]. Type I collagen cross-linked with enzymes such as transglutaminase [65] or temporarily supported by an internal silicone sleeve [66] have shown potential for vascular tissue engineering applications, however, suboptimal mechanical properties still remain problematic. Hybrid constructs obtained with mixtures of collagen and fibrin gel or elastin have shown a significant improvement in mechanical properties over collagen alone [59, 67]. These approaches are limited by the length of the process—a common roadblock to clinical feasibility. Using a different construction technique, mixtures of collagen and elastin have been electrospun on mandrels to obtain tubular three-layered fibrous constructs that mimic the natural morphology and structure of arteries and have demonstrated good cell integration [68]. Other biological molecules such as GAGs have also been used for TEVGs. In particular, scaffolds derived from the esterification of the hyaluronic acid have been used to conduct studies *in vitro* [61] and *in vivo* [69].

Another alternative for natural polymers are those derived from decellularized tissue ECM such as small intestinal submucosa or urinary bladder matrix [70, 71]. This approach has been extensively studied in several tissue engineering applications and the ease of processing and

good biocompatibility has led to wide acceptance in the clinical community. During the process of tissue regeneration, the implanted native ECM-derived scaffold is gradually degraded until, eventually, only the cells and tissues that have been deposited by the host remain in place of the scaffold. The scaffold consists of a collection of both structural and functional proteins, which fundamentally alters the healing response [70]. The ECM serves as an inductive scaffold for deposition of organized tissues, rather than simple scar tissue formation, similar to that which occurs during fetal development. The acellular nature of the scaffold removes the antigenic stimulus that would otherwise cause an adverse immune response [72]. Although cell loading might be an alternative to enhance regeneration for this type of approach, the nonporous nature of these scaffolds makes cell incorporation *in vitro* difficult. Furthermore, the highly thrombogenic nature of collagenous ECM-based constructs might lead to graft failure for small diameter vascular constructs [70].

A third type of approach consists of intact decellularized veins or arteries. In this approach, native vessels are harvested and processed to extract all the cellular components usually by means of detergent solutions, and are then subsequently sterilized. The acellular nature of the scaffold partially eliminates the immune response as in the ECM-derived scaffolds, but the mechanical and structural integrity of the original vessel is preserved [73, 74]. Although different animal species or cadavers can be used as sources to obtain these grafts, the procedure is labor intensive, difficult to scale-up, and raises some concerns for the possibility of disease transmission.

Clinically relevant features for the scaffolds described above are ranked and summarized in **Table 1-1**.

Table 1-1 Ranking of scaffolds for four key considerations of clinical viability for use in creating a TEVG. Table from [75].

	Mechanical properties	Cell seeding	Biocompatibility	Scale-up
Synthetic polymers	Very good	Very good	Fair	Very good
Biological gels	Fair	Very good	Very good	Fair
Decellularized ECM scaffolds	Good	Poor	Very good	Very good
Decellularized vessels	Very good	Poor	Very good	Fair

Mechanical properties were ranked based on published work. Cell seeding was ranked based on off-the shelf availability. Biocompatibility was ranked taking into account cell incorporation and the inflammatory reaction triggered after implantation. Scale-up was based on the feasibility to industrialize the construction process.

1.4.3 Surface modifications

The surface of most scaffolds can be engineered to interact with cells at the molecular level. For example, covalent incorporation of cell adhesion-promoting oligopeptides such as RGD, YIGSR, or REDV on the surface of polymers can increase the steric availability of these ligands to cell-membrane integrin receptors [76]. The concentration and distribution of adhesive ligands influence the strength of cell attachment, extent of cell spreading, and the speed of cell migration [77], and allows for the modulation and control of these parameters. Cell-specific ligands can be used, for example, to foster cell adhesion of targeted cell types in desired locations while inhibiting the adhesion of undesirable cell types [78].

Enhancement of adhesion can also be obtained with deposition of self-assembled films. Nanopolyelectrolyte films made of poly(D-lysine) or poly(allylamine hydrochloride) have been shown to increase adhesion of ECs in a controllable manner without protein precoating [79].

Another desirable feature of such films is their ability to incorporate enzymatic recognition sites to give to the scaffold a specific proteolytic sensitivity that can help direct the desired remodeling of the scaffold upon *in vivo* implantation [78].

Incorporation of growth factors into the scaffold is another strategy to control cell attachment and regulate cell proliferation, migration, differentiation, and protein expression. For example, collagen matrices covalently incorporated with heparin and loaded with vascular endothelial growth factor (VEGF) have been shown to significantly enhance angiogenesis in the collagen matrices, thereby increasing EC proliferation [80].

More recently, polymeric gene delivery has been considered to induce the expression of functional proteins, thereby avoiding the cytotoxicity and immunogenicity issues related to the use of viral gene delivery systems [81]. This approach might allow a controlled overexpression of anticoagulant and anti-inflammatory proteins such as thrombomodulin and/or inhibitors of procoagulant and proinflammatory proteins such as vascular cell adhesion molecule-1 (VCAM-1) and intracellular adhesion molecule-1 (ICAM-1).

1.5 CELL SOURCE

Two different cell sources have been used to produce a cellular TEVG: terminally differentiated cells or stem cells.

1.5.1 Adult differentiated cells

The use of terminally differentiated vascular cells permits the fabrication of a TEVG with the same cellular constituents of a native artery, which may potentially reproduce functionality. However, this approach requires a very large initial number of cells and their retrieval might be difficult to accomplish without an invasive procedure for the patient and the harvesting of significant amounts of functional, native tissues (for autologous approaches). Non-autologous cells, derived from different donors (including cadavers), would require an undesirable (or even unacceptable) immunosuppression therapy or other interventions to prevent rejection. Differentiated cells have usually a low proliferative rate and a limited number of divisions available due to cell senescence; therefore these cells have restricted possibilities of expansion [82]. Although some groups have tried to genetically manipulate the proliferation kinetics of differentiated cells by reintroducing the reverse transcriptase telomerase subunit into the adult cell genome [83], the genetic intervention remains a major concern for the scientific community and, therefore, an obstacle to clinical feasibility.

Luminal seeding of endothelial cells (ECs) to confer antithrombogenic properties to the conduit lumen is also a common approach for biodegradable scaffolds. Human umbilical vein ECs cells have been used in this manner, though bovine and porcine aortic ECs have also been used [84, 85]. Smooth muscle cells (SMCs) have been utilized in several approaches to create a TEVG, including seeding on synthetic biodegradable scaffolds [46], culture in biological gels [60], or as component of cell-based constructs [30, 31]. Dermal fibroblasts have been used to construct a ‘‘self-assembled’’ TEVG, using extensive cell culture and relying on accelerated ECM production by the cells [32].

1.5.2 Adult stem cells

Stem cells have a great potential for use in tissue engineering applications and may circumvent many of the shortcomings associated with other solutions to cell sourcing. A first distinction should be made between adult stem cells and embryonic stem cells. Almost all tissues possess latent populations of adult stem cells that become active in determined circumstances such as in case of injury or remodeling, and are chemo-attracted to determined sites by specifically released cytokines [86]. Adult stem cells can be harvested from several autologous tissue sources with varying levels of invasiveness including bone marrow, body fat, and striated muscles [87-89] without compromising the functionality of the donor tissue. Adult stem cells usually display a rapid, almost endless expansion capability when cultured in expansion media (usually rich in fetal serum) and therefore, are ideal candidates for tissue engineering which requires availability of large amount of undifferentiated cells in a short amount of time.

The therapeutic use of bone marrow (BM) (*e.g.*, in bone marrow transplantation) has created an extensive background of knowledge on this particular cell source. BM contains different types of progenitor cells at various stages of differentiation. BM includes hematopoietic stem cells (positive for the protein markers CD34, Sca-1, and c-Kit) [90], mesenchymal stem cells (CD105+ and CD73+ and negative for CD34) [91], and endothelial progenitor cells (EPCs; CD133+, CD34+, and VEGFR-2+) [92]. Hematopoietic stem cells are responsible for the generation of all blood cells including erythrocytes, leukocytes and thrombocytes. Mesenchymal stem cells, instead, can differentiate into many different cell types including osteocytes, adipocytes, neurocytes, chondrocytes, and myocytes and have high proliferative kinetics [93]. Mesenchymal stem cells have also been shown to differentiate to

SMCs, making them a valid candidate for vascular applications [94]. EPCs, finally, have been shown to differentiate into ECs and produce capillary networks *in vitro* [95].

Several TEVG approaches have used BM progenitor cells (BMPCs). Some of them have relied on an *in vitro* maturation and pre-differentiation of BMPCs into ECs and SMCs [73]. Other approaches utilized undifferentiated BMPCs relying on their *in vivo* differentiation and remodeling [96].

Adipose-derived stem cells (ASCs) are another promising candidate for tissue engineering since the availability of autologous fat is high and does not require highly invasive procedures for harvesting (liposuction) [89]. ASCs have been shown to differentiate into multiple cell lines, including bone, fat, smooth muscle, and cartilage [97], as well as endothelial cells [98].

The skeletal muscle is another source of progenitor cells. Muscle-derived stem cells (MDSCs) isolated from the striated muscle exhibit multipotentiality toward vascular lineages (SMCs and ECs), self-renewal capabilities, and have a direct role in tissue remodeling and regeneration both *in vitro* and *in vivo* [99-101]. MDSCs are SCA-1+, CD34+, and they represent a promising alternative for vascular tissue engineering applications.

1.5.3 Embryonic stem cells

Embryonic stem cells (ESCs) are pluripotent cells capable, with the appropriate environmental cues, either generating any cellular lineage or self-renew. Self-renewal is the capacity of making a perfect cellular copy an unlimited number of times. ESCs are obtained from the inner cell mass of the blastocyst (a very early developmental stage of the embryo) causing the loss of the fertilized egg. Therefore, the use of human ESCs has raised a number of ethical dilemmas,

thereby limiting their use. Differentiation of ESCs cells into ECs and SMCs has been achieved showing angiogenesis and formation of microvascular structures *in vitro* [102] and *in vivo* [103, 104]. However, beyond the ethical issues, immunogenic and tumorgenic problems continue to represent obstacles to clinical applications of ESCs.

1.6 SEEDING TECHNIQUES

Cell seeding represents a fundamental step in any tissue engineering application that incorporates cells into or onto scaffolds prior to culture or implantation [105]. Desirable features for any seeding technique include, minimized cell injury, uniform cell distribution, high seeding efficiency, reduced seeding time, high reproducibility, and user independence. The incorporation of cells into tubular scaffolds is generally more challenging than the one into flat sheets of scaffolds, and it is desirable in a variety of tissue engineering applications such as those for the vascular, cardio-respiratory, urological, neurological, and gastrointestinal systems. A distinction should be made between surface seeding, e.g., lining cells on a luminal surface, and bulk seeding, which implies delivery of cells through the thickness of the scaffold. Most of the current seeding techniques have involved the seeding of cells onto surfaces. Previously described seeding techniques take advantage of different, single driving forces such as sedimentation [106], electric/magnetic fields [107, 108], rotation [109], or vacuum/filtration [110, 111]. Recently, acoustic waves have been used to increase the depth of cell penetration into the scaffold surface as well [112]. The use of a seeding device is often challenging since mechanical forces are usually involved in seeding procedures and can be responsible for damage

via membrane lysis or triggering of apoptotic pathways [113, 114]. Bulk seeding is a more difficult task to accomplish especially in a controllable manner.

The complex micro-architecture of the scaffolds often hampers the passive incorporation of cells within them. In a three dimensional environment it might be beneficial to provide a uniform and controllable distribution of cells to foster homogeneous tissue remodeling and to avoid competition for nutrients in areas with a higher density of cells [111]. Surface seeding by dripping a cell suspension on the matrix is a very simple, and the most common technique for bulk incorporation of cells into scaffolds [115, 116]. However, this technique neither produces a high yield of cells included within the scaffold nor affords a "quality control" on the final engineered tissue due to the manual nature of the procedure. Incorporation of cells in matrix suspensions such as collagen or fibrin gel or a synthetic hydrogel [60] is an easy and effective seeding technique but the applications are limited by the poor mechanical properties of hydrogels (recall **Section 1.4.2**). Recently a novel technique called "microintegration" based on simultaneous electrospinning of polymer and a cell suspension to produce a cellularized construct was reported [117]; this technique may affect cell viability due to the strong electrical field and to the cytotoxicity related to the polymer solution solvent. A technique called "cell printing" allows for a multilayered deposition of cells and hydrogels in complex 3D shapes via a modified ink-jet printing technology [118]. This technique allows for detailed control of scaffold and cell deposition but the process is still complex and costly.

Figure 1.4 summarizes the seeding methods previously described in the literature.

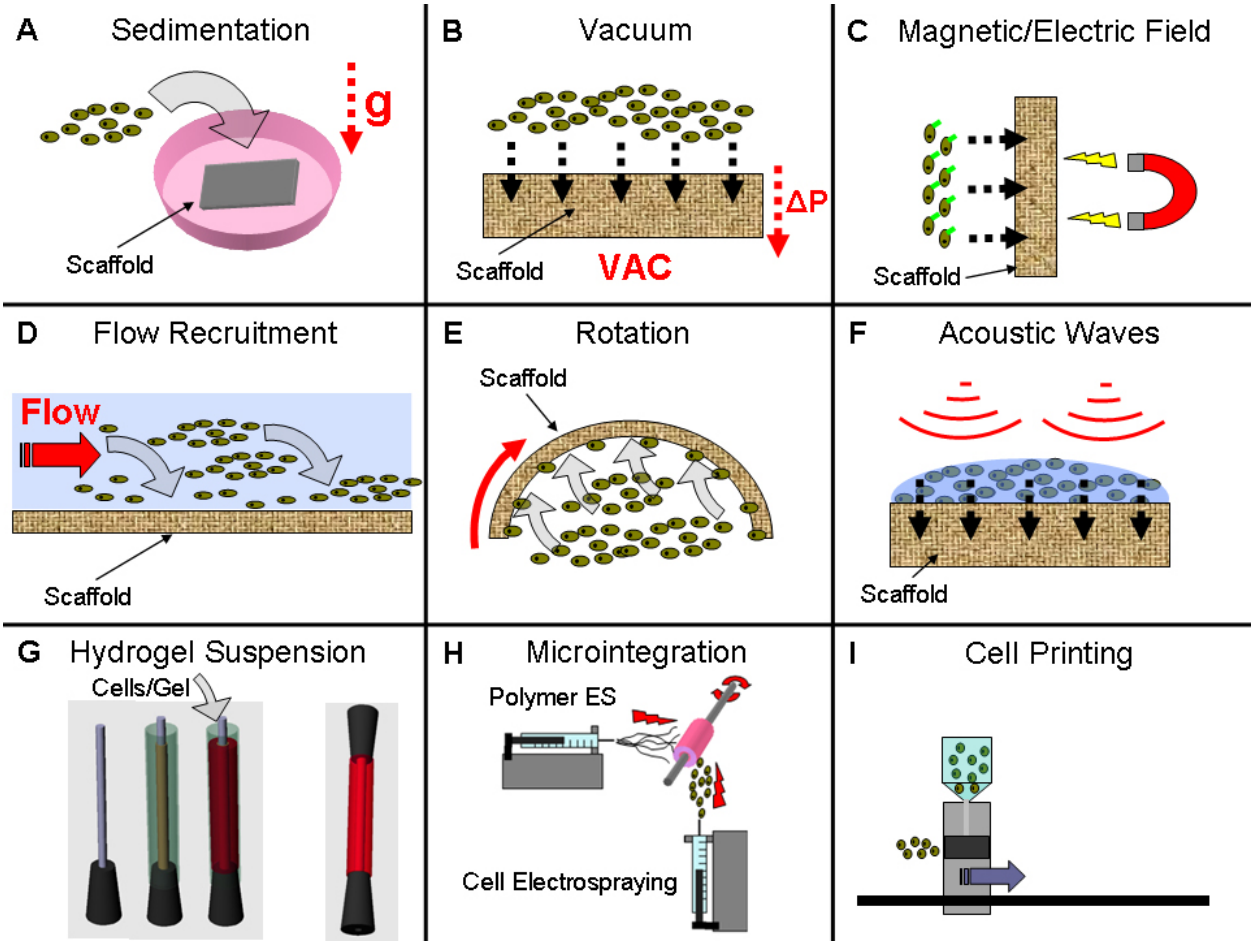

Figure 1.4 Overview of previously reported seeding techniques. **A.** Pipetting cells suspensions on top of flat sheets of scaffold materials allows for gravity-mediated cell sedimentation onto the surface. **B.** When a porous scaffold is placed in a column between a seeding suspension and an applied vacuum, a transmural flow is generated by the pressure gradient resulting in an entrapment of cells in the scaffold matrix. **C.** Immuno-labelling cells with electrical of magnetic particles allows for scaffold seeding driven by electric or magnetic fields. **D-E.** Cell suspensions cyclically moved on top the scaffold (either via flow generated by a pump of via rotation of the scaffold) will induce the progressive recruitment of cells onto its surface. **F.** Acoustic waves oriented toward a cell suspension in contact with a porous scaffold improve the penetration of cells into the pores. **G.** Pouring cell/hydrogel suspensions into molds will cause the creation of a cellularized scaffold upon gelation. A similar concept is pursued with the "cell sheets" technique in which the cells are initially embedded in their own produced ECM in forms of sheets. The sheets are then used to create different shapes by means of external supports. **H.** The concurrent deposition of polymer via electrospinning and cells via electrospraying has been shown to produce densely cellularized constructs. **I.** Ink-jet printer modified systems allowed a highly controlled 3D deposition of cell/hydrogel suspensions to create scaffolds with a seeded micro-architecture.

1.7 *IN VITRO* STUDIES OF TEVGS

In vitro approaches requiring mechanical or biochemical conditioning regimens rely on the cellular remodeling mechanisms of the engineered tissue to build the ECM structure, increasing the mechanical properties of TEVGs, or inducing cell proliferation and/or differentiation before implantation. However, these natural processes are often slow to occur *in vitro*, requiring culture times (weeks to months) that might not be compatible with the clinical translation in which the ideal paradigm is to provide "off-the-shelf" or at least readily available products. Therefore, extenuating *in vitro* culture and maturation times for engineered tissues, while providing very valuable insights on controlled tissue formation, might not be ideal for a translational approach.

1.7.1 Bioreactors

Most tissue-engineered constructs lack mechanical and functional properties necessary for a successful *in vivo* implantation immediately following seeding. Therefore, the use of bioreactors for *in vitro* culture and maturation has become a major area of investigation in tissue engineering. The goal of a bioreactor is to create a sterile physiological environment in which TEVG constructs can be cultured and exposed to biochemical (*e.g.*, growth factors, cytokines, *etc.*) and biophysical stimuli (*e.g.*, mechanical forces, *etc.*). Bioreactors can guide the tissue development and growth until complete maturation of the engineered tissue before implantation. Several bioreactors for TE have been described in the literature with various levels of complexity and performance. Basic types of bioreactors include spinner flasks [119] and rotational culture systems [120]. These devices enhance mass transport of nutrients and gases by adding convective components to the mass transport equations [121] (induced by the constant

stirring/movement of culture media within the bioreactor), and have the relevant advantage of being simple, cost effective, and promptly useful following seeding due to their delicate culture conditions. These bioreactors are not designed to exert mechanical forces on tubular constructs or to perfuse them with a continuous flow. More complicated perfusion bioreactors, instead, can subject tubular constructs to steady or time-varying mechanical stresses such as shear stress, hydrostatic pressure, and circumferential stress, thus mimicking the cardiovascular environment [37, 66, 122]. Both the magnitude and frequency of mechanical stimulation have effects on the development of the tissue *in vitro* [123].

1.7.2 Biochemical stimulation

Mechanical stimulation has been coupled with biochemical factors in order to recreate the complex natural milieu encountered during tissue development. Bioactive chemicals such as ascorbic acid, copper sulfate, and amino acids have been shown to enhance matrix deposition and cross-linking [37] and ultimately, the strength of the engineered tissue. Growth factors such as basic fibroblastic growth factor (bFGF), platelet-derived growth factor (PDGF), transforming growth factor-beta (TGF-β), and vascular endothelial growth factor (VEGF) have been utilized to stimulate engineered tissues. Both bFGF and PDGF are mitogens for SMCs and ECs [124, 125], which allows for faster proliferation of cells into the engineered tissue. TGF-β is involved in mitogenesis and morphogenesis and increases ECM matrix deposition [126]. TGF-β has also shown to increase α-SMA expression and matrix production in collagen gels exposed to both static and dynamic culture [127, 128]. TGF-β also induces differentiation of BMPCs toward SMC lineages [129]. VEGF has mitogenic effects for ECs and progenitor cells [125] and can induce EC differentiation in progenitor cells [130].

1.8 *IN VIVO* STUDIES OF TEVGS

Several studies have focused on the body's ability to restore and regenerate functional tissues starting with temporary engineered tissues [72, 131, 132]. In these works, the living organism has been utilized as a ''bioreactor'' to complete the formation of the engineered graft via host-mediated remodeling mechanisms. The role of the scaffold in this approach is to provide temporary structural and mechanical support, and in some cases, to provide biochemical cues to direct remodeling [133]. Several approaches have successfully utilized this model for vascular applications with different levels of success.

Acellular biological grafts have been implanted in dogs showing good patency rates, absence of infections and intimal hyperplasia. However, several of these grafts developed aneurysms within the first 48 weeks of implantation thus limiting this application in future studies [134, 135]. TEVGs were obtained via host-response (encapsulation) to Silastic tubes implanted into the peritoneal cavity of rats and rabbits [33]. This approach might be limited by the need of an additional surgery to retrieve the TEVG introducing additional morbidity to the process. Cho *et al.* [73] seeded scaffolds with labeled BMPCs pre-differentiated *in vitro* into SMCs and ECs. Eight-week follow-up showed increase in patency rate of the seeded grafts compared to the unseeded controls. Moreover, the seeded cells where engrafted into the remodeled grafts showing their contribution in the vascular remodeling process. With a similar approach, another group reached a 100-week post-implantation period with positive outcome in a

growth model in lambs, thus showing also the ability of the TEVG to growth with the host animal [136].

The architectural structure of the scaffold, such as pore size, porosity, and interconnectivity, has a significant impact on the *in vivo* mechanisms of remodeling [137]. The cellular component incorporated into the scaffolds prior to implantation also plays a critical role in the TEVG remodeling and functionality *in vivo* [138]. Despite years of research, the *in vivo* mechanisms of remodeling remain not completely understood and no clear consensus on the best approach to pursue has been achieved yet.

1.9 CLINICAL TRANSLATION

To be clinically viable, a TEVG must meet several requirements extending beyond its successful preclinical testing. From a commercial standpoint, a short overall fabrication time for the TEVG is a critical prerequisite for its future clinical translation. A long manufacturing process would generate high production and quality control costs consistently affecting the price of the final product and its chance to be reimbursed by insurance companies. The cost of a TEVG will be an important indicator of its capacity to penetrate the market, thus becoming available to patients. Reproducibility of the TEVG characteristics and functionality is also critical for quality control purposes and in order to test and predict clinical outcomes in different patient populations. Therefore, research efforts should be focused on a manufacturing process in which most of the steps involved in the construction of the TEVG are automatic and user independent. This is a very important consideration especially when dealing with complex bioreactors that require a high degree of skill for their use. From a clinical standpoint, a product's availability off-the-

shelf would be the ideal situation mainly because it would be widely accepted by the vascular and cardiac surgical community. Moreover, for the approximate 50% of the patients requiring urgent or emergent CABG surgery [139] or for the trauma patients, an off-the-shelf, or more feasibly, a short time-frame approach would be the only possible answer.

Those TEVG approaches using cellular components have intrinsic constraints for their complete off-the-shelf availability due to their need for cell isolation and expansion; ideally, they should rely on a manufacturing process being completed within the sterile operating room setup where the patient's own cells would be integrated into an off-the-shelf available scaffold before the implantation. This model would require operative infrastructures that are not currently implemented in hospitals. While many within the vascular tissue engineering field believe that we are at least a decade away from a complete clinical application of TEVG, some clinical trials have already been conducted with promising results. Shin'oka and coworkers [38, 115] have successfully implanted a porous P(CL/LA) scaffold reinforced with an external sleeve of nonwoven PGA seeded manually with autologous BMPCs. The cells were isolated concurrently with the procedure to repair single ventricle anomalies using a total cavopulmonary connection. They reported eight patients who were asymptomatic and with no need of reoperation at an average follow-up of 13 months. L'Heureux *et al.* [140] reported six hemodialysis patients with failing arteriovenous shunts implanted with autologous TEVGs as arteriovenous graft with a follow up of 13 months. Three of the patients successfully completed the follow-up period with no issues, resisting repeated needle punctures.

These encouraging results provide evidence that although widespread clinical applications of vascular tissue engineering may be a long way off, clinical translation of this emerging science is clearly feasible.

1.10 HYPOTHESIS AND SPECIFIC AIMS

A critical analysis of the literature with a particular emphasis on the pitfalls that limited the positive outcome of previous TEVG approaches led to the formation of the following hypothesis:

Working Hypothesis: *A novel scaffold optimally seeded with stem cells, acutely cultured and stimulated* in vitro*, and ultimately implanted* in vivo *will remodel into a functional vascular tissue.*

This hypothesis was addressed in this dissertation by the following specific aims:

Specific Aim 1: *Development and optimization a seeding device to rapidly and efficiently deliver cells uniformly and reproducibly through porous, tubular scaffolds.* One of the challenges in the tissue engineering of tubular tissues and organs is the efficient seeding of porous scaffolds with the desired cell type and density in a short period of time, and without affecting cell viability. Though different seeding techniques have been investigated, a fast, reproducible, and efficient bulk seeding method with uniform cellular distribution was yet to be reported. The purpose of this aim was to overcome the limitations of the previous seeding techniques for porous tubular constructs.

Specific Aim 2: *Development of a composite scaffold to mimic the mechanical and structural properties of native arteries.* The use for vascular tissue engineering of two different types of PEUU scaffolds (TIPS PEUU and ES PEUU) has been

previously investigated. Each of these scaffolds have shown distinct positive features such as excellent cell integration upon seeding (TIPS) or excellent mechanical properties (ES). A rationally-guided, hybrid ES-TIPS PEUU scaffold was designed and developed to incorporate both these features into the same scaffold.

Specific Aim 3: *Determination of the ideal acute culture conditions to optimize the construct via cellular proliferation, migration, and spreading.* Upon seeding, the TEVGs require a transitional quasi-static culture period before any flow or mechanical force can be applied. The purpose of this aim was to investigate the ideal culture protocol to consistently achieve a completely populated and undifferentiated stem cell-based construct suitable for *in vivo* implantation.

Specific Aim 4: *Assessment of the remodeling, patency, phenotype, and mechanical properties following in vivo remodeling.* Natural mechanisms of vascular healing and remodeling are the results of the synergistic action of multiple biochemical and biomechanical factors. We have adopted a "black box" approach to evaluate the final result at different time points rather than establishing a mechanistic model of remodeling which was beyond the scope of the current dissertation.

In this research work, we have explored a multidisciplinary framework incorporating adult stem cells, biomaterial technologies, a novel seeding device, and preclinical animal studies

to develop and test TEVGs. The aforementioned framework was rationally designed and oriented to meet clinical translation criteria (described in **Section 1.9**) with respect to the TEVG fabrication time frame, reproducibility, and practical feasibility. The goal of the proposed research was to develop a viable and functional TEVG in time periods compatible with the clinical practice. Therefore, the following dissertation can be considered a translational (or applied) research project involving a wide variety of research disciplines and subjects. Naturally, many points of this work have been carried out deliberately refraining from establishing mechanistic bases of functioning. In many circumstances, only an observational ("black-box") approach has been pursued, thus introducing several limitations to the study.

The following two chapters (**Chapter 2** and **3**) will explore the development of several versions of a seeding device for porous tubular scaffolds (**Specific Aim 1**), which can be considered the pillar of this research endeavor and the basis for a possible future commercial venue for the development of a TEVG. **Chapter 4** will focus on the development of the ES-TIPS PEUU scaffold (**Specific Aim 2**) with a particular emphasis to its mechanical characterization in comparison with its two single components (TIPS and ES PEUU) and native blood vessels. **Chapter 5** will describe the interactions between cells (MDSCs) and PEUU-based scaffolds within dynamic culture conditions (**Specific Aim 3**). The chapter will also cover the development and testing of a novel perfusion bioreactor. **Chapter 6** will be dedicated to the *in vivo* preclinical studies (**Specific Aim 4**) performed in rats (allogeneic approach), while **Chapter 7** will describe the pilot study perfomed in pigs (autologous approach). The chapter will also mention about the isolation of a heterogeneous population of adult stem cells derived from the striated muscle of pigs. Finally, **Chapter 8** will draw conclusions from the results obtained in each specific aim, describing the advantages and limitations of each, and propose

future directions and improvement of the technologies based on lessons learned from this dissertation work.

2.0 SPECIFIC AIM 1, PART 1: DEVELOPMENT OF A SEEDING DEVICE FOR TUBULAR SCAFFOLDS

The seeding of porous scaffolds is a fundamental part of our tissue engineering paradigm, and should comply with a number of requirements. For example, tissue engineered scaffolds should be uniformly bulk-seeded with cells to promote rapid, homogeneous, full-thickness tissue formation. A homogeneous cell distribution is critical since regions in which cells are not seeded will likely have a delay in tissue formation and remodeling. In addition, if used as a vascular graft, the luminal surface of an engineered tubular construct should ideally be lined with a confluent endothelial layer to inhibit thrombosis and maintain graft patency. When cell availability is an issue (*e.g.*, when autologous differentiated cells are used), it is necessary to seed the scaffold with a high efficiency in order to deliver the highest percentage of the initial cell count used. Finally, to be clinically viable, a tissue engineered construct should be fabricated in a minimal amount of time and in a reproducible and user-independent fashion.

2.1 INITIAL DESIGN OF A VACUUM SEEDING DEVICE FOR TUBULAR SCAFFOLDS

2.1.1 Design principles

The initial design of a novel device to incorporate cells into the wall of tubular scaffolds was focused on two main design criteria: rapid bulk cellular integration and seeding uniformity. The need for rapid cell penetration into the wall of a porous conduit suggested the need for a transmural flow of a cell suspension through the scaffold wall. In this way, the cells are transported into the bulk of the material along with the liquid solution, and the resulting scaffold acts as a filter for the seeding suspension (*i.e.*, the scaffold retains cells within its pores via the process of cell suspension filtration). This filtration process makes the seeding outcome intrinsically correlated to the physical and structural characteristics of the scaffold (*e.g.*, hydrophilicity, permeability, porosity, pore size, *etc.*). A seeding process utilizing a filtration mechanism inherently requires a permeable scaffold to allow for transluminal flow. Creation of a transmural flow across a permeable media (filter) requires a transmural pressure gradient. The vacuum applied downstream to a filter creates a positive pressure gradient upstream to the porous media, thereby inducing a movement of fluid across the filter. This method is commonly used in a variety of laboratory applications such as bottle-top filter devices for the sterilization of fluids, or DNA purification columns. The same concept has been described in literature for surface cell seeding of mostly flat scaffolds [141, 142], but also commercially available vascular grafts [110].

Inducing a transmural flow through the wall of a porous tubular scaffold with the specification of uniform distribution of the flow rate along the longitudinal and circumferential

directions is not a trivial task. To address these challenging specifications, it was proposed to apply the vacuum externally to the tubular scaffold while the liquid cell suspension was fed internally via two opposite tees connected to syringes.

2.1.2 First prototype and bench-top testing

The first prototype of vacuum seeding device (**Figure 2.1**) served as a proof of concept, and consisted of an airtight chamber modified from a previously developed tissue housing chamber for vascular segments and two stainless steel (SS) tees, each connected distally to a 5 mL syringe filled with a seeding suspension. An additional 30 mL syringe filled with saline was connected to one tee via a three-way stopcock (along with one of the two seeding syringes) with the purpose of flushing the remaining luminal seeding suspension throughout the scaffold wall at the end of the seeding process. The syringes were used as collapsible containers to allow for passive withdraw of the fluid contained within upon application of vacuum inside the chamber.

Several bench-top tests of the first working prototype allowed for a better understanding of the seeding mechanisms and to troubleshoot several issues related to the initial design of the vacuum seeding device. The lesson learned from these initial experiments was paramount for the development of the first generation of the functional seeding device later described in **Section 2.2**.

The application of a negative pressure inside the chamber directly from the laboratory vacuum line (as shown in **Figure 2.1A**) induced a passive withdraw of seeding suspension from the two seeding syringes and its exudation throughout the scaffold wall, as expected. The flow rate across a porous media is normally described by the Darcy's law, given here in its extended form as:

$$Q = -A\alpha \frac{\Delta P}{\mu L} n \qquad \textbf{2-1}$$

where A is the exudation area, α is the permeability of the porous media, ΔP is the pressure gradient across the porous media, μ is the dynamic viscosity, L is the thickness of the porous media, and n is the porosity.

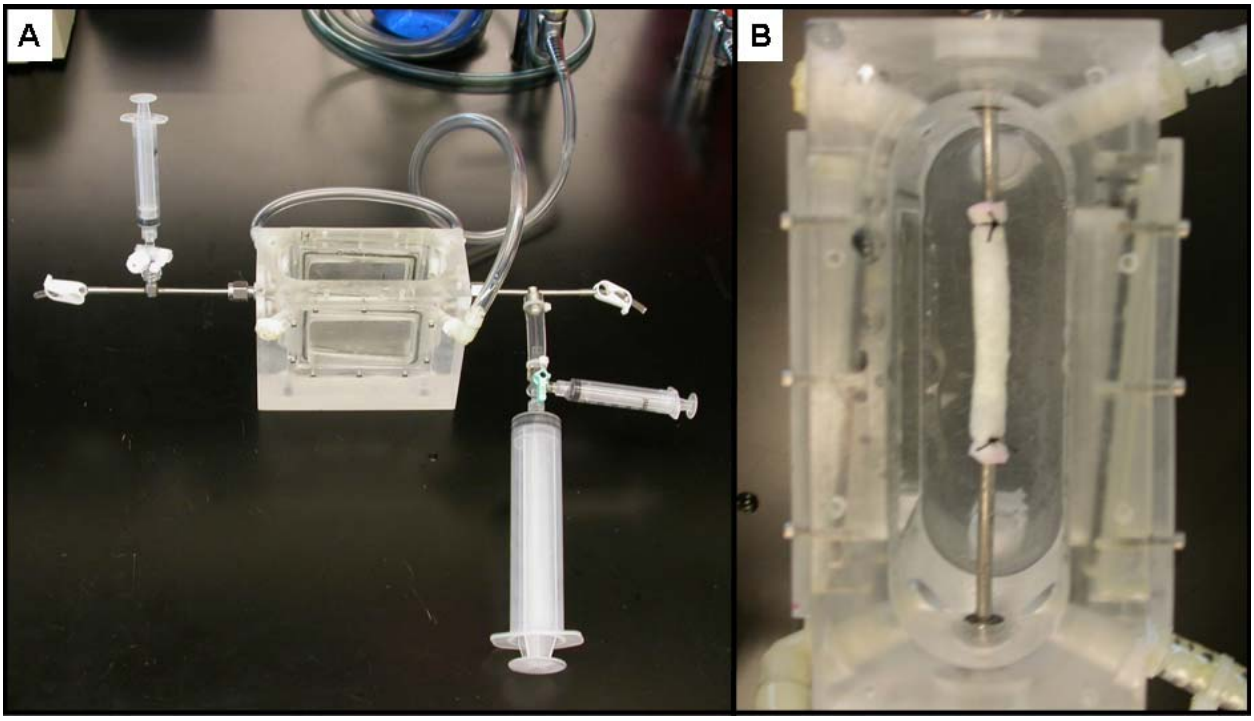

Figure 2.1 First working vacuum seeding device prototype. **A**. The device consists of an airtight chamber directly connected to the laboratory vacuum line. The chamber holds two aligned tees connected to two seeding and one flushing syringe. A lid with an intermediate rubber gasket is secured via thumb screws (not shown) to retain the internal pressure. **B**. The tubular scaffold is reversibly secured internally to the chamber to the two opposite tees via silk suture ligations allowing for exudation of the seeding suspension throughout its wall. The chamber acts also as a reservoir to recollect the exuded seeding suspension for cell counting purposes to measure seeding efficiency. Seeding efficiency is defined as the ratio between the number of cells recollected into the chamber and the number of seeded cells.

However, the presence of the seeding syringes upstream to the flow path in the first prototype did not allow this formula to correctly model the flow rate for a given ΔP. This effect was due to the energetic cost required to overcome the drag force necessary to move the syringe rubber piston. This force has different values depending on the size and type of syringe used. Therefore, **Equation 2-1** grossly overestimates the flow rate throughout the porous media in such a case. Note that the pressure gradient across the porous wall is equal to the applied vacuum inside the chamber (*i.e.*, "downstream pressure" = vacuum level, "upstream pressure" = atmospheric pressure).

Additionally, the absence of a regulator system for the vacuum was causing the seeding flow rate to be too high since the chamber was directly connected with the maximum available vacuum level (usually ~ -30 inHg (-760 mmHg)) from the laboratory vacuum line. Therefore, the need for an external vacuum regulator system was evident. For this purpose, a regulator circuit was designed and built (see **Figure 2.2**). The circuit consists of a multi-turn needle valve (Cole-Parmer, Vernon Hills, IL) acting as a flow regulator connected in series to the circuit, a 0.2 μm ePTFE filter (Acro® 50, Pall Corporation, East Hills, NY) placed in parallel to the circuit, a digital vacuum gauge (ACSI, Irvine, CA), a switch represented by a three-way stopcock, and a quick-disconnect tube coupling with shut-off valves (McMaster-Carr) to rapidly connect and disconnect the circuit to the seeding chamber. All the components are connected to each other and to the laboratory vacuum line via polyvinyl chloride (PVC) tubing. The vacuum regulator circuit takes advantage of flow-dependent, localized pressure losses into the flow regulator valve and into the ePTFE filter to reduce the level of available vacuum into the seeding chamber. The reduction of the vacuum level is created by inducing a flow of air moving from the ePTFE filter outlet into the vacuum line (dashed arrows in **Figure 2.2**), leading to a controllable pressure loss.

The vacuum level can be adjusted with the flow regulator and observed with the vacuum gauge while the downstream switch is in an off position. Immediately after the switch is turned on, a transient flow of air (dotted line in **Figure 2.2**) is mobilized from the chamber to the vacuum line until a steady vacuum level (equilibrating the vacuum level previously selected with the switch in its off position) is reached into the chamber. The recorded vacuum range for the developed vacuum regulator circuit was 0 to -16 inHg obtained with either a fully closed or open regulator valve. The flow rate inside the chamber for different levels of vacuum was recorded by measuring the time necessary to release 10 mL of water from the two 5 mL syringes with increasing levels of vacuum from -1 to -8 inHg (**Figure 2.3**).

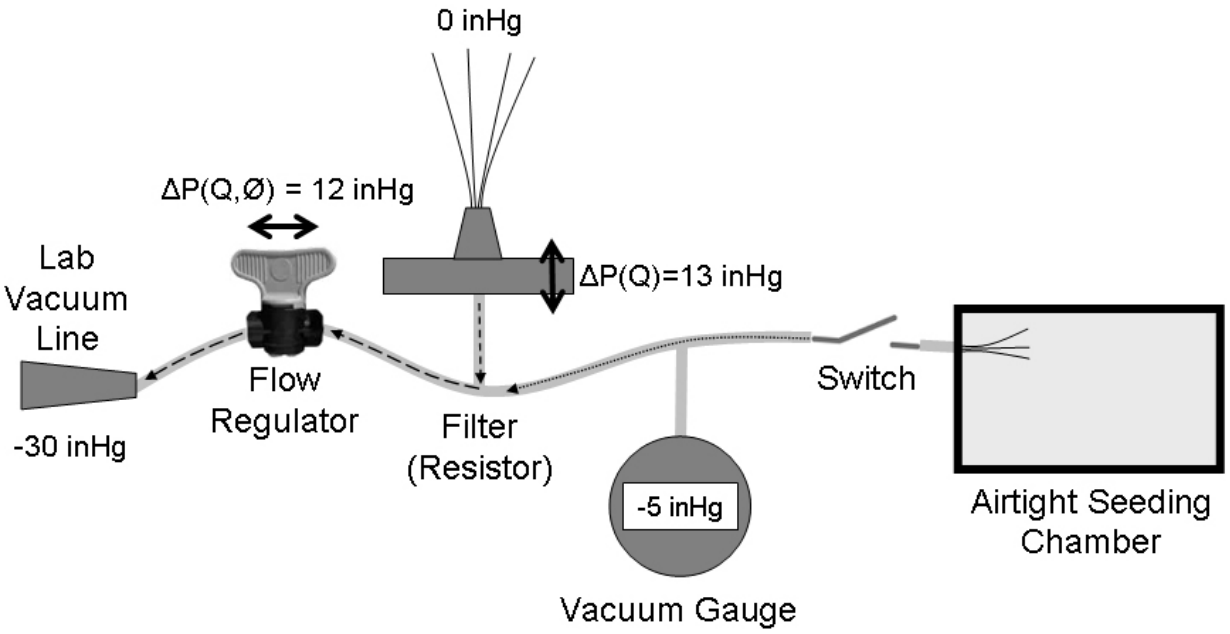

Figure 2.2 Vacuum regulator circuit. By increasing the level of closure of the needle valve (flow regulator), it is possible to increase the localized pressure drop across it (reducing the flow of air) leading to a reduction of available vacuum in the chamber.

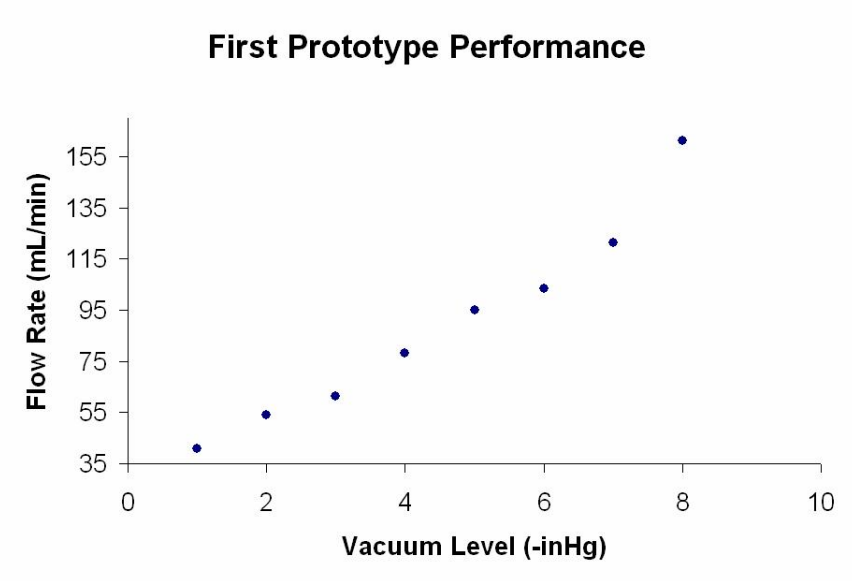

Figure 2.3 Flow rate generated inside the vacuum seeding device for different levels of vacuum. The data represented was obtained with the same TIPS PEUU scaffolds used in the initial seeding experiments.

While developing the first prototype, it was also determined that there was need for scaffold adaptors for a rapid and effective connection and disconnection of the tubular scaffolds to the two tees without the use of a direct suture ligation. The purpose was also to limit the direct handling of the scaffold with surgical instruments after seeding to avoid squeezing of the porous matrix and accidental cell loss. To this end, adaptor tips were designed and built by modifying common micropipette tips (**Figure 2.4**). The distal end of the conical micropipette tip was cut with a razor to enlarge its opening. Polypropylene tubing (Intramedic) was pressure-fit inside the central channel by pulling a guiding silk suture string through it (**Figure 2.4B**) which was previously ligated to the tip of the small tubing. The scaffold ends were subsequently ligated to two custom tips with silk suture strands. Before applying the sutures, a SS wire was

inserted into the channel of the custom-made tips to avoid the collapse of the tubing while tightening the knots. The concept of tee adaptor was applied to a large variety of scaffold sizes with several different design modifications covering a wide range of tube IDs (1-25 mm). An example of a custom made adaptor used to seed a large diameter scaffold (see **Section 2.2.6.1**) is shown in **Figure A.1**.

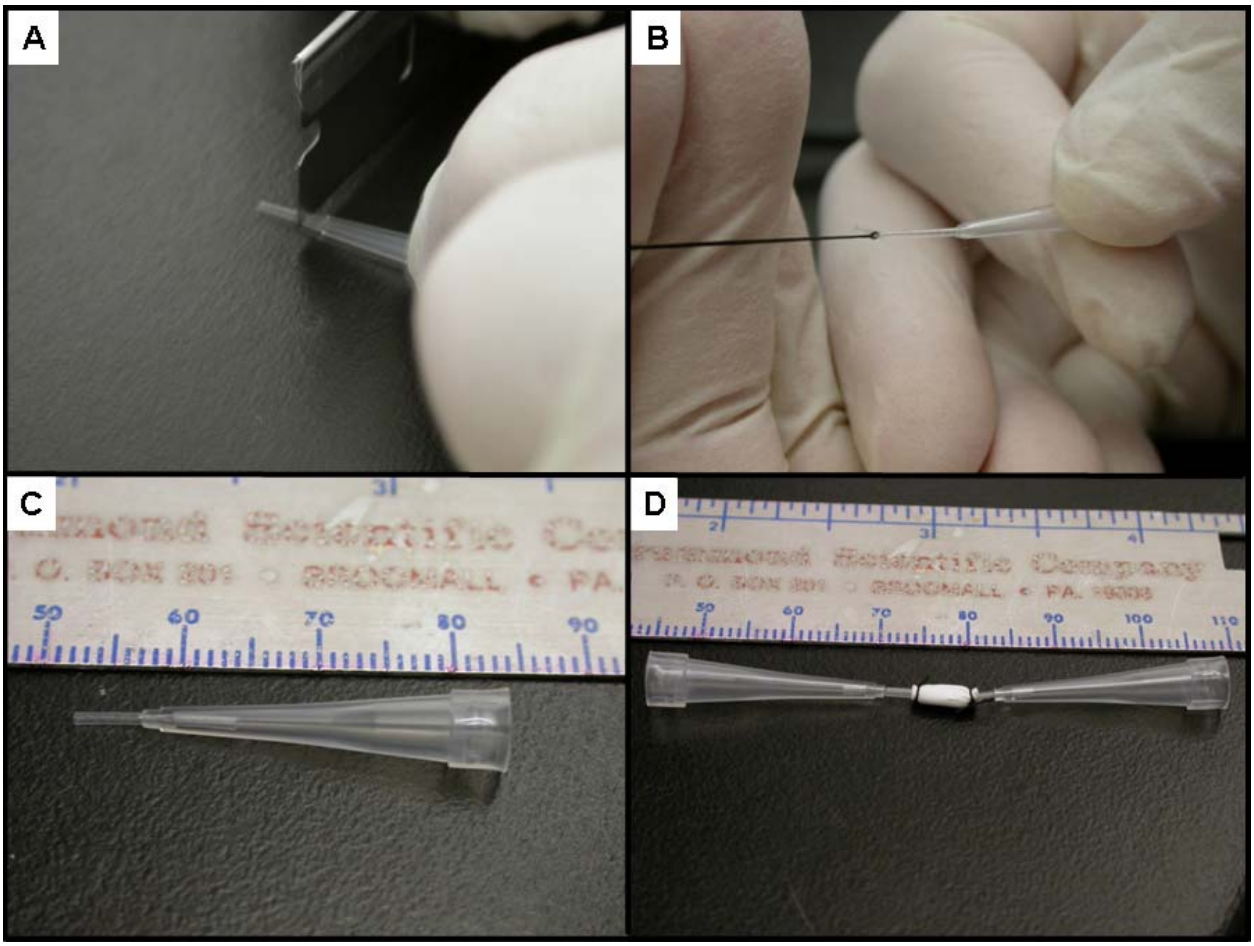

Figure 2.4 Adaptor tips fabrication for scaffold ID of ~1 mm. **A.** The pipette tip was cleaved with a razor. **B.** A silk strand was used as a guide to pull and pressure-fit an internal small tubing. **C.** Appearance of the completed custom-tip. **D.** The scaffold attached to two tips for a rapid connection/disconnection to the seeding tees.

2.1.3 Seeding testing

The first seeding experiments (**Figure 2.5**) were performed using the vacuum regulator circuit (**Figure 2.2**) and custom-made adaptors (**Figure 2.4)**. The device was sterilized prior to seeding by ethylene oxide (EtO) gas diffusion for 16 hours (Andersen Product Inc.). The scaffolds used for the initial testing were porous PEUU obtained via TIPS [53] (Length = 2.5 cm, ID = 3.3 mm, thickness = 1 mm; see **Chapter 4** for a detailed description of this scaffold).

Rat bone marrow derived progenitor cells (rBMPCs) were isolated using a previously reported technique [143]. Briefly, the bone marrow obtained from the femurs of Sprague-Dawley rats was mixed in a 1:1 volume with Dulbecco's modified Eagle's medium (DMEM) (Sigma), supplemented with 10% fetal calf serum (FCS) (Gibco, Invitrogen Corporation) and 1% penicillin/streptomyocin (P/S) (Gibco, Invitrogen Corporation), filtered with a 70μm cell strainer filter (BD Biosciences) and centrifuged at 1000 rpm for 5 min. The resulting cell pellet was resuspended and the cells were plated in 175 cm^2 flasks and cultured for 7 days at 37°C in 5% CO_2. After 7 days of culture, non-adherent cells and floating debris were removed, and the remaining rBMPCs were then expanded to the required cell number for each seeding experiment. Cells were suspended in DMEM supplemented with 10% FCS and 1% P/S. Initial seeding assessment was performed by seeding three tubular scaffolds with 2 million rBMPCs, each suspended in 10 mL of culture media. The vacuum level applied to the chamber was -5 inHg. Immediately after seeding, each scaffold was cultured in static conditions for 2 hours, and then fixed in 4% paraformaldehyde for 1 hour.

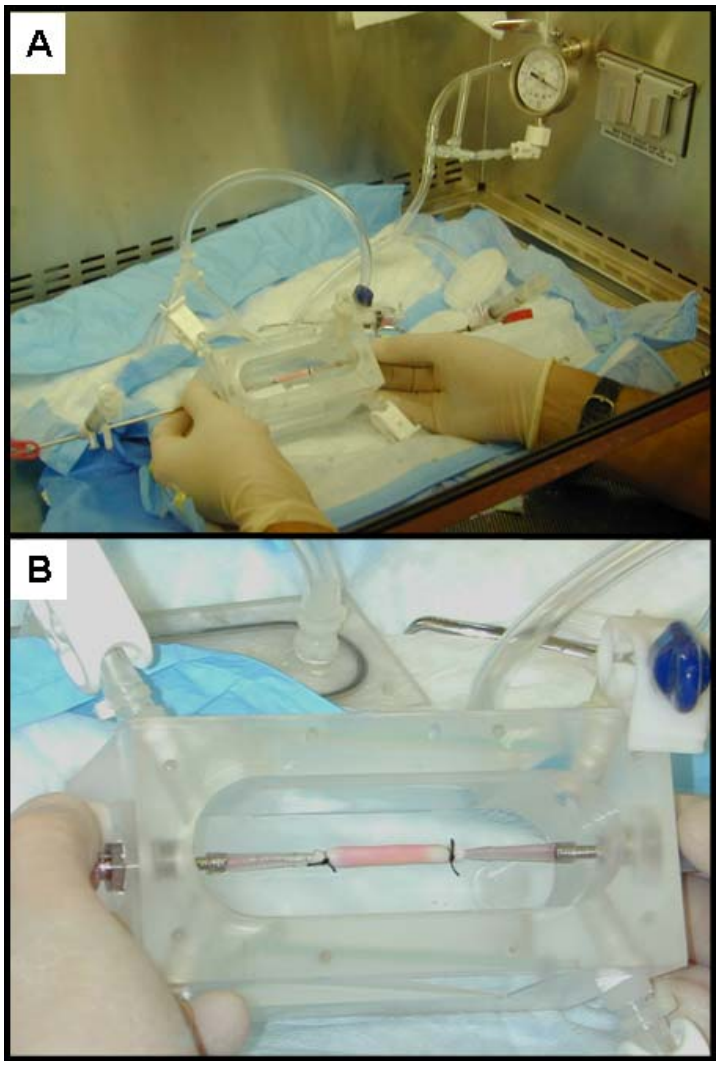

Figure 2.5 Initial seeding experiments performed with the first prototype of vacuum seeding device. The process was performed under a laminar flow hood to avoid contamination (A). Note the pinkish color of the scaffold (B) (cell culture media) following seeding due to the transmural flow of cell suspension.

After washing in phosphate buffered saline (PBS) and overnight immersion in 30% sucrose solution, the specimens were embedded in tissue freezing medium (TBS, Triangle Biomedical Sciences, Durham, NC) and sectioned with a cryostat (Cryotome, ThermoShandon, Pittsburgh, PA). The 10-μm sections were stained with the nuclear stain DAPI (bisbenzimide, Sigma) for

one minute. The sections were observed via epifluorescence microscopy using an Eclipse E800 (Nikon, Melville, NY) with a UV filter.

Simple qualitative assessment of the seeding results (**Figure 2.6**) suggested an imbalance between the amount of cells seeded in the two hemi-cylinders of the scaffold (top and bottom), likely due to a cell sedimentation effect induced by gravity. Therefore, a basic image-based quantification of cell nuclei was performed via ImageJ software (NIH, Bethesda, MD) demonstrating that the bottom of the scaffold was receiving 60.8±2.9% of the total cell number compared to the 39.2±2.9% (mean ± standard deviation, n = 3) incorporated in the top half.

Additional important observations were made following the initial seeding experiments. First, the two seeding syringes were not synchronous during the seeding. In particular, one of the two syringes started and almost completed its run before the second syringe started its release, jeopardizing the symmetry of the outflow from the two tees and theoretically, the longitudinal uniformity of cell distribution. Second, the flow rate of the seeding suspension for a determined vacuum level and for a given pair of syringes was not consistent (the average flow rate was calculated dividing the total volume of seeding suspension by the time necessary to complete the release of seeding bolus from both the syringes). Both these effects were unpredictable, and presumably due to slight differences in the resistance that the rubber tip of different syringe pistons were exerting on their relative internal plastic syringe body.

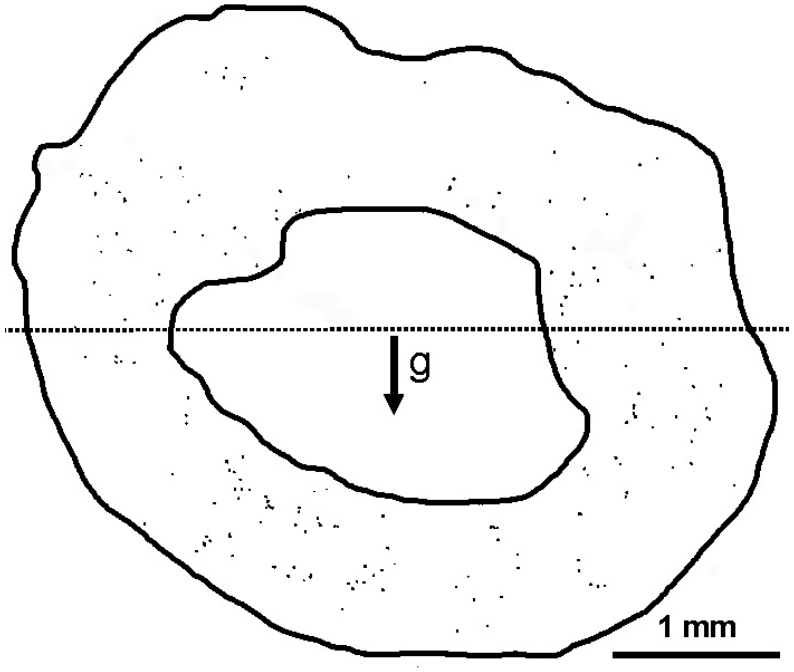

Figure 2.6 Representative section showing nuclear stain following seeding with the first seeding device. The picture was inverted to increase the contrast. The external and internal scaffold perimeter was highlighted artificially in black. Note a qualitative increase in cell number in the lower portion of the scaffold due to cell sedimentation. The arrow indicates the gravitational axis during seeding.

A lower resistance of one of the two syringes would explain the earlier cell suspension release starting by upon application of vacuum inside the chamber. Moreover, an average increase in resistance in a given pair of syringes used for one seeding would result in a lower average flow rate compared to another pair of syringes with less average resistance for a given vacuum level inside the chamber, affecting the reproducibility of seeding. Both of these relevant shortcomings were the result of the use of the vacuum as the sole driver for the flow of seeding suspension released from syringes.

It was clear that the first prototype of the seeding device required additional modifications to improve the seeding capabilities and the reproducibility of the seeding. In

particular, the issue of cell sedimentation in the lower half of the scaffold (qualitatively shown in **Figure 2.6**) suggested the use of a rotating scaffold around its longitudinal axis while the seeding suspension was released throughout its wall. Moreover, the variability in flow rate from the syringes for a given level of vacuum suggested the use of a precision syringe pump to reproducibly control the flow rate of the seeding suspension for each seeding process.

The incorporation of these two additional features driven by rationally- and empirically-based criteria applied to the design of an initial vacuum seeding device led to the fabrication of the first generation of a rotational vacuum seeding device (RVSD) as described in the following section.

2.2 FIRST GENERATION OF RVSD

The RVSD was designed to take advantage of the synergistic actions of the vacuum applied inside the chamber and the flow generated by a syringe pump to induce a transmural flow through the porous polymer scaffold wall. During this phase, the cells infused by the syringe become entrapped within the pores of the scaffold while the liquid phase of the cell suspension exudes through its wall. The tubular scaffold simultaneously rotates around its longitudinal axis during the seeding in order to increase the uniformity of seeding along its circumferential direction.

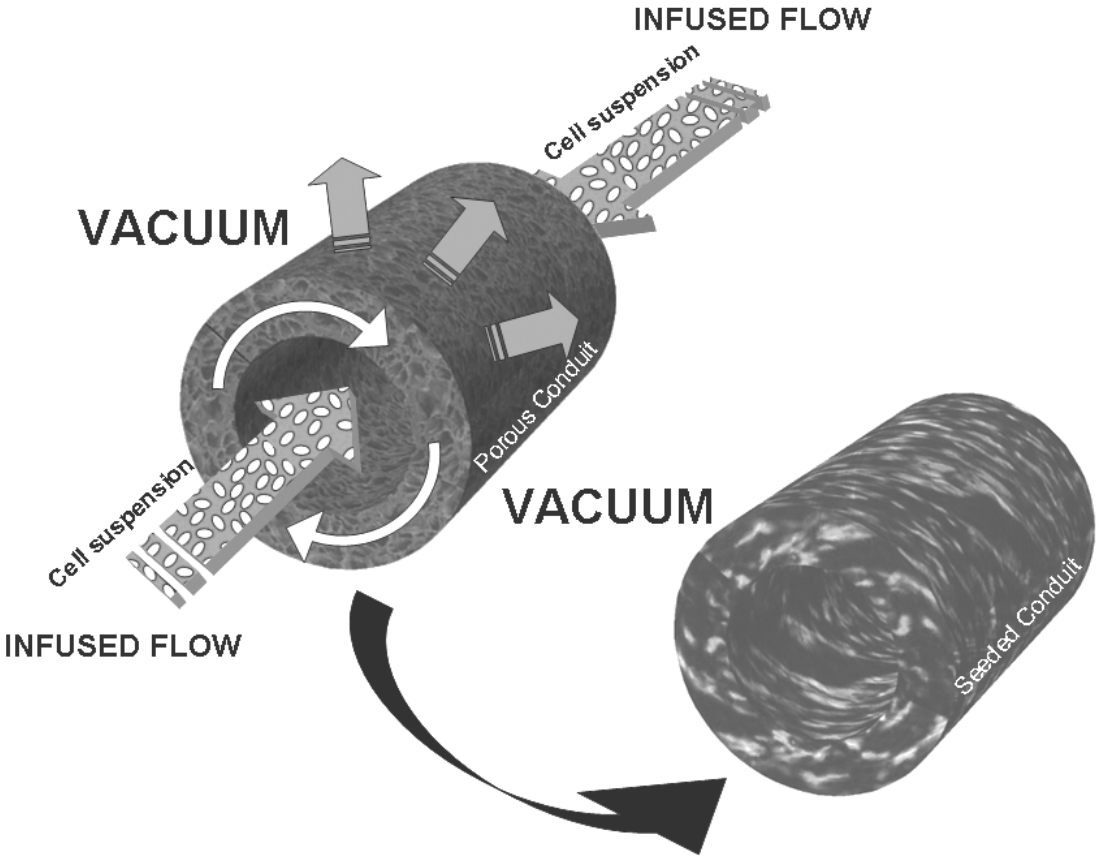

Figure 2.7 Operating principle of the seeding technique. A transmural flow is induced by an external vacuum and intraluminal infusion of a cell suspension. The porous nature of the scaffold allows for the liquid phase to exude through while the cells become entrapped in the pores. Rotation is employed to yield a uniform circumferential seeding distribution. Image from [55].

2.2.1 Chamber design

Several incremental steps were performed to complete the transition between the very first prototype described previously (**Figure 2.1**) and the final, functional prototype of first generation of RVSD. Most of these steps consisted in replacements of used materials or components, or in

the custom-modifications of determined parts. Therefore, for brevity, while describing the first generation of RVSD, only the final materials and components used will be described here.

The creation of the first RVSD required the design of several custom-made components. The design and drawing of all the parts was made with Solidworks 2005 software (Solidworks Corp., Concord, MA). Drawings are shown in **APPENDIX A**. A new airtight chamber (internal dimensions: 10x3x5 cm, **Figure A.2**) was machined with a computer-controlled milling machine from a solid block of cast acrylic. A cast acrylic top lid was created for the chamber (thickness = 5 mm, **Figure A.3**) and secured to its top opening via 8 SS thumb screws (McMaster-Carr) and an intermediate rubber gasket laid on top of the chamber aperture to avoid pressure loss during seeding.

A cast acrylic sheet (45x30x1.5 cm) was used as a base for the RVSD. Feet (5x5x2 cm) made of cast acrylic were solvent-welded with methylene chloride (Sigma) to each of the four corners of the base (**Figure A.4**). Two threaded holes were made in the chamber in order to allow for horizontal placement of two identical, coaxial SS tees (OD = 6.35 mm, ID = 2 mm, length = 10 cm, **Figure A.5**) by means of two intermediate sealed joints. These joints were obtained by modifying SS Yor-Lock compression tube fittings (male pipe adapter, McMaster-Carr) by removing the internal double-sleeve, and machining a bore (Ø = 6.4 mm) throughout the main body of the adapter (to remove the default internal step), enabling its use as a sleeve bearing for the rotating SS tees. An airtight seal between the sleeve bearing and the rotating tee was obtained by inserting a fluoroelastomer V-ring seal (SKF, Göteborg, Sweden) between the body of the tube fitting and its back nut. PTFE grease (Magnalube-G, Saunders Enterprises, Inc., Long Island City, NY) was used to lubricate the custom sealed sleeve bearings and the rotating

tees (shafts). The sealed joints were screwed into the threaded hole made in the chamber and allowed for the rotation of the tees across the wall of the acrylic chamber without pressure loss.

The two tees were coupled inside the chamber by a custom-built SS 316L torque transmission device (**Figure A.6** and **Figure A.7**) transferring the rotary movement from an externally rotated tee ("Driving Tee") to the other ("Driven Tee") (**Figure 2.8** and **Figure 2.9**). This component creates a mechanical connection between the two tees by expanding them peripherally to its axis leaving a central gap between the two tees (where the scaffold can be connected). The torque transmission was provided to the tees via two opposite SS socket set screws for each side. Another threaded hole was made laterally in the chamber wall to host a nylon barbed port to connect the chamber to the laboratory vacuum line via the described vacuum regulation system (**Figure 2.2**). The goal of the regulator was to maintain a constant and controllable negative relative pressure inside the chamber.

A precision aluminum timing belt pulley (SDP/SI, New Hyde park, NY) was mounted on the Driving Tee and driven by a polyurethane/kevlar timing belt (SDP/SI, New Hyde park, NY) by an identical pulley mounted on the shaft of a base mount geared AC motor (Rex Engineering, Titusville, FL). The tees were connected distally, outside the chamber, to hydraulic rotating joints (Deublin Co., Waukegan, IL) via Kynar® compression tube fitting adapters (McMaster-Carr). The rotating joints were mounted with a barbed port and connected via PVC tubing to syringes mounted onto a programmable precision syringe pump (Model: PHD 22/2000, Harvard Apparatus Inc., Holliston, MA). Each RVSD inlet port was provided with a disposable shut-off valve (Clearlink Luer Activated Valve, Baxter) to prevent loss of fluid from the RVSD when syringes were not connected. The rotating joints allowed for the uninterrupted flow of seeding

suspension from a stationary tube to a rotating tee without pressure loss or seeding suspension spills.

The RVSD chamber mounted with all its components was fixed to its base via two custom-made Delrin® mounting towers for the rotating joints (**Figure A.8**), and anchored to the RVSD base via thumb screws. The mounting towers provided a circular socket for the rotating joints to be laid on and to be firmly held by a semicircular cap tightened by knurled thumb screws (**Figure A.9**). Both mounting towers were provided with two 3 cm-long tracks to enable their translation on the RVSD base to modify the distance between the two tees when seeding different scaffold lengths. The chamber was aligned to the base via two machined cone-shaped Delrin® pins secured onto the base and matching two holes on the bottom of the RVSD chamber. **Figure 2.8** provides an expanded schematic of the first generation of RVSD, while **Figure 2.9** shows most of the technical features described above.

The RVSD was subsequently tested to demonstrate its fluid dynamics performance and its cell seeding capabilities. The following paragraphs will provide a comprehensive description of such testing.

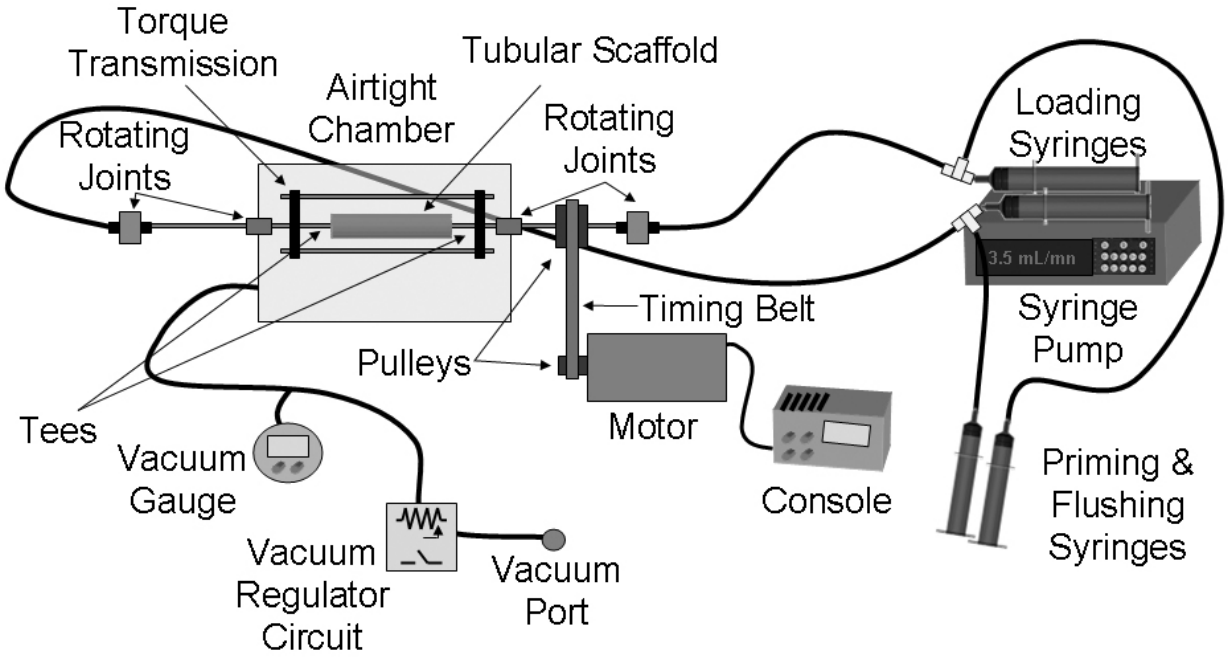

Figure 2.8 Schematic of the RVSD. A cell suspension is infused intra-luminally into both ends of a porous tubular scaffold by means of a syringe pump. Applied vacuum in the chamber fosters the radial exudation of the liquid phase of the cell suspension across the thickness of the polymer. An electrical motor rotates the construct, promoting a homogeneous distribution of cells around the circumference. Image from [55].

2.2.2 Fluid dynamic modeling

2.2.2.1 Methods

The computational fluid dynamics (CFD) software Fluent (version 6.2, Fluent Inc., Lebanon NH) was used to calculate the fluid shear stresses acting on the cells in the lumen of the rotating scaffold and to visualize the complex internal fluid dynamics during seeding.

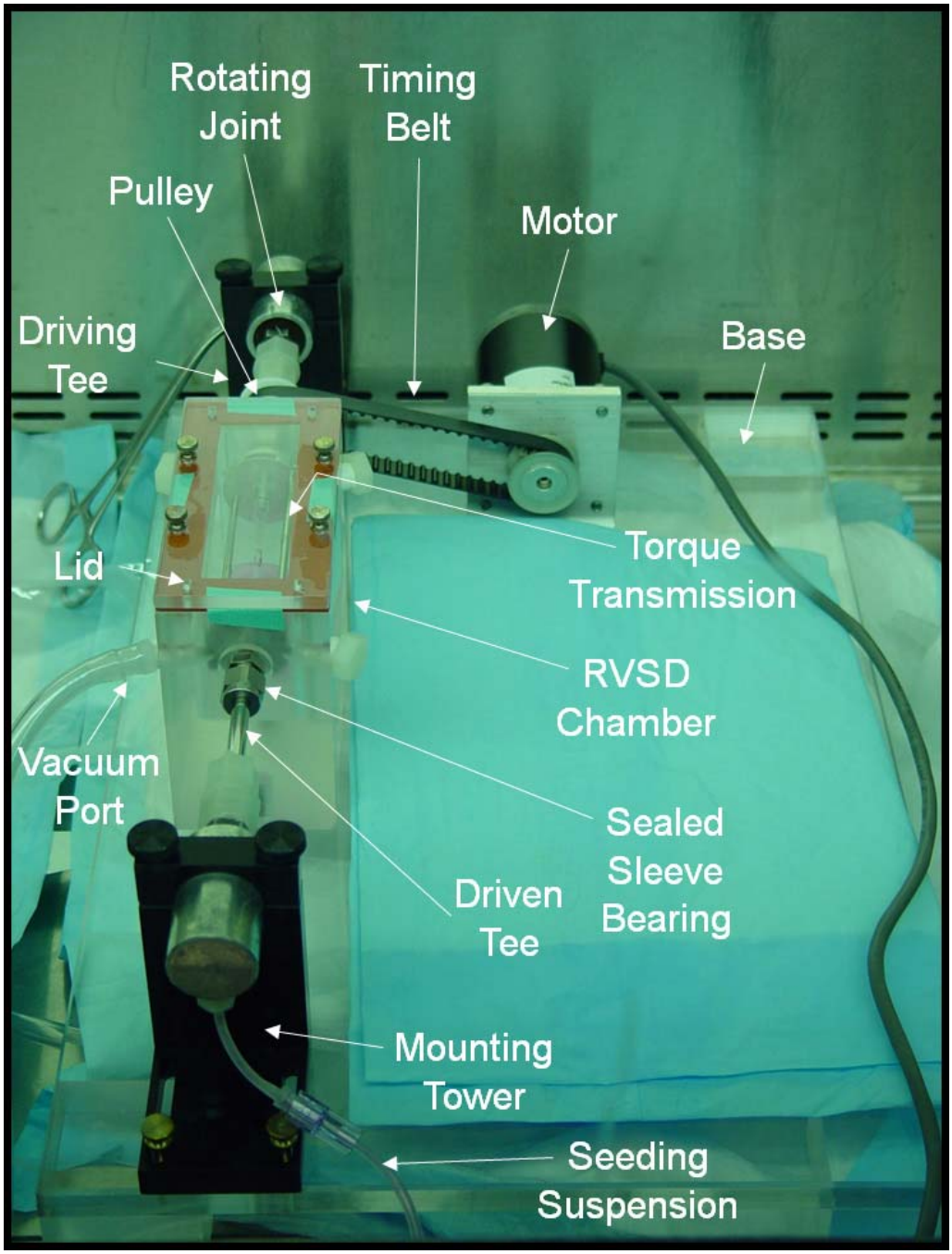

Figure 2.9 RVSD under a laminar flow hood during a seeding process.

For this purpose a $4.5x10^5$ wedges volume mesh was created (Gambit 2.2, Fluent Inc., Lebanon, NH) with boundary layers on the luminal surface of the area of interest (scaffold lumen). The model consisted of a series of adjacent cylinders modeling the fluid domain of the two tees and the lumen of the central scaffold. The fluid domain of the scaffold lumen was surrounded by an external, concentric tube representing the scaffold **Figure 2.10**.

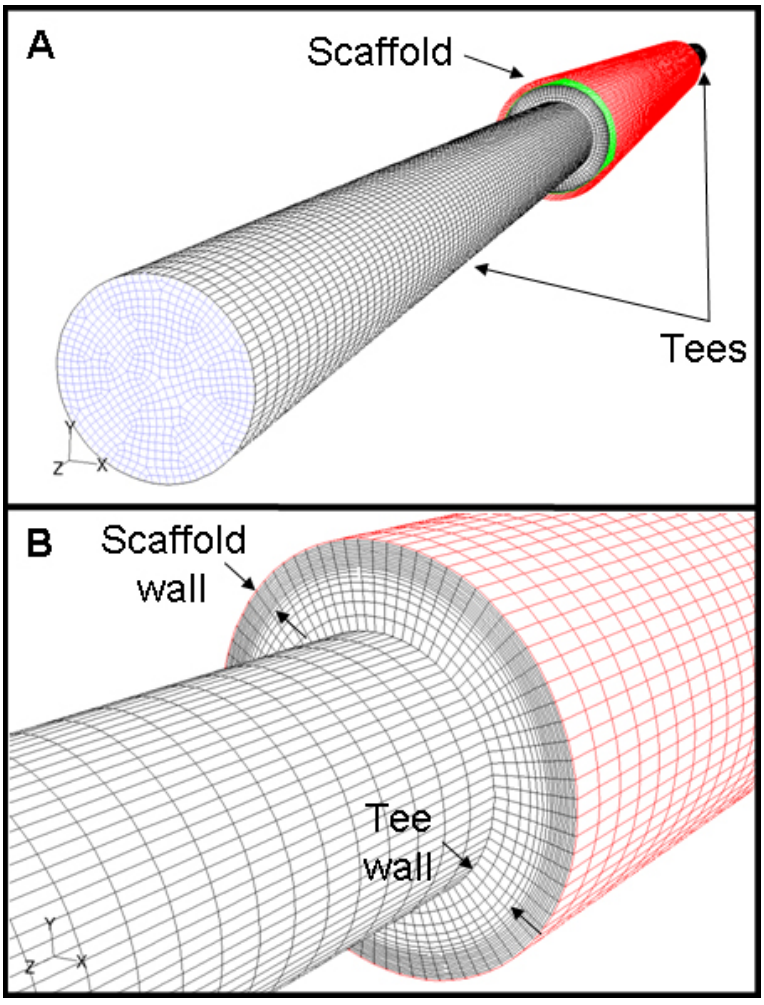

Figure 2.10 3D Mesh used during the CFD analysis. **A.** Perspective of the whole fluid domain including the two tees and the central scaffold. **B.** Close-up of the boundary layer used to model the transition between the lumen of the scaffold and its wall.

The tubular volume of the scaffold was modeled as a "porous medium" which is an implicit function provided by the software. This function adds a local energetic loss. Analytically, this model introduces an additional source of momentum to the Navier-Stokes equations, which describe the motion of fluids. This consists of two terms, a viscous loss and an inertial loss, which are completely described as [144]:

$$S_i = \sum_{j=1}^{3} D_{ij} \mu v_j + \sum_{j=1}^{3} C_{ij} \frac{1}{2} \rho |v_j| v_j \qquad \textbf{2-2}$$

where S_i is the additional source of momentum for the i-direction, μ is the dynamic viscosity of the fluid, v_j is the j component of the fluid velocity, ρ is the desity of the fluid, and D_{ij} and C_{ij} are components of defined matrices representing the 3D components of permeability and inertial resistance, respectively. This term of loss contributes to the resolution of the pressure gradient within the cells defined as "porous media" with a linear and second-order proportionality to the velocity of the fluid crossing those elements. In case of homogenous porous media, the matrices D and C are diagonal with $1/\alpha$ and C_2, respectively on the diagonals and zero for the other elements. **Equation 2-2** becomes:

$$S_i = \frac{\mu}{\alpha} v_i + C_2 \frac{1}{2} \rho |v_i| v_i \qquad \textbf{2-3}$$

where α is the permeability of the porous media and C_2 is a term representing the inertial loss. In the case of laminar flow, the pressure loss is typically proportional to the velocity of the fluid crossing the porous media, and the constant C_2 can be considered negligible.

Finally, ignoring the convective acceleration and the diffusive terms due to the low velocities involved, the Navier-Stokes equation becomes the Darcy's law which describe the flow of a fluid through a porous media:

$$\nabla p = -\frac{\mu}{\alpha} v \qquad \textbf{2-4}$$

The software uses this equation for each of the three directions associated to the porous volume. **Equation 2-4** in a finite form becomes:

$$\Delta p_i = \mu \cdot D_{ij} v_j \Delta n_i \qquad \textbf{2-5}$$

where i = x,y,z, the terms $1/\alpha_{ij}$ are the elements of the matrix D, μ is the dynamic viscosity, v_j are the components of the velocity vector, and Δn_i are the thicknesses of the "porous" elements in the three directions.

The permeability α of the polymer scaffold was calculated empirically using Darcy's law by measuring the average pressure loss per unit of surface area of the scaffold for a set exudation rate of saline (flow rate = 16 mL/min, n = 3). A simple circuit was created by connecting a syringe to the scaffold via tubing and a tee, and clamping the scaffold downstream with a surgical clamp. The set flow rate was produced via a precision syringe pump (Model: PHD 22/2000, Harvard Apparatus Inc., Holliston, MA), and the resulting pressure was monitored via an in-line pressure transducer (model TJE, Honeywell Sensotec, Columbus, OH). The dimensions of the scaffold were measured via a digital caliper (Fisher Scientific) to calculate the luminal area of the internal surface (with the assumption of homogeneous exudation flow rate within the internal surface of the scaffold). The dynamic viscosity μ of the cell suspension was

measured with a capillary viscometer (Cannon-Manning, Cannon Instruments Company, State College, PA), and a rheologic curve was generated with a digital cone and plate rheometer (DV-III, Brookfield Engineering Labs, Middleboro, MA) in order to demonstrate the Newtonian properties of the fluid under shear rate ranges obtained with the device. Both measures were performed at 21ºC, consistently with the conditions used during seeding.

The CFD simulation was performed assuming steady state conditions. The solver was segregated with implicit formulation and SIMPLE pressure-velocity coupling. A spatially uniform velocity (corresponding to a flow rate of 8 mL/min for each tee) was assigned to the two tee inlets with 10 diameters of flow extension to allow for complete flow profile development. The rotation of the tees and the scaffold around their longitudinal axis was simulated with a moving mesh function (rotational speed = 350 rpm). Convergence of the solution was demonstrated with residual values $\leq 10^{-4}$, and confirmed with the stability of two surface monitors (the average absolute pressure on the outlet surface and the average velocity on the interior surface). The outlet (outer surface of the scaffold) was modeled with a constant negative pressure equal to the vacuum pressure inside the chamber (-5 inHg). The wall shear stress (WSS) on the luminal surface of the model was determined during post-processing by the software, while the WSS acting on the scaffold pores was estimated analytically. In brief, the conservation of momentum in laminar flow conditions was considered for a rigid, cylindrical pore and modified with the Hagen-Poiseuille equation for a determined pressure drop [121]. The resulting equation for the WSS is:

$$\tau_{rz,\max} = \frac{Q \cdot 4 \cdot \mu}{\pi \cdot R^3} \qquad \textbf{2-6}$$

where Q is the flow rate in the pore, μ the dynamic viscosity, and R the pore radius, which was taken as 10 μm (consistent with the smallest pores of the porous polymer). The flow rate in the pore was set by considering the total flow rate entering the scaffold (from both tees) divided by the effective open area of the luminal surface of the scaffold (effective open area = porosity x internal luminal cylindrical area) multiplied by the average pore area, with the assumption of even distribution of the inlet flow rate in the porous luminal surface of the scaffold.

2.2.2.2 Results

The permeability of the polymer scaffold used for seeding was found to be $2.6\pm0.2\text{x}10^{-13}$ m^2, while the dynamic viscosity was found to be 1.03 cP. The cell suspension was found to be approximately Newtonian due to its relatively flat rheological curve (**Figure 2.11**).

The density of the fluid was proportionally calculated for a 10% serum (1025 kg/m^3) solution in culture media (1008 kg/m^3) and determined to be 1010 kg/m^3 (*i.e.*, density of fluid = 1/10 · density of serum + 9/10 · density of culture media).

The wall shear stress distribution on the luminal surface of the CFD model was negligible (*i.e.* < 1 $dyne/cm^2$). The calculated wall shear stress in the representative smallest pore diameter was 5.4 $dyne/cm^2$. The CFD simulation also described the pathlines of the seeding suspension during seeding (**Figure 2.12**). The liquid suspension starts to twist inside the tees due to the viscous transfer of momentum to the fluid from the rotating walls. Once entered the rotating scaffold lumen the cell suspension starts to expand toward the scaffold wall and to gradually exude throughout the entire length of the scaffold.

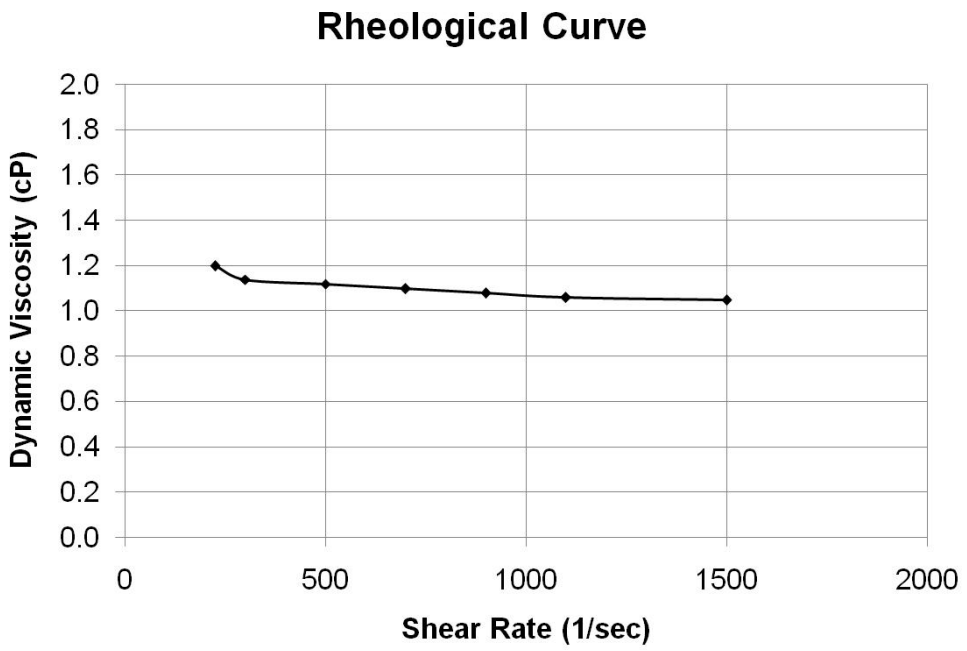

Figure 2.11 Rheological curve measured for the seeding suspension at 21ºC. Note the near-Newtonian behavior of the fluid.

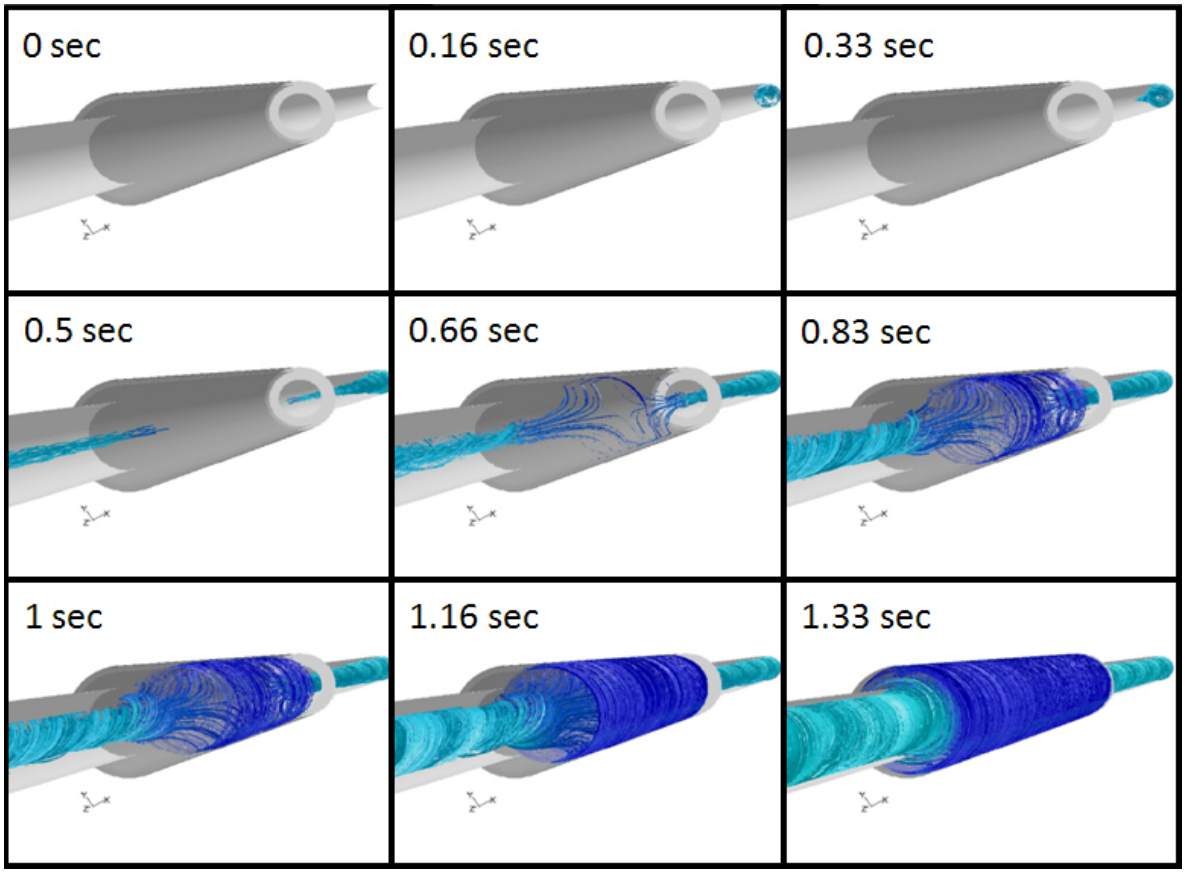

Figure 2.12 Pathlines of the fluid flow into the RVSD obtained via CFD. The sequence was obtained by releasing pathlines from the two surfaces representing the tee inlets within a total timeframe of 1.33 seconds.

2.2.3 Bulk seeding performance

2.2.3.1 Qualitative and quantitative assessment of bulk seeding

The performance and reproducibility of the RVSD was qualitatively and quantitatively investigated. The scaffolds used for the bulk seeding experiments (porosity 90%, pore size range 10-200 μm) were prepared via TIPS processing of PEUU as previously described [53] to 2 cm length, 4.0 mm ID, and 200-300 μm wall thickness. Two different cell types were used in this evaluation. Murine muscle-derived stem cells (MDSCs) obtained from the laboratory of Dr. Johnny Huard via an established pre-plating technique [99] were cultured and seeded in DMEM (Sigma) supplemented with 1% P/S (Gibco, Invitrogen Corporation, Carlsbad, CA), 10% FCS (Atlanta Biologicals, Norcross, GA), and 10% horse serum (HS; Gibco, Invitrogen Corporation). rBMPCs isolated as previously reported [143] were cultured and seeded in DMEM (Sigma) supplemented with 10% bovine serum (Gibco, Invitrogen Corporation) and 1% P/S (Gibco, Invitrogen Corporation).

Qualitative evaluation of the seeding was performed by seeding three TIPS tubular scaffolds with $10x10^6$ rBMPCs or MDSCs suspended in 10 mL of culture media using a flow rate of 6.8 mL/min (the flow rate in the RVSD is referred to each syringe; therefore, the total flow rate exuding through the scaffold is $2 \cdot Q$), a rotation speed of 120 rpm, and an applied vacuum of -5 inHg. These parameters were chosen empirically by a qualitative assessment of the seeding suspension exudation patterns during seeding (data not shown). The total seeded cell number was obtained by multiplying the cell density of the seeding suspension by the set seeding volume (volume released by the syringe pump in each seeding).

Immediately after seeding constructs were removed from the RVSD and left in static culture for two hours. The samples were fixed in 4% paraformaldehyde for 1 hour and subsequently washed in PBS. After embedding a small ring of each construct in tissue freezing medium (TBS, Triangle Biomedical Sciences, Durham, NC), the specimens were frozen and sectioned (thickness = 10 μm). Sections were stained for cytoskeleton (F-actin) by permeabilizing in Triton-X-100 solution (Fisher Scientific, Fair Lawn, NJ) for 15 minutes, and incubating with 1:250 dilution of phalloidin conjugated to Alexa 488 (Molecular Probes, Eugene, OR) for an hour in a moist chamber to prevent drying of the samples. Unbound phalloidin was removed by subsequent washes in PBS. The sections were then counterstained with the nuclear stain DAPI (bisbenzimide, Sigma) for one minute and mounted in gelvatol. The sections were observed via epifluorescence microscopy using an Eclipse E800 (Nikon, Melville, NY) with UV filter for the DAPI stain and with FITC filter for the phalloidin stain.

Quantitative evaluation of the seeding was performed by calculating the seeding efficiency of seeded scaffolds and also via the two dedicated experiments described below. The seeding efficiency (percent of the total number of cells incorporated into the scaffold) was calculated by determining the cell count in the seeding solution after seeding using a hemocytometer, and comparing to the cell count prior to seeding.

The first experiment was designed to assess the cell distribution along the longitudinal direction of the scaffold. For this, $15x10^6$ MDSCs were suspended in 20 mL of culture media (2 10mL syringes) and infused into TIPS tubular scaffolds (n = 6, flow rate = 8 mL/min, rotation speed = 350 rpm, vacuum = -5 inHg). The increased flow rate (compared to the previous qualitative testing) was chosen to guarantee a good longitudinal ejection of seeding suspension,

while the increased rotational velocity was similarly chosen to improve the circumferential uniformity of seeding.

After seeding, each construct was kept for two hours in static culture and subsequently cut into 9 serial equi-sized rings. Each ring underwent metabolic-based cell counting (MTT) as described below, in order to measure the cell number in each ring and, therefore, in each longitudinal location of the seeded constructs. Those rings from the bulk seeding experiments dedicated for viability and cell number analysis were placed in 200 μL of media supplemented with 20 μL of MTT solution [3-(4,5-dimethylthiazol-2-yl)-2,5-diphenyltetrazolium bromide] (Sigma) into a single well of a 96 multiwell plate immediately after culture. The specimens were kept for 4 hours at 37°C. Samples were then immersed in 200 μL of 0.04 N HCl in 2-propanol solution and kept for 24 hours at 4ºC. The adsorbance was read at 570 nm with a microplate reader (model 680, Bio-Rad, Hercules, CA) and normalized to the dry weight of each ring and the total cell number in each construct. The cell number was obtained with a previously derived standard curve for the cell type of interest. Statistical analysis of the data, as described below, allowed assessment of the uniformity of the longitudinal distribution of cells in the constructs and the reproducibility of the device.

The second experiment was designed to assess the cell distribution along the circumferential direction. For this, a single TIPS tubular scaffold was seeded using the same conditions as the first experiment described above, cultured, and cut using the same cells, conditions and parameters as the first experiment. However, the construct was slit open with a single longitudinal cut in order to identify the relative circumferential position among different cross-sections. Nine total serial rings were processed for nuclear staining as previously described in this section. Each stained section was digitally photographed and reconstructed

from 16 consecutive fields of view at 200X. Subsequently, the images were reconstructed and used to generate four composite images representing the four circumferential quadrants (0°-89°, 90°-179°, 180°-269°, 270°-359°), where the 0°-89° quadrant was the first quarter of the circumference clockwise from the longitudinal slit that was cut and so on. Each quadrant of each section underwent image-based quantification of the cell number with an intensity threshold filter (Scion Image 4.0, Scion Corporation). The cell number in each quadrant was assessed by dividing the total measured area occupied by the nuclei divided by the average area occupied by one nucleus. This was calculated by averaging the area of 30 different nuclei in a field of view.

2.2.3.2 Statistical analysis

The Kolmogorov-Smirnov test (Matlab 7.0) was used to check the normality of the data. The Kruskal-Wallis test (Matlab 7.0) was used for assessing longitudinal and circumferential uniformity and reproducibility. To assess longitudinal uniformity, comparisons were made of the percentage of total cell number among each longitudinal portion of each seeded construct (rows analysis). For the reproducibility assessment, instead, comparisons were made of the percentage of total cell number per general location (any of the 9) among the different seeded constructs (columns analysis). Therefore, reproducibility was considered as the capacity of consistently incorporating the same fraction of the total cell number, ideally 1/9 of the total available (11.11%). Finally, to assess circumferential uniformity, comparisons were made of the number of cells in each circumferential quadrant of each section used.

2.2.3.3 Results

A representative section of a TIPS scaffold bulk seeded with rBMPCs and stained for cell nuclei, 1 hour after seeding, is shown in comparison with a native rat aorta in **Figure 2.13**. Note the similarity in cell distribution and density throughout the thickness. The MDSCs incorporated into the scaffolds maintained a spherical shape two hours after seeding **(Figure 2.14**) demonstrating incomplete cell attachment. The morphology and spreading of the MDSCs as shown here was representative of the other two cell types used.

The cell seeding efficiency was 77.2±12.5 % in the tested constructs. The viability 2 h after seeding was > 95% of the initial effective cell number incorporated into the scaffold. Each seeding procedure took approximately 1–2 min.

The bulk seeding experiments (n = 6) exhibited a high level of longitudinal uniformity represented by the comparison of the normalized average cell number percentage for each of the 9 longitudinal segments (**Figure 2.15**, $p = 0.99$). The seeding was also reproducible as represented by the comparison of the average cell number per longitudinal location among different constructs (**Figure 2.16**, $p = 0.24$). The seeded scaffolds also exhibited circumferential seeding uniformity based on a similarity in cell numbers in the four quadrants of the seeded construct (**Figure 2.17**, $p=0.25$).

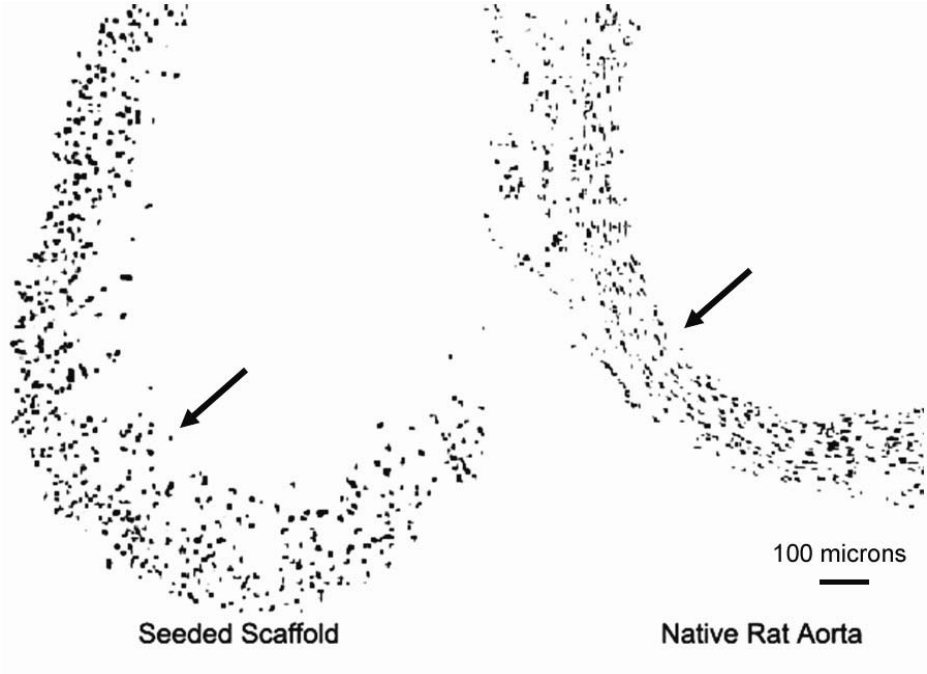

Figure 2.13 Comparison between the nuclei distribution of a rBMPC-seeded tube and a native rat aorta 1 hour after seeding. The arrows indicate the luminal surface of the conduits. Magnification = 100X. Image from [55].

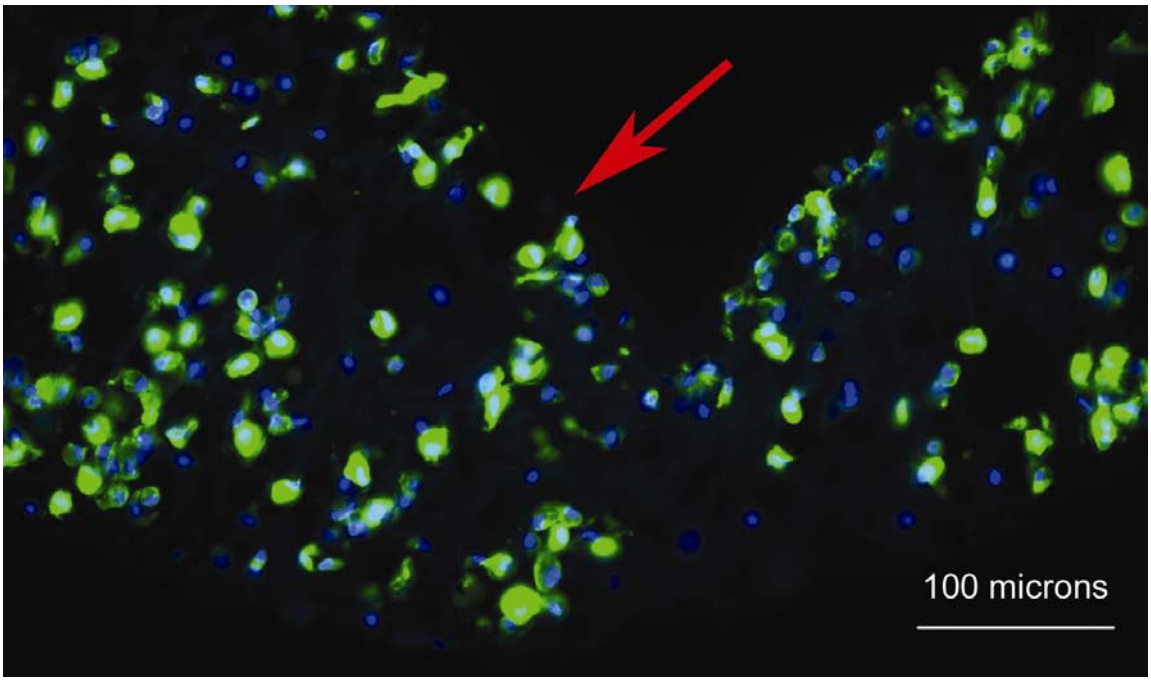

Figure 2.14 MDSC morphology 2 hours after seeding. Note that the cells still maintain a spherical shape. The arrow indicates the luminal surface of the scaffold. Blue = nuclei, Green = F-actin, Magnification = 200X. Image from [55].

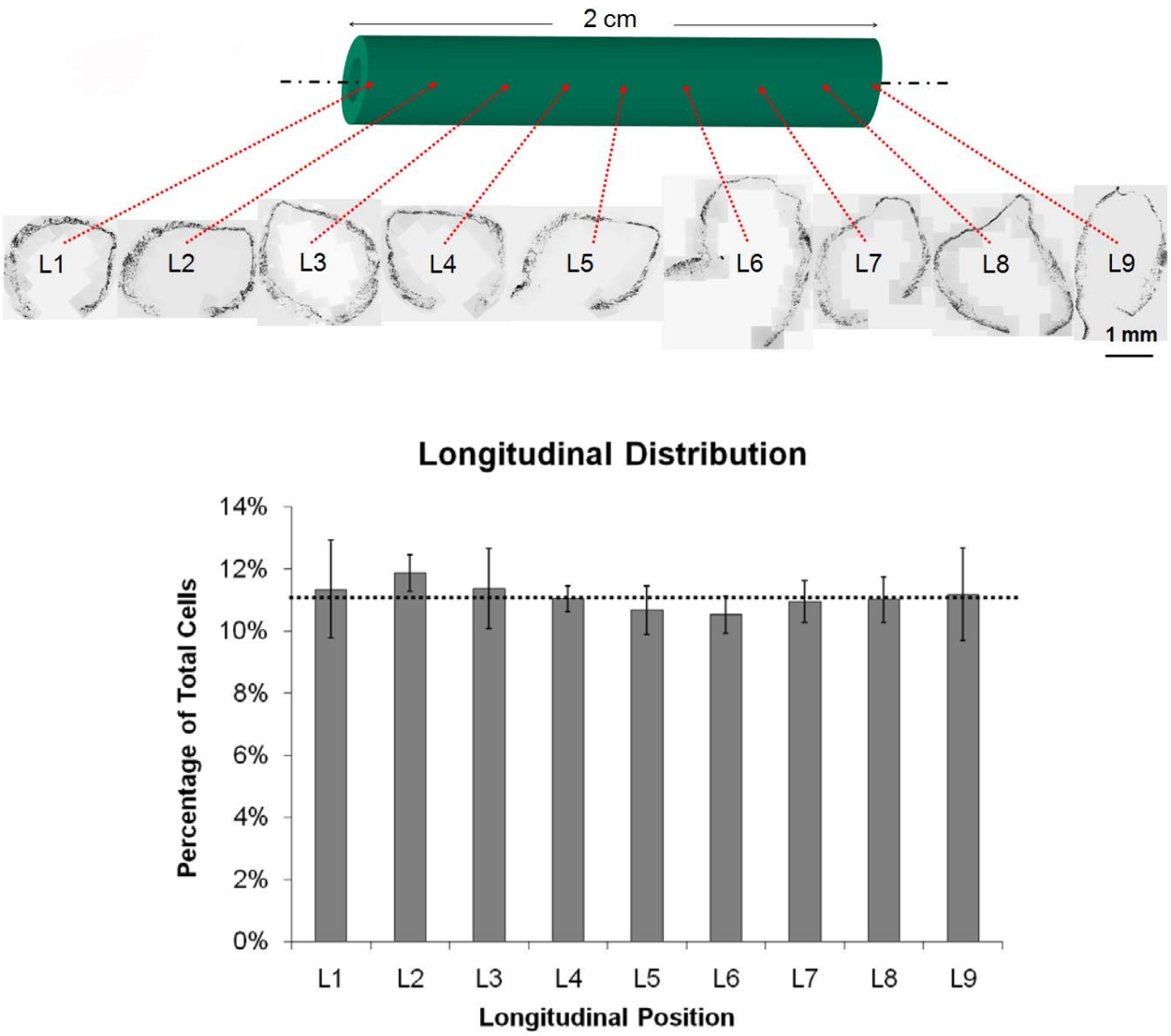

Figure 2.15 Assessment of longitudinal bulk cell seeding uniformity of MDSCs into 2 cm long TIPS PEUU scaffolds. **Top**. Representative nuclear staining of the 9 longitudinal positions of the scaffold (qualitative assessment). **Bottom**. Longitudinal cell distribution indicated by the percentage of cells present in each of 9 longitudinal segments of the seeded scaffolds (mean ± standard deviation; n = 6). The dashed line shows the ideal case of perfect distribution correspondent to the 11.11% of the total cell number included in each longitudinal location of the scaffold. Image adapted from [55].

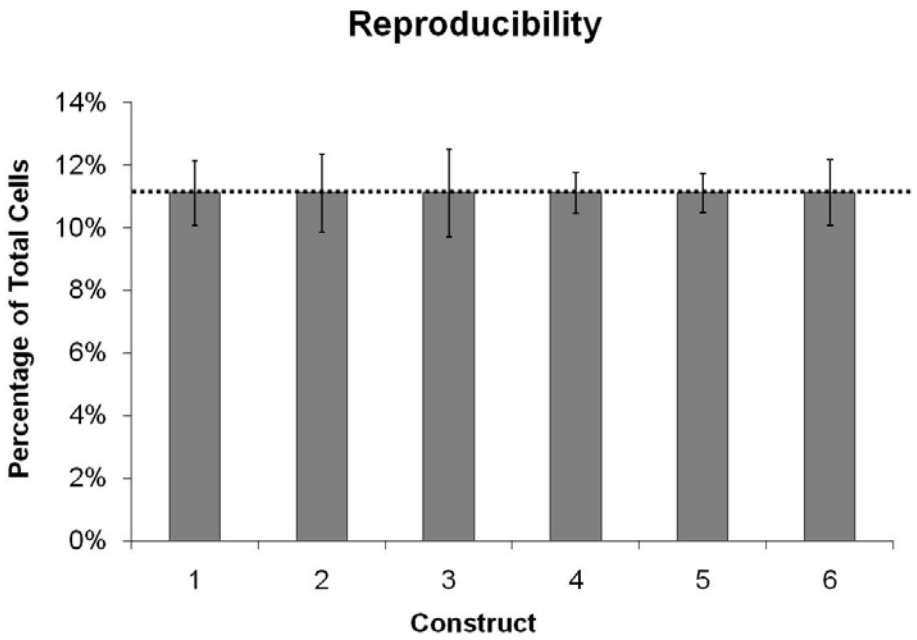

Figure 2.16 Assessment of reproducibility. Each of the 6 seeded constructs received the same percentage of total cells per average longitudinal location (mean ± standard deviation; n = 9). The dashed line shows the ideal case of perfect reproducibility corresponding to 11.11% of the total cell number included in the average longitudinal location of the scaffold. Image adapted from [55].

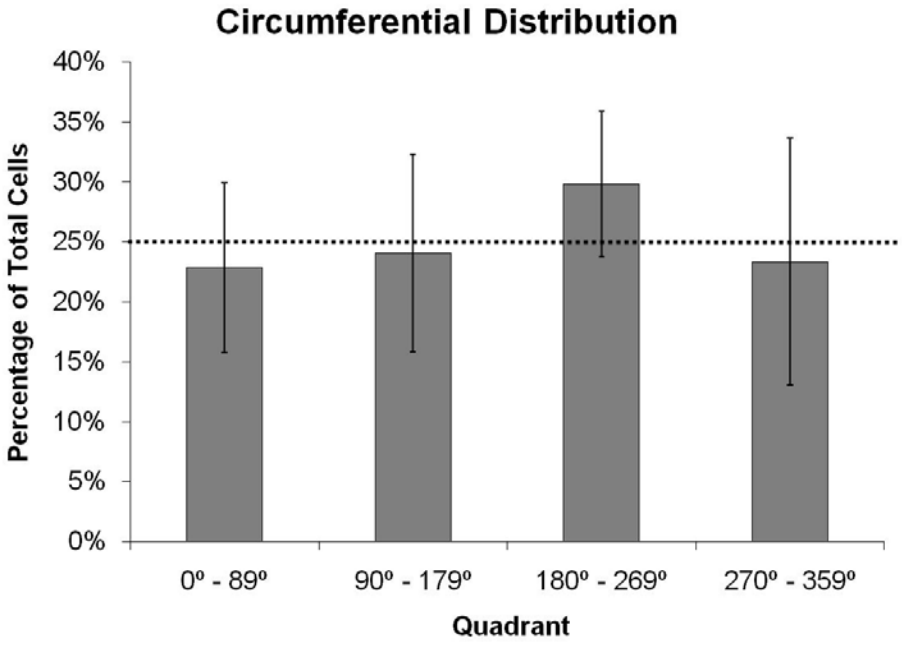

Figure 2.17 Assessment of circumferential cell distribution. Average percentage of the total cells included in each of the four circumferential quadrants of the scaffold. The dashed line shows the ideal case of perfect circumferential distribution corresponding to 25% of the total cell number included in each quadrant. Image adapted from [55].

2.2.4 Surface seeding performance

2.2.4.1 Qualitative assessment of surface seeding

The scaffold utilized for assessing the surface seeding capabilities of the RVSD was fabricated by electrospinning PEUU onto a rotating 3.5 mm SS mandrel to a length of 2 cm, and a wall thickness of 200 μm (porosity 90%, pore size ~5 μm) using a previously described method [57]. Bovine aortic endothelial cells (bAECs) (Cambrex Corporation, East Rutherford, NJ) were cultured and seeded in endothelial microvascular growth media (EGM-MV) (Cambrex).

The luminal surface seeding capability of the device was tested with dedicated experiments where in three 2 cm long, electrospun tubular constructs were seeded with either rBMPCs, bAECs, or MDSCs. The small pore size of the electrospun polymer scaffold prevented the passage of cells through the conduit wall but not the passage of the liquid phase, thereby allowing for luminal surface seeding. The constructs were seeded with $8x10^6$ cells suspended in 20 mL of culture media using the same seeding parameters used for the bulk seeding experiments. A ring of each seeded construct was cut 1 hour after seeding, fixed, and stained with nuclear stain, while the remainder was kept for 12 hours in static culture conditions to allow the cells to spread on the surface.

After 12 hours of static culture, the specimens were fixed in 2.5% glutaraldehyde for one hour, washed in PBS and re-fixed in 1% osmium tetroxide (OsO_4) for another hour. After multiple washes in PBS the specimens were dehydrated with an ethanol gradient (from 30% to 100%), and subsequently processed with critical point drying (Emscope CPD 750, Emscope Lab., Ashford, UK) with 4 cycles of liquid CO_2 soaking and venting at 10ºC before reaching the critical point for CO_2 at 31.1ºC at 1100 psi. After complete dehydration the specimens were

gold/palladium sputter coated (Sputter Coater 108 auto, Cressington Scientific Instruments Inc., Cranberry Twp., PA) with a 3 nm thick layer of gold. The luminal surfaces in different locations of the seeded scaffolds were observed with field emission scanning electron microscopy (SEM) (JSM-6330F, JEOL ltd. Tokyo, Japan). The constructs were then fixed and processed for fluorescent markers (F-actin, nuclear staining) and qualitatively analyzed. Different fields of view in the SEM and fluorescence microscopy images were analyzed to provide a qualitative assessment of seeding uniformity. The scaffolds seeded with MDSCs were also processed for confocal microscopy. Briefly, samples were rinsed with PBS, fixed with 4% paraformaldehyde, permeabilized with 0.1% Triton x-100 and stained with rhodamine phalloidin (Molecular Probes) for F-actin and draq-5 (Biostatus Ltd) for nuclei. Imaging was done on a Leica TCS-SL laser scanning confocal microscope (Leica Microsystems Inc., Bannockburn, IL) acquiring a stack of images relative to a 30μm depth from the luminal surface of the scaffolds.

2.2.4.2 Results

Shortly after seeding (1 hour), the three electrospun PEUU constructs each seeded with a different cell type (rBMPCs, bAECs, or MDSCs) showed an accumulation and passive adhesion of cells on the luminal surface (**Figure 2.18**). Cells were homogeneously distributed in both the circumferential and the longitudinal direction of the constructs (qualitatively assessed only). After 12 hours of static culture, the luminal surface was completely lined with spread cells that formed a continuous layer on the electrospun polymer (**Figure 2.19**). The other three cell types similarly covered the luminal surface of the electrospun scaffold after 12 hours of static culture (**Figure 2.20**). Maximum intensity projection (MIP) image generated from the stack of confocal images taken from the MDSC-seeded scaffolds confirmed the spreading of cells **Figure 2.21**.

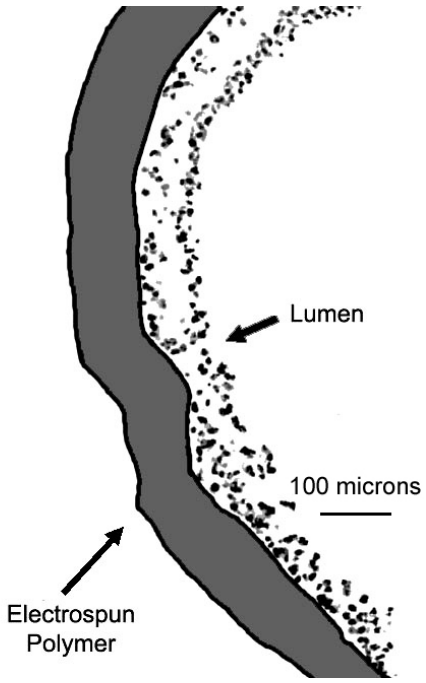

Figure 2.18 Accumulation of MDSCs on the luminal surface of the electrospun PEUU 1 hour after seeding. Cell nuclei appear black. The polymer was visualized under UV light and is artificially indicated by the grey region. These results are representative, as those for rBMPC, bAEC are similar. Magnification = 100X. Image from [55].

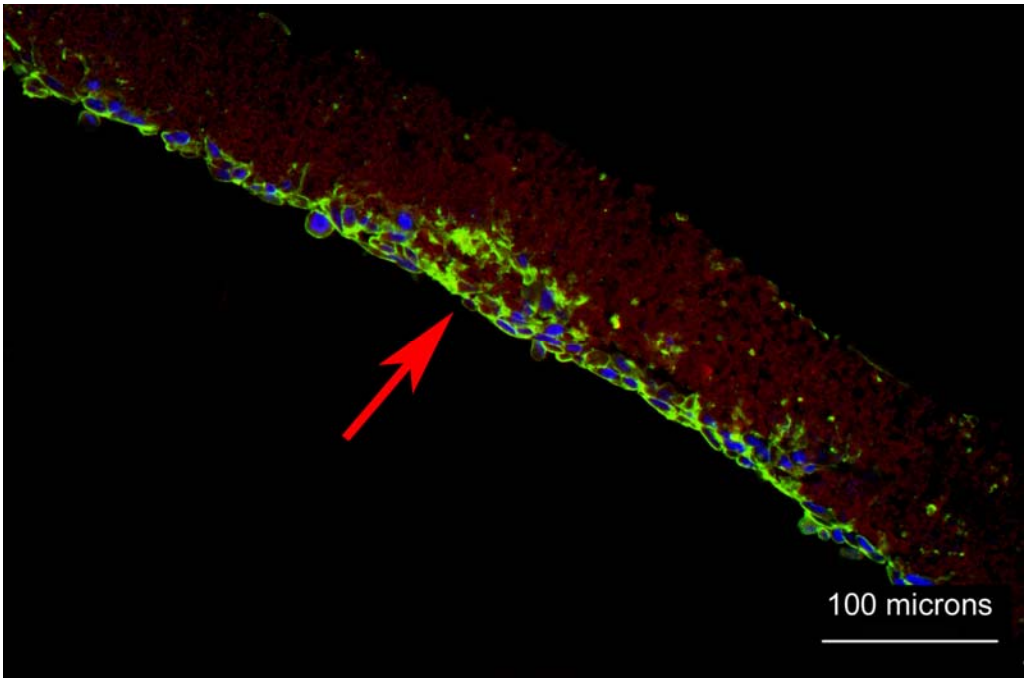

Figure 2.19 MDSCs distribution (blue = nuclei, green = F-actin) on the luminal surface of the electrospun PEUU scaffold (red) after 12 hours of static culture. The arrow indicates the luminal surface of the scaffold. These results are representative, as those for rBMPC, bAEC are similar. Magnification 200X. Image from [55].

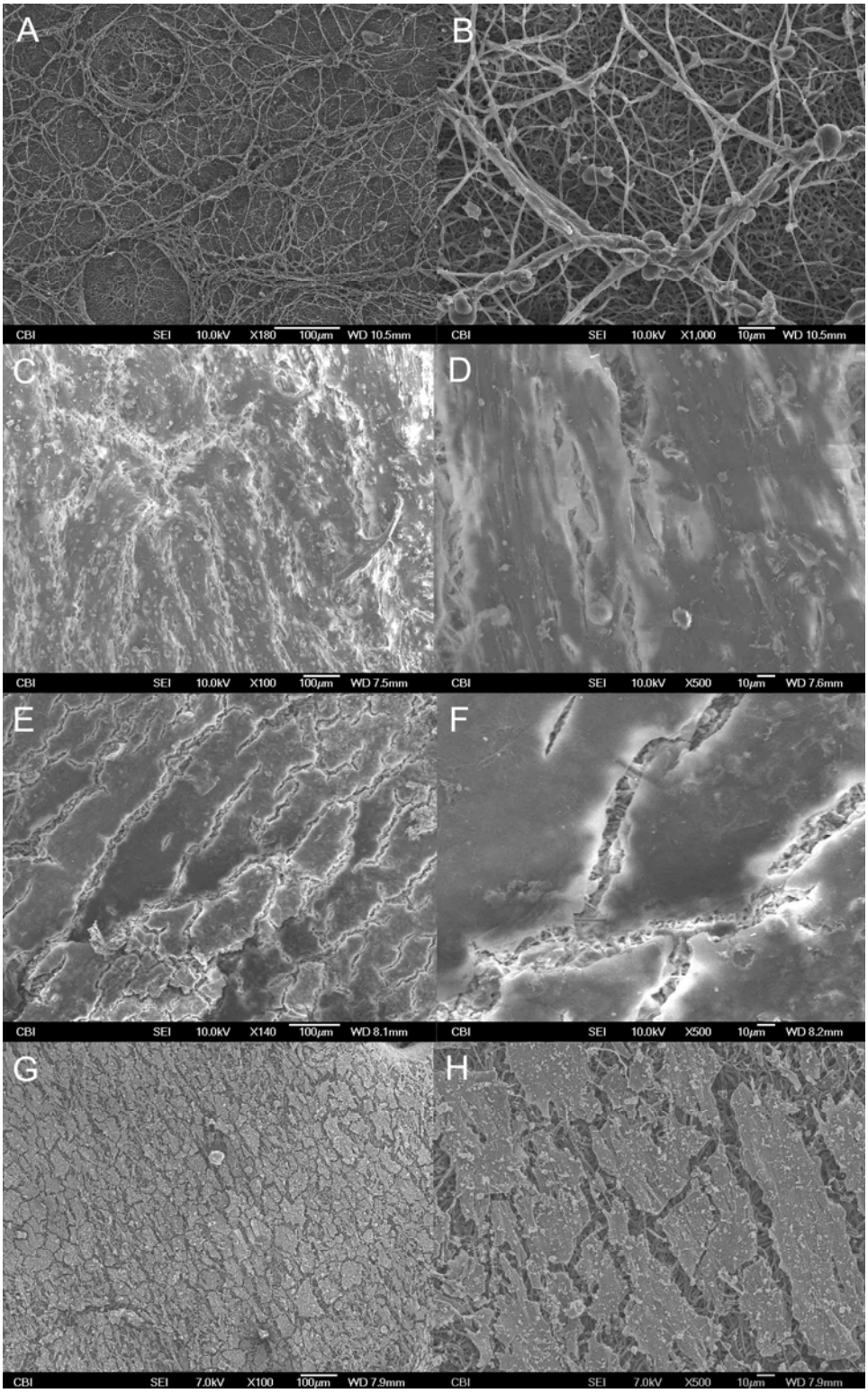

Figure 2.20 Representative SEM images of luminally surface-seeded electrospun PEUU scaffolds. **Left.** Low magnification. **Right.** High magnification. **A-B.** Control, unseeded scaffold. **C-D.** Seeded BMPCs after 12 hours of static culture. **E-F.** Seeded bAECs after 12 hours of static culture. **G-H.** Seeded MDSCs after 12 hours of static culture. **A-F.** from [55].

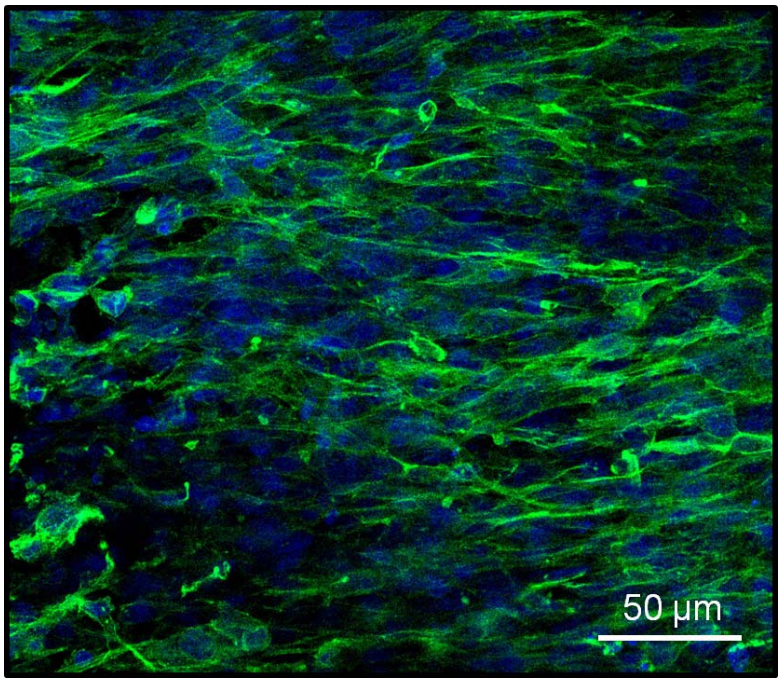

Figure 2.21 Confocal microscopy of MDSC-surface-seeded ES PEUU scaffolds. MIP 3D reconstruction on the lumen of the scaffold. Blue = nuclei, green = F-actin on the luminal surface of the electrospun PEUU scaffold after 12 hours of static culture. Magnification 200X.

2.2.5 Summary and limitations

The compact seeding device developed, combining the synergistic action of vacuum, rotation, and flow, was able to produce a rapid, efficient, reproducible, and uniform seeding of tubular porous constructs without generating injurious mechanical conditions for the cells. The analysis of the shear stresses generated inside the rotating scaffold during seeding performed with computational and analytical tools suggested absence of damaging conditions for the cells. The

metabolic-based viability assay performed after seeding (MTT) confirmed the absence of deteriorating conditions for the cells during seeding.

The quantitative analysis of the RVSD performance described in **Sections 2.2.2** and **2.2.3** was carried out using only a few combinations of relevant seeding parameters (*i.e.*, vacuum level, rotational speed, and flow rate) based on empirical observations. The chosen combination of parameters delivered more than acceptable results in terms of bulk seeding uniformity, reproducibility, and efficiency (see **Section 2.2.3)**; however, an analytical characterization and its empirical validation would provide a better understanding of the functioning of the device, and it would possibly lead toward performance optimization. This concept will be expanded in **Section 2.2.6**.

A theoretical limitation in the design of the first generation of RVSD is the length of the construct suitable for quantitatively uniform longitudinal seeding. This is not only due to the size of the seeding chamber, but also to the physical, structural, and geometrical features of the scaffold. In fact, the seeding process is likely affected by the scaffold characteristics. This can be considered another intrinsic limitation of the current design. The bulk cell seeding assessment was performed using only one type of polymer scaffold (TIPS PEUU) with cell types mostly relevant for muscular tube applications; therefore, further experiments are required to demonstrate the flexibility of RVSD use for different scaffold materials or tissue engineering applications. We will address these concerns and limitations in the following sections.

2.2.6 Additional studies toward functional characterization

An analytical model of the hydrodynamic forces involved in the cell seeding of TIPS PEUU porous scaffolds via the RVSD with and without rotation was implemented to better understand the mechanisms behind the seeding process.

2.2.6.1 Analytical model of the hydrodynamic forces involved in the RVSD operation

The transmural pressure drop, δP_w, across the tubular scaffold wall during cell seeding can be estimated by assuming the luminal surface, S, of the TIPS PEUU scaffold made of cylindrical pores of average diameter, d_p, through which Poiseuille flow of culture media occurs, governed by [121]:

$$\delta P_w \cong 128 \frac{\mu \cdot t \cdot q_p}{\pi \cdot d_p^4} \qquad \textbf{2-7}$$

where μ is the dynamic viscosity of the seeding suspension, t is the length of the pore (the scaffold wall thickness), and q_p is the volumetric flow passing through one pore. q_p can be estimated by dividing the total flow rate Q infused through the scaffold by the total number of pores n_p (assuming homogeneous distribution of flow within the scaffold) as:

$$q_p = \frac{Q}{n_p} = \frac{1}{4} \frac{Q \cdot \pi \cdot d_p^{\,2}}{\varepsilon \cdot S} \qquad \textbf{2-8}$$

where ε is the porosity of the scaffold. Substituting q_p into **Equation 2-7** results in:

$$\delta P_w \cong 32 \frac{\mu \cdot t \cdot Q}{d_p^2 \cdot \varepsilon \cdot S} \qquad \textbf{2-9}$$

If we assume a pore diameter of 20 μm (typical smallest pore size of TIPS PEUU scaffolds), then, using the same parameters used for the bulk seeding experiments in **Section 2.2.3** (*i.e.*, μ = 1.03 cP, t = 250 μm, Q = 16 mL/min, ε = 0.95, S = 2.5 cm^2) $\delta P_w \approx 20$ dyne/cm^2 or 0.02 mmHg. In a horizontal tubular scaffold, the hydrostatic pressure variation from the top to bottom of the scaffold lumen is given by $\delta P_h = \rho g D_i$, where ρ is the density of the seeding suspension and D_i is the internal diameter of the scaffold. For D_i = 4 mm, $\delta P_h \approx$ 400 dyne/cm^2 or 0.3 mmHg. With a uniform vacuum imposed on the outside of the scaffold, the large intraluminal hydrostatic pressure variation relative to this transmural pressure variation will drive a radial perfusion of cell suspension through the tubular porous scaffold. This perfusion varies significantly from the top to the bottom of the lumen, leading in turn to non-uniform cell seeding around the circumference of the scaffold as previously observed (see **Section 2.1.3**, **Figure 2.6**). This model underscores the need of rotation during seeding.

There are two possible mechanisms through which rotating the tubular scaffold can improve the uniformity of cell seeding as observed. First, as initially thought, centrifugal forces are generated by rotation and produce circumferentially uniform radial media flow. For this to occur, centrifugal forces would need to create a pressure gradient from the center of rotation to the scaffold wall which is large enough to overcome the hydrostatic pressure variation from the top to bottom of the tubular lumen (*i.e.*, to render hydrostatic pressure variation negligible compared to the centrifugal pressure variation). The pressure variation due to centrifugal forces, δP_c, is approximately given by (**APPENDIX B**):

$$\delta P_c \cong \frac{1}{4}\rho\omega^2 (D_i / 2)^2 \qquad \textbf{2-10}$$

where ω is the angular velocity. For our case this results in $\delta P_c \approx 15$ dyne/cm^2 or 0.01 mmHg. As this is an order-of-magnitude less than the hydrostatic pressure variation, centrifugal forces are unlikely to be large enough to produce a circumferentially uniform radial perfusion of the scaffold wall and uniform cell seeding. Scaffold rotation rates would need to be 10-100 times faster to create centrifugal forces that could impact cell media perfusion and cell seeding of the scaffold.

The second possible mechanism underlying the effect of rotation on cell seeding is simply that the rotation brings all circumferential sectors of the scaffold wall to the bottom position, where gravitationally drive cell media perfusion is predominately occurring. For this mechanism to be effective, the rotation period should be small compared to the time for gravitationally-driven flow to occur from the top to the bottom of the tubular conduit. An order-of magnitude estimate of the top-to-bottom velocity of gravitational flow is $V_g \sim Q/(D_i L)$, L being the length of the scaffold, and for the time from top to bottom is $t_g \sim D_i / V_g$. Using these estimates, we the required frequency of rotation would be:

$$\frac{1}{f} << \frac{D_i^2 L}{Q} \qquad \textbf{2-11}$$

For the parameters used in **Section 2.2.3** $f >>$ 0.8 s^{-1} or 50 rpm. The performed bulk-seeding study which demonstrated circumferential cell uniformity (**Figure 2.17**) was performed at an even higher rotation speed (350 rpm).

If centrifugal forces are not playing a direct role in cell seeding within rotating tubular scaffolds (as hypothesized), and if the role of rotation is merely to compensate for the hydrostatic variation in luminal pressure and the resulting imbalance in top-to-bottom flow of media, then the possibility exists for an alternative approach to bulk cell seeding that could also produce circumferentially uniform cell distributions within a tubular porous scaffold. For example, one alternative approach would be if the vacuum pressure is not applied directly to the scaffold, as in the current configuration, but through culture media (or an isotonic liquid in general) within which the tubular scaffold is submersed (**Figure 2.22**).

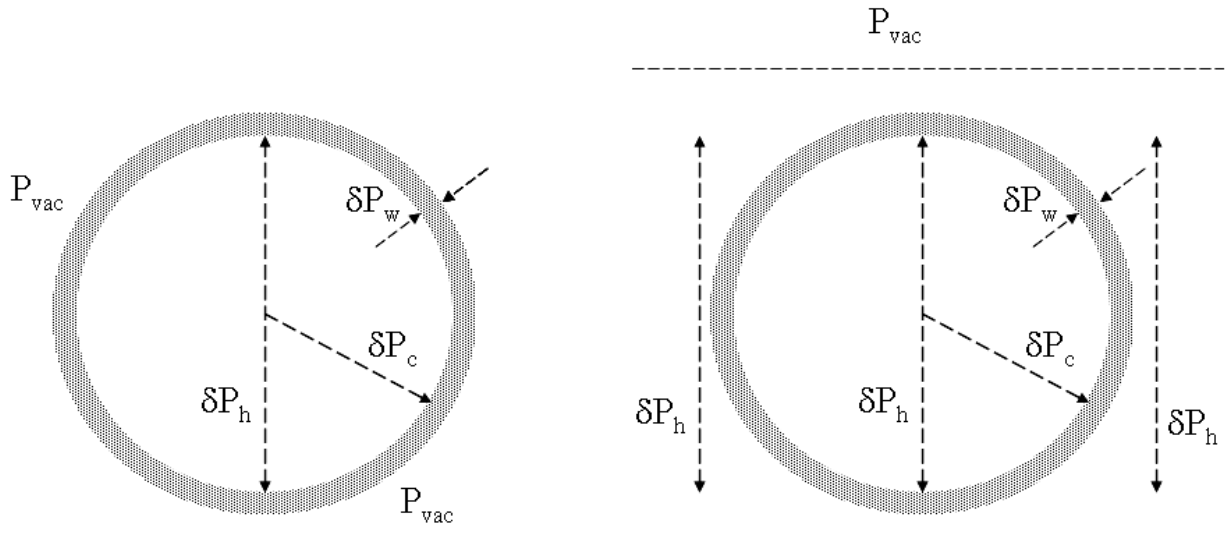

Figure 2.22 Schematic of a cross-section of the tubular scaffold showing the hydrodynamic forces involved in the seeding process with (Right) and without (Left) immersion into a liquid media.

In this case, the extraluminal liquid will transmit the vacuum pressure to the scaffold but will also eliminate a transmural hydrostatic pressure variation. Thus, in theory, the transmural variation in hydrostatic pressure within and outside the tubular scaffold will cancel one another and allow a circumferentially uniform transmural pressure and cell media flow to exist across the wall of the tubular scaffold. Such an approach would have the advantage of obviating the need for rotation of the tubular scaffold, or at least significantly diminishing the required rate of rotation.

2.2.6.2 Methods for the empirical validation of the analytical model

Based on the analytical model presented in **Section 2.2.6.1**, a dedicated experiment was conducted to assess the hypothesis of improved circumferential distribution within immersion conditions for the scaffold. To this end, tubular scaffolds (length = 1 cm, ID = 4 mm, thickness = 250 μm, porosity = 90%, pore size range = 20-200 μm, permeability = 2.6×10^{-13} m^2) made of TIPS PEUU were seeded with MDSCs via the RVSD with four different seeding conditions defined as follow:

1. **Rot/Dry:** Rotation speed = 150 rpm, Vacuum level = -5 inHg, Flow Rate = 2 mL/min, seeding chamber dry (currently used configuration).
2. **Rot/Wet:** Rotation speed = 150 rpm, Vacuum level = -5 inHg, Flow Rate = 2 mL/min, RVSD chamber filled with saline.
3. **Still/Dry:** Rotation speed = 0 rpm, Vacuum level = -5 inHg, Flow Rate = 2 mL/min, seeding chamber dry.

4. **Still/Wet:** Rotation speed = 0 rpm, Vacuum level = -5 inHg, Seeding Flow Rate = 2 mL/min, Seeding chamber filled with saline.

Scaffolds (n = 3 per condition for a total of 12 scaffolds) were seeded with ~$8x10^6$ MDSCs each released from a single 30 mL syringe loaded with a total of 113 million cells suspended in 28 mL of media (*i.e.*, each scaffold was seeded/infused with 2 mL of seeding suspension). After each seeding, the syringe was gently agitated to avoid sedimentation of cells on the bottom of the syringe and consequent reduction of seeding suspension cell density.

Scaffolds were fixed in 4% paraformaldehyde immediately after seeding for 1 hour and then washed in PBS. Scaffolds were subsequently processed for cell nuclear imaging as previously described in **Section 2.2.3**. Seven consecutive pictures for each section were taken at 40x and digitally reconstructed (Photoshop 7.0) to represent the whole section in one single image. Five reconstructed sections per seeded construct were processed via ImageJ in order to quantify the cell density for each seeding condition. The calculated cell density for each seeding condition was obtained dividing the cell number in each section by the total area occupied by the scaffold in each section. To assess cell distribution along the circumferential direction, the constructs were initially marked with a line running along the longitudinal extension of the scaffold to denote the gravitational axis within experimental groups 3 and 4. From the previously reconstructed sections the four circumferential quadrants (0°-89°, 90°-179°, 180°-269°, 270°-359°) were identified as described in **Section 2.2.3**. Each quadrant of each section underwent image-based cell density quantification via a three-step normalization process. First, the cell number in each quadrant of each section (measured as described in **Section 2.2.3**) was normalized by the total number of cells in that entire section to give a percentage (*i.e.*, % of the

total cell number incorporated in each quadrant). This step was performed to take into account the possible variability in cell number released within different constructs and variations in seeding efficiency. Second, the area of each quadrant of each section was normalized by the total area of that entire section to give a percentage of the total area occupied by each quadrant. This was done to consider local variability in seeding due to different wall thickness and, therefore, variations in permeability. Finally, the first two steps were combined to give a normalized cell density (*i.e.*, % cell/% area for each quadrant), taking into account errors introduced by possible variations in area and initial cell number.

A reference axis was arbitrarily chosen to identify the four quadrants in the two experimental groups using rotation (**Rot/Dry** and **Rot/Wet**) and to quantify the circumferential variability in cell number. Moreover, the quadrants were combined (Top = 0°-179°; Bottom = 180°-359°) in order to show the overall sedimentation effect due to gravity (*i.e.*, bottom versus top portion of the scaffold) for the experimental groups.

2.2.6.3 Results

According to the cell density assessment, the different experimental conditions affected the overall seeding efficiency (percentage of the initial cell number included in the construct after seeding). In particular, group 1 had a statistically higher ($p = 0.027$) seeding efficiency than any of the other groups while no significant differences were detected among the other groups (**Figure 2.23**). Also, although not statistically significant, group 3 seems to have an increased cell density compared to group 2 and 4. This observation suggests that seeding in dry conditions results in a higher seeding efficiency compared to the ones performed in an immersed state. A possible explanation to this phenomenon may be a cell loss from the scaffold while removing it

from the seeding device. In fact, the surrounding liquid media would rapidly rinse the internal surface of the scaffold immediately after its disconnection from the two tees. The pulling of the scaffold out of the media, combined with the large concentration gradient (proteins and cells) between the dense seeding suspension within the scaffold lumen and wall and the solution inside the chamber, might foster such cell loss from the scaffold wall. The phase immediately following seeding is very delicate; the cells are only passively incorporated into the pores without cell attachment. This preliminary observation reinforced the need for a normalization of the cells counted in each quadrant of the scaffold (as we will see below) based on the total cell number counted in its entire circumferential area.

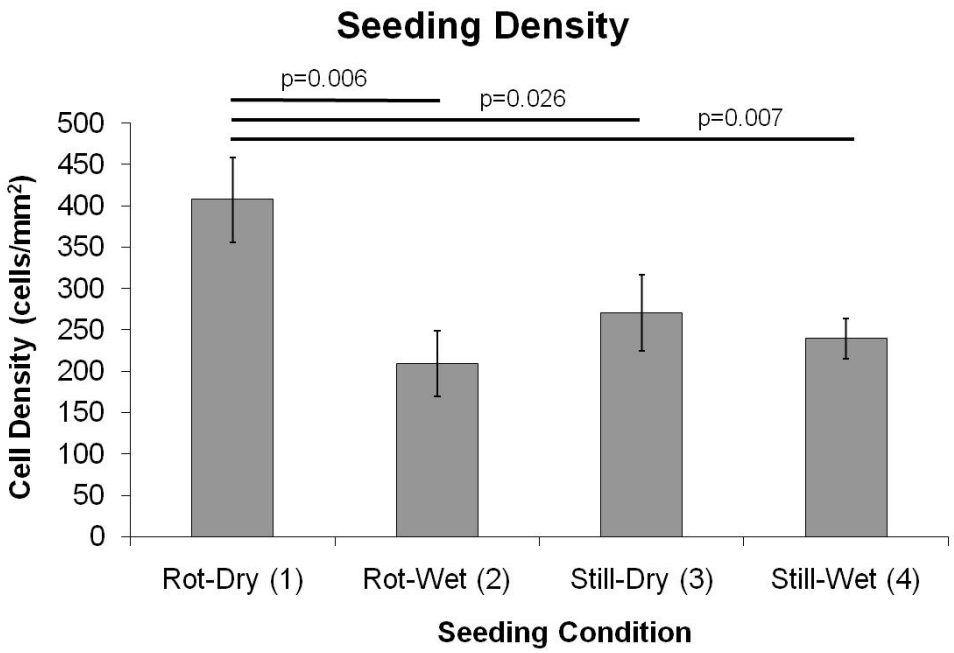

Figure 2.23 Measured seeding densities for the four different seeding conditions tested (mean ± standard deviation; n = 3). The bars indicate statistical difference with p-values as indicated.

Qualitative assessment of cell seeding distribution (**Figure 2.24)** confirmed the increased cell density obtained by seeding with the original configuration (**Rot/Dry**). A quantitative analysis of cell distribution in the four quadrants is shown in **Figure 2.25**. Moreover, the overall sedimentation effect due to gravity is shown in **Figure 2.26**.

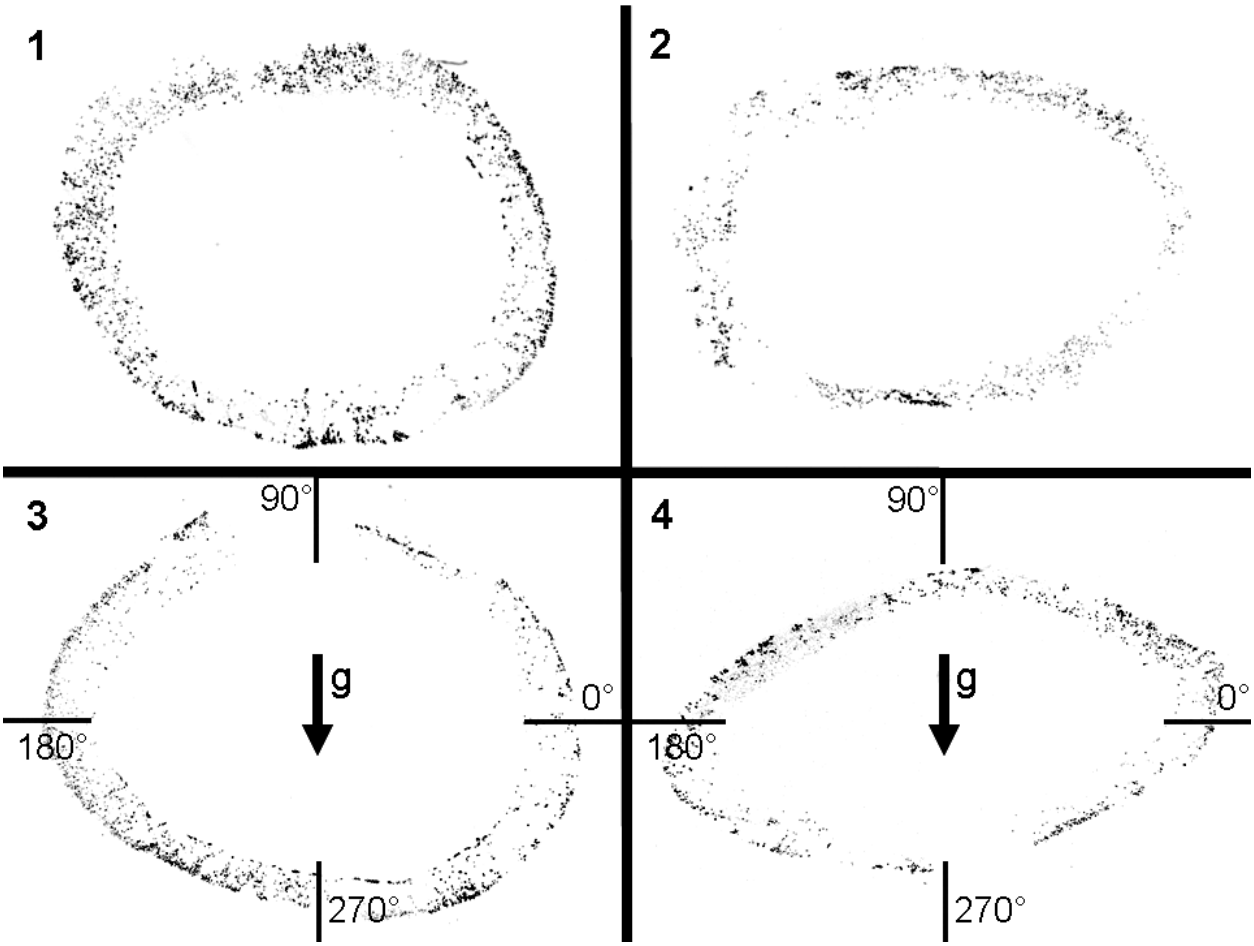

Figure 2.24 Representative sections of seeded TIPS PEUU scaffolds within the different seeding conditions: 1) Rot/Dry; 2) Rot/Wet; 3) Still/Dry; 4) Still/Wet. The initial reference point (0°) used for circumferential cell seeding quantification is shown. The arrows indicate the direction of the gravitational axis.

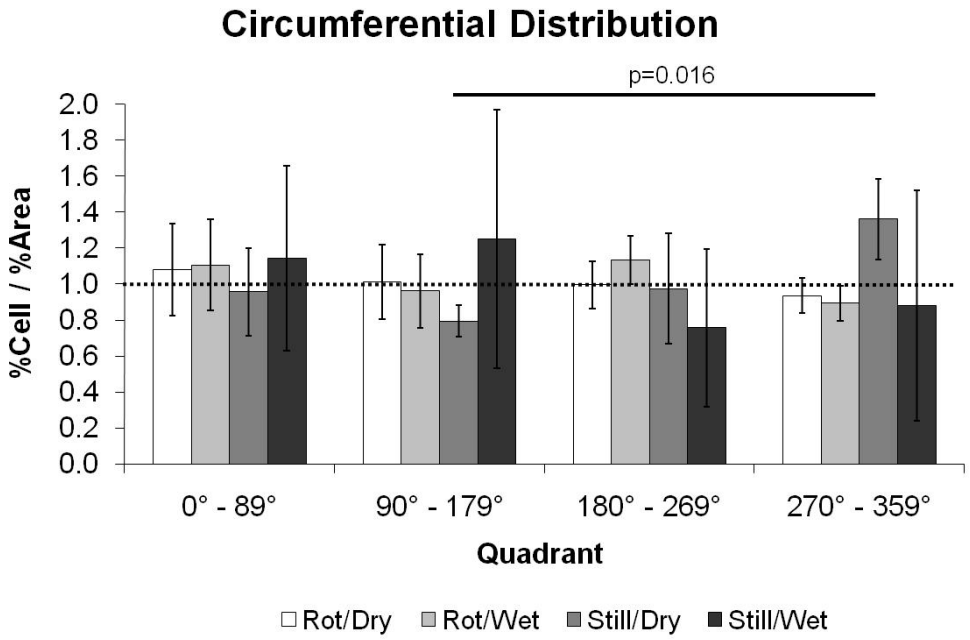

Figure 2.25 Normalized cell density in the four circumferential quadrants of the seeded scaffolds (mean ± standard deviation; n = 3). The dashed line indicates the ideal seeding.

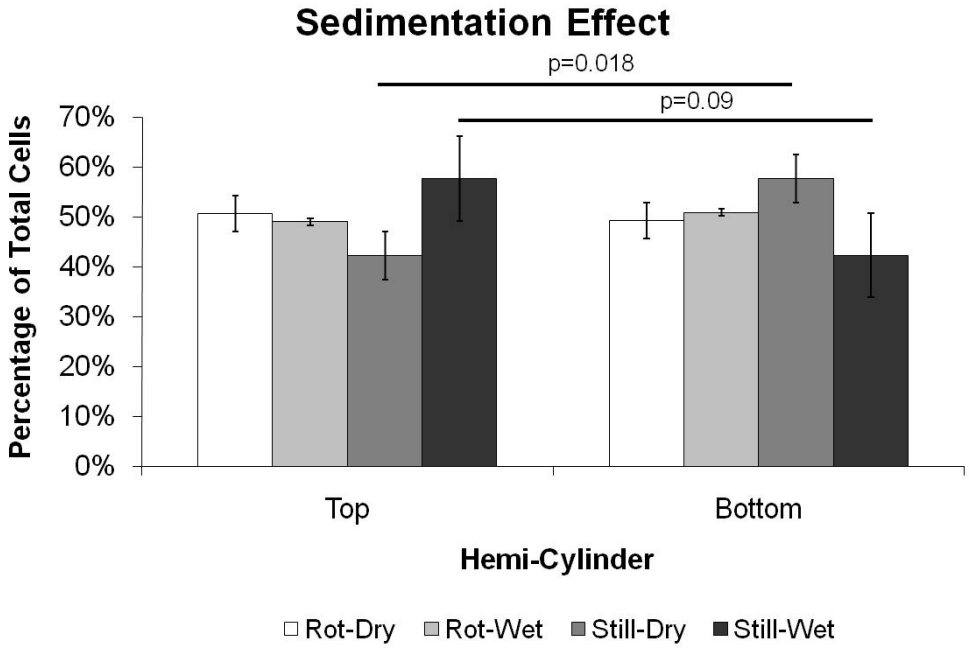

Figure 2.26 Percentage of total cells for the two circumferential hemi-cylindrical portions of the scaffolds (mean ± standard deviation; n = 3).

These results show that the rotation is indeed critical to reach a homogeneous circumferential distribution as predicted by the analytical model (see **Section 2.2.6.1**). The results of condition **Still/Dry** showed a statistically relevant imbalance between measured normalized cell densities in the top and bottom portions of the scaffold ($p = 0.018$) confirming the validity of the model and the previously observed gravity effects (see **Section 2.1.3** and **Figure 2.6**). However, the distribution obtained without rotation in immersed conditions (**Still/Wet**) did not agree with the analytical model. In fact, unexpectedly, the results showed an almost statistically significant ($p = 0.09$) inversion rather than a reduction of the trend noted in **Still/Dry**. However, a theoretical speculation for the observed increase in cell number in the top portion of the scaffold would suggest that the reduced cell sedimentation within the lumen of the scaffold observed in the immersed seeding conditions (as explained by the analytic model), coupled with the overall reduced cell density observed within the scaffold wall in immersed conditions (**Figure 2.23**), might demonstrate the presence of a stagnant luminal cell suspension media with an increased cell density. Fresh seeding suspension entering the scaffold lumen with a stagnant, denser media may tend to float due to a buoyancy effect, resulting in a higher flow rate in the top half of the scaffold and, therefore, a higher seeding density.

These experiments showed that seeding in immersed conditions might introduce undesirable effects including lower seeding efficiency, and higher seeding variability (note the higher standard deviations observed in the group **Still/Wet**). This feature was thus abandoned in the future implementations of the RVSD.

The characteristics of the scaffold would likely affect the seeding distribution. For example, the length-to-diameter (*L/ID*) ratio of the scaffold more than its absolute dimensions provides a relevant geometrical characterization of the scaffold. This parameter will likely

influence the scaffold internal fluid dynamics and therefore, the seeding distribution outcome. High values for this ratio (*e.g.*, long tubular constructs with small IDs) will likely generate an imbalance between the flow rate exuding through the scaffold in proximity of the tees and that exuding through the scaffold within its central portion. Due to the relatively high permeability of the scaffold (which results in a low hydraulic resistance for flows exuding through its wall) the resulting distributed pressure loss along the length of the scaffold (after few units of length) would be higher than the pressure loss caused by the exudation through the scaffold wall.

The flow entering the scaffold during the seeding process has two possible pathways: either proceeding longitudinally toward the center of the scaffold or exuding radially through the scaffold wall. The flow rate within these two pathways will be inversely proportional to their respective hydraulic resistances, with the greater flow favoring the path with the lower resistance (radial). Furthermore, in proximity of the tees the flow has elevated radial components (generated to maintain the mass continuity) due to the sudden expansion experienced by the fluid. This creates an additional outflow effect which facilitates the imbalance in longitudinal cell distribution. To test this limitation a simple experiment was performed as a proof-of-concept. One TIPS PEUU scaffold (length = 40 mm, ID = 2.2 mm, thickness = 250 μm) was seeded with the $10x10^6$ MDSCs suspended in 10 mL of media with seeding parameters consistent with what was previously used in **Section 2.2.3**. The scaffold size was chosen to emphasize the hypothesized longitudinal seeding imbalance with relatively high *L/ID* ratio of 18. **Figure 2.27** shows the results obtained and it demonstrates the suspected limitations of the RVSD implementation. Before this seeding device could be utilized in clinically relevant applications (where high *L/ID* ratios are desirable) this severe limitation needed to be addressed.

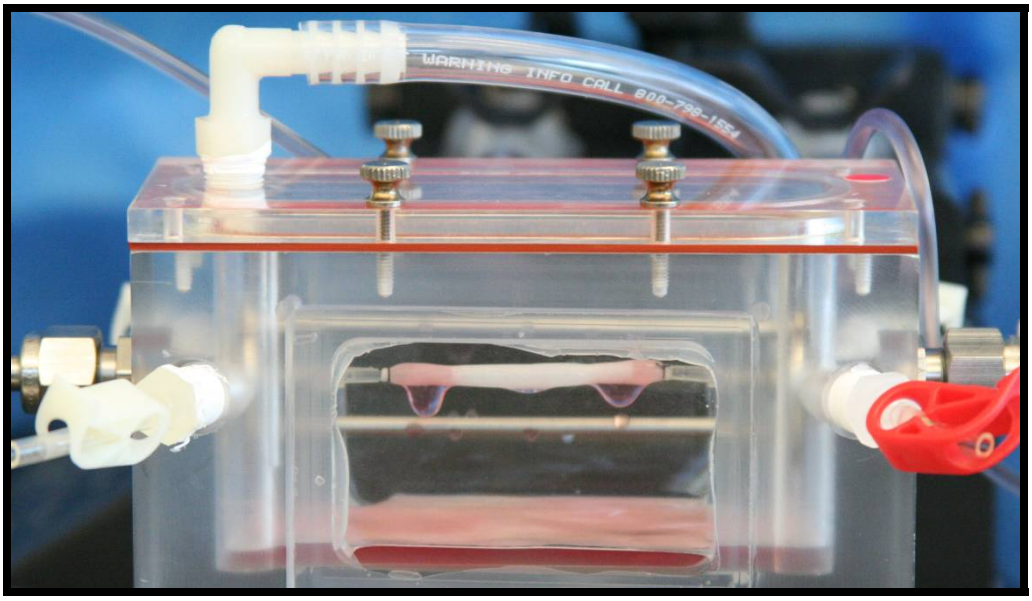

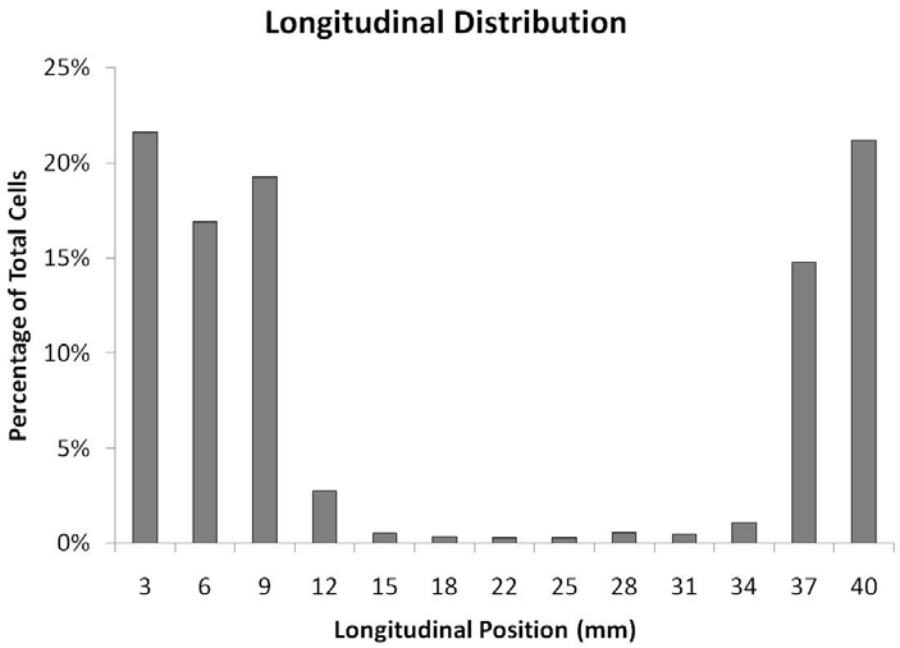

Figure 2.27 Seeding experiment demonstrating the limitation in longitudinal seeding capabilities of the RVSD for scaffolds with high *L/ID* ratios. **Top.** Representative picture taken during the seeding. Note how the pinkish media exudes mostly in proximity of the peripheral regions of the scaffold. **Bottom.** MTT-based cell quantification along the longitudinal direction of the scaffold.

2.2.7 Flexibility for different materials and applications

An additional concern mentioned above was the use of scaffolds based on only one type of polymeric material (PEUU) and targeting only vascular tissue engineering applications for all the seeding tests performed. To prove the ability of the RVSD to seed any porous material allowing for transluminal flow, and at the same time, its suitability for different tissue engineering applications, additional biodegradable polymeric scaffolds and cell types originating from collaborating laboratories and a Japanese biomaterial company, were tested. A detailed description of these scaffold fabrication techniques and cell types is beyond the scope of this dissertation, therefore, only a brief explanation will be provided.

First, polycaprolactone (PCL) scaffolds (a generous gift from Dr. Kacey Marra) with porosity obtained via salt leaching technique (length = 15 mm, ID = 1 mm, thickness = 500 μm, pore size = 35-70 μm), were seeded with $3x10^6$ human Foreskin Fibroblast Cells (hFFCs) (also provided by Dr. Marra). The scaffolds were mounted with tips (recall **Figure 2.4**) and seeded using the same seeding parameters described in **Section 2.2.3**. A sample of the scaffold was observed via SEM prior to seeding. Following seeding, the construct was processed for nuclear and cytoskeletal staining and observed via fluorescence and confocal microscopy as described in **Section 2.2.4**.

The scaffold appeared homogeneously integrated with hFFCs throughout the thickness of the wall (**Figure 2.28-B**). Cytoskeletal staining showed a cellular spreading aspect (**Figure 2.28-C**).

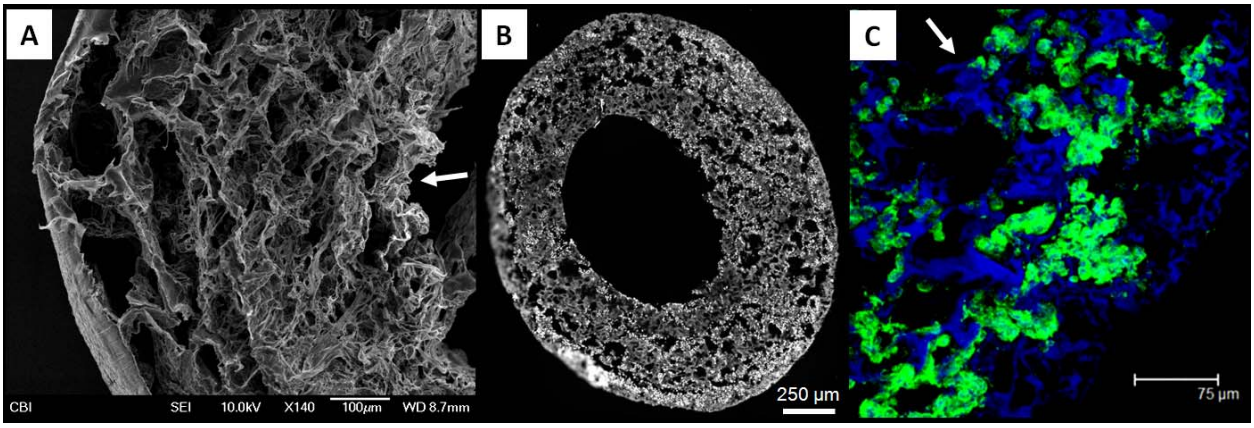

Figure 2.28 Utilization of the RVSD for seeding hFFCs in a PCL porous scaffold. **A.** SEM of the unseeded scaffold wall. **B.** Nuclear staining of a cross-section of the hFFC-seeded scaffold. **C.** Confocal microscopy of the hFFC-seeded scaffold. The arrows indicate the lumen of the scaffold.

Second, a commercially available large-diameter, bi-layered PGA-P(LA/CL) scaffold (length = 3 cm, ID = 1.5 cm, thickness = 600 μm) donated by a Japanese company (Gunze LTD, Kyoto, Japan) was seeded with $20x10^6$ rat MDSCs (rMDSCs) and processed for nuclear staining with the seeding parameters and technique as described in **Section 2.2.3**. Qualitative seeding results are shown in **Figure 2.29**.

Finally, Rosa26 mouse hepatocytes (generously provided by Dr. Eric Lagasse) were bulk-seeded (cell density: $0.3x10^6$ cells/mm^3) into TIPS PEUU scaffolds (ID = 3 mm, length = 10 mm, thickness = 0.2 mm) and processed for nuclear staining with the seeding parameters and technique as described in **Section 2.2.3**. The seeding device produced again a uniform distribution of cells throughout the thickness of the scaffolds (**Figure 2.30-A**). The ability of the RVSD to seed the cells without damaging them was again confirmed by the intact cell morphology of the delicate hepatocytes (**Figure 2.30-B**).

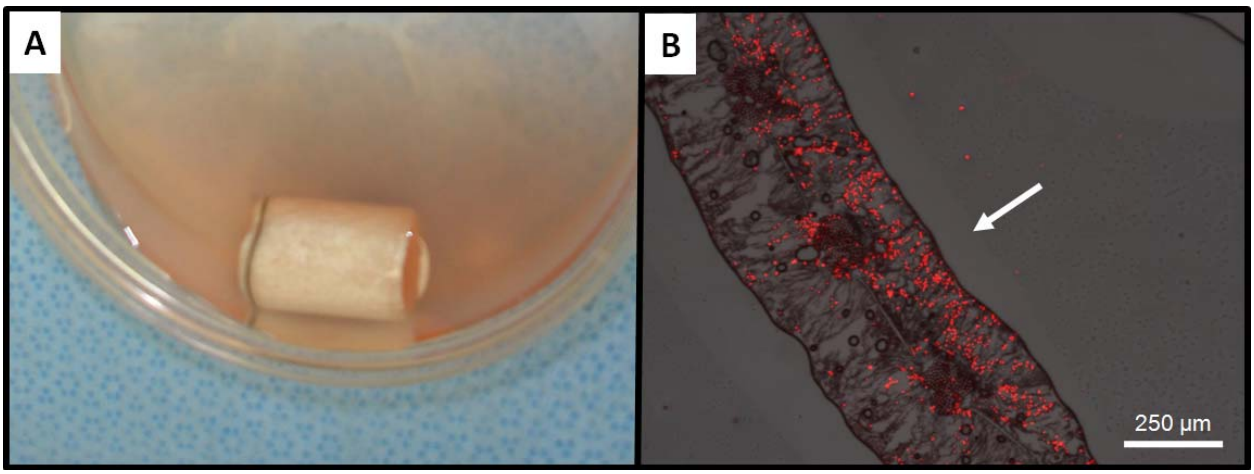

Figure 2.29 Utilization of the RVSD for seeding large-diameter PGA-P(LA/CL) porous scaffold. **A.** Macroscopic appearance of the scaffold immediately following seeding. **B.** Nuclear staining of a cross-section of the rMDSCs-seeded scaffold. Red = Nuclei. The arrow indicates the lumen of the scaffold.

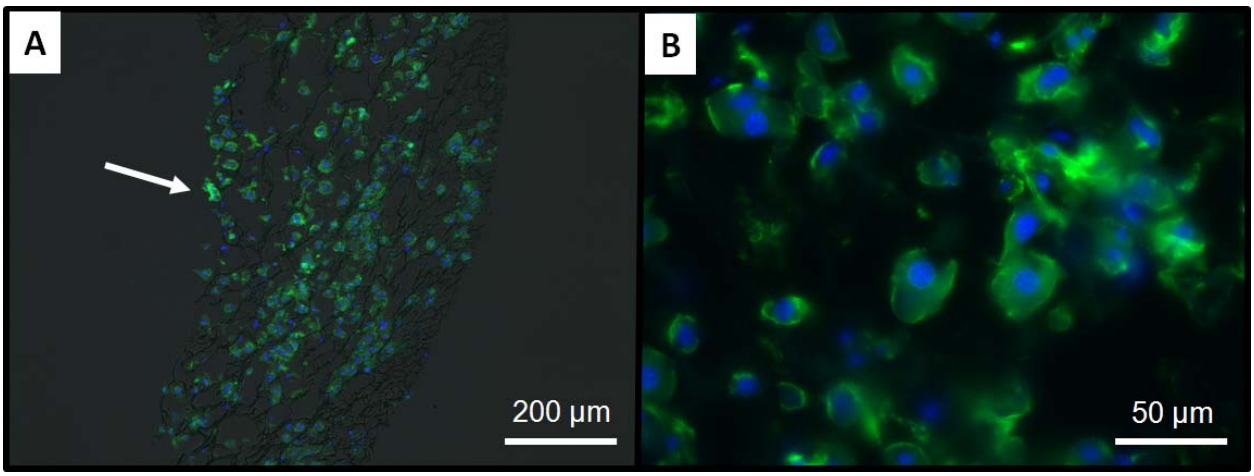

Figure 2.30 Utilization of the RVSD for seeding mouse hepatocytes into a TIPS PEUU scaffold. **A.** Nuclear and F-actin staining of a cross-section of the hepatocytes-seeded TIPS PEUU scaffold. Blue = Nuclei, green = F-actin, dark grey = scaffold. The arrow indicates the lumen of the scaffold. **B.** Higher magnification. Picture taken at 400X.

These additional tests demonstrated the RVSD capability of seeding any type of porous tubular scaffolds and any cell types, hence showing its suitability as a platform technology for future clinical applications.

3.0 SPECIFIC AIM 1, PART 2: SECOND GENERATION OF SEEDING DEVICE FOR PRECLINICAL APPLICATIONS: THE S-RVSD

3.1.1 Modification of the cell seeding system

Due to the limitation of the RVSD to seed scaffolds of clinically-applicable *L/ID* ratios (see **Section 2.2.6.3** and **Figure 2.27**), some design modifications of the seeding device were required. To deliver cells uniformly along the longitudinal direction of tubular scaffolds, it was necessary to create a system that performed successfully, independent of the length of the scaffold.

3.1.1.1 The flow distribution problem and possible solutions

A problem in hydraulics – commonly referred as the "flow distribution problem" – , is the achievement of a uniform distribution of flow rates into lateral branching channels distributed along the longitudinal axis of a common central pipe [145]. This problem is analogous to our present case; *i.e.*, the scaffold is analogous to the central pipe, and the pores of the scaffold represent the branching channels. A solution to this problem consists of the rationally-guided variation of the lumen of the lateral channels to obtain uniform departing flow rates throughout the entire length of the central pipe [146]. In particular, lateral branches (or pores) should have gradually increasing diameters moving away from the central lumen inflow area resulting in a

gradual decrease in the localized pressure losses associated with the lumen restriction encountered for each branch. If properly designed, it is possible to balance the distributed (central pipe length) and localized (lateral branches) pressure losses in order to obtain uniform flow rates in each lateral branch.

Following the analogy of scaffold (central pipe) and pores (lateral branches), this solution is not directly applicable to our problem. In fact, this would imply a modification of the scaffold porosity, consisting of a gradual increase in the scaffold pore size along the longitudinal direction, which is not desirable for obvious reasons. However, the same solution could be utilized by machining an intermediate custom-made distributor placed coaxially inside the lumen of the scaffold. This components would have a long tubular shape with several radially-oriented orifices (with variable diameters as explained), and it would extend throughout the whole length of the scaffold providing uniform radial flow rates along its longitudinal direction (**Figure 3.1**).

However, the machining of this component should be specific for each scaffold size (length), meaning that different distributors should be fabricated to seed different scaffold sizes. For example, any different scaffold length would require a specifically-designed component to satisfy the condition of equal distribution of flow rate. Moreover, the described solution is intrinsically limited because of the variability in radial velocity for different locations in the longitudinal direction of the scaffold (as a direct consequence of consistent flow rates but different radial efflux areas). Different radial flow velocities will likely affect the radial distribution of cells within the scaffold wall in different longitudinal locations (possibly this limitation affects also the current design of RVSD).

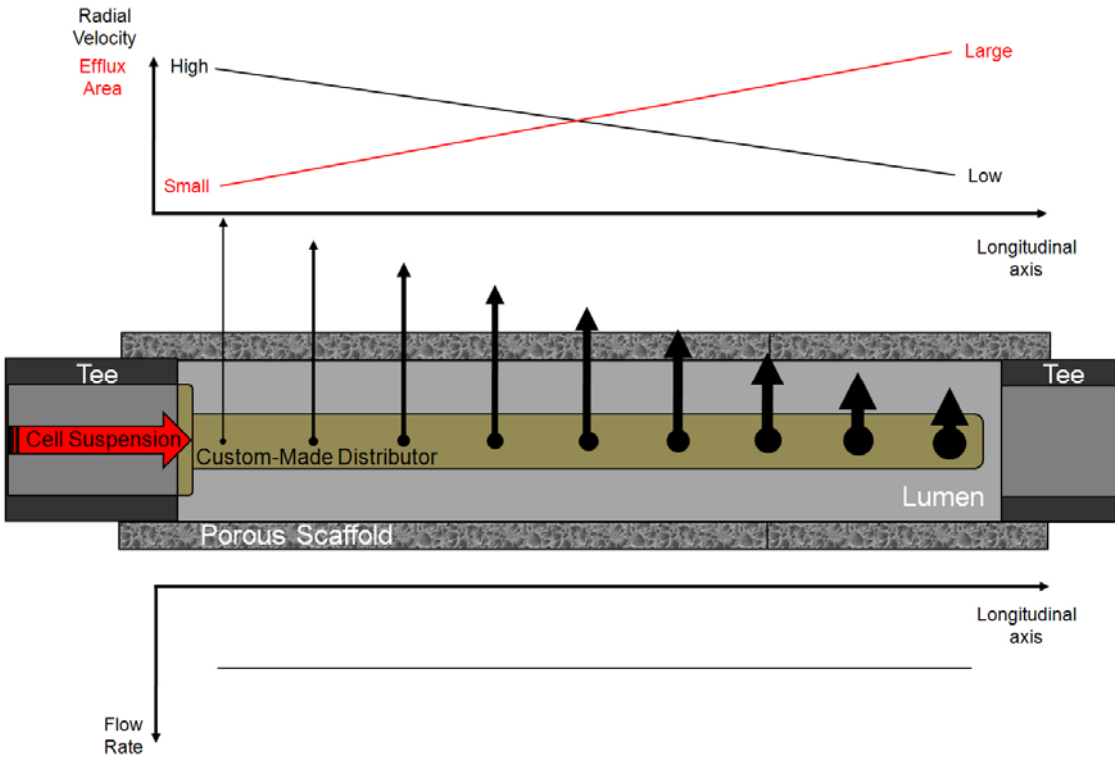

Figure 3.1 Schematic demonstrating the thoughts and rationale behind the custom-made distributor proposed as a solution to address the limitations in longitudinal seeding seen with the RVSD.

Another way to solve this problem would be to globally increase the hydraulic resistance provided by the scaffold wall (*i.e.*, to decrease the scaffold permeability). In this way the pressure loss along the longitudinal direction of the scaffold would be negligible compared to that in the radial direction, and the radial flow would then be longitudinally uniform. This solution could be implemented in two ways, either by decreasing the scaffold permeability directly by altering the scaffold characteristics (*e.g.*, decreasing the pore size), or by applying an external, conformal, and slightly water permeable wrap around the scaffold (properly sealed to allow only the flow across its wall) in order to produce a reversible increase in overall wall permeability. Neither of these solutions are ideal. The implementation of the first solution would

affect the cell-scaffold interaction by significantly reducing the nutrient diffusion into the scaffold wall (affecting viability) and by providing incompatible pore sizes to allow for cell penetration (as seen for the ES PEUU scaffolds in **Section 2.2.4**). The second would introduce a user-dependency and risk of contamination due to the manual application of an external wrap. Moreover, significantly decreasing the permeability of the scaffold wall may lead to other problems, especially for scaffolds with elevated *L/ID* ratios. For example this can lead to an increase in luminal pressures during seeding, potentially affecting cell viability.

3.1.1.2 Chosen solution: The Stylet and Diffuser system

The above considerations led to the idea of a local delivery of cells by means of a mobile internal sliding body able to release cells locally in a controllable manner. This system would include a single cell releasing "Diffuser" provided with radial nozzles attached to an arm or "Stylet". The Stylet has the double function of driving the Diffuser along the axis of the tubular scaffold and transporting the cell suspension in its internal lumen. The sliding Stylet and Diffuser would translate along the longitudinal axis of the scaffold while the scaffold is rotating externally on around it. The working principles of such a system are summarized in **Figure 3.2**.

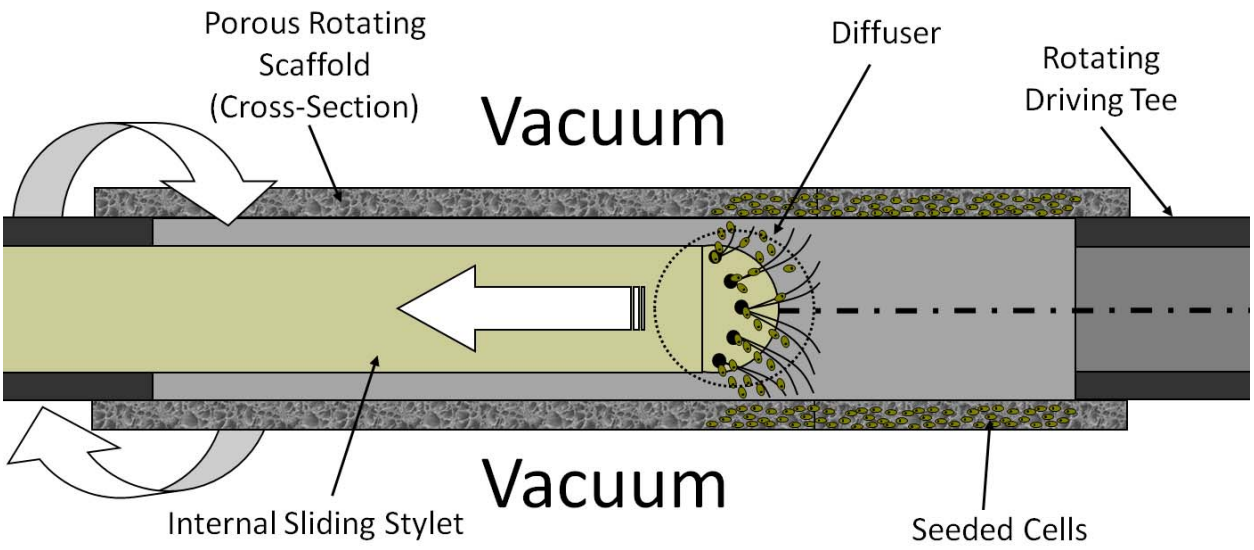

Figure 3.2 Schematic of the Stylet sliding internally to the rotating scaffold.

The hypothetical advantage of such a system consists in its possible ability to infuse cells locally into the scaffold wall with constant overall flow rate and a uniform radial component of the velocity. The basic principle of the RVSD including the rotation, the vacuum, and the infusion of the seeding suspension via a syringe pump would be preserved. The implementation of this new concept would only add a single but fundamental feature to the first generation: the sliding internal body. As such, the second generation of seeding device arose, referred to as the sliding-rotational vacuum seeding device (S-RVSD). One consequence of the implementation of this new concept is the adoption of a single cell infusing syringe instead of the two utilized in the original design.

The implementation of the sliding Stylet and Diffuser required several modifications to the design of the original RVSD. The first regarded the achievement of a translational

movement for the Stylet/Diffuser component. To this end, a linear sliding stage with scale and vernier (Series A15, Velmex Inc., Bloomfield, NY) was utilized to translate the Stylet and to visualize the position of the stage and the subsequent position of the Diffuser inside the scaffold. The linear sliding stage converts the rotational movement of its central screw into a translation of the stage (**Figure 3.3**). The linear sliding stage was fixed to the RVSD base via SS screws with careful alignment of its central leading screw to the axis of the RVSD tees. Custom-made components were designed and drew via Solidworks 2005 software (Solidworks Corp., Concord, MA). Drawings are shown in **APPENDIX A**. A custom-made Stylet holder to transmit the translational motion from the sliding stage to the Stylet was machined from a single sheet of black Delrin® (**Figure A.10**). The base of the Stylet holder was mounted on top of the sliding stage via two SS socket cap screws (**Figure 3.3**). On top of the Stylet holder, a set screw holds the Stylet tightly into a bore (Ø = 3.2 mm) running across the full thickness of the component.

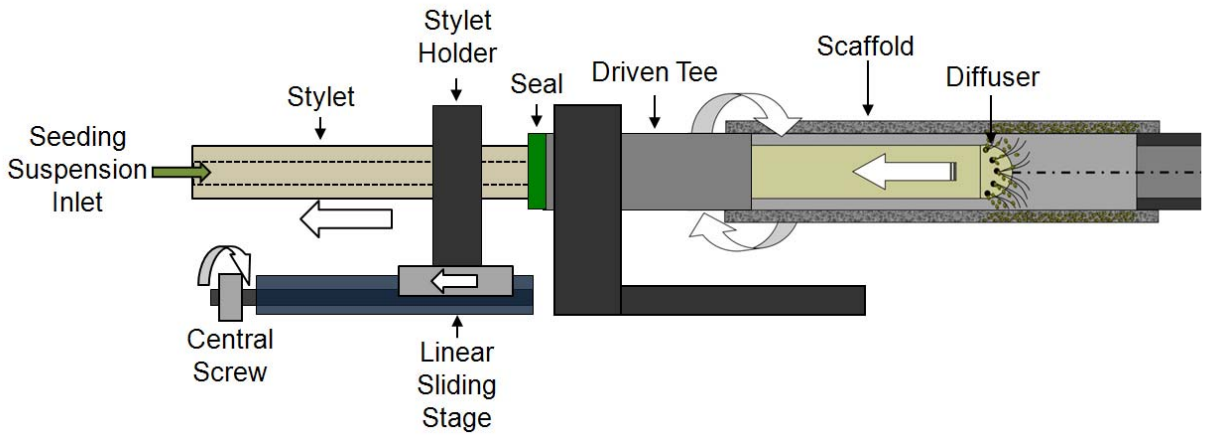

Figure 3.3 Schematic of the linear sliding stage system used to translate the Stylet/Diffuser component during seeding with the S-RVSD.

The motion control necessary for the movement and positioning of the linear slide stage suggested the use of a stepper motor ("Motor 2") (S57-83, Parker Compumotor, Rohnert Park, CA) which was anchored on the RVSD base via an aluminum support (**Figure A.11** and **Figure A.12**). A precision aluminum timing belt pulley (SDP/SI, New Hyde park, NY) was mounted on the central screw of the Unislide and driven by a polyurethane/kevlar timing belt (SDP/SI, New Hyde park, NY) using an identical pulley mounted on the shaft of the Motor 2. At this stage of the S-RVSD development, it was decided to also control the rotation of the scaffold via another stepper motor ("Motor 1") (S57-83, Parker Compumotor, Rohnert Park, CA) capable of delivering a strictly controlled rotational velocity and replacing the original AC motor. Also Motor 1 was anchored to the RVSD base via a custom-made support (**Figure A.13** and **Figure A.14**). The design of an electronic control box for the computer-controlled S-RVSD operations will be described in **Section 3.1.2**.

The Stylet was fabricated from a thick-walled SS 316L tube (OD = 3.175 mm, ID = 0.98 mm, length = 25.4 cm). The Diffuser was machined from a single PTFE cylindrical rod (final dimensions: OD = 4.65 mm, length = 5 mm); (**Figure A.15**). A central lumen was created through 3/4 of its length. Eight equi-spaced radially-distributed bores (Ø = 0.62 mm) were drilled to connect the central lumen of the Diffuser to its cylindrical lateral wall. Threads on both the internal lumen of the Diffuser and the end of the Stylet allow for a firm coupling of the two components (**Figure 3.4**).

The Driven Tee of the original RVSD (see **Figure 2.9**) was replaced by a 7 cm-long SS 316L tube (OD = 6.35 mm, ID = 5 mm) to allow for a concentric sliding of the Stylet within its internal lumen (see **Figure 3.3**). Two solid PTFE cylindrical rods (Ø = 5 mm; length = 1.5 cm) were pressure fit in the two opposite ends of the new Driven Tee. A bore (Ø = 3.18 mm) was

machined in the center of the two ends in order to re-establish an internal central lumen (**Figure A.21**). This created a concentric alignment of the Stylet within the Driven Tee and a low-friction sleeve bearing allowing for the mutual movement (rotation and translation) of the two components. An adapter made of Delrin® was fabricated to reduce the external diameter of the Driven Tee from 6.35 mm to 4.7 mm in proximity to the scaffold ligation site (**Figure A.22**). Also the Driving Tee was replaced with a larger and longer tee (**Figure A.23**).

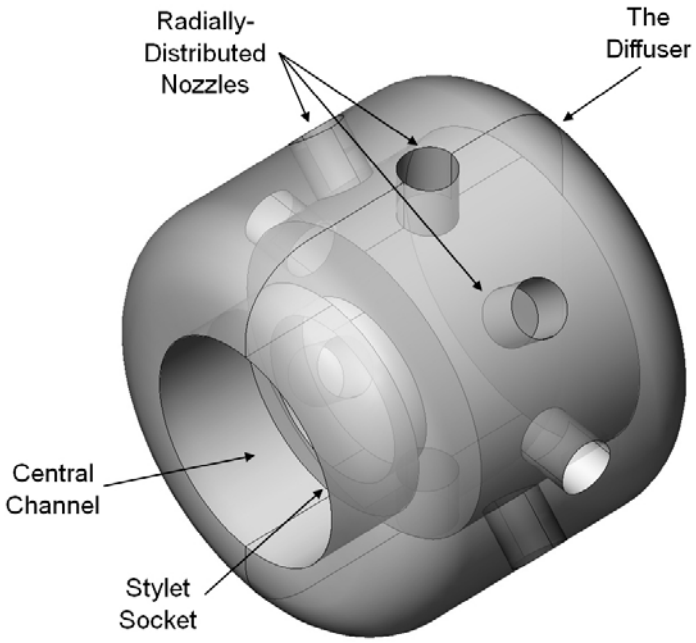

Figure 3.4 The Diffuser 3D modeling.

Two custom-made SS 316-L inline swivel joints (007-10211-ZAT, Rotary Systems, Inc., Ramsey, MN) with internal Armoloy plating and Teflon seals were used to replace the rotating joints in the RVSD design. The inline feature of these rotating joints was necessary to allow for the sliding of the Stylet across the swivel extension while the Driven Tee was rotated. The mutual movement of the two components would have been otherwise impossible in the previous 90º rotating joint configuration, in which the bend would not allow for the translation of the rigid Stylet within its internal channel.

The connection between the tees and the new rotating swivel joints were made with SS compression fittings (McMaster-Carr) replacing the previous plastic ones. A SS Yor-Lock compression tube fitting (male pipe adapter, McMaster-Carr) was modified (similar to what was previously done for the rotating joints crossing the RVSD chamber) by removing its internal double-sleeves. Machining a bore (Ø = 3.2 mm) throughout the main body of the tube fitting to remove the internal shoulder (originally designed to stop the fitted tube from further longitudinal sliding), enabled its use as a sleeve bearing for the sliding SS Stylet. The back nut of the compression tube fitting was also machined to reduce its overall length. A fluoroelastomer V-ring seal (SKF, Göteborg, Sweden) seal was placed between the compression tube fitting and its back nut component to create an airtight seal between the translating Stylet and the interior of the S-RVSD chamber. This sealed joint was screwed into the back threaded bore of the inline swivel. A schematic of the assembly is shown in **Figure 3.5**.

Two different custom-made supports for the new rotating joints were machined from a thick sheet of black Delrin®. The support for rotating joint connected to the Driving Tee was similar in shape with the one of the old rotating joints (**Figure A.17**), while the rotating joint connected to the Driven Tee was re-designed to bridge the sliding stage component with a

double base (**Figure A.19)**. Both supports were provided with caps to hold firmly the rotating joints (**Figure A.20**), and were anchored to the RVSD base via SS socket cap screws. Two slots were made on both support bases (**Figure A.16** and **Figure A.18**) to allow for regulation of the distance between the rotating joints and the S-RVSD chamber (*i.e.*, to allow for the regulation of the scaffold length) (**Figure 3.6**). The Driving Tee side maintained the same basic features as that used in the RVSD except for the presence of a three-way stopcock directly attached to a polypropylene Luer Lock female port screwed in the back of the rotating joint to close the circuit downstream after saline priming just before seeding.

A detailed overall schematic of the S-RVSD depicting all of its major components as well as a photograph of the S-RVSD are shown in **Figure 3.7** and **Figure 3.8**, respectively.

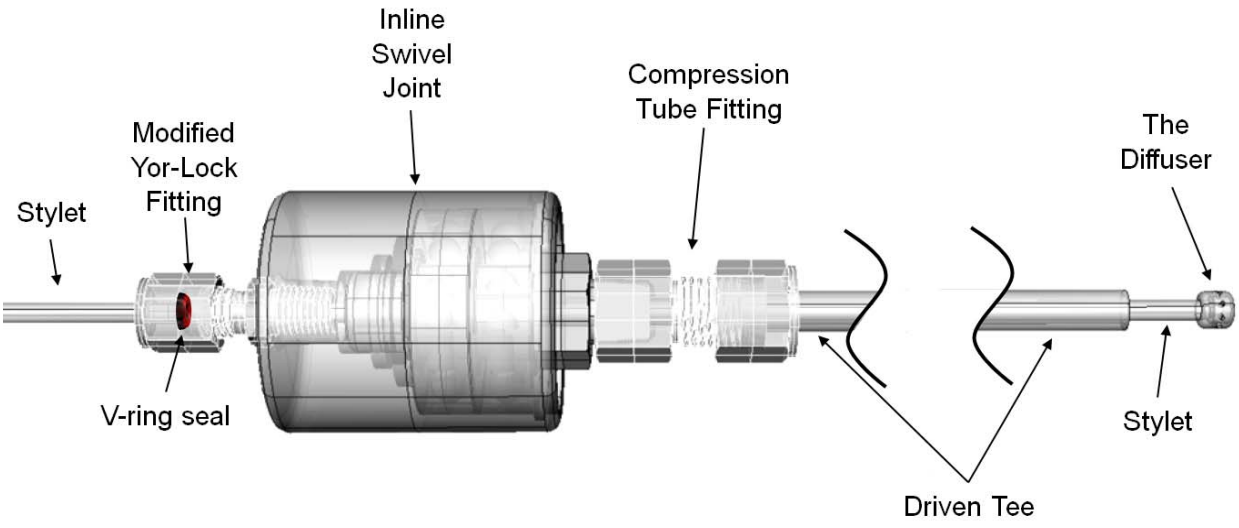

Figure 3.5 3D model of the assembly for the S-RVSD Driven Tee.

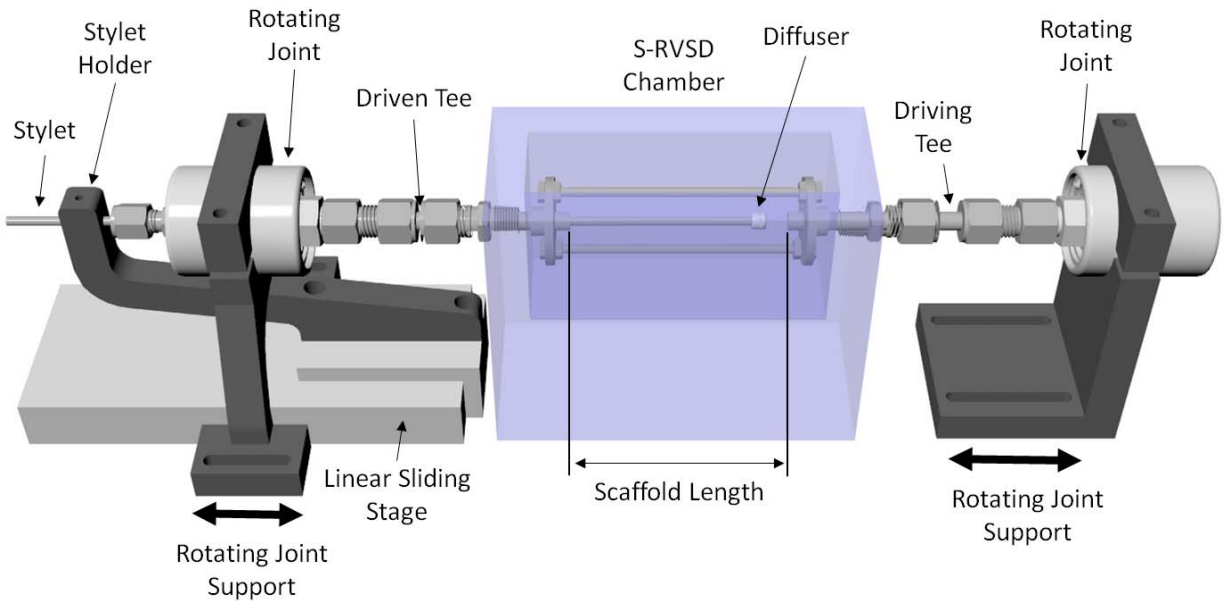

Figure 3.6 3D model of the S-RVSD. Note the regulation of the scaffold length by changing the position of the rotating joint supports.

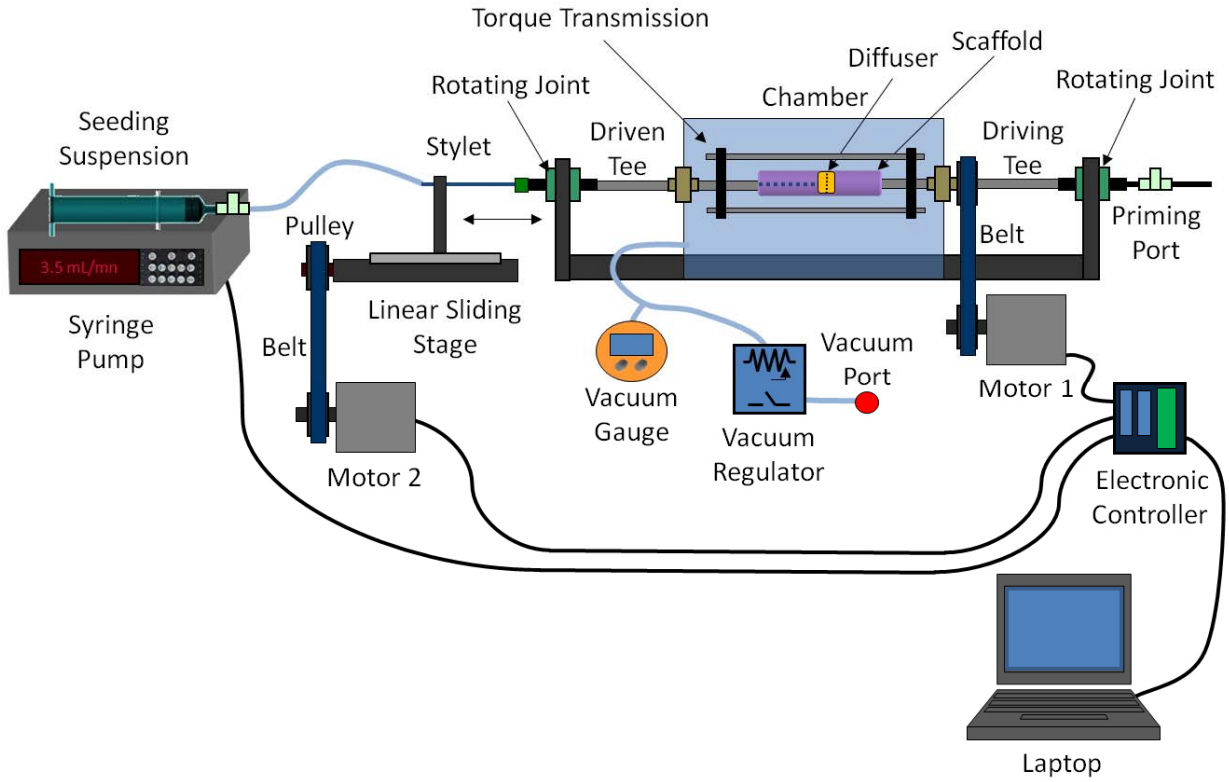

Figure 3.7 S-RVSD schematic.

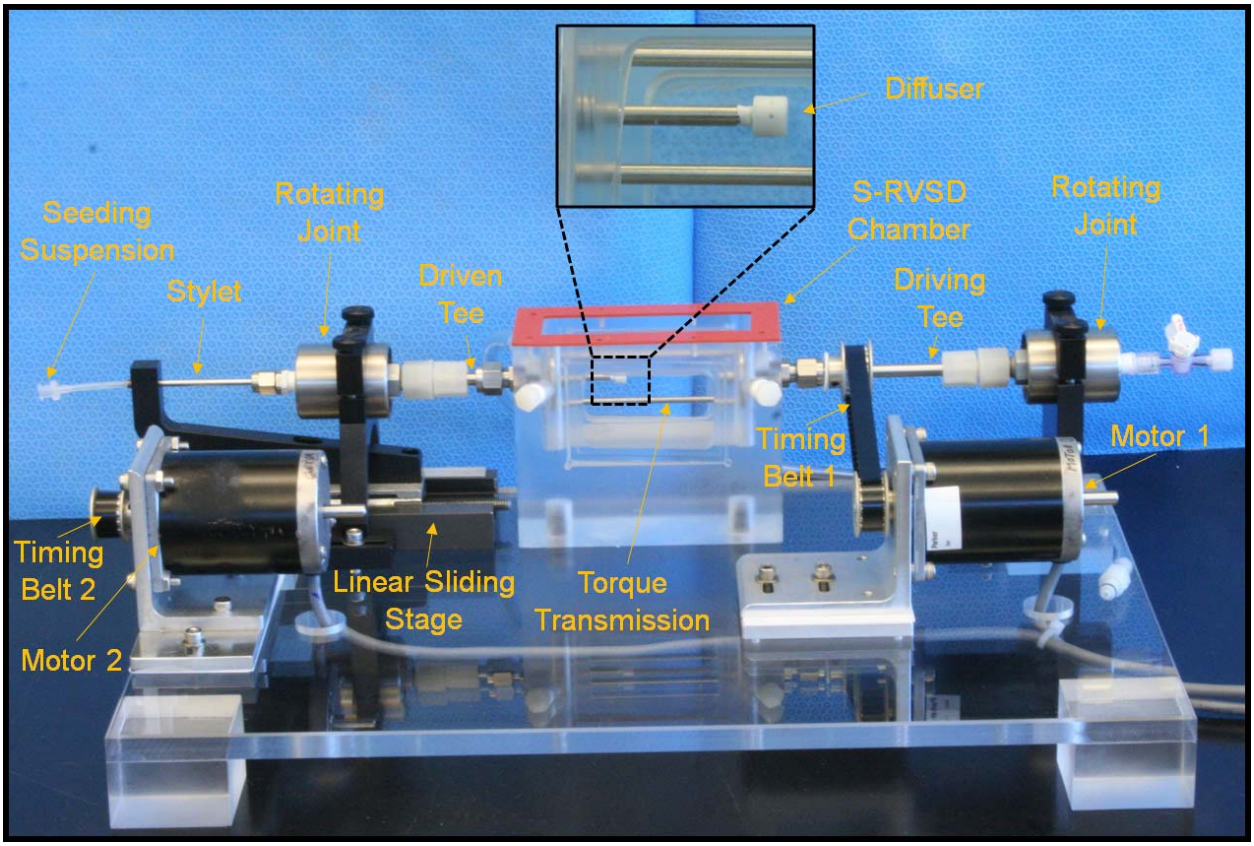

Figure 3.8 Actual photograph of the S-RVSD. Inset shows a close-up of the Diffuser.

3.1.2 Electronic control box

The introduction of a second motor in the design of the S-RVSD and the adoption of stepper motors required the incorporation of electronic drivers to provide the proper motion signal for the motors and to control the overall function of the device. To this end, a control box was built to operate the device and the syringe pump in a coordinated fashion.

A 20x25 cm electronic enclosure base made of painted steel with 5 cm-tall vertical edges was provided with 4 rubber feet on its bottom to allow space for the placement of screws used to anchor the internal electronic components. A power supply (XL-PSU, Parker Compumotor, Rohnert Park, CA) was positioned on the base. This component transforms the 115 V AC (60Hz) signal into a stable 24 V DC power supply. The DC source was used to energize two digital micro-stepping drivers (ViX IM250, Parker Compumotor, Rohnert Park, CA). These three components were secured with screws and nuts on the steel base parallel to each other with a distance of approximately 2 cm to allow for heat dissipation as per product specifications. The two drivers were connected to each other in a "daisy chain" configuration via a short RJ-45 cable. In this configuration, the first driver ("Driver 1") receives the instructions from a PC via a RS-232 communication protocol and transfers the pertinent information to the second driver ("Driver 2") (**Figure 3.9**). This configuration also allows for two-way communication among motors, drivers, and the computer in case of the future need for implementation of a feedback control system such as digital encoders.

A relay circuit was custom-made to enable the control of the syringe pump. In particular, Driver 1 is provided with a user I/O port (15-Position HD male D-Sub connector). The internal electronics of the driver allows trigger for up to three 24 V output signals upon request. The syringe pump has the option of being remotely controlled. The basic functions of infuse/refill and pump start/stop signals are triggered by the simple opening or closing of two different electrical circuits. To match these two different specifications a relay circuit was custom-made on two of the three output pathways available from Driver 1.

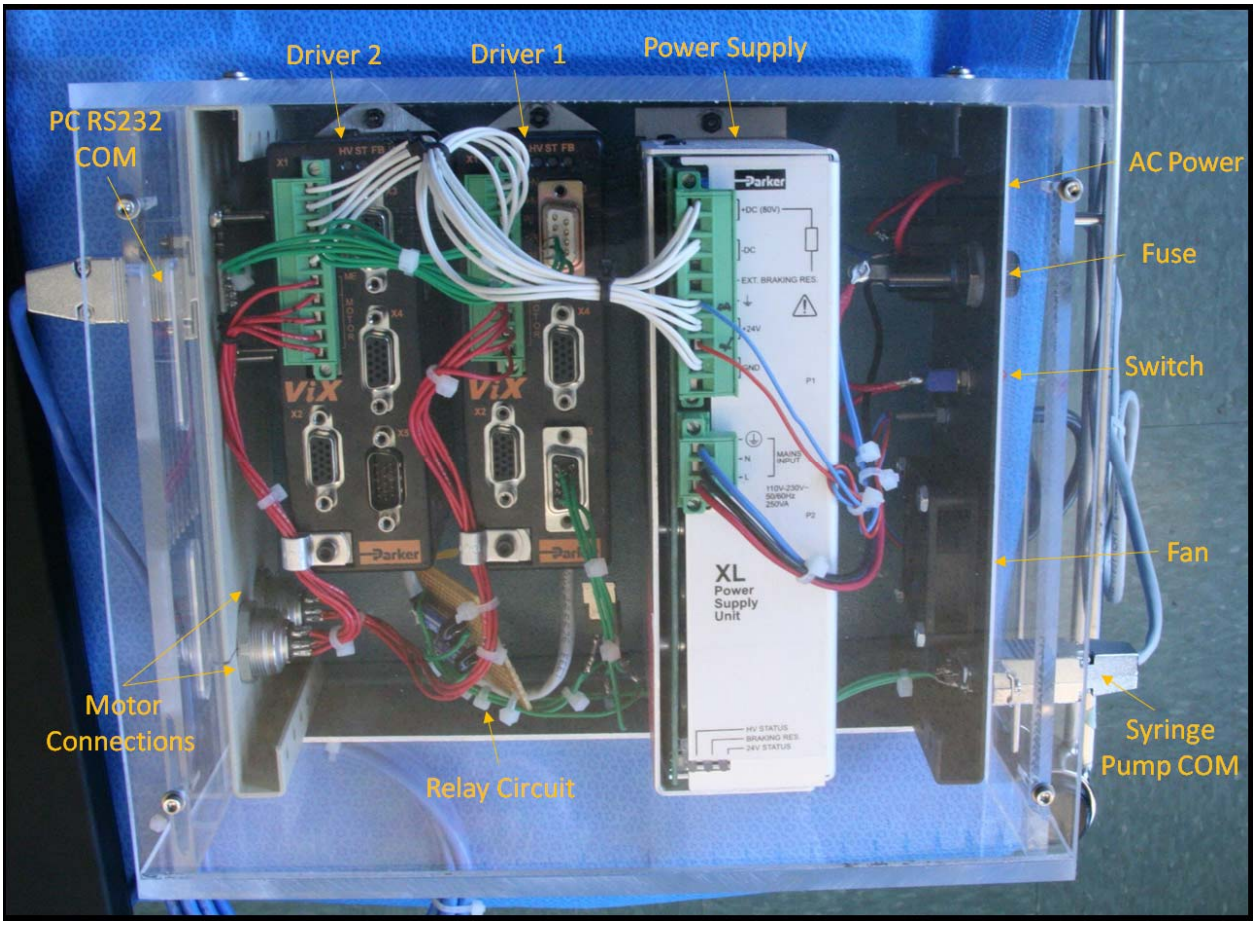

Figure 3.9 S-RVSD Electronic Control Box. Top view. Back wall is to the right, front wall to the left.

Each of the two circuits consisted in a voltage regulator (276-1770, Radioshack Corp., Forth Worth, TX) to convert 24 V DC output from the driver into a 5 V DC output followed by a 5 V DC SPST Reed Relay (275-232, Radioshack Corp., Forth Worth, TX) to control the electrical connection mechanism necessary to operate the syringe pump. These two components were connected in a series configuration (**Figure 3.10**).

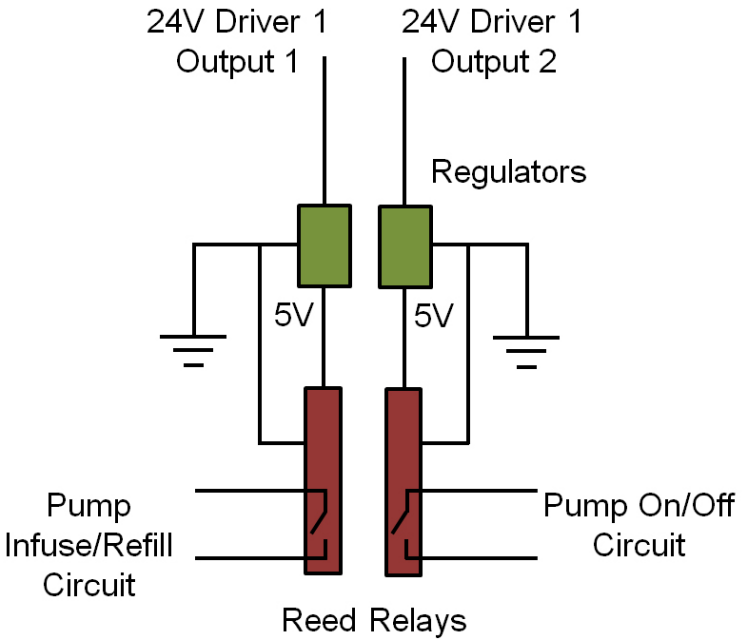

Figure 3.10 Schematic of the S-RVSD relay circuit utilized to control the syringe pump.

The power supply was also used to energize a 5x5 cm 24 V cooling fan (514F, ebmpapst, Inc., Farmington, CT) mounted on the aluminum back wall (20x10 cm) of the S-RVSD box. The back wall of the electronic box was also provided with a standard panel-mount IEC 320 plug for the AC power, an in-line fuse holder, a switch, and a 9-position female D-Sub connector used to operate the syringe pump through the aforementioned circuit. The front aluminum wall (20x10 cm) was mounted with another 9-position female D-sub connector for the serial communication with the PC, and two 6-contacts shielded miniature circular female sockets (series 440, Binder-USA, LP, Camarillo, CA) for a rapid connection/disconnection with the two stepper motors

necessary to operate the S-RVSD. The box was finally covered with a transparent cast-acrylic, vented cover (**Figure 3.9**).

The drivers were controlled via serial communication from a PC. Software (Easi-V, Parker Compumotor, Rohnert Park, CA) converted a specific, proprietary language into instructions for the driver. Examples of common instructions include energizing/de-energizing and starting/stopping the motors, defining rotational velocity and acceleration, defining the numbers of revolutions before stopping, starting/stopping the syringe pump, *etc.* While the drivers used are fully themselves programmable (being provided with an internal hardware memory allowing for stand-alone operations, without direct connection with a PC), the seeding testing and subsequent experiments were conducted in a PC-tethered mode allowing for constant control of the operational parameters. The software allowed for the programming of several "buttons" through a graphic interface to respond to basic and more complex commands. **Table 3-1** shows most of the commands used to operate the S-RVSD before, during, and after the seeding procedures. Most of these commands are a combination of single instructions.

Table 3-1 Commands used to operate the S-RVSD during seeding procedures.

Command	Micro-Stepper Instruction
Energize Motors	0ON;2A100;2V10
De-Energize Motors	0OFF
Stop Motors	0K
Motor 1: Rotation CW 45º	1MI;1A50;1V10;1D3125;1G
Motor 1: Rotation CCW 45º	1MI;1A50;1V10;1D-3125;1G
Motor 1: Rotate for Seeding	1MC;1V0.167;1G
Motor 2: Zero Position	2MA;2W(PA,0);1W(PA,0)
Motor 2: Forward Step (5mm)	2MI;2D98425;2V100;2G;2TR(MV,=,0);2R(PT)
Motor 2: Backward Step (5mm)	2MI;2D-98425;2V100;2G;2TR(MV,=,0);2R(PT)
Motor 2: Go to Zero Position	1MA;1V5;1D0;2MA;2A100;2V5;2D0;1G;2G
Motor 2: Slide and Seed	2MI;2D-98425;2V0.1;1O(00X);2G;2TR(MV,=,0)
Syringe Pump: Refill	1O(10X)
Syringe Pump: Infuse	1O(00X)
Syringe Pump: Start	1O(X00)
Syringe Pump: Stop	1O(X01)

3.1.3 Considerations and calculations for the correct use of the system

3.1.3.1 Definition of the motion regimen

The new "sliding" feature of the S-RVSD required some considerations to identify the appropriate parameters for its correct operation. In particular, it was important to identify a suitable motion regimen for the Diffuser (*i.e.*, motion type, direction and velocity) and for the scaffold (*i.e.*, rotational velocity) in order to yield an optimal seeding.

Though very simple to implement with the computer-controlled drivers for the stepper motors, a non-steady movement for the Diffuser and scaffold (*e.g.*, multiple passages from the same longitudinal location for the Diffuser, periodic rotations of the scaffold, accelerations/decelerations, *etc.*) might be difficult to model and would require optimization studies beyond the scope of this work. Therefore, a decision was made early on to perform the seeding with steady movements of the Diffuser and the scaffold, in which the movement of the Diffuser occurs in a single direction with a steady linear velocity and the scaffold rotates with a constant rotational velocity during the entire seeding process.

Once these basic specifications were established, qualitative bench-top testing (no data was recorded) suggested several protocol to adopt for the correct use of the device. When considering the Diffuser component, these tests suggested that the "pulling configuration" (*i.e.*, with the seeding occurring with the Diffuser initially placed in proximity of the Driving Tee and pulled back toward the Driven Tee during the seeding; recall **Figure 3.2**) was more efficient than the opposite "pushing configuration". This conclusion was based on the observation that the Diffuser, while pushed from the Driven Tee toward the Driving Tee, was causing an increase in intraluminal pressure due to the compression of the proximal liquid volume. This resulted in to an increase in the scaffold luminal diameter and a subsequent loss of proximity between the Diffuser and the scaffold wall. The delicate contact between the Diffuser and the scaffold lumen was designed to maximize the localization of cells based on the Diffuser position during seeding. As a consequence of the pushing configuration, the seeding suspension was partially diffusing beyond the Diffuser position, resulting in a loss of seeding precision as observed using colored solution during testing. Conversely, in the pulling configuration, the scaffold wall was in good adherence with the Diffuser for the entire duration of seeding. This contact effect was fostered

by the gentle intraluminal suction caused by the retraction of the Diffuser through the lumen of the scaffold which induced contact between the two bodies, allowing for localized transmural exudation of seeding suspension (in correspondence of the Diffuser nozzles).

3.1.3.2 Definition of the operational parameters

Once the type and direction of the Diffuser movement was defined, it was necessary to establish the appropriate relationship between the translational and rotational speeds for the Diffuser and the scaffold, respectively. These two parameters are required to be linked based on a specific relationship because the cell suspension is released discretely by the 8 radial nozzles. If the Diffuser would release cell suspension without moving and without the external scaffold rotation, the seeding pattern within the scaffold cross-section would resemble 8 radially-oriented lines crossing the scaffold longitudinal wall corresponding with the 8 cell-releasing nozzles. If the Diffuser would slide without scaffold rotation, this seeding pattern would extend longitudinally, resulting in 8 longitudinal "planes" of seeded scaffold. Finally, if the tangential velocity of the scaffold wall (due to the rotation) is significantly slower than the longitudinal velocity of the Diffuser, the seeding pattern would be elicoidal with 8 seeded helical cell patterns twisting along the length of the scaffold. Therefore, it is important to slide the Diffuser with a speed that allows for circumferential homogeneity throughout the whole length of the scaffold.

This problem can be solved by considering that the time (t_{arc}) necessary to rotate the scaffold for 1/8 of the circumference (arc length included between two adjacent nozzles with the assumption that the eight nozzles release the same flow rate of seeding suspension) starting from any initial time (t_0) has to be at most equal to the time (t_{nozzle}) necessary to remove (during the translation of the Diffuser) the extension of the seeding nozzle from the initial longitudinal

location of the Diffuser at t_0. That is, $t_{arc} \leq t_{nozzle}$. Performing few calculations (**APPENDIX C**), it is possible to demonstrate that the value of the angular velocity for the scaffold ($\omega_{Scaffold}$) has to comply with the following expression:

$$\omega_{Scaffold} \geq 12 \cdot v_{Diffuser} \qquad \textbf{3-1}$$

The angular velocity and velocity of the Diffuser are expressed as rpm and mm/sec, respectively.

Once the type of movement for the Diffuser (steady, unidirectional, pulling configuration) and a relationship between the rotational velocity of the scaffold and the translational velocity of the Diffuser (**Equation 3-1**) were both established, it was apparent that these velocities would be dictated by the overall seeding time. For example, a long seeding time (t_s) would require a low $v_{Diffuser}$ in order to cover the length of the scaffold in exactly t_s. Furthermore, once established t_s (and therefore $v_{Diffuser}$), also $\omega_{Scaffold}$ results partially defined (inferior limit) by **Equation 3-1**. One of the design criteria for the original RVSD was the rapidity of seeding. This was achieved, as the seedings using the RVSD took between 1 and 3 minutes. Another *a priori* decision for the design of the S-RVSD was to complete the seeding process in 5 minutes. This set seeding time defined the translational velocity for the Diffuser and suggested the rotational velocity of the scaffold. The translational velocity of the diffuser was set to 0.167 mm/sec required to cover the 5 cm of scaffold length in exactly 5 minutes. The rotational speed for the scaffold was set to be 10 rpm in agreement with **Equation 3-1**, which exceeded the minimum required value (~2 rpm) of a factor ~5. This was decided as a safety feature to take into account the possibility that the 8 nozzles of the Diffuser would not release the same flow rate (as originally assumed) as a consequence of gravity.

An additional consideration for the S-RVSD regards the direction of rotation for the scaffold, which needs to be consistent with the direction in which the Diffuser is screwed on the Stylet. Rotating the scaffold in the opposite direction might cause a disconnection of the Diffuser leading to seeding failure. Additionally, the presence of the sliding feature eliminated the possibility of keeping the previous design of using custom-made tips for the scaffold (recall **Figure 2.4**). Therefore, prior to each seeding, each scaffold needed to be reversibly secured to the S-RVSD tees via silk suture ligation.

3.1.3.3 Definition of the S-RVSD seeding protocol

The protocol for seeding with the S-RVSD was defined and described as follows. The scaffold was secured to the device, the tubing, Stylet, Diffuser, scaffold, and Driving Tee circuits were primed by infusing Dulbecco's modified phosphate buffered saline (DPBS) from a priming syringe (priming volume = 4.5 mL). Subsequently, the Stylet, Diffuser and scaffold were primed with the seeding suspension to initiate scaffold seeding precisely upon activation of the syringe pump. The Diffuser was positioned in proximity to the Driving Tee and the seeding was initiated by applying vacuum to the chamber, starting scaffold rotation, and starting the infusion of cell suspension concurrently with the movement of the Stylet (this operation is synchronized by the S-RVSD electronic controller). The seeding was automatically terminated once the Diffuser reached the end of the scaffold by synchronously stopping of sliding Stylet and Diffuser, the cell infusion, and the rotation of the scaffold.

3.1.4 Seeding performance

3.1.4.1 Qualitative assessment of seeding functionality

Once the criteria and protocol for seeding the S-RVSD were established, a mock seeding was performed using a PTFE porous vascular graft (W. L. Gore & Associates, Inc., Flagstaff, AZ) and a bromophenol blue dye (Sigma) to assess the effectiveness of the device qualitatively. The dye was used to mimic the seeding suspension for simplicity, and it also allowed visualizing the exuding flow with high contrast to demonstrate the efficacy of the system in terms of local delivery of seeding suspension. The seeding parameters were consistent with those defined in **Section 3.1.3.**

3.1.4.2 Quantitative assessment of bulk seeding uniformity

As previously done for the RVSD, a complete quantitative assessment of the bulk seeding capabilities of the S-RVSD was performed. To this end, 5 cm-long, hybrid ES-TIPS PEUU scaffolds (n = 3, ID = 4.7 mm; a detailed description of this scaffold type is provided in **Chapter 4**) were seeded in order to show the absence of significant differences in cell number along the longitudinal, circumferential, and radial directions of the scaffolds, similar to that described in **Section 2.2.3** for the RVSD. This analysis also focused on the assessment of apoptosis activation to confirm absence of damaging conditions during seeding. The scaffold ratio (*L/ID*) for these experiments was equal to 11, suitable to demonstrate the ability of the S-RVSD to overcome the limitation of the RVSD shown in **Figure 2.27**.

Pig muscle-derived slowly adhering cells (SACs) obtained from a modification of an established pre-plating technique [147] were cultured and seeded in DMEM (Sigma) supplemented with 20% serum (a detailed description of the isolation technique, and culture reagents is provided in **Section 7.3**). Three scaffolds were seeded with $30x10^6$ cells suspended in 20 mL of media, with a flow rate of 4 mL/min. The vacuum level was maintained consistent with the value, which was that used with the RVSD (-5 inHg), and the translational speed of the Diffuser and the rotational velocity of the scaffold were set to 0.167 mm/sec and 10 rpm, respectively as previously described (recall **Section 3.1.3**).

After seeding, a ring (~ approximately 4 mm in width) was cut from each of the two ends of the scaffold to exclude the portions of scaffold ligated to the tees and not reached by the nozzles of the Diffuser from subsequent analysis. The longitudinal cell distribution was assessed via MTT assay (as previously described in **Section 2.2.3**) performed on scaffold segments (~4 mm) taken from 9 longitudinal portions (*i.e.*, L1-L9 in **Figure 3.11**). The MTT absorbance was normalized by the actual length of each portion to account for cut length variations. The circumferential distribution was assessed (as previously described in **Section 2.2.3**) from 3 longitudinal sections of the scaffold (~3 mm); namely from a proximal (in proximity of the Driven Tee), medial, and distal locations (in proximity of the Driving Tee) of the scaffold (see **Figure 3.11)**. A portion (~ 1 mm in length) of each of these three segments was dedicated to histology (H&E) for both qualitative circumferential assessment and quantitative (radial) analysis. Briefly, the radial distribution was assessed by creating a rectangular mask, split in three equal areas by two perpendicular segments along its long edge, using Rhinoceros 3.0 (Robert McNeel & Associates, Seattle, WA). Five random nuclear staining images previously used to quantify the circumferential distribution from each of the three seeded scaffolds were

imported in PowerPoint 2003 (Microsoft Corp.). The mask was superimposed onto each image and manually rotated and scaled to be perpendicular to and fit to a portion of cross-section. In this manner, the mask compartmentalized three regions of interests across the scaffold radius (*i.e.*, luminal, medial, and abluminal). The cell number in each of the three radial regions was counted manually and recorded on a spreadsheet. The same operation was repeated three times for three different, random, locations within each image.

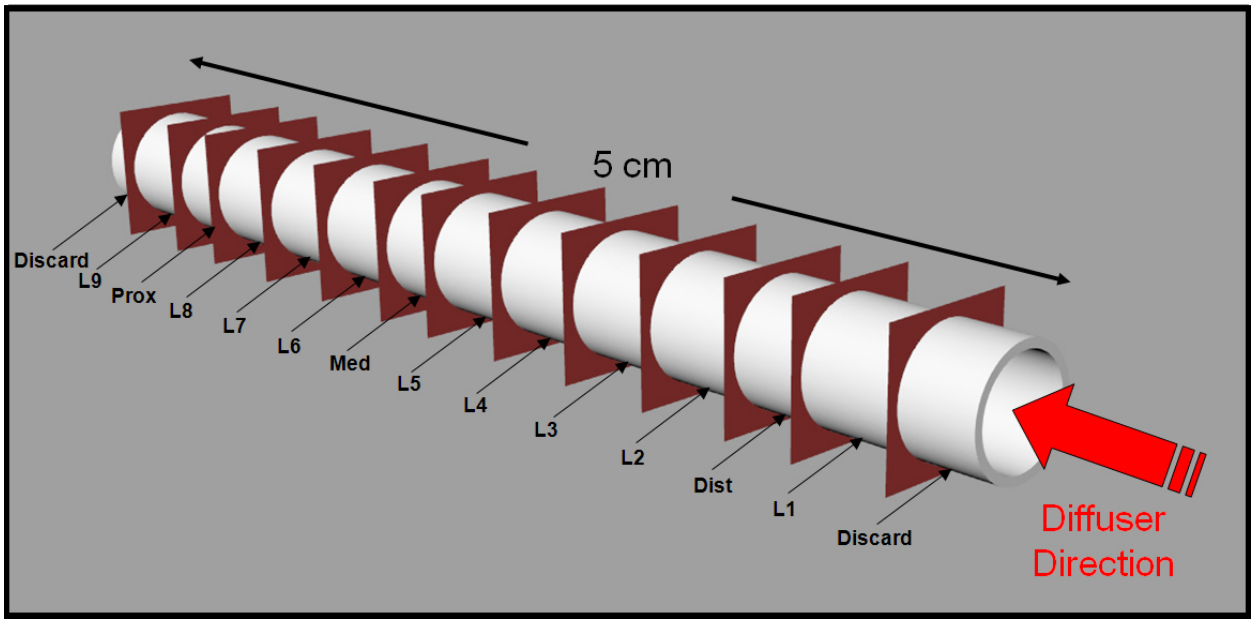

Figure 3.11 Schematic of serial cut on the scaffold for the quantitative assessment of the S-RVSD seeding uniformity.

3.1.4.3 Quantitative assessment of apoptosis

Apoptosis, which is an early marker of cell injury, was quantified from the same three frozen sections dedicated to circumferential and radial cell distribution analysis using the In Situ Cell Death Kit (Roche Applied Science, Indianapolis, IN). This assay utilizes the fluorescein-based TUNEL method to identify cleavages in the genomic DNA produced as a consequence of apoptosis. Briefly, frozen cross-sections were dried at 37˚C for 30 minutes, and rehydrated in PBS for 30 minutes. Samples were then incubated at room temperature for 10 minutes each in 10μg/ml Proteinase K followed by a freshly prepared solution of 0.1% Triton X-100 and 0.1% sodium citrate for permeabilization of cell membranes. DNA strand breaks were identified by incubation at 37˚C for one hour with Terminal deoxynucleotidyl transferase and fluorescein labeled dUTP (both provided in the kit from Roche). Nuclei were counterstained with DAPI.

A section from each slide was treated with 100 U/ml of DNase I to serve as positive controls each time the assay was performed to ensure efficacy of the kit. All sample preparation parameters including incubation times, temperatures, and reagent concentrations were optimized using DNase I treated positive controls. Negative controls were incubated with labeled dUTP without the transferase enzyme. All slides were mounted in gelvatol and imaged at 200X using a Nikon Eclipse E800 epifluorescent microscope and Spot image acquisition software. For each scaffold in the three described locations (Prox., Med., and Dist.), 5 images at 200x were quantified from at least 3 sections. Quantification of the number of TUNEL positive cells was performed by manual counting, while the total number of cells per image was counted via ImageJ softwar (as previously described in **Section 2.2.3**). The percentage of positive cells was obtained by dividing the manually-counted positive cells by the total cell number in each image.

3.1.4.4 Statistical analysis

All statistical analyses of the quantitative cell distribution measurements were performed with SPSS v.13 (SPSS Inc., Chicago, IL) software. All the datasets were tested for normality via the Kolmogorov-Smirnov test. Comparison for different groups was performed using one-way ANOVA. Results are given as mean ± standard deviation. A confidence interval greater than 95% ($p<0.05$) was considered significant.

3.1.4.5 Results

The initial qualitative mock seeding test using the blue dye demonstrated that the device was inducing a localized exudation of dye along with the position of the Diffuser, as expected (**Figure 3.12**).

The MTT assay results (both qualitative and quantitative) for the longitudinal distribution of cells are shown in **Figure 3.13**. Statistical analysis showed no significant differences in the longitudinal distribution of cells ($p = 0.77$).

The quantification of the circumferential cell distribution revealed no statistical differences in the four quadrants of the scaffolds, neither among the three different locations along the longitudinal direction of the scaffolds (**Figure 3.14**), nor among the whole scaffolds in general (**Figure 3.15**).

Radial distribution was homogeneous, showing no significant differences among the three radial portions of the scaffold wall (**Figure 3.16**).

The percentage of apoptotic cells following seeding via the S-RVSD was 5.0±7.1%. A qualitative assessment of apoptosis is shown in **Figure 3.17.**

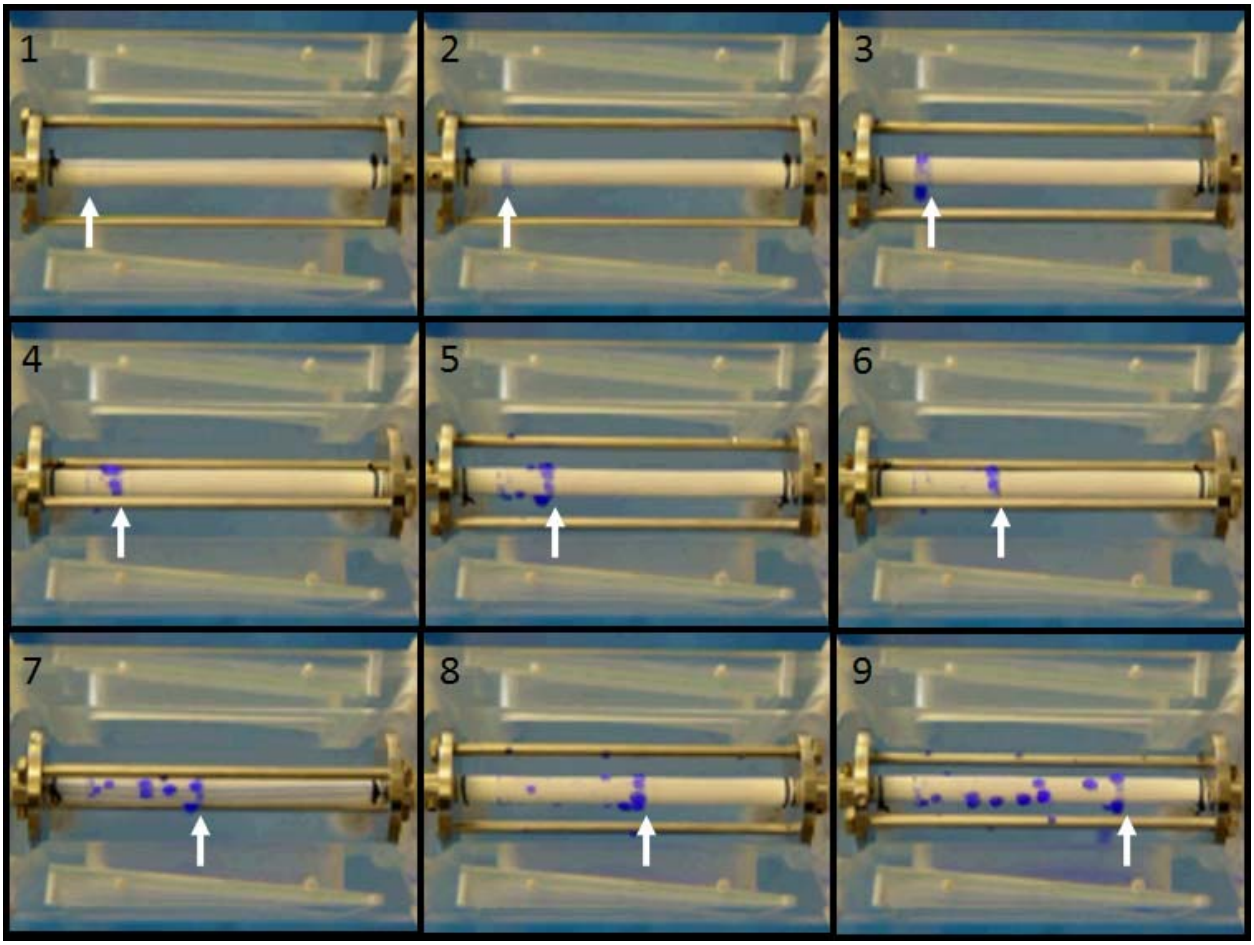

Figure 3.12 Mock seeding sequence (**1-9**) of the S-RVSD demonstrating the functioning of the device. A commercially available vascular graft and a blue ink were used for this purpose. The arrows indicate the current position of the internal Diffuser. The overall seeding time was 5 min. The frames of the sequence are spaced approximately 40 sec from each other.

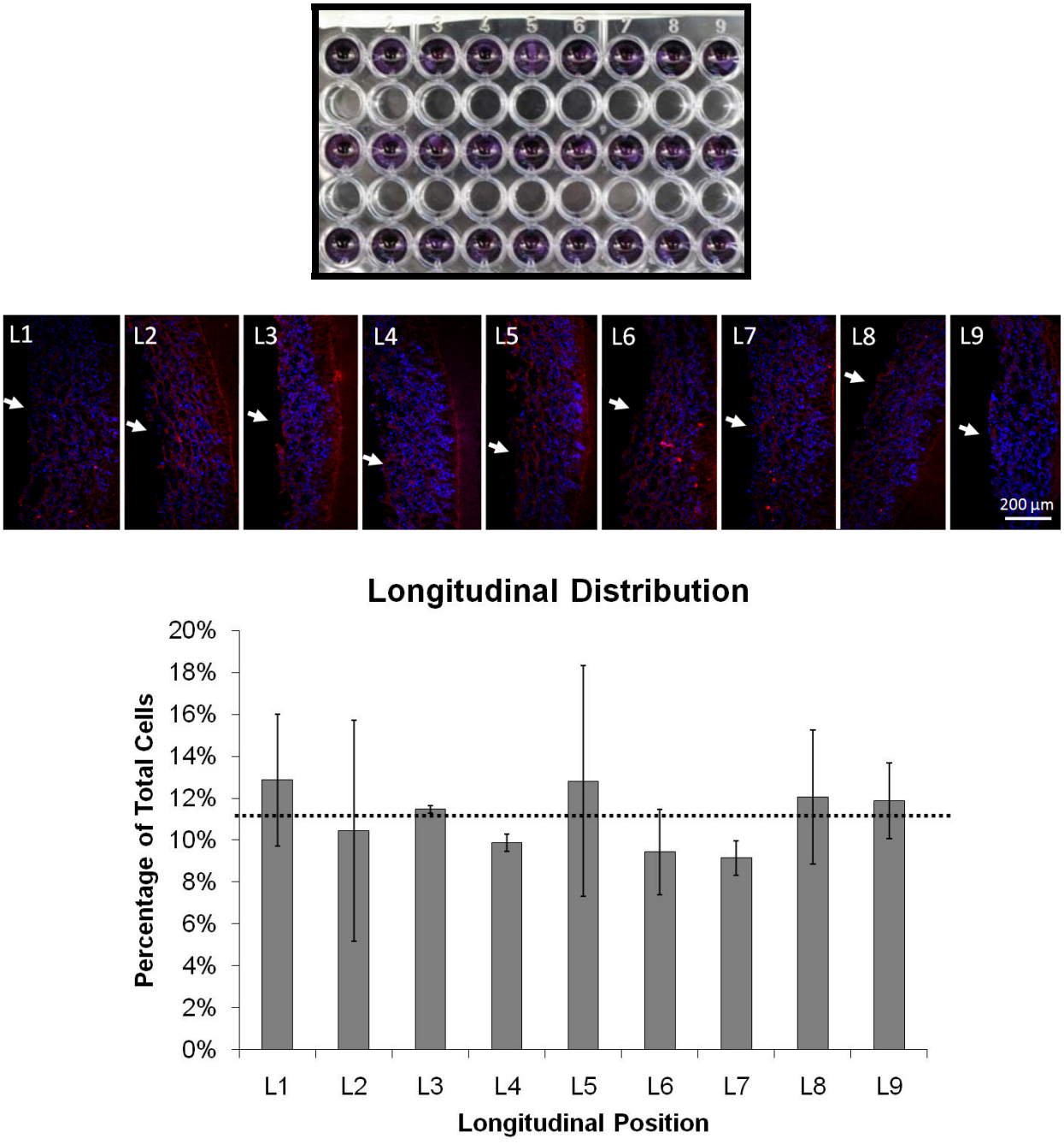

Figure 3.13 Longitudinal distribution of cells seeded via the S-RVSD. **Top**. Qualitative assessment of MTT signal for the three scaffolds seeded in the 9 longitudinal positions. **Center.** Representative sections stained for nuclear staining. Blue = nuclei, red = scaffold. The arrows indicate the lumen of the scaffold. **Bottom.** Quantification of the MTT assay (mean ± standard deviation; n = 3). The dashed line shows the ideal case of perfect distribution correspondent to the 11.11% of the total cell number included in each longitudinal location of the scaffold.

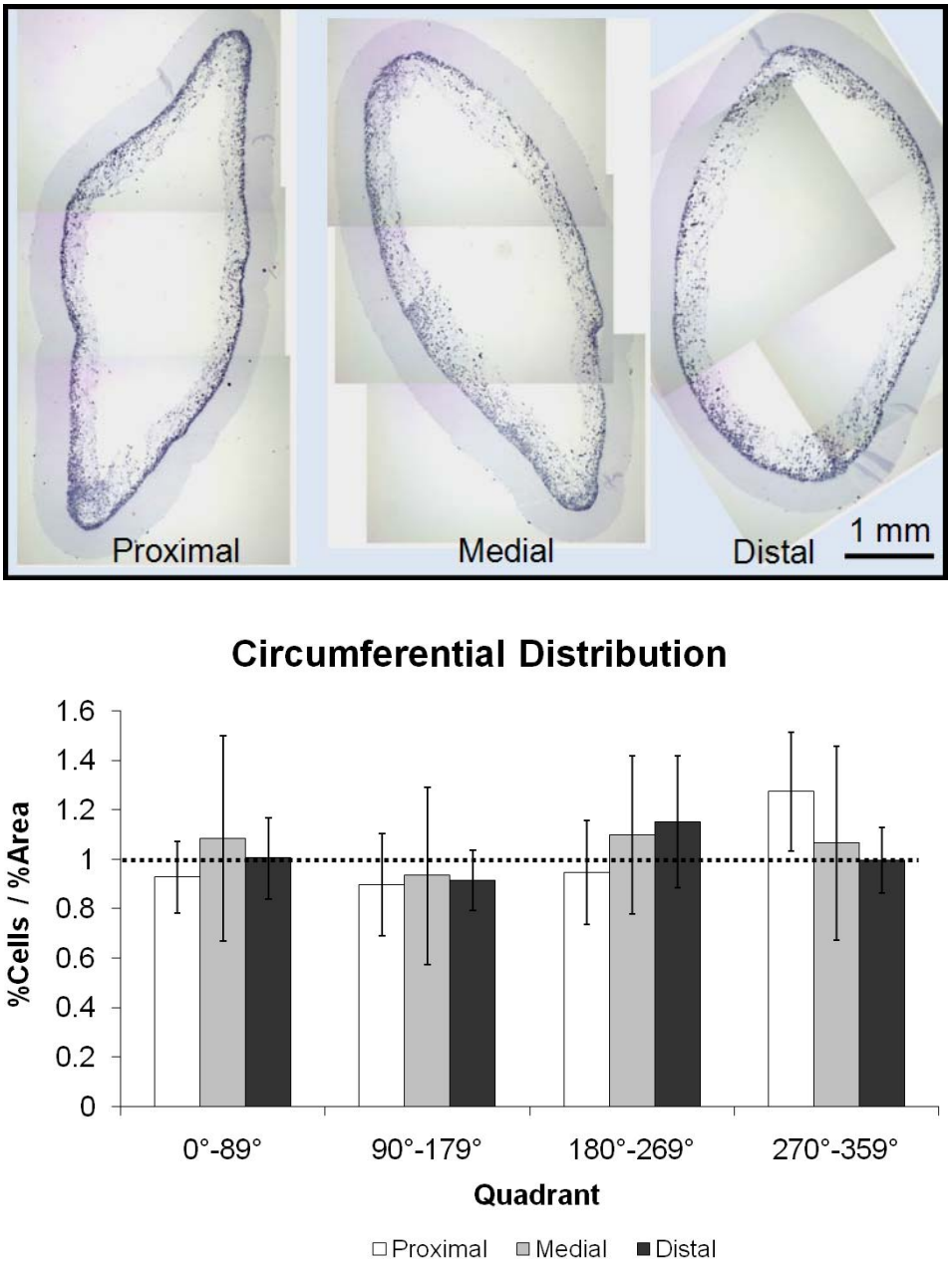

Figure 3.14 Local circumferential cell distribution after seeding via S-RVSD. **Top**. Representative H&E sections of the three locations used to quantify the circumferential distribution valid as a qualitative assessment. **Bottom.** Normalized cell density in the four circumferential quadrants of the scaffolds (mean ± standard deviation; n = 3). Note that the value 1.0 (dashed line) corresponds to the ideal seeding in which the cells are perfectly equi-distributed around the circumferential direction.

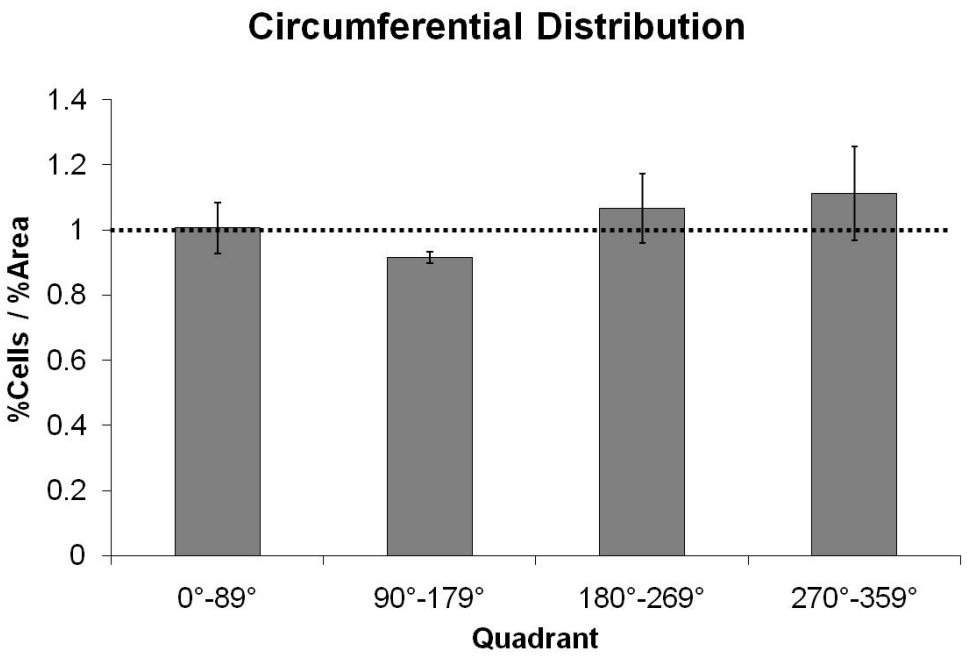

Figure 3.15 Global circumferential cell distribution after seeding via the S-RVSD (mean ± standard deviation; n = 3). Note that the value 1.0 (dashed line) corresponds to the ideal seeding in which the cells are perfectly equi-distributed around the circumferential direction.

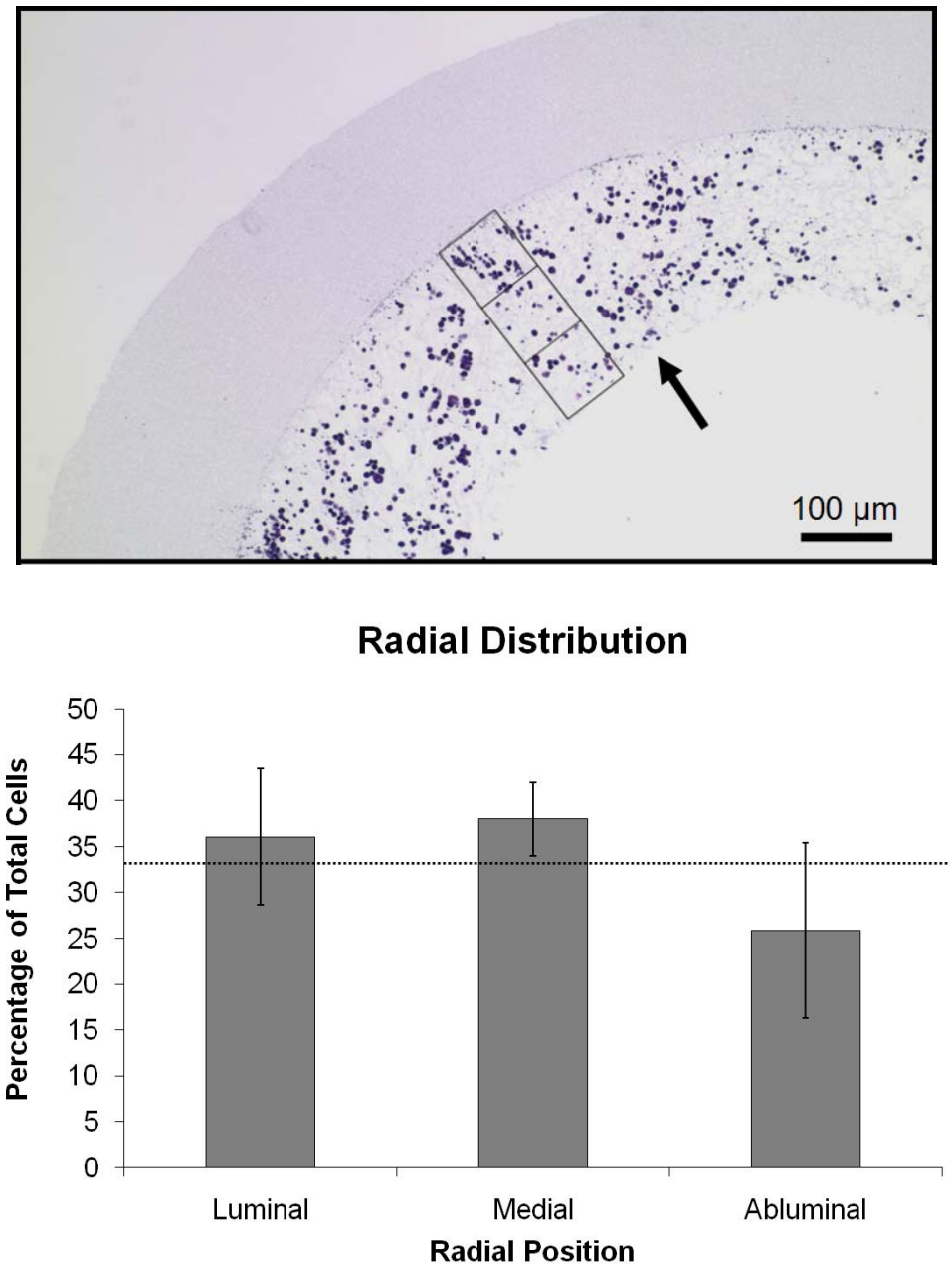

Figure 3.16 Radial cell distribution after seeding via the S-RVSD. **Top.** Representative H&E showing the mask used to quantify the cell number. The arrow indicates the lumen of the scaffold. **Bottom.** Quantification of radial cell distribution (mean ± standard deviation; n = 3). The dashed line indicates the ideal 33% corresponding to a perfectly uniform radial distribution of cells.

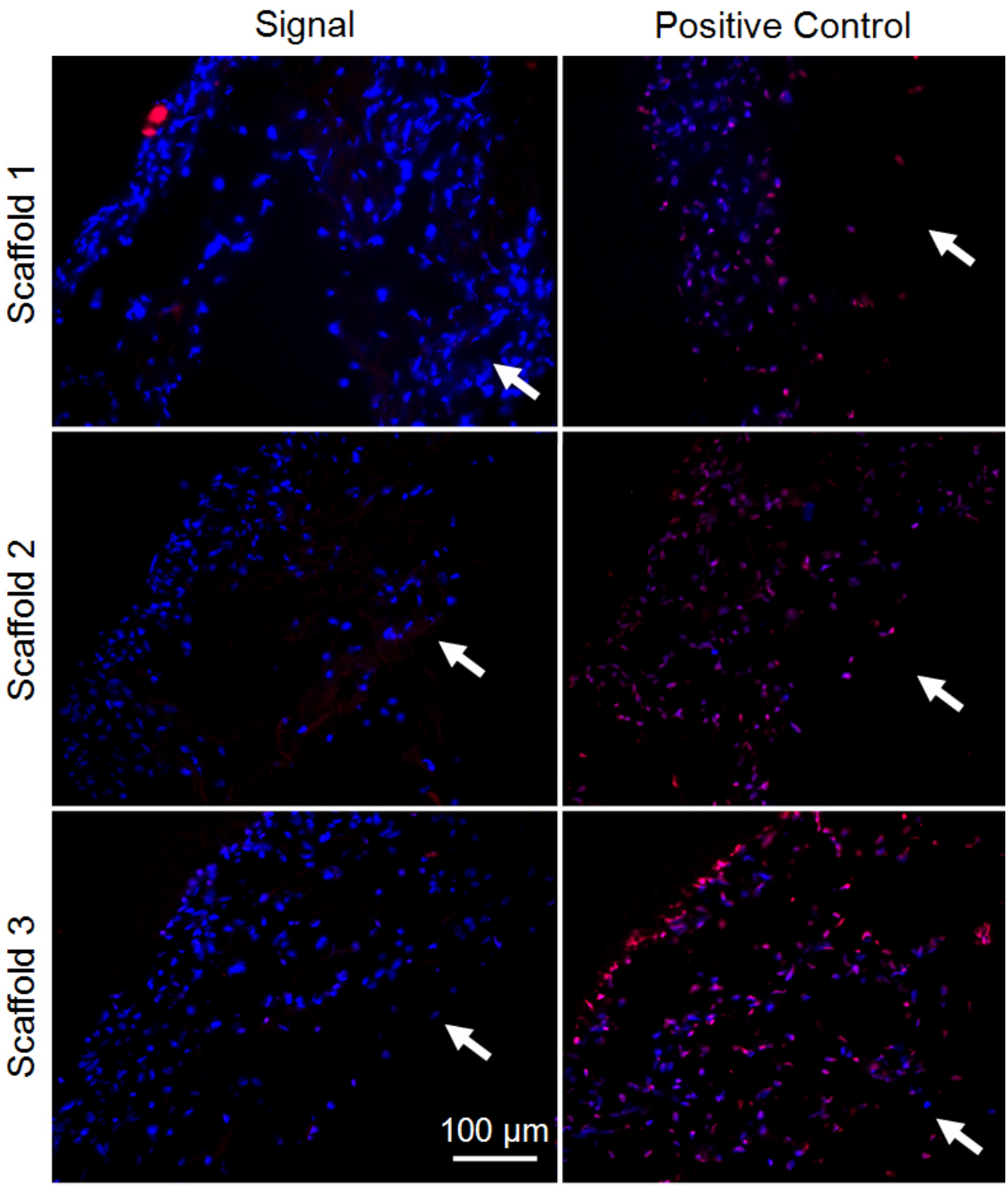

Figure 3.17 Apoptosis detection after S-RVSD seeding testing. **Left Column.** Representative images of the three scaffolds seeded. **Right Column.** Representative pictures of the three positive controls used. Blue = Nuclei. Purple = Apoptotic nuclei. Arrows indicate the lumen of the scaffolds. Pictures were taken at 200X.

3.1.5 Discussion and limitations

The new internal sliding, local cell delivery feature implemented in the S-RVSD has proven to overcome the previous seeding length limitations seen with the RVSD. The modified device was able to deliver cells uniformly throughout the length of 5 cm scaffolds with *L/ID* ratio of approximately 11 (**Figure 3.13**), whereas the original device failed to do this for scaffolds with *L/ID* > 5 (**Figure 2.27**). In fact, the length of the scaffold used in the S-RVSD assessment was only limited by the dimension of the chamber. In theory, with properly scaled chamber and Stylet, there is no limit for the scaffold length. The device has also shown to provide uniform circumferential distribution of cells along the circumferential direction of the scaffold (recall **Figure 3.15**).

Additionally, these series of tests of the S-RVSD has also proven to deliver cells in a uniform manner across the radial direction of the scaffolds (recall **Figure 3.16**). The radial distribution is likely affected by the flow rate of cell seeding suspension. No study has been performed to understand the role of the flow rate in the radial cell distribution, as that was beyond the scope of this work. However, showing the ability to control cell distribution might be critical for future applications, where different layers of cells could be serially deposited across the thickness of the scaffold to mimic the cell components present in the arterial vasculature (*e.g.*, fibroblasts in the *adventitia*, smooth muscle cells in the *media*, and endothelial cells in the *intima*).

The low level of apoptosis detected supported the hypothesis of the absence of cell injury following seeding (see **Figure 3.17**). There was initial concern that the shear stress, to which the cells would be exposed within the S-RVSD could be high enough to adversely affect cell viability. In particular, the flow within the Stylet central lumen is likely to generate the

highest shear stress due to the small caliber of the lumen (~0.9 mm) and the high flow rate. The pores of the scaffold, though much smaller, receive a reduced flow rate due to the permeation of flow across a very high numbers of pores. The shear stress within the Stylet lumen was estimated using **Equation 2-6** in **Section 2.2.2.1** to be 9.6 dynes/cm^2 (**APPENDIX D**), confirming the physiologic magnitude of the forces involved with the seeding process of the S-RVSD.

Another important improvement of the S-RVSD was the implementation of computer-controlled motors and syringe pump. This feature increased the precision of the seeding process with strict control of the scaffold rotation and translation of the Diffuser while reducing the human interactions and therefore, improving upon the reproducibility of the seeding outcomes.

In summary, the S-RVSD developed here appears to have ideal features to seed porous tubular scaffolds for preclinical applications of a TEVG. One such application will be extensively explored in **Chapter 7** in which a large animal model (pig) will be the recipient of a TEVG seeded with the S-RVSD. The S-RVSD may represent a technology suitable for future clinical applications as well. However, the current prototype needs modifications to be compliant with the requirements of a medical device. In **Section 8.4.1.2** one possible modification is proposed, along with a description of a prototype of a disposable "product" that can be utilized in the system for future clinical applications.

4.0 SPECIFIC AIM 2: DEVELOPMENT OF A NOVEL SCAFFOLD FOR VASCULAR TISSUE ENGINEERING APPLICATIONS

The scaffold is one of the most critical components in tissue engineering, as it should provide a temporary structure and milieu for regeneration, *i.e.*, gradual replacement of the scaffold with native-like tissue. Furthermore, the scaffold should provide mechanical support to withstand physiologic conditions over an extended period of time. The matching of mechanical properties with those of native vessels is a critical requirement for any small-diameter vascular graft, as mechanical mismatch has been associated with perturbation in the local hemodynamics, establishing the basis for restenosis and graft failure [148].

Throughout the last two decades many endeavors have been made to develop a mechanically and functionally sound TEVG to replace or bypass arterial segments. Extensive research has been dedicated, in particular, to the development of scaffolds with the right combination and compromise of mechanical, structural, and biological properties suitable for cardiovascular applications. Different approaches have been explored for this purpose, spanning from biological materials [31, 66, 149], to completely synthetic materials with [150, 151] or without [45, 46] surface modifications, to approaches [152]. Biological scaffolds (*e.g.*, collagen and fibrin gels) can exhibit an intrinsic capacity for biocompatibility and bioactivity; however, they have also been associated with suboptimal mechanical properties [67] and have the potential for disease transmission and immunogenicity. Decellularized biological tissues tend to offer

improved mechanical properties, however, incomplete removal of exogenous materials has been attributed to severe immunological reactions in early human clinical trials [153] and thus these scaffolds, while clearly promising, require significant care in their preparation and characterization. Moreover, the seeding of these scaffolds is not feasible, owing to their low porosity. Synthetic scaffolds have the capacity of exhibiting tunable and reproducible properties. However, the most commonly used aliphatic polyesters such as poly(glycolic acid), poly(L-lactic acid), and their copolymers are generally much stiffer than native soft tissues and can, under some conditions, induce a transient or chronic inflammatory response due to the acidity of their degradation products [43]. Another common challenge in tissue engineering is the difficulty of obtaining highly bulk-cellularized scaffolds due to intrinsic scaffold limitations such as insufficient pore size or interconnectivity, or to inadequate seeding techniques [112].Critical to the majority of vascular tissue engineering approaches is the scaffold component [40], which provides, as a temporary 3-D template, structural, mechanical and possibly biological support and guidance throughout the tissue formation and remodeling processes. Foremost, the scaffold should allow for cell infiltration, adhesion, and proliferation, followed by cell-mediated remodeling leading to ECM deposition [154]. Other requirements for the scaffold include mechanical strength, compliance, and suture retention strength comparable to physiologic values [35]. Moreover, the scaffold should not possess significant plastic behavior since this could lead to aneurysm formation upon chronic implantation. Additionally, toward a more "biomimetic" approach the scaffold should hypothetically possess anisotropic structural and mechanical properties similar to native blood vessels [155, 156].

4.1 PEUU: AN ELASTOMERIC POLYMER FOR VASCULAR TISSUE ENGINEERING

The PEUU represents a valid candidate as a scaffold for TEVG scaffold due to its elasticity and tunable mechanical and degradation properties [51, 52]. This polymeric material is cytocompatible and processable into scaffolds via several techniques. A TIPS process, for example, has been used to fabricate highly porous scaffolds [53] able to promote efficient cell integration, cell attachment, and diffusion of nutrients *in vitro* [54, 55]. The same polymer was electrospun to obtain similar nanofibrous architecture and mechanical properties to those of native, structural soft tissues [56, 57].

Due to the promising properties and flexibilities for different processing techniques, the PEUU was defined as a scaffold of choice for our approach.

4.1.1 The use of TIPS PEUU for TEVG applications

Initial studies toward the creation of a TEVG were performed using the TIPS PEUU as the scaffold of choice [54, 55]. This scaffold has been previously described and characterized in the form of tubular scaffolds with a wall thickness of approximately 2.0 mm [53]. Tubular scaffolds with reduced wall thickness (obtained by modifying the size of the mold used) were used for the testing and validation of the initial vacuum seeding device (**Section 2.1.2**), the bulk seeding testing of the RVSD (recall **Section 2.2.3**, [55]), *in vitro* testing of cell proliferation, spreading, and phenotype within the scaffold both immediately following seeding with the RVSD and after several days of dynamic culture (this characterization will be properly described in **Section 5.1** [54]), and finally the initial *in vivo* testing as an aortic interposition graft in a rat model

(described in **Chapter 6**). The chronology of the mentioned studies did not follow the order of this dissertation since most of the testing was performed within overlapping time frames and not following a rigid sequential structure. A comprehensive description of this scaffold fabrication technique, morphology, and mechanical properties has been provided in the literature and therefore, is beyond the scope of the current dissertation. However, a mechanical characterization of the material will be described in **Section 4.2.5** in comparison to the newly developed scaffold (ES-TIPS PEUU) and to native arteries. Furthermore, an indirect characterization of the TIPS scaffold will be provided as a part of the composite ES-TIPS scaffold.

The use of TIPS PEUU was discontinued when, during *in vivo* testing, significant evidence of scaffold dilation, leading to aneurysm formation, emerged (this will be properly described in **Chapter 6**). An initial heat treatment was performed to increase the strength of the material but was not enough to lead to *in vivo* scaffold stability.

4.1.2 The use of ES PEUU for TEVG applications

The ES PEUU has remarkable mechanical features due to its fibrous structural nature, which replicates the anisotropic properties of native soft tissues [56]. The use of the ES PEUU scaffold was limited in our approach due to its small pore size, not allowing for the desired bulk cell seeding and integration. However, the material was used to successfully test the surface seeding capabilities of the RVSD (recall **Section 2.2.4**). Furthermore, the ES PEUU scaffold has been utilized to test the response to shear stress of` rMDSCs surface-seeded onto the luminal surface of scaffolds and subjected to media flow perfusion by a perfusion bioreactor system (see **APPENDIX E**).

Small ES PEUU scaffolds (length = 10 mm, ID = 1 mm) were also used to evaluate their *in vivo* performance as an aortic interposition graft in a rat model. Different configurations were attempted in this model, including unseeded scaffolds, scaffold luminally coated with a covalently bound hydrophilic layer (MPC), and scaffold surface seeding with rMDSCs. These first two acellular approaches are the subject of a publication in preparation and are certainly beyond the subject of the current dissertation due to their lack of stem cell-based features.

As for the TIPS PEUU scaffold, no special characterization or description will be dedicated to the ES PEUU scaffolds since this appear elsewhere [57], however the mechanical properties of this scaffold were measured in comparison with the newly developed ES-TIPS PEUU scaffolds and a morphological characterization was performed as part of the composite ES-TIPS PEUU scaffold as described in the following section.

4.2 ES-TIPS PEUU: A NOVEL SCAFFOLD FOR VASCULAR TISSUE ENGINEERING APPLICATIONS

To match the scaffold requirements of seedability and sound mechanical properties, a novel PEUU-based scaffold was developed and tested. Both TIPS and ES processing were applied sequentially to obtain a composite (*i.e.*, bi-layered) tubular conduit scaffold, integrating the positive features of both scaffolds. In particular, the desirable microstructural and mechanical characteristics yielded by TIPS and ES, respectively, were rationally integrated for the purpose of creating a novel scaffold for small-diameter vascular tissue engineering applications. A thorough morphological and mechanical characterization was performed to test compatibility of the scaffold relative to the native vasculature. The scaffolds were then seeded with adult muscle-

derived stem cells, via the RVSD to assess the efficiency of cell inclusion within a short seeding duration time.

4.2.1 PEUU polymer synthesis

Most of the reagents utilized for the synthesis of the PEUU polymer were processed prior to their use. In particular, solvents dimethyl sulfoxide (DMSO) and N,N-dimethylformamide (DMF) were dried over 4-A molecular sieves. Polycaprolactone diol (PCL, Aldrich, MW ¼ 2000) was dried under vacuum for 48 hours at 50°C. Putrescine (Sigma) and 1,4-diisocyanatobutane (BDI, Fluka) were distilled under vacuum. Stannous octoate (Sigma) catalyst and 1,1,1,3,3,3-hexafluoroisopropanol (HFIP, Oakwood) solvent were used as received. Biodegradable and biocompatible PEUU was synthesized from BDI and PCL with putrescine chain extension using a two-step solution polymerization as described previously [51]. Briefly, 250 ml roundbottom flask under dry nitrogen with reactant stoichiometry of 2:1:1 BDI:PCL:putrescine molar ratio were used. BDI at 15wt% in DMSO was continuously stirred with 25wt% PCL in DMSO followed by stannous octoate addition. The reaction was allowed to proceed for 3 h at 80ºC followed by cooling at room temperature. Putrescine was then added drop wise with stirring and the reaction was continued at room temperature for 18 h. The resulting PEUU solution was precipitated in distilled water, the wet polymer was immersed for 24 h in isopropanol to remove unreacted monomers, and the polymer was dried under vacuum at 50°C for 24 h.

4.2.2 Scaffold preparation

Two different small-diameter sizes of composite scaffolds were made, both a larger diameter (ID-4.7: length = 30 mm, ID = 4.7 mm), and a smaller diameter (ID-1.3: length = 10 mm, ID = 1.3 mm). The rationale behind the choice of these two sizes was their relevance for planned preclinical studies in rats (abdominal aorta) (**Chapter 6**) and pigs (carotid artery and internal jugular vein) (**Sections 7.6** and **7.**7). The ID-4.7 scaffold was also used for testing the S-RVSD as described in **Section 3.1.4**.

The internal layer (*i.e.*, intima/media equivalent) of the composite scaffolds consisted of porous PEUU, obtained via TIPS as previously described [157]. Briefly, PEUU solutions in DMSO (10% w/v) were poured at 80°C into custom-made molds, accordingly dimensioned for the two different scaffold sizes. Each mold consisted of an internal SS (for the ID-4.7 mold) or tungsten carbide mandrel (for the ID-1.3 mold) covered by PTFE tubing. The mandrels were concentrically aligned into a tubular glass sheath via two custom-machined PTFE sealing stoppers (**Figure 4.1**). The molds were filled with hot polymer solution and then rapidly cooled to -80°C for 3 hours, inducing the separation of the phases (solvent/polymer). The molds were subsequently uncapped and immersed in ethanol for 1-2 weeks at 4°C to allow the solid solvent crystals to completely dissolve, yielding an interconnected pore structure. The scaffolds were washed for 48 hours in demineralized water to remove residual solvent, and freeze-dried for an additional 48 hours.

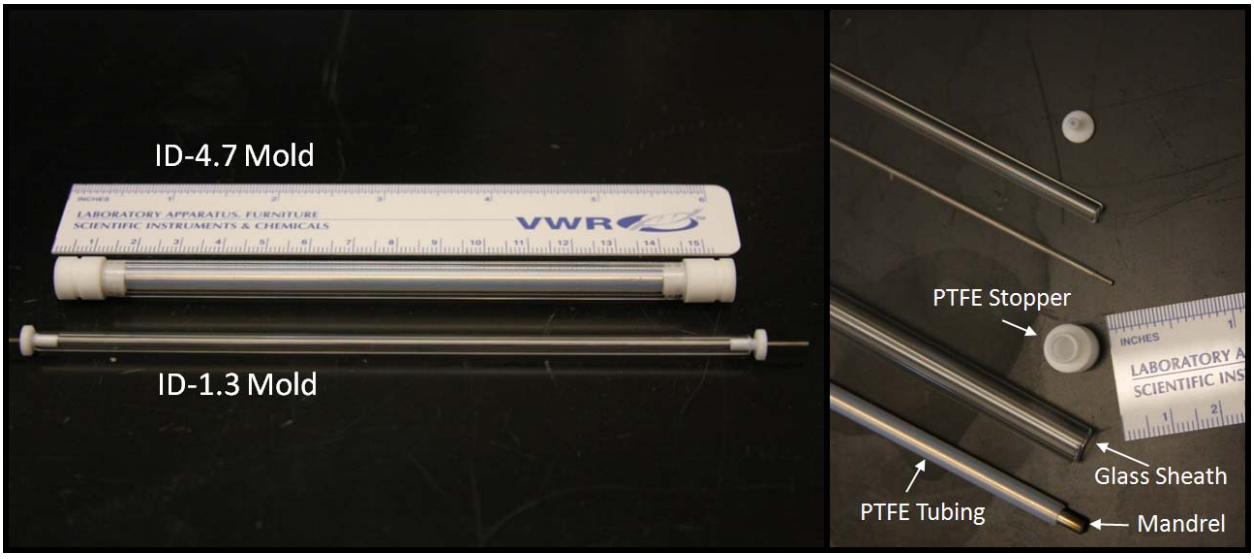

Figure 4.1 Custom made molds used for creating the internal TIPS PEUU layer of the ES-TIPS scaffolds.

The TIPS conduits were subsequently coated by ES of PEUU using an apparatus and technique previously described [57]. Briefly, the TIPS conduits were slipped onto mandrels (diameters: 4.0 mm, 1.0 mm) in conjunction with an intermediate thin sleeve made of PTFE tubing to facilitate insertion and removal. PEUU solution in HFIP (8% w/w) was prepared and loaded into 10 mL syringes connected via plastic tubing to a steel capillary (ID = 1.2 mm), which was suspended 7 cm over the target TIPS tubular scaffold/mandrel.

The mandrels were rotated at 250 rpm and simultaneously translated on an x-y stage (Velmex Inc., Bloomfield, NY) along the longitudinal direction of the mandrels in a cyclic manner (translational speed = 6 cm/s, amplitude = 8 cm, frequency = 0.4 Hz). The mandrels were charged with -3 kV, while the capillary was charged with 10 kV. High voltage was supplied for each component using a combination of two high voltage generators (Gamma High Voltage Research, Ormond Beach, FL). The polymer solution was infused via a precision

syringe pump (Harvard Apparatus, Holliston, MA) at 1 mL/hr. The ES time for the ID-4.7 scaffold was 1 hour while for the ID-1.3 was 15 minutes.

A schematic of the entire process is shown in **Figure 4.2**. At the end of the process, electrospun polymer deposited beyond the extension of the underlying TIPS scaffold was removed with a razor. The scaffolds were dried within a vacuum chamber for 24 hours. Sterilization was performed by immersing the scaffolds in 70% ethanol solution for 24 hours followed by multiple washes with sterile DPBS.

4.2.3 Statistical methods

All statistical analysis was performed using SPSS v.15 software (SPSS Inc., Chicago, IL). All datasets were tested for normality via the Shapiro-Wilk test. Comparison of the mean values of the data sets was performed using one-way ANOVA. Post hoc analysis was performed via Bonferroni test. Student's t-test was used to determine significant differences between different set of data. All measures are presented as mean ± standard deviation. A confidence interval greater than 95% was considered significant ($p<0.05$).

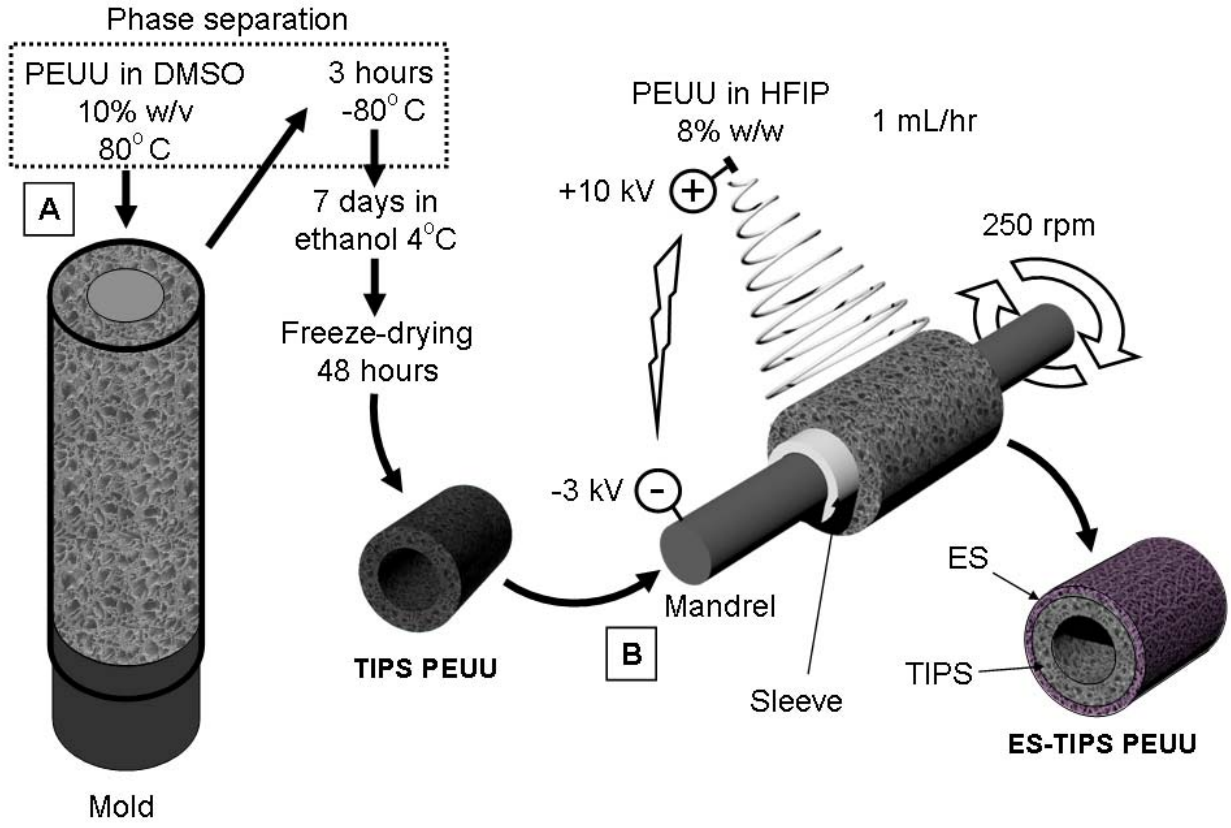

Figure 4.2 ES-TIPS PEUU scaffold fabrication. **A.** The inner layer of the compound scaffold is obtained by pouring hot polymer solution into a custom-made mold and rapidly freezing it to induce solvent-polymer phase separation (TIPS). **B.** After freeze drying, the resulting tubular scaffolds are mounted onto a mandrel in order to deposit an external micro-fibrous PEUU layer via electrospinning (ES). An intermediate sleeve between the TIPS scaffold and the mandrel is used to facilitate removal of the ES-TIPS scaffold at the end of the procedure.

4.2.4 Morphological assessment

4.2.4.1 Methods

ES-TIPS PEUU scaffolds were immersed in liquid nitrogen and rapidly cut with a cold razor to generate a sharp fracture, exposing a cross-section with preserved structural features. The specimens were mounted dry on aluminium stubs with a double adhesive copper tape and sputter coated with a 3.5 nm thick layer of gold/palladium (Sputter Coater 108 auto, Cressington Scientific Instruments Inc., Cranberry Twp., PA). The cross-sections were imaged by field emission SEM (JSM-6330F, JEOL ltd. Tokyo, Japan). Image-based analysis (ImageJ) was used to measure the thickness of the two layers, the dimension of the pores, and the thickness of the ES nanofibers. A total of 10 to 30 measurements were used for each scaffold analyzed (n = 3). Pore size was measured as the maximum diameter of all void spaces visible in the image.

4.2.4.2 Results

ES-TIPS PEUU scaffolds appeared macroscopically smooth and without any gross defects (**Figure 4.3-A**). Observed under SEM, the scaffolds exhibited a morphology characterized by two distinct layers: a highly porous internal layer (TIPS) and a fibrous external layer (ES) (**Figure 4.3-Figure 4.4**). The measured thickness of the TIPS layer in the ID-1.3 and the ID-4.7 scaffolds was 345±55 μm and 481±74 μm, respectively. No statistical difference in thickness was detected for the TIPS scaffolds before and after ES ($p = 0.79$), demonstrating absence of a

significant compression effect due to the ES process.The external ES layer in the ID-1.3 and the ID-4.7 scaffolds had a thickness of 73±26 μm and 253±60 μm, respectively. The two layers appeared to be firmly adhered to each other with no grossly visible delaminations (*i.e.*, disconnections larger than the average TIPS pore size; see, *e.g.*, **Figure 4.3-C**).

The observed adherence between the layers was presumably due to the combined effects of the many localized fusions of the ES nanofibers with the pore walls of the TIPS scaffolds (**Figure 4.3-D**). The TIPS layers of the ID-1.3 scaffolds had pore sizes measuring 5.1±3.2 μm while for the ID-4.7 scaffolds the pore size was 123±20 μm. The pore size of the ES layer (for both scaffold sizes) was 5.1±3.2 μm while the diameter of the ES nanofibers was 743±201 nm.

A summary of morphological properties is shown in **Table 4-1**.

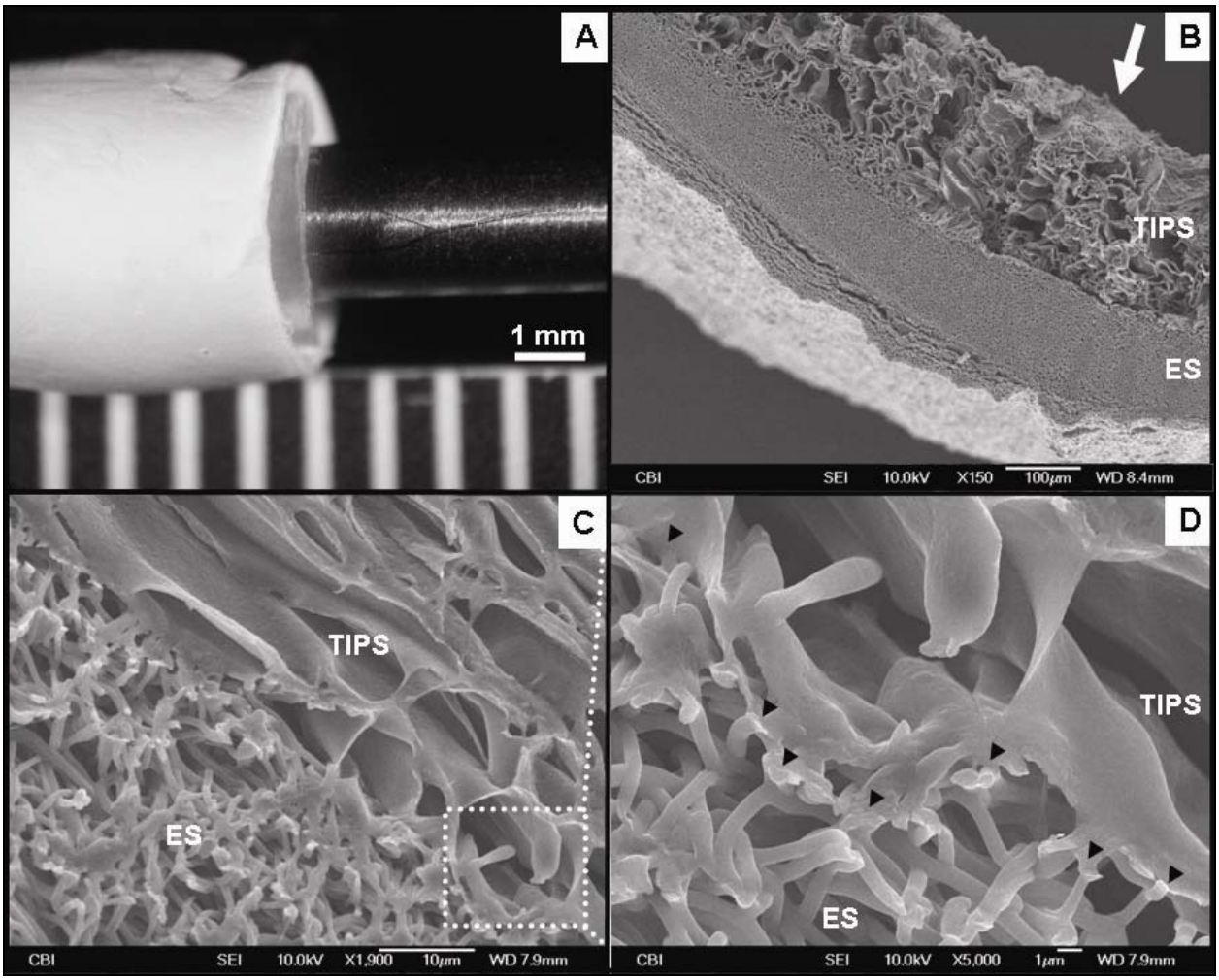

Figure 4.3 Representative morphological assessment of the ID-4.7 ES-TIPS PEUU scaffold. **A.** Macroscopic appearance after electrospinning. **B.** Micrograph representing a cross-sectional portion of the compound scaffold. The arrow indicates the lumen. **C.** Interface between the two layers of the scaffold. **D.** Adhesion points (indicated by black arrow heads) in which electrospun fibers are fused with the pore structures of the TIPS.

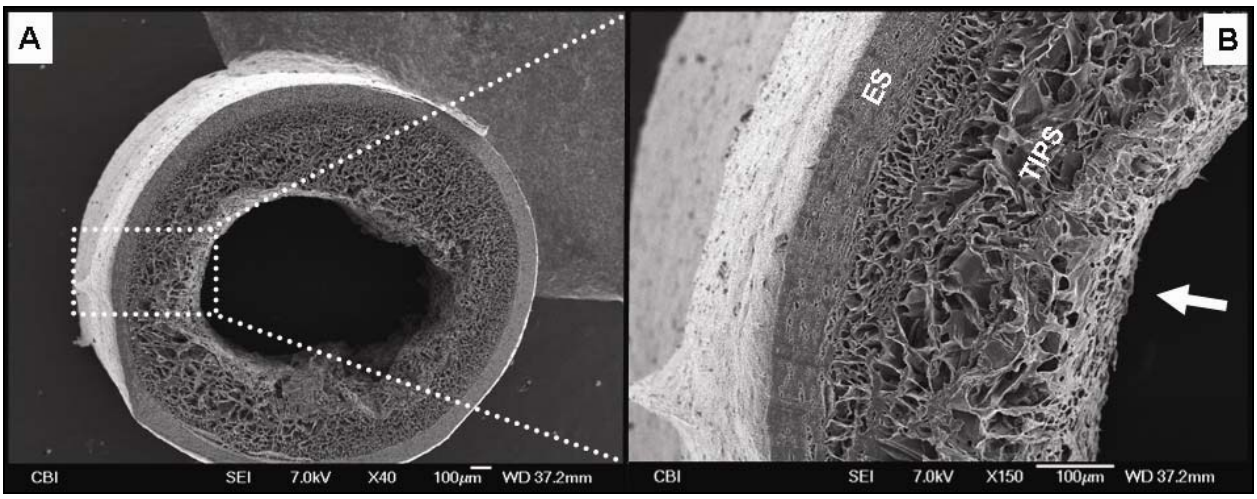

Figure 4.4 Representative morphological assessment of the ID-1.3 ES-TIPS PEUU scaffold. **A.** Micrograph of the whole cross-section. **B.** Magnification of the boxed area in A. The arrow indicates the lumen of the scaffold.

Table 4-1 Summary of morphological properties of the ES-TIPS PEUU scaffolds.

	N	Mean	Standard deviation
Thickness of Uncoated Small TIPS Scaffolds (μm)	3	389.9	48.9
Thickness of Uncoated Large TIPS Scaffolds (μm)	3	489.3	45.1
Thickness of TIPS Layer for Small Scaffolds (μm)	3	345.8	55.1
Thickness of TIPS Layer for Large Scaffolds (μm)	3	481.4	74.4
Thickness of ES Layer for Small Scaffolds (μm)	3	73.9	26.8
Thickness of ES Layer for Large Scaffolds (μm)	3	253.2	60.1
Pore Size of TIPS Layer for Small Scaffolds (μm)	3	50.8	3.1
Pore Size of TIPS Layer for Large Scaffolds (μm)	3	123.3	20.1
Pore Size for ES Layer (μm)	3	5.1	3.2
Diameter of ES Fibers (nm)	3	743.2	201.7

4.2.5 Mechanical properties

Mechanical testing was performed only on the ID-4.7 ES-TIPS conduits due to size limitations of the ID-1.3 scaffolds (~3 mm for the circumferential direction), which did not allow for a complete characterization. In addition, a batch of ID-4.7 TIPS PEUU and ES PEUU was tested to assess uniaxial mechanical properties in order to assess the mechanical contribution of each component of the ES-TIPS Scaffolds. Additionally, human saphenous veins (hSVs) and porcine internal mammary arteries (pIMAs) (generously provided by Dr. Marco Zenati) were obtained from remaining portions of vein grafts used in CABGs procedures and from animals used for unrelated acute surgical studies, respectively. These native vessels were assessed to compare the mechanical properties of the ES-TIPS PEUU scaffolds with those of native vessels and determine the suitability of the scaffold for *in vivo* applications.

4.2.5.1 Uniaxial tensile testing

To measure uniaxial material properties of the scaffold conduits, a tensile tester (Tytron TM250, MTS System Corp., Minneapolis, MN) mounted with a 10 lb force transducer (Model 661.11B-02, MTS System Corp., Minneapolis, MN) was used. Dry scaffolds were cut into strips (width ~2 mm, length ~15 mm) along their circumferential or longitudinal directions. Adjacent samples were paraffin embedded and sectioned to retrieve accurate thickness measurements of each specimen via image-based techniques.

To ensure a firm but delicate retention of the scaffold within the metal tensile system clamps, each specimen was mounted via a sandwich of thin cardboard and hot glue [158]. Specimen length and width were measured with a digital caliper (Thermo Fisher Scientific,

Waltham, MA). The specimens from each direction were pulled at 10 mm/min crosshead speed until rupture following 10 cycles of preconditioning to 20% strain. Load–displacement curves were computed to obtain stress–strain relationships according to current length and cross-sectional area with the assumption of incompressibility [58]. This assumption implies that the measurable initial volume of the tested specimen remains constant throughout testing. Therefore, knowing the stretch $\lambda = L/L_0$ (ratio between the current, deformed specimen length (L) and the initial length (L_0)) of the tested strip, it is possible to retrieve the deformed cross-sectional area as: $A = A_0/ \lambda$. The Cauchy stress is then calculated as $\sigma = F/A$ (load/deformed cross-sectional area). The strain was conventionally calculated as: $\varepsilon = \lambda - 1$.

Ultimate tensile stress (UTS) and strain to failure (STF) were considered, respectively as the maximum stress value before failure and its corresponding value of strain. Elastic modulus was estimated by calculating the slope of the stress-strain curves using a linear regression fitting curve for levels of circumferential strain measured while pressurizing (see the experimental setup description in **Section 4.2.5.5**) the scaffolds from physiologic diastolic to systolic values of arterial pressure (80-120 mmHg).

4.2.5.2 Ring testing

Native vessels were tested uniaxially only in the circumferential direction following a slightly different experimental setup (ring strength [159]). This was due to size limitation of the native vessels and to the difficulty in establishing a firm grip of the wet and slippery native tissue as done for the dry scaffolds. In particular, to measure ring strength, an ATS uniaxial tensile tester (10 mm/min crosshead speed according to ASTM D638-98 until sample failure) mounted with a 10 lb force transducer (SM-10, Interface) was modified to surround the two clamps with a

custom-fabricated sealed chamber filled with saline. A recirculation circuit composed of a roller pump, PVC tubing, and heat exchanger was constructed in order to maintain a constant temperature of 37ºC during the tests (**Figure 4.5**).

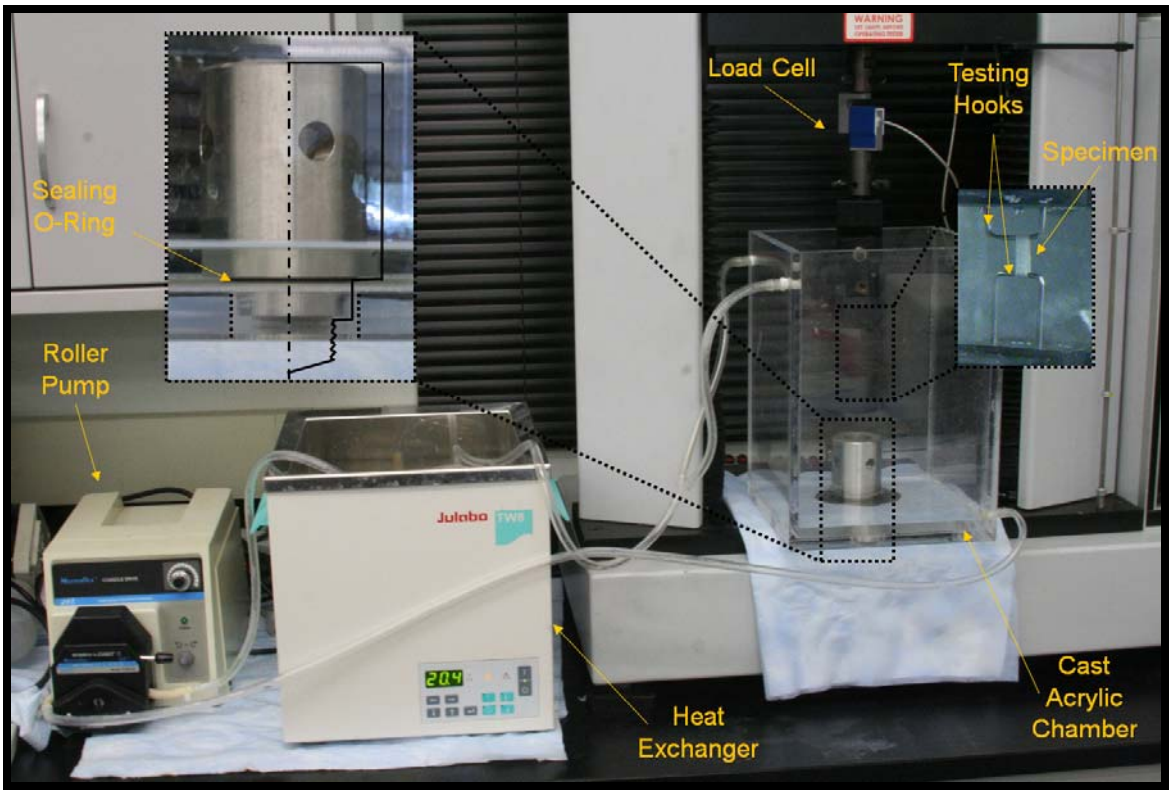

Figure 4.5 Custom-made ring test setup provided with recirculation saline chamber.

A ring of each vessel was cut (1-2 mm length) and diameter, thickness, and width was measured with a dial caliper. The rings were inserted with two custom made stainless steel flat

hooks that were subsequently attached to the clamps of the testing device. All specimens were preconditioned prior to testing with 10 cycles at 5% circumferential stretch. Load-displacement curves were computed to obtain stress-strain relationships according to initial length and current cross-sectional area with the assumption of incompressibility, as previously described. The stress-strain relationships were derived to calculate the instantaneous elastic modulus. A schematic of the ring testing procedure is shown in **Figure 4.6**.

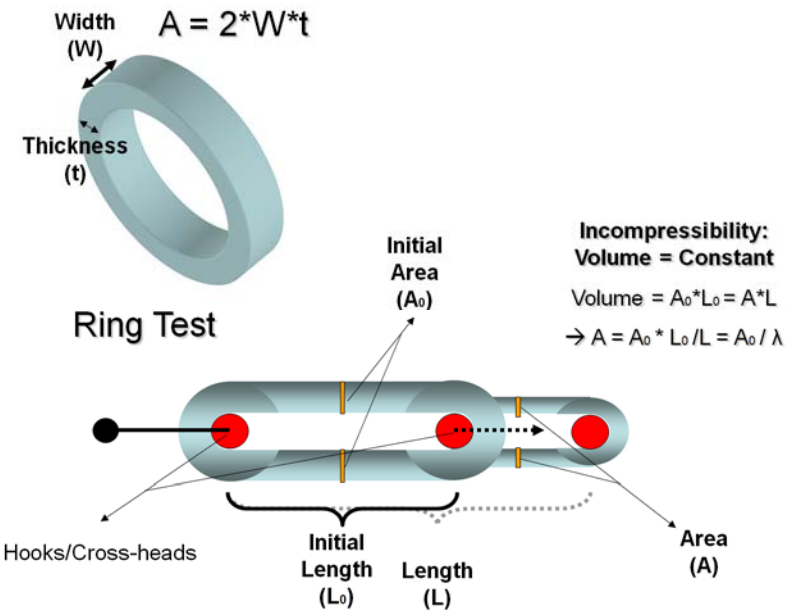

Figure 4.6 Ring test schematic. Image from [58].

4.2.5.3 Burst testing

Burst pressure was measured by pressurizing the scaffolds and the native vessels with a controlled flow of compressed air within a simple closed circuit (**Figure 4.7**). Scaffolds were loaded internally with high viscosity freezing medium (TBS, Triangle Biomedical Sciences) immediately prior to testing in order to clog the pores avoiding transluminal flow for complete pressure retention [58]. This gel has no significant mechanical properties as evidenced by a simple mechanical testing experiment in which the pressure required to burst a bubble of gel was measured to be smaller than 4 mmHg. Air was infused at 100 mL/min as recommended by previous work [156]. Pressure was measured via a high pressure gauge (pressure range = 0-60 PSI, Noshok, Berea, OH) after clamping the downstream line (**Figure 4.7**). The maximum pressure before rupture was taken as the burst pressure.

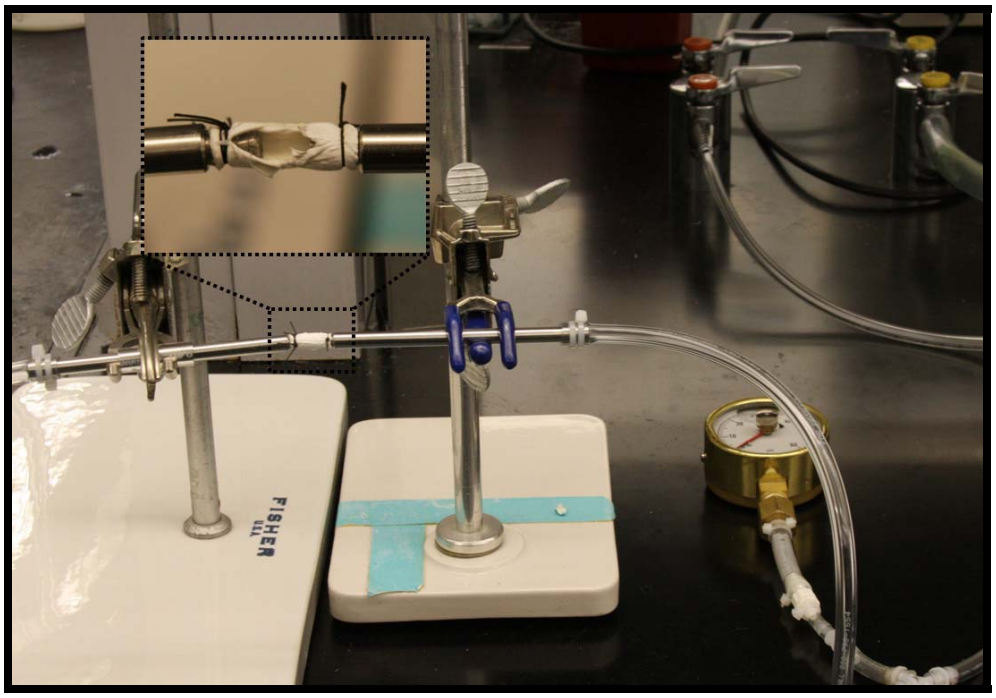

Figure 4.7 Burst test setup.

4.2.5.4 Suture retention testing

Suture retention testing was performed according to American National Standard Institute-Association for the Advancement of Medical Instruments (ANSI/AAMI) VP20 standards [32] using the same testing apparatus as for the uniaxial testing. Briefly, each tubular scaffold and native tissue was cut to obtain rectangular strips (n = 4, length = 10 mm, width = 4 mm). The short edge of each specimen belonged to the circumference of the original tubular scaffold to replicate the direction of the actual pulling force involved in an end-to-end anastomosis. A single 5-0 PDS™ (Ethicon, Inc.) loop was created 2 mm from the short edge of each sample and

secured to a hook connected to the clamp of the testing device. An extension rate of 2 mm/sec was used to pull the suture. Suture retention force was considered to be the maximum force recorded prior to pull–through of the suture. Suture retention strength was obtained by normalizing the suture retention force to the thickness of each scaffold.

4.2.5.5 Compliance and β stiffness testing

Dynamic compliance and β stiffness measurements were performed via a previously described vascular perfusion system [160]. The flow loop was filled with saline at room temperature, and delivered physiologic, arterial, pulsatile intraluminal pressure (120/80 mmHg) and flow (100 mL/min). Briefly, a pulsatile centrifugal pump (Biomedicus 520D, Medtronic, Minneapolis, MN) was used to provide a sinusoidal pulsatile flow to tees enclosed into a testing chamber. Two pressure transducers (Model TJE, Honeywell – Sensotec Co., Columbus, OH) placed equidistant upstream and downstream of the vessel central point were used to measure intraluminal pressure. The pressure in the center of the vessel was then calculated as the average between the proximal and distal pressure transducer measurements. The outer diameter of the pressurized scaffolds was measured with a He-Ne laser micrometer (Beta LaserMike, Dayton, OH). Both pressure and diameter signals were automatically recorded at 30 Hz for 1 minute every hour over 24 hours via an acquisition card connected to a personal computer. Compliance, C, was calculated from recordings of pressure, P and inner diameter, ID_p as:

$$C = \frac{\left(ID_{120} - ID_{80}\right)}{ID_{80}} \frac{1}{P_{120} - P_{80}} \qquad \textbf{4-1}$$

where $P_{120} = 120$ mmHg and $P_{80} = 80$ mmHg.

The inner diameter at a given pressure P, ID_p, was estimated via an assumption of incompressibility from the cross sectional area, A, of the scaffold (measured from histological sections of the same construct using ImageJ software), and the outer diameter OD_p of the scaffold (measured via a laser micrometer) by the expression:

$$ID_p = 2 \cdot \sqrt{\left(\frac{OD_p}{2}\right)^2 - \frac{A}{\pi}} \qquad \textbf{4-2}$$

Recordings of OD_p for each time point were also used to calculate the percentage of scaffold dilation over time ($\Delta OD_{\%}$) to quantify possible plastic deformations due to creep. This value was calculated by dividing the average pressurized external diameter at each time point by the initial average pressurized external diameter for each tested scaffold.

Native vessels were tested also for static compliance; briefly, the constructs were subjected to a pressure ramp (0-200 mmHg) by means of a syringe pump (Harvard Apparatus), and the circuit was clamped downstream while the pump infused saline at a constant rate (4 mL/min).

Pressure-diameter relationships during compliance measurements were also used to compute the dimensionless stiffness index, β, via:

$$\beta = \frac{\ln\left(\frac{P_{120}}{P_{80}}\right)}{\left[\frac{\left(OD_{120} - OD_{80}\right)}{OD_{80}}\right]} \qquad \textbf{4-3}$$

Finally, the percentage of variation of the initial, average external diameter over the pulse was plotted over 24 hours of perfusion. This was done to demonstrate the absence of plastic

deformations of the scaffolds, which could possibly lead to dilations during sustained exposure to pulsatile arterial pressures.

4.2.5.6 Results

All scaffolds exhibited anisotropy for supra-physiologic values of distension reached throughout the uniaxial testing. The circumferential properties were generally characterized by a lower slope (stiffness) and lower UTS compared to the longitudinal properties for all three scaffolds. In particular, TIPS and ES PEUU scaffolds exhibited very different uniaxial properties with different shapes of the stress-strain curve. The TIPS curve had an almost linear behavior (**Figure 4.8**) while the ES curve had an exponential trend more similar to native tissues (**Figure 4.9**), as expected. The uniaxial curve for the ES-TIPS PEUU scaffolds revealed a behavior that was in between that for the TIPS and ES alone, suggesting a balanced contribution of the two components (**Figure 4.10** and **Figure 4.11**).

A comparison of the three different scaffolds is shown in **Figure 4.12**.

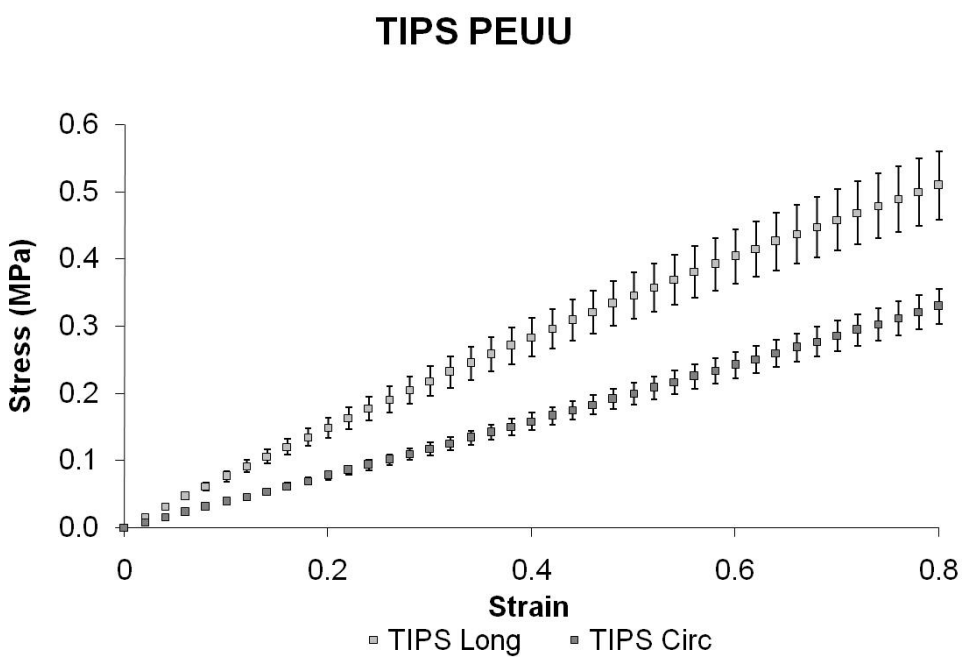

Figure 4.8 TIPS PEUU uniaxial mechanical properties within a physiologically-relevant range of strain (mean ± standard deviation; n = 3).

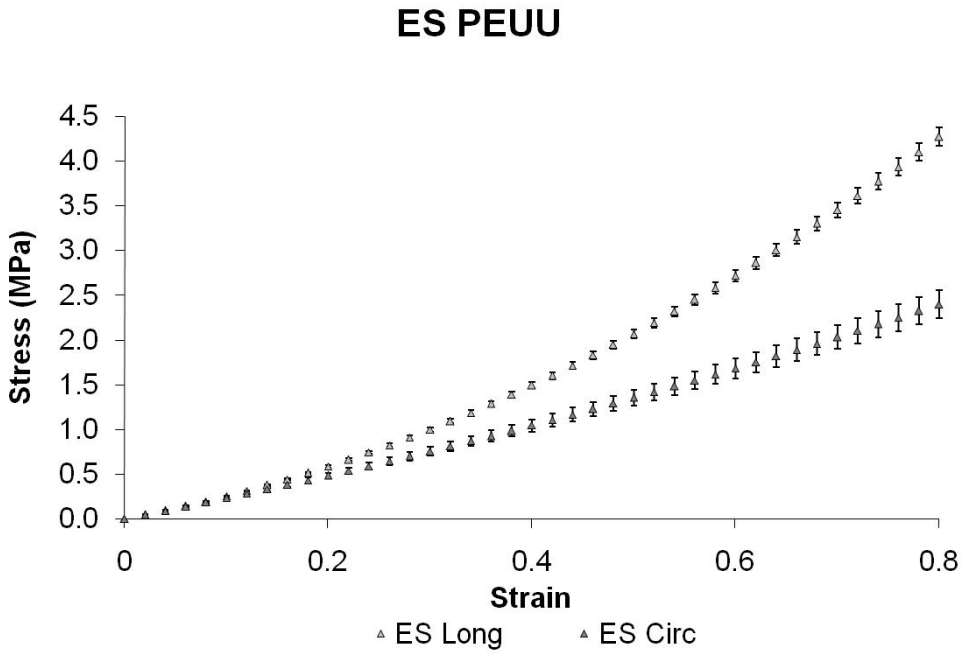

Figure 4.9 ES PEUU uniaxial mechanical properties within a physiologically-relevant range of strain (mean ± standard deviation; n = 5).

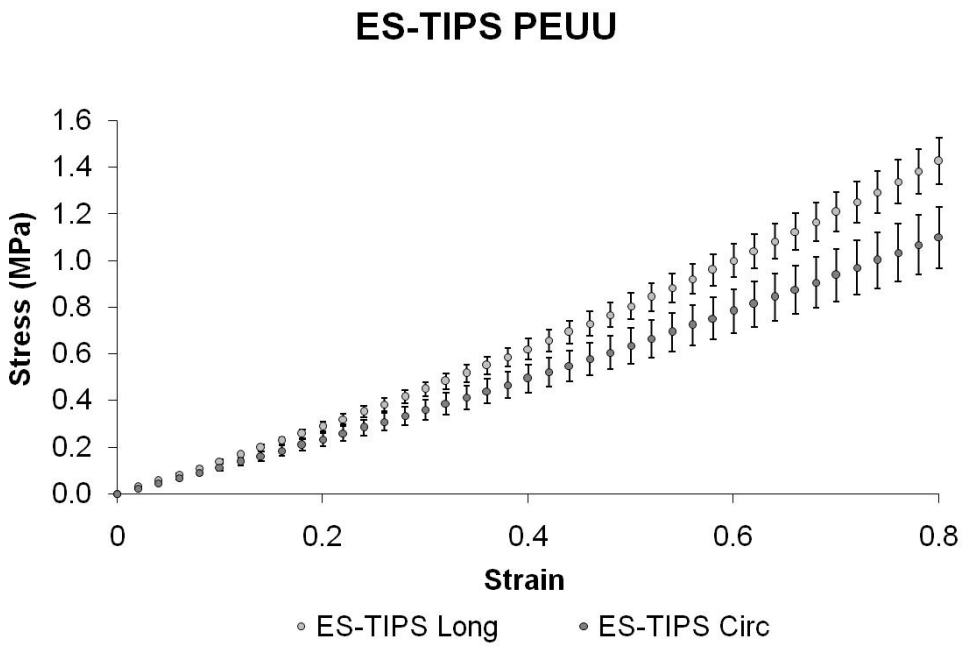

Figure 4.10 ES-TIPS uniaxial mechanical properties within a physiologically-relevant level of strain (mean ± standard deviation; n = 3).

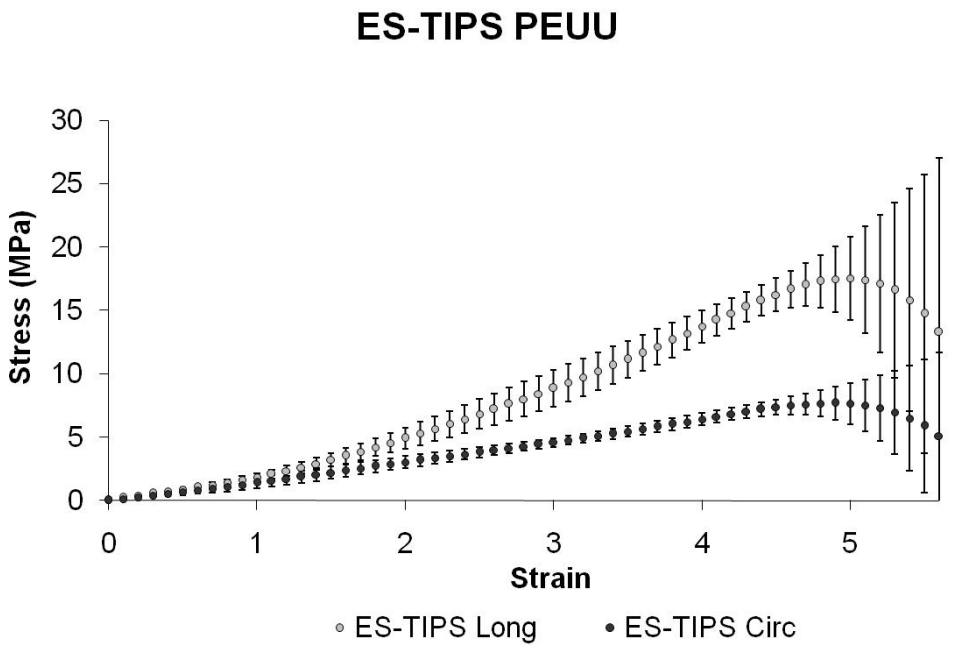

Figure 4.11 Circumferential and longitudinal uniaxial tensile properties of ID-4.7 scaffolds (mean ± standard deviation; n = 3) along the complete testing range. The scaffold shows significant anisotropy ($p<0.05$; n = 3) with stiffer and stronger mechanical properties in the longitudinal direction. The level of strain to failure is comparable in the two directions.

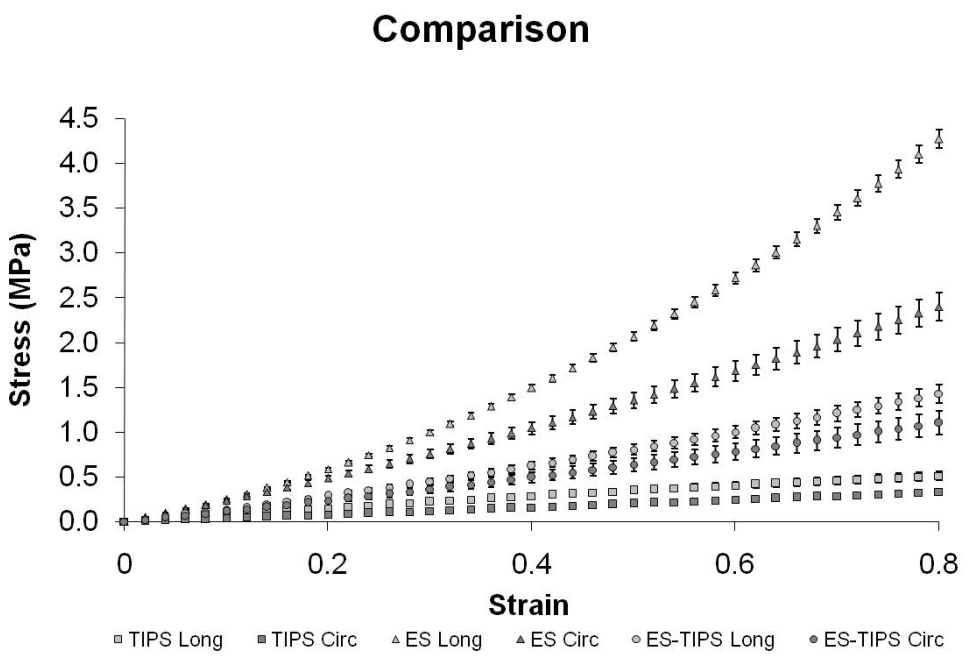

Figure 4.12 Comparison of uniaxial properties of the three scaffolds. Note how the ES-TIPS material properties fall between those of its two individual components, as expected. (TIPS PEUU: n = 3; ES PEUU: n = 5; ES-TIPS PEUU: n = 3)

The circumferential and longitudinal UTSs for the TIPS scaffolds were statistically different ($p = 0.038$) with values of 0.4±0.1 MPa and 0.7±0.2 MPa, respectively; while this values were not statistically different ($p = 0.21$) for the ES scaffolds UTSs, with values of 14.0±2.9 MPa and 17.2±5.7 MPa, respectively. For the ES-TIPS, the circumferential UTS was statistically weaker (8.3±1.7 MPa; p 0.013) than the longitudinal UTS (21.1±4.8 MPa). The ES and ES-TIPS scaffolds were significantly stronger ($p < 0.001$) than the TIPS PEUU, regardless of the direction. **Figure 4.13** summarize the strength comparison among the three different scaffolds. The circumferential UTS of the hSVs and pIMAs were 3.7±2.0 MPa and 10.4±7.1 MPa, respectively (**Figure 4.14**).

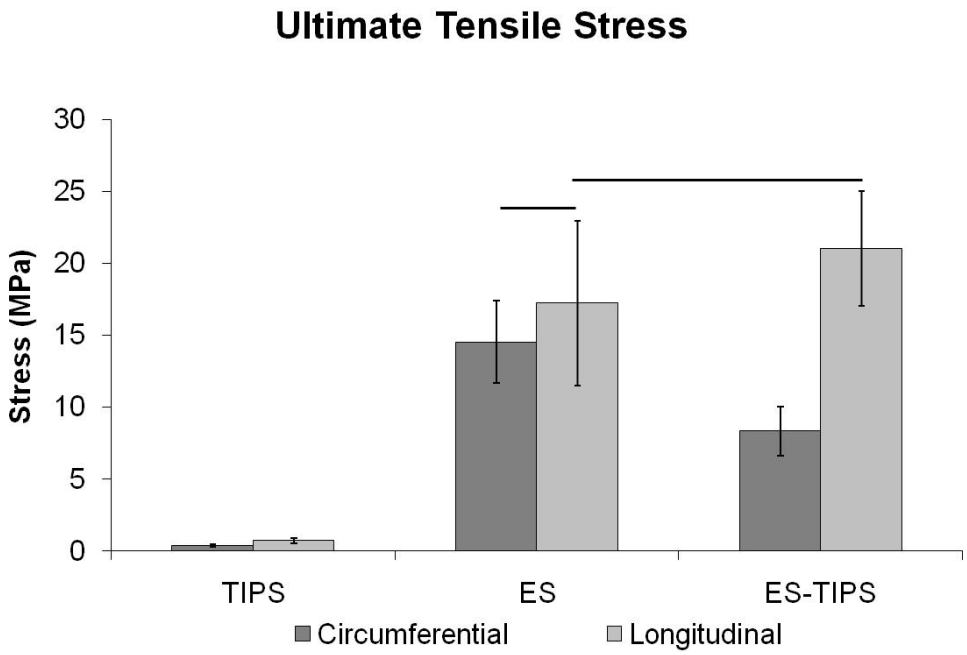

Figure 4.13 Comparison of strength among the three different scaffolds. The bars indicate the absence of statistical significance between two groups; all the other comparisons are statistically significant ($p < 0.05$). (TIPS PEUU: n = 3; ES PEUU: n = 5; ES-TIPS PEUU: n = 3).

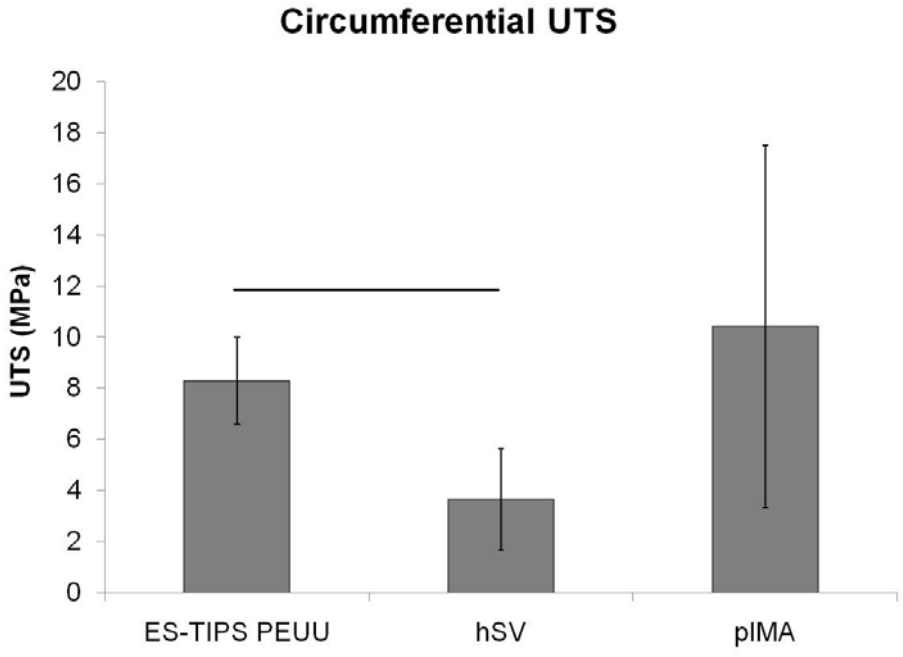

Figure 4.14 Comparison in circumferential UTS between ES-TIPS PEUU scaffolds and native vessels. The bar indicates statistically significant difference ($p < 0.05$) between two groups; all the other comparisons are not statistically significant. (ES-TIPS PEUU: n = 3; hSV: n = 4; pIMA: n = 6).

The STF of the TIPS scaffolds was not statistically different in the two directions ($p = 0.59$) with circumferential and longitudinal values of 1.0±0.1 and 1.3±0.4, respectively. Similarly, the ES PEUU STF was not statistically different in the circumferential and longitudinal directions ($p = 0.35$) with values of 2.8±0.3 and 2.5±0.5, respectively. The ES-TIPS scaffolds were significantly more distensible (*i.e.*, greater STF; $p < 0.05$) than the two other scaffolds with no significant differences in the two directions (circumferential STF = 5.3±0.5, longitudinal STF = 5.6±0.7; $p = 0.56$) (**Figure 4.15**). The circumferential STF for the hSVs and pIMAs were 1.7±0.7 and 1.5±0.2, respectively (**Figure 4.16**).

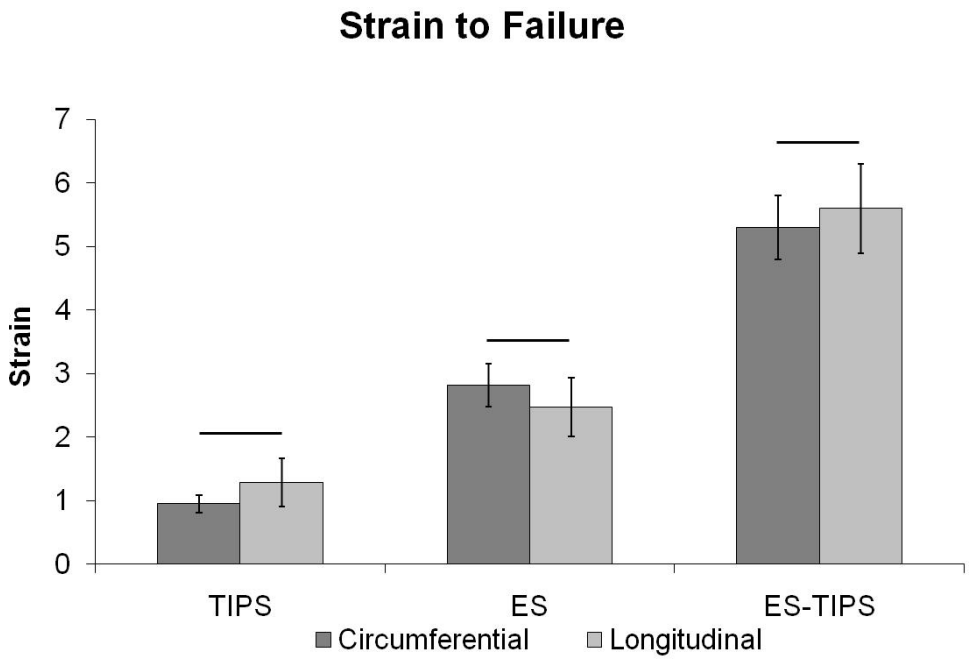

Figure 4.15 Strain to failure results from uniaxial tensile tests for the three different scaffolds. The bars indicate the absence of statistical significance between two groups; all the other comparisons are statistically significant ($p < 0.05$). (TIPS PEUU: n = 3; ES PEUU: n = 5; ES-TIPS PEUU: n = 3).

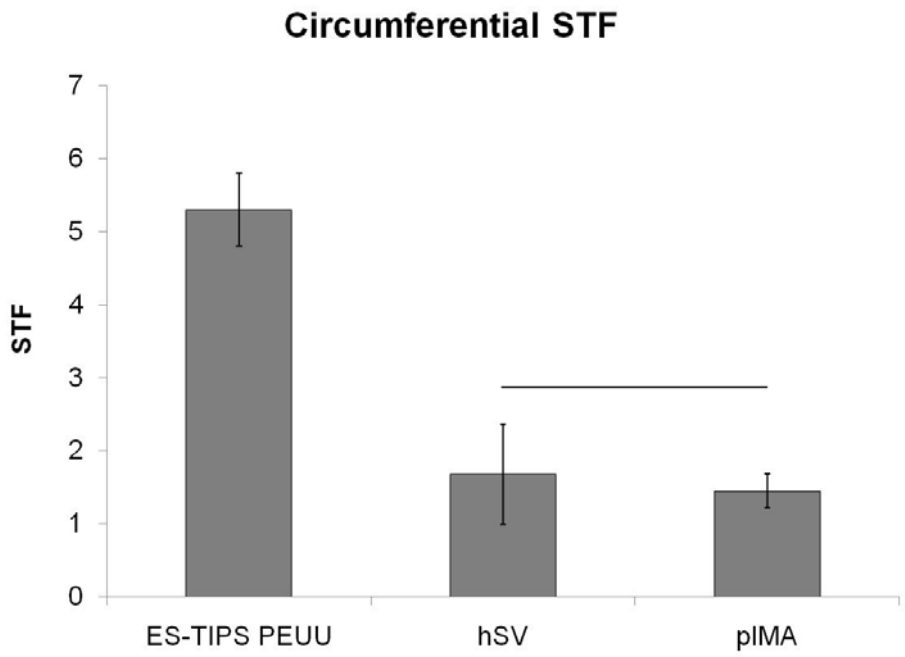

Figure 4.16 Comparison in circumferential STF between ES-TIPS PEUU scaffolds and native vessels. The bar indicates absence of statistically significant difference between two groups; all the other comparisons are statistically significant ($p < 0.05$). (ES-TIPS PEUU: n = 3; hSV: n = 4; pIMA: n = 6)

The approximated elastic modulus was not significantly different in the two directions for TIPS ($p = 0.41$) and ES-TIPS ($p = 0.23$) scaffolds, while the ES PEUU scaffolds exhibited statistically different moduli ($p = 0.0008$) (TIPS: circumferential = 0.4±0.03 MPa, longitudinal = 0.76±0.1 MPa; ES: circumferential = 2.9±0.3 MPa, longitudinal = 4.7±0.5 MPa; ES-TIPS: circumferential = 1.4±0.4 MPa, longitudinal = 1.8±0.3 MPa) (**Figure 4.17**). The circumferential elastic modulus for the hSVs and pIMAs was 2.3±1.3 MPa and 0.4±0.2 MPa (**Figure 4.18**). A summary of the uniaxial properties for ES and TIPS PEUU is shown in **Table 4-2**.

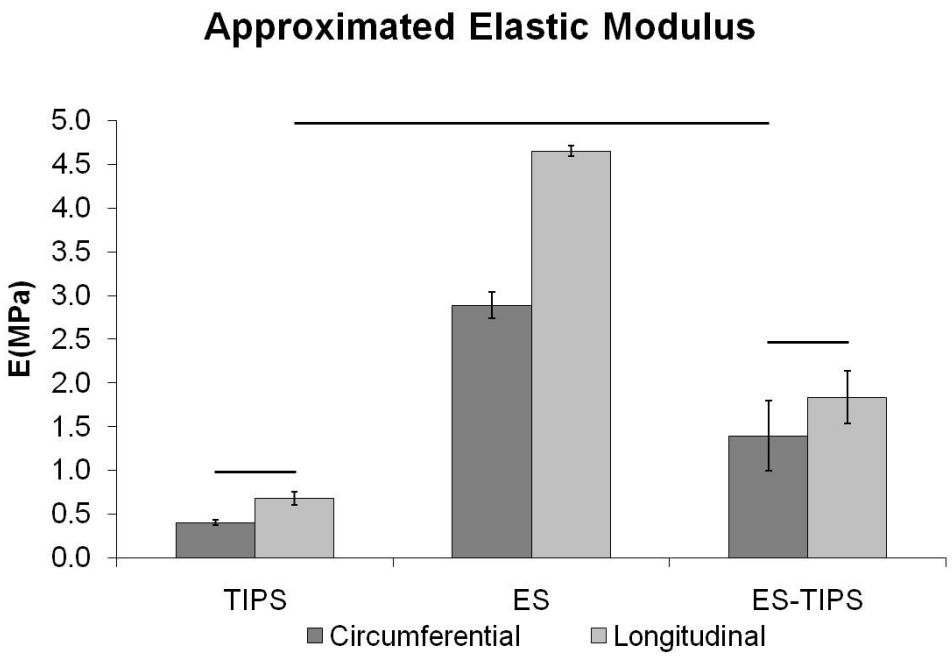

Figure 4.17 Approximated elastic modulus for the three different scaffolds. The bars indicate absence of statistically significant difference between two groups; all the other comparisons are statistically significant ($p < 0.05$). (TIPS PEUU: n = 3; ES PEUU: n = 5; ES-TIPS PEUU: n = 3).

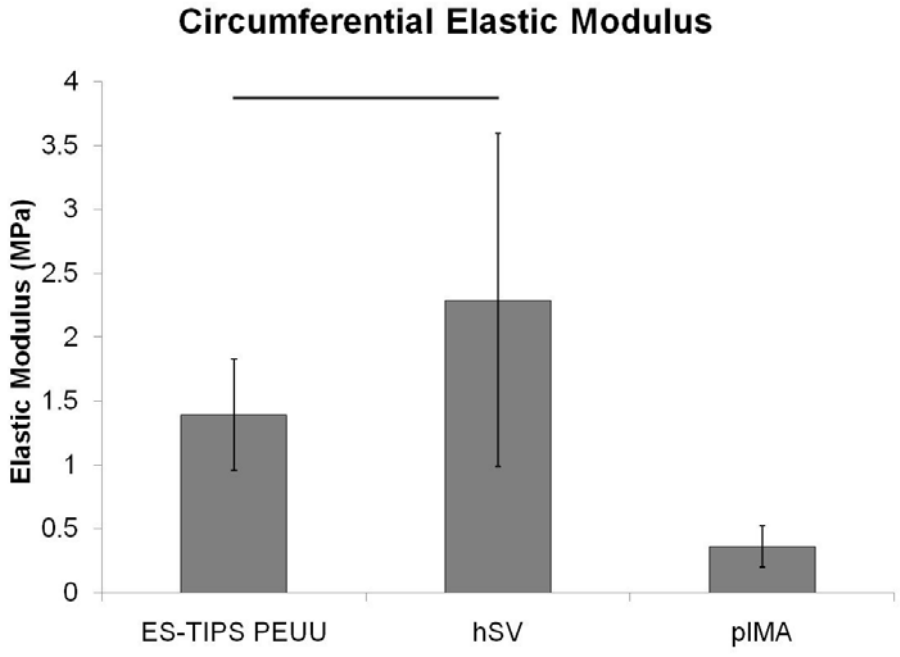

Figure 4.18 Comparison in approximated circumferential elastic between the ES-TIPS scaffolds and the native vessels. The bar indicates absence of statistically significant difference between two groups; all the other comparisons are statistically significant ($p < 0.05$). (ES-TIPS PEUU: n = 3; hSV: n = 4; pIMA: n = 6).

Table 4-2 Summary of uniaxial tensile properties for the two single components of the ES-TIPS PEUU scaffolds.

	N	Mean	Standard deviation
ES PEUU Circumferential ultimate tensile stress (MPa)	5	14.5	2.2
TIPS PEUU Circumferential ultimate tensile stress (MPa)	3	0.4	0.1
ES PEUU Longitudinal ultimate tensile stress (MPa)	5	17.2	5.7
TIPS PEUU Longitudinal ultimate tensile stress (MPa)	3	0.7	0.2
ES PEUU Circumferential strain to failure	5	2.8	0.3
TIPS PEUU Circumferential strain to failure	3	1.2	0.2
ES PEUU Longitudinal strain to failure	5	2.5	0.5
TIPS PEUU Longitudinal strain to failure	3	1.3	0.4
ES PEUU Circumferential elastic modulus (MPa)	5	2.9	0.3
TIPS PEUU Circumferential elastic modulus (MPa)	3	0.4	0.1
ES PEUU Longitudinal elastic modulus (MPa)	5	4.6	0.4
TIPS PEUU Longitudinal elastic modulus (MPa)	3	0.7	0.2

The burst pressure for the ID-4.7 ES-TIPS PEUU scaffolds was 2292±599 mmHg. The burst strength for hSVs and pIMAs was 1267±569 mmHg and 2146±263 mmHg, respectively (**Figure 4.19**). Suture retention force for the ES-TIPS scaffold was 3.4±0.3 N, while the suture retention tension was $5.1\pm0.4\text{x}10^3$ N/m. The suture retention force for the hSVs and pIMAs was 2.6±0.8 N and 1.0±0.3 N (**Figure 4.20**), while the suture retention tension was $6.2\pm2.4\text{x}10^3$ N/m and $4.3\pm1.9\text{x}10^3$ N/m, respectively (**Figure 4.21**).

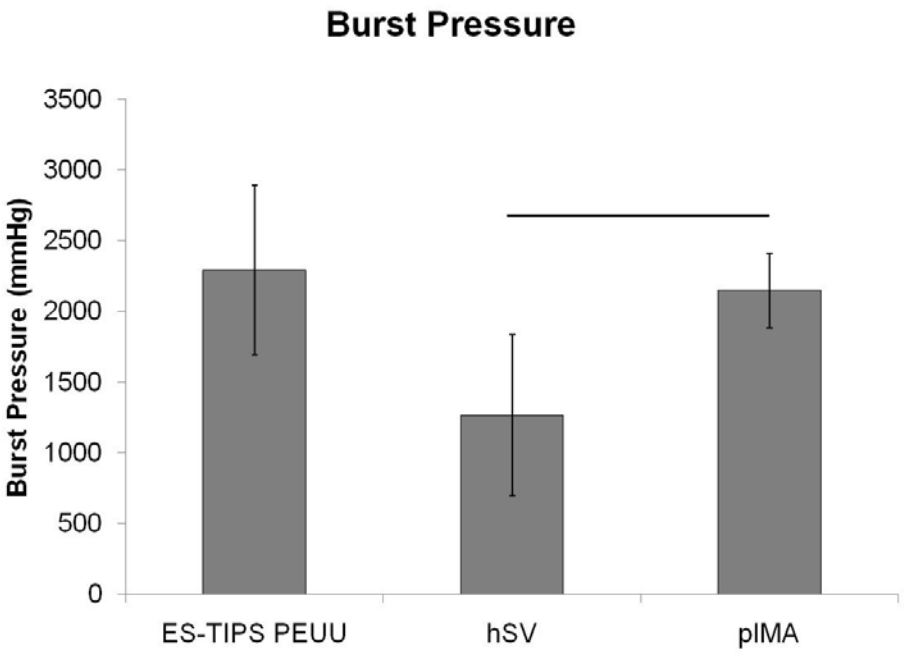

Figure 4.19 Comparison in burst pressure between ES-TIPS PEUU scaffolds and native vessels. The bar indicates statistically significant difference between two groups ($p < 0.05$); all the other comparisons are not statistically significant. (ES-TIPS PEUU: n = 3; hSV: n = 4; pIMA: n = 6).

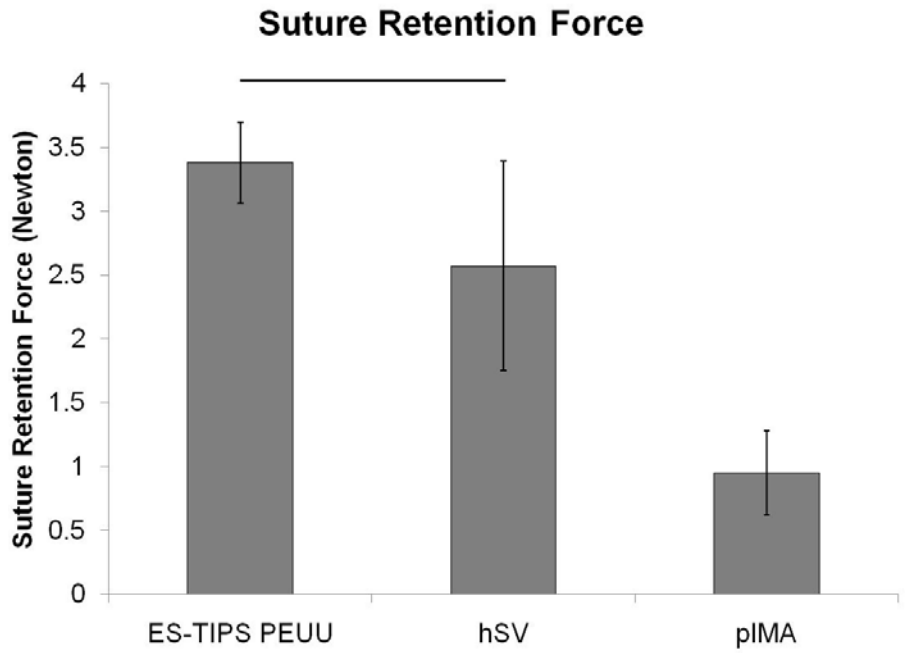

Figure 4.20 Comparison in suture retention force between the ES-TIPS PEUU and native vessels. The bar indicates absence of statistically significant difference ($p < 0.05$) between two groups; all the other comparisons are statistically significant. (ES-TIPS PEUU: n = 3; hSV: n = 4; pIMA: n = 6).

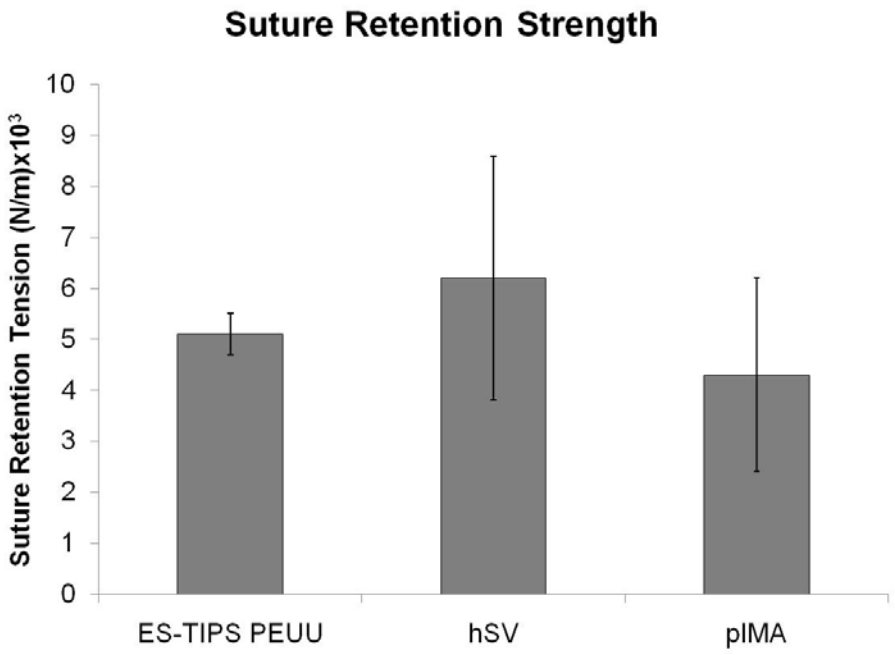

Figure 4.21 Comparison in suture retention strength between ES-TIPS PEUU and native vessels. None of the differences are statistically significant. (ES-TIPS PEUU: n = 3; hSV: n = 4; pIMA: n = 6).

Comparison of the pressure-diameter (P-D) relationships for the ES-TIPS PEUU scaffolds before (**Figure 4.22**) and after (data not shown) 24 hours of perfusion, showed no significant differences. P-D curve for the ES-TIPS scaffolds were compared to those obtained with the native vessels (**Figure 4.23**). The dynamic compliance for the hSVs and pIMAs was $3.4\pm2.0\text{x}10^{-4}$ mmHg^{-1} and 11.2 ± 6.0 $\text{x}10^{-4}$ mmHg^{-1}, respectively.

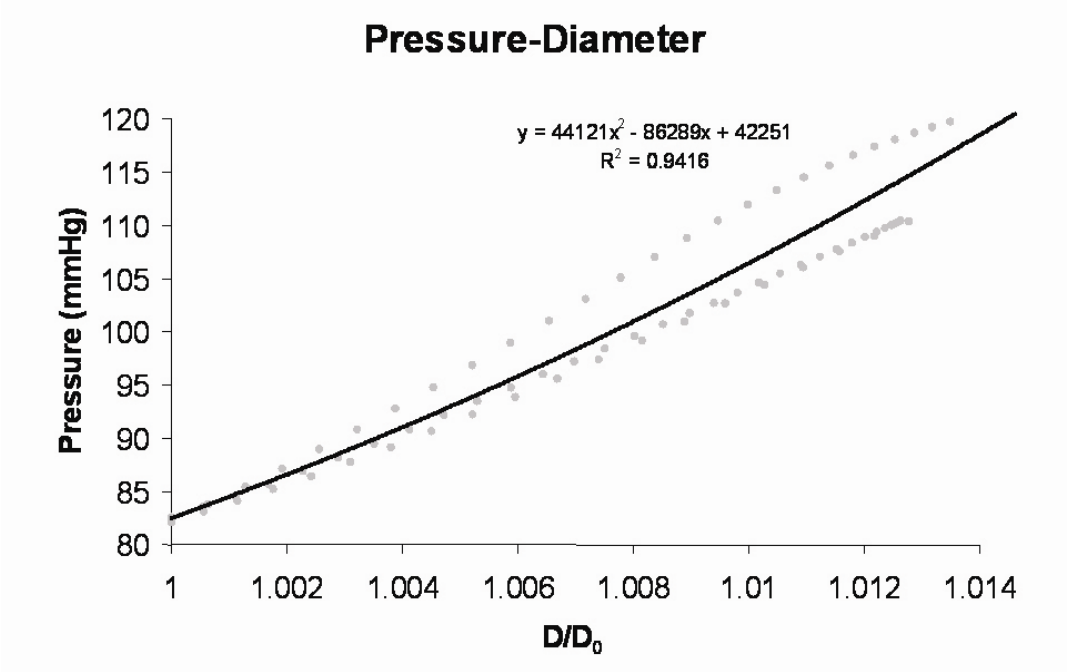

Figure 4.22 Pressure-diameter relationship under physiologic pulse pressures for the ID-4.7 scaffolds at the beginning of the 24 hour perfusion. The curve is a second-order polynomial interpolation of the data points from n = 3 tested scaffolds.

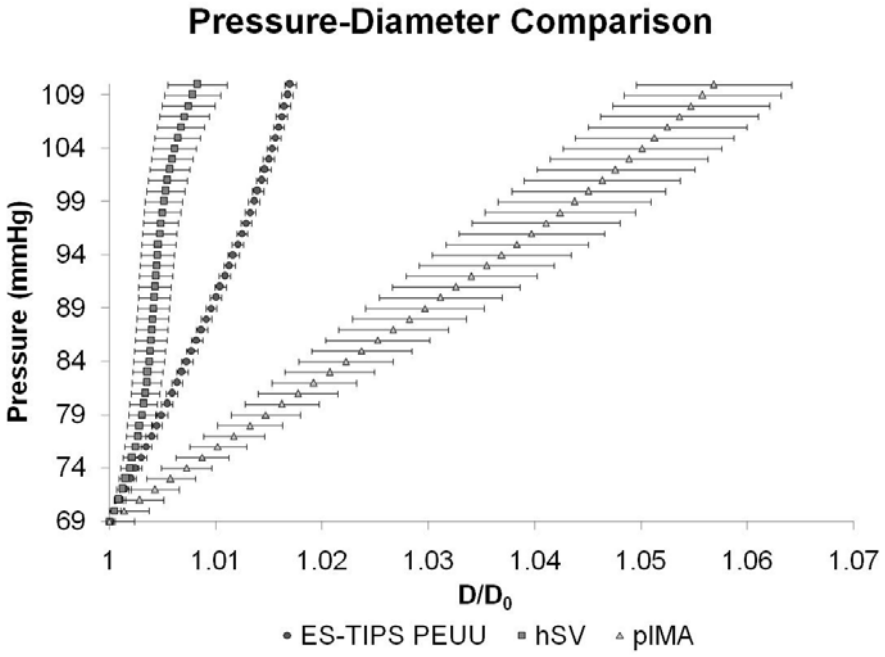

Figure 4.23 Comparison of P-D curves between ES-PEUU scaffolds and native vessels. The results are presented as Average ± SEM. (ES-TIPS PEUU: n = 3; hSV: n = 4; pIMA: n = 6).

Recordings of the percentage of variation of the initial average *OD* over 24 hours of perfusion, detected a non-significant increase in average diameter (**Figure 4.24**).

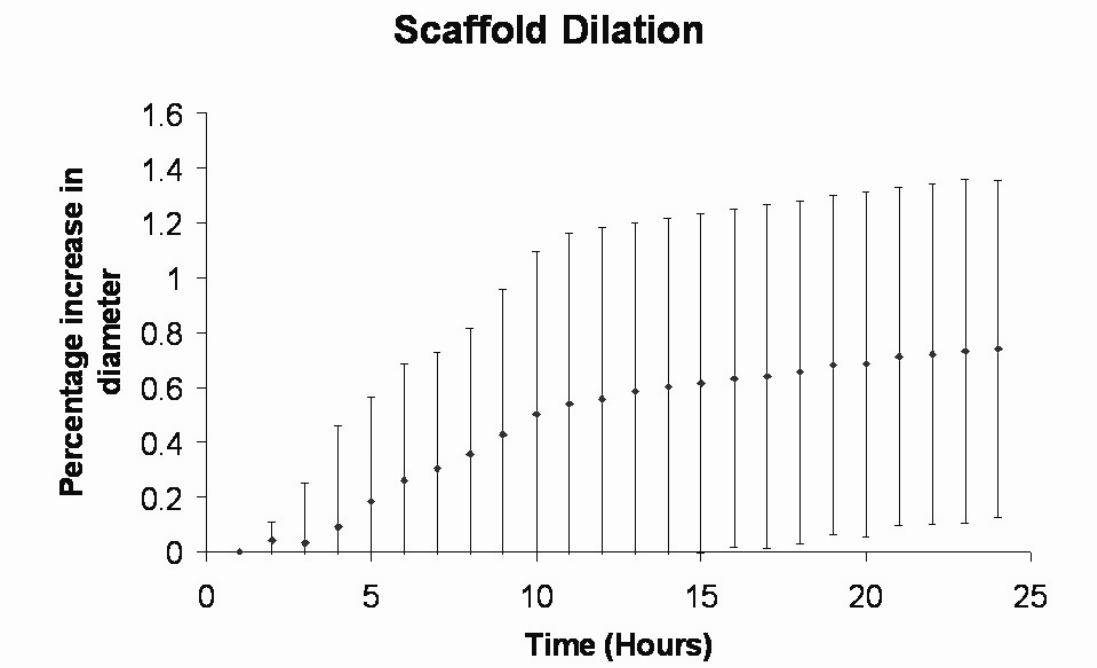

Figure 4.24 Percent variation of average external diameter for the ID-4.7 scaffold over the pulse during 24 hours of arterial perfusion ex vivo (mean ± standard deviation; n = 3). No significant differences were noted between any time points over 24 hours of cyclic pressure

Though a slight, non-significant dilation occurred (<1% over 24 hrs), the diameter at the end of the 24 hours was not statistically different from that recorded at the beginning. Compliance also did not change significantly over 24 hours from its initial value of $4.6\pm0.5\times10^{-4}$ $mmHg^{-1}$ (**Figure 4.25**). The compliance for the hSVs and pIMAs were $3.4\pm2.0\times10^{-4}$ and $11.2\pm6.0\times10^{-4}$ $mmHg^{-1}$, respectively (**Figure 4.26**).

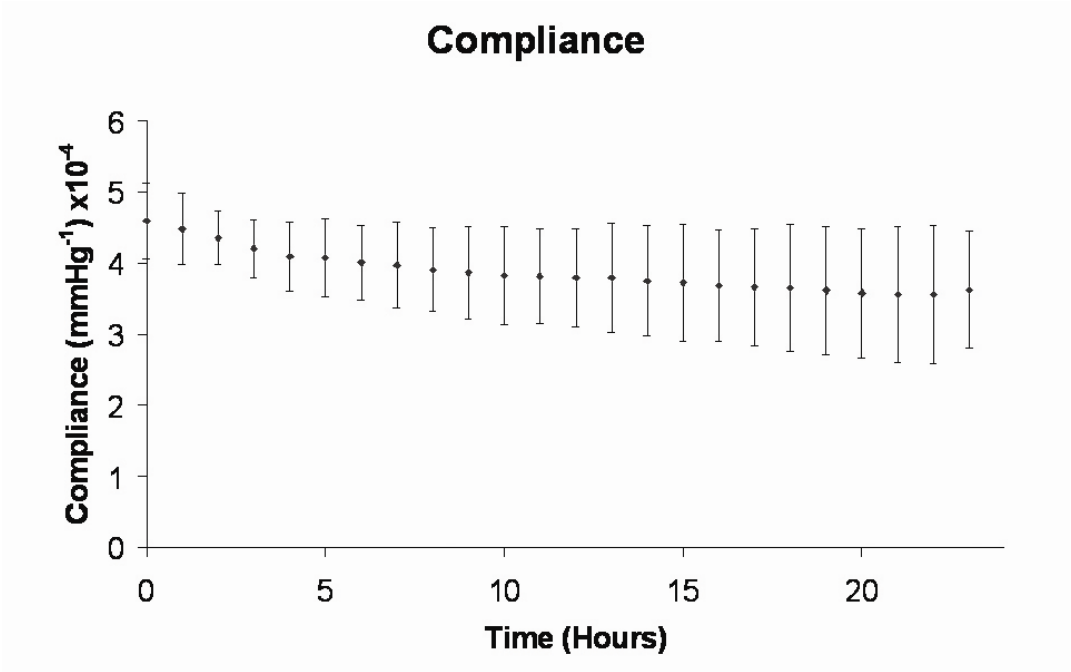

Figure 4.25 Dynamic compliance of the ID-4.7 scaffold measured over 24 hours of mechanical training under arterial physiologic pulsatile pressure (mean ± standard deviation; n = 3). No significant differences were detected between any time points.

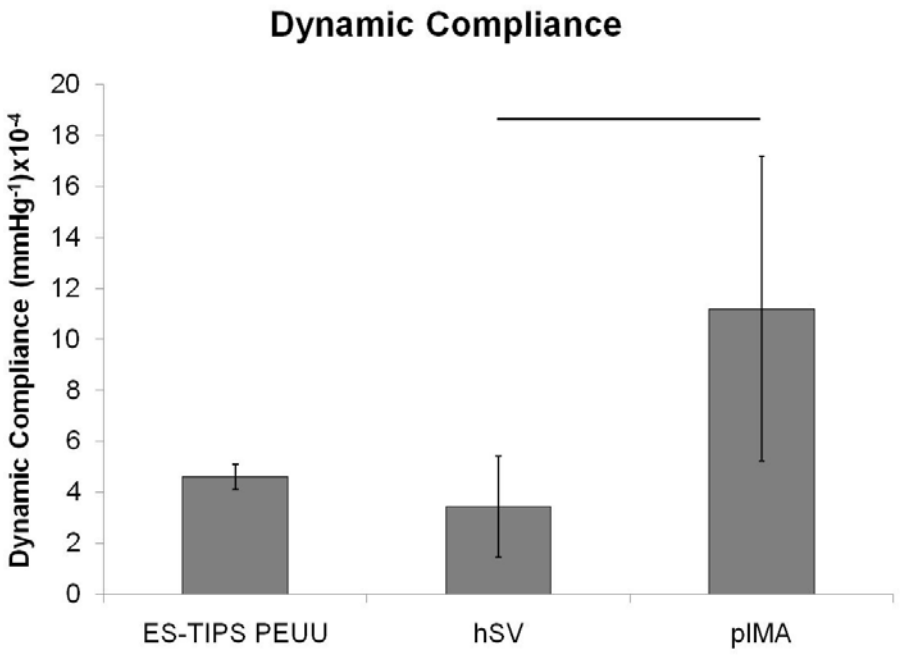

Figure 4.26 Comparison in dynamic compliance between ES-TIPS PEUU scaffolds and native vessels. The bar indicates statistically significant difference between two groups; all the other comparisons are not statistically significant (ES-TIPS PEUU: n = 3; hSV: n = 4; pIMA: n = 6).

Similarly, the dimensionless stiffness index β did not change significantly over the 24 hour perfusion, with an initial value of 21.6±2.9 (**Figure 4.27**). The stiffness index for the hSVs and pIMAs were 46.0±11.9 and 14.0±11.9, respectively.

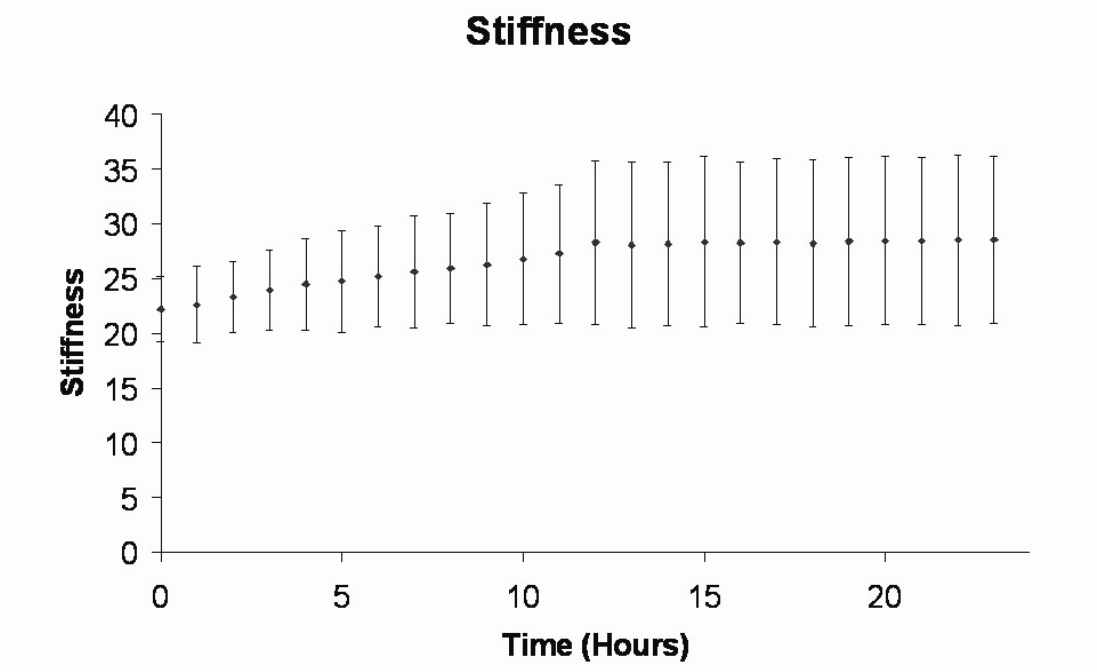

Figure 4.27 β stiffness of the ID-4.7 scaffold measured over 24 hours of mechanical training under arterial physiologic pulsatile pressure (mean ± standard deviation; n = 3). No significant differences were detected between any time points.

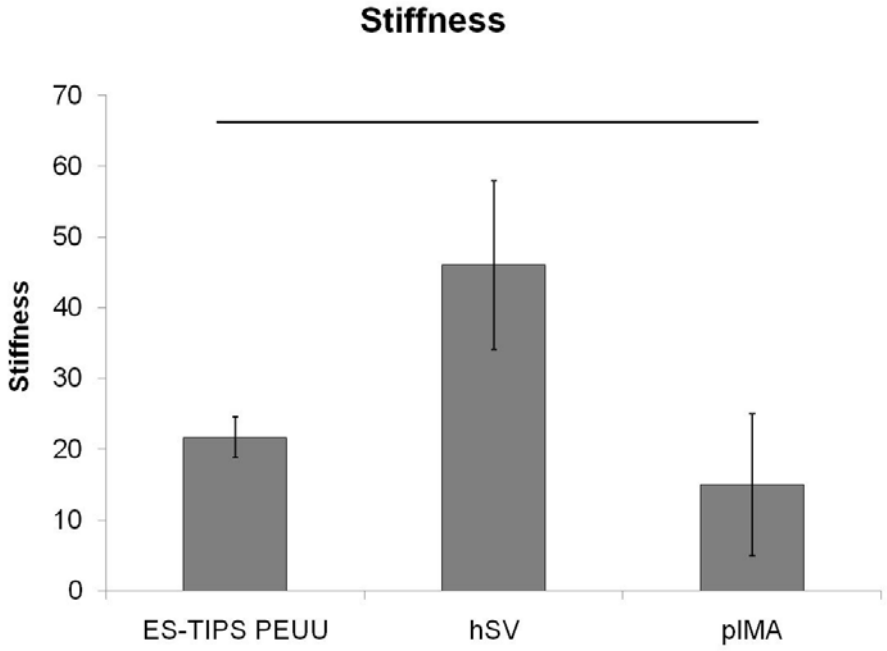

Figure 4.28 Comparison in β stiffness between the ES-TIPS PEUU scaffolds and the native vessels. The bar indicates absence of statistically significant difference between two groups; all the other comparisons are statistically significant ($p < 0.05$). (ES-TIPS PEUU: n = 3; hSV: n = 4; pIMA: n = 6).

A summary of biomechanical values measured for the ES-TIPS PEUU scaffolds and for the native vessels is shown in **Table 4-3** and **Table 4-4**.

Table 4-3 Summary of biomechanical properties of the ES-TIPS PEUU scaffolds.

	N	Mean	Standard deviation
Circumferential ultimate tensile stress (MPa)	3	8.3	1.7
Longitudinal ultimate tensile stress (MPa)	3	21.1	4.8
Circumferential strain to failure	3	5.3	0.5
Longitudinal strain to failure	3	5.6	0.7
Circumferential elastic modulus (MPa)	3	1.4	0.4
Longitudinal elastic modulus (MPa)	3	1.8	0.3
Burst pressure (mmHg)	3	2292	599
Suture retention force (N)	4	3.4	0.3
Suture retention tension (N/m)x10^{3}	4	5.1	0.4
Dynamic compliance ($mmHg^{-1}$)x10^{-4}	3	4.6	0.5
Stiffness index	3	22.2	3.1

Table 4-4 Summary of biomechanical properties of native hSVs and pIMAs.

	N	Average	Standard Deviation
hSV thickness (μm)	4	436	121
pIMA thickness (μm)	6	231	38
hSV circumferential UTS (MPa)	4	3.7	2.0
pIMA circumferential UTS (MPa)	6	10.4	7.1
hSV circumferential STF	4	1.7	0.7
pIMA circumferential STF	6	1.4	0.2
hSV circumferential E (MPa)	4	2.3	1.3
pIMA circumferential E (MPa)	6	0.4	0.2
hSV burst pressure (mmHg)	4	1267	569
pIMA burst pressure (mmHg)	6	2146	263
hSV suture retention force (Newton)	6	2.6	0.8
pIMA suture retention force (Newton)	6	1.0	0.3
hSV suture retention tension (Newton/m)	6	6.2	2.4
pIMA suture retention tension (Newton/m)	6	4.3	1.9
hSV dynamic compliance ($mmHg^{-1}$)$x10^{-4}$	4	3.4	2.0
pIMA dynamic compliance ($mmHg^{-1}$)$x10^{-4}$	6	11.2	6.0
hSV β stiffness index	4	46.0	11.9
pIMA β stiffness index	6	15.0	10.0

4.2.6 Cell seeding capabilities

The ES-TIPS PEUU scaffolds were bulk-seeded via the RVSD with rMDSCs, obtained and cultured as previously described for the murine MDSCs in **Section 2.2.3**. To avoid longitudinal distribution issues (recall **Figure 2.27**), the ID-4.7 scaffolds were cut to a length of 2 cm prior to seeding. Both scaffold sizes were seeded using custom made tee adapters with $3x10^6$ (ID-1.3) or $30x10^6$ (ID-4.7) rMDSCs (corresponding to an equivalent seeding density of approximately

$1.5x10^5$ cells/mm^3). The seeding parameters were: a vacuum of -5 inHg, an infusion rate of 2.5 mL/min and a rotational speed of 150 rpm (for the ID-1.3 scaffolds), or an infusion rate of 4 mL/min and a rotation speed of 10 rpm (for the ID-4.7 scaffolds). Immediately after the seeding of each sample, the media exuded through the scaffold into the RVSD chamber was collected and used for cell counting via a hemocytometer to calculate seeding efficiency (percentage of initial cell number entrapped within the scaffolds). Subsequently, the scaffolds were placed in static culture in Petri dishes for two hours and then processed for fluorescence-based cytoskeletal and nuclear staining and imaging as shown in **Section 2.2.3**. The scaffolds were visualized with high exposure times (~10 sec) under a TRITC filter.

After two hours of culture, following seeding, fluorescent staining showed high cellular density inside the internal TIPS layer for both the ID-1.3 and ID-4.7 constructs (**Figure 4.29)**. Cell distribution was qualitatively uniform across the entire thickness (radial direction) of the internal layer of the TEVG, and throughout the circumferential and longitudinal direction. An extensive quantitative analysis of seeding uniformity was beyond the scope of this exercise. However, this type of analysis has been shown for the ID-4.7 scaffolds seeded with the S-RSVD in **Section 3.1.4**. The external ES layer did not exhibit the presence of any cells, as expected, due to its small, restrictive pore size, not allowing passive cell penetration. Cell seeding efficiency in the ID-4.7 and ID-1.3 scaffolds was 91.3±1.6% and 93.2±1.7%, respectively. The seeding procedure took 1.5 min for the ID-1.3 scaffolds and 5 min for the ID-4.7.

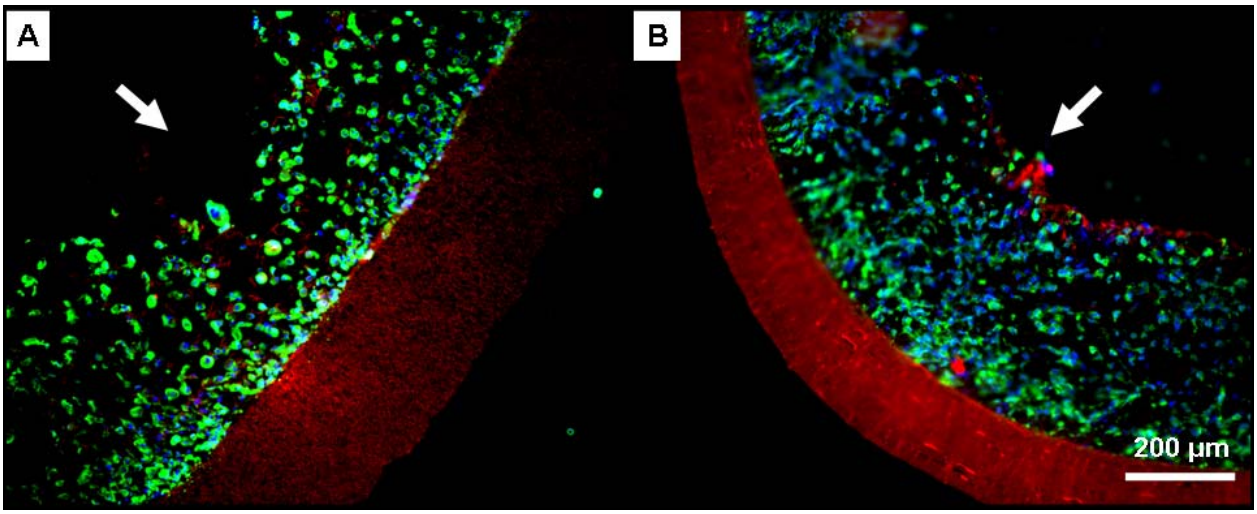

Figure 4.29 Representative cell density into the TIPS layer of the ES-TIPS PEUU scaffolds 2 hours after seeding (n = 3). **A**. ID-4.7 scaffolds. **B.** ID-1.3 scaffolds. The arrows indicate the luminal surface. Blue = nuclei, green = F-actin, red = scaffold. Magnification = 100X.

4.2.7 Discussion and limitations of ES-TIPS scaffold

We developed and tested a PEUU-based scaffold for vascular tissue engineering obtained by combining two previously developed PEUU-processing techniques: TIPS [53] and ES [57]. The biocompatibility, cell attachment, and tunability of degradation rate and mechanical properties for the PEUU were previously demonstrated [51]. Moreover, recent *in vivo* studies showed how the same material did not produce detrimental host inflammatory response due to its degradation products but rather fostered remodeling [161, 162]. Morphologically, the scaffold was biomimetic, presenting two concentric layers with the highly cellularized, porous TIPS layer mimicking the functional *tunica media* and the fibrous, external ES layer acting as the adventitial layer providing mechanical support (see **Figure 4.3** and **Figure 4.4**). We speculate that these

features might be able to guide the process of neo-tissue formation toward native-like features upon remodeling *in vivo*. In **Chapter 6** we will address this point in detail.

Mechanically, the ES-TIPS PEUU scaffolds showed a predictable compromise between the mechanical properties of its two single components (TIPS PEUU and ES PEUU), leading to ideal mechanical properties for arterial vascular applications. In particular, the ES-TIPS values of UTS (**Figure 4.14**), elastic modulus (**Figure 4.18**), dynamic compliance (**Figure 4.26**), and β stiffness (**Figure 4.28**) were between those of hSVs and pIMAs. The ES-TIPS PEUU had physiologically-compatible values of burst pressure (**Figure 4.19**) and suture retention strength (**Figure 4.20** and **Figure 4.21**). When compared with previously described mechanical properties of human arteries, the ES-TIPS PEUU scaffolds showed comparable burst strength and suture retention force values (burst pressure = 2031-4225 mmHg, suture retention force = 2.0±1.1 N) [32]. Furthermore, the ES-TIPS PEUU scaffold exhibited compliance, β stiffness, and elastic modulus similar to those measured for healthy human coronary arteries (compliance = 14.1±5.9x10^{-4} $mmHg^{-1}$, β stiffness = 16.9±7.1, elastic modulus = 1.4±0.7 MPa) [163]. These characteristics suggest that the ES-TIPS PEUU scaffold may represent an ideal substitute for matching the mechanical properties of native arteries. Indeed, in light of the previously demonstrated ability to reproducibly control the anisotropy of ES PEUU by varying the rotational speed of the mandrel [56], it is expected that a similar degree of control will be possible in the context of ES-TIPS PEUU scaffolds, thus potentially allowing for TEVG anisotropy to be tailored to that of the particular vessel targeted for replacement. However, a comprehensive study toward the optimization of mechanical properties and anisotropy of the ES-TIPS scaffold was beyond the scope of this dissertation and, therefore, was not performed.

The ES-TIPS PEUU scaffolds maintained their geometry and mechanical properties over time while perfused *ex vivo* for 24 hours with physiologic, pulsatile pressure waveforms (see **Section 4.2.5.5**). This feature may be critical for the *in vivo* applications of the scaffold as a TEVG. Aneurysm formation, for example, is a possible drawback of TEVGs and may be due to the intrinsic viscoelastic behavior of thermoplastic polymers (creep) and weakening associated with degradation kinetics. The relatively slow *in vitro* degradation previously reported for PEUU [51] would likely help the host remodeling mechanisms to gradually replace the scaffold with native tissue while the scaffold provides mechanical integrity over an extended period of time. *In vivo* studies for extended implant periods will address this concern in **Chapter 6**.

The seeding via the RVSD yielded high cell density (~$1.5x10^5$ cells/mm^3) in both the ID-1.3 and the ID-4.7 scaffold sizes (**Figure 4.29**) within a few minutes of seeding procedures and with high seeding efficiencies (>92%). These features are critical for the future clinical translation of TEVGs, where rapid turn-around time is desired, and any amount of donor cells wasted due to inefficient seeding could be unacceptable. **Chapter 5** will present longer-term biological endpoints regarding the incorporation of cells into TIPS PEUU [54] and ES-TIPS PEUU scaffolds following seeding and *in vitro* culture. These endpoints include cell viability, proliferation, phenotype and ECM deposition. The assessment of these endpoints is clearly important prior to pre-clinical animal studies. The scope of the cell seeding studies conducted herein had only the aim of demonstrating feasibility, with the primary focus being the mechanical characterization of the construct.

While the ES-TIPS PEUU scaffold exhibited material properties similar to native arteries, these results were limited to some of the tests performed in a dry state at room temperature and without cellular components for ease of testing. These testing conditions are different from those

that the scaffold would experience when implanted *in vivo,* where the material would be hydrated, infiltrated with cells, at body temperature, and in contact with a complex biological milieu. It has been shown that the material properties of synthetic scaffolds might vary depending on the hydration conditions of the scaffold [164]. The reported differences in mechanical properties between dry and wet samples were within the same order of magnitude. Therefore, testing in simplified environmental conditions might not significantly affect the mechanical properties of the scaffold reported here. Once implanted, the scaffold will undergo degradation and remodeling which will affect the mechanical properties over time. In **Chapter 6** we will quantify the performance of these scaffolds following *in vivo* remodeling.

5.0 SPECIFIC AIM 3: *IN VITRO* STUDIES TO UNDERSTAND CELL-SCAFFOLD INTERACTIONS AND "MATURATION" OF THE TEVG

5.1 BIOLOGICAL ANALYSIS OF MURINE MDSCS INCORPORATED INTO TIPS PEUU SCAFFOLDS AND CULTURED *IN VITRO*

5.1.1 Initial considerations toward the development of a stem cell-based TEVG

The development of the first generation seeding device (RVSD, see **Section 2.1**) – which allowed for an effective, fast, and reproducible cell integration within porous, tubular scaffolds (*i.e.*, the fabrication of a TEVG) – initiated a series of subsequent studies investigating the culture and maturation of cells into a 3D porous tubular matrix. The purpose of these studies, described in this chapter, was to assess the cell/scaffold interactions over a defined period of culture time within different culture conditions in preparation for the *in vivo* studies.

As described in **Section 1.9**, time is a critical factor for the future clinical translation of a TEVG, and it is a recurrent key consideration throughout this work. Short fabrication times are essential to propose future products compatible with the standard clinical practice for two basic reasons: first, a long fabrication time is likely to translate into expensive production processes, which might be also prone to issues or failure. Second, from the clinical perspective, it is important to allow a consistent percentage of patients among elective and emergent cases to

benefit from a TEVG approach. This group of patients might not be able to wait extended periods of time for a TEVG. Normal histogenesis processes produced *in vitro* can demand very extensive time frames (several months) to produce a native-like ECM structure "mature" enough to withstand *in vivo* implantation with a basic functionality [30]. Therefore, when deciding "how good is good enough?" for undergoing implantation of a tissue engineered construct, it is necessary to accept or define a compromise between functionality and fabrication time [165].

As described in **Section 4.2**, a novel scaffold for vascular applications was developed and tested (ES-TIPS PEUU) with the purpose of mimicking the mechanical and structural features of native vessels. The extensive mechanical characterization performed, suggests its suitability to withstand the demanding arterial mechanical environment and to match the elastic behavior of the native arterial wall. Behind the development of the biodegradable scaffold was the goal of providing a synthetic substrate, which was mechanically suitable for immediate implantation, without requiring extended culture time.

The development of the RVSD was also oriented toward a rapid fabrication time, and implantation readiness. Upon incorporation of cells within the scaffold via the RVSD, it is critical to allow cells to settle into the pores, attach, spread, and proliferate before substantial mechanical perturbation (such as that experienced with *in vivo* implantation) can be applied. This necessity was realized early on in this work by performing *in vitro* perfusion experiments of the TEVG constructs (data not shown).

The cells represent the second critical part of our TEVG paradigm and should allow for antithrombogenicity once implanted *in vivo*. In theory, cells should contribute to the remodeling of the TEVG, leading to native-like structural and functional features upon degradation and remodeling *in vivo*. Progenitor cells show great potential for use in tissue engineering

applications and may circumvent many of the shortcomings associated with other options in cell sourcing (see **Section 1.5**). Progenitor cells are easier to harvest than terminally differentiated cells for vascular applications where a muscle biopsy, a bone marrow aspirate or a blood aspirate are usually preferable to a blood vessel biopsy to collect endothelial or smooth muscle cells. Stem cells also usually display a rapid, almost limitless expansion capability. The skeletal muscle is a valid source of stem cells for tissue and genetic engineering applications. MDSCs are a population of long-term proliferating cells, expressing hematopoietic stem cell markers. They have previously shown the ability to retain their phenotype for more than 30 passages with normal karyotype and were able to differentiate into muscle, neural, and endothelial lineages both *in vivo* and *in vitro* [99-101]. MDSCs are a unique population of multipotential cells distinct from the well-studied satellite cells, and characterized by more plasticity when compared with the satellite cell. It has been hypothesized that MDSCs could actually be a precursor of the satellite cell itself [101]. MDSCs have also been shown to have both a strong self-renewal capacity and have proved to be useful in myogenic regeneration models [101, 166, 167]. MDSCs are SCA-1+, CD34+, and they represent a promising alternative for vascular tissue engineering applications [99]. For these reasons MDSCs were used as the cell source of choice for our approach.

The goals of the studies described in this section were to evaluate the interaction of MDSCs with the PEUU scaffold, and to identify suitable culture criteria to allow for MDSCs proliferation and possibly ECM deposition within the scaffolds prior to implantation within scaffolds.

5.1.2 Dynamic culture of a MDSC-based TEVG in spinner flasks

5.1.2.1 Methods

The first experiments were performed to evaluate the behavior of murine MDSCs in TIPS PEUU scaffolds. The rationale behind the use of mouse cells relied essentially on their extensive phenotypic and behavioral characterization, which allowed detecting variations induced by the TEVG approach proposed here.

The synthesis of the polymer was consistent with that previously described in **Section 4.2.1**. That is, the obtained PEUU polymer solution was injected into a cylindrical mold consisting of an outer glass tube (ID = 5.5 mm) and an inner PTFE mandrel (OD = 4.5 mm), coaxially fixed by two rubber stoppers. The mold filled with hot PEUU solution underwent TIPS processing as described in **Section 4.2.2** to obtain porous tubular scaffolds. Scaffold length, ID, and wall thickness were measured with a digital caliper and were nominally 2 cm, 4 mm, and 300 μm, respectively.

Mouse MDSCs were isolated via an established pre-plating technique [99]. Cells were then plated at low density (200 cells/cm^2) on 175 cm^2 flasks and cultured at 37 ºC and 5% CO_2 with complete DMEM media (described in **Section 2.2.3**). Cells were expanded to the desired number and were only used between passages 10 and 15. Media changes were performed every 48 h during culture. Before use, MDSC monolayers were washed three times in DPBS and then incubated with 0.1% trypsin for 5 min to detach them from the flasks. MDSCs were then centrifuged at 1200 rpm for 5 min to form a pellet, and resuspended in DMEM to the desired concentration in preparation for seeding.

MDSCs were incorporated into the fabricated TIPS PEUU scaffolds (total cell number = $10x10^6$ cells, seeding suspension density = $2x10^6$ cell/mL) via the RVSD. Seeding parameters were consistent with what was previously described in **Section 2.2.3**, except for the seeding flow rate, which was 5 mL/min. The constructs (n = 12) were then flushed with 5 mL of plain DMEM in order to wash residual cells from the lumen of the scaffolds, and were then removed and incubated in a Petri dish for 1 h. After seeding, the TEVGs were placed in 500 mL spinner flasks (196580575, Bellco Glass Inc., NJ) with 100 mL of culture media, supplemented with 50 mg/mL of ascorbic acid, and stirred at 15 rpm for 7 days. Control constructs were cultured either within the spinner flasks without ascorbic acid or in static culture in a Petri dish.

To assess cell spreading and distribution, ring segments for different areas of each construct were fixed, processed, and imaged for F-actin and nuclear staining as previously described in **Section 2.2.3**. To assess collagen production and TEVG histology, separate ring segments were fixed in 10% neutral buffered formalin for 1 hour. They were then embedded in paraffin blocks and 5 μm sections were cut using a microtome (Thermo Shandon Inc., Pittsburgh, PA). Sections were mounted on slides, stained with H&E and Masson's trichrome and viewed under bright light optics using a Nikon Eclipse E600 microscope. Collagen production was qualitatively assessed on acquired images using Adobe Photoshop (v. 7.0, Adobe Systems Inc., USA).

To assess proliferation and viability within the constructs, samples were analyzed with MTT mitochondrial activity assay at days 1, 3 and 7 [168]. Briefly, before the TEVG was fixed, three rings of approximately equal size (normalized by weight) were randomly sectioned from each construct and placed in the wells of a 96-well plate with 200 μl of serum free a-MEM and 20 μl of MTT solution (Sigma Aldrich, St. Louis, MO) and processed as described in **Section**

2.2.3. The number of contained cells was estimated by using a standard curve previously generated for known cell concentrations and by transforming absorbance to cell number using the equation generated by the slope of the curve. The average reading of the three rings was used as the result for each construct. Comparisons between groups (ascorbic acid supplemented and nonsupplemented constructs) were made by a two-tailed paired t-test and results were expressed as difference in cell number. Population doubling time (PDT) and number of population doublings (PD) were calculated from those values as: PD = log (cell number at day 3/cell number at day 1), PDT = time/PD.

Cells were characterized at day 0 (prior to seeding) and after 7 days of TEVG culture by flow cytometry for CD34 and Sca-1 expression. Briefly, TEVGs were incubated with 0.1% trypsin for 5 min to remove MDSCs from the scaffolds. The cells were then pelleted and blocked with 10% mouse serum for 15 min. Some cells were then labelled with rat anti-mouse Sca-1 (phycoerythrin (PE) anti-mouse Ly6A, 1 ml stock, 553336, Pharmingen, USA) and CD34 (biotinylated, 1 ml stock Purified Rat Anti-Mouse CD 34(1HC)) monoclonal antibodies for 15 min. The same proportion of cells were treated with equivalent amounts of isotype control antibodies PE-Mouse IgG 2b (33805X, Pharmingen, USA) and biotin purified Rat IgG (11021D, Pharmingen, USA). Both fractions were then washed with PBS and labelled with streptavidin–allophycocyanin (APC, 1:300, 13049A, Pharmingen, USA), 7-Amino-actinomycin D (7-ascorbic acid D), or Via-Probe (555816, Pharmingen, USA) to exclude non-viable cells from the analysis. Appropriate gating was performed to determine Sca-1 and CD34 expression via flow cytometry with a FACS Aria (Becton Dickinson, San Jose, CA). Cells at day 0 were processed following the same protocol, but without the need for removal from the scaffold.

Immunofluorescence was performed to corroborate Sca-1 expression and to assess myotube formation (fusion) by myosin heavy chain (MHC) expression. Briefly, frozen sections were obtained as described above and incubated with 0.1% Triton-X 100 in PBS for 10 min. Non-specific binding of antibodies was blocked by incubating the samples for 45 min with 5% normal donkey serum in PBS with 0.5% bovine serum albumin (Fraction V, Sigma-Aldrich, St. Louis, MO) and 0.15% glycine (Sigma- Aldrich, St. Louis, MO). Following this, the sections were incubated at room temperature with the primary antibodies (Sca-1 (1:500) and MHC (1:500) Sigma-Aldrich, St. Louis, MO) diluted in blocking solution for 60 min. Unbound primary antibody was removed by subsequent washes in PBS. Next, the samples were incubated with a Cy3-conjugated (Sigma-Aldrich, St. Louis, MO) secondary antibody (1:500) for 1 h at room temperature and then rinsed three times for 15 min with PBS. For nuclear visualization, cells were counter-stained with DAPI. The samples were then mounted in gelvatol and viewed under confocal microscopy using an Olympus F1000 confocal microscope. Positive controls were MDSCs cultured at high density for 7 days with low serum. Under these conditions, MDSCs undergo myogenic differentiation readily [169].

Uniaxial mechanical characterization and suture retention tests were performed on the seeded scaffolds following the same protocols described in **Section 4.2.5.2**.

5.1.2.2 Results

Immediately after seeding, nuclear staining showed a high number of cells inside the constructs. Distribution was qualitatively even along the length and across the entire thickness of the TEVG (**Figure 5.1-A**), confirming the results previously shown in **Section 2.2.3**. After 3 days of static culture, cells appeared to migrate from the center of the wall toward the inner and outer edges

during this timeframe (**Figure 5.1-B**). In contrast, the TEVGs cultured in dynamic conditions appeared completely populated with cells that were clearly spread throughout the scaffolds (**Figure 5.1-C**). Macroscopically, the scaffolds appeared to have a tissue-like aspect and texture (**Figure 5.2**).

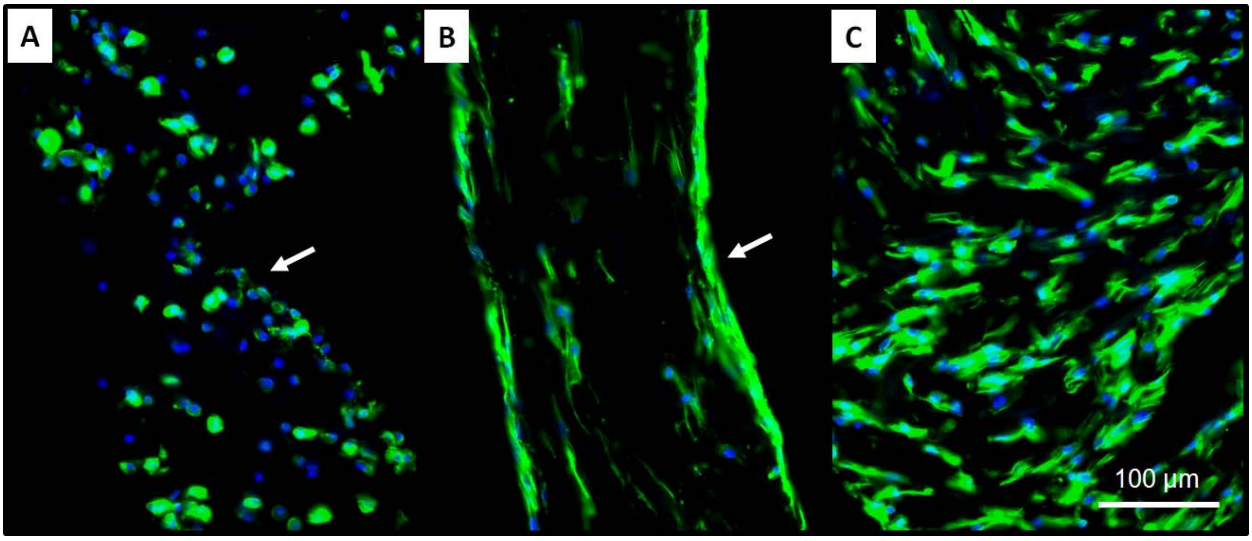

Figure 5.1 Representative microscopic aspect of MDSC-seeded TEVG. **A.** The constructs showed uniform transmural cellular distribution immediately after seeding. **B.** Appearance after 3 days of static culture showing cell accumulation at the edges of the polymer. **C.** Appearance after 3 days of culture in spinner flasks showing cell spreading throughout the wall thickness. Green = F-actin, blue = nuclei. The arrows, indicate the scaffold lumen. Image adapted from [54].

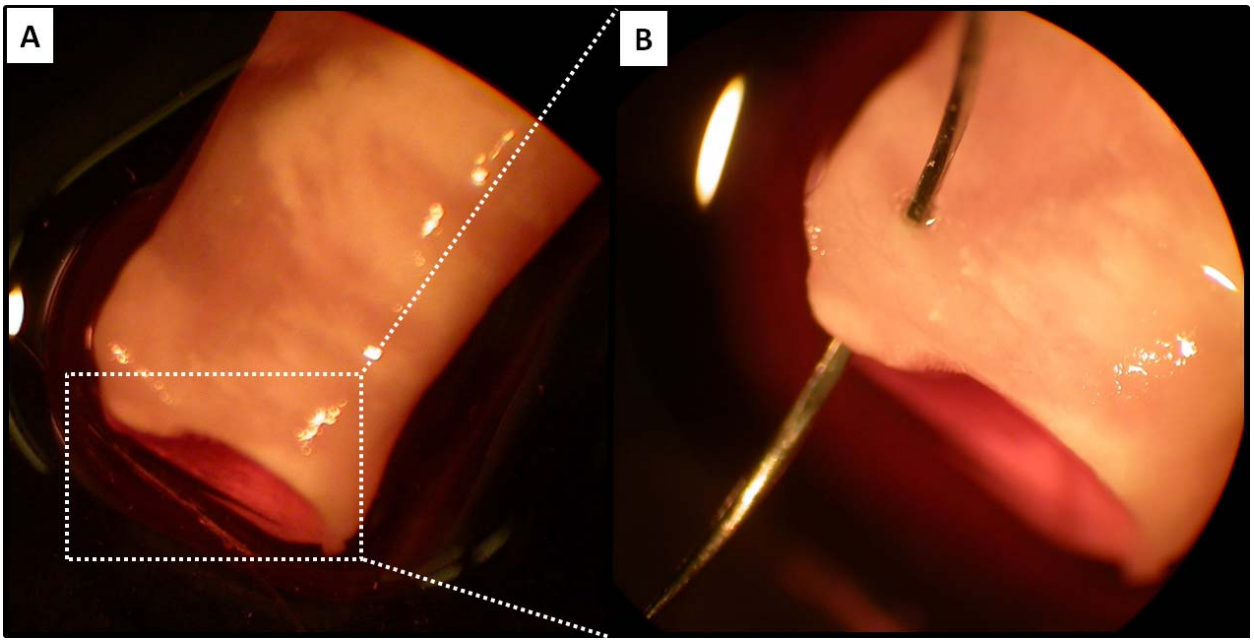

Figure 5.2 Representative macroscopic aspect of the TEVG after 3 days of dynamic culture. Image adapted from [54].

Proliferation analysis showed that the cells within the constructs supplemented with ascorbic acid in spinner flask culture exhibited a rapid proliferation, starting from $116\pm76x10^3$ cells/mg (cell number per weight of construct) at day 0 and reaching $491\pm145x10^3$ cells/mg at day 3 (n = 3) (**Figure 5.3** and **Figure 5.4**).

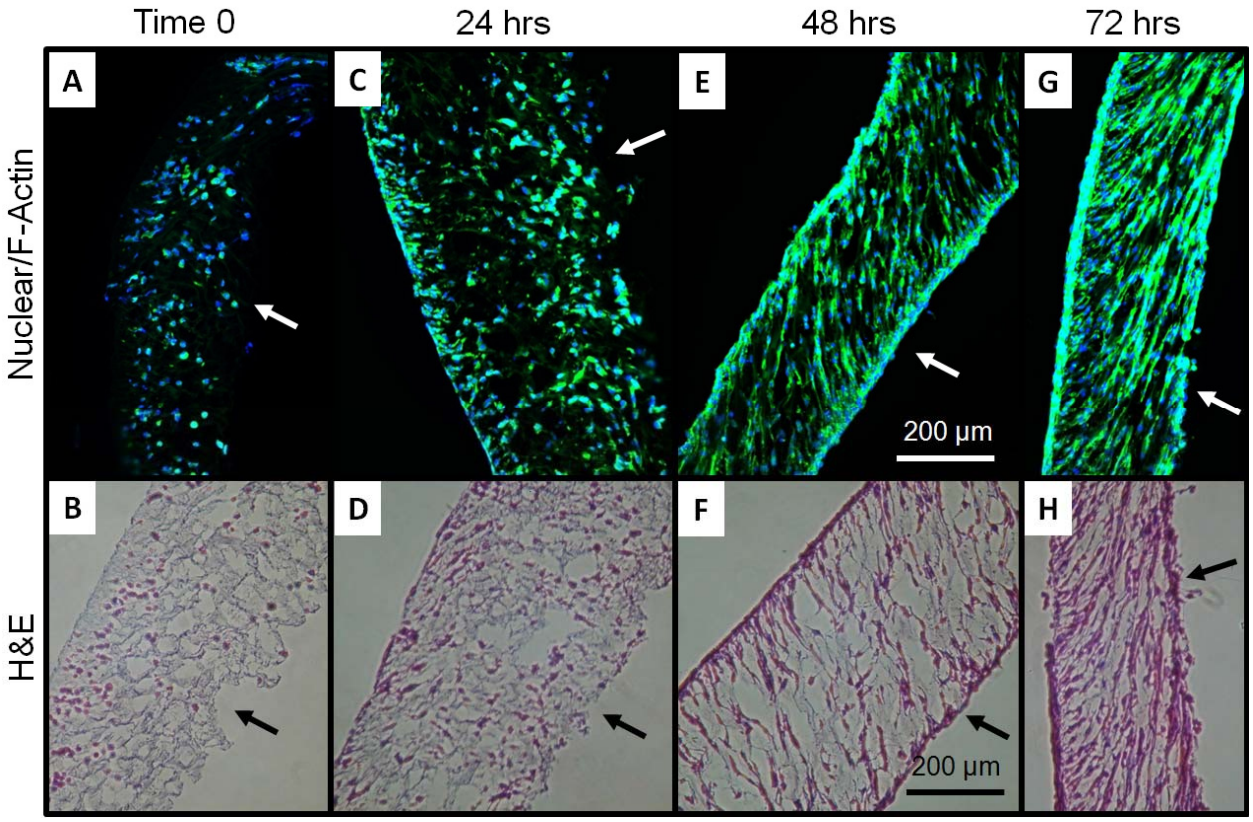

Figure 5.3 Representative nuclear/f-actin and H&E staining images showing cell proliferation over three days of dynamic culture. **A-B.** Immediately after seeding. **C-D.** After 24 hours of dynamic culture. **E-F.** After 48 hours of dynamic culture. **G-H.** After 72 hours of dynamic culture. Note how the constructs are now completely populated with cells. The arrows indicate the lumen of the scaffolds.

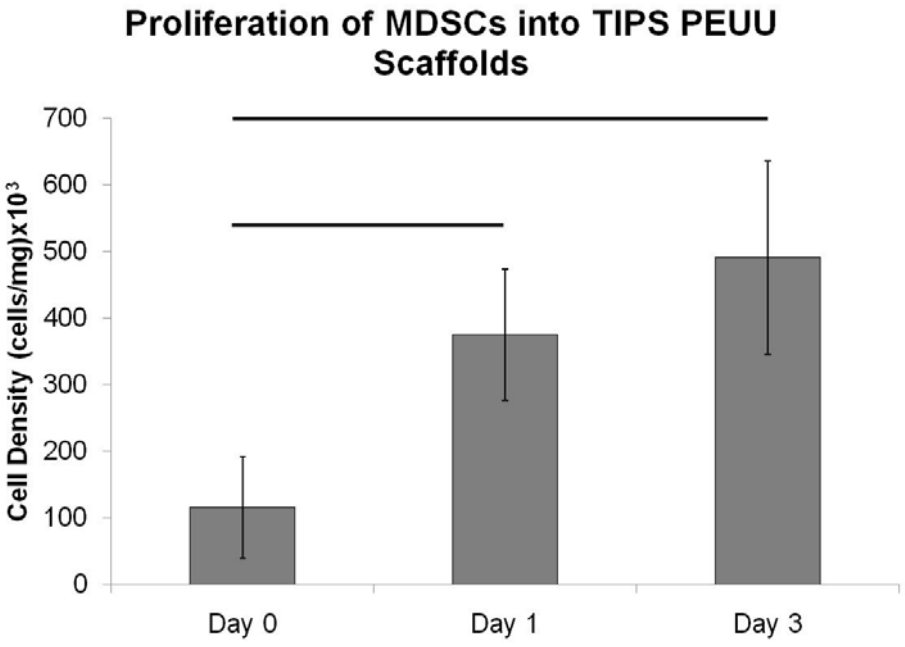

Figure 5.4 Quantification of cell proliferation following culture in spinner flasks. The bars indicate statistically significant difference between two groups ($p < 0.05$; Day 0: $n = 5$; Day 1: $n = 3$; Day 3: $n = 5$). Image adapted from [54].

The calculated number of PD was 2.1 while the PDT was 35 hours. A significant difference in proliferation was detected between the constructs supplemented with ascorbic acid and the non-supplemented controls. At day 1 the TEVGs supplemented with ascorbic acid had $174\pm30x10^3$ more cells/mg than those not supplemented ($p<0.05$; $n = 3$), and at day 3 the difference was $121\pm75x10^3$ cells/mg ($p<0.05$; $n = 5$) (**Figure 5.5**). The ascorbic acid supplemented TEVGs exhibited collagen production by day 7, while the non-supplemented constructs did not show any collagen production (**Figure 5.6**).

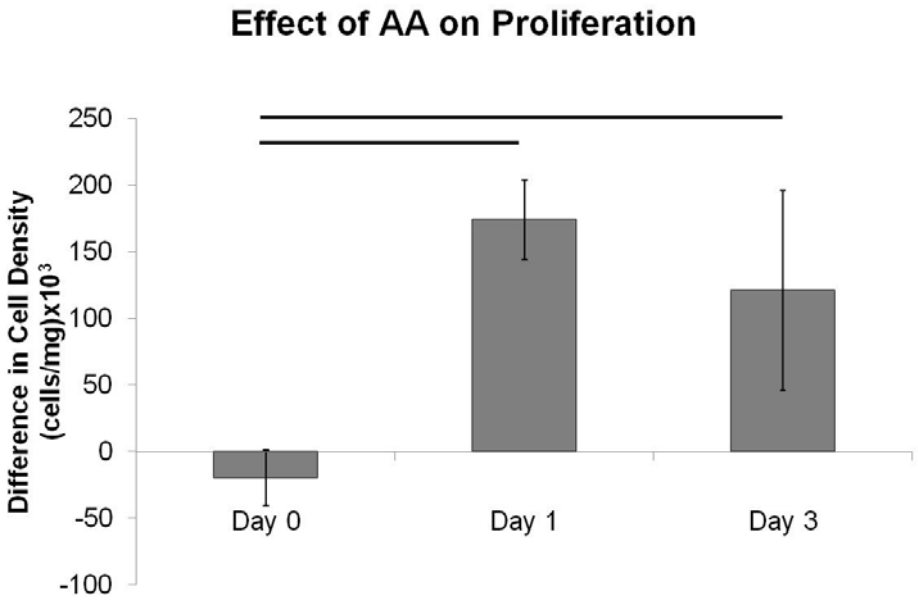

Figure 5.5 Quantification of effect of AA on cell proliferation following culture in spinner flasks. The values represent the differences in cell number between constructs supplemented with ascorbic acid and non-supplemented controls. The bars indicate statistically significant difference between two groups ($p < 0.05$; Day 0: $n = 5$; Day 1: $n = 3$; Day 3: $n = 5$). Image adapted from [54].

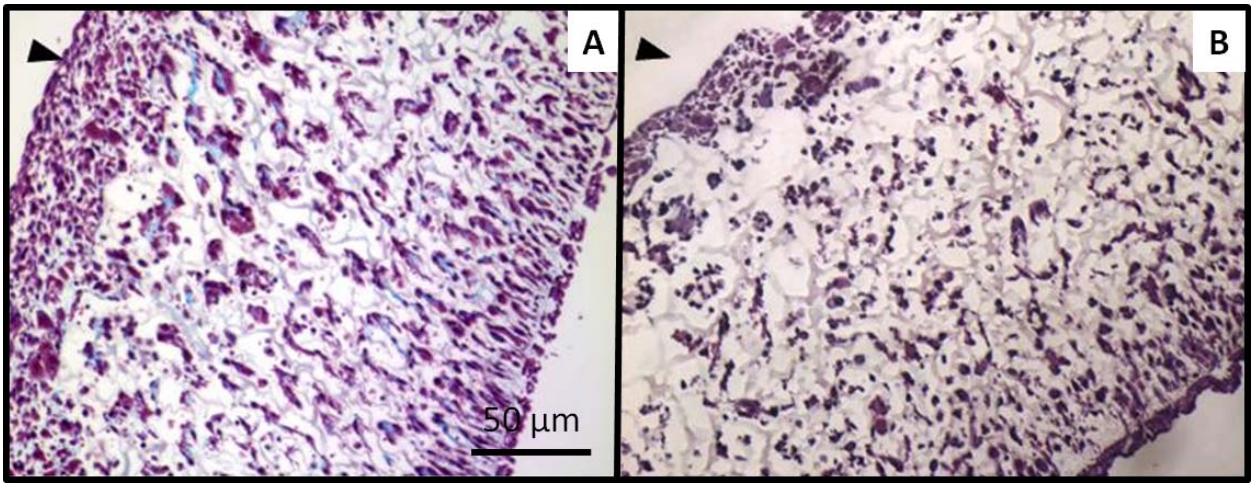

Figure 5.6 TEVG histology with Masson's trichrome. After 7 days, the constructs supplemented with ascorbic acid (**A**) had visible collagen deposition, differently from the controls (**B**) with no ascorbic acid. Blue = collagen, arrowheads indicate the lumen. Image adapted from [54].

The stem cell characterization at day 7 showed no significant difference in positive expression of Sca-1 in MDSCs compared to that at day 0 (77±20% compared to 66±6%, respectively; $p < 0.05$; $n = 3$). Initial CD34 expression level was 61±10%, while at 7 days it was 19±12% ($p < 0.011$; $n = 3$) (**Figure 5.7-A/B**). Sca-1 positive expression by immunofluorescence was consistent with the flow cytometry analysis (**Figure 5.7-C**). MHC expression was only scarcely noted in MDSCs after 7 days of culture (**Figure 5.7-D**).

Suture retention strength was measured to be 1.32±0.30 N ($n = 5$).

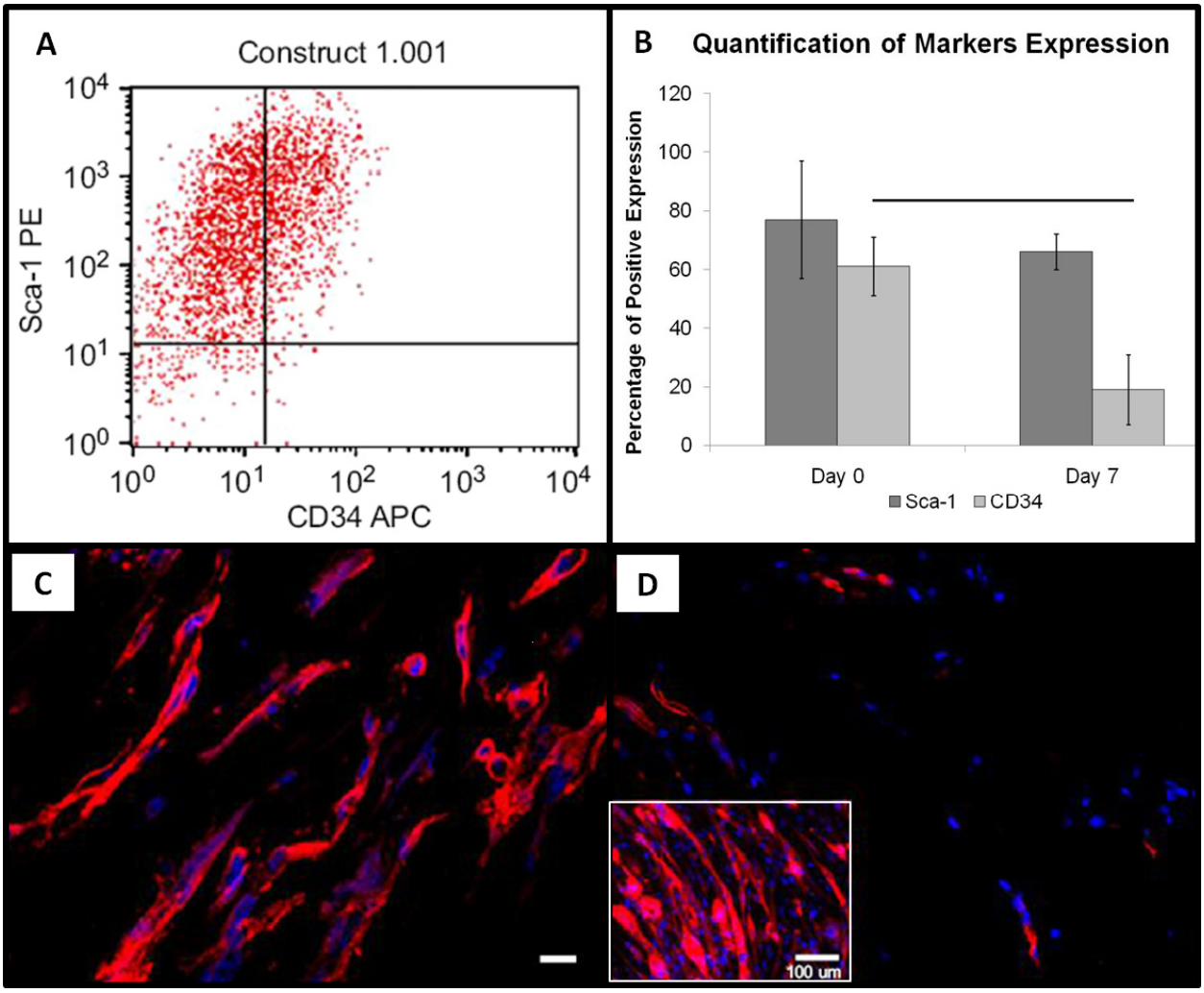

Figure 5.7 Stem cell characterization. **A.** Sca-1 and CD34 expression measured by flow cytometry. **B.** Sca-1 remained high and unchanged while CD34 expression was decreased ($p = 0.011$; $n = 3$) after 7 days in culture. **C.** Sca-1 expression was confirmed by immunofluorescence. Red = Sca-1, blue = nuclei, scale bar = 10 μm. **D.** MHC expression was scarce, suggesting a low incidence of fusion and myotube formation. Positive control (inset) shows myotube formation of monolayer MDSCs. Red = MHC, blue = nuclei. Image adapted from [54].

5.1.2.3 Discussion

In this acute (3-7 days) assessment of cell-scaffold interactions, it was demonstrated that following seeding via the RVSD, cells were able to proliferate and populate the polymer scaffold while in dynamic culture (**Figure 5.1**), retaining their stem cell features (**Figure 5.7**) and producing collagen when stimulated with ascorbic acid (**Figure 5.6**). The seeding procedure was completed in minutes and the scaffolds were fully populated with healthy-looking cells within 3 days (**Figure 5.4**). Collagen deposits were evidenced after 7 days (**Figure 5.6**), demonstrating initial secretion of ECM. With these premises, this approach, as opposed to a completely cellular-based approach requiring months to obtain an implantable engineered blood vessel [32], would allow the TEVG to be implanted shortly after seeding, provided that the cells are incorporated successfully and that the scaffold is mechanically sound to withstand arterial circulation.

While the mechanical properties of the TIPS PEUU scaffolds, are in some aspects similar to those of native arterial vessels (*e.g.*, STF (**Figure 4.15**), elastic modulus (**Figure 4.17**), and suture retention (**Figure 4.20**)), the strength of the material might not be ideal for vascular applications as seen in **Figure 4.13**. This concern was confirmed by the initial *in vivo* studies in which the TIPS PEUU scaffolds were associated with aneurysm formation and failure (this will be described in detail in **Chapter 6**). However, the high porosity and pore interconnectivity of the TIPS PEUU scaffolds are believed to play an important role in the observed cellular proliferation and spreading, and might constitute a critical feature for the development of a TEVG. The development of the ES-TIPS scaffold (**Section 4.2**) was highly driven by these considerations.

The behavior of the MDSCs incorporated into the PEUU scaffolds was consistent with the high proliferative features described in 2D culture [167]. The values for Sca-1 and CD34 expression in monolayer are similar to previous reports [99, 169, 170]. However, this is the first report to characterize the cells for their expression of CD34 and Sca-1 in a 3D environment. The observation that MDSCs maintain Sca-1 (**Figure 5.7**) suggests that these cells maintain their stem cell phenotype throughout the seeding and culture process. CD34 is a surface glycoprotein which functions in hematopoiesis and hematopoietic cell adhesion [171, 172]. The role of CD34 expression in MDSC function has not been fully elucidated [167, 173], although this marker is routinely used to characterize MDSCs [174, 175]. A possible speculation regarding the loss of CD34 expression (**Figure 5.7-B**) following cell incorporation in a TEVG could be related to a change in the cell adhesion characteristics due to a 3D environment (scaffold pores). Furthermore, in another type of muscle stem cell, it has been shown that CD34 varies with the activation state of the cell [176]. The scarce expression of MHC noted after 7 days (**Figure 5.7-D**) suggests that cells are not forming myotubes, as shown in the positive controls, indicating that spontaneous differentiation to myogenic lineage is not occurring. Maintaining the stem cell phenotype during culture is desired in order to profit from the compelling regenerative capabilities of the cells when exposed to the actual vascular environment upon implantation. The performance of MDSCs within the TIPS PEUU scaffolds described in this section adds to their previously reported potential in cell transplantation, making them an attractive source for vascular tissue engineering and confirming them as a cell type of choice for our approach.

It is widely accepted that a successful TEVG will require dymanic culture conditions [40, 177] due to the need for increased nutrient transfer inside the walls of the scaffold compared to static culture. Indeed, this possibly explains the cell migration toward the edges, which was

observed in the controls of the current study (**Figure 5.1-B**). Several studies have utilized perfusion bioreactors to overcome this problem and to provide the TEVG with a more realistic mechanical environment, which is also thought to be important to drive the cells into the desired phenotypic lineage [75, 127, 128, 178]. We have demonstrated in this section that spinner flask culture has the ability to increase nutrient transfer inside a 2-cm long TEVG while maintaining the simplicity of a standard culture method, making it more attractive for clinical applications, where the set-up of a complex bioreactor might represent a limiting factor. However, this simple bioreactor setup might not be suitable for longer constructs, where the need for a coherent media flow inside the lumen of the TEVG is necessary to provide uniform nutrient transport. Therefore, longer scaffolds will require a modification of the culture system in order to achieve the same nutrient transfer observed in the experiments described in this section. The development and testing of such system will be described in **Section 5.3.**

5.2 BIOLOGICAL ANALYSIS OF RAT MDSCS INCORPORATED INTO ES-TIPS PEUU SCAFFOLDS AND CULTURED *IN VITRO*

5.2.1 Considerations toward species-specific *in vitro* studies in preparation for animal studies

In the previous section an extensive *in vitro* characterization of cell/scaffold interaction was provided for murine MDSCs. These studies were designed to test a spectrum of endpoints comprehensively including viability, proliferation, matrix deposition, and phenotype for a well characterized type of MDSCs such as the murine one. In order to translate the performed

analysis toward *in vivo* studies (**Chapter 6**), it was necessary to replicate part of the endpoints performed for murine cells with species-specific cells for each model of interest. Providing a phenotypic analysis before and after a very short *in vitro* culture period was considered to be beyond the scope of the current dissertation. Therefore, it was decided, for the sake of time and feasibility, to focus on the most critical aspects of cell/scaffold interactions: first, the capacity of species-specific cell incorporation into the designated scaffold of interest, and second, the ability of the incorporated cells to proliferate and populate the matrix in a short amount of time. A densely cellularized scaffold was considered the premise for implantation.

5.2.2 Incorporation and dynamic culture of rat MDSCs into ES-TIPS scaffolds

5.2.2.1 Methods

MDSCs were isolated from striated muscle biopsies of Lewis rats by means of a previously described pre-plating technique [99]. The cells were then transfected with the LacZ reporter gene following a previously described method [100]. Briefly, a plasmid encoding for the β-galactosidase (LacZ), minidystrophin and the neomycin resistance gene was transfected for 24 hours using the lipofectamine reagent (GIBCO BRL) according to the manufacturer's instructions. The transfection was made to be consistent with the future *in vivo* implantation in Lewis rats (see **Section 6.1.1**) ruling out the possibility of a cell behavioral change as a result of the transfection. Cells were then plated, cultured, and expanded (as described in **Section 5.1.2**). Before seeding, rat MDSCs were trypsinized and put in suspension as described in **Section 5.1.2** and prepared to the desired concentration in preparation for seeding.

The cells were seeded into ID-1.3 ES-TIPS PEUU scaffolds (length = 1 cm) prepared as previously described in **Section 4.2.2**. The number of cells and seeding parameters used were consistent with that previously described in **Section 4.2.6**. Briefly, $3x10^6$ LacZ+ rat MDSCs suspended in 5 mL of complete culture media (as described in **Section 2.2.3**) were seeded into each scaffold via the RVSD (a total of 9 ES-TIPS PEUU scaffolds were seeded).

Immediately after seeding, TEVGs were cultured in static conditions at 37°C in standard incubators for 2 hours and then placed into spinner flasks at 15 rpm for 7 days. Three constructs were fixed and processed for F-actin and nuclear staining (as explained in **Section 2.2.3**) immediately after the 2 hours of static culture. An additional three constructs were removed from spinner flask after 3 days of dynamic culture and processed identically. Finally the last three constructs were processed in the same manner after 7 days. The cell density, proliferation, and spreading into the ES-TIPS scaffold were quantified via an image-based technique. In particular, nuclear staining images were taken at 10x and processed with the ImageJ software. Grayscale images were thresholded and subsequently processed with a watershed filter to indentify and separate overlapping nuclei. The number of nuclei was automatically counted with a particle count function. The cell density was obtained by dividing the measured scaffold area by the counted number of nuclei. Cell spreading was quantified by measuring the area of F-actin staining and dividing it by the number of counted nuclei in each image. The F-actin area was obtained by threshholding images obtained with the FITC filter and by measuring the resulting total area. Merged images were used to evaluate the results qualitatively at each time point. Statistical analysis was performed consistently with that described in **Section 4.2.3**.

5.2.2.2 Results and discussion

The 1.3-ID ES-TIPS scaffolds were highly cellularized immediately after seeding (**Figure 5.8-A**), confirming the results previously obtained with the same cell type and scaffold (**Figure 4.29-B**). After 3 days of dynamic culture, the constructs had a significant reduction in cell number followed by a non-significant variation at 7 days (**Figure 5.8-B/C**, and **Figure 5.9**). After 3 and 7 days it was possible to notice, in some luminal areas, multilayered accumulations of cells, eventually detaching from the TEVGs during dynamic culture (**Figure 5.8-C**). These results provide insights about the reduction in cell number detected after the achievement of cell confluency into the scaffolds, suggesting cell migration toward areas with higher nutrient concentration (*e.g.*, the lumen).

A set of experiments was performed to understand the role of the initial seeding density on the maturation time of the TEVG (data not shown). In those experiments it was noted that by increasing the initial cell number during the seeding process, the time required for obtaining cell confluency was reduced (Note: the concept of confluency in a 3D environment is here intended as complete cell coverage detected retrospectively with any cytoskeletal markers within histological assessment; an example of 3D scaffold confluency is shown in **Figure 5.3-G/H**). Upon achievement of confluency, cells migrated toward areas of increased nutrient concentration (likely due to nutrient competition) and ultimately fell off the constructs, leading to reduced cell densities. Based on those results is was concluded that using 3 million cells as the initial concentration and a period of three days of dynamic culture exceeded the ideal "maturation" time leading to cellular loss. Therefore, it was established that the ideal *in vitro* culture period prior to *in vivo* implantation (see **Section 6.1.1**), when seeding $3x10^6$ into 1.3-ID ES-TIPS scaffolds should have been less than 3 days (*e.g.*, 24-48 hours following seeding).

The spreading quantification over 7 days of dynamic culture showed a positive trend, though not significant (**Figure 5.10**). This result is consistent with cell adhesion and partial spreading into the 3D pores of the scaffold. An important insight learned from this and some unrelated experiments (data not shown) was that the TIPS PEUU porous structure is supportive of proliferation, as seen extensively in **Section 5.1.2**, but it might hamper the free cell rearrangement including full spreading, and more importantly cell alignment. This is caused by the spongy-like, though interconnected, porous matrix of the TIPS PEUU scaffolds, which results in the presence of physical polymer walls between pores, avoiding cell penetration.

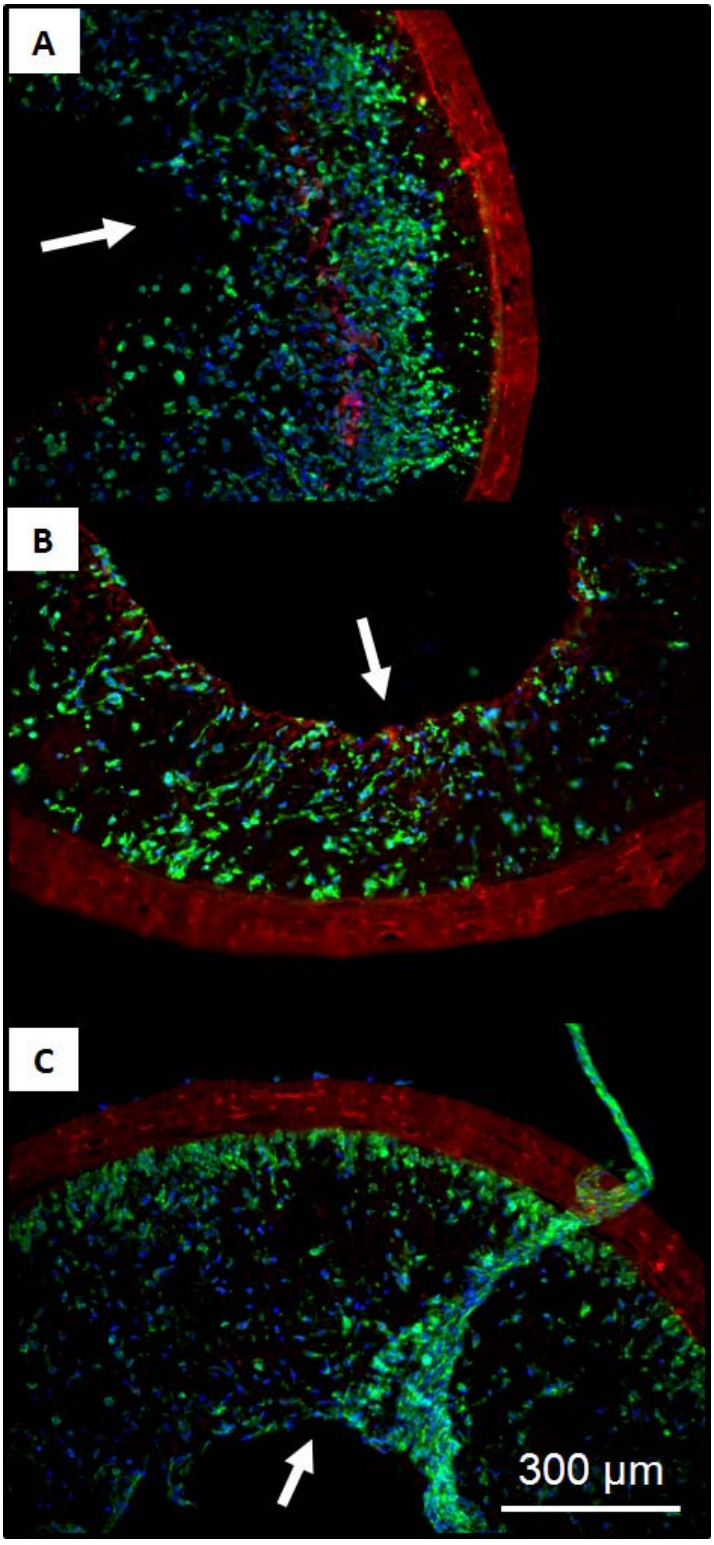

Figure 5.8 Representative qualitative results of rat MDSC-incorporated ES-TIPS PEUU scaffolds. **A.** Results after 2 hours of static culture. **B.** Results after 3 days of dynamic culture. **C.** Results after 7 days of dynamic culture. The arrows indicate the luminal surface. Blue = nuclei, green = F-actin, red = scaffold. Images taken at 100X.

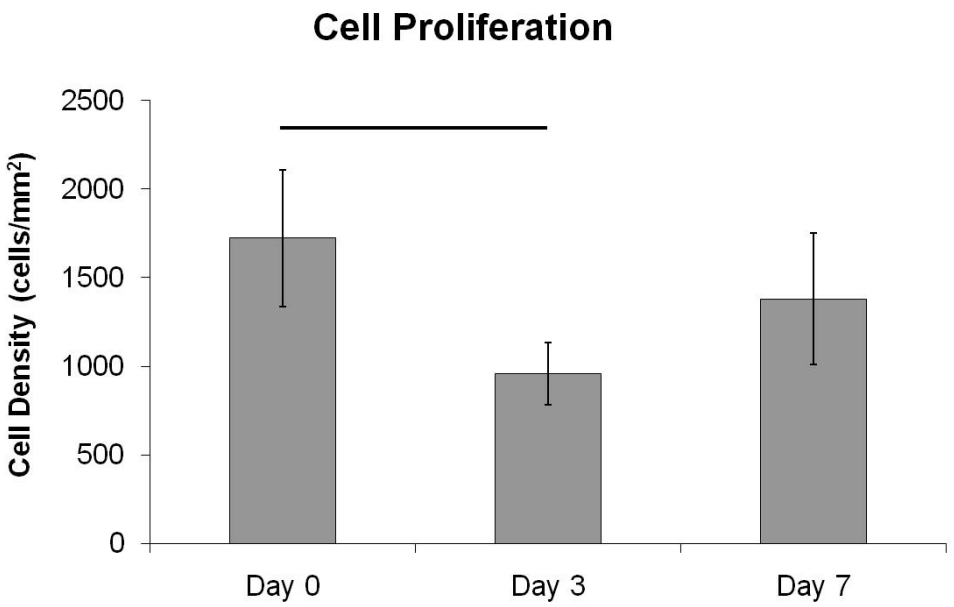

Figure 5.9 Quantification of rat MDSC density into ES-TIPS PEUU scaffolds at different time points. The bar indicates statistically significant difference between two groups ($p < 0.05$; $n = 3$); all the other comparisons are not statistically significant.

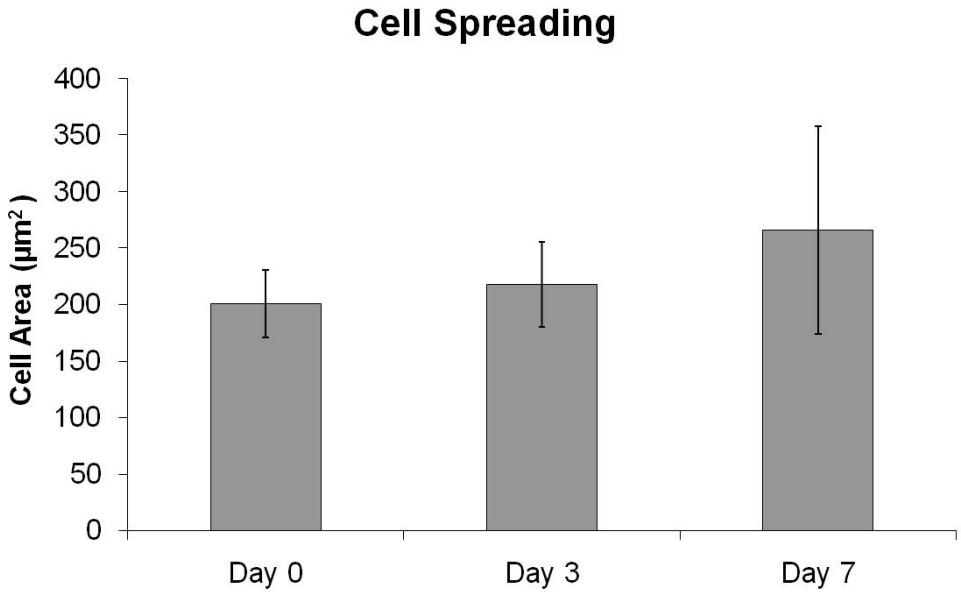

Figure 5.10 Cell spreading (intended as average area positive for F-actin for each cell) at different time points. None of the differences are statistically significant ($n = 3$).

5.3 DEVELOPMENT OF A NOVEL BIOREACTOR FOR TISSUE-ENGINEERED TUBULAR CONSTRUCTS: THE PERFUSER

Described in **Sections 5.1.2** and **5.2.2** was the dynamic culture of TEVGs using spinner flask bioreactors in order to improve nutrient transport to the constructs via convection. With this technique, cells were able to spread and populate the constructs within three days without compromising their stem cell phenotype. However, these culture conditions are likely to be suitable only for small *L/ID* ratios (*L/ID* for the TEVGs described in **Section 5.1.2** was approximately 5, while that for those described in **Section 5.2.2** was approximately equal to 6). Longer constructs (*L/ID* > 8) are likely to receive a poor amount of nutrients in their central region compared to the end regions, and this could lead to inhomogeneous tissue development. This potential issue is confounded by the folding of the tubular scaffolds following placement in the rotational fluid dynamic field of the spinner flask. Therefore, media has little chance of reaching the entire lumen during culture in spinner flasks. With this in mind, a novel, cost-effective bioreactor was designed in order to homogeneously perfuse tubular constructs by creating a continuous flow of media into their lumen.

5.3.1 Design principles

The main design specification for the bioreactor was the creation of a controllable, continuous flow into tubular scaffolds without generation of relevant intraluminal pressures. This feature

was required to create a continuous turnover of nutrients along the entire length of the scaffolds, which is paramount to cell survival, attachment, and proliferation in the delicate phase immediately following cell seeding. Upon incorporation of cells into the scaffolds via the seeding devices (see **Chapters 2** and **3**), cells are essentially passively suspended in culture media within the scaffold pores, and it is necessary to provide nutrient transport without generating forces that could flush them away from the scaffold before an initial attachment can be achieved. Another design specification was the compatibility in size with a standard incubator. This specification allows for a considerable reduction in complexity and variability compared to a need for temperature and pH control by simply being exposed to the incubator environment. Finally, another important feature being sought was cost-effectiveness. Complex bioreactors for vascular applications usually require very expensive components to perfuse tubular structures (*e.g.*, centrifugal or roller pumps) and measure and control the flow rate (*e.g.*, ultrasonic flowmeters and resistors) which are incompatible with easy clinical translation. The device should also allow for independent experiments by separating completely the culture environment for each TEVG, and have a limited culture media volume to reduce the costs associated with the use of expensive culture reagents.

To meet these requirements a modification of the simple spinner flask design was proposed, utilizing the concept of a wind sock in an inverted fashion. Wind socks are normally used in aviation to detect wind direction and strength by allowing a tapered fabric tube to rotate on a hinge and spontaneously align with the direction of the wind. The tapered shape is used to enhance the inlet flow rate (by increasing the inflow area) and to progressively increase the internal air velocity proceeding further into the conical geometry until the outlet (in which it reaches the maximum air flow velocity). This phenomenon allows for a horizontal placement

(lifting effect) of the sock against the gravity due to a net reduction of the internal pressure (induced by the increased internal velocity according to Bernoulli's law).

If the relative velocity of the two components (wind and wind sock) is inverted (*i.e.*, moving the sock against a static volume of fluid) the result will be intuitively the same: the sock will have an internal fluid flow and will undergo the same lifting effect (**Figure 5.11**). We can utilize this concept by connecting a tubular conduit (TEVG) at the end of the sock and moving the system with a linear velocity *v* within the liquid (cell culture media). The resulting internal flow generated by the movement of the sock will have an inflow velocity of approximately *v* as well, and it will continue its path inside the downstream conduit, "perfusing" the conduit itself . This is the basic concept utilized in the design of the Perfuser.

The natural following step was to eliminate the space-requirement from this design principle involving the need of continuous, linear movement into a fluid. This could be accomplished by making the movement itself periodical (*i.e.*, rotational). The simple spinner flask design is suitable to serve this purpose by performing some simple modifications (described in **Section 5.3.2**). Spinner flasks are ideal bioreactors for a number of applications due to their simplicity, cost-effectiveness, low-maintenance, and functionality, and they are an ideal candidate to comply with the required design specifications of this project. Spinner flasks are also ideal for performing independent experiments (more flasks can be used contemporarily), and require a limited amount of cell culture media for their functioning.

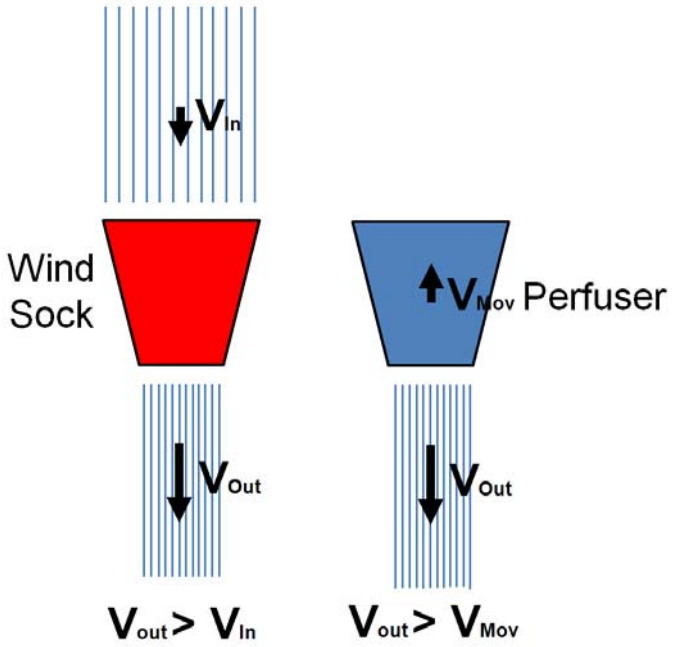

Figure 5.11 Analogy of the Perfuser principle (right) to the wind sock (left). V_{In} represents the velocity of the wind entering the wind sock. V_{Out} is the outflow velocity (increased by the tapered shape of the wind sock). If the Perfuser is moved with velocity $V_{Mov} = V_{in}$ in a static environment filled with air, the resulting outflow velocity should be the same as V_{Out}.

A system able to create the wind sock effect by taking advantage of the rotation provided by the internal rotating body of a spinner flask was the key concept in the design of the Perfuser. However, one important aspect to consider while utilizing a rotational velocity around a pivot was the relative velocity. This conceptual system, rotating inside an enclosed space such as the spinner flask, will likely create a circular, whirpool motion of the surrounding fluid, reducing the relative velocity between the wind sock and the rotating fluid leading to reduction/loss of relative velocity and thus net effective flow inside the sock. Therefore, it was important to design the rotating body in a hydrodynamically-efficient fashion to reduce the perturbation of the flow created by the rotating components, while maximizing the internal perfusion. The presence of a

neck in the spinner flask glass containers suggested the design of a geometrically-variable system able to retract while being inserted through the neck of the bottle and expand in a controllable fashion once needed. It was also necessary to provide each spinner flask with the capability of perfusing two TEVGs at the same time instead of one. This was implemented to allow the culture of each TEVG with a backup construct for the prospective large animal studies planned (**Chapter 7**).

5.3.2 Fabrication of the device

Commercially available 500 mL spinner flasks (196580575, Bellco Glass Inc, NJ) were completely unmounted in their basic components including a glass bottle, a central vertical PTFE stem with internal glass tube, a PTFE-coated magnetic bar and, a PTFE paddlewheel. An assembly (Perfuser system) formed by five components was fabricated for each spinner flask used (**Figure 5.12**). Custom-made components were designed and drawn via Solidworks 2005 software (Solidworks Corp., Concord, MA). Drawings are included in **APPENDIX A**.

In particular, the Perfuser system consisted of a cylindrical cuff made of Delrin® (external diameter = 3 cm, internal diameter = 1.6 cm, thickness = 1 cm, **Figure A.24**) allowing for a connection with the spinner flask stem, two arms, and two plugs acting as wind socks. The cuff was provided with two opposite rectangular slots to host foldable arms. Each arm (length = 2.5 cm, width = 1 cm, thickness = 3 mm, **Figure A.25**) was made of Delrin® and was provided with hydrodynamically-efficient lateral profiles (rounded) on their long edges, designed to avoid fluid perturbation while rotating within the fluid. Each arm was coupled with the cuff via SS pins (hinges) allowing for variable angle orientation between the arms and the cuff. Both hinges were

provided with small custom-made SS hinge springs working in a self-opening configuration (*i.e.*, when unconstrained, both arms extend fully, reaching a mutual angle of 180º). On top of the two hinges, two small SS screws were inserted vertically through the wall of the cuff reaching the wall of each arm. By modifying the depth of each screw it was possible to regulate precisely the maximum angle of the arm with respect to the cuff by defining the upper limit for the extension of the arm induced by the spring.

Distally from the cuff, each arm was connected via a hinge to a Delrin® plug designed to take advantage of the wind sock effect (**Figure A.26**). Each plug was made from a solid cylinder of material, and oriented in order to generate internal flow by rotating in a clockwise direction. A conical cavity (maximum internal diameter = 1 cm) was machined throughout its longitudinal axis and a bore was drilled to create a channel (ID = 3 mm) in the distal end of the plug. All edges were made rounded and smooth, again for minimizing the creation of a rotational flow inside the flask. On the back of the external wall of the plug, some material was removed via a lathe until an attachment tee with external diameter of 4.7 mm was created. The tee was provided with several circumferential grooves to allow for a secure ligation of the TEVG.

The Perfuser assembly was then connected to the PTFE vertical stem of the spinner flask by sliding the cuff onto the stem and tightening a SS set screw to secure the cuff at the desired height (~ 6 cm from the bottom of the stem; **Figure 5.12**). The original Teflon-coated stirrer bar was replaced with a longer one (Fisher Scientific) (shape = octagonal, diameter = 1 cm, length = 5.4 cm) to increase the torque transmitted to the rotating body inside the spinner flask. The original paddlewheel was discarded as its use would tend to generate rotational velocity in the fluid field.

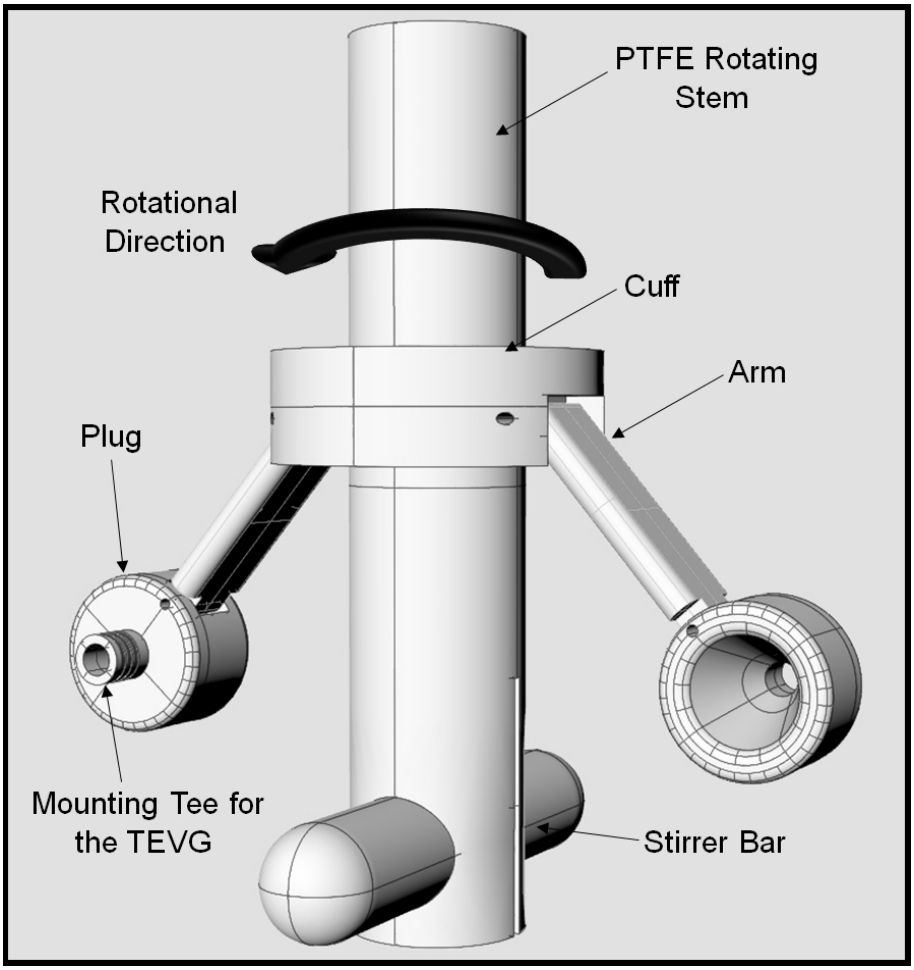

Figure 5.12 3D model of the Perfuser illustrating the major components of the device.

The rotating Teflon and glass stem is reconnected to the cap of the spinner flask and the assembly inserted into the spinner flask glass container. To insert the assembly, the arms and plugs are temporarily retracted, reducing the angle between the arms and the stem, thereby reducing the radial dimension of the assembly. The angle between the arm and the stem was set in order to have the plug positioned at approximately 2 mm (*i.e.,* minimum geometrical clearance to allow unconstrained rotation) from the interior wall of the glass. As a result, the radial distance between the centerline of the central PTFE stem and the longitudinal axis of the Perfuser plug was approximately 2.9 cm. The rotation of the Perfuser internal rotor was obtained by a precision multi-plate magnetic stirrer platform (D2005 Stirrer, BELLCO Biotechnology) which communicates the torque via magnets across the glass container of the spinner flask.

5.3.3 Performance and flow visualization

Once the Perfuser prototype was developed, it was necessary to demonstrate the consistency between the expected behavior of the Perfuser and the actual one via a validation process. To this end, a series of experiments was performed to show effective functioning of the device and to characterize the fluid dynamics inside the spinner chamber and the forces involved with the operation of the device.

The first experiment was designed to verify the absence of issues related to the movement of the internal rotating system with the attached TEVG scaffolds. Two 5 cm-long ID-4.7 TIPS PEUU scaffolds were ligated with a single 4-0 silk suture to the tees of the Perfuser. The system was then filled with 250 mL of water and put in rotation at different rotational speeds. The system was able to rotate smoothly over a range of rotational speeds between 8 and 200 rpm.

Slower rates were characterized by loss of fluidity in the movement while higher speeds caused the rotating body to freeze, falling out of phase with the underneath driving rotating magnet. The scaffold followed the curvature of the internal glass wall while rotating, as expected. No kinks or entanglements were detected in the scaffolds.

The second experiment was performed to demonstrate flow inside the tubular scaffolds during the Perfuser operation. To this end, the rotating body, including the PTFE stem and the Perfuser assembly, was coupled with an ink reservoir formed by a 1.6 microcentrifuge tube (with the cap-end cut off) and a capillary tube (see **Figure 5.13-A**). The reservoir was connected via transparent tape to the PTFE stem approximately 2 cm higher than the Perfuser cuff, and about 5.5 cm higher than the centerline of the plug. On the bottom of the tube a small hole was drilled and a small polypropylene capillary tube (Intramedic) was pressure fit into it by pulling a silk suture previously knotted to the tube. The capillary tube was aligned with the rounded edge of the Perfuser arm and secured to it with transparent tape in order to cross the centerline of the underneath Perfuser plug. The capillary tube was cut slightly before the center of the plug to allow for release of dye just in front of the plug. Two PTFE vascular grafts (length = 6 cm, ID = 6 mm ID, *L/ID* = 10) (W. L. Gore & Associates, Inc., Flagstaff, AZ) were connected to the Perfuser plugs for the purposes of flow visualization testing (**Figure 5.13-A**). The hydrophilic nature of the PEUU scaffolds was not ideal for testing purposes due to a consistent absorption of ink (data not shown) causing loss of the contrast necessary for testing.

The reservoir was filled with a CDI tissue marking dye (Cancer Diagnostics, Inc., Birmingham, MI) and the rotating portion of the Perfuser was rapidly inserted into the glass container of the spinner flask and rotated at 12 rpm. A sequence of pictures was taken with a SLR camera (Canon 40D) provided with a macro lens (28 mm USM Canon) at the rate of 6

pictures per second and with a shutter speed of 1/2500 sec and an aperture of 4.5 to capture qualitatively the ink released by entering the plug and leaving the scaffold.

The images clearly show the path of the dye entering the Perfuser plug (**Figure 5.13-B**), and exiting the scaffold (**Figure 5.13-C**), confirming the generation of flow inside the conduit. After interruption of the rotation the dye was again released, but this time it fell vertically to the bottom of the glass container (**Figure 5.13-B**). **Figure 5.14** shows a photo sequence capturing a half of a revolution during the Perfuser testing.

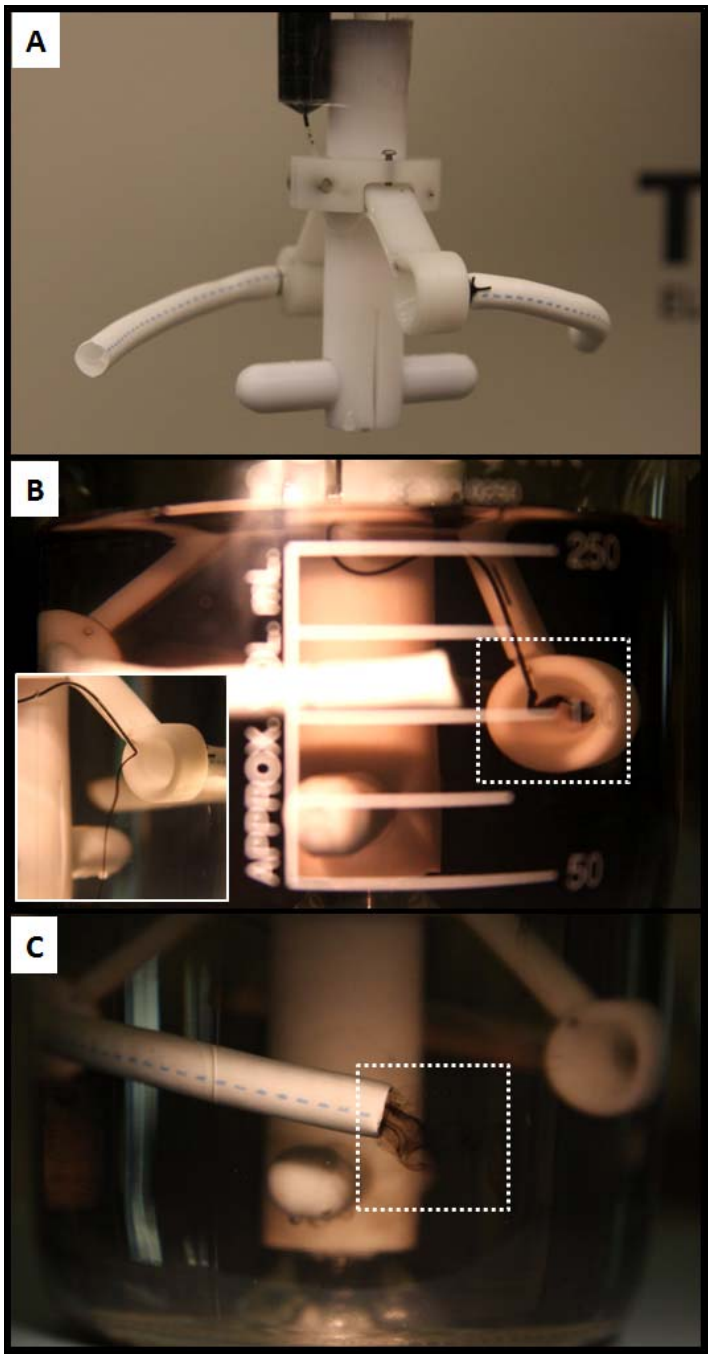

Figure 5.13 Testing of the Perfuser. **A.** Modification of the Perfuser by an ink releasing system composed by a small cylindrical reservoir and a capillary tube slowly infusing dye in the center of the Perfuser plug. **B.** Image demonstrating flow within the inlet of the plug (dashed box) while spinning at 12 rpm and after the rotation was halted (inset). **C.** Image of the distal tip of a conduit showing outflow of ink (dashed square) confirming the establishment of flow inside the tubular scaffold.

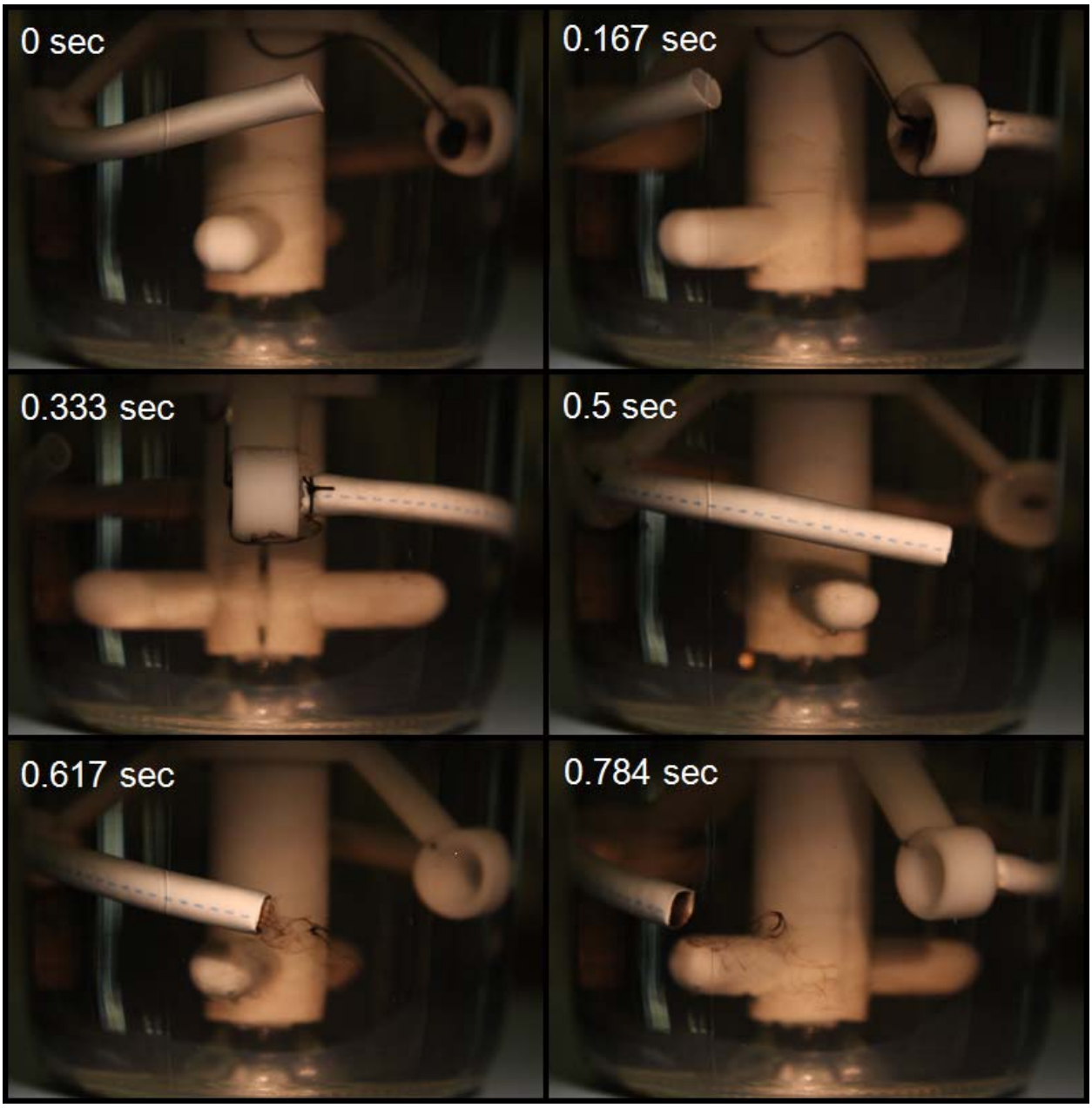

Figure 5.14 Perfuser testing: photo-sequence of the dye release over approximately a half of a revolution.

After this qualitative assessment of flow was completed, some additional testing was performed to quantify the flow performance of the system. To this end, a machine vision system – comprising of a high/resolution camera (A504K, Basler AG, Ahrensburg, Germany) mounted with a Telecentric 55 mm lens and a 2x converter (Computar TEC-M55, CBC (AMERICA) Corp., Commack, NY), and a XCap acquisition board and software (Epix, Inc., Buffalo Grove, IL) – was used with a high-performance machine (System: XP 64, Processor: Intel Xeon, memory: 6 Gb).

High-speed (500 fps), high-resolution (1280x1024 pixels) videos of the Perfuser were acquired at different rotational speeds using the same dye releasing system and dye described above. The exposure time for each frame was 2 msec, and the aperture of the lens was set to 2.8. The camera was oriented perpendicularly to the glass container and was focused on the centerline of the rotating plug to capture the tangential component of velocity of the released dye into the plug during rotations at different rotational speeds (12, 20, 43, 62, and 83 rpm). The system was illuminated by two opposite Fiber-Lite high intensity illuminators (Dolan-Jenner Industries, Boxborough, MA). A sheet of white paper was placed between each light source and the glass container to increase the diffusion of the light avoiding glass reflections. Each video was processed with the Xcap software to retrieve two snap shots depicting arbitrary initial and final positions of the plug during its motion. The pair of images for each rotational velocity were stored and processed with ImageJ to measure the horizontal distance between an arbitrary, recognizable feature in the dye flow (*i.e.*, a curl) and the edge of the plug inlet (**Figure 5.15**).

The measure of distance was corrected taking into account the error introduced by the phenomenon of parallax. This effect is defined as an apparent change in an object's position (in this case the measured distance) due to a change in the observer's position, or equivalently due to

a movement of the observed object. In this case the camera was the observer, while the plug and dye were the observed objects changing positions. The nontrivial model used to perform this optical correction is described in **APPENDIX F**. By measuring the number of frames between the initial and the final snap shot and by measuring the variation in corrected distance between the moving plug and the released dye, it was possible to quantify the relative velocity between the dye and the plug. The measured relative velocity was used to quantify the flow rate entering into the front cone of the plug (and therefore the perfused conduit) by simply multiplying the measured velocity by the known inlet area of the plug. This method is justified also in the case of a rotational velocity field such as the one generated into the Perfuser. In fact, a rotational field with rotational velocity (ω) is characterized by linearly increasing tangential velocities (v) moving distally from the center of rotation along the radial direction (r) (according to $v = \omega\, r$). The velocity measures were taken in the centerline of the Perfuser plug, therefore, the measures reflected the average flow velocity over the entire area of the plug opening. The inner hemi-portion of the plug was naturally exposed to lower tangential flow velocities but it was balanced by the outer hemi-portion, which was perfused with higher tangential flow velocities. Additionally, a measurement error for each rotational velocity acquisition was calculated. This error reflected the discrepancy in value between the angular velocity of the plug defined according to the spinner flask platform setup and the correspondent angular velocity measured via machine vision calculations. The error value was obtained by dividing the nominal rotational velocities tested by the respective values obtained from high-speed measurements and provided an indication of the possible variability of the results. The measurement error calculated for all the rotational velocities used was 12.5±6.3% (n = 5).

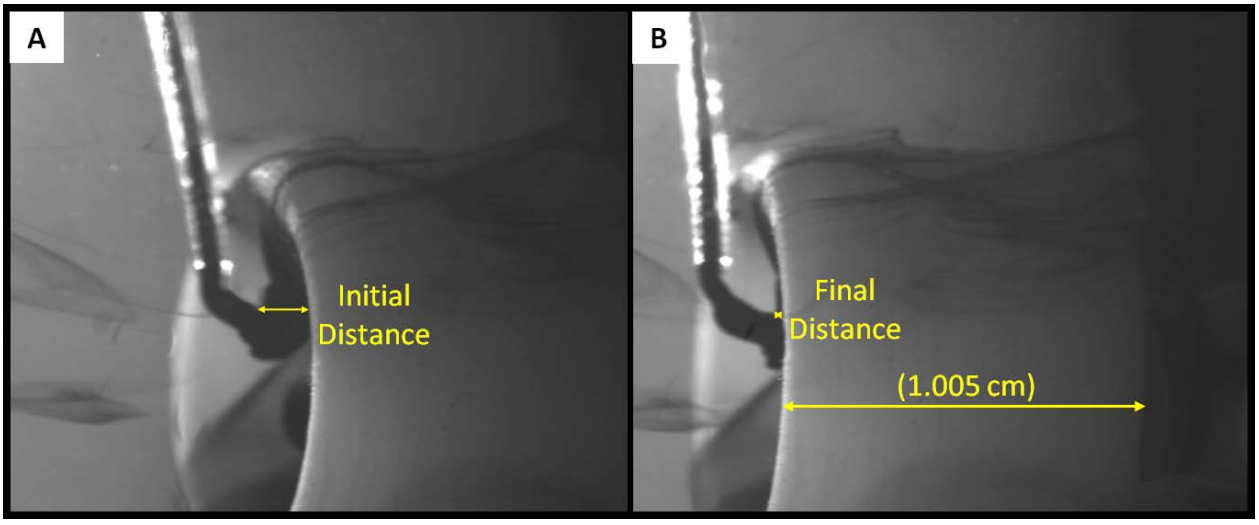

Figure 5.15 Sample pair of images used in the Perfuser flow visualization. **A.** The initial snapshot taken for the flow quantification at 12 rpm. The horizontal distance between a selected curl in the dye and the edge of the perfuser plug is indicated. **B.** The paired snapshot shows the reduction in distance following a known time frame. Each pair of images (initial and final shot) was scaled by measuring the know length of the plug.

The flow rates calculated for each angular velocity of the Perfuser are shown in **Figure 5.16**. A second order polynomial fit was made via Excel showing a good agreement with the experimental data (R^2 = 0.97). Using the measured tangential velocities and **Equation 2-6**, it was possible to calculate the wall shear stress inside the lumen of ID-4.7 scaffolds for different rotational speeds (**Figure 5.17**). Also in this case a second order polynomial curve showed a good fit (R^2 = 0.97).

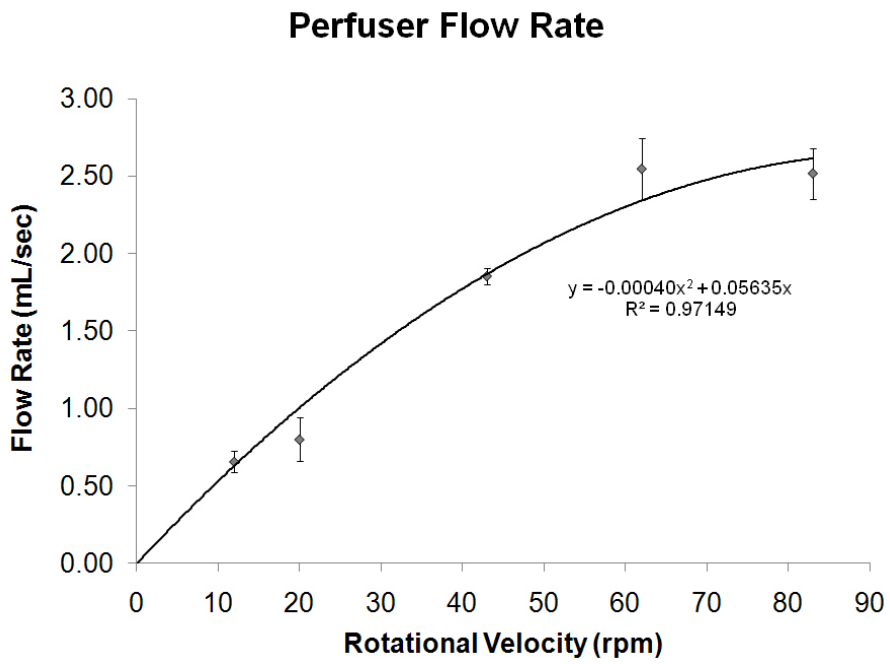

Figure 5.16 Perfuser flow rates measured for different rotational velocities via a flow visualization technique. The solid line represents a second order polynomial fit of the data. Given as measure ± error; n = 1. Note that the "error" is 12.51% of the measure as described above.

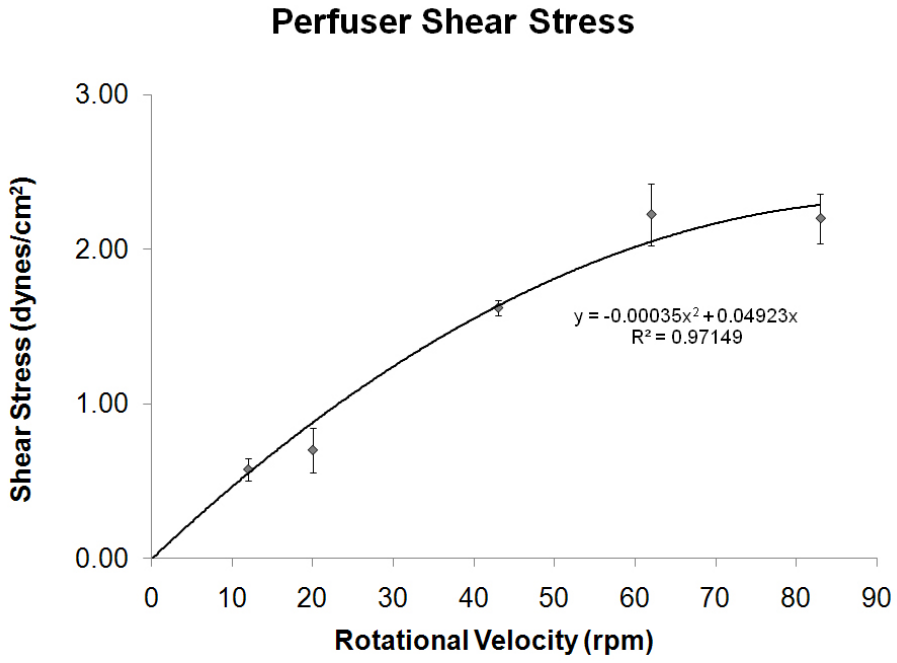

Figure 5.17 Shear stresses generated into a 4.7-ID scaffold while connected to the Perfuser rotating at different rpm levels. The solid line represents a second order polynomial fit of the data. Given as measure ± error; n = 1.

A summary of the values obtained for each rotational velocity is shown in **Table 5-1**.

Table 5-1 Summary of flow visualization analysis.

Rotational speed (rpm)	12	20	43	62	83
Relative tangential velocity of the dye (cm/sec)	0.94	1.14	2.64	3.63	3.59
Flow rate into the scaffold (mL/sec)	0.66	0.80	1.85	2.55	2.52
Wall shear stress into a 4.7-ID scaffold (dynes/cm^2)	0.57	0.70	1.62	2.22	2.20
Tangential velocity of the plug (cm/sec)	3.65	6.09	13.09	18.87	25.26
Ideal flow rate (mL/sec)	2.56	4.27	9.19	13.25	17.73
Fluid dynamic efficiency	25.66%	18.75%	20.19%	19.22%	14.20%

5.3.4 Discussion

The results obtained with the Perfuser indicated the achievement of controllable and physiologically relevant values of flow rate and shear stress in the TEVG by varying the rotational velocity of the system. The flow rate and the related shear stress increased with the rotational velocity, apparently reaching an asymptomatic value after 83 rpm. Flow visualization results demonstrated that the rotating components of the Perfuser indeed created a rotational velocity field in the fluid. This effect was clearly due to the drag force exerted on the fluid by the rotating components. This phenomenon generated a reduction in the overall fluid dynamic efficiency of the Perfuser. In fact, if the plug would spin into a fluid media completely and permanently static, the resulting flow and shear stresses would be greatly enhanced by the

increased net relative velocity entering the Perfuser plug. Calculating the ratio between the ideal (corresponding to a Perfuser plug moving within a static fluid) and measured flow rates, it was possible to quantify the fluid dynamic efficiency of the system, which was equal to 19.6±4.1% (*i.e.*, the system with its defined geometrical features and working principles, at the current status of development, was able to perfuse the scaffolds with about 20% of its physical potential based on the aforementioned concept of the wind sock). It was observed that the efficiency was generally decreasing for higher angular velocities (**Table 5-1**). This data was consistent with the observed asymptotic behavior of the flow rate (**Figure 5.16**). By performing more complex CFD optimization studies of the profiles of the rotating components it should be possible to increase the overall fluid dynamic efficiency of the Perfuser. However, this subject was beyond the scope of this work and it was, therefore not further addressed.

The results that were obtained suggested that the Perfuser might represent an ideal tool for the temporary dynamic culture of TEVGs or any tissue engineering tubular constructs (TETCs) due to its simplicity, cost-effectiveness, and functionality. Mass transport, in fact, is widely believed to be primary limiting factor in tissue engineering [179], which often requires dynamic conditions to allow for culture of cells in a 3D environment. The Perfuser was able to provide intraluminal perfusion of nutrients in long TETCs, thus presumably enhancing mass transport. It was also able to provide physiologically relevant levels of shear stress with very limited resources. A variety of costly and complex bioreactors were previously described [180], however, since time is an important factor in the development of a TEVG, a device such as the Perfuser appears to be an ideal candidate to serve the purpose of a short, inexpensive, and effective period of dynamic culture required before *in vivo* implantation in a large animal model.

In the following section an additional validation of the performance of the Perfuser involving actual TEVG culture is described.

5.4 BIOLOGICAL ANALYSIS OF PIG SLOWLY ADHERING CELLS INTO ES-TIPS PEUU SCAFFOLDS CULTURE *IN VITRO*

In summary of the work to this point, the development of the RVSD (**Chapter 2**) opened the possibility to incorporate efficiently and without damage cells into porous tubular scaffolds to be used as TEVGs. The initial investigations toward a characterization of the device (**Section 2.2.3**) and the following comprehensive *in vitro* culture (**Section 5.1**) used murine cells due to their extensive characterization [99-101, 166, 167, 169]. A basic phenotypic assessment following seeding with the RVSD and subsequent acute dynamic culture in a spinner flask was performed to understand the influence of these processes in the maintenance of stem cell phenotypic markers.

In preparation for small animal *in vivo* studies (**Chapter 6**), rat cells were used to test the capacity of the RVSD to incorporate efficiently cells originating from a different species into the ES-TIPS PEUU scaffold, and the spreading and proliferation of those cells into the scaffolds (**Section 5.2.2**). The phenotypic characterization of rat MDSCs and their modification as a result of the seeding procedure and/or dynamic culture was considered beyond the scope of the work due to the poor characterization available in literature for rMDSCs and therefore, the lack of comparative standards.

In preparation for a large animal *in vivo* study in pigs (**Chapter 7**) autologous slowly adhering cells (SACs) were isolated and characterized for their morphology and proliferation

kinetics (**Sections 7.3** and **7.4**) and used to test the functionality of the newly developed S-RVSD (**Section 3.1.4**). Those studies served two the purposes; providing a quantitative demonstration of the seeding uniformity along the three cylindrical directions of the scaffolds (longitudinal, circumferential, and radial), and demonstrating the ability for pig late SACs to be incorporated with a high density into the pores of the ES-TIPS PEUU scaffolds. Furthermore, the TUNEL assay showed the absence of significant apoptosis following seeding, providing additional evidence of cell viability.

The remaining step toward *in vivo* implantation in pigs was to test the proliferation of pig SACs within ES-TIPS PEUU scaffolds following dynamic culture in the newly developed Perfuser bioreactor.

5.4.1 Pig SACs-containing scaffold cultured in dynamic conditions via the Perfuser

Pig SACs were cultured to confluency in 175 cm^2 flasks (a detailed description of the isolation technique, cell characterization, and culture reagents is provided in **Sections 7.3** and **7.4**), trypsinized, counted, and suspended in 20 mL of complete culture media. Cells were then seeded into 5 cm long ID-4.7 ES-TIPS PEUU scaffolds (see **Section 4.2)** via the S-RVSD. Each scaffold was seeded with $15x10^6$ pig SACs (n = 3) using seeding parameters consistent with those described in **Section 3.1.4**. Briefly, the feed rate for the seeding suspension was 4 mL/min, the rotational speed of the scaffold was 10 rpm, the translational velocity of the Diffuser was 0.167 mm/sec, and the vacuum was set to -5 inHg.

Immediately after seeding, the scaffolds were placed into 50 mL conical tubes filled with 40 mL of media and were cultured statically for 2 hours in a standard incubator. The cap was left untightened to allow for gas exchange in the incubator's 5% CO_2 atmosphere. Following

static culture, a ring of each scaffold (~8 mm in width) was cut with a scalpel blade and split into four smaller rings (~2 mm in width). Three from each scaffold were processed for MTT (3 repeated measurements per sample) with the same protocol described in **Section 2.2.3**. The fourth ring was processed for histology (H&E) as previously described in **Section 2.2.3**.

Each scaffold was then aseptically mounted on a dedicated Perfuser (to perform independent experiments), ligated with 4-0 silk and cultured for 48 hours while rotating at 20 rpm in standard incubators. At 24 and 48 hours additional rings from each scaffold were again harvested, split, and processed for histology and MTT.

Immediately after seeding, the scaffolds appeared homogeneously populated with pig SACs with a relatively low density and the usual spherical shape (**Figure 5.18-A**). After 24 hours of dynamic culture, the scaffold appeared densely populated with spread cells (**Figure 5.18-B**). After 48 hours of dynamic culture into the Perfuser, the histology showed an elevated number of cells into the TIPS layer of the scaffold but a generalized loss of cell spreading (**Figure 5.18-C**). The MTT results showed a significant 3-fold increase in cell number (**Figure 5.19**) after 24 hours, confirming the qualitative histological results. There was no significant difference detected in cell number between the 24 and 48 hour time points.

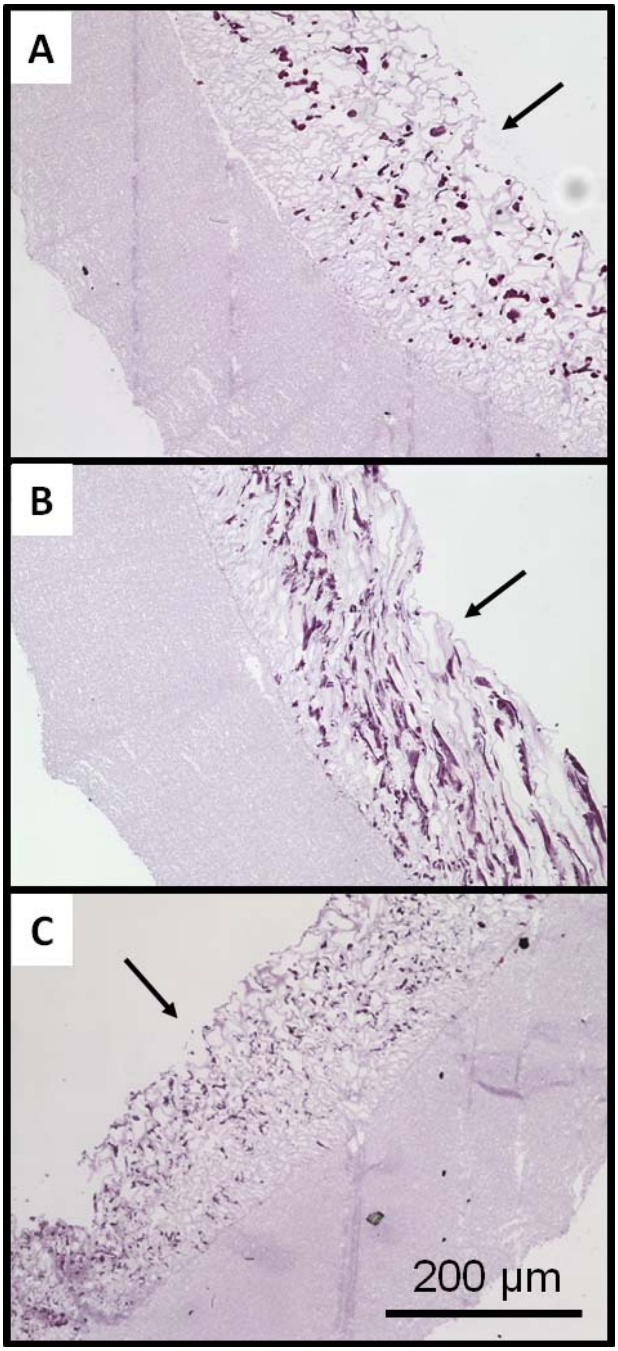

Figure 5.18 Qualitative assessment of pig SACs culture within the Perfuser. **A.** Representative results after 2 hours of static culture immediately following seeding. **B.** Representative results after 24 hours of dynamic culture within the Perfuser. **C.** Representative results after 48 hours of dynamic culture within the Perfuser. The arrows indicate the lumen of the ES-TIPS PEUU scaffolds.

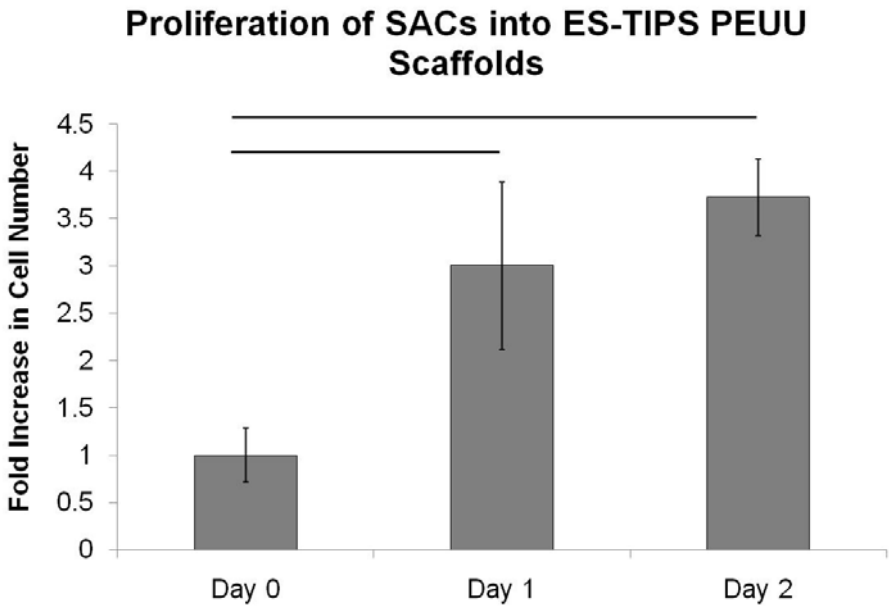

Figure 5.19 Proliferation analysis of SACs cell within ES-TIPS PEUU scaffolds following dynamic culture in the Perfuser.

This experiment confirmed the capability of the S-RVSD to incorporate effectively pig SACs into ES-TIPS scaffolds. It also demonstrated SACs proliferation within the scaffolds scaffolds following dynamic culture in the Perfuser. According to what was established in **Section 5.2.1** these two characteristics represent critical requirements to perform *in vivo* studies.

While the subject would deserve further investigations (in particular a better understanding of the lack loss of additional cell spreading observed after 48 hours, and an analysis of different initial cell densities, time points, and rotational velocities for the Perfuser), additional related studies were not performed in this dissertation work. This was mostly due to a very limited availability of pig cells as well as time and budget constraints, which did not allow for performing additional, complementary studies. As mentioned in the **Section 1.10** this work

is not free of limitations due to its deep interdisciplinary features, and this is just another example.

In the next Chapter the lessons learned from seeding device validation, scaffold development and testing, and acute *in vitro* dynamic culture experiments were directly applied toward preclinical translation with *in vivo* experiments both in small and a large animal models.

6.0 SPECIFIC AIM 4, PART 1: SMALL ANIMAL ALLOGENEIC TEVG STUDY

6.1 INITIAL CONSIDERATIONS ON *IN VIVO* STUDIES

Several accomplishments contributed to the initiation of the *in vivo* studies of the TEVG in a small animal model and, subsequently in a large animal model as well. As mentioned, the actual order of experiments did not follow the rigid structure of this dissertation. In particular, the first implantations in Lewis rats were performed using TIPS PEUU scaffolds seeded with rat MDSCs. This was possible following the development and testing of the RVSD (**Section 2.1**). Thorough *in vitro* testing using murine MDSCs within dynamic culture conditions (**Section 5.1.2**), and some validation studies to reproduce the results using rat MDSCs and TIPS PEUU scaffolds (**Figure 6.1-B**) were then performed. As explained in **Section 5.2.1** the established criteria for implantation were the achievement of a densely and uniformly cellularized scaffold in a short amount of time. The goal was to provide a viable, stem cell-based TEVG with the potential to remodel and regenerate *in vivo* into a functional native-like artery.

To corroborate the validity of the established criteria for implantation, it is useful to refer to another approach led by Dr. Toshiharu Shin'oka. This group used similar basic requirements for implantation, and obtained successful results in both preclinical and clinical studies. In these studies, autologous BMPCs were harvested and isolated in the operating room. A cell suspension was prepared using BMPCs and autologous plasma, and was manually seeded,

intraoperatively, on a commercially available, medical grade, biodegradable scaffold just prior to implantation [38, 39, 96, 115]. The resulting conduit was tested in large-caliber applications such as an inferior vena cava interposition graft, or the cavopulmonary connection. These applications are characterized by a less demanding mechanical environment than that in the systemic arterial tree, and therefore a reduced occlusive rate due to neo-intimal tissue formation compared to those of small-diameter arteries.

While the technique described by Shin'oka *et al.* seems ideal from the clinical standpoint due to its off-the-shelf availability and promising results, their cell seeding efficiency was very poor. The seeding and culture protocols described in this dissertation (seeding via the RVSD and the acute dynamic culture of the scaffold, leading to cell attachment, proliferation, and spreading) might add value to it. In particular, the advantages of having an efficient, cost-effective, rapid, and reproducible seeding method has been widely speculated in **Section 1.6**, and the need for a transient, acute, and delicate period of dynamic culture has been demonstrated in **Chapter 5**. For example, when comparing our results immediately after seeding with those published by Shin'oka *et al.* (**Figure 6.1**), the potential benefit of our approach is apparent. Not only does the seeding density and the seeding uniformity across the scaffold wall appear higher in our approach, but also the seeding efficiency. It is likely that the manual nature of the seeding technique described by Shin'oka *et al.* will lead to less efficient incorporation of cells (*i.e.*, many available cells are likely wasted). Furthermore, in both approaches, cells have a spheroidal shape immediately after seeding, denoting poor or no attachment to the scaffold pores. In these conditions, an abrupt exposure to physiological levels of pressures and flow might lead to cell loss. Therefore, a short period of culture within delicate dynamic conditions, such as the one

described in this approach, might contribute to a more effective cell retention and functionality upon implantation.

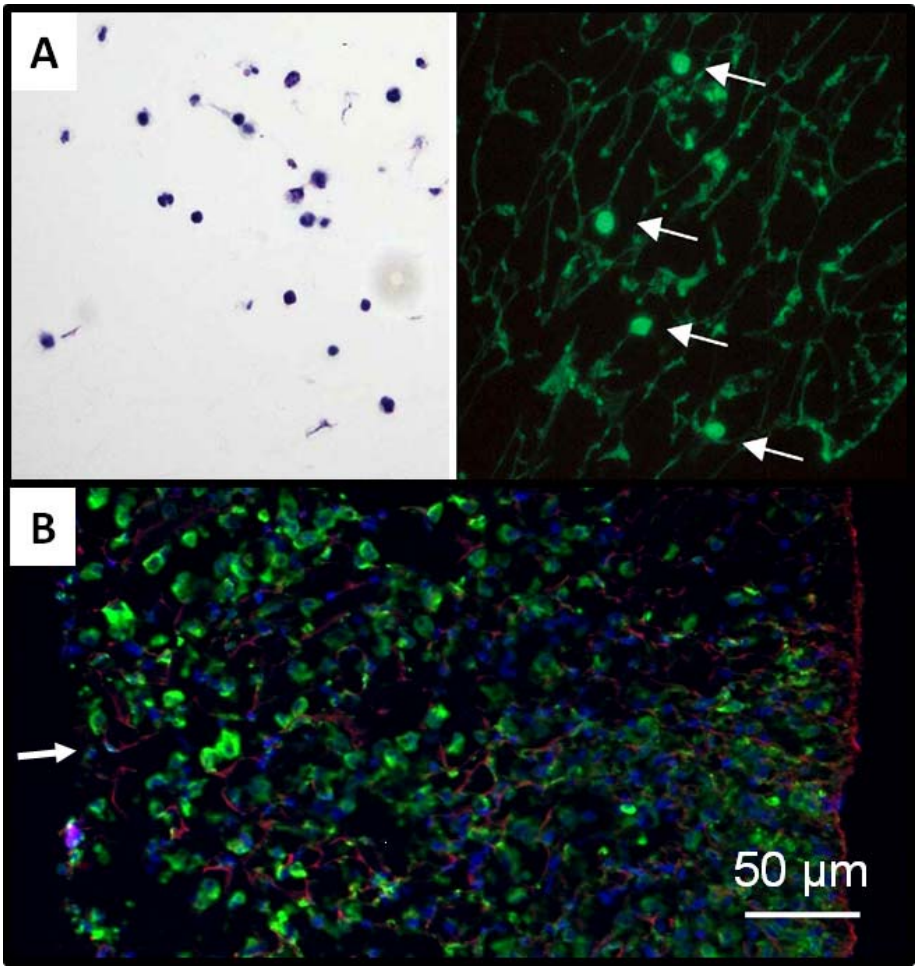

Figure 6.1 Comparison of cellular density between the seeding the approach described by Shin'oka *et al.*[115] (**A – left and right panels**), and a TIPS PEUU scaffold seeded with rat MDSCs via the RVSD (**B**). The arrow in the bottom image indicates the luminal surface. Blue = nuclei, green = F-actin, red = scaffold. Image taken at 200x.

Within this framework, the animal studies were initiated as a natural subsequent step in our translational approach.

In the following sections a comprehensive analysis of the *in vivo* studies will be provided.

6.1.1 Preparation of allogeneic TEVGs for *in vivo* studies

To test the working hypothesis of this dissertation work (recall **Section 1.10**), the *in vivo* remodeling of porous biodegradable elastomeric scaffolds (initially TIPS PEUU, and subsequently ES-TIPS PEUU) seeded with allogeneic rMDSCs in a rat model for a period of 8 weeks was evaluated.

Lewis rat MDSCs were isolated and transfected with the LacZ reporter gene as described in **Section 5.2.2**. Cells were then plated, cultured, and expanded as described in **Section 5.1.2**. Before use, rMDSC monolayers were detached from the culture flasks between passages 10 and 15, counted, and then resuspended in culture media to the desired concentration in preparation for seeding as described in **Section 5.1.2**. Each seeding bolus consisted of 5 mL of complete media and $3x10^6$ rMDSCs.

ID-1.3 TIPS PEUU (length = 1 cm, *ID* = 1.3 mm, thickness = 350 μm) and ES-TIPS PEUU (length = 1 cm, *ID* = 1.3 mm, thickness = 420 μm) scaffolds were fabricated as described in **Section 4.2.2**. Each scaffold was provided with a pair of tips (recall **Figure 2.4**), and sterilized in 70% ethanol solution for 24 hours, in preparation for seeding. Each scaffold was then rinsed multiple times in sterile Dulbecco-modified phosphate-buffered saline (DBPS), to remove residual ethanol solution, and stored in cold DPBS in 15 mL tubes until use. Prior to seeding, each scaffold was warmed to 37°C in a water bath.

Each scaffold was seeded via the RVSD as described in **Section 4.2.6**. Briefly, each scaffold was mounted into the RVSD via simple pressure fitting of the scaffold tips onto the RVSD tees. The RVSD fluid circuit was de-aired and primed by the injection of warm DPBS. The prepared seeding suspensions were fed equally into two 3 mL syringes. Both syringes were then connected to the RVSD and mounted on the rack of a syringe pump to begin the seeding process. The seeding parameters consisted of a feed rate of 2.5 mL/min, a rotational speed of 150 rpm, and a vacuum level of -5 inHg. The constructs were then flushed with 5 ml of plain DMEM to seed the residual cells from the tubing and the lumen of the scaffolds.

Immediately after seeding, the constructs were removed and incubated in a Petri dish for 1 hour with the tips still attached to prevent cell loss from the scaffold during handling. After this short period of static culture, the plastic tips and a small portion of overlapping scaffold were carefully removed. Constructs were then placed in 500 mL spinner flasks (Bellco Glass) with 100 mL of culture media and stirred at 15 rpm for 48 hours before implantation.

6.1.2 *In vivo* small-animal study design

The rat is an established model for vascular disease and has been extensively studied. This model has the advantage of being available at low-cost, and having a rapid and reproducible vascular response to injury [181]. Due to its characteristics, the rat is usually used as an initial model to test the effects of novel vascular therapeutic approaches, including those leading to migration and proliferation of smooth muscle cells and the formation of neointima *in vivo* [181]. In particular, the infrarenal portion of the rat aorta has been used in a number of small-diameter vascular studies due to its relatively easy access, and the low number of lateral branches. These

studies include the testing of TEVGs [69, 182], synthetic vascular grafts [183, 184], or surgical techniques [185, 186].

The Lewis rat is an inbred, albino strain, normally used for transplantation and endocrinology studies [187]. This rat strain was chosen for its suitability for transplantation due to its inbred feature, which could potentially result in immune-tolerance to recipient of an allogeneic cell source, not requiring immune suppression.

Adult Lewis rats (n = 42; weight ~ 300 g; (Charles River Laboratories, Inc., Boston, MA) received aortic interposition grafts as described in **Section 6.1.3**, and were divided in 4 groups. The first group (rG-1; n = 15) received TIPS PEUU scaffolds seeded with rMDSCs. The second group (rG-2; n = 17) received ES-TIPS PEUU scaffolds seeded with rMDSCs. The third group (rG-3; n = 10) received either an acellular TIPS PEUU scaffold as a control for rG-1 (n = 5), or an acellular ES-TIPS (n = 5) as a control for rG-2.

Animals were electively sacrificed at 8 weeks or euthanized earlier if ambulatory impairment or distress was evident due to construct occlusion or thromboembolic events. Following euthanasia, a comprehensive set of endpoints were evaluated to assess the performance and the remodeling of the scaffolds, including fluoroscopy, gross pathology, histology, SEM, and immunohistochemistry.

6.1.3 Infrarenal aortic interposition graft in rats

All animal procedures and treatments were performed in compliance with the Institutional Animal Care and Use Committee (IACUC) of the University of Pittsburgh guidelines.

Animals were anesthetized in a 2% isofluorane in pure oxygen atmosphere (induction chamber) followed by a single dose of 50 mg/kg ketamine, injected interperitoneally. Animals

were then placed on a warming pad (40-45°C) in supine position and ventilated with 1% isofluorane in pure oxygen administered via a rat-sized rubber cone positioned on the animal's nose.

Surgeries were performed using aseptic techniques and sterile instruments. The skin of the anterior abdomen was aseptically prepped, without previous fur shaving, with povidone-iodine solution. A midline laparotomy incision was made through the skin and abdominal muscles. The wound and viscera were retracted and held in place by a small screw retractor. The abdominal aorta was exposed below the renal arteries and carefully separated from the inferior vena cava. Sodium heparin (40 IU) was given intravenous through a tributary vein of the inferior vena cava. Two micro-vascular clamps, held by a microapproximator, were applied to the infrarenal aorta proximally (5-8 mm downstream to the renal arteries) and distally (about 15 mm from the first clamp), and the aorta was sectioned in between the clamps creating a gap of approximately 1 cm, due to the relief of the physiological longitudinal vascular tension. The TEVG was trimmed on both edges to obtain a 1 cm-long construct and then sutured in place to the native aorta, in an end-to-end, interrupted anastomotic pattern with 10-0 polyamide monofilament (Arosurgical, Newport Beach, CA). An average of 6 stitches per anastomosis was required. The trimmed edges of each TEVG were fixed in 4% paraformaldehyde and processed for cytoskeletal and nuclear staining as described in **Section 4.2.6** to assess the pre-implantation cell density.

After the graft was anastomosed, the clamps were released and patency was verified by direct observation. Clamping time was approximately 25-35 minutes. Finally, the muscle layer and skin were closed with 3-0 polyglactin absorbable suture (VICRYL, Ethicon, Inc.), and a

povidone-iodine ointment was applied on the sutured abdominal incision to prevent post-operative infections.

The rats were observed in the surgical suite until fully recovered from the anesthesia and then returned to the housing area. Standard analgesic and antibiotic therapy was administered following the surgery. In particular, for the first 3 days after surgery, buprenorphine (0.5 mg/kg twice a day) and cefuroxime (100 mg/kg twice a day) were administered subcutaneously. Antiaggregation therapy was started after the surgery with aspirin and dypiridamole (200 mg via mouth daily during the first week and 100 mg via mouth daily after the first week until elective sacrifice).

A schematic of the surgical procedure is shown in **Figure 6.2**.

6.1.4 Performance after 8 weeks *in vivo*

6.1.4.1 Patency

After 8 weeks, animals were anesthetized with 5 % isofluorane in pure oxygen, anticoagulated and concurrently euthanized with a lethal intracardiac injection of heparin/KCl (40 IU of heparin in 5 ml of KCl). Following euthanasia, the thoracic descending aorta was exposed via median sternotomy and by displacement of the heart and lungs, and then cannulated with a 22 G Angiocath (BD, Sandy, UT) secured with a 4-0 silk ligation. The animals were placed under a dynamic angiography system (OEC 9800 Plus, GE Healthcare, Piscataway, NJ) and iodine constrast media (Renografin-60, Bracco Diagnostics, Princeton, NJ) was manually infused through the angiocath during irradiation and acquisition to assess graft patency. Patency rate was calculated as the ratio between the number of animals with positive contrast flow through

the construct and the total number of animals within each experimental group. Statistical differences in patency rate between groups were detected via an exact Fisher test for non-parametric variables. Mechanical failure was assumed when obvious dilation could be observed at the time of fluoroscopy.

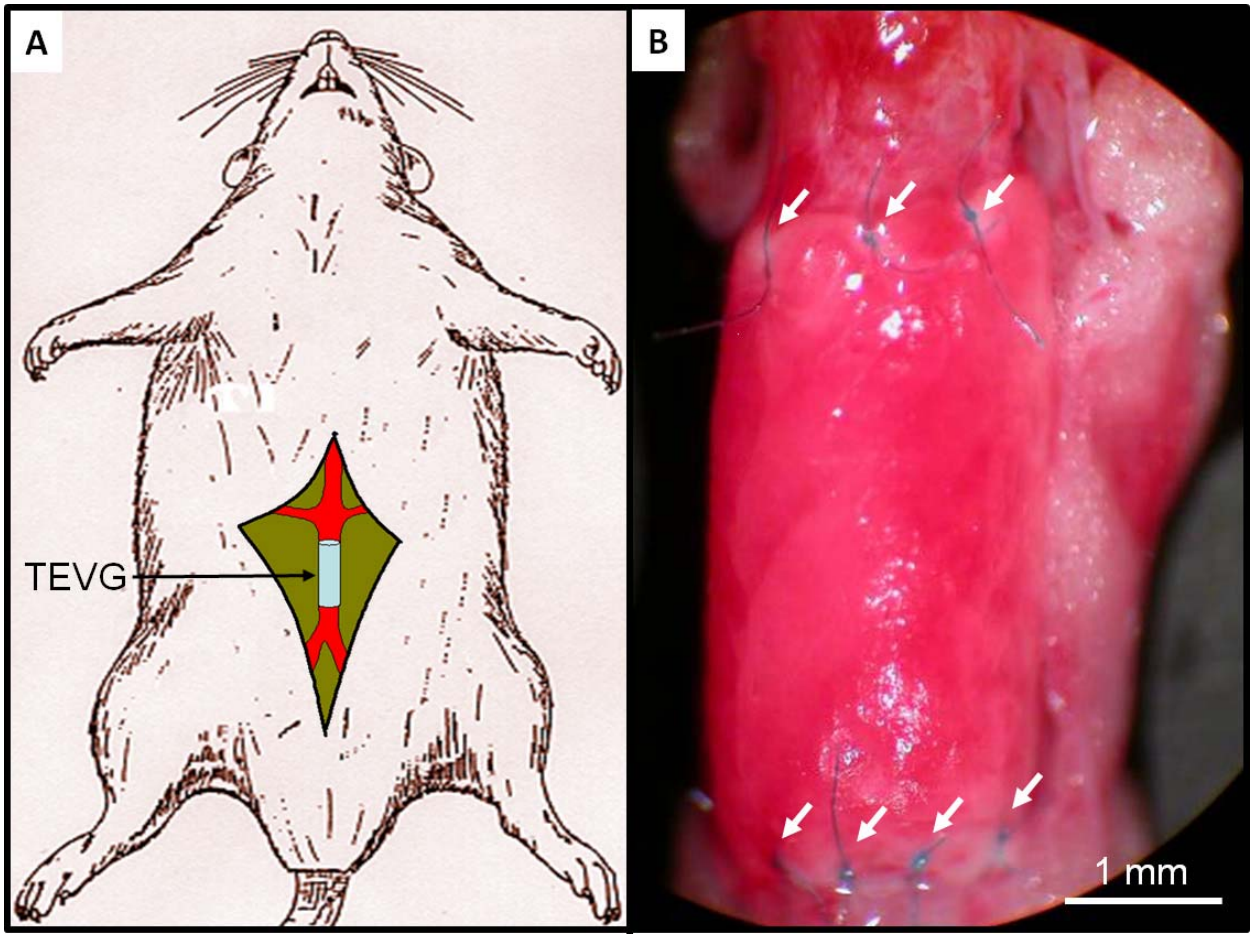

Figure 6.2 Rat infrarenal aortic interposition graft surgery. **A.** Schematic showing the location of the TEVG as an interposition graft in the abdomen of the animal. **B.** Close-up showing the graft at the end of one representative vascular procedure. The arrows indicate the 10-0 stitches used to anastomose the graft to the native aorta. Note the good size matching.

6.1.4.2 Gross macroscopic appearance

After angiography, a midline laparotomy was performed and the constructs were dissected, explanted from the animal along with approximately 5 mm of native aorta within each anastomosis and stored in saline until processing. All of the specimens were initially observed at 10x under a zoom stereomicroscope (SMZ660, Nikon Instruments Inc., Melville, NY), in order to detect gross macroscopic remodeling, signs of infections, abscess formation, presence of intraluminal thrombus and vessel wall thickening. The TEVGs were subsequently cut in several longitudinal portions for the various other endpoints.

6.1.4.3 Histology

For histological assessment, separate ring segments were fixed in 10% formalin for 1-2 hours and immersed in 30% sucrose solution overnight at 4°C, before standard paraffin embedding and sectioning (section thickness = 5 μm) via microtome (Thermo Shandon Inc., Pittsburgh, PA). Hematoxylin and eosin and Masson's trichrome were performed following standard histological protocols. Histological slides were observed and imaged within bright field microscopy via an Eclipse E600 microscope (Nikon Instruments Inc., Melville, NY) provided with a digital color CCD camera (Model 2.3.1, Diagnostic Instruments Inc., Sterling Heights, MI).

Phenotypic assessment of newly formed tissue was assessed via immunofluorescence using a previously described protocol (see **Section 5.1.2**). Briefly, dedicated sections were incubated for 60 minutes at room temperature with the following primary antibodies: smooth muscle alpha-actin (1:500) (Sigma-Aldrich, St. Louis, MO), calponin (1:200), (Sigma-Aldrich, St. Louis, MO), myosin heavy chain (1:500) (Sigma-Aldrich, St. Louis, MO) and Von

Willebrand Factor (vWF) (1:100) (Dako). Unbound primary antibody was removed by subsequent washes in PBS. The samples were then incubated with a Cy3-conjugated (Sigma-Aldrich, St. Louis, MO) secondary antibody (1:500) for 1 hour at room temperature and subsequently rinsed 3 times for 15 minutes each with PBS. For nuclear visualization, cells were counter-stained with DAPI. The samples were then mounted in gelvatol and viewed and imaged with the aforementioned microscope and camera.

Cell tracking, using the LacZ reporter, was performed on 5 μm frozen sections fixed in 2% glutaraldehyde, according to a previously described protocol (recall **Section 5.2.2**) using the X-gal stain overnight and eosin counterstain where blue nuclei was only found in LacZ+ cells.

The luminal surface of the explanted constructs was examined by SEM. Dedicated samples were processed as described in **Section 2.2.4**.

6.1.4.4 Results

After 48 hours of dynamic culture, the constructs of rG-1 (rMDSC-seeded TIPS PEUU scaffold) and rG-2 (r-MDSC-seeded ES-TIPS PEUU scaffold) appeared completely populated with cells that were spread inside the scaffolds (**Figure 6.3**).

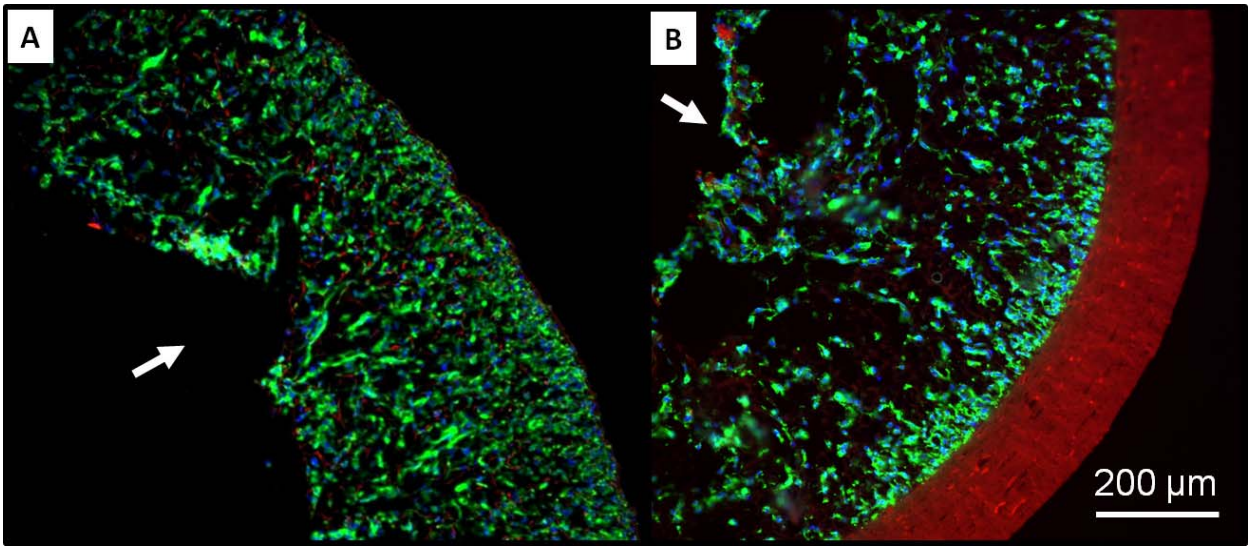

Figure 6.3 Pre-implantation microscopic aspect of the TEVG for small animal studies. **A.** rMDSC-seeded TIPS PEUU scaffold. **B.** rMDSC-seeded ES-TIPS PEUU scaffold. The arrows indicate the luminal surface. Blue = nuclei, green = F-actin, red = scaffold.

Surgical implantation was feasible in all cases and no differences were noted between the groups in the surgical features of the constructs (*i.e.*, tissue handling and suturability). Upon implantation, all TEVGs clearly appeared to have strong pulsatility, with no oozing or leaking of blood. All animals recovered well from surgery and showed no signs of distress immediately post-operatively. In rG-1, two animals showed signs of lower limb impairment, absence of pulses, and lower limb necrosis within the first 72 hours, requiring early sacrifice. Another animal had an aneurysmatic rupture leading to the death at day 4. In rG-2, three animals were sacrificed before 8 weeks due to ischemia of the lower limbs. In rG3, five animals showed evidence of lower limb ischemia, which required early sacrifice within the first week. All remaining animals were electively sacrificed at 8 weeks with no need of premature euthanasia. Four animals (two in rG-1, and two in rG-2) that had a self-limited necrotic plaque in the

medial/distal part of the tail but positive femoral pulses, were treated with a partial resection of the tail following standard amputation techniques, and were electively sacrificed after 8 weeks.

The angiograms performed to evaluate patency rate showed that in rG-1, eight out of fifteen animals (53.3%) had an open construct with no signs of stenosis. However, four of these animals showed aneurysmatic dilation (50%) of the TEVG (**Figure 6.4-A**). In rG-2, eleven out of seventeen animals (64.7%) were patent with no signs of stricture, dilations, or mechanical failure (**Figure 6.4-C**). In contrast, only one out of ten animals (10%) in the combined rG-3 was patent while the remainder showed a complete obstruction of the graft (**Figure 6.4-E**). There were no significant differences in patency rate between rG-1 and rG-2 ($p = 0.22$), but when compared to the acellular controls in rG-3, both groups had a significant difference ($p = 0.03$ for rG-1 vs rG-3, $p = 0.007$ for rG-2 vs rG-3).

All patent constructs in rG-1 and rG-2 showed a tissue-like appearance with clear remodeling of the scaffold without signs of scar tissue at the level of the anastomoses (**Figure 6.4-B/D**). No signs of infection or abscess formation were detected in any of the explants, regardless of patency outcome. Non-patent constructs in these groups had white organized tissue in the lumen, mainly at the anastomoses level, suggestive of intimal hyperplasia formation. In rG-3, all constructs but one, showed clear intraluminal thrombus formation with little or no remodeling of the scaffold (**Figure 6.4-F**).

SEM analysis for the explanted TEVG in rG-1 and rG-2 revealed no signs of stricture at the anastomosis level in the patent constructs (**Figure 6.5-A/B**), and a clear integration between the native vessel wall and the implanted polymer (**Figure 6.5-B**. In rG-1 and rG-2 groups, an endothelial-like layer was observed on the luminal surface, with a smooth transition from the

native endothelium to the tissue engineered graft (**Figure 6.5-C**). The luminal surface in rG-3 constructs was completely covered by adherent platelets (**Figure 6.5-D**).

Histological analysis of rG-1 and rG-2 showed formation of an external collagenous capsule, as well as an internal tissue layer with collagen and cellular components characteristic of smooth muscle cells (**Figure 6.6-A/B**). The scaffold showed a good remodeling in the TIPS layer in both groups and less remodeling in the electrospun layer in rG-2 group (**Figure 6.6-B**). There was evidence of giant cells, characteristic of a foreign body response, together with a population of mononuclear cells inside the scaffold, suggesting an active degradation process. Although not quantified, the cell density inside the polymer appeared to be lower than the pre-implant analysis suggesting cell migration out of the scaffolds. In rG-3, there were almost no cellular components inside the scaffold with scarce remodeling and a clear organized fibrin structure in the lumen, characteristic of thrombus formation.

X-gal staining of the sections from the rG-1 and rG-2 groups showed LacZ+ cells that participated in the remodeling, corroborating the remaining presence of the implanted cells at 8 weeks (**Figure 6.7**).

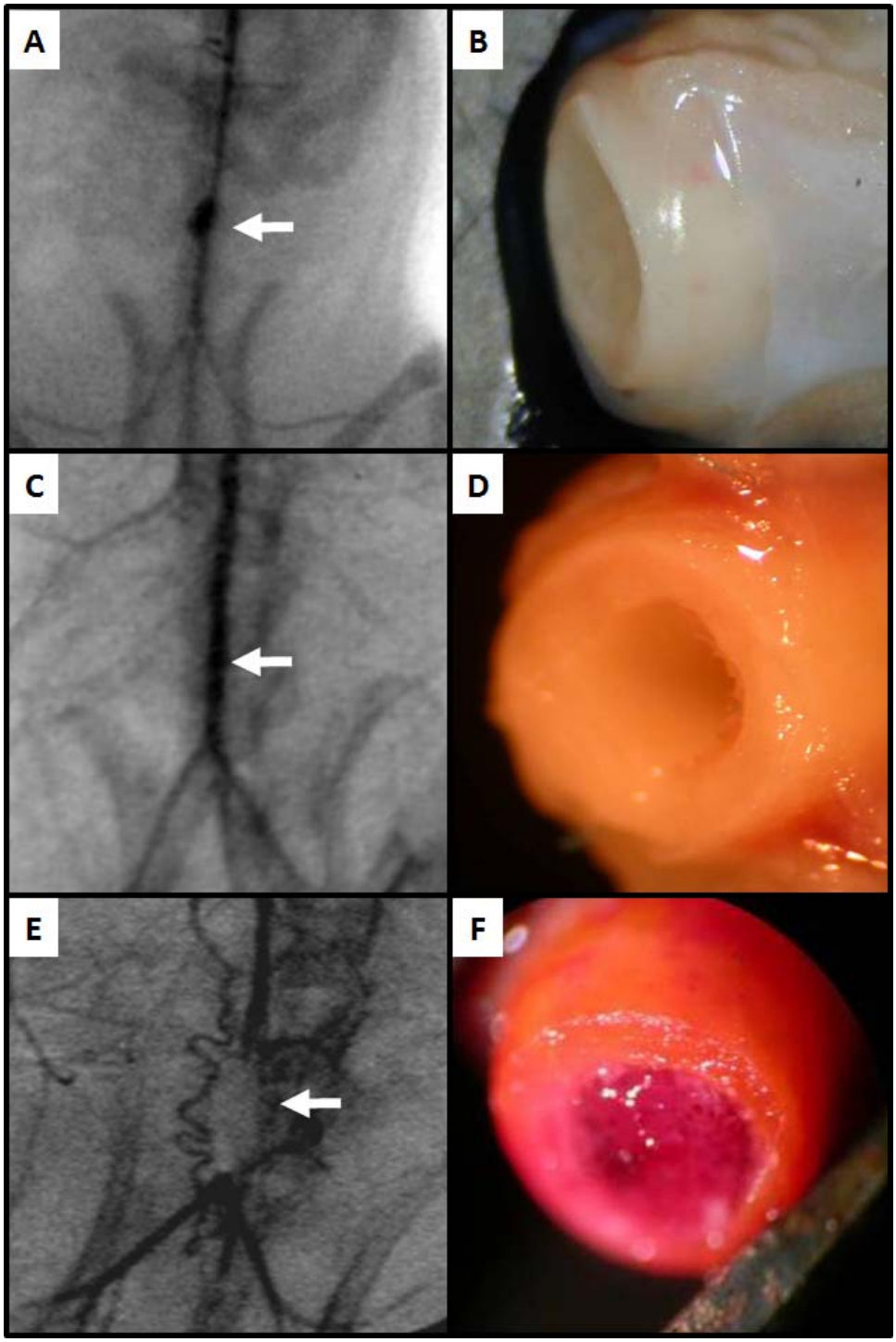

Figure 6.4 Fluoroscopy and gross pathology after 8 weeks *in vivo*. Representative fluoroscopy and gross pathology, respectively, of rG-1 (**A**, **B**), rG-2 (**C**, **D**), and rG-3 (**E**, **F**). The arrows in the left panels indicate the position of the TEVG. Note aneuryrism formation of the TIPS scaffold (**A**) and complete occlusion of acellular scaffolds (**E**).

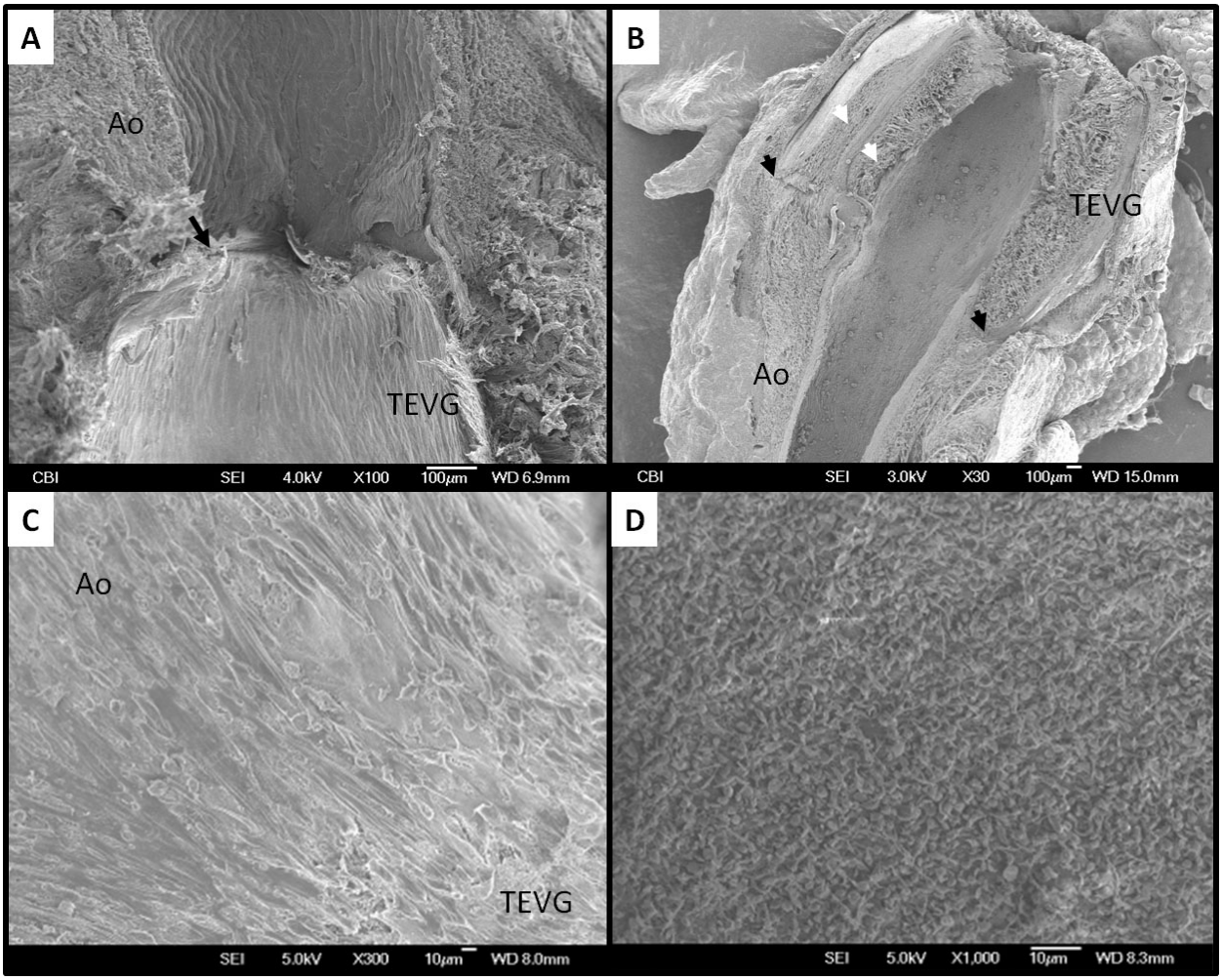

Figure 6.5 SEM of the luminal surface of the TEVG following 8 weeks *in vivo*. **A.** Representative micrograph of a patent TEVG from rG-1. The black arrow indicates the anastomosis between the aorta (Ao) and TEVG. **B.** Representative micrograph of a patent TEVG from rG-2. The white arrows indicate the two layers of the ES-TIPS PEUU scaffold. **C.** Representative close-up on the lumen of a patent TEVG from rG-2. The image is also representative for rG-1 TEVGs. **D.** Representative micrograph of the lumen of the scaffold from rG-3.

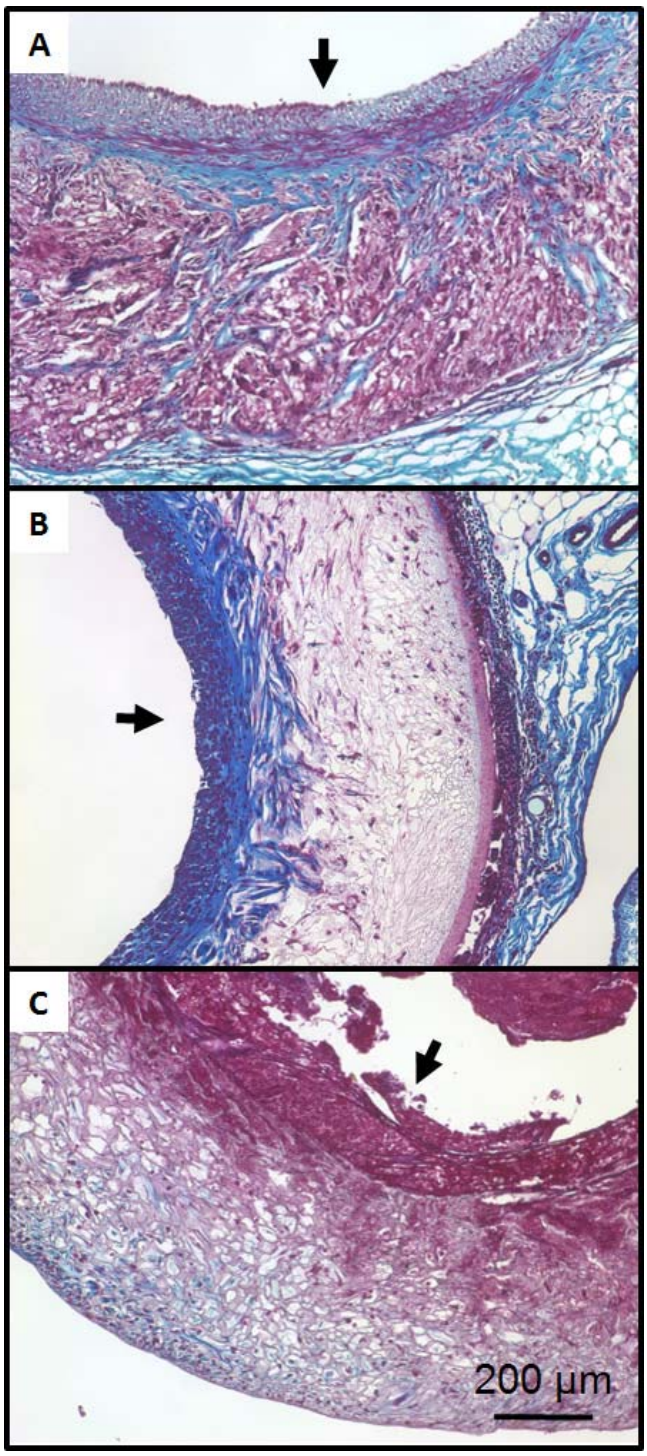

Figure 6.6 Histological analysis following *in vivo* remodeling. Representative Masson's trichrome results for rG-1 (**A**), rG-2 (**B**), and rG-3 (**C**) groups. The arrows indicate the lumen of the TEVG.

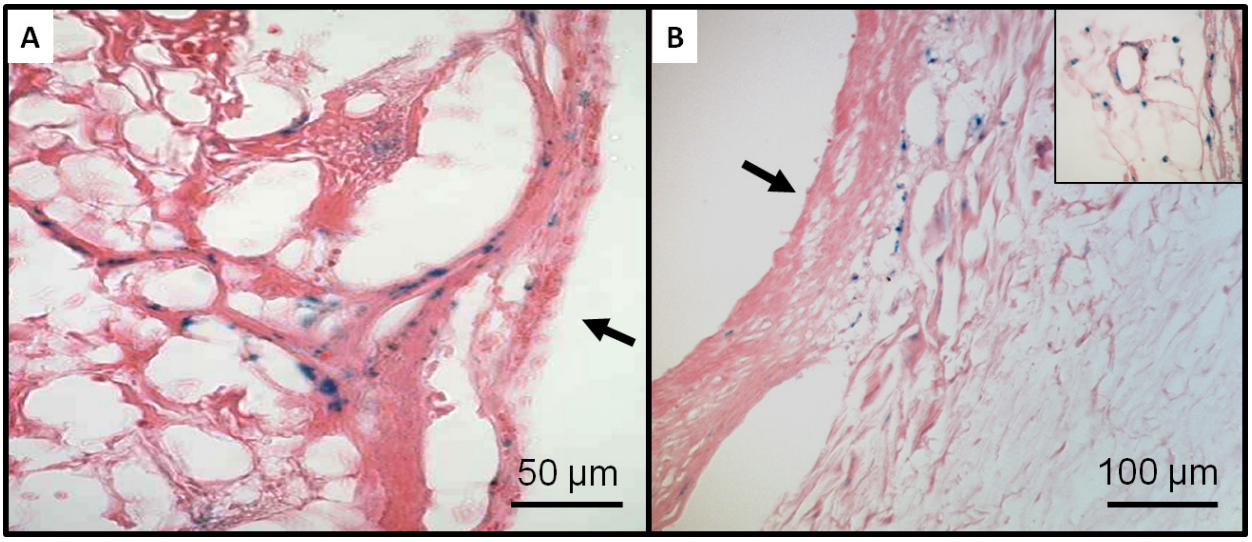

Figure 6.7 Representative X-Gal staining after *in vivo* remodeling revealing LacZ+ cells in rG-1 (**A**), and rG-2 (**B**) groups. **B.** Representative results of rG-2. The inset in **B** is a different region (same scale) showing LacZ+ cells participating in capillary formation in the rG-2 group. The arrows indicate the lumen of the TEVGs.

The immunohistochemical analysis showed that the inner tissue layer noted in rG-1 and rG-2 was positive for smooth-muscle alpha actin and calponin, suggesting a smooth muscle cell phenotype. The cell layer lining the luminal surface stained positive for vWF, corroborating the presence of endothelial cells. No differences were noted between rG-1 and rG-2 groups. Myosin heavy chain was negative in all of the samples.

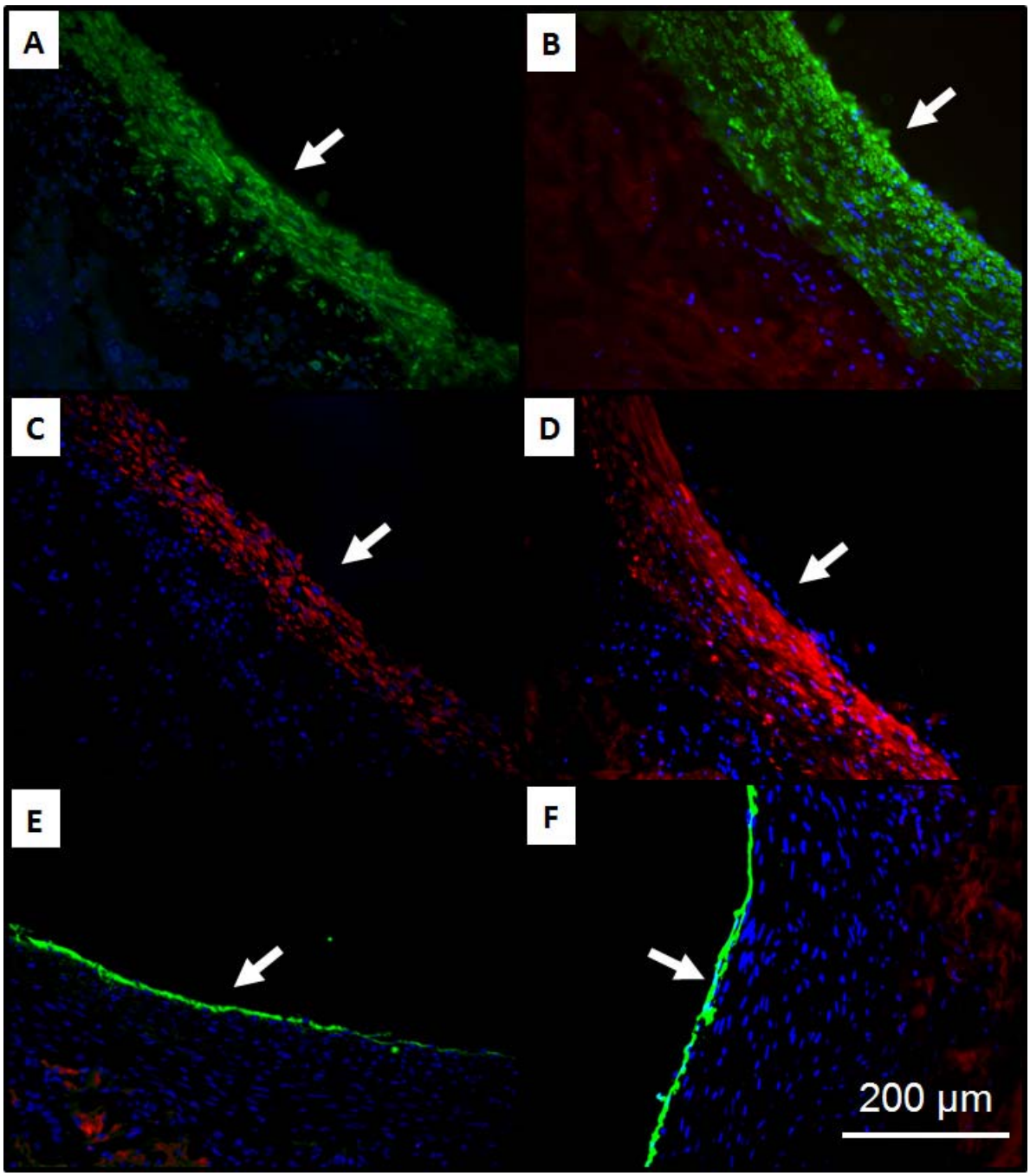

Figure 6.8 Immunohistochemistry after *in vivo* remodeling in rG1 (**left column**) and rG-2 (**right column**). **A-B**. α-SMA (green) and cell nuclei (blue). **C-D.** Calponin (red) and cells (blue). **E-F.** vWF (green) and cell nuclei (blue). The arrows indicate the lumen of the TEVGs.

6.1.5 Discussion

The remodeling of rMDSC-based TEVGs *in vivo* has been investigated in this section and compared to the behavior of acellular scaffolds. Marked differences in patency rates were detected between cellular and acellular constructs, suggesting antithrombotic properties of the seeded cells, leading to maintenance of patency. LacZ+ seeded cells (LacZ+) were detected in the TEVGs after 8 weeks *in vivo* (**Figure 6.7**), demonstrating the role of MDSCs in the remodeling process. The presence of the seeded cells in the scaffold after 8 weeks also supports the utility of acute dynamic culture to allow for cell retention, attachment, and spreading.

The presence of neo-tissue formation within the TIPS layer of the scaffolds, characterized by densely cellularized, collagenous tissue (**Figure 6.6**), and positive markers for smooth muscle cells (α-SMA and calponin; **Figure 6.8**), and for endothelial cells (vWF; **Figure 6.8**) suggests the remodeling of the TEVG toward an artery-like structure.

The TIPS PEUU scaffold proved to be mechanically inadequate for arterial applications as evidenced by the high dilation/failure rate (50%) leading to aneurysm formation and, in one case, to rupture. Conversely, the compound ES-TIPS PEUU scaffold demonstrated suitability for arterial applications. The combination of the two PEUU processing techniques in the ES-TIPS scaffolds provides the necessary porosity for cell support and tissue ingrowth, while providing the mechanical properties to withstand systemic circulation at least for a period of 8 weeks. Moreover, the absence of detectable differences in remodeling within the TIPS layers of rG-1 and rG-2 suggests that the electrospun layer does not affect either the cellular activity or diffusion of nutrients.

The engraftment of MDSCs in TEVGs after 8 weeks (**Figure 6.7**) provides only initial evidence to suggest the role of the seeded cells in the remodeling process *in vivo*. Direct

comparison between histology and LacZ+ images did not allow for the establishment of a direct relationship between the engrafted cells and the new tissue formation. Follow-up co-localization studies, molecular endpoints, and functional tests are necessary to elucidate the mechanisms of action by which the cells prevent thrombosis of the grafts and contribute toward the detected presence of vascular cell phenotypes. However, it is possible that the signaling released by the implanted cells plays a key role in the remodeling and recruitment of host endothelial cells.

The use of allogeneic cells without immune suppression represents another limitation of this study. Though Lewis rats are inbred, thus limiting the chances of a strong immune response, this might have caused the sub-optimal patency rate detected. A careful investigation, assessing macrophage infiltration, and other markers denoting the immune response, should be performed in additional studies.

The rat model represents another intrinsic limitation of this study. Unless genetically-modified to develop a particular condition, the rat is normally more resistant to cardiovascular disease than humans [188]. Therefore, while this study may have suffered an underestimation of the patency rate due to the allogeneic cell source, it may have overestimated patency rate due to the intrinsic resistance of rats to vascular disease.

Another limitation of this study is the amount of polymer degradation noticed in the long term endpoint at 8 weeks. Although the TIPS portion appears heavily remodeled and infiltrated, supporting the hypothesis that TIPS PEUU degradation occurs concurrently with tissue deposition and regeneration, the ES layer remains intact with no visible degradation after 8 weeks. This evidence did not allow for the assessment of whether the TEVG is supportive of a conservative remodeling as a whole (*i.e.*, the degradation kinetics are comparable with the deposition of structurally- and mechanically-sound native ECM leading to a stable TEVG until

complete scaffold degradation occurred), and hence did not allow for proving its suitability as an arterial substitute. We have observed in a separate study (data not shown) that electrospun constructs implanted as an arterial vascular graft can resist *in vivo* degradation for more than six months, without failing mechanically. While it is possible that, by that time, the TIPS layer would be sufficiently remodeled and the newly formed tissue would be strong enough to withstand systemic circulation, concerns arose regarding the degradation properties of the ES PEUU material. Therefore, a comprehensive study to describe and optimize the degradation kinetics of the ES PEUU, and longer-term *in vivo* studies to test the resulting TEVG as a vascular substitute, are required, but was beyond the scope of this dissertation.

Most of the previously described cellular approaches for vascular tissue engineering have relied on a long-term culture period to reach the desired cell density and mechanical strength. It has been shown in this work that the combination of an effective seeding technique (**Chapter 2**) followed by a short term *in vitro* culture period in a dynamic environment (**Chapter 5**) effectively yields a TEVG suitable for arterial applications within a clinically relevant period of time, without adversely affecting the phenotype of the seeded stem cells. In this *in vivo* study within the rat model, some evidence has been provided that such an approach is a suitable alternative to obtain an arterial vascular substitute.

7.0 SPECIFIC AIM 4, PART 2: LARGE ANIMAL AUTOLOGOUS TEVG STUDIES

The allogeneic, small animal study described in the previous sections showed very promising results. Moreover, it answered critical questions demonstrating most of the articulated hypothesis of this work (recall **Section 1.10**). However, the rat model, though inexpensive and practical, might be significantly distant in pathophysiology from the human model [181]. Therefore, a more complex model was subsequently used to bring the approach a step further toward clinical translation. To this end, an autologous study was designed and performed in a clinically relevant, large animal model using pigs.

The domestic pig model has the advantage of having better cardiovascular anatomic and phenotypic similarities with humans than rodents. It is cost-effective and readily available [189]. Domestic pigs have been used for a variety of vascular grafting approaches, including several TEVG studies both for small- [190, 191], and large-diameter [192] applications, and synthetic vascular graft studies [193, 194].

Since time is a key factor to consider when designing a clinically viable approach for tissue engineering, all of the techniques in this work have been designed to take place in a short amount of time. Indeed, the seeding process takes only minutes, the scaffold is readily available off-the-shelf because it can be produced and in stock well ahead of time, and the acute culture within a spinner flask or the Perfuser requires 1 to 3 days to populate the scaffolds with spread cells. The limiting factor, when translating the allogeneic study performed in rats into a fully

autologous approach in pigs, is represented by the cell source. The striated muscle is a valid source of adult stem cells [166], and was chosen for the approach presented. (recall **Section 5.1.1)**. However, the isolation of MDSCs using the preplating technique as previously described [99], is time consuming, requiring approximately 6 days to extract the PP6 fraction of cells (MDSCs) as a small percentage of the total cell number available, before the expansion process can be initiated. While the possibility of MDSC isolation and characterization utilizing more complex methods, such as the fluorescence-activated cell sorting, is certainly an ideal option to obtain the stem cell fraction rapidly [54], due to limited funding and the preclinical nature of these studies, a period of 2 weeks for the stem cell isolation via the preplating technique and their expansion was chosen.

The validity of this approach and time frame was tested in prior pilot studies, which demonstrated its feasibility, and allowed time to troubleshoot a number of issues related to the initial study design (**APPENDIX G**). Specifically, the autologous cell isolation/expansion and scaffold fabrication protocols were modified to accommodate requirements learned during the course of the pilot study.

7.1 STUDY DESIGN

Once the amount of time dedicated to obtain cells was established, the design and the time frame of the study were designed accordingly. In particular, the study entailed a muscle biopsy performed on each animal the first day (Day 0) to isolate autologous stem cells. The following 2 weeks were used to isolate (Days 0-5), and expand and transfect (Days 6-13) the cells with the LacZ promoter for *in vivo* tracking purposes. On Day 14, cells were seeded into ES-TIPS PEUU

scaffolds (recall **Section 4.2**) via S-RVSD (recall **Chapter 3**). After a short period of static culture, the seeded scaffold was transferred in the Perfuser (**Section 5.3**), and cultured dynamically for a 24 hour period prior to implantation on Day 15.

The seeded scaffolds were then implanted either as a carotid interposition graft (CIG) or as an arteriovenous (vascular access) graft (AVG) in a carotid-to-internal jugular vein configuration. The implantation side was randomly selected for each animal. The contralateral side was implanted in a paired-control fashion with a carotid sham for the CIG animals or with a PTFE graft for the AVG animals. The study can thus be divided in three different experimental groups. The first group (pG-1) consisted of animals receiving an autologous TEVG as a CIG for 1 month (n = 5). The second group (pG-2) was animals receiving a CIG for 3 months (n = 4), and the last group (pG-3) was animals receiving a TEVG as an AVG for 1 month (n = 2). It important to note that in the pilot studies (**APPENDIX G**), an additional 9 pigs were used; 7 pigs in pG-1, one pig in pG-2, and another pig in pG-3. These animal could not be included in the final study since they required the variation of several study parameters to address a number of issues encountered during the course of the study. Furthermore, the pilot study did not entail the use of the Perfuser bioreactor (recall **Section 5.3**), but rather a simple culture in spinner flask, as described for the small animal study (**Section 6.1.1**), was utilized.

Recall that the rat study demonstrated very poor patency rates for the unseeded scaffolds (**Section 6.1.4**), suggesting a role of seeded stem cells in the maintenance of patency. For this reason, no unseeded scaffolds were used as controls in this study due to the high cost of the pig model and the apparent lack of usefulness of the unseeded scaffold. Instead, more clinically-relevant controls (*i.e.*, the carotid sham and the PTFE graft) were used. The carotid sham control was used to test the pathogenic effect of the surgical access and manipulation, and the resulting

effects on native healthy tissue due to the presence of foreign suture material at the anastomoses (*i.e.*, iatrogenesis). This was performed to substantiate or rule out the generation of adverse effects as a consequence of the surgery itself, instead of to the properties of the TEVG in the CIG experimental groups. For example, the commonly used, non-resorbable suture for vascular applications, Prolene, has been associated with inflammation and intimal hyperplasia triggered by a foreign body inflammatory reaction [195]. The PTFE control for the AVG group was chosen based on it being the current standard for hemodialysis access requiring arteriovenous connection [196].

A summary of the study design described here is shown in **Figure 7.1.**

After the selected survival period, pigs were sacrificed and a comprehensive set of endpoints were assessed, to evaluate the performance and the remodeling of the TEVG. The planned endpoints included: fluoroscopy to test the patency and the structural consistency of the TEVG (absence of dilations or pseudo-aneurysms); gross pathology to detect the presence of infections, abscess formation, scaffold degeneration, and the formation of thrombus or intimal hyperplasia; histology to assess the TEVG remodeling; SEM to analyze the luminal surface of the scaffold and demonstrate endothelial coverage; immunohistochemistry to evaluate the phenotype of the remodeled TEVG; and, finally, mechanical testing to quantify the degradation/effective remodeling of the TEVG .

A schematic of the endpoints evaluated for the explanted TEVGs is shown in **Figure 7.2**.

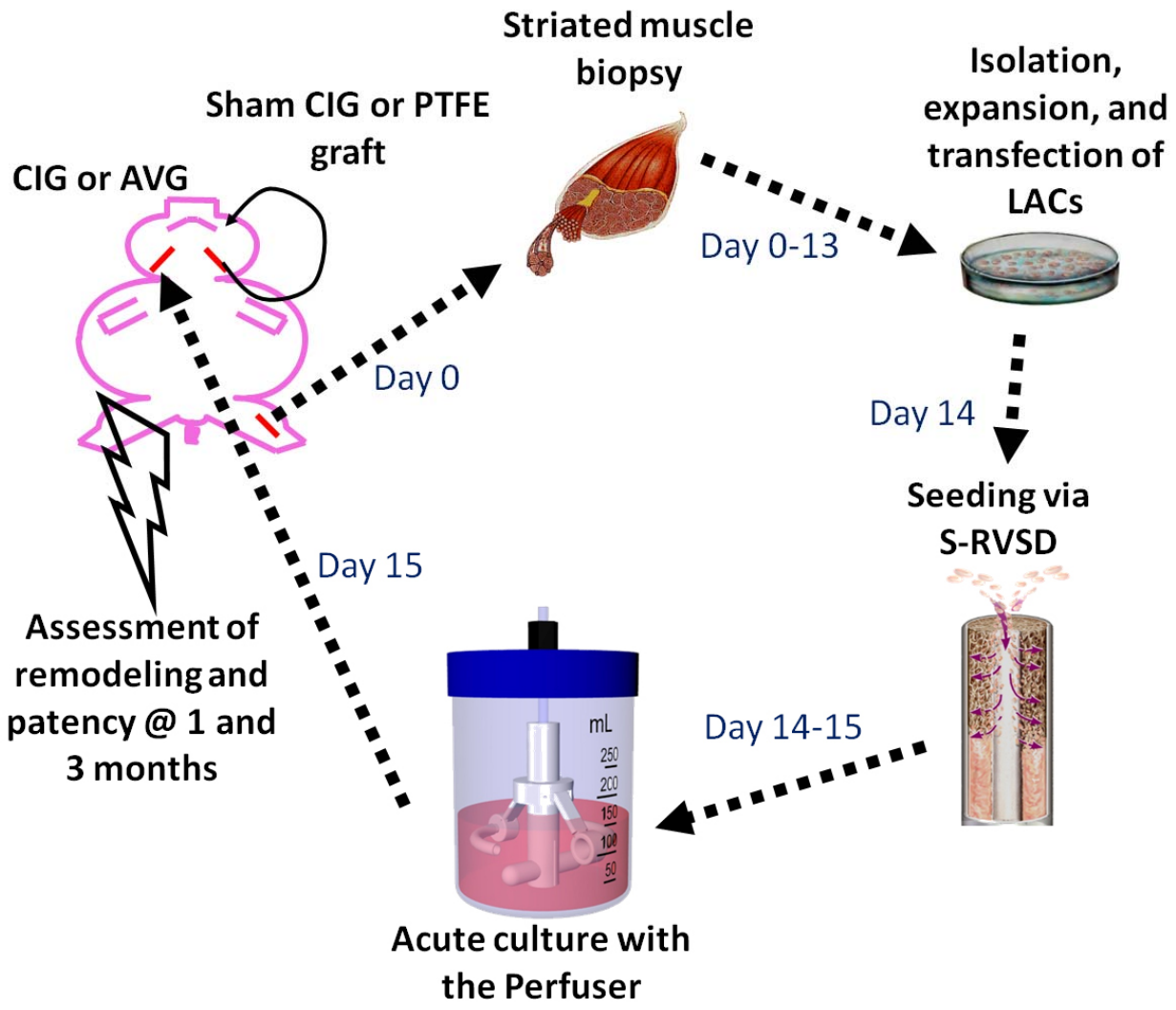

Figure 7.1 Schematic of the pig study design.

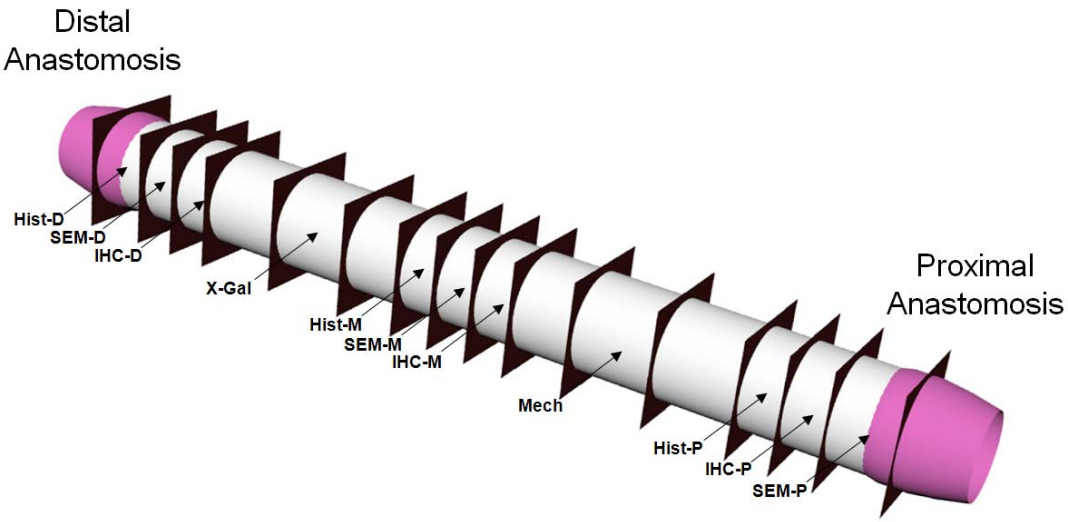

Figure 7.2 Summary of the endpoints assessed for the explanted TEVGs. For each portion of the TEVG (*i.e.*, D = distal, M = middle, or P = proximal), the evaluation of three main endpoints – histology (Hist), SEM, and immunohistochemistry (IHC) was performed.

7.2 PIG MUSCLE BIOPSY PROCEDURE

All animal procedures and treatments were performed in compliance with the IACUC of the University of Pittsburgh.

Pigs (domestic crossbred, weight = 30-35 kg, age = 4-6 months of both sexes) were brought into the animal facility at least 2 days prior to the day of the biopsy procedure, and kept *nil per os* 12 hours prior to surgery. In preparation for the surgery, animals were anesthetized with acepromazine, 0.15 mg/kg, and ketamine, 15.0 mg/kg (both intramuscular) combination, intubated, and maintained at a surgical plane of anesthesia with isoflurane (1-3% in oxygen).

Once each animal was clipped and prepped for the procedures it was moved into the surgical suite and placed on positive pressure ventilation and instrumented with monitoring equipment (ECG). Pulse oximetry and blood pressure were monitored throughout the surgical procedure. After the induction of anesthesia, aseptic surgery was performed.

A monolateral, full thickness, semilunar skin incision (diameter ~ 8 cm) on the gluteus of the animal was performed by a Bovie in order to expose the underlying fat layer (**Figure 7.3-A**). The subcutaneous fat and muscle fascia were carefully dissected within a single flap to expose the lean striated muscle. A superficial muscle biopsy (approximately 5x2x1 cm) was resected with a 10-blade scalpel following the natural orientation of the muscle fibers (**Figure 7.3-B**). The harvested tissue was subsequently placed in cold DPBS supplemented with 5% antibiotic/antimycotic (A/A) solution (Gibco, Invitrogen Corporation, Carlsbad, CA) and stored in ice until processing for cell isolation as described in **Section 7.3**. The resulting muscle cavity was carefully observed for bleeding and cauterized or temporarily packed with sterile gauzes as needed to interrupt minor bleeding (**Figure 7.3-C**). The skin and fat flaps were repositioned and sutured with 3-0 polyglactin absorbable suture (VICRYL, Ethicon, Inc.) with approximately 12-15 separate stitches (**Figure 7.3-D**). A povidone-iodine ointment was applied on the sutured incision at the end of the procedure to avoid post-operative infections upon return in the animal cage. More details on the post-operative care of the animals is provided in **Section 7.6**.

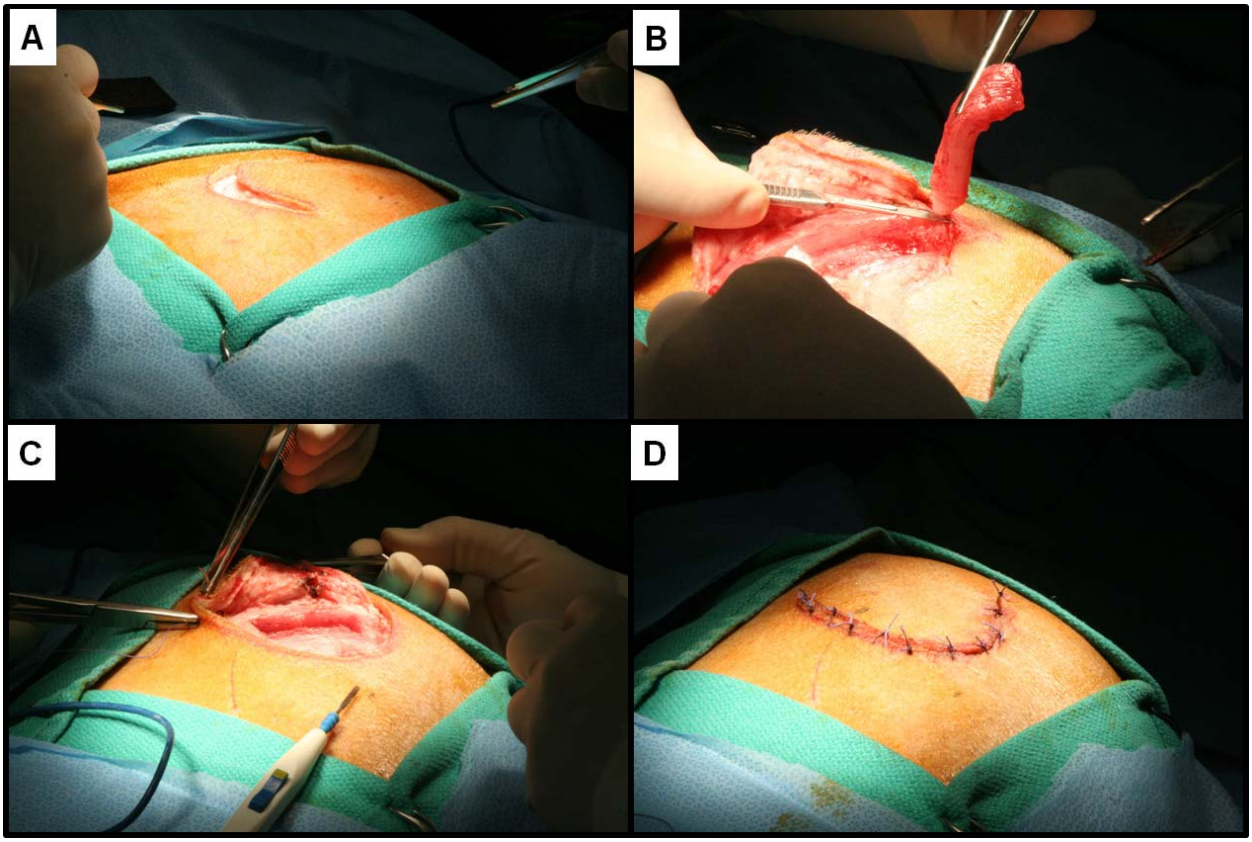

Figure 7.3 Pig muscle biopsy procedure. **A.** A semilunar incision is made with a Bovie. **B.** A flat muscle biopsy following the natural muscle fiber orientation is resected with a scalpel. **C.** The resulting cavity is inspected and dried from oozing blood before closure. **D.** The skin is closed with separate stitches.

7.3 ISOLATION OF PIG SLOWLY ADHERING CELLS

7.3.1 Methods

The muscle tissue was processed within 1 hour from the harvesting. The sterile tube filled with cold DPBS and antibiotic/antimycotic used to transport each biopsy was weighted prior to and

after storing the tissue to retrieve the weight of each biopsy. The isolation procedure was performed in sterile conditions under a laminar flow hood. The tissue was cleaned from macroscopic superficial fat residues with a sharp iris scissor and then serially washed in Petri dishes filled with Hank's balanced salt solution (HBSS) (Gibco) (**Figure 7.4-A**). Each biopsy was then meticulously minced into a coarse slurry in a Petri dish with HBSS (**Figure 7.4-B**), transferred into a 50 mL tube and centrifuged at 3500 rpm for 5 min (**Figure 7.4-C**) before undergoing a three-step enzymatic dissociation. The supernatant solution with additional fat residues was removed and the pellet was resuspended in 0.2% collagenase-type XI (Sigma) and placed in a standard incubator at 37ºC for 1 hour (**Figure 7.4-D**). Every 15 min the tube was gently shaken to facilitate the enzymatic digestion and then replaced in the incubator. The tube was then centrifuged at 3500 rpm for 5 min and resuspended in dispase solution (Gibco; 2.4 units/mL in HBSS) for 45 minutes. After another centrifugation the tissue was finally incubated for 30 minutes in 0.1% trypsin-EDTA (Gibco).

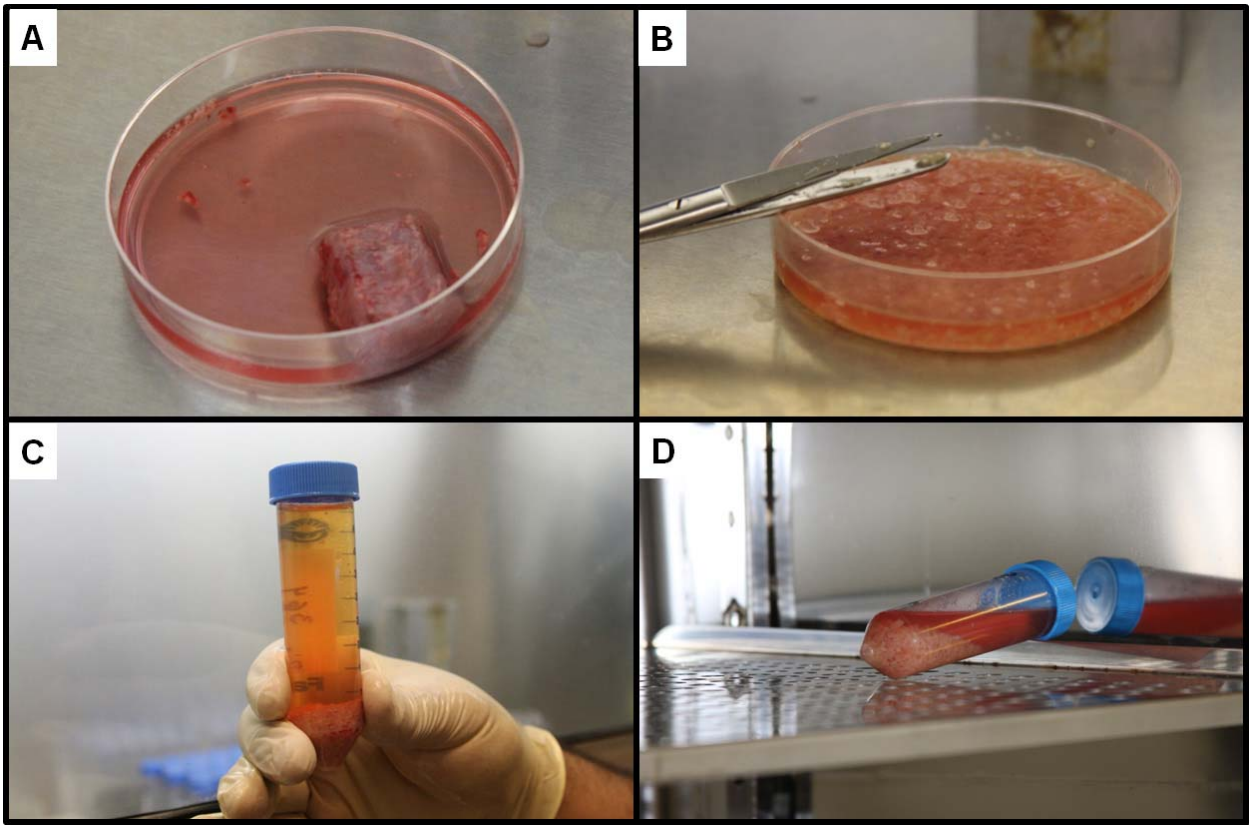

Figure 7.4 Pig SACs isolation via enzymatic dissociation. **A.** The muscle biopsy is cleaned and washed in separate Petri dishes under the laminar flow hood. **B.** The tissue is minced into a coarse slurry. **C.** The processed tissue is centrifuged to remove additional fat residues into the supernatant. **D.** A three-step enzymatic dissociation allows the cells to separate from the muscle ECM.

After completion of the enzymatic dissociation, cells were centrifugated and resuspended in DMEM (Gibco) supplemented with 10% HS (Gibco), 10% FBS (Gibco), 0.5% chicken embryo extract (Gibco), and 1% penicillin/streptomycin (Sigma) and plated into collagen-coated (collagen type I, Sigma) T175 culture flasks for 2 hours. The media with a large number of non-adherent floating cells was then removed and replated into another T175 flask for 24 hours, while cells attached to the first flask received additional fresh media. This process, called "pre-plating", was repeated 5 times every 24 hours. Cells attached to the first flask are defined as

preplating 1 (or PP1), those attached to the second flask PP2, and so on for the remaining 4 days of preplating. The reported protocol is essentially that described for mouse cells [99], in which the PP6 cells are considered to be MDSCs; however, to increase the cell yield, preplatings 3, 4, 5, and 6 were trypsinized and pooled in equal proportions into a single culture flask and expanded (**Figure 7.5**). This population was defined as pig SACs; the name was derived from the variability in time of the adhesion properties of these cells. This decision was made after initial pilot studies (**APPENDIX G**) suggested that the sole yield of the PP6 fraction, following isolation and expansion, was not sufficient to provide enough cellular density into the TEVG within the desired time frame. A limited phenotypic characterization and comparison between the pooled population of PP3, PP4, and PP5 and the PP6 cells (see **Section 7.4**) did not allow us to draw reliable conclusions. However, a speculation in favor of this approach relies on the potentially increased phenotypic heterogeneity of the pooled population compared to the more homogeneous PP6 fraction. The heterogeneity might, in fact, translate to a better *in vivo* outcome, as suggested by the increasing body of evidence supporting developmental heterogeneity more than plasticity as the main mechanism behind the broad therapeutic efficacy of mesenchymal stem cells *in vivo* [197].

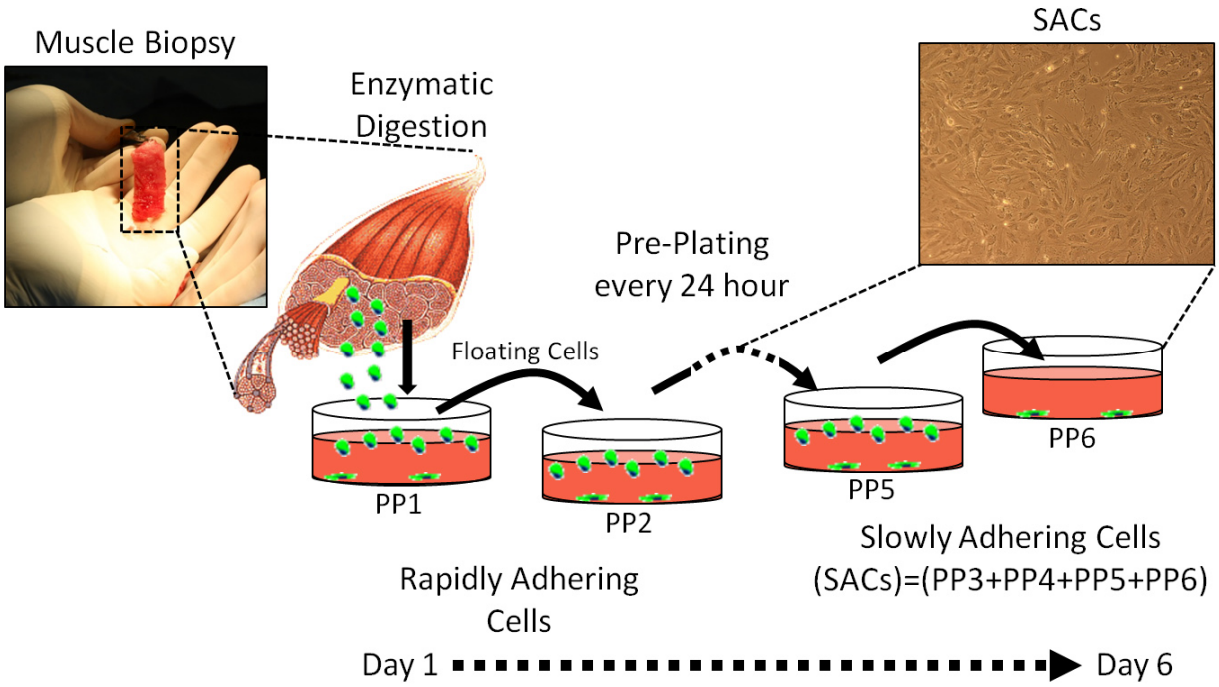

Figure 7.5 Pig SACs isolation via the pre-plating technique.

However, the initial number of SACs plated on the sixth day was still limited by the number of PP6 cells available due to the established requirement of equal cell proportions for each preplating in the pooled culture (*e.g.*, total number of PP6 cells obtained on the sixth day = x, plated number of SACs plated on the sixth day = $4x$).

Two days prior to seeding, SACs were transfected with a retrovirus carrying the gene encoding for β-galactosidase (LacZ) for 24 hours using a protocol previously described in **Section 5.2.2,** and used as needed. A small amount of cells from different isolations (n = 5) were plated in 6-well plates, growth to confluency, and fixed for 10 minutes in 2.5% glutaraldheyde followed by multiple washes with PBS. The plates were then stained with X-Gal overnight to

retrieve the efficiency of LacZ transfection by counting the percentage of transfected cells over the total number of cells visible per field of view.

7.3.2 Results

The isolation and expansion process (starting from the day of the biopsy to the day of cell use lasted 14.2±1.9 days. While two week period was defined *a priori*, as previously explained in **Section 7.1**, the variability was due to schedule constraints. The weight of the muscle biopsy was consistent (10.5±1.6 gr). The total number of PP6 cells obtained on the sixth day, however, was quite variable, being equal to $3.1\pm4.0\text{x}10^5$ cells. This yield corresponded to a PP6 cell isolation density (number of cells per unit of weight of tissue) of $3.2\pm4.6\text{x}10^4$ PP6 cells/gr. The SACs populations were pooled 9.5±1.2 days after the muscle biopsy was harvested, and the time available for expansion of the SACs was 4.4±1.3 days. Within the available expansion time the SACs PD and PDT (as defined in **Section 5.1.2**) were 1.3±0.6, and 93.4±36.3 hours. The resulting transfection efficiency was < 1%.

7.4 CHARACTERIZATION OF PORCINE SACS

No comprehensive characterization of porcine MDSCs is available in the literature. A complete characterization of this cell type, which would require an extensive number of resources and experiments, was considered beyond the scope of the current work. However, a limited characterization based on immunohistochemistry and FACS was performed for pig PP6 cells, as well as a qualitative and quantitative morphological analysis of pig SACs. Due to the complexity and inherent variability in cell biology, this analysis was performed with a pure, phenomenological approach, limiting it to a description of the results obtained without establishing statistical relationships in order to define patterns of generalized features.

7.4.1 Methods

Dedicated pig PP6 isolations (n = 4) were processed for immunohistochemistry against a variety of cell markers for a basic phenotypic screening. Immunostaining was performed following a protocol identical to what was previously described in **Section 5.1.2**. In particular, a general endothelial antibody (APG993, Antigenix), and CD31 (555027, DB Biosciences), were used to detect endothelial markers, desmin (D1033, Sigma) and vimentin (V4630, Sigma) were used as a striated muscle markers, and finally GFAP (G3893, Sigma) was used as a nerve marker. The percentage of positive cells was quantified via an image-based technique as previously described in **Section 3.1.4.3** for the apoptosis quantification.

The percentage of expression of an additional number of surface markers was quantified via FACS in different isolations (n = 5) using the same protocol used in **Section 5.1.2**. In particular, VE-Cadherin (CD144) (V1514, Sigma) was used as an endothelial cell marker, CD45

(APG450F, Antigenix) as a hematopoietic cell marker, CD56 (304610, Biolegend) as a neural cell marker, CD146 (MCA2141F, Serotec) as a pericyte/endothelial cell marker, and finally CD34 (348801, BD Biosciences) as a hematopoietic and myogenic marker.

A qualitative and quantitative morphological characterization of pig SACs in culture prior to their use *in vivo* was also performed. In particular, a series of at least five 100x images per isolation (n = 8) was taken with an inverted, phase-contrast microscope (Nikon TS100, Nikon Digital Sight DS-L1). Each image was quantified via a semi-automatic image processing technique performed with ImageJ, in order to recognize and quantify the size and circularity of cells. To this end, an edge recognition algorithm was used, followed by a threshold filter and a binary filter to eliminate small gaps into well defined shapes. Each image was then assessed with a particle analysis function for area and circularity. The shape index is a shape function that is calculated for each cell as: shape index = 4π (cell area/cell perimeter^2) [198]. This parameter approaches a value of 1 in cases where cells have a circle-like shape, while the value and to 0 in cases of spindle-shaped cells.

7.4.2 Results

All markers used for immunohistochemistry except for vimentin were negative for all tested isolations though no positive controls were used to determine the specificity of the antibodies. The percentage of cells positive for vimentin was 62.3±29.9% (mean ± standard deviation; n = 3).

FACS results showed that pig PP6 cells expressed a variety of markers in different percentages. Positivity for CD144 was 29.2±21.3%, while for CD45 it was 2.9±3.5%, for CD56 it was 18.4±13.7%, for CD146 it was 15.1±19.9%, and finally for CD34 it was 19.5±15.2%.

These results are summarized in **Table 7-1**.

Table 7-1 Percentage of expression of phenotypic markers for pig SACs.

	N	Mean	Standard deviation
CD144	4	29.2	21.3
CD45	4	2.9	3.5
CD56	4	18.4	13.7
CD146	4	15.1	19.9
CD34	4	19.5	15.2

These results do not provide a robust phenotypic characterization of pig PP6 cells isolated via preplating. However, they demonstrate the heterogeneity of the population, which might be desirable for *in vivo* applications as described in the previous section.

A qualitative, morphological assessment of pig SACs for several isolations is shown in **Figure 7.6**, while the results of the image-based cell morphology quantification are summarized in **Figure 7.7** and **Figure 7.8**.

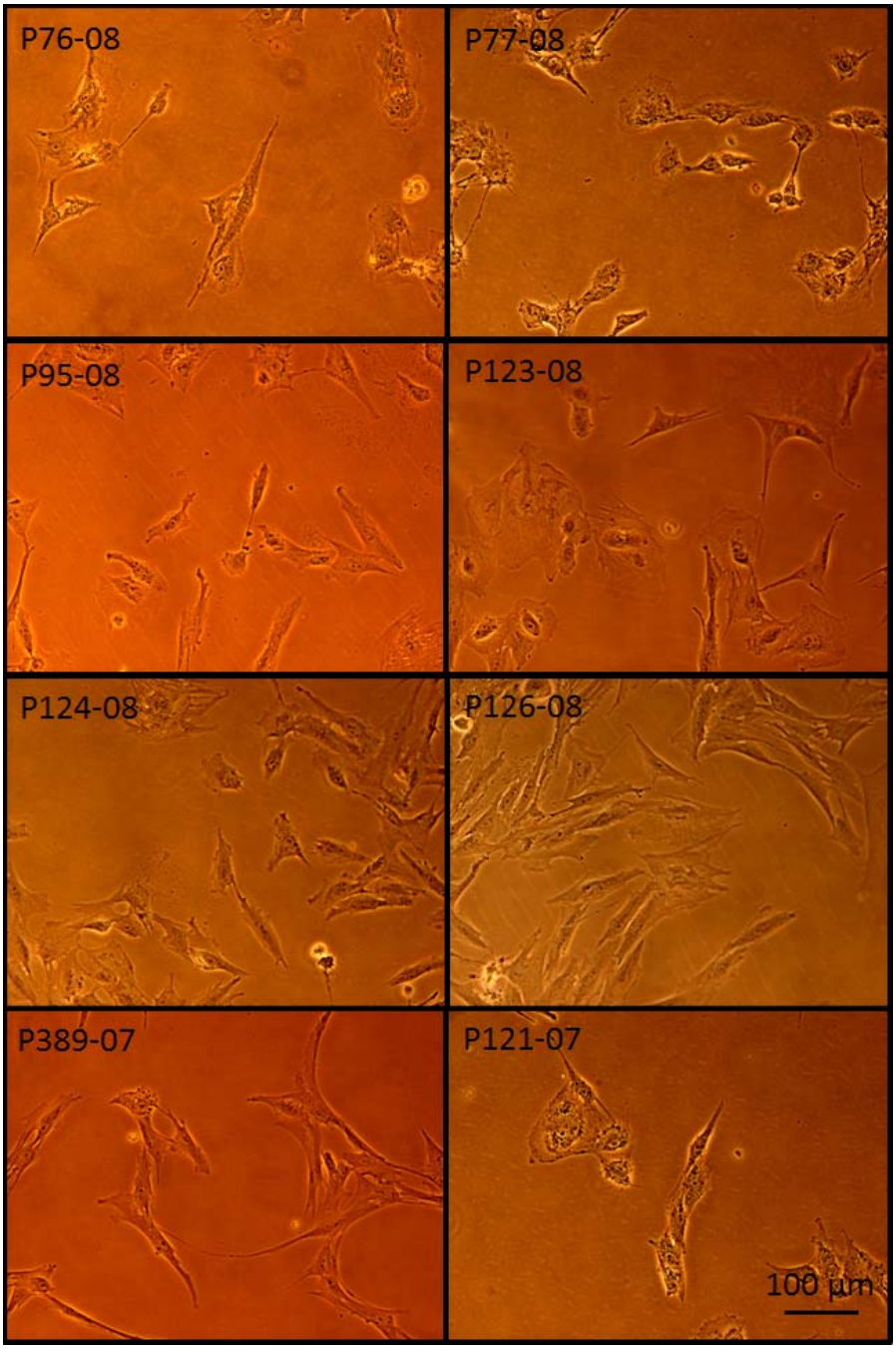

Figure 7.6 Pig SACs morphology. The label on the top left corner of each panel represents the isolation ID of the 8 isolations used for this purpose. Pictures were taken at 200X.

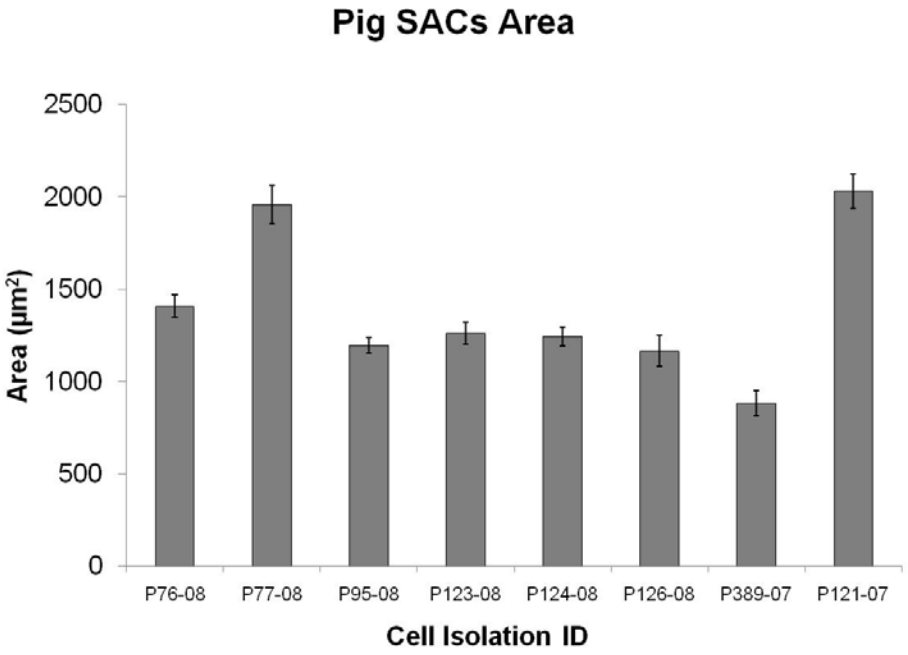

Figure 7.7 Average cell area quantification for 8 different isolations of pig SACs. Measures are presented as mean ± SEM; n > 50.

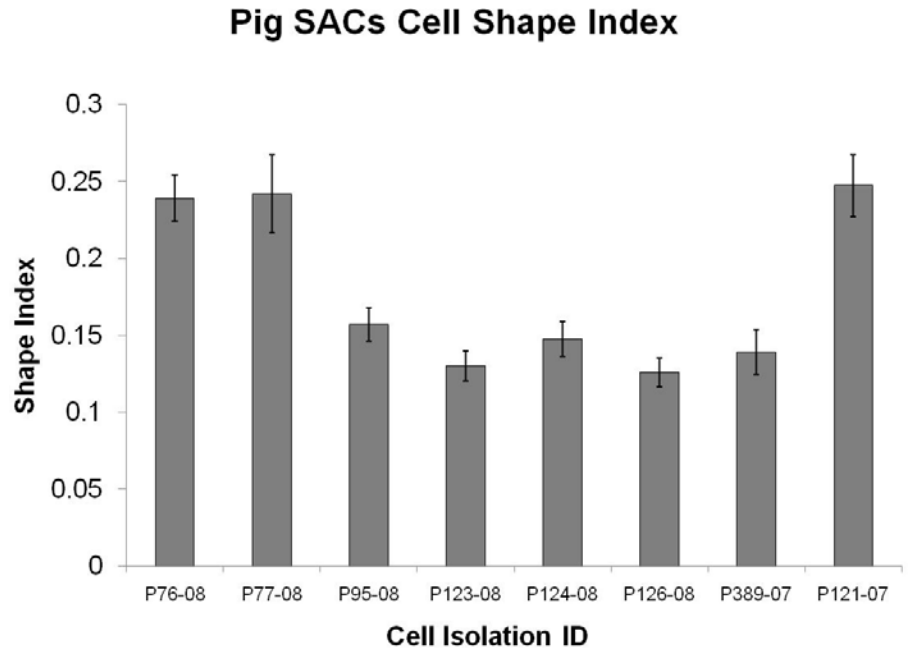

Figure 7.8 Shape index quantification for 8 different isolations of pig SACs. A value of 1 would represent a circular cell, while a value of 0 is linear of highly spindle-shaped. Measures are presented as mean ± SEM.

7.5 SEEDING AND DYNAMIC CULTURE OF PIG AUTOLOGOUS TEVGS

At the end of the 2 week period allocated to isolating and expanding autologous SACs, a TEVG was prepared for each animal one day prior to implantation. SACs from each isolation were trypsinized from the culture flasks and counted on the 14th day post-muscle biopsy. The number of autologous pig SACs available on the designated day of seeding was 14.0±8.0x10^6 cells, far less than the expected 30 million. **Table 7-2** provides the number of SACs available from each isolation used for the TEVG seedings.

Table 7-2 Summary of the number of seeded cells for each of the TEVGs implanted in the pig model. * indicates animals that died shortly post-operatively.

Pig ID	Experimental Group	Seeding Date	Seeded Cell Number (x10^6)
P75-08	pG-2	04/13/08	6.53
P76-08	pG-2	04/14/08	11.01
P77-08	pG-2	04/15/08	4.52
P95-08	pG-2	05/05/08	10.35
P100-08	pG-1	05/14/08	13.65
P101-08	pG-3	05/15/08	15.61
P102-08*	pG-1	05/15/08	14.83
P123-08	pG-1	06/10/08	5.78
P124-08	pG-1	06/11/08	22.57
P125-08	pG-1	06/10/08	22.75
P126-08*	pG-3	06/10/08	27.61

The average yield for the isolations obtained in these studies was significantly lower ($p = 0.0095$) than that obtained previously in the pilot study ($37.3 \pm 24.7 \times 10^6$ cells). The reasons for this are unknown. The combined low number of available cells and the high variability in cell yield among different isolations caused each TEVG to receive a low and variable number of autologous cells. This limitation, although undesirable in the paradigm of the study, was unavoidable. The low yields obtained in the isolations of the first TEVGs implanted needed to set the standard for cell number in all subsequent TEVGs to be consistent. However, as suggested by the rat study, seeded MDSCs have a critical role in the maintenance of patency and in the remodeling of the TEVG *in vivo* (**Section 6.1.5**). Despite this, due to the large number of people needed to be coordinated for each experiment, and to the tight schedule of the animal surgical suites and housing space, the time flexibility allowed for this study was minimal. As a result, we were forced to settle for the cell yields obtained in each isolation.

The scaffolds used for the pig study were the ID-4.7 ES-TIPS PEUU, prepared to a length of 5 cm. At least two scaffolds per cell isolation were fabricated and sterilized as previously described (**Section 4.2.2**) in preparation for each seeding. The availability of two scaffolds per isolation was originally planned for two purposes. One was to provide a backup scaffold in case of inherent, macroscopic (*e.g.*, delaminations, tears, *etc.*), or microscopic (*e.g.*, low porosity, *etc.*) defects of the other, which could potentially have affected the seeding outcome. The other was to serve as a TEVG backup in case of unexpected issues after the seeding was completed (*e.g.*, contaminations, damages caused by handling or by surgical manipulation, *etc.*). This redundant approach was also thought to simulate the scenario of a future clinical application of this technology. However, the unexpected low cell yield obtained

from each isolation did not allow for a TEVG backup approach and, therefore, only a scaffold backup approach was utilized.

More than 95% of the total cell number available was suspended in 20 mL of complete SACs media (see **Section 7.3**) in preparation for seeding. The remaining percentage of cells was replated and expanded for cell characterization purposes as described in **Section 7.4**.

The scaffold for each animal was mounted onto the tees of the S-RVSD, secured with 2-0 silk ligations, and primed with warm DPBS with the priming valve in the open position. While infusing the DPBS for priming the lumen of the scaffold, the Diffuser was brought in the initial seeding position (in proximity of the Driving Tee; recall **Figure 3.2**). The seeding parameters were consistent with those described in **Section 3.1.4** for the testing of the S-RVSD. The seeding process used for the TEVGs for the pig studies is shown in **Figure 7.9**.

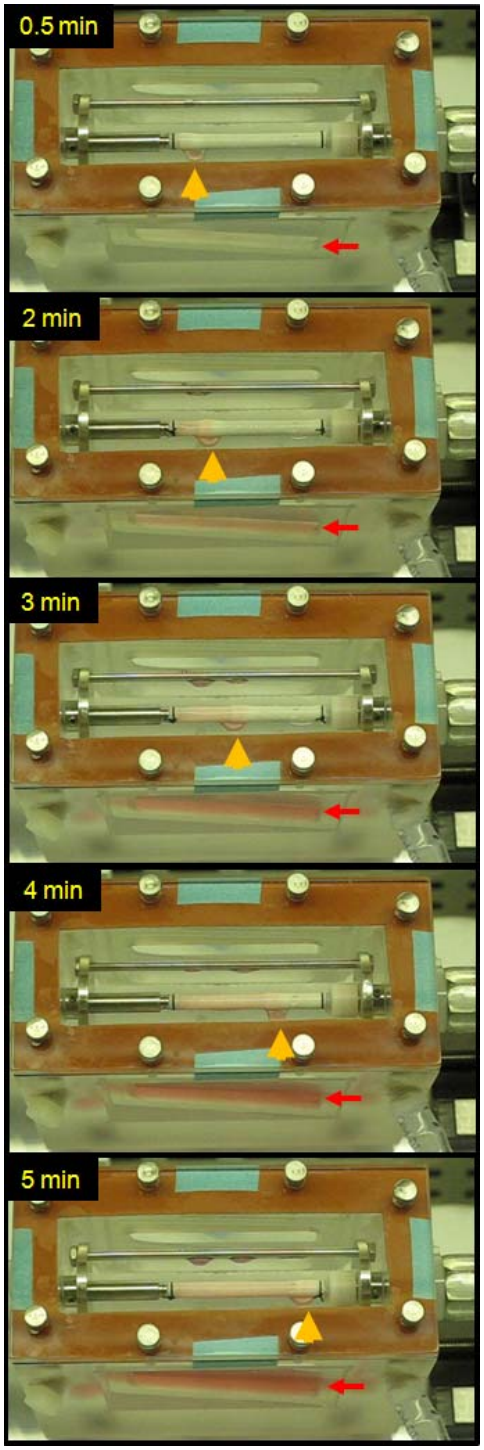

Figure 7.9 Representative seeding of a 5 cm-long ID-4.7 ES-TIPS PEUU scaffold seeded with pig SACs for one of the TEVGs. The sequence is in chronological order during the seeding process. The yellow arrows indicate the current position of the internal Diffuser identified by the local exudation of seeding suspension drops. Note how the scaffold has two distinct colors during seeding: a left pink side denoting the portion already seeded, and a right white side denoting the portion yet to be seeded. The red arrows indicate the increasing level of media exuded out of the scaffold and collected into the chamber during seeding.

Immediately after seeding, the scaffolds were left in the S-RVSD for approximately 10 min to let the cell settle into the pores of the scaffold, and then transferred with minimal manipulation into a 50 mL tube filled with complete media and cultured in static condition for 2 hours in a standard cell culture incubator specifically devoted for these preclinical tests. The cap of the tube was partially unscrewed to allow for gas exchange between the cell culture media and the incubator. Due to the lack of a TEVG control, no spare portion of the constructs (*e.g.*, a small ring) could be dedicated for analysis of the seeding results. Based on the S-RVSD testing results from **Section 3.1.4**, it was felt that this decision was fully justified. Concurrent with the beginning of static culture, a Perfuser system for each TEVG was primed with 200 mL of complete culture media, placed with unscrewed caps into the same incubator on top of its electronic platform, and put in rotation at 20 rpm to equilibrate temperature and pH of the media.

After the 2 hour period of static culture, each construct was mounted into its dedicated Perfuser via 4-0 silk ligation and placed in rotation for 24 hours at 20 rpm. At the end of the this acute dynamic culture, scaffolds were transported to the surgical suite directly in the Perfuser, which was enclosed in an aluminum foil-coated styrofoam container to prevent heat loss and contamination during transport.

Just prior to implantation, each TEVG was trimmed at the two ends for surgical sizing purposes, and the excised portions were fixed in 10% formalin, dehydrated following standard histological protocols, and embedded in paraffin blocks. Sections (5 μm-thick) were cut and processed with H&E staining and imaged at 40x to evaluate the pre-implantation cellularity of each scaffold as well as the consistency in size between the scaffolds (**Figure 7.10**).

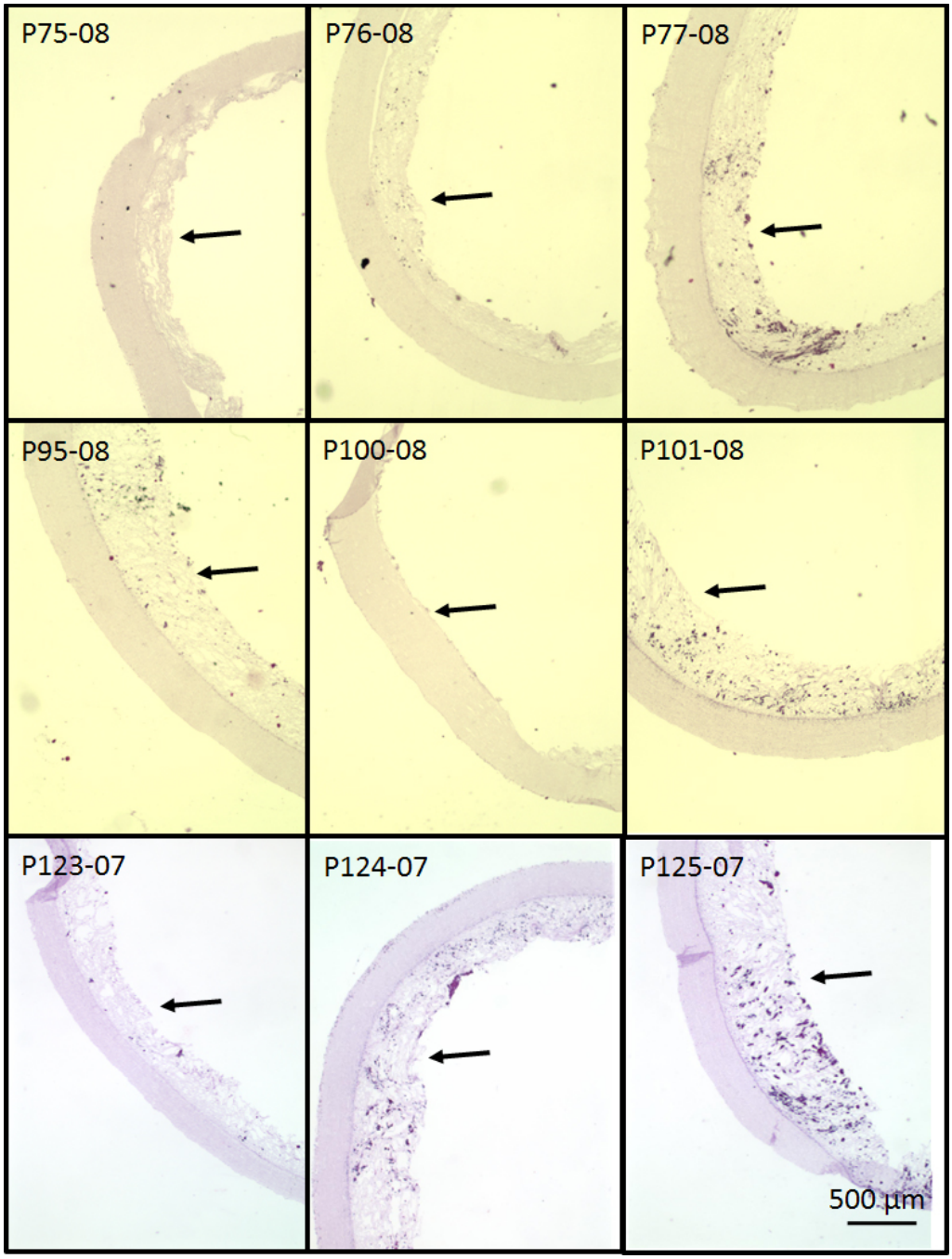

Figure 7.10 Pre-implantation histology of the TEVGs used in the pig study. The label in the top left corner of each panel represents the animal ID number. The arrows indicate the lumen of the scaffolds. Note that the sections cut for the P100-08 scafold experienced delamination between the ES and TIPS layers, due to inherent scaffold defect, leading to loss of the TIPS layer during the histology processing. Therefore, only the ES layer is visible.

Consistent with the low cell numbers available for seeding (**Table 7-2**) all TEVGs exhibited a low level of cellularity prior to implantation, resulting in nearly acellular implants. The ES layers of the scaffolds were approximately (qualitatively) uniform in thickness from scaffold to scaffold, while the TIPS layer exhibited variability between scaffolds (*e.g.*, different thicknesses, densities, *etc*). Moreover, some partial or complete delaminations between the two layers were observed (**Figure 7.10**). These defects were presumably generated by some variability in the ES-TIPS fabrication process and not due to the seeding, the dynamic culture of the TEVG, or sectioning artifacts. Significant discrepancies in scaffold quality between what was observed during the testing of the S-RVSD (recall **Section 3.1.4.5**) and the Perfuser (recall **Section 5.4.1**), and the pre-operative results of these *in vivo* studies were observed. While it is difficult to identify univocally the reasons for these discrepancies, some speculations will be provided in **Section 7.10**.

7.6 CAROTID INTERPOSITION GRAFT PROCEDURE

Following the consclusion of the seeding and dynamic culture approximately 2 weeks after the muscle biopsy procedure, each pig received an autologous TEVG. Three days prior to the implantation, animals started receiving prophylactic platelet aggregation inhibitor therapy (clopidogrel, 75 mg by mouth, daily). Animals were prepared and anesthetized for surgery as described in **Section 7.2**, and then placed in the supine position, and prepped. A surgical field was created in the cervical area. Bilateral cervical incisions (~ 15 cm) were made with a Bovie through the skin and the underlying Platysma. In one side, a cannulation was performed on the

external jugular vein as an intravenous access during surgery. For each side, the sterno-cleido-mastoid was dissected and retracted from the underlying trachea and tissues by two Weitlaners. The common carotid arteries were exposed and completely dissected from the internal jugular veins for a length of approximately 8 cm. Concurrently, the autologous TEVG was removed from the Perfuser and washed in a basin containing ~300 mL of sterile saline supplemented with ~100 IU mL of heparin to remove culture media residues.

One carotid (side randomly selected) chosen to receive the TEVG was operated on first, while the other exposed carotid was temporarily packed with saline-impregnated gauzes. After a baseline ACT time was acquired, the animal was heparinized with an initial dose of 150 IU/kg, and subsequently re-heparinized as needed to maintain an ACT level higher than 2.5-fold the baseline level. The carotid was then clamped with two Cooley's vascular clamps, and a 2 cm portion was excised between the vascular clamps. The subsequent retraction of the carotids created a gap of length ~5 cm due to the residual vascular longitudinal tension. Vascular spasm due to the surgical manipulation was relieved with papaverine solution applied locally, as needed.

The autologous TEVG was then interposed to the carotid gap and sized to a length of approximately 4 cm by cutting the ends. These TEVG rings were fixed in 10% formalin and processed to assess pre-implantation histology. The two ends of the graft and carotid were spatulated with Potts scissor to correct any size mismatch due to the onset of vascular spasm. The TEVG was then anastomosed in an end-to-end fashion with separate 7.0 Prolene (Ethicon) stitches. Before completing the distal anastomosis and permanently resuming blood flow, the graft was carefully de-aired by briefly releasing the proximal vascular clamp. The TEVG was pliable, simple to handle and to suture, and exhibited visible pulsatility under arterial blood flow.

In two animals, the graft required removal of small thrombi by internal release of a few boluses of heparinized saline with a syringe before completion of the distal anastomosis. This issue was apparently caused by an erratic and unpredictable coagulatory behavior of these two animals, leading to sudden drops in ACT level during surgery, and unresponsiveness to additional administration of heparin.

The contralateral side was then operated on in the same fashion, but using as a graft a 2 cm portion of native carotid (*i.e.*, a portion of carotid was excised and immediately reconnected via two end-to-end vascular anastomosis).

Before closing the surgical access incisions, the surgical field was carefully checked for bleeding or oozing and cauterized or treated accordingly. In some instances the anastomotic sites of the grafts were treated with absorbable hemostats (Surgicel, Ethicon) to address minimal blood leaking, or additional stitches were made to stop more significant bleeding from the anastomosis. A summary of the surgical vascular procedure is shown in **Figure 7.11**.

The Platysma was then closed with 2-0 Vicryl (Ethicon) with full thickness bites in a running fashion, while the skin was closed with intradermal running suture using 3-0 Vicryl (Ethicon).

Following the surgical procedure and cessation of inhalation anesthesia, animals were extubated after exhibiting swallowing and protective cough reflexes, and kept warm and dry for the following post-operative hour to prevent hypothermia. The animals were then monitored hourly for 24 hours.

Analgesia (buprenorphine hydrochloride, 0.005-0.01 mg/kg, intramuscular, twice a day), and antibiotics (cefuroxime, 100 mg/kg, intramusclular, twice a day) were administered at

regular intervals for 4 days post-operatively, and were continued as needed if signs of pain or infection were noted.

Anti platelet aggregation therapy (clopidogrel, 75 mg, and aspiring, 325 mg, per mouth, once a day) was maintained for the first 4 weeks to ensure proper tissue remodeling and endothelialization and to reduce chances of acute graft occlusion. Aspirin administration was continued for the entire survival period.

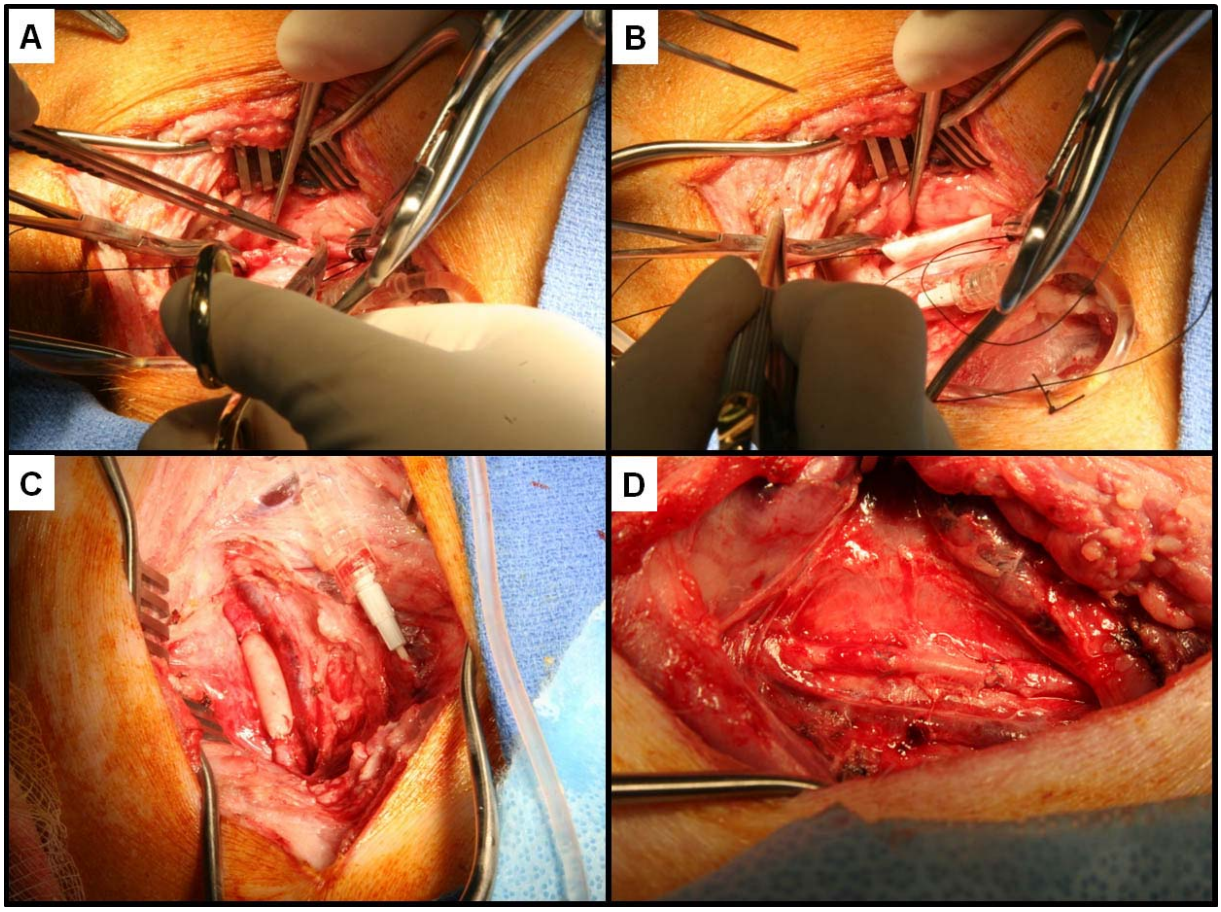

Figure 7.11 Summary of the carotid interposition graft procedure. **A.** Both carotids are dissected from the underlying internal jugular veins and pneumogastric nerves and a 2-cm portion is excised. **B.** The TEVG is properly sized to a length of 4 cm and anastomosed with separated stitches. **C.** Appearance of the TEVG after the blood flow is resumed. **D.** Appearance of the carotid sham after the blood flow is resumed.

7.7 PIG CAROTID-TO-INTERNAL JUGULAR ARTERIOVENOUS GRAFT PROCEDURE

The preparation of the animal and the surgical access for the AVG procedure was identical to that described in **Section 7.6** for the CIG configuration. The carotid was dissected from the internal jugular vein (IJV). The TEVG was sized to a length of 4.5 cm and spatulated at its ends. After administration of heparin, a 2 cm portion of carotid was isolated by two Cooley's clamps in proximity of the distal end of the dissection from the underlying IJV. The adventitial layer of the carotid was thinned with Potts scissors and access to the lumen of the carotid was gained via a short incision made with a #11 scalpel blade through the medial and intimal layers. The incision was enlarged with a clean longitudinal cut by Potts scissors to a length of approximately 8 mm. The carotid incision was oriented laterally toward the IJV (*i.e.*, the cut was positioned 45° from the anterior wall of the carotid (taken as 0°)). A four-quarter running suture was performed with 7-0 prolene to anastomose the TEVG to the distal portion of the carotid. After the arterial (proximal) anastomosis was performed, vascular clamps were briefly released to check for patency and immediately reclamped. Likewise, an identical anastomosis was performed on the proximal portion of the dissected IJV. The venous (distal) anastomosis was oriented at an angle of 225º from the anterior wall of the IJV (**Figure 7.12-A**).

An identical procedure was performed contralaterally using a commercially available, 6 mm-ID PTFE vascular graft (W. L. Gore & Associates, Inc., Flagstaff, AZ) as control (**Figure 7.12-B**). Following the completion of both anastomoses, the grafts were manually felt to check for the characteristic vibrations generated by the transitional flow at the venous anastomoses [199], demonstrating graft patency and high flow. This effect is due to the reduced vascular

resistance following AVG shunting, which generates a supraphysiologic flow through the AVG leading to turbulences perceivable through the wall of the graft.

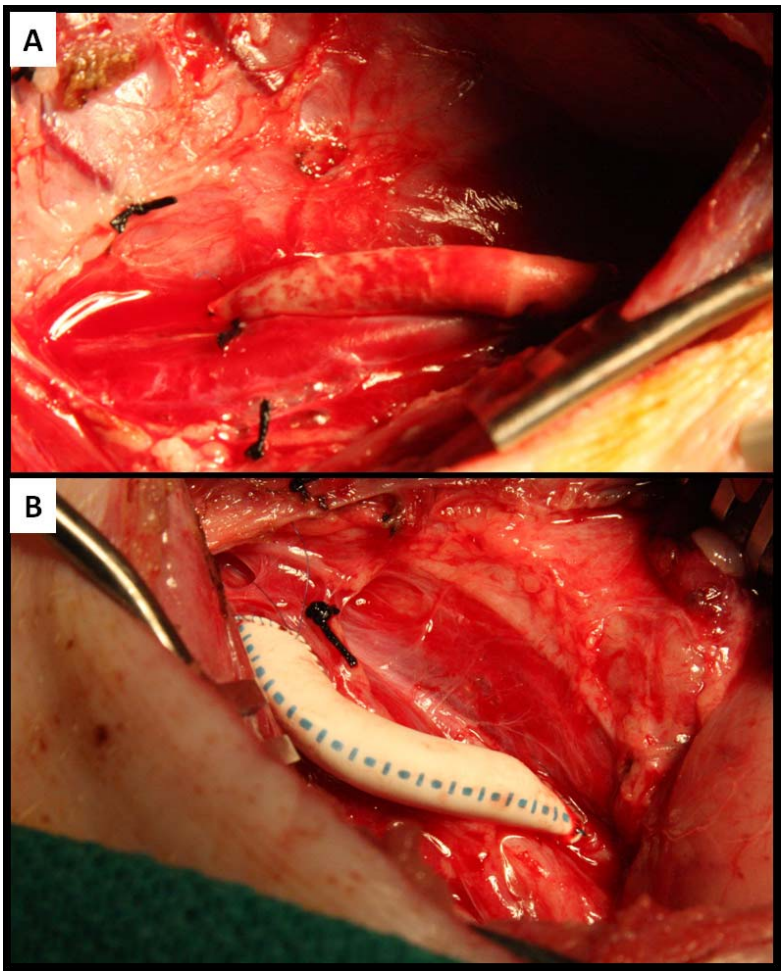

Figure 7.12 AVG procedure. **A.** Aspect of the TEVG after completion of both anastomoses. **B.** Contralateral PTFE graft used as control.

7.8 PIG CAROTID ARTERY HISTOMORPHOLOGICAL AND PHENOTYPIC ANALYSIS

A qualitative histomorphological and phenotypic study was performed on porcine native common carotid arteries. The purpose of the study was to define positive controls for any of the histological and immunohistochemical endpoints originally planned after *in vivo* remodeling, and to define some dimensional landmarks in terms of wall thickness and internal diameter. This was considered paramount to demonstrate univocally the characteristics of the remodeled TEVG and, at the same time, to create a basis of comparison between native and tissue engineered vessels after remodeling.

To this end, native porcine carotid arteries, harvested from pigs within the initial pilot studies, were processed following standard laboratory protocols for a set of histological staining including H&E, Movat's pentachrome (fibrin and muscle), Masson's thricrome (collagen), Verhoeff's (elastin), and picrosirius red (collagen organization/maturation and orientation). The results are shown in **Figure 7.13**.

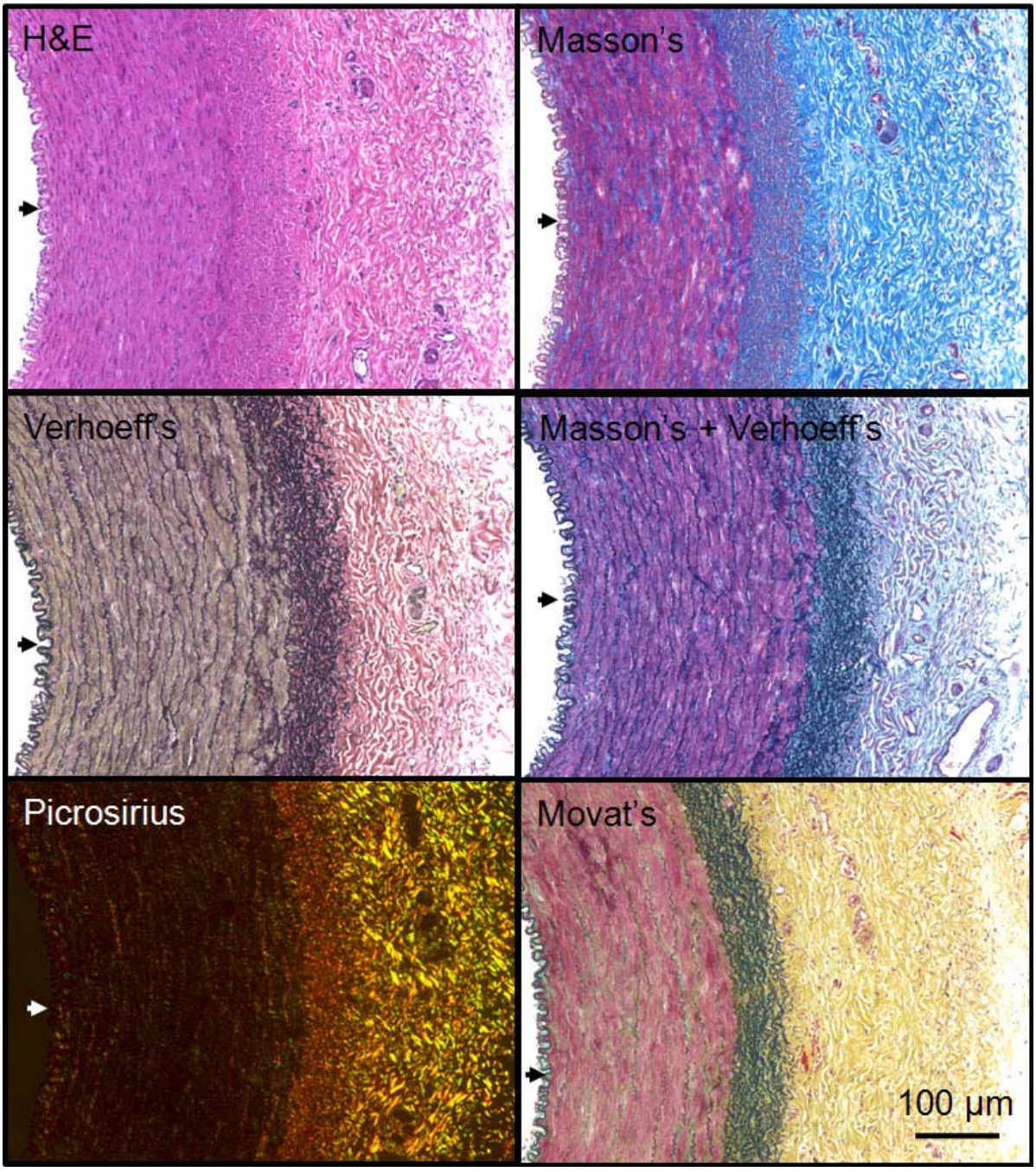

Figure 7.13 Histological positive control for porcine carotid arteries. The arrows indicate the lumen of the artery. The images were taken at 10X. Color codes: H&E: purple = nuclei, pink = tissue; Masson's: same as H&E and blue = collagen; Verhoeff's: same as H&E and black = elastin; picrosirius: green = immature collagen fibers, yellow = partially mature collagen fibers, red = completely mature collagen fibers; Movat's: black = elastin, red = muscle, yellow = collagen, blue = glycosamino-glycans.

Additional freshly excised porcine carotid arteries were fixed in 4% paraformaldehyde and processed for immunohistochemistry following the protocol previously described in **Section 5.1.2**. Several primary antibodies against smooth muscle and endothelial markers were used. In particular, as smooth muscle markers, α-SMA (1:500) (A5228, Sigma), and h1-calponin (1:400) (M3556, Dako) were employed. As an endothelial marker vWF (AB6994, AbCam) was used. Additional antibodies were previously attempted against MHC (1:400) (M3558, Dako), vWF (1:200) (A0082, Dako), and CD31 (1:40) (M0823, Dako) without success, so they are not reported here.

The results are shown in **Figure 7.14**.

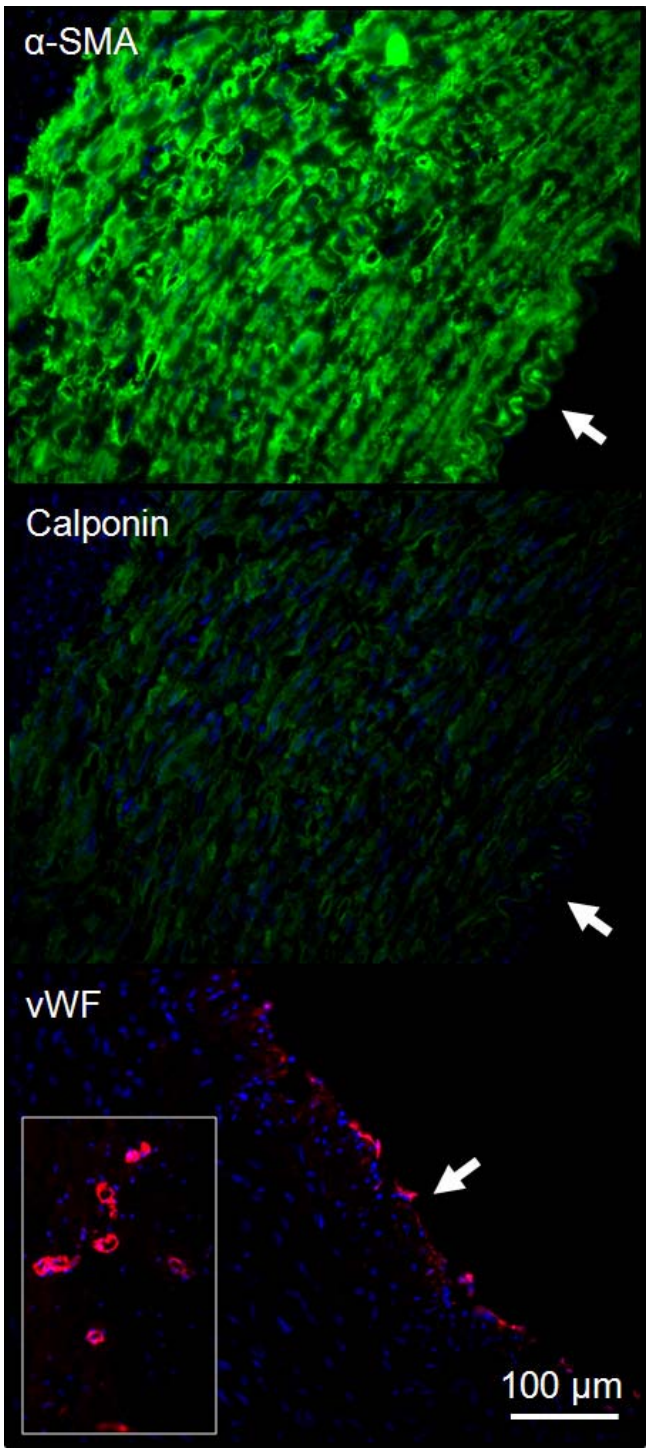

Figure 7.14 Immunohistochemistry positive control for porcine carotid arteries. The arrows indicate the lumen of the artery. In the top and middle panes green = marker, blue = nuclei. In the bottom panel red = vWF, bleu = nuclei. The inset in the vWF panel shows positivity for *vasa-vasorum* in a peri-adventitial location of the artery. The images were taken at 20X. The scale bar in the bottom panel applies to all panels.

7.9 PERFORMANCE AFTER *IN VIVO* REMODELING

Two animals did not complete the expected survival period. The first pig (from pG-1) died overnight, approximately 12 hours after the TEVG implant surgery. During necropsy, a very large volume of blood clot (~ 400 mL) was found in proximity to the carotid sham and allegedly caused a fatal trachea compression leading to asphixia. The animal was replaced, in order to maintain the originally planned number of animals for pG-1. The second animal (from pG-3) died within the first hour post-surgery. The cause of death is not clear, however, due to some coagulatory anomalies recorded during the surgery, it is likely that the animal had a fatal stroke. Unfortunately, this animal could not be replaced due to financial constraints and therefore, only one animal was used for pG-3. All the other animals completed the planned survival period without relevant issues.

At the end of the designated survival period, each animal was euthanized. To this end, anesthesia was induced with an intramuscular injection of telazol ketamine xylazine (0.03 mL/kg). The animal was then put on a mask infusing 5% isofluorane in 100% oxygen, a catheter was inserted into an ear vein, and systemic administration of heparin (30,000 IU) was followed by a lethal injection of KCl (120 mL).

Each animal was then prepared for necropsy. A circular cervical incision was made to remove completely the anterior skin and muscle wall of the neck, for easy access to the grafts. For both CIG and AVG configurations, the Sterno-cleido-mastoids were retracted and both carotids were exposed 2-5 cm upstream to the original surgical area and ligated with a 2-0 silk.

Downstream to the ligation (~ 1 cm) a barbed cannula provided with a unidirectional valve was inserted into the lumen of the carotids and held in place by 2-0 silk suture. The animals underwent dynamic angiography (OEC 9800 Plus, GE Healthcare, Piscataway, NJ), while contrast media (Renografin-60, Bracco Diagnostics, Princeton, NJ) was contemporaneously infused in both carotid arteries.

According to fluoroscopy findings, the patency rate of the TEVG for all three experimental groups was 0%. The patency rate for the carotid sham control in pG-1 and pG-2 was 100%, while the only animal from pG-3 had a control PTFE graft patent after one month.

Figure 7.15 shows a representative fluoroscopy of each experimental group.

Following the fluoroscopy, the grafts were completely exposed and imaged with a digital camera by dissecting the adherent scar tissue resulting from the previous surgical procedure. All the TEVGs were surrounded by a thick collagenous capsule, which created an external layer spanning between the anostomoses (**Figure 7.16-A/C**). This finding suggests a foreign body response generated by the presence of the biomaterial (PEUU). No signs of infection, abscess, or chronic inflammation were noticed in any of the grafts or in the surrounding tissues. None of the TEVGs had any signs of mechanical failure or dilations, suggesting that, while patent, TEVGs were structurally stable and, in part therefore, met the design goals for scaffolds described in **Chapter 4**. The sham carotid controls did not exhibit the same surrounding collagen capsule nor any sign of infection or inflammation (**Figure 7.16-B/D**). The TEVG and PTFE grafts in the only successful animal from pG-3 were hidden by a very thick and rigid capsule which did not allow reasonable exposure of the grafts by further dissection; therefore, they were not photographed for inclusion in **Figure 7.16**.

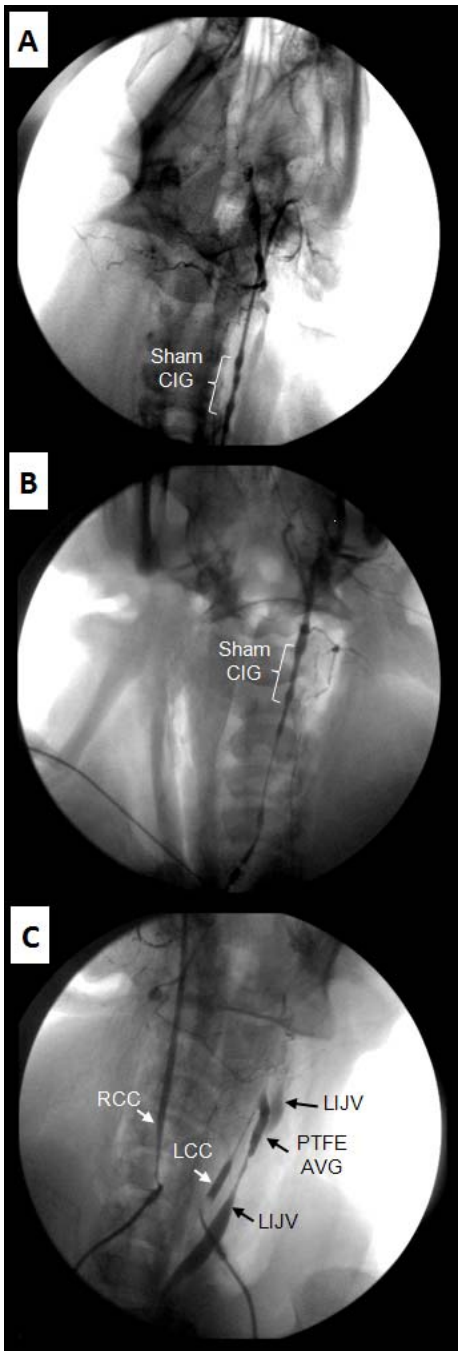

Figure 7.15 Fluoroscopies representing each group in pig studies. **A.** Representative aspect of a fluoroscopy from pG-1. **B.** Representative aspect of a fluoroscopy from pG-3. **C.** Fluoroscopy of the only animal from pG-3. RCC = right common carotid artery, LCC = left common carotid artery, LIJV = left internal jugular vein. None that none of the contralateral TEVGs can be visualized

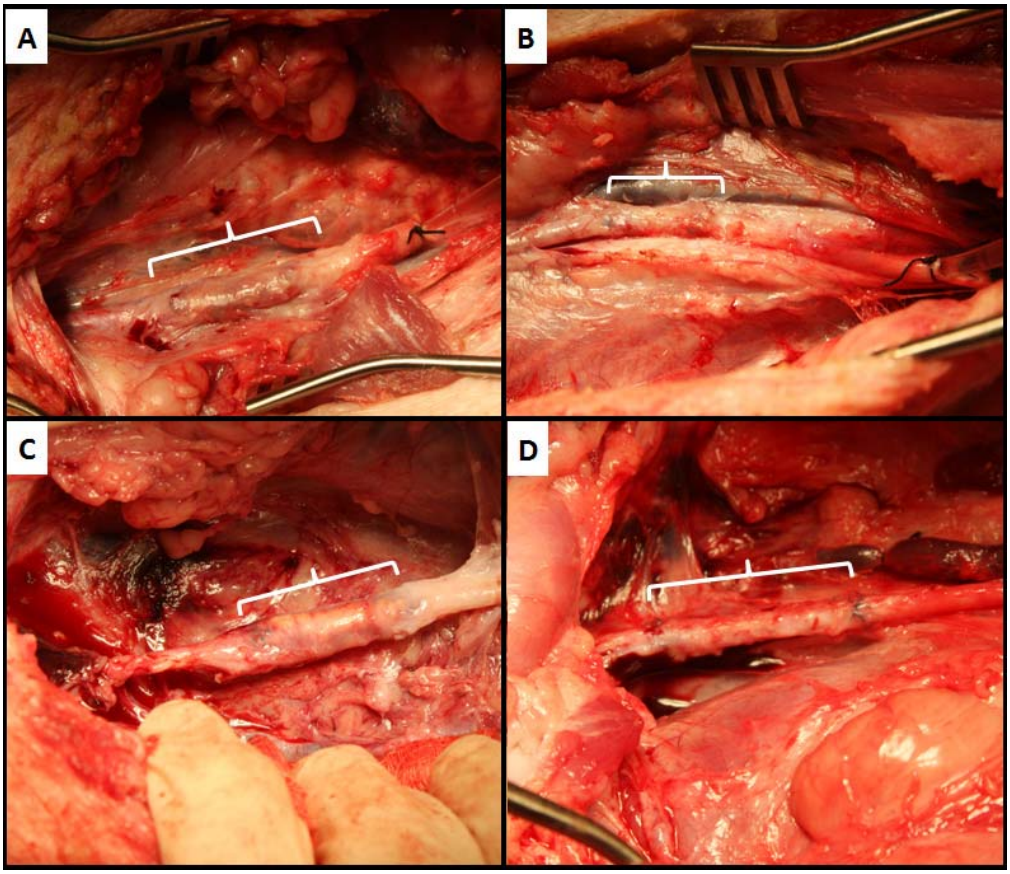

Figure 7.16 Pig necropsy. **A.** Representative aspect of a TEVG from pG-1. **B.** Representative aspect of a carotid sham from pG-1. **C.** Representative aspect of a TEVG from pG-2. **D.** Representative aspect of a carotid sham from pG-2. The braces indicate the location and extension of the grafts. Note the presence of the underlying blue stitches used for the anastomosis at the extremities of each graft. The right side of each picture corresponds to the proximal portion of the graft.

The grafts were then excised and cut in three equi-sized sections (*i.e.,* proximal, middle, and distal) with a razor. The graft consistency under the razor was firm, supporting the presence of ECM within the TEVG lumen in all groups. The external collagenous capsule was not adherent to the external surface of the TEVG in all groups. After the cuts were made, the external capsule retracted consistently in all groups, presubably due to the presence of residual stress. Each segment was then observed on end under a dissecting zoom stereo microscope (SMZ660, Nikon Instruments Inc., Melville, NY) and imaged.

All TEVGs appeared obstructed by a glistening, pinkish matter consistent with intimal hyperplasia (**Figure 7.17**, **Figure 7.18**, and **Figure 7.19**). In most of the specimens it was possible to detect a small lumen in the center of the TEVG, likely a sign of a progressive reduction of internal diameter along with the development of intimal hyperplasia.

The carotid sham grafts for both time points appeared free of thrombuses or any other irregularity. The lumen seemed glistening and whitish, consistent with the presence of a healthy endothelium. The observed internal diameter of this group was highly variable among animals, likely due to the presence of a residual spasm (**Figure 7.17** and **Figure 7.18**).

The PTFE graft appeared partially occluded by irregularly-shaped, organized thrombi adherent on a portion of the lumen. The remaining luminal area seemed free of major issues (**Figure 7.19**).

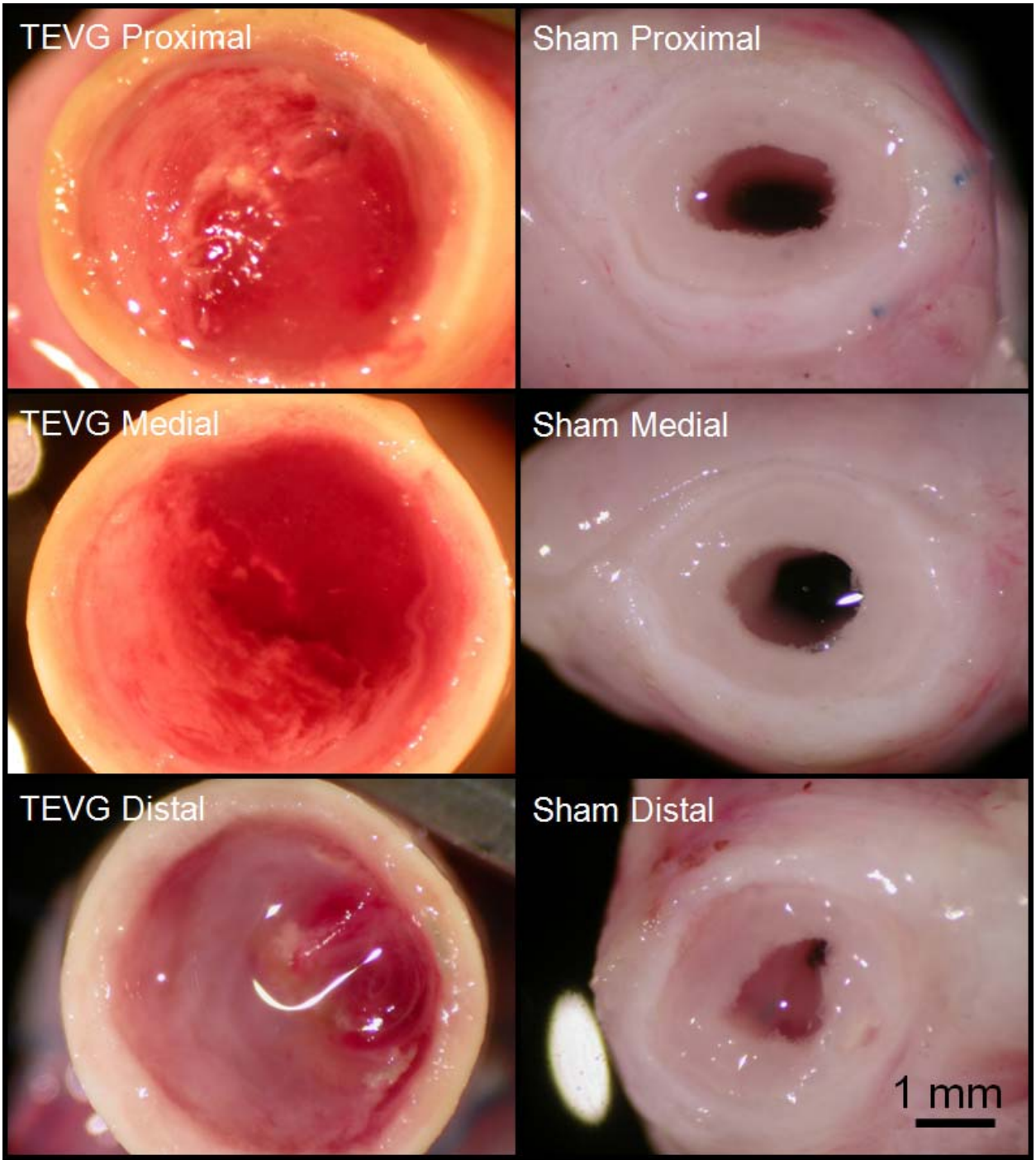

Figure 7.17 Representative gross pathology images of pG-1.

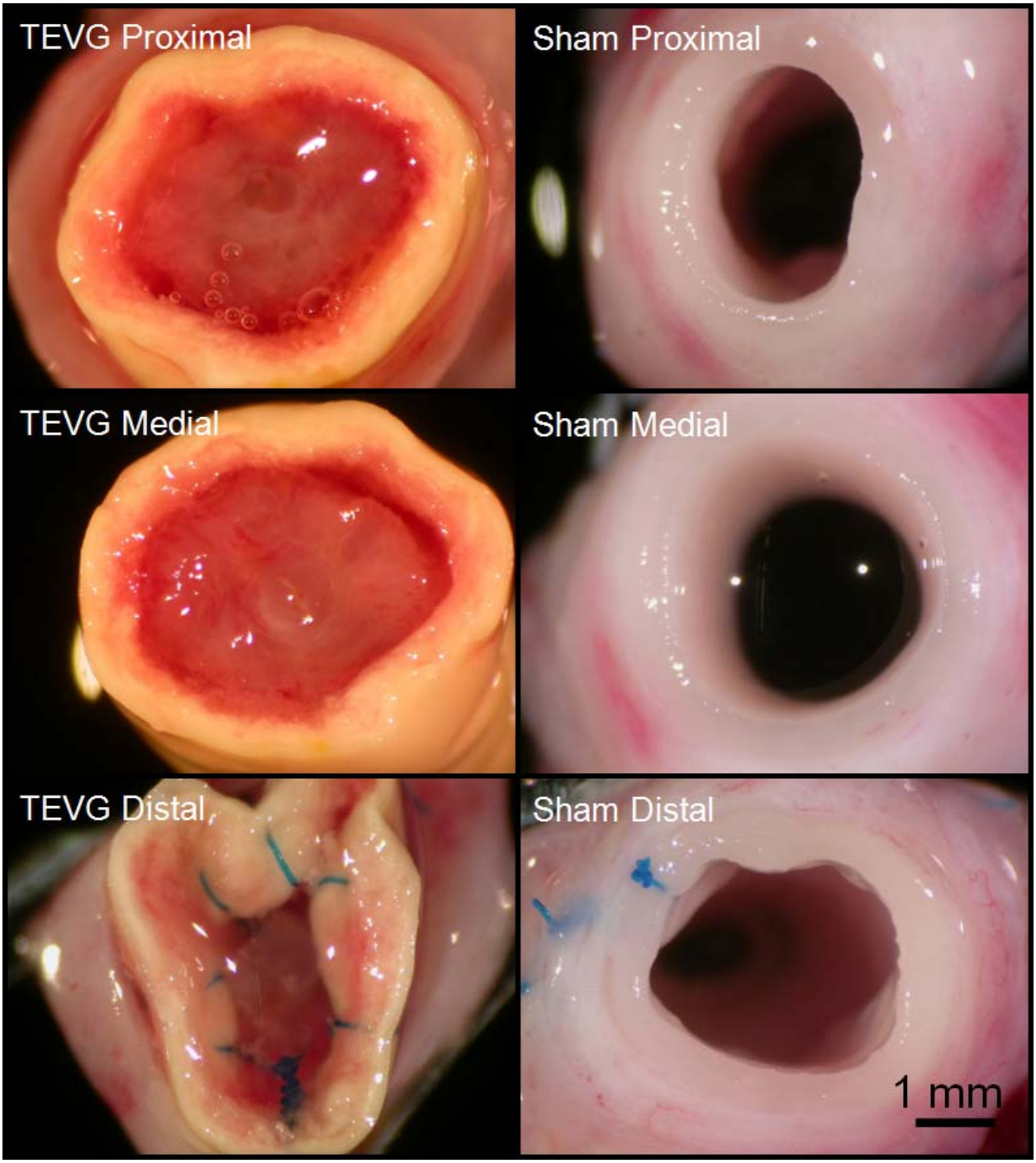

Figure 7.18 Representative gross pathology images of pG-2.

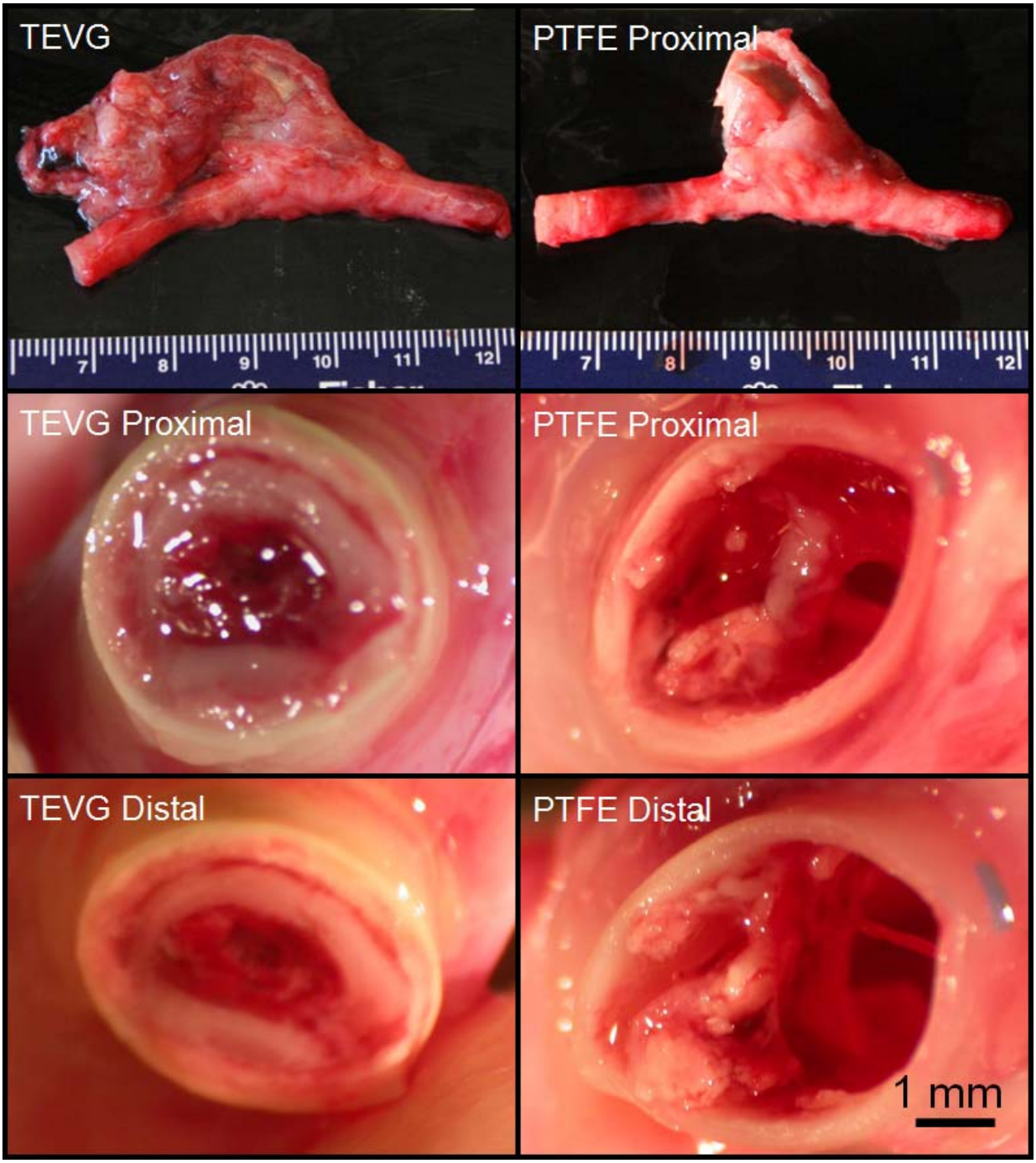

Figure 7.19 Gross pathology images of pG-3. Top panels show the macroscopic aspect of the explanted grafts. Note that the middle portion of the graft was not imaged.

Following gross pathological analysis, grafts were finally processed for histology. Due to the lack of patency in each of the implanted TEVGs, only the Masson's thricrome was performed; the planned additional endpoints (recall **Figure 7.2**) were not performed due to the graft failure.

Histological findings of the TEVGs from pG-1 and pG-2 suggest the formation of intimal hyperplasia at the two anastomotic levels (**Figure 7.20** and **Figure 7.21)**. This likely led to progressive reduction of the graft internal diameter and blood flow, leading to subsequent thrombus formation. The presence of intimal hyperplasia at the anastomotic levels was consistent with that found from the initial pilot studies. At both 1 and 3 months the TIPS layer of the TEVGs appeared coarse, swollen, and highly infiltrated with biological matrix, suggesting remodeling and scaffold degradation. However, the ES layer seemed to retain its original density and shape. This effect confirms the role of the ES PEUU in providing mechanical and structural integrity as expected (recall **Chapter 4**).

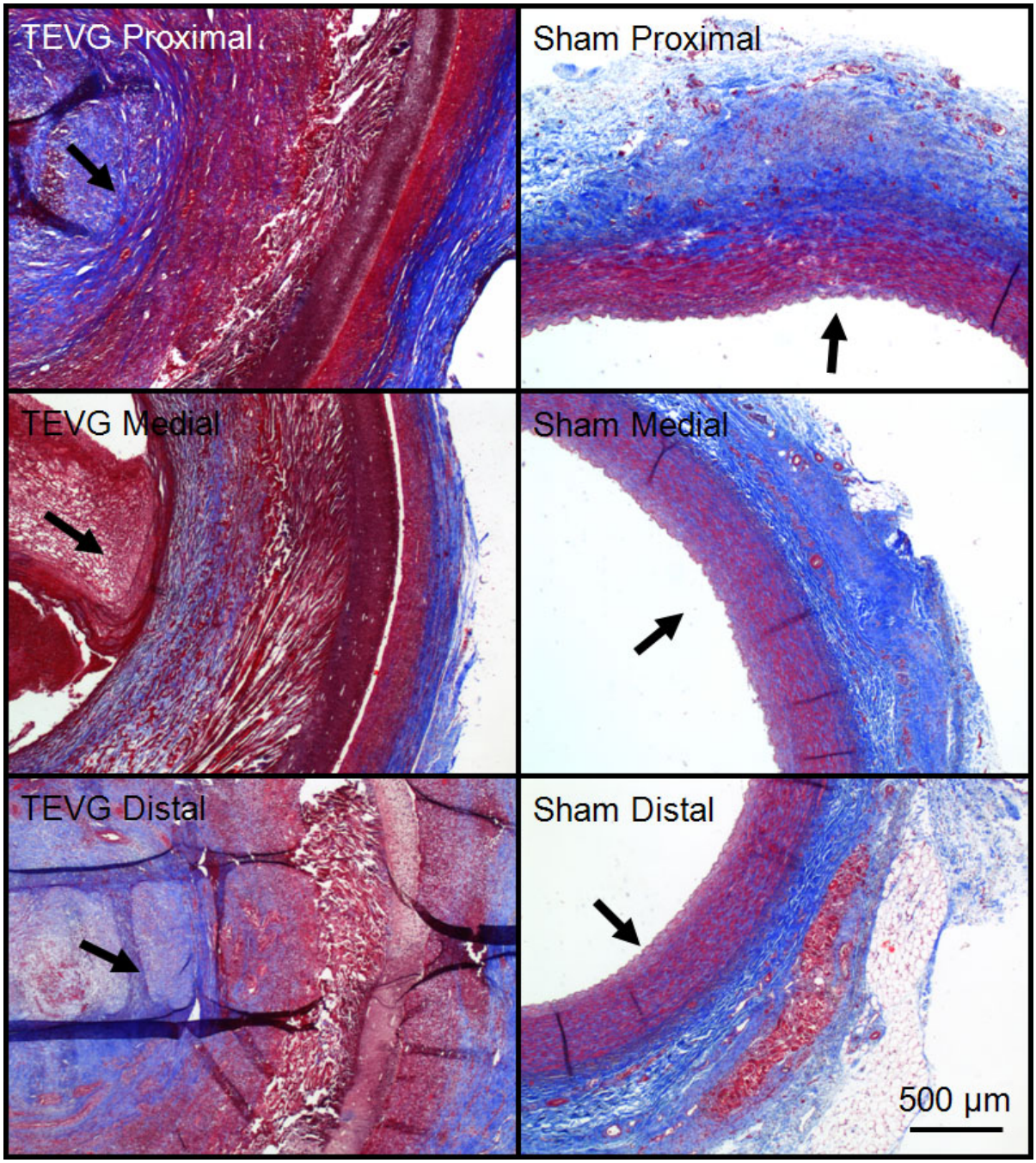

Figure 7.20 Representative Masson's trichrome images of pG-1. The arrows indicate the lumen.

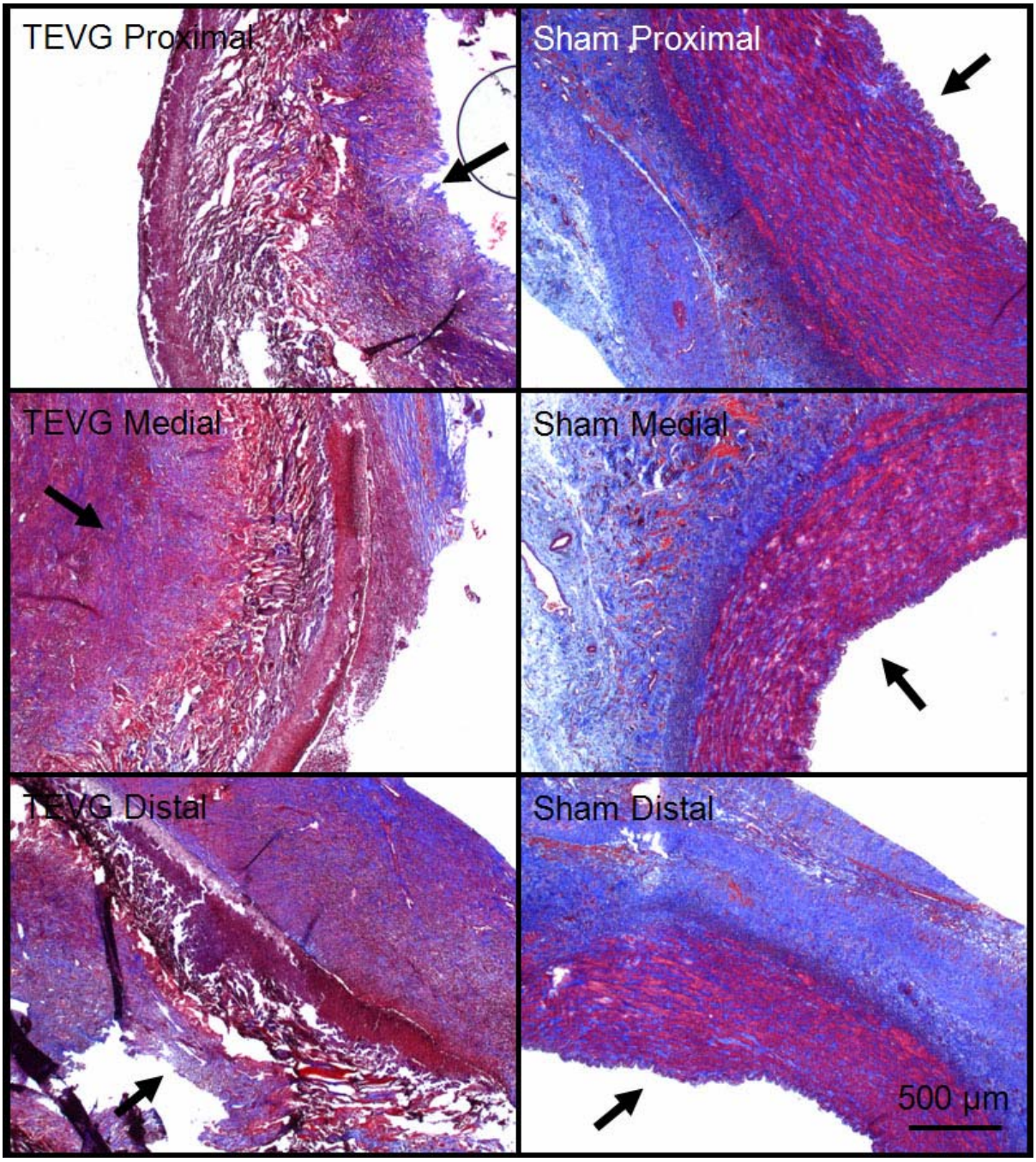

Figure 7.21 Representative Masson's trichrome images of pG-2. The arrows indicate the lumen.

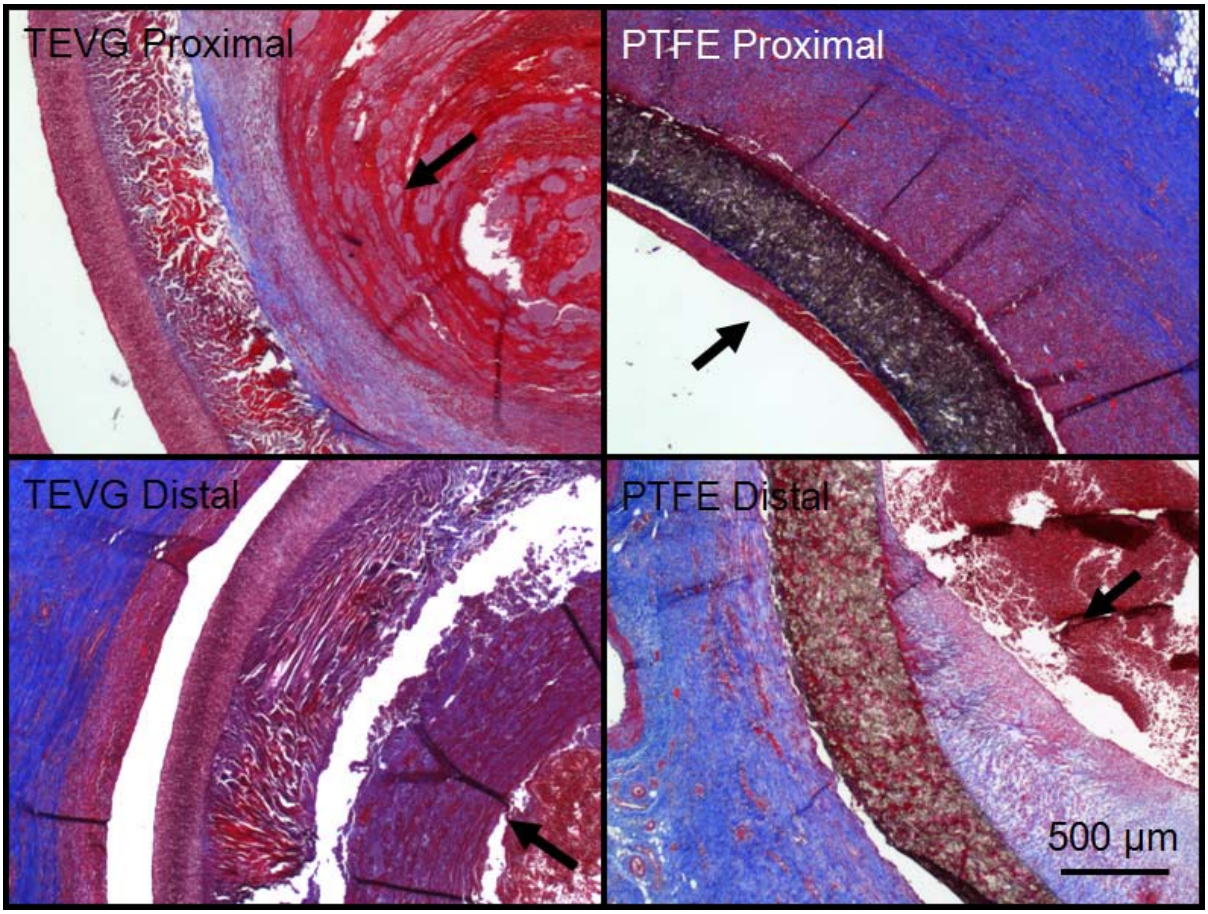

Figure 7.22 Histology Masson's trichrome of pG-3. The arrows indicate the lumen.

7.10 DISCUSSION AND LIMITATIONS

This chapter described the *in vivo* testing of an autologous pig LAC-based TEVG, implanted as a CIG or AVG in a paired fashion along with a native carotid artery or a standard PTFE graft, respectively. This study was designed to test a paradigm to provide an autologous small-

diameter TEVG suitable for implantation within a 15 day time frame from an initial muscle biopsy. The time frame was defined in attempt to compromise the limited resources involved for cell isolation and the need for an off-the-shelf approach to meet clinical viability standards. The paradigm developed to accomplish this goal included the use of several technologies developed throughout this research effort including the S-RVSD (**Chapter 3**), the ES-TIPS PEUU scaffold (**Section 4.2**), the Perfuser bioreactor (**Section 5.3**), and several lessons learned from *in vitro* (**Sections 5.1**, **5.2**, and **5.4**) and *in vivo* (**Chapter 6**) testing, including the use of murine, rat, and porcine cells.

This study did not produce the expected results in terms of patency rate and remodeling. A 0% patency rate recorded for all the TEVGs and the development of high levels of intimal hyperplasia clearly suggested the presence of one or more important issues to be addressed. It is difficult to demonstrate the causes for the poor *in vivo* performance of TEVGs due to the complexity of the *in vivo* remodeling and regeneration mechanisms, and to the lack of a mechanistic characterization of the biological processes involved with the TEVG culture and the *in vivo* remodeling. However, some speculations based on evidence collected during the studies presented here suggests that the lack of seeded cells prior to implantation (**Figure 7.10**) played a major role in the graft failure.

The results from the previous rat *in vivo* study defined a clear role for the cells incorporated into the scaffold in the maintenance of patency. A similar patency rate was in fact obtained for the acellular control grafts implanted in rats. Furthermore, the pig model is likely to be more prone than the rat to intimal hyperplasia and graft failure for genetic reasons. Results obtained with the PTFE graft, which was patent but clearly affected by major thrombus formation, is supportive of a high tendency for the development of intimal hyperplasia in pigs. A

number of reports in the literature have shown elevated intimal hyperplasia formation both in vein and PTFE arterial grafts in pigs [200, 201]. From this evidence it is inferable that the porcine model, although anatomically and genetically similar to humans, might be significantly more hyperplastic. Therefore, some concerns arise when defining the validity of this model as a pre-clinical tool for vascular disease.

The limited amount of cells found in the scaffolds prior to implantation was consistent with the low yield of cells after the isolation from the pig striated muscle. However, some of the isolations yielded almost 100% of the expected 30 million cells (**Table 7-2**), but the associated TEVG still exhibited a lower-than-expected cellular density prior to implantation. Therefore, while the cell isolation requires some optimization, in order to increase the cell yield while reducing the necessary time frame, it is not proper to identify it as the cause of the lack of cellularity prior to implantation. Other possible causes for the observed lack of cellularity are: the seeding process through S-RVSD, the quality of the scaffolds used, or dynamic culture in the Perfuser. It is prudent to rule out the S-RVSD since it has been extensively tested, showing consistent and reproducible results.

The scaffold is instead a possible reason for this failure. Many of the available ES-TIPS scaffolds for the pig studies had to be discarded due to macroscopic issues including delaminations between the two layers or poor quality (*i.e.*, cracks, disseminated small holes, or suboptimal wall thickness). Furthermore, the TIPS scaffold was the object of prior intensive optimization studies (data not shown) to solve some consistent microscopic issues, which resulted in a lack of porosity and transmural penetration of cells during seeding via the RVSD. Therefore, it is possible that the batches of scaffold used for the pig study were affected by any of the microscopic issues.

Finally, the Perfuser seems to be another possible cause for the observed lack of cellularity. The limited characterization of its functioning in combination with a pig LAC-based TEVG (**Section 5.4**) might have caused oversight of some unexpected issues. The most probable of those involves the premature exposure to intraluminal flow. It is possible in fact, that a 2 hour period of static culture was not enough for pig SACs to establish proper adhesion into the scaffold pores, resulting in a significant cell loss when experiencing flow.

This study, although affected by negative *in vivo* results, served the purpose of demonstrating the feasibility of the overall approach proposed here in a pre-clinical setup. In particular, it showed that it was possible to coordinate several professionals spanning from biomaterial scientists, vascular surgeons, stem cell scientists, and animal facility and laboratory technicians in a synergistic manner, so that the approach proposed here was successfully put into practice. This is probably the single most important accomplishment of this entire dissertation.

Furthermore, the 0% infections observed proved that the whole process was performed with proper sterile techniques. Finally, the ES-TIPS scaffold proved to be structurally and mechanically suitable to withstand the demanding arterial environment and to exhibit proper suture retention properties without exhibiting any mechanical failure.

8.0 SUMMARY, CONCLUSIONS AND FUTURE DIRECTIONS

A multidisciplinary framework for the creation of a stem cell-based tissue-engineered vascular graft has been developed and investigated in this study. Along the way, several technologies were developed that may have wider applications. A summary of the key accomplishments and findings as a result of this research project is provided next, followed by a description of the advantages and limitations of this study. Finally, some recommendations for future studies are discussed.

8.1 SUMMARY OF RESULTS

8.1.1 Summary of Specific Aim 1

Development and optimization of a seeding device to rapidly and efficiently deliver cells uniformly and reproducibly through porous, tubular scaffolds.

Two generations of a rotational vacuum seeding device were designed, fabricated, and qualitatively and quantitatively tested for bulk cell seeding capabilities of porous tubular scaffolds. Both device generations were compact and combined the synergistic action of vacuum, rotation, and controlled flow to produce a rapid, efficient, reproducible, and quantitatively uniform seeding (*i.e.*, in the longitudinal, circumferential, and radial directions of

the scaffold wall). The shear stresses, generated inside the rotating scaffolds, were analyzed with computational and analytical tools. These results, combined with those of both a metabolic-based viability assay and an apoptosis assay suggested the absence of injurious conditions for the cells during seeding. The new features implemented in the second generation (*i.e.*, the S-RVSD), including a controllable local delivery of cells and computer-controlled operations, improved upon the first generation by extending the seedable length of the scaffold and increasing the precision and the reproducibility of the seeding process by reducing human interaction.

8.1.2 Summary of Specific Aim 2

Development of a composite scaffold to mimic the mechanical and structural properties of native arteries.

A novel, bi-layered scaffold for vascular tissue engineering (*i.e.*, the ES-TIPS PEUU) was fabricated and tested for morphological (*i.e.*, microstructure, porosity, *etc.*), mechanical (*i.e.*, tensile properties, compliance, burst strength, *etc.*), and biological (*i.e.*, cell seeding via the S-RVSD developed in **Specific Aim 1**) properties. Morphologically, the scaffold was biomimetic mimicking the functional *tunica media* and the fibrous, external ES layer acting as the adventitial layer providing mechanical support. Mechanically, ES-TIPS PEUU scaffolds showed suitable mechanical properties for arterial vascular applications, exhibiting appropriate strength, compliance, and suture retention properties when compared with native vessels. Biologically, the scaffold was supportive of uniform cell integration with high seeding efficiencies.

8.1.3 Summary of Specific Aim 3

Determination of the ideal acute culture conditions to optimize the construct via cellular proliferation, migration, and spreading.

MDSC-based TEVGs were acutely cultured in dynamic conditions to understand general cell-scaffold interactions. Cells derived from three different species – mice, rats, and pigs – were used for this purpose. In all three studies, cells were seeded into the scaffold via either the RVSD or the S-RVSD developed in **Specific Aim 1**, and cultured within dynamic conditions for up to 3 days. Mouse MDSCs proliferated within the scaffold during dynamic culture, retained their stem cell features, and produced collagen when stimulated with ascorbic acid. Rat cells were seeded successfully into the ES-TIPS, developed in **Specific Aim 2**. Constructs cultured in spinner flasks showed proliferation and spreading, demonstrating readiness for the subsequent rat *in vivo* study of Specific Aim 4.

A novel perfusion bioreactor (the Perfuser) was developed and tested for the *in vitro* culture of larger scaffold sizes such as those required for the subsequent pre-clinical study in pigs of Specific Aim 4. The device was able to induce physiologically relevant flow rates and shear stresses into the scaffolds, as expected.

Finally, ES-TIPS scaffolds were seeded via the S-RSVD with pig SACs and cultured for up to 48 hours in the Perfuser. After 24 hours, the scaffolds were populated with spread SACs, validating the capability of the Perfuser, and demonstrating achievement of the established requirements for implantation.

8.1.4 Summary of Specific Aim 4

Assessment of the remodeling, patency, phenotype, and mechanical properties following in vivo remodeling.

The remodeling of a MDSC-based TEVG was tested *in vivo* in both small (*i.e.*, rats; allogeneic cell source; 8 weeks survival), and large (*i.e.*, pigs; autologous cell source; 1 and 3 months survival) animal models. The allogeneic-based TEVG approach in rats has been investigated and compared to the behavior of acellular scaffolds. Significant differences in patency rates were detected between seeded and acellular constructs, suggesting antithrombotic properties of the seeded MDSCs. The presence of a neo-tissue formation within the TIPS layer of the scaffolds, characterized by densely cellular, organized collagen, and positive markers for smooth muscle and endothelial cells, demonstrated the remodeling of the TEVG toward an artery-like structure. Seeded cells were engrafted in the remodeled TEVGs after 8 weeks *in vivo*, suggesting a role of MDSCs in the remodeling process toward a functional blood vessel. The study confirmed the promising mechanical characteristics of the ES-TIPS PEUU scaffolds developed in **Specific Aim 2**, by showing absence of mechanical failure after 2 months *in vivo*.

Following the promising results obtained in rats, an autologous study involving LAC-based TEVGs, implanted as a CIG or AVG in a paired fashion in pigs along with a native carotid artery or a standard PTFE graft, was performed. The study was designed to test a framework in which the animal received an autologous small-diameter TEVG suitable for implantation within a 15 day time frame from an initial muscle biopsy. This study resulted in a 0% patency rate for all the TEVGs, and in the development of high levels of intimal hyperplasia, clearly suggesting the presence of one or more important issues to be addressed. While the cause is yet to be demonstrated, it is quite likely that the limited amount of cells found in the scaffolds prior to

implantation was the main contributing factor for the poor *in vivo* performance. Although affected by negative results in a large animal model *in vivo*, this study served the purpose of demonstrating the feasibility of the overall autologous approach.

8.2 ADVANTAGES OF THE APPROACH

The inherent advantage of the approach proposed here relies on its initial definition of criteria necessary for clinical viability, and on the *ad hoc* development of a number of innovative technologies based upon those criteria. This advantage can be described by the expression "translational research". In particular, the basic driving guidelines for this research effort, toward the development of a clinically viable TEVG, were: time/cost efficiency, reproducibility/seeding efficiency, and autologous cell sourcing. Each of these basic requirements forced the development of several solutions in a "clinically meaningful" way. For example, the time factor and the concept of reproducibility were fundamental specifications in the design of the RVSD/S-RVSD, which lead to unique technologies and methodologies emphasizing, for the first time, the importance of cell seeding and the quantification of its results. Any future "product" in regenerative medicine entailing the combination of cells and scaffolds, in fact, will certainly need to comply with those requirements. The need for an efficient use of the available cells, suggested (along with other factors) the need of a new scaffold, able to retain almost 100% of the seeded cells immediately after seeding. From a clinical perspective, the number of "wasted" cells might be a viable indicator of the success for a determined approach. Finally, the requirement of autologous cell sourcing fostered the creation of a model of collaborative effort between surgical facilities, "manufacturing" and testing facilities (*i.e.*,

laboratories), and stem cell isolation facilities, which is paramount for the clinical success of any stem cell-based tissue-engineered product.

Two additional advantages of this approach are in its characteristics as a "platform technology" and the multidisciplinary nature of the subjects investigated, resulting in the development of a plethora of solutions. Although, the approach presented here was conceived and tested for small-diameter vascular applications, it is conceivable to use the same approach for a variety of applications requiring tissue-engineered tubular grafts, either using the entire paradigm proposed here, or only some parts of it.

8.3 LIMITATIONS OF THIS APPROACH

Paradoxically, the general limitation of this approach is also in its translational nature. Technology-oriented research, such as the one proposed here, characterized by the development of a number of innovative technologies across a wide spectrum of subjects has, unavoidably, the downside of possessing many limitations. First, many of the studies performed here were carried out with a phenomenological approach, limited to the description of the methods and results of experiments based on reasonable assumptions or *a priori* decisions, but unable to establish a mechanistic, functional model. Second, the large diversity of studies necessary to develop and test a new approach in a preclinical animal model, spanning from device fabrication, biomaterial science, molecular biology, and surgical studies, leads to a large number of possible complications.

Specific limitations are now summarized for each specific aim.

8.3.1 Limitations of Specific Aim 1

Due to the development of two generations of a seeding device, in which the second was designed to solve most of the limitations of the first generation, Specific Aim 1 suffers the least amount of limitations within this framework. However, one limitation consists in the lack of a rigorous sensitivity analysis to determine how the different seeding parameters (*i.e.*, rotational velocity, vacuum level, flow rate, *etc.*) affect the seeding outcome, and an optimization study to determine, for a specific scaffold type, which are the best seeding parameters to obtain the most efficient seeding.

8.3.2 Limitations of Specific Aim 2

The major limitation affecting the ES-TIPS scaffold was the absence of a quality-controlled manufacturing process. This often led to batch-to-batch variability in mechanical and structural properties, as well as the presence of defects, such as delaminations between the two layers, tears or small holes, skins preventing cell penetrations, *etc*. Furthermore, the porous nature of the TIPS PEUU, which allows for excellent cell penetration and proliferation, might hamper, to a certain extent, processes such as cell spreading and alignment.

8.3.3 Limitations of Specific Aim 3

The *in vitro* studies utilizing rat and pig cells suffered from a lack of a rigorous cell characterization. In fact, while mice MDSCs have been extensively characterized in the literature, both rat MDSCs and pig SACs do not have any supportive background available.

These circumstances are not ideal since they imply the loss of the reference values that are normally used to understand the influence of exogenous factors, such as their incorporation into a 3D scaffold or the subsequent dynamic culture *in vitro*. The biological characterization of the Perfuser was also affected by a very limited availability of porcine cells, which did not allow additional studies to corroborate or confute the loss of spreading detected after 48 hours of dynamic culture.

8.3.4 Limitations of Specific Aim 4

The rat *in vivo* study was limited by the use of allogeneic cells, which might have resulted in a decreased patency rate. Furthermore, the study failed to demonstrate a fundamental theoretical milestone for a tissue-engineered vascular graft, "the constructive remodeling", which implies full degradation of the scaffold material and replacement with mechanically, structurally, and functionally sound neo-vessel formation. Longer time points are therefore necessary to complete the degradation of the ES-TIPS *in vivo* and demonstrate long-term patency. The pig study was affected by major limitations including: poor cell yield from the muscle biopsy isolations, poor to null phenotypic and behavioral characterization of the cell population, very slow population doubling time, very low transfection efficiency for the LacZ promoter, and the lack of a comprehensive characterization of the *in vitro* culture on pig cells into the Perfuser. These limitations resulted in very low pre-implantation cellularity into the ES-TIPS scaffolds, which might have directly caused the poor *in vivo* performance detected. Therefore, the cell source used, while promising due to supposed heterogeneity of the SACs, might not represent the best candidate for our approach.

8.4 FUTURE WORK

Each specific aim of the framework proposed here would benefit from several areas of potential future work. In general, future studies should focus on the troubleshooting of the limitations summarized in **Section 8.3**.

8.4.1 Future work for Specific Aim 1

8.4.1.1 Sensitivity and optimization study

The S-RVSD should be further assessed using a sensitivity study with medical grade scaffolds having reproducible permeability and pore size distribution. This characteristic is critical to test how the three main variables of the device (rotational speed, vacuum level, and flow rate) affect the seeding outcome eliminating "the noise" introduced by the batch-to-batch variability of the scaffolds. A thorough sensitivity study would allow us to better understand the underlying mechanisms of functioning for the device and possibly lead to rationally-guided modifications or simplifications. Once defined, the scaffold of interest and the cell type (depending on each specific application) would need to undergo a separate optimization study to understand which combination of seeding parameters would lead to an optimal seeding outcome. The definition of an optimal target outcome depends on each specific application and represents the starting point of any optimization study. The problem of the "optimization" is a complex subject involving the use of algorithms based on mathematical and stochastic formulations. These algorithms allow one to navigate through the space of the available variables (in this case three) with a relatively

small number of attempts (experiments or simulations) in order to identify the location within the variables space corresponding to the absolute or relative maximum of the performance indicator.

8.4.1.2 Design of a disposable cartridge for clinical applications

An additional effort should be made toward a more clinically-realistic implementation of the S-RVSD consisting of a disposable component. While the technology of cell seeding was conceived, built, tested, and validated with the multiple prototypes of the RVSD, the development of the prototype of a possible clinical "product" was not pursued or implemented, despite the patenting of the technology (USPTO Appl. No.: 11/243,818. See **Appendix H**). However, a preliminary conceptual design of a seeding system for possible future clinical use was prepared.

The conceived system consists of two units: 1) a disposable, sterile seeding cartridge incorporating within its design most of the key features of the S-RVSD; and 2) a reusable base unit device. This conceptualization follows a very common model for medical devices: the razor-razor blade model. A new cartridge containing a porous scaffold would be inserted into the base unit for each seeding and then disposed of, following removal of the seeded construct.

The perceived disposable cartridge consists of an external, cylindrical clear polycarbonate shell with two vented, removable end caps (**Figure 8.1**). Each cap has a central, circular opening sealed externally with a 0.2 μm PTFE filter, to maintain the internal sterility while allowing for gas transfer and pressure equilibration. The internal side of the cap is pressure fit with a plastic contact bearing component, including a short central cylindrical socket supported by radially-oriented prongs in contact with the internal side of the cap. An internal rotating body is fit between the two cap contact bearings. When the cartridge is closed, it is free

to rotate around its longitudinal axis (**Figure 8.2**). The internal rotor is a single plastic component, obtained by injection molding techniques and consists of two aligned tees, connected by a three-arm torque transmission. The hollow space within each of the two tees has a thin, medical grade polyurethane tubular sac, having a diameter equal to the internal diameter of the scaffold (**Figure 8.1**).

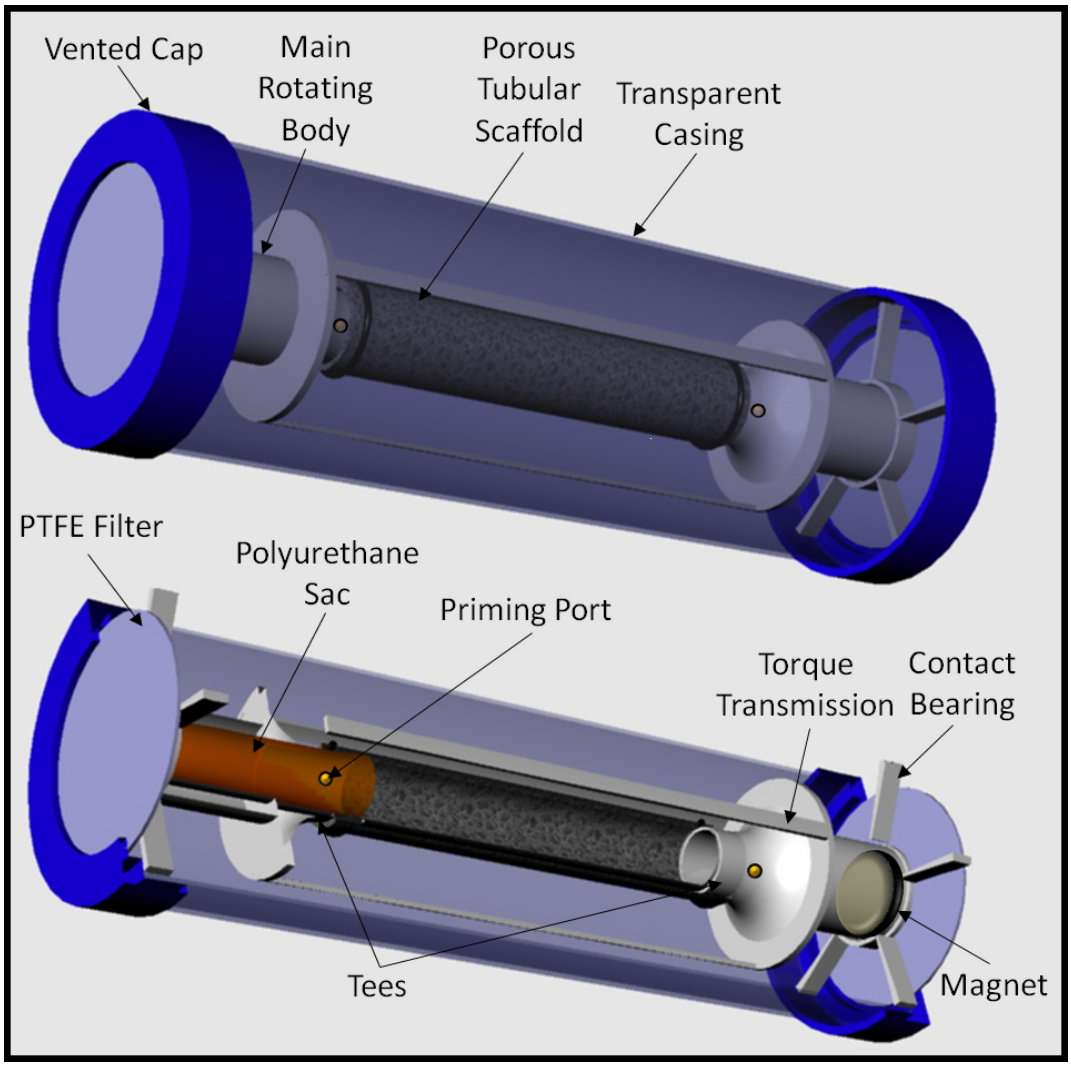

Figure 8.1 Schematic of the disposable cartridge for the perceived S-RVSD modified for clinical use.

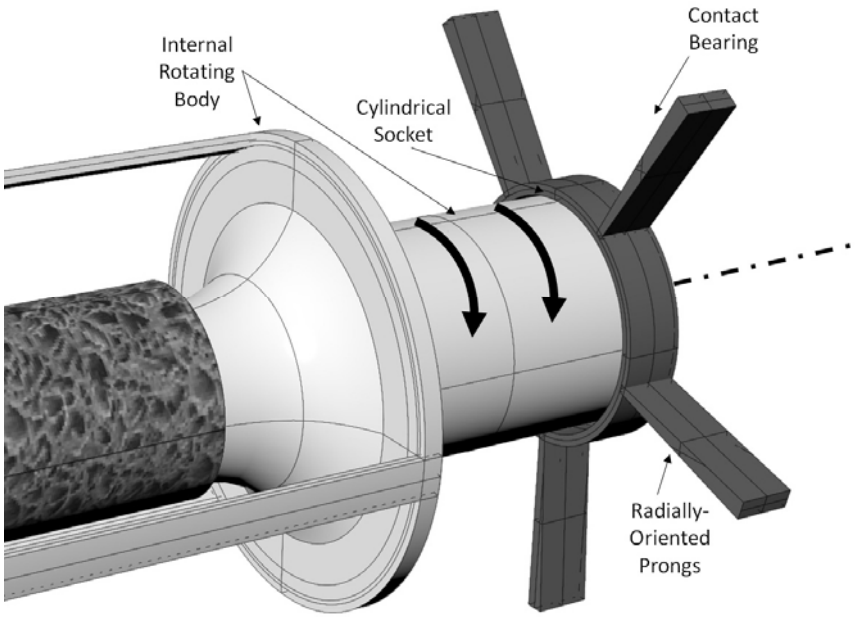

Figure 8.2 Schematic of the internal bearing of the perceived S-RVSD cartridge.

The open sides of the two sacs are sealed to the internal edge of the opening of the tees, while the opposite ends of the sacs are initially placed inside the tees at the periphery of the rotating body. Each tee has a small rubber port able to be punctured by a syringe needle. One side of the rotating body has a magnetic plate embedded within it, which transfers the torque to the rotating body from a rotating magnetic stage placed in the base unit.

The base unit is an electronically-controlled system, incorporating a vacuum regulator system, a DC motor, a power supply, and a socket for the seeding cartridge, enclosed in an illuminated air-tight compartment. The device receives vacuum from an external source, such as a hospital line, and automatically regulates the vacuum levels to the desired value inside the cartridge socket upon receiving the seeding signal. The internal electrical motor rotates a

magnetic stage, in proximity of the cartridge magnetic plate, to transfer the rotational motion to the internal rotating body of the cartridge.

Prior to seeding, a porous tubular scaffold is mounted on the two tees by opening one cap of the cartridge and removing the rotating body. The scaffold is attached to the rotating body tees by a custom-designed sealing ring device. The inflatable seal consists of a cylindrical plastic case and an internal inflatable, toroidally-shaped polyurethane bag. A small rubber valve is attached to the toroidal bag and is exposed externally to the casing by a small aperture in the plastic (**Figure 8.3**). Once one end of the scaffold is inserted onto one tee, the sealing ring device is overlapped with the scaffold and inflated by puncturing the rubber valve with an air-filled syringe until a firm compression of the scaffold on the tee is obtained. The rotor with the attached scaffold is then primed with a cell suspension via the priming port and reintroduced in the cartridge. The cartridge is then inserted in the dedicated base unit socket and the seeding is initiated.

During seeding, the base unit applies an external vacuum to the cartridge while putting its internal body in rotation. The vacuum is transferred to the interior of the cartridge via the PTFE filters and initiates a transmural flow of seeding suspension, similar to that seen in the RVSD. While exuding through the scaffold wall, the cell suspension causes a progressive inward collapse of the internal polyurethane bags from the rotating central body toward the center of the scaffold, mimicking the function of the Diffuser in the S-RVSD. During the exudation of the liquid phase of the cell suspension through the scaffold, the two collapsible bags retract into the scaffold until they touch each other in the center, completing the seeding procedure.

At the end of the process, the disposable cartridge is removed from the base unit, the scaffold is retrieved by unscrewing the cartridge cap and deflating the inflatable ring devices, and the cartridge is discarded.

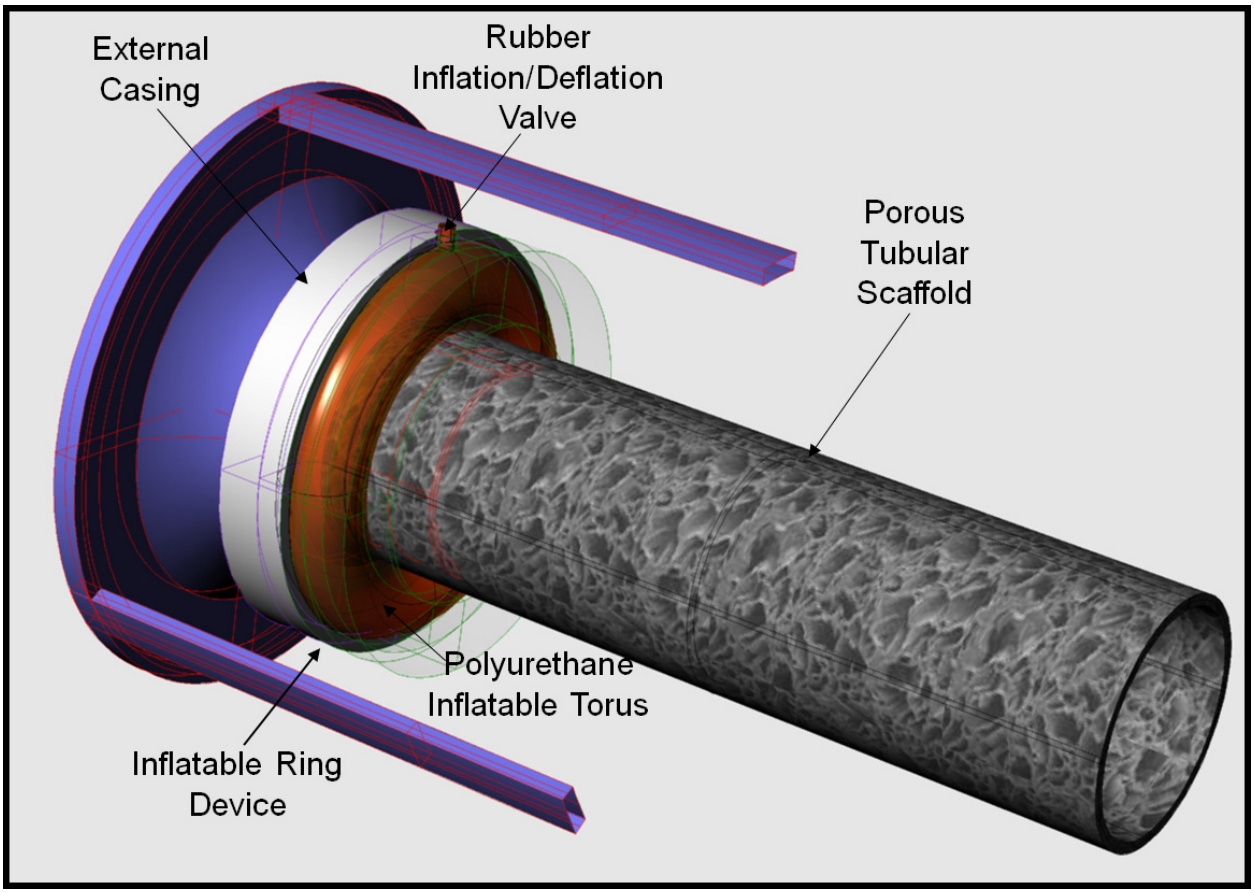

Figure 8.3 Schematic of the inflatable ring device within the cartridge of the perceived S-RVSD modified for clinical use.

8.4.2 Future work for Specific Aim 2

The ES-TIPS PEUU scaffold should be further characterized by a predictive analytical model. A constitutive structural and mechanical model of the composite scaffold could be obtained by coupling the properties of its two distinct layers via a parametric model of which parameters would be estimated through empirical data. It would also be important to perform oxygen diffusivity experiments to define the influence of the scaffold thickness on the cell viability within the scaffold to identify a rational compromise between nutrient diffusivity and mechanical properties.

Moreover, the bi-layered scaffold should be better characterized for its biodegradation properties with standard *in vitro* and *in vivo* degradation assays, and this should be optimized for the specific application in which it would be used.

Basic thrombogenicity assays should be performed *in vitro* to evaluate the inherent tendency of the scaffold (with and without seeded cells) to cause clot formation. Perfusion with animal whole blood and quantification of platelets adherence would be a cost-effective way to quantify thrombogenicity. A possible improvement to reduce thrombogenicity could be the surface modification of the luminal layer in order to inhibit platelet adhesion with biomimetic molecules such as phospholipidic substrates, or heparin binding domains.

8.4.3 Future work for Specific Aim 3

A complete species-specific phenotypic characterization of MDSCs used for future *in vitro* or *in vivo* experiments is paramount to univocally identify the cell population used, to demonstrate the reproducibility of the isolation technique, and to define phenotypic landmarks to show the effects

of different culture conditions or the course of the remodeling *in vivo*. A possible solution to this end could entail the utilization of mRNA microarrays and proteomics microarrays to identify patterns of phenotypic (transcriptional and traslational) expression from isolations obtained from a large number of animals (*i.e.,* rats or pigs) with exact same isolation protocols and baseline conditions. This would allow to point out a number of surface markers that can be used to sort cell populations via flow cytometry hence reducing the isolation time (without the need for the preplating technique), and increasing the reproducibility of the cell population.

An alternative to the use of adult stem cells derived from the striated muscle would be the adoption of bone marrow- or adipose-derived progenitor cells. For example, mesenchymal stem cells obtained from these two tissue sources would be valid candidates for tissue engineering applications due to their multipotentiality, self-renewal capabilitites (recall **Section 1.5.2**), and accessibility. The relatively low invasiveness of the procedures required to harvest bone marrow (*e.g.,*. iliac crest aspiration), or fat (*e.g.,* liposuction), and the relatively loose consistency of both tissues, which eliminates or reduce the need for enzymatic digestions, are important indicators of their potentially successful use for TEVG applications.

Furthermore, it is recommendable the utilization of human stem cells to provide a further step toward clinical feasibility which require functional characterization of human cells behavior *in vitro* and *in vivo* (*e.g.,* implantation into immune-tolerant or immune-suppressed animals). In fact, our laboratory has already begun initial investigations toward this end [202].

The Perfuser would require a more rigorous biological characterization to demonstrate its full potentiality as a bioreactor for tissue-engineered tubular constructs. In particular, its capability to foster cell growth within the engineered tubular construct along the longitudinal

direction of the scaffold, and the possibility of stimulating luminally seeded cells via shear stress-mediated mechanotrasduction should be demonstrated.

8.4.4 Future work for Specific Aim 4

8.4.4.1 General considerations

Future animal studies (regarless of the animal model used) should be aimed at demonstrating constructive remodeling (see **Section 8.3.4**). Therefore, longer time points should be tested to allow complete degradation of the scaffolds. Ideally, medical imaging techniques (*e.g.,* ultrasound-based imaging) would be used to track patency and the degradation of the scaffold over the duration of the study.

A quality control study should be directed toward the achievement of high levels of cell density into the ES-TIPS PEUU scaffolds prior to implantation in an autologous animal model. The aim of this study would be to substantiate or confute the speculative conclusions made in this work (see **Section 7.10**) based on the inconsistent results obtained in the pig study. It is likely, in fact, that the lack of patency in those grafts was caused mainly by the quasi-acellular characteristic of the implanted TEVG. Additionally, a more clinically-relevant control should be used for the carotid interposition graft, such as the IJV as an arterial vein graft. Arterial vein grafts, in fact, are still the gold standard for revascularization in CABG and peripheral bypass surgeries [203, 204].

Upon remodeling, a number of functional characterizations should be performed to demonstrate the functionality of the remodeled TEVGs for both vascular lineages. Endothelial function can be tested with specific assays such as the uptake of acetylated low-density

lipoprotein, or antithrombogenicity assays such as platelet adhesion quantification or indirectly via immunohistochemistry, by detecting specific markers including CD31 and e-NOS. Both endothelial and smooth muscle function can be tested with a vasoactivity assay. The TEVG response to endothelial-independent vasoconstrictors (*e.g.,* epinephrine, *etc.*), and endothelial-dependant vasodilators (*e.g.,* sodium nitroprusside, *etc.*) would represent an excellent indicator of the capacity of the TEVG to respond to environmental stimuli [205].

8.4.4.2 Autologous bone marrow to enable full off-the-shelf use of a TEVG

Finally, an autologous *in vivo* approach involving an alternative cell source should be considered to allow for an effective off-the-shelf approach and to avoid the hurdles and time constraints of an inefficient stem cell isolation technique. Based upon the approach of Shin'oka *et al.*[38], consisting of the use of autologous bone marrow-derived mononuclear cells, manually seeded onto porous scaffolds, a large animal pilot study was performed in dogs to investigate this possible cell source within our framework. Conceptually, the patient needing a TEVG would receive a bone marrow aspiration in the morning under local anesthesia (**Figure 8.4-A**), a simple Ficoll gradient would be performed to isolate the mononuclear fraction of the bone marrow by centrifugation [206] (**Figure 8.4-B**) within a 1-2 hour time frame. The cells would then be seeded intra-operatively via the disposable implementation of the S-RVSD described in **Section 8.4.1.2** (**Figure 8.4-C**) and, shortly thereafter, the seeded scaffold would be implanted into the patient.

This proposed approach appears ideal for three basic reasons. First, the patient would be able to receive an autologous blood vessel completely off-the-shelf, requiring only a same-day non-invasive bone marrow isolation, while the disposable seeding cartridge would be available at

any time with an extended shelf life. Second, bone marrow cells have been extensively investigated and characterized in a number of cell therapy studies [207, 208] and, due to their heterogeneity and/or plasticity, have resulted in a number of successes in terms of re-establishment of *in vivo* functionality for several clinical applications [209]. Third, from a regulatory standpoint, the intraoperative use and handling of cells would be subjected to a lesser burden of requirements since it would be likely perceived as a minimal manipulation procedure according to FDA standards (*i.e.*, autograft instead of a processed (cultured), autologous cell source) and, therefore, it might result in a more tractable regulatory approval pathway.

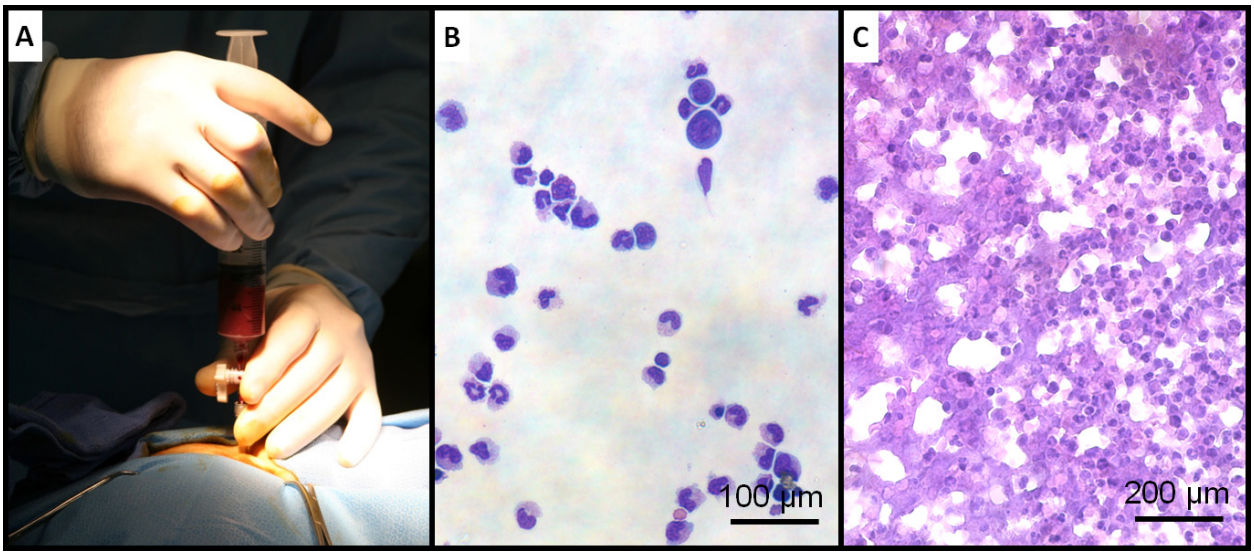

Figure 8.4 Sequence showing the main steps of the study design proposed as a future study. **A.** Aspiration of the bone marrow. **B.** Cytospin of the mononuclear fraction of the bone marrow. **C.** Seeded bone marrow in the large scaffold described in **Figure 2.29**.

APPENDIX A

APPENDIX A: MECHANICAL DRAWINGS

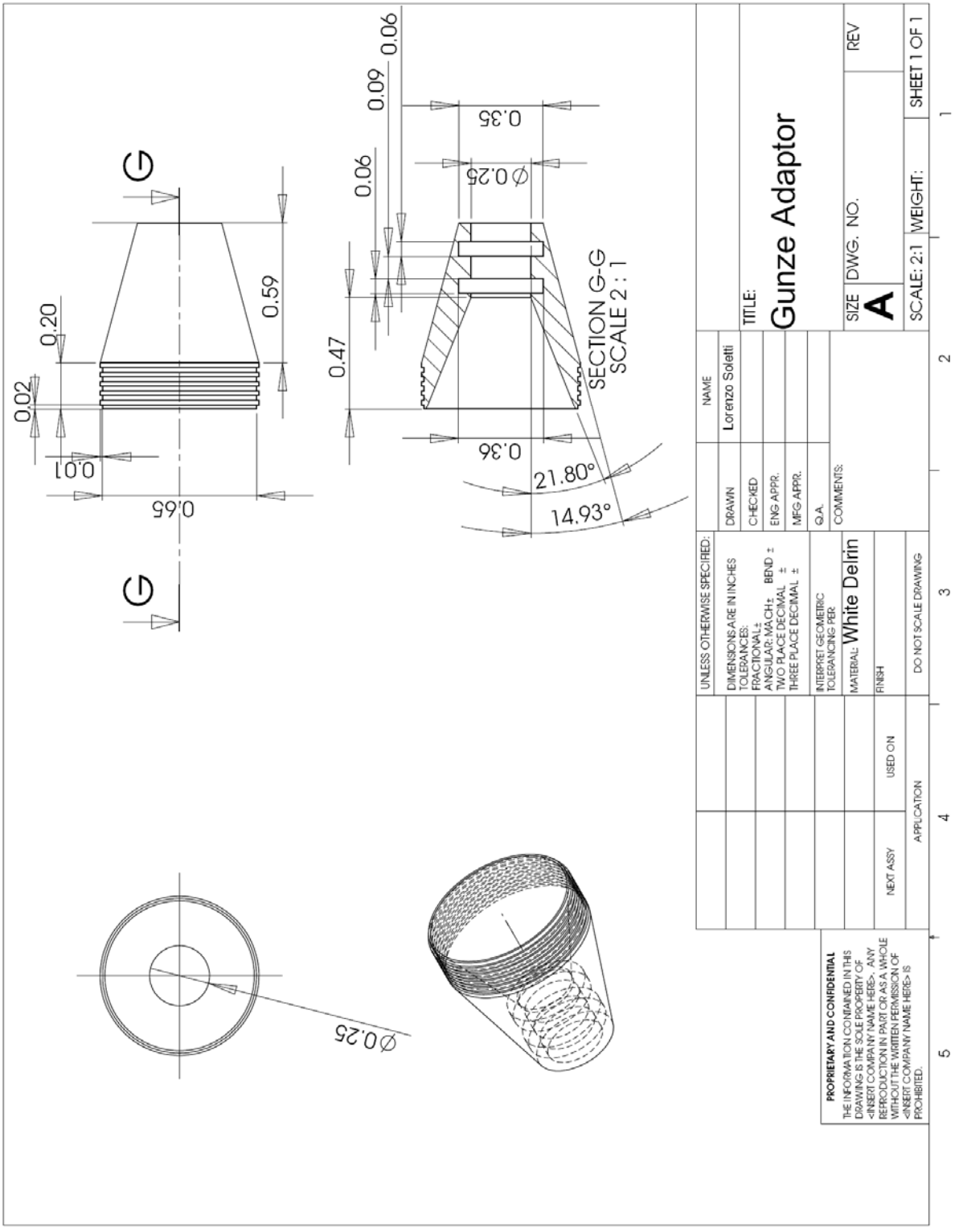

Figure A.1 Mechanical drawing of a truncated cone-shaped tip designed to adapt the RVSD to a 17 mm of ID scaffold (see **Section 2.2.6.1**).

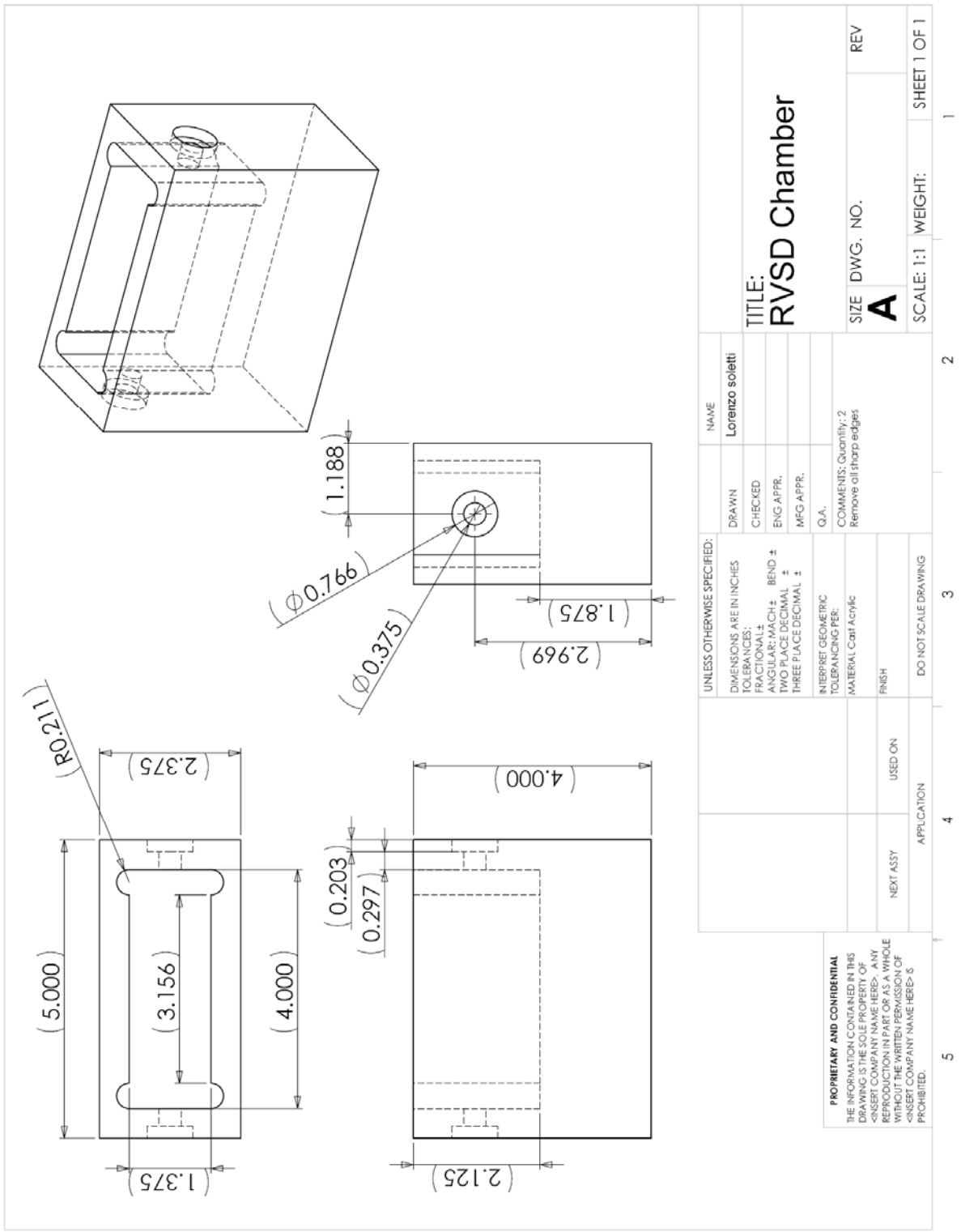

Figure A.2 RVSD chamber.

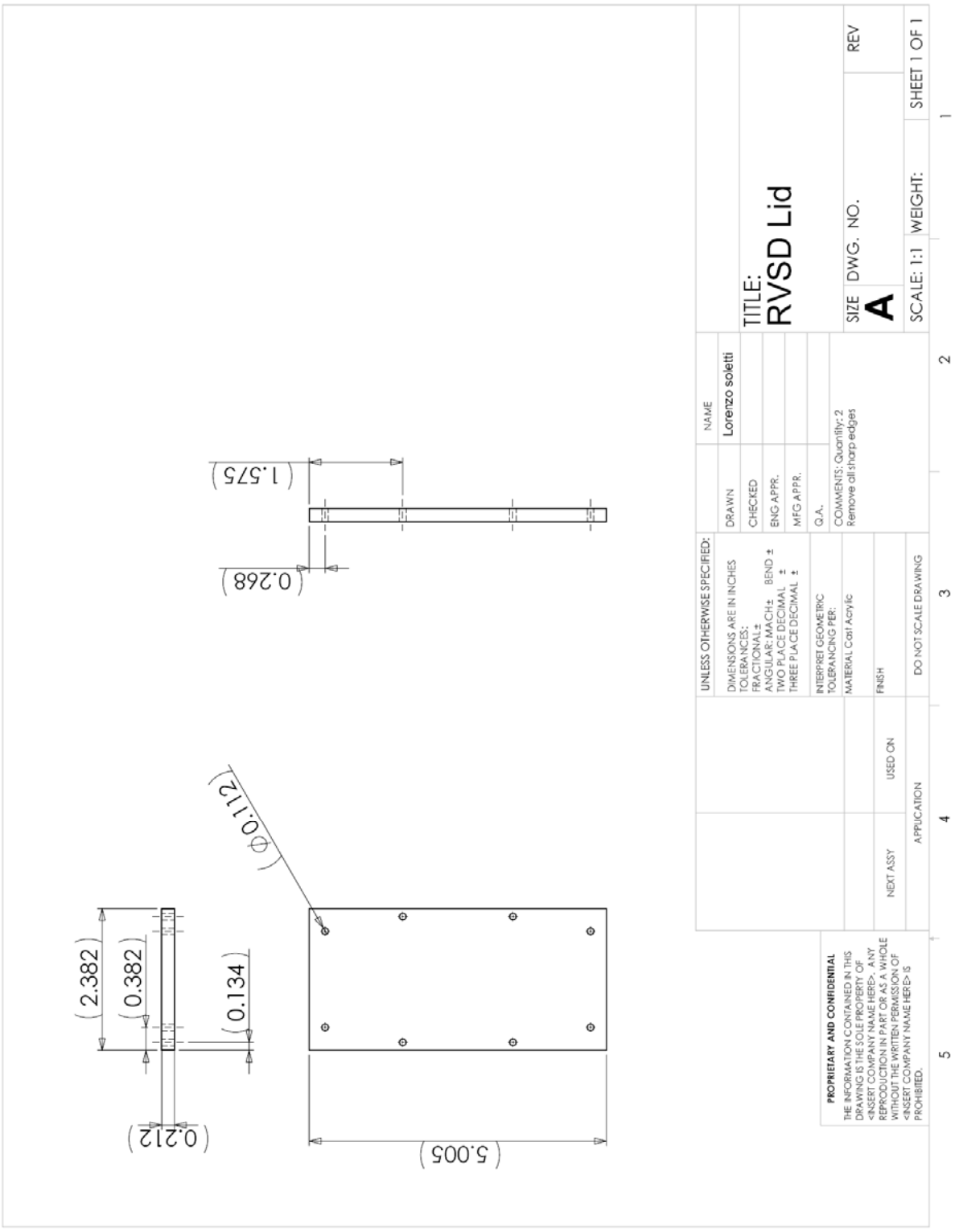

Figure A.3 Lid for the RVSD chamber.

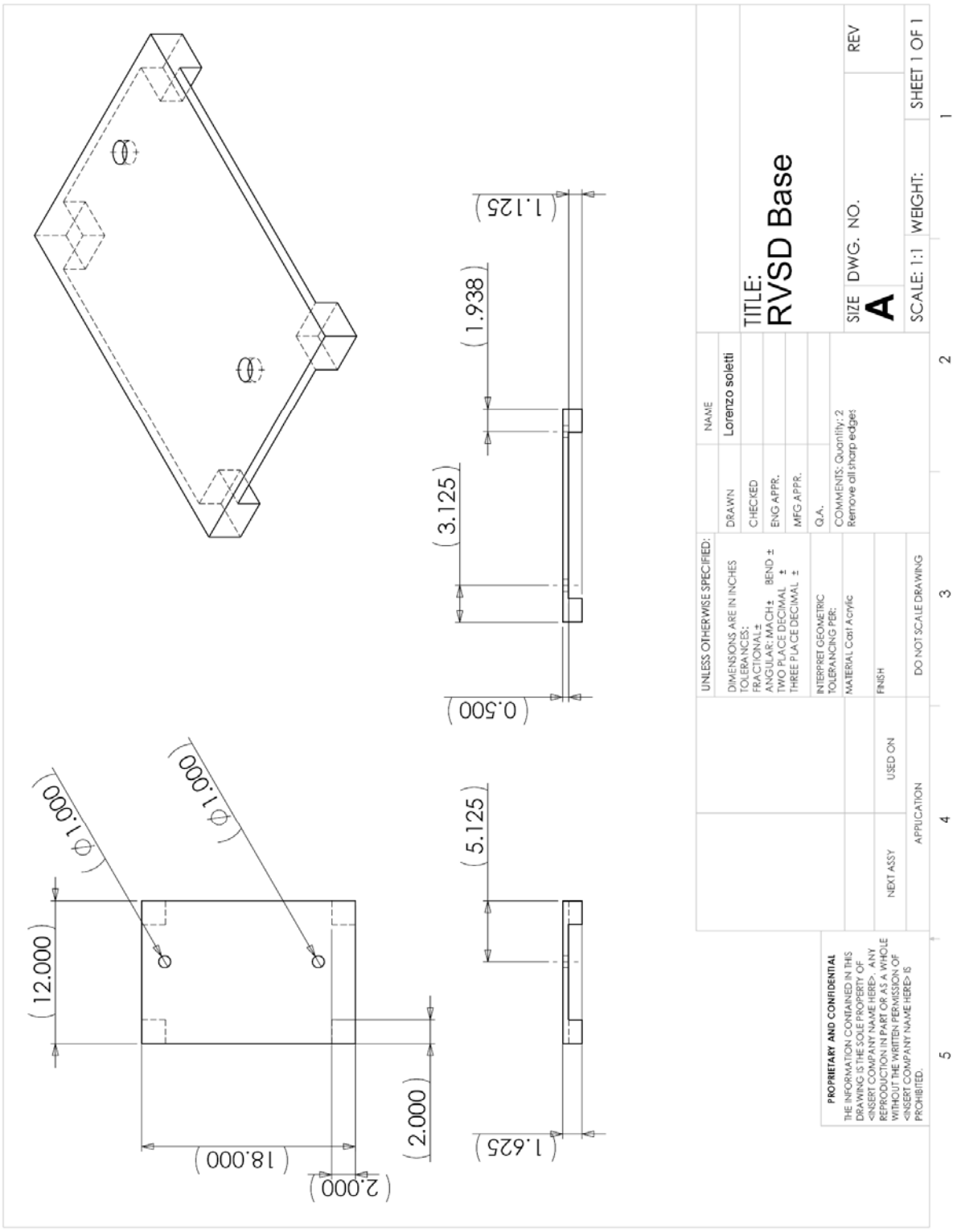

Figure A.4 RVSD Base

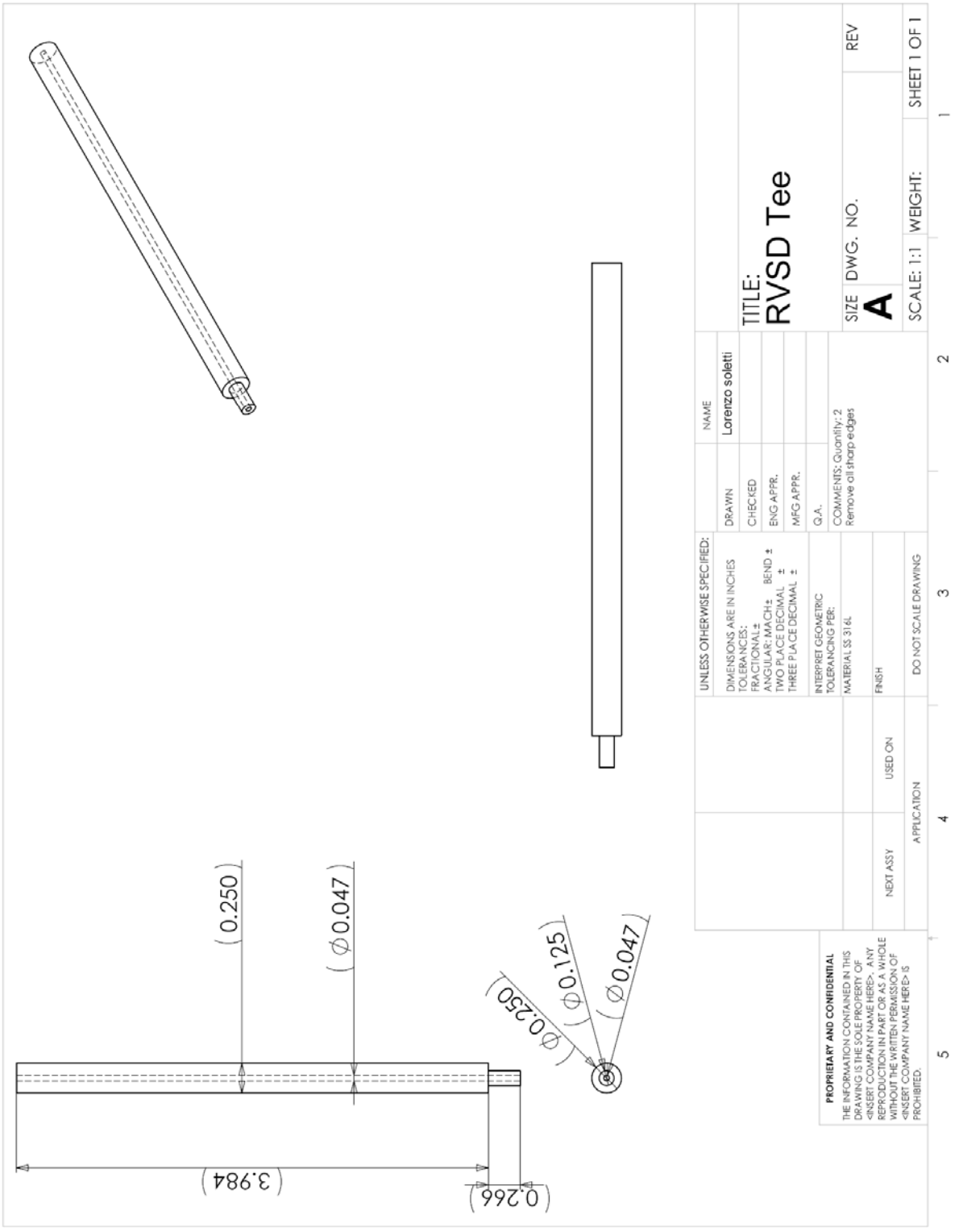

Figure A.5 Design of both the Driving and the Driven Tees for the RVSD.

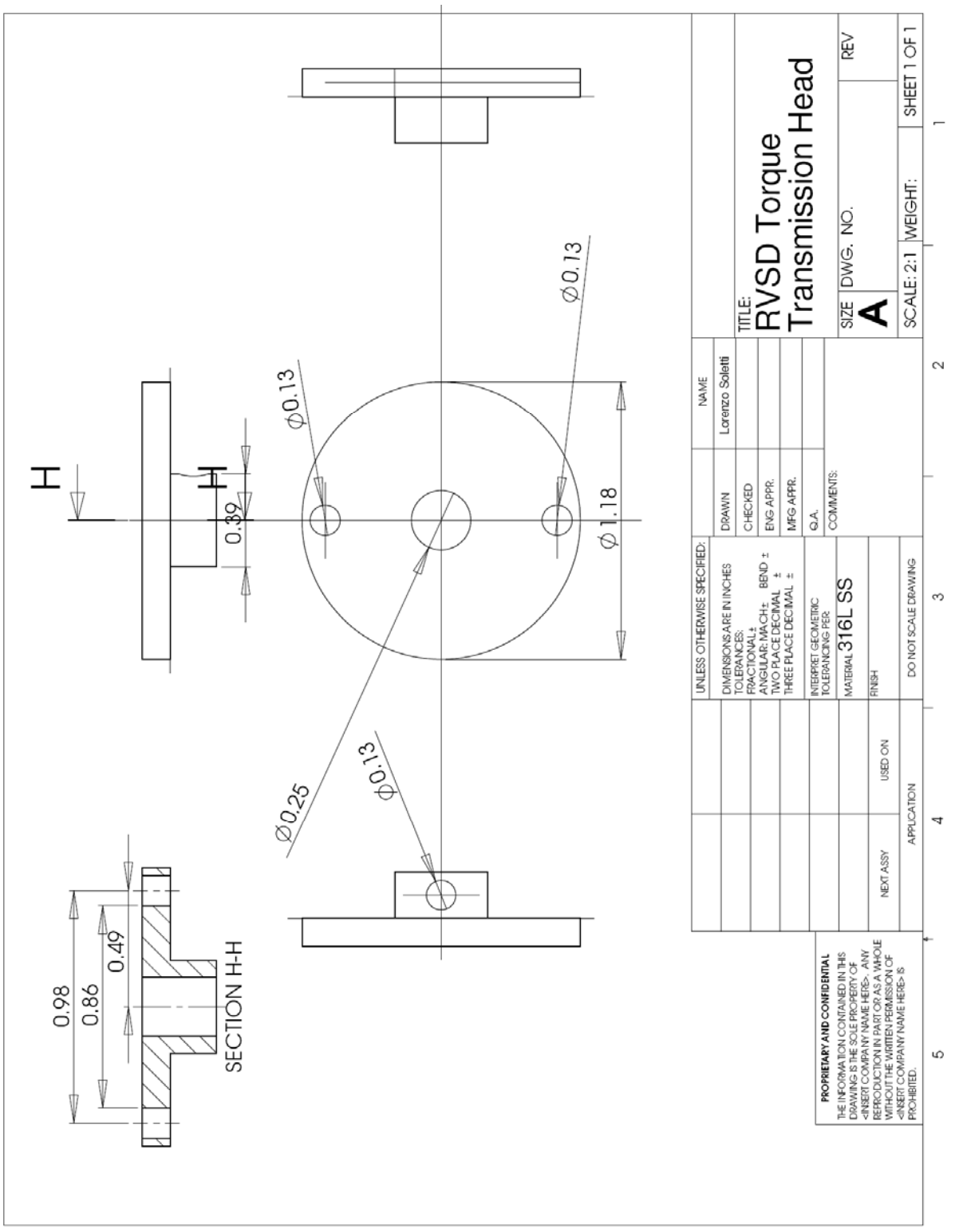

Figure A.6 Head for the RVSD torque transmission.

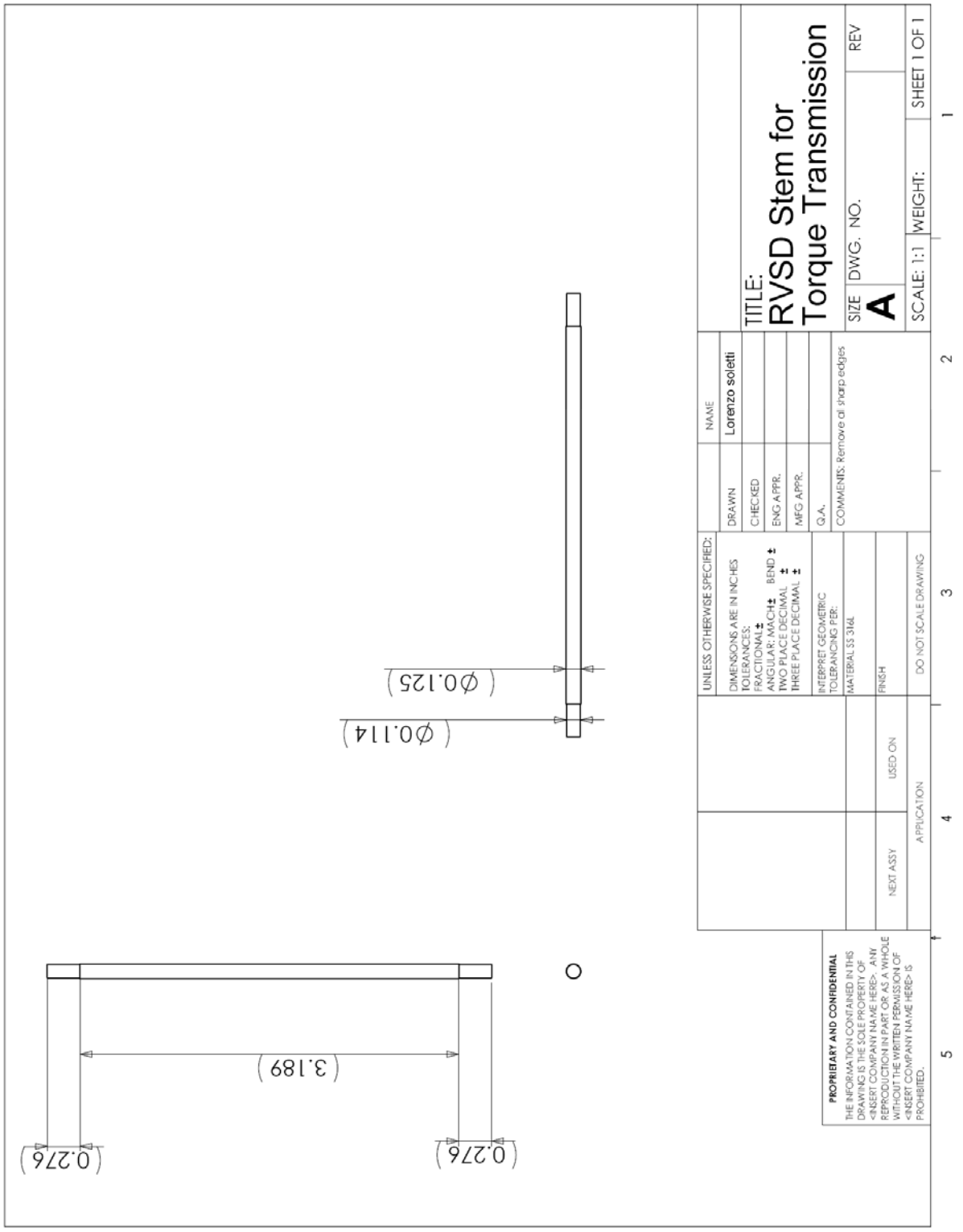

Figure A.7 Stem for the RVSD torque transmission.

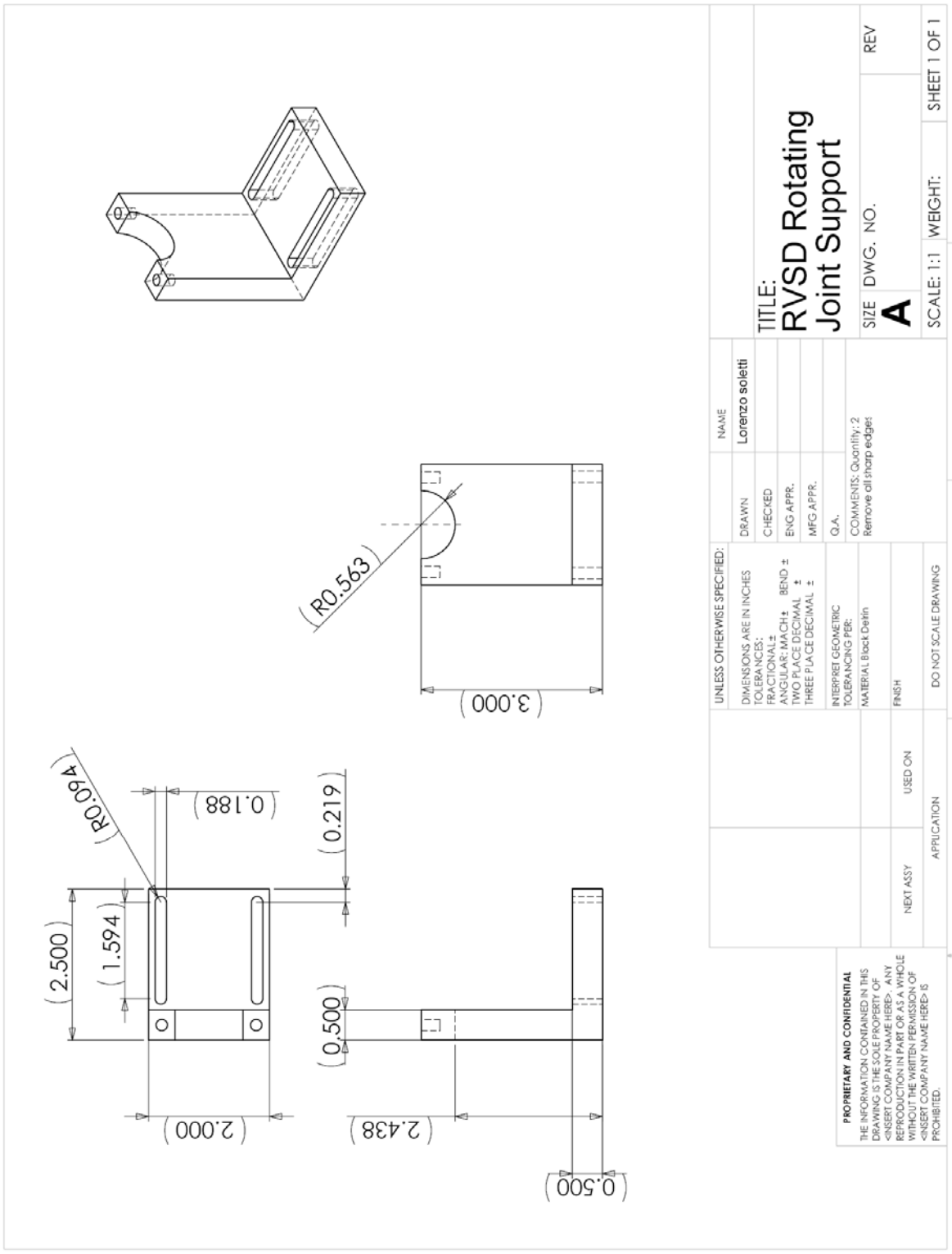

Figure A.8 Joint support for the RVSD.

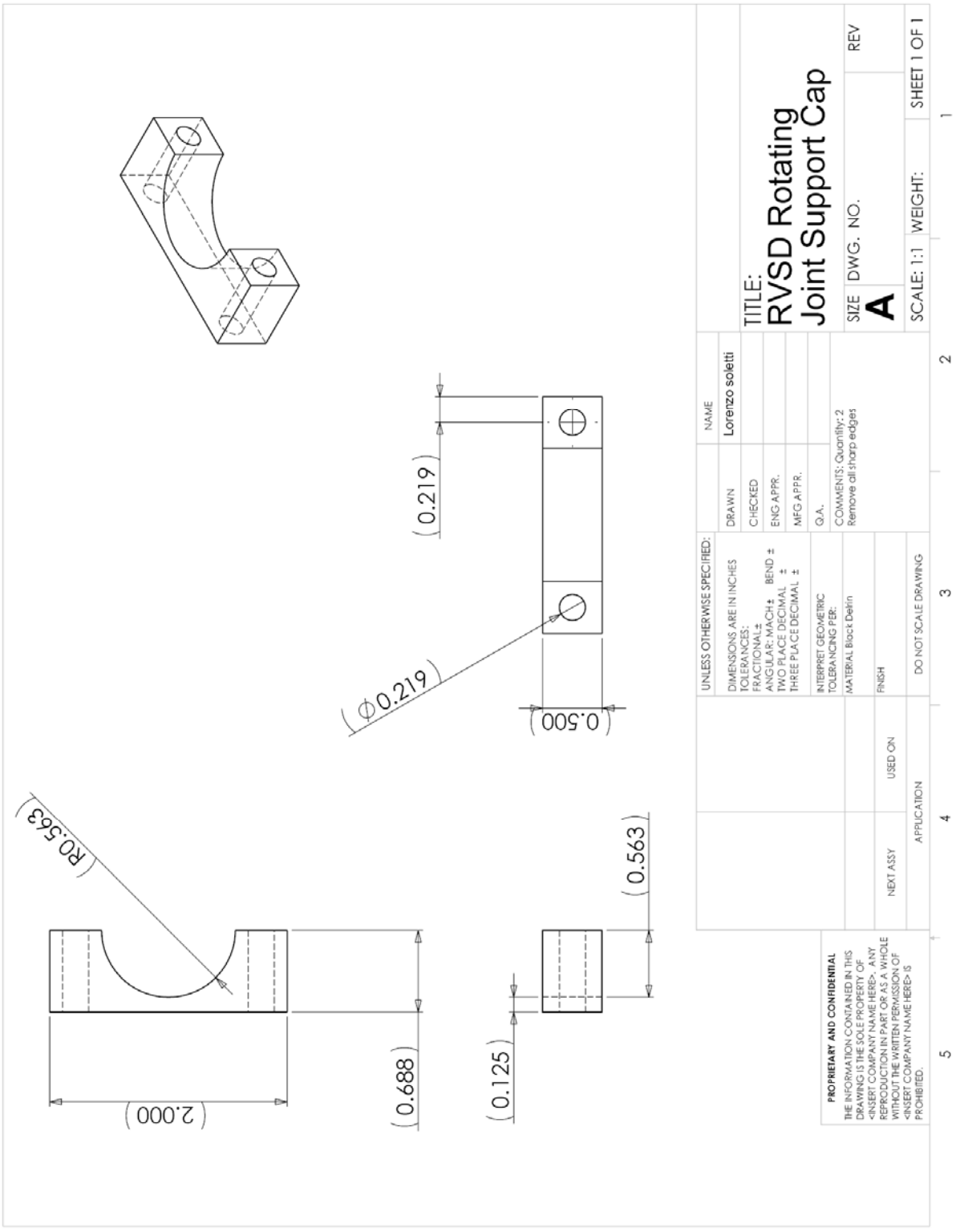

Figure A.9 Cap for the rotating joint support for the RVSD.

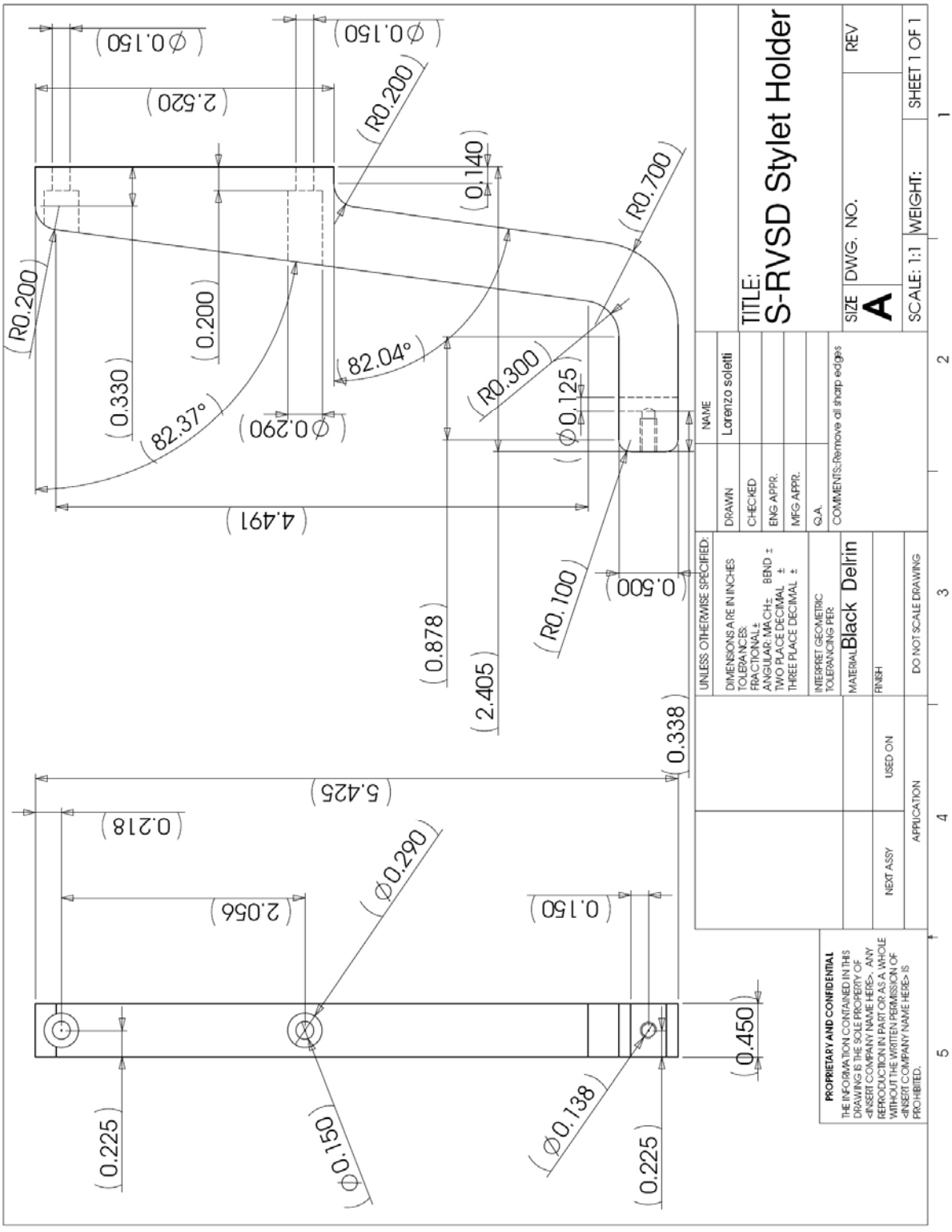

Figure A.10 Stylet holder for the S-RVSD.

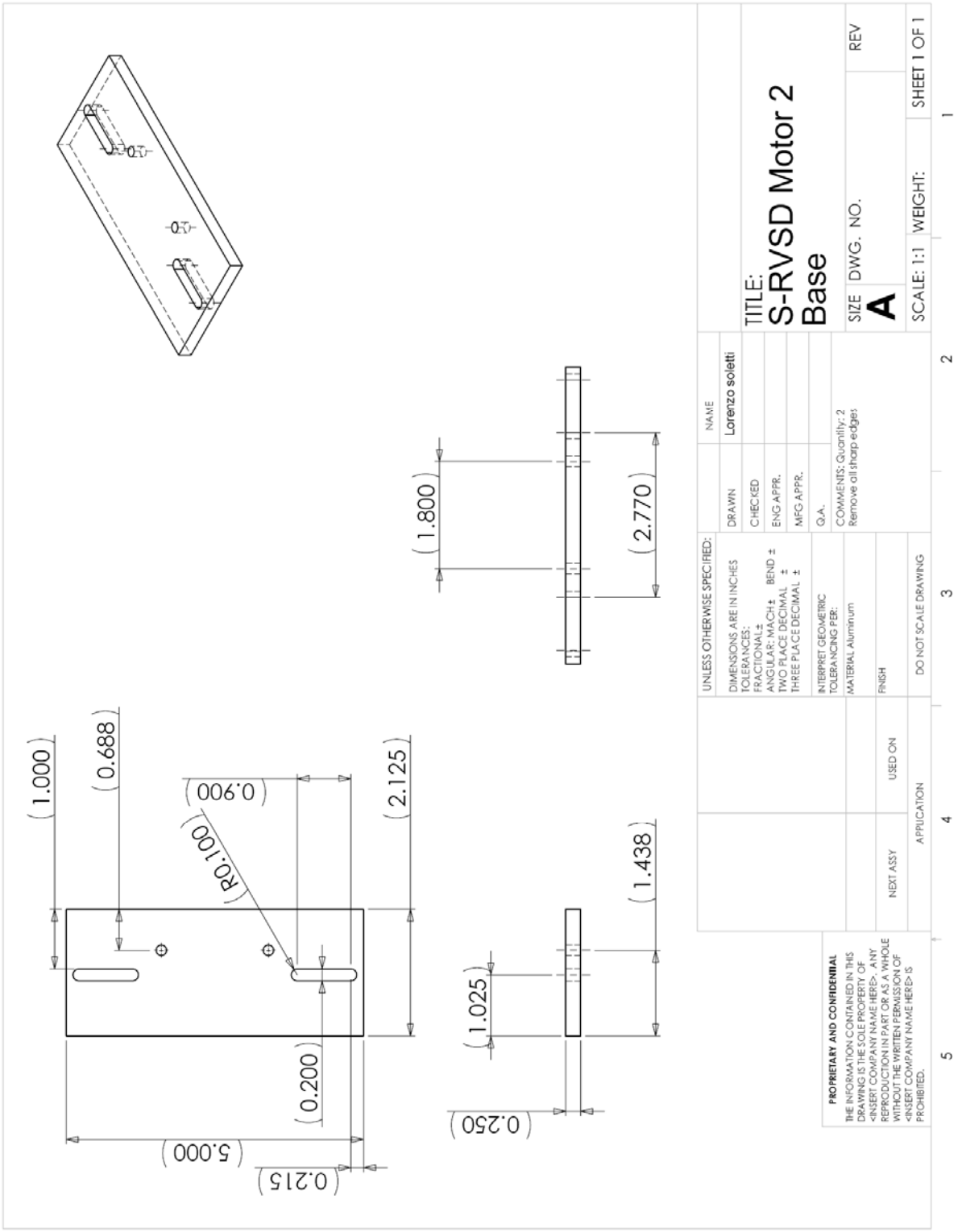

Figure A.11 Motor 2 base support for the S-RVSD.

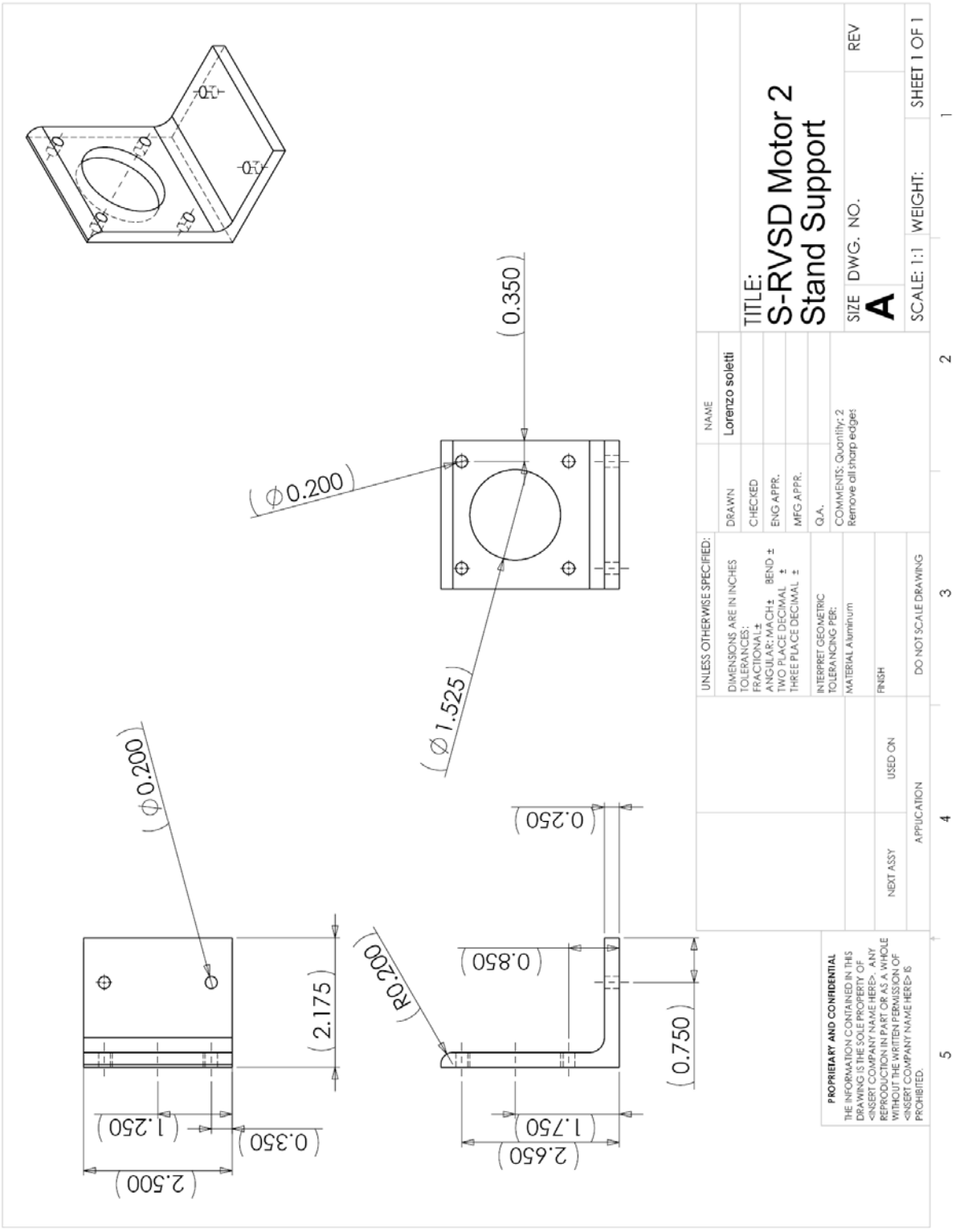

Figure A.12 Motor 2 stand support for the S-RVSD.

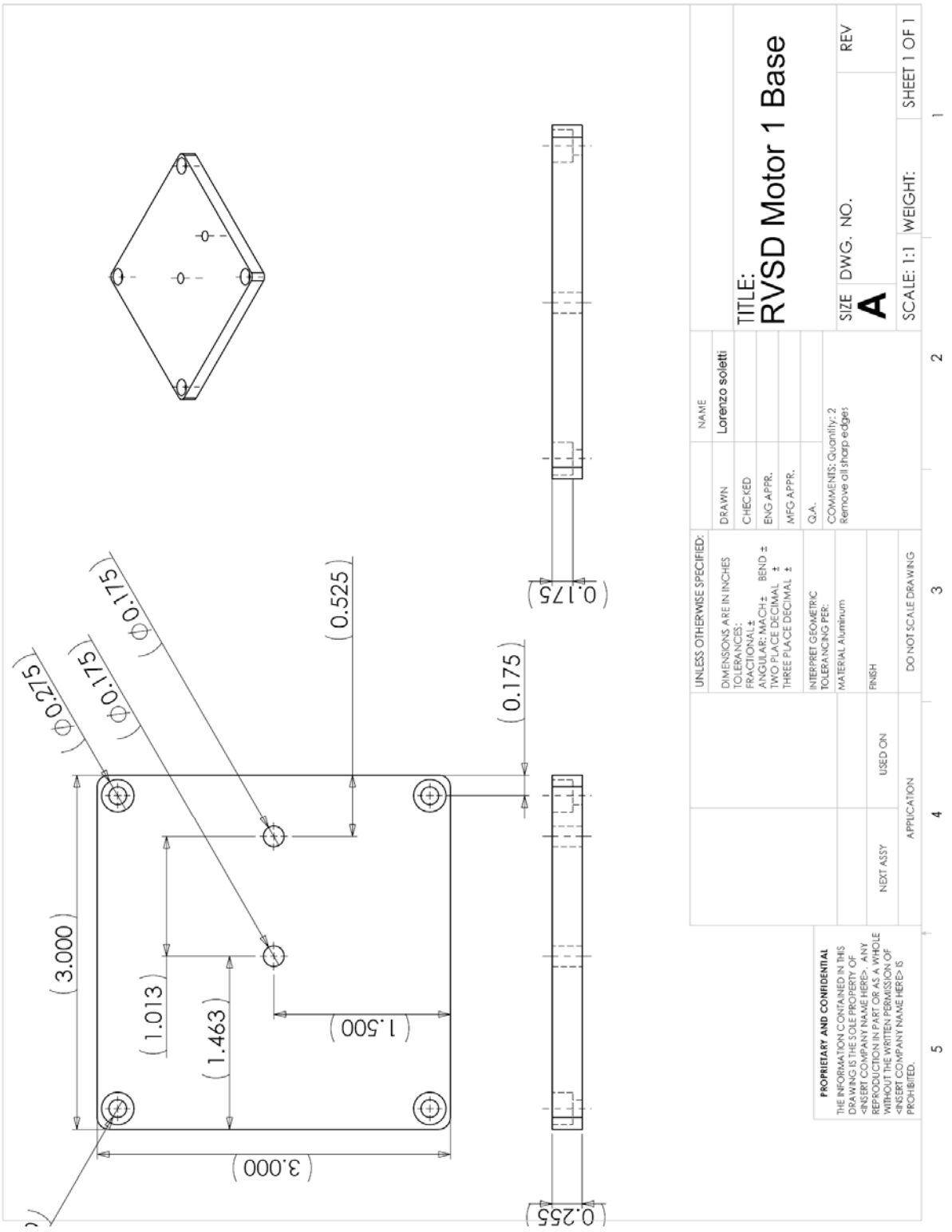

Figure A.13 Motor 1 base support for the S-RVSD.

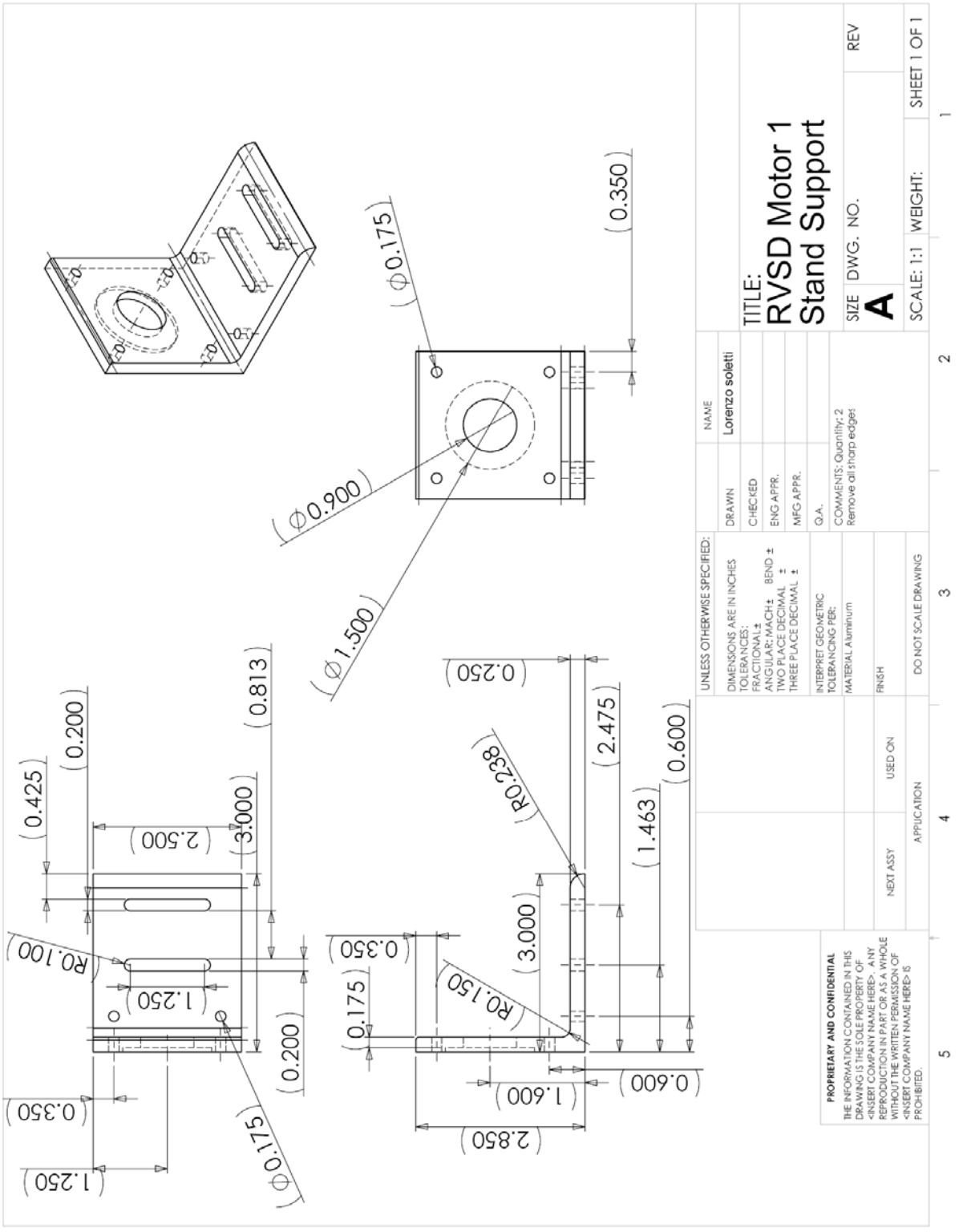

Figure A.14 Motor 1 stand support for the S-RVSD.

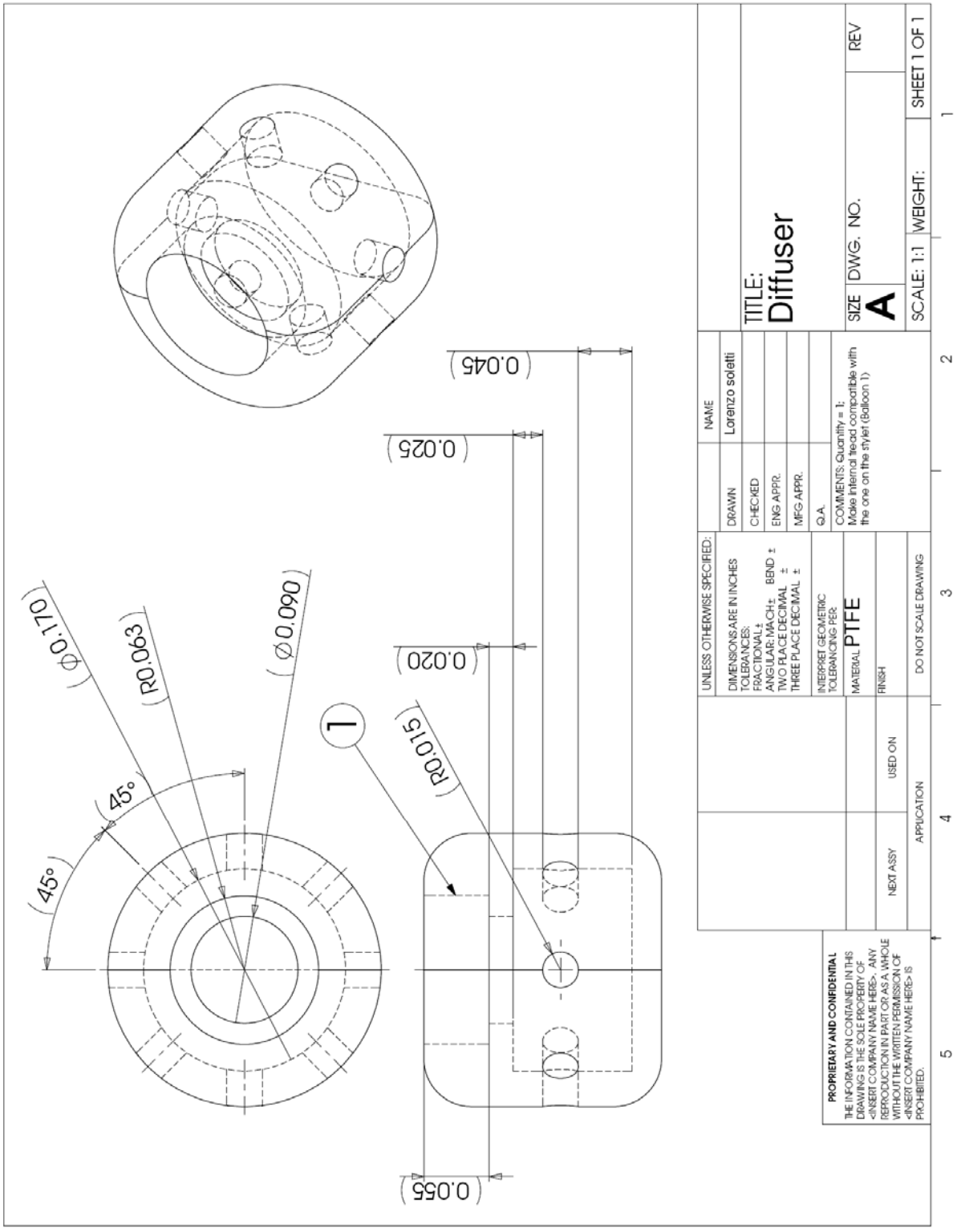

Figure A.15 Diffuser for the S-RVSD.

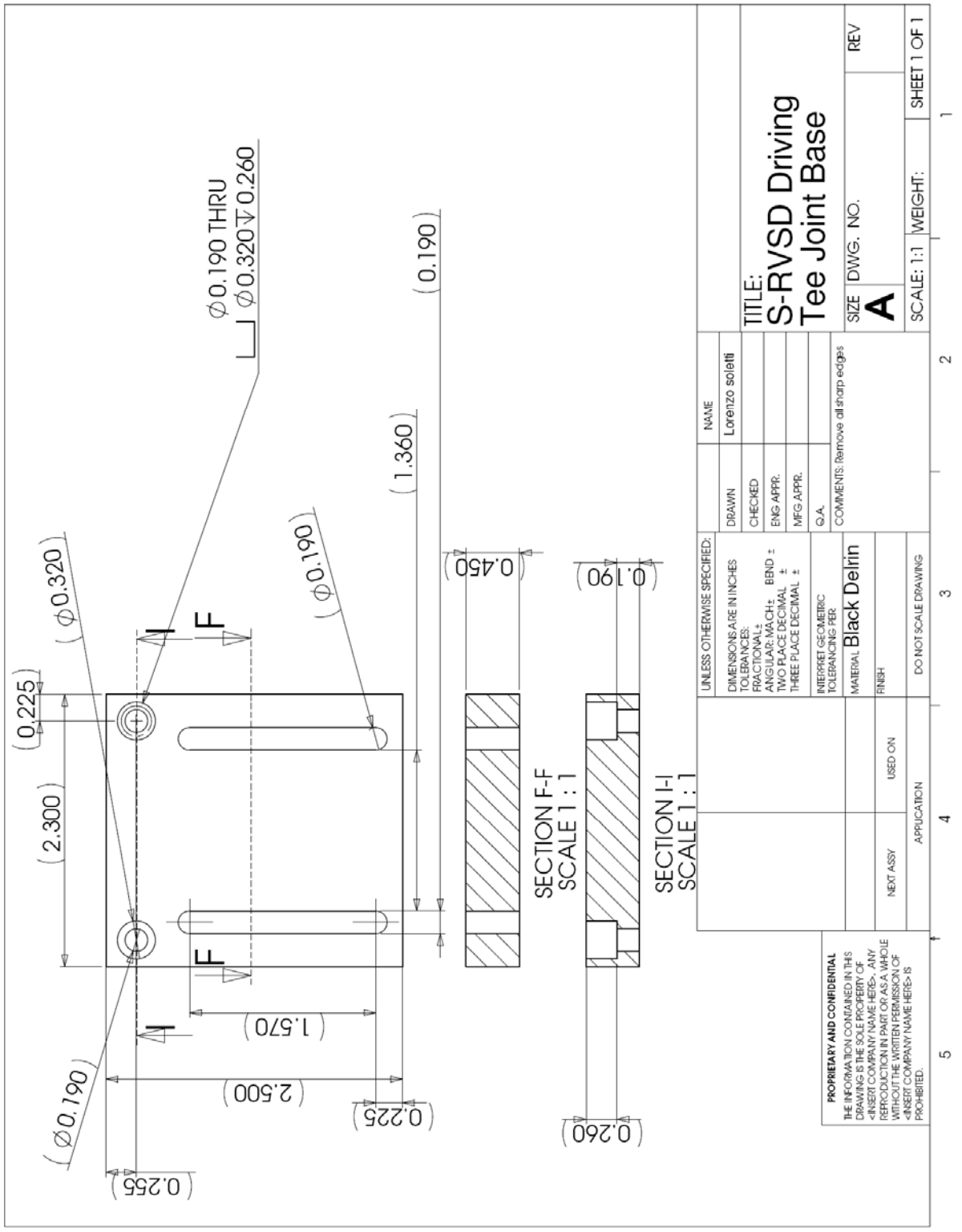

Figure A.16 Base for Driving Tee rotating joint support for the S-RVSD.

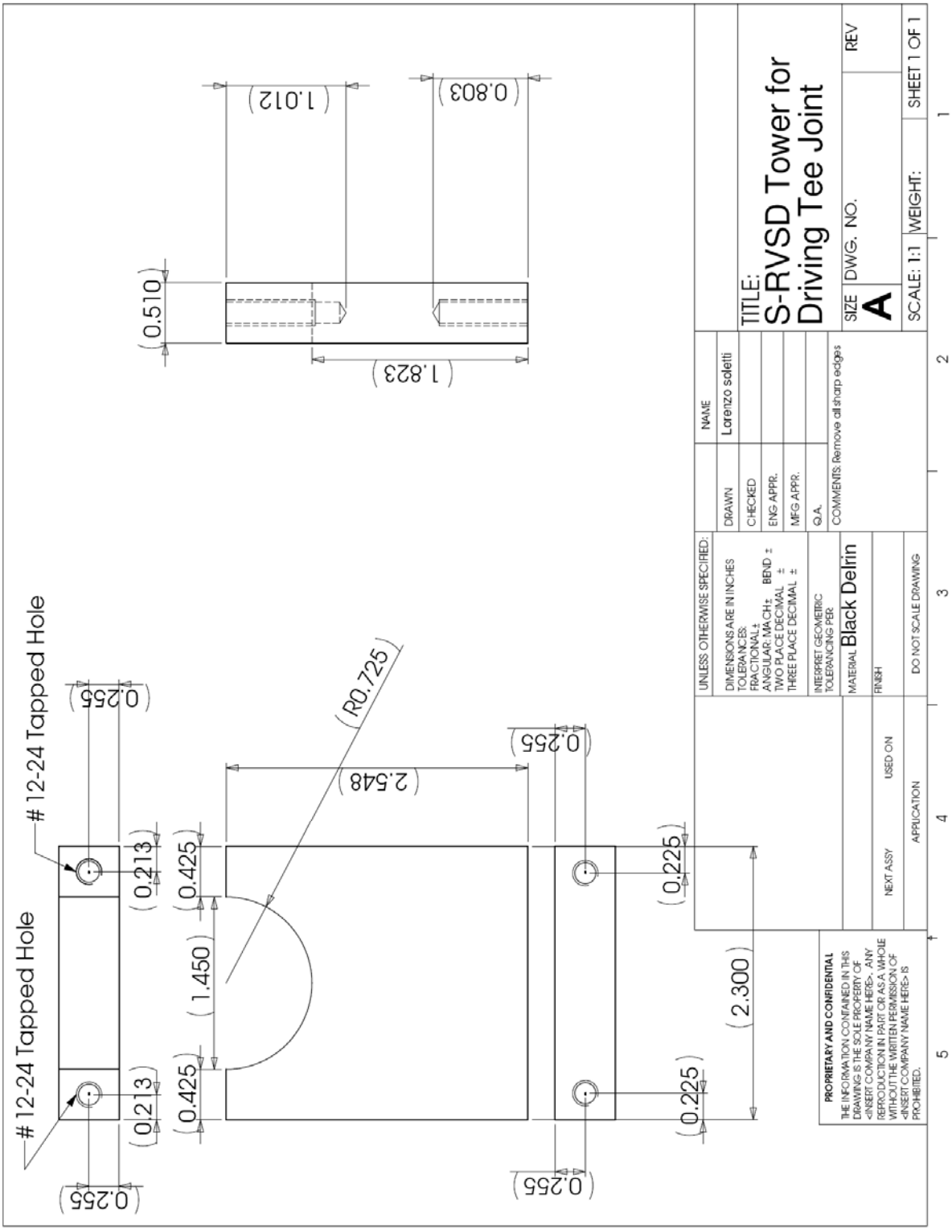

Figure A.17 Support for Driving Tee rotating joint for the S-RVSD.

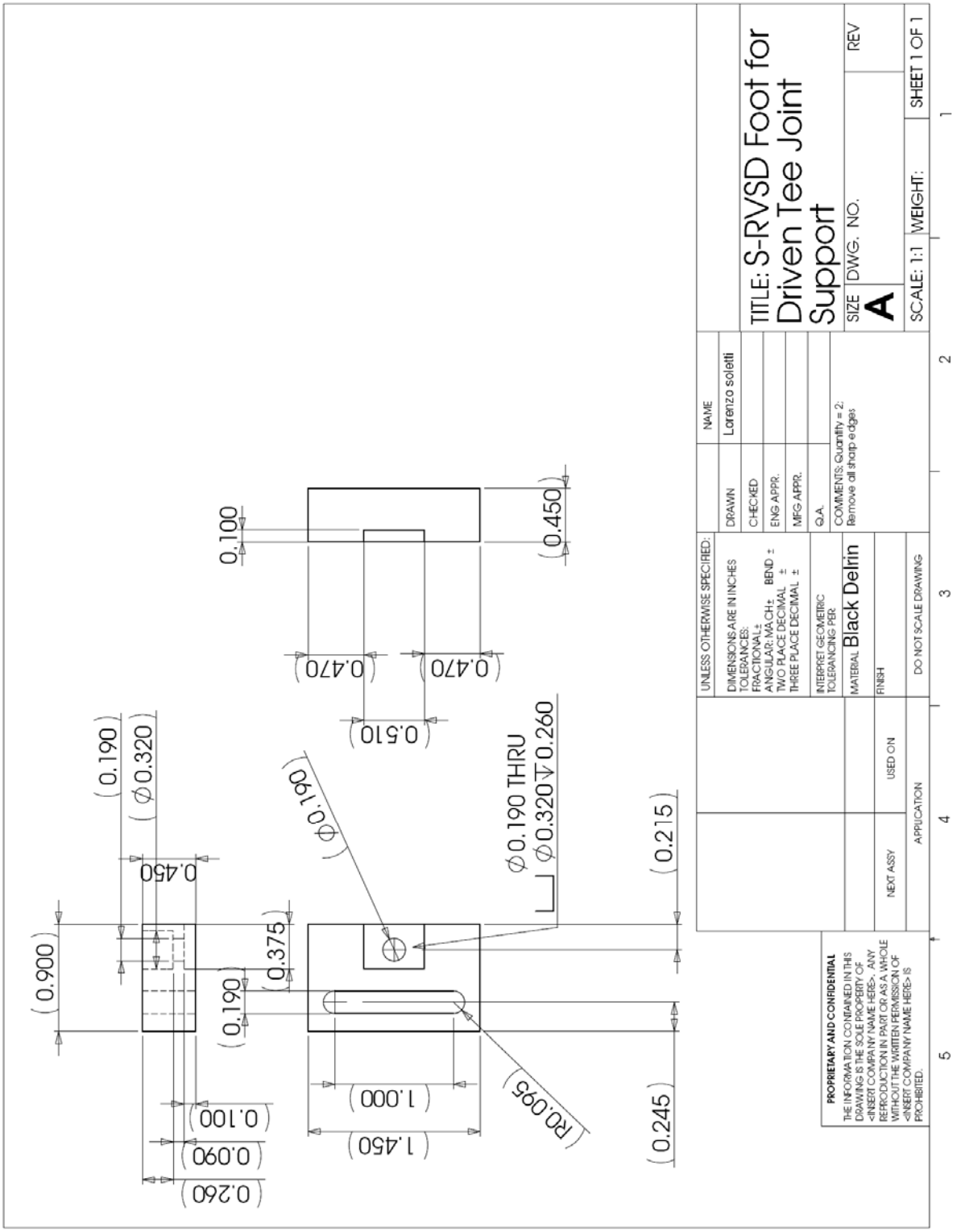

Figure A.18 Feet for Driven Tee rotating joint support for the S-RVSD.

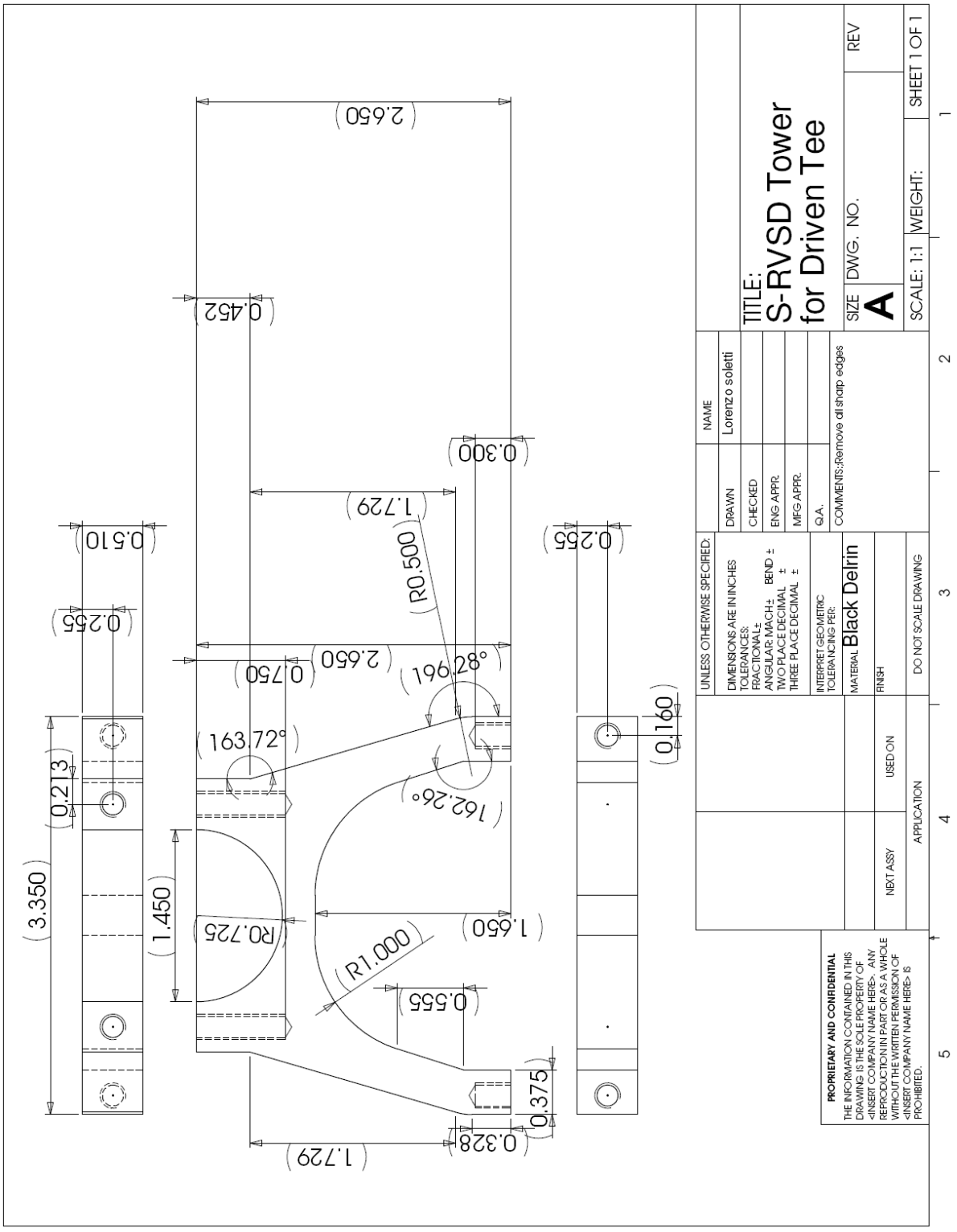

Figure A.19 Support for Driven Tee rotating joint for the S-RVSD.

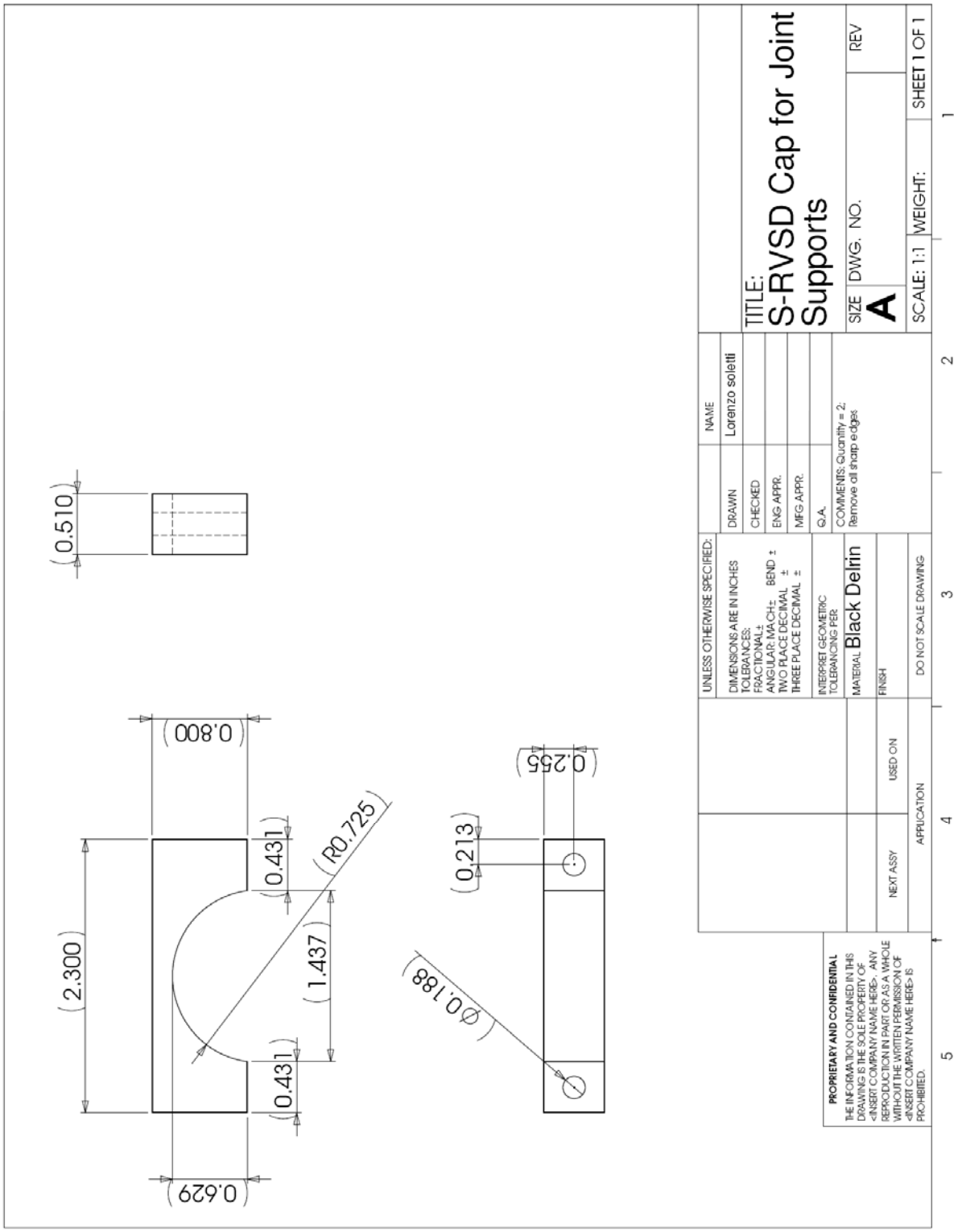

Figure A.20 Cap for rotating joints supports for the S-RVSD.

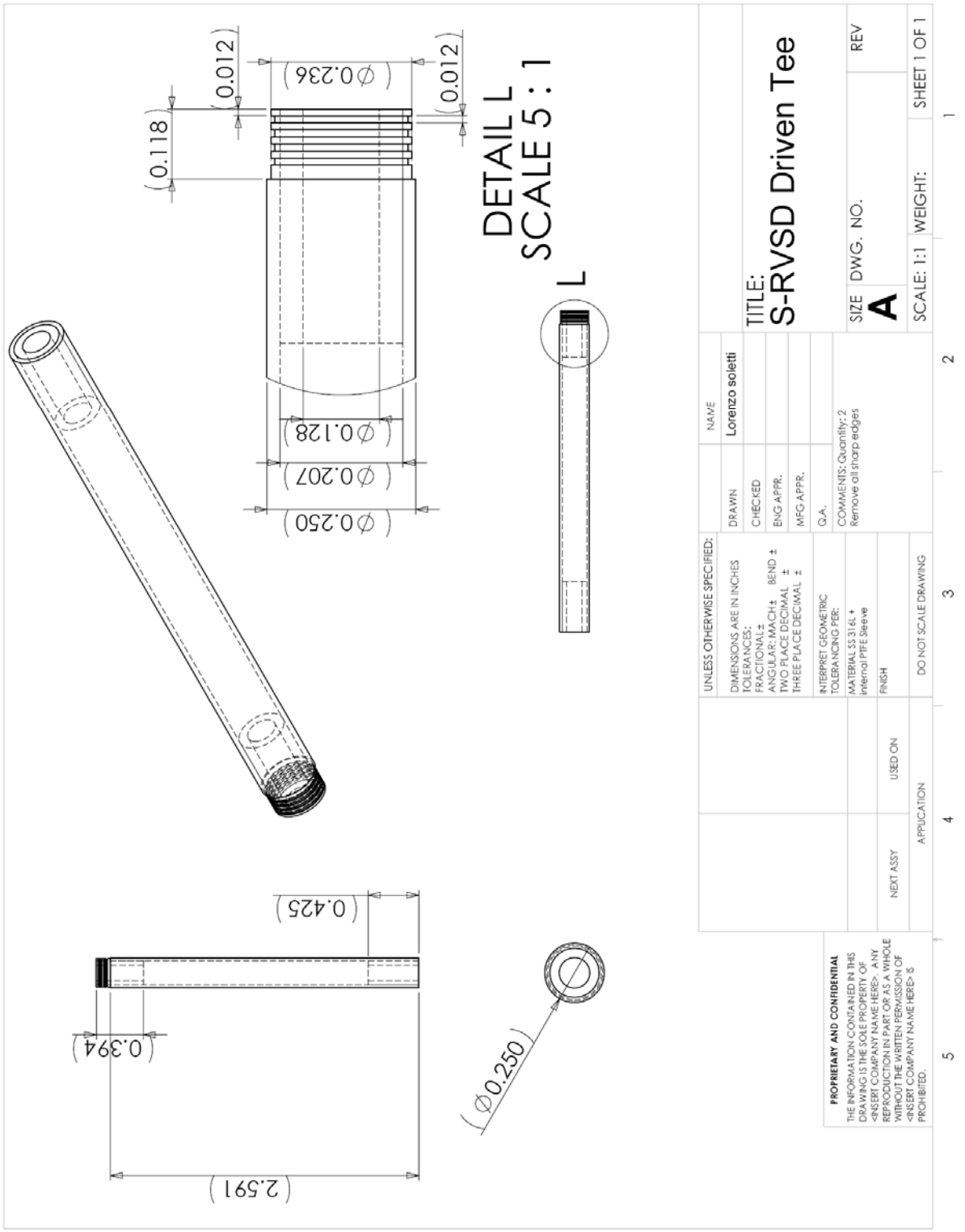

Figure A.21 Driven Tee for the S-RVSD.

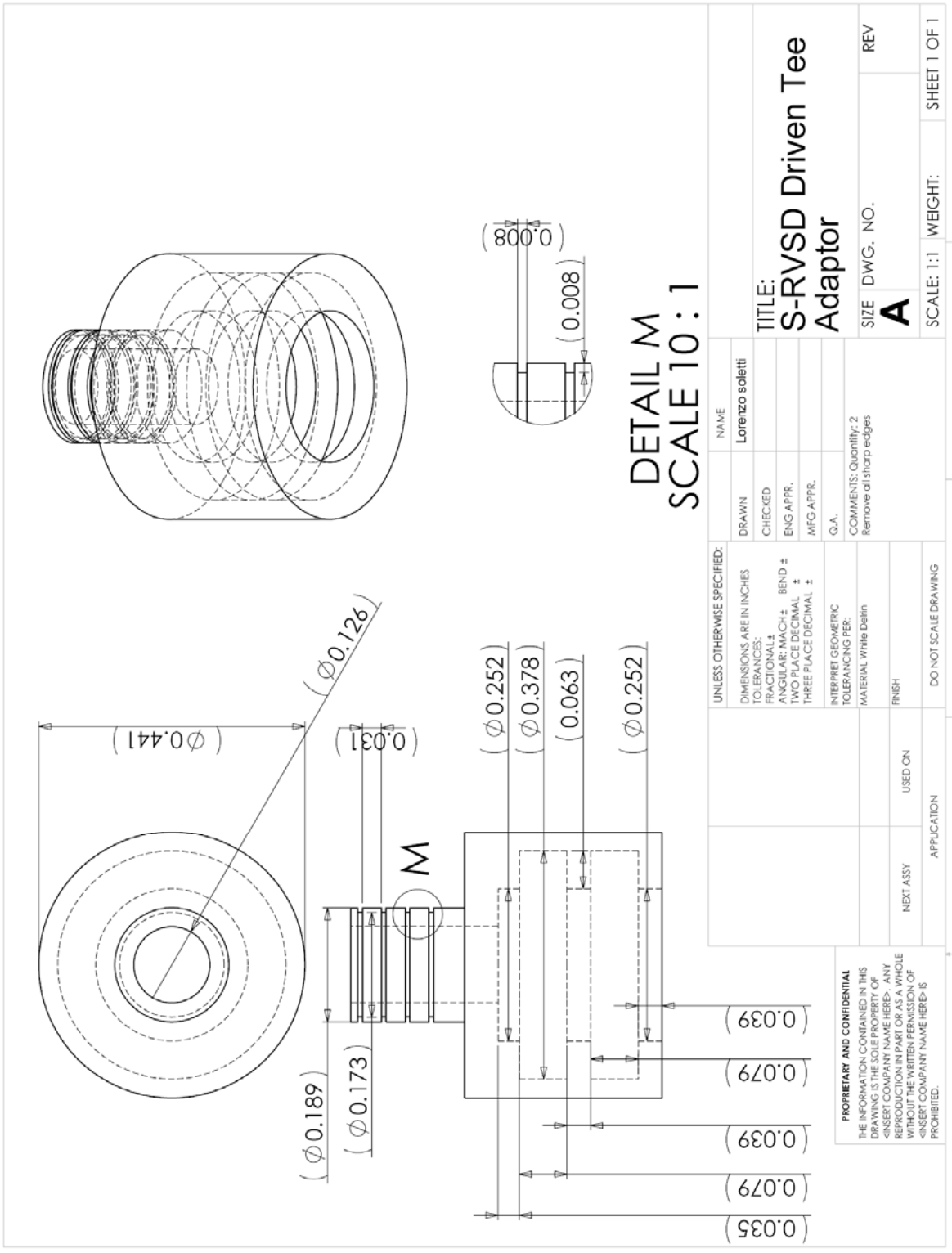

Figure A.22 Tee adaptor for the Driven Tee of the S-RVSD.

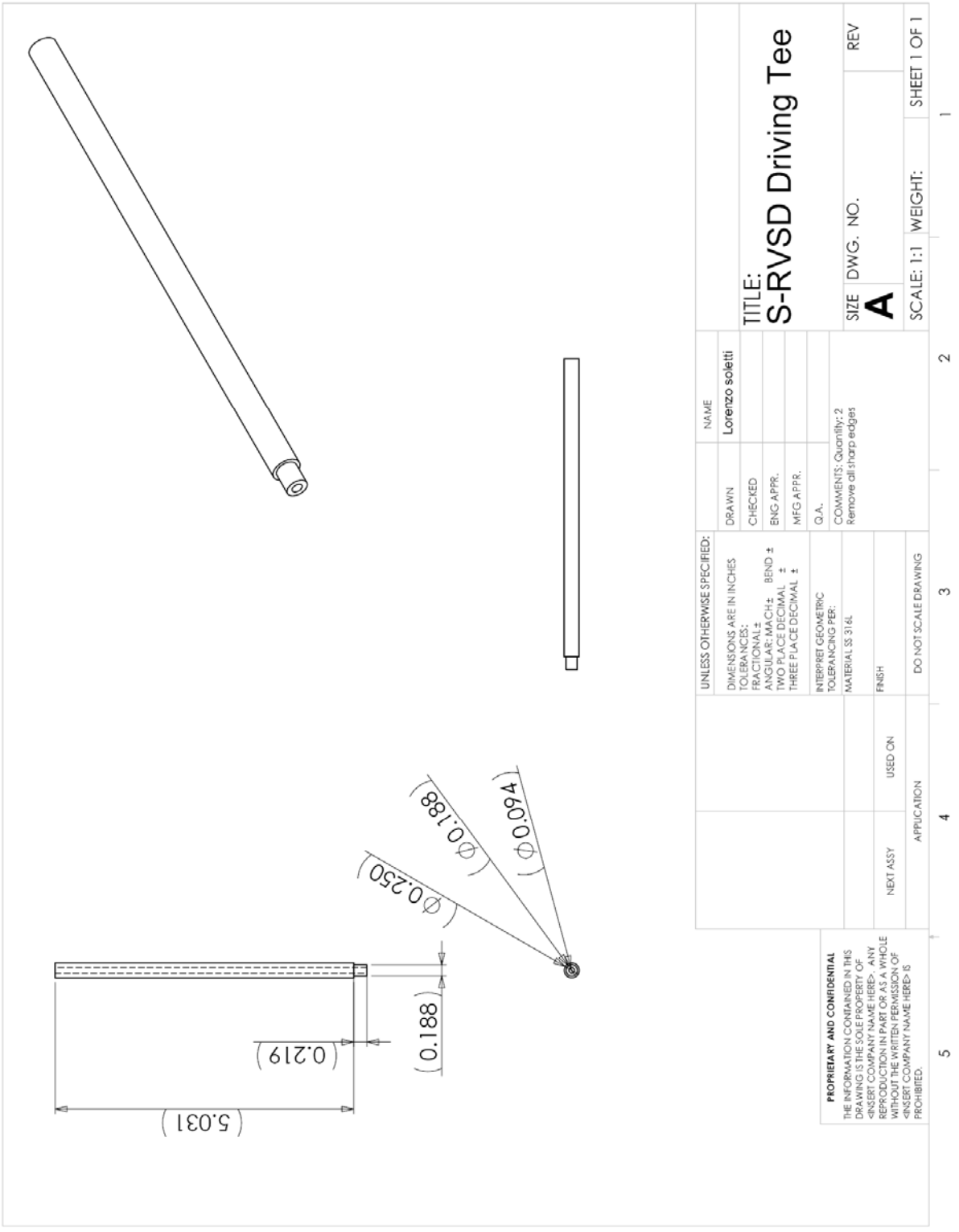

Figure A.23 Driving Tee for the S-RVSD.

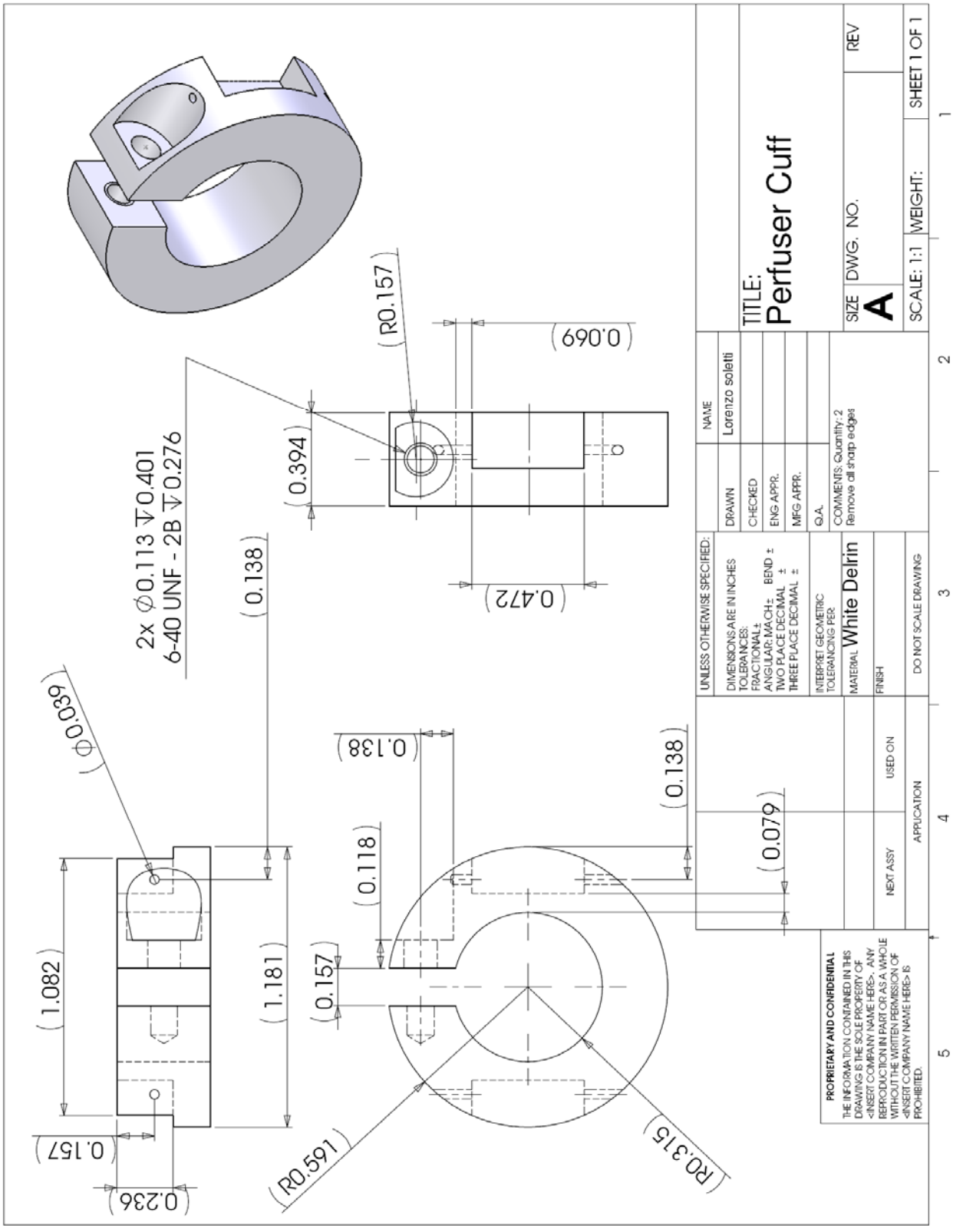

Figure A.24 Cuff for Perfuser.

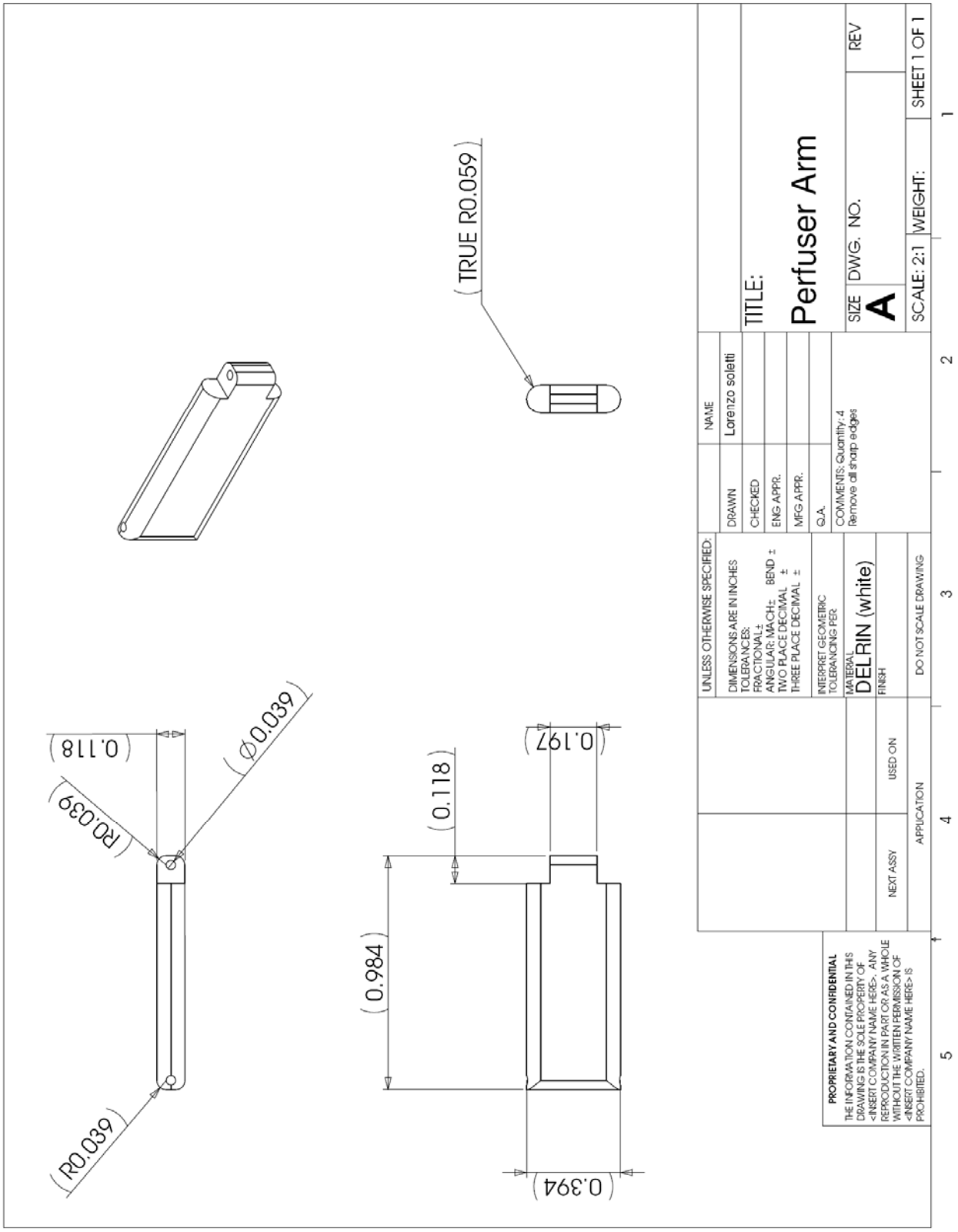

Figure A.25 Arm for Perfuser.

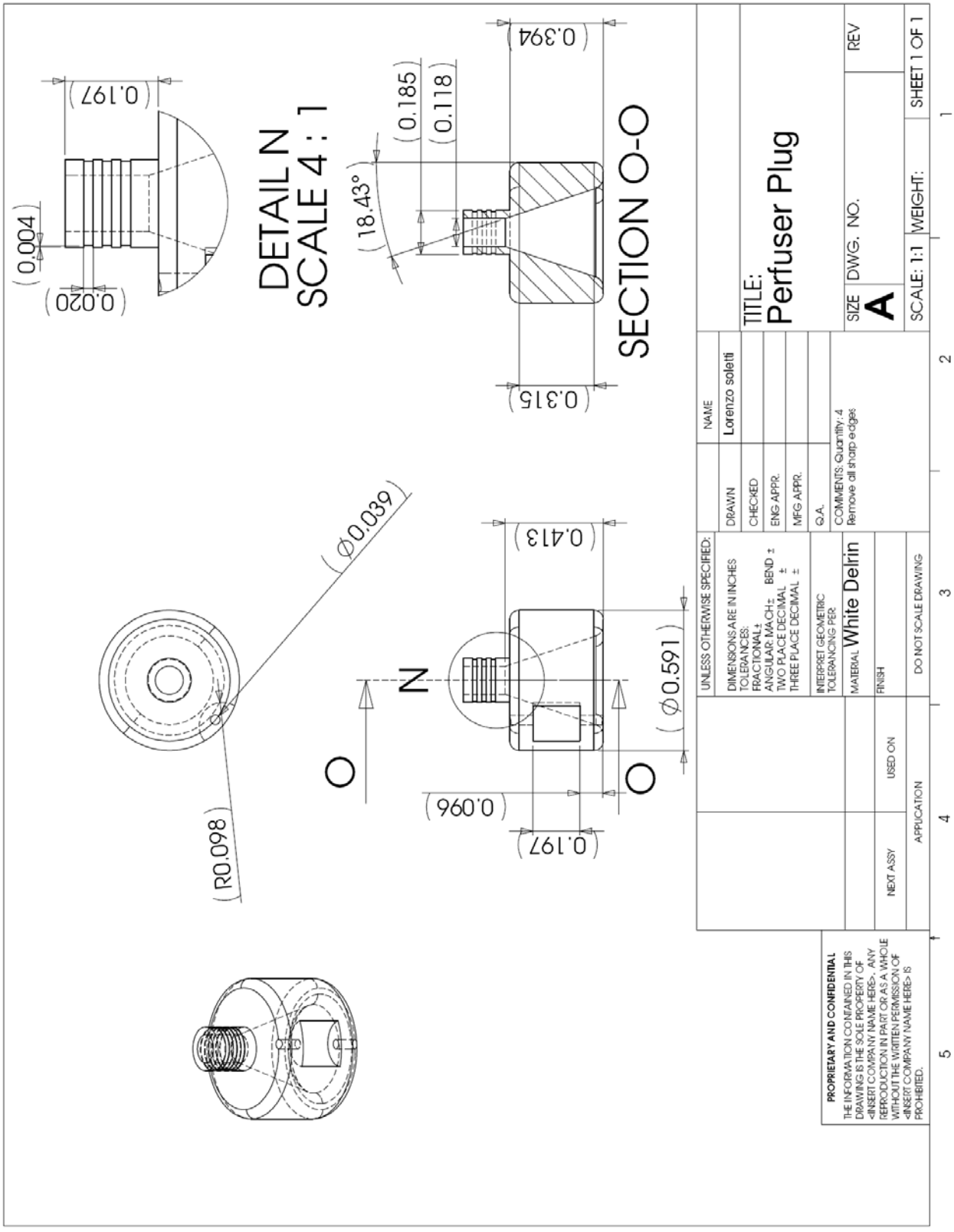

Figure A.26 Plug for the Perfuser.

APPENDIX B

APPENDIX B: ΔP DUE TO THE CENTRIFUGAL ACCELERATION

These calculations are in support of the material presented in **Section 2.2.6.1**.

Area of a circular sector shown in **Figure B.** 1:

$$A = \frac{1}{2} r^2 \theta$$

Mass of the circular sector:

$$m = A\rho = \frac{1}{2} \rho \cdot r^2 \theta$$

Centrifugal acceleration:

$$a(r) = \omega^2 r$$

Centrifugal force acting on the center of inertia of a sector of angle θ:

$$F_c = \int_0^R ma(r)dr = \frac{1}{2}\theta \int_0^R r^3 \omega^2 dr = \frac{1}{8}\theta \cdot R^4 \omega^2$$

Pressure variation due to centrifugal forces:

$$\delta P_c = \frac{F_c}{A} = \frac{1}{4} \cdot R^2 \omega^2 = \frac{1}{4} \omega^2 \left(\frac{D_i}{2} \right)^2$$

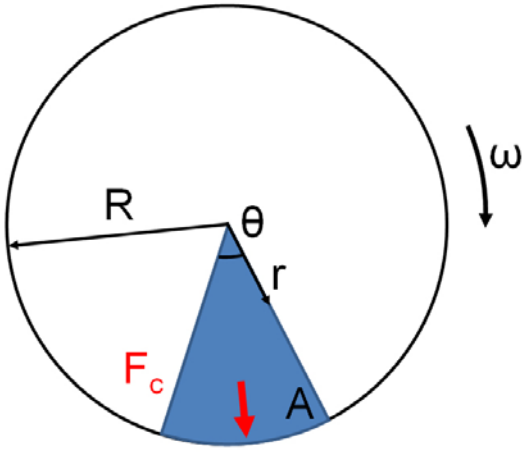

Figure B. 1 Schematic showing the terminology used in the calculations.

APPENDIX C

APPENDIX C: RELATIONSHIP BETWEEN ROTATIONAL AND TRANSLATIONAL VELOCITIES IN THE S-RVSD

These calculations are in support of the material presented in **Section 3.1.3.2**.

Number of nozzles in the Diffuser = 8

Angular velocity of the scaffold [rpm] = $\omega_{Scaffold}$

Period of revolution [sec] = $T_{Scaffold} = 60 / \omega_{Scaffold}$

Time required to rotated the scaffold of 1/8 of a revolution = $t_{arc} = 1/8\ T_{Scaffold} = 7.5 / \omega_{Scaffold}$

Diameter of a nozzle of the Diffuser = 0.62 mm

Translational velocity of the Diffuser ($v_{Diffuser}$) = Translational velocity of the nozzle (v_{Nozzle})

Time required to move the Diffuser of a length equal to its nozzle diameter = $t_{Nozzle} = 0.62 / v_{Diffuser}$

Relationship to satisfy: $t_{arc} \leq t_{Nozzle}$

Substituting: $7.5 / \omega_{Scaffold} \leq 0.62 / v_{Diffuser}$

Therefore: $\boldsymbol{\omega_{Scaffold}}$ **[rpm]** $\geq 12\ \boldsymbol{v_{Diffuser}}$ **[mm/sec]**

APPENDIX D

APPENDIX D: ESTIMATION OF THE SHEAR STRESS WITHIN THE STYLET

These calculations are in support of the material presented in **Section 3.1.5**.

The shear stress inside the lumen of the Stylet was estimated using **Equation 2-6** (cross-ref) valid for steady laminar flows in a rigid cylinder (Poiseuille equation assumptions) substituting the values of dynamic viscosity of the cell culture media (1.03 cP) and the radius of the internal channel of the Stylet (0.45 mm) for a range of flow rates (1-10 mL/min).

$$\tau_{rz,\max} = \frac{Q \cdot 4 \cdot \mu}{\pi \cdot R^3}$$

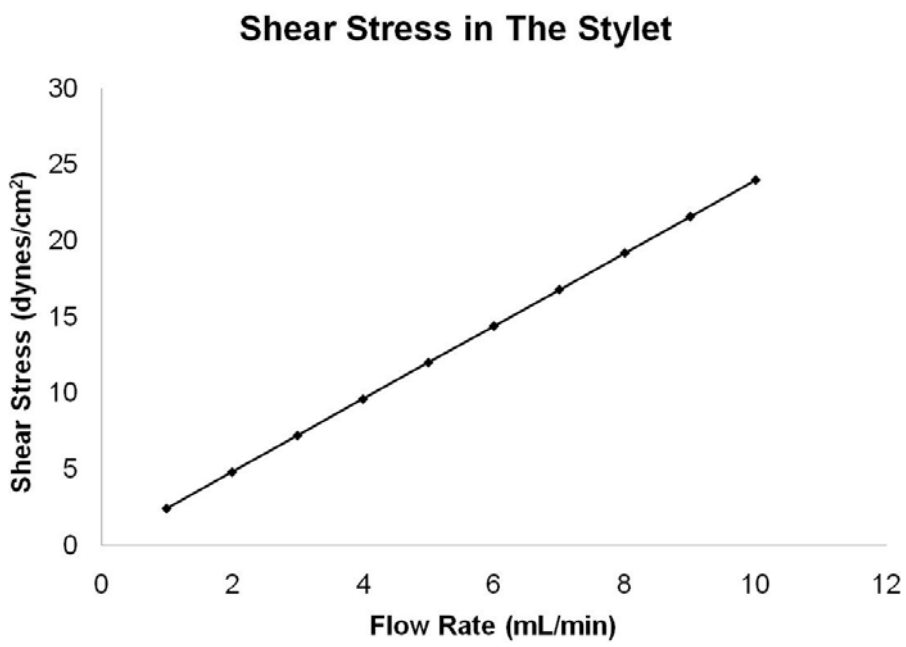

Figure D. 1 Estimation of the shear stress in the Stulet for different flow rates.

APPENDIX E

APPENDIX E: *IN VITRO* ASSESSMENT OF A ES PEUU SCAFFOLD SURFACE-SEEDED WITH MDSCS AND SUBJECTED TO SHEAR STRESS

This preliminary study investigated the response to shear stress of MDSCs surface-seeded onto the lumen of ES PEUU scaffolds in support of the material presented in **Section 4.1.2**. To this end, a simple perfusion bioreactor allowing for independent control of pressure and flow was fabricated. Briefly, a perfusion chamber was machined from a cast acrylic block (external dimensions: 25x25x7 cm) to perfuse up to 6 tubular conduits simultaneously in a sterile environment (**Figure E. 1**). The system holds internally 6 pairs of stainless steel tees in a parallel fashion, which constitute the perfusate circuit. The tees are immersed in a bath of media internally to the chamber. The compact chamber can be kept in standard incubators during culture to maintain a physiologic temperature and pH in the culture media. Both perfusate and bath circuits are fed by a roller pump (Masterflex) provided with two pump heads (Masterflex, Cole-Palmer, Vernon Hills, IL) connected to the same shaft (one pump for each circuit) to provide accurate control of the flow. A common reservoir feeds both circuits and is vented by a 0.2 micron PTFE filter to allow for gas exchange within the incubator, and to prevent contaminations. Gas permeable silicone tubing (Masterflex) was used to allow for additional gas

exchange into the incubator. Additionally, the perfusate circuit was provided with a pulse dampener (placed immediately after the pump head) to eliminate the inherent high frequency pulsatility of the roller pump, a flow resistor (placed immediately after the perfusion chamber) to control the pressure inside the perfused conduits, a pressure transducers and a flow probe to control the pressure and flow rate, respectively.

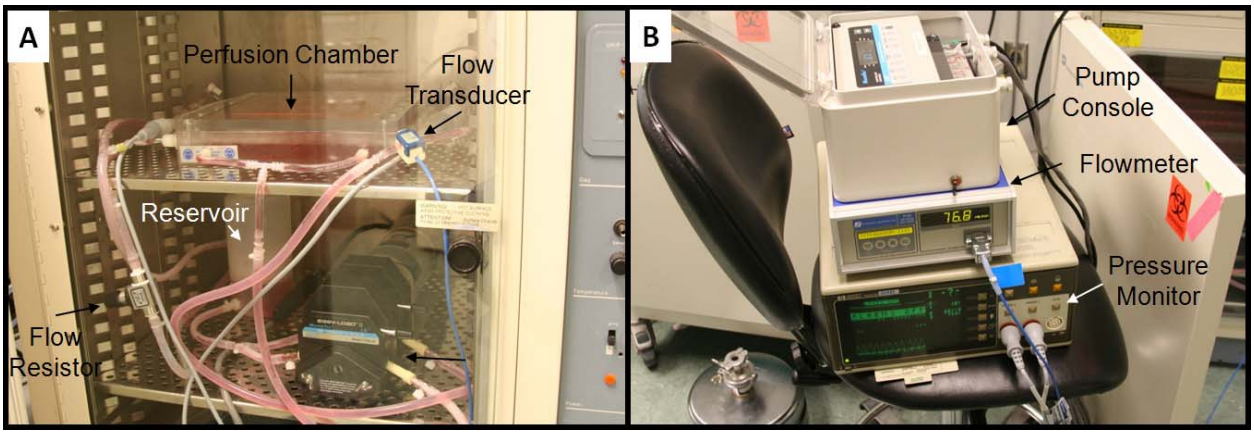

Figure E. 1 Perfusion bioreactor system. **A.** Perfusion setup into a standard incubator. **B.** Flow/pressure control consoles.

ES PEUU scaffolds (recall **Section 4.1.2**) (length: 10 mm, ID: 4.7 mm, thickness: 150-200 μm, porosity: 80-95%, pore diameter: 5-20 μm) were surface-seeded with $20x10^6$ mouse MDSCs via the RVSD using the same protocol described in **Section 2.2.4**. Immediately after seeding, the constructs were cultured in Petri dishes for 24 hours. Constructs were then mounted in the flow bioreactor and subjected to ~1 dynes/cm^2 shear stress under steady flow (100

mL/min) for another 24 hours, while a control group was maintained in static conditions. Cell viability was assessed with MTT assay, while cell morphology, distribution, and alignment were assessed using nuclear (DAPI, Draq5) and cytoskeletal (rhodamine phalloidin) staining with fluorescence microscopy.

Immediately after seeding, a high number of cells adhered on the luminal surface of the scaffolds. The distribution appeared (qualitatively) uniform along the length and the circumference of the constructs. After the first 12 hours of static culture, the scaffolds appeared lined with attached cells that started to spread on the luminal surface surface (**Figure E. 2**).

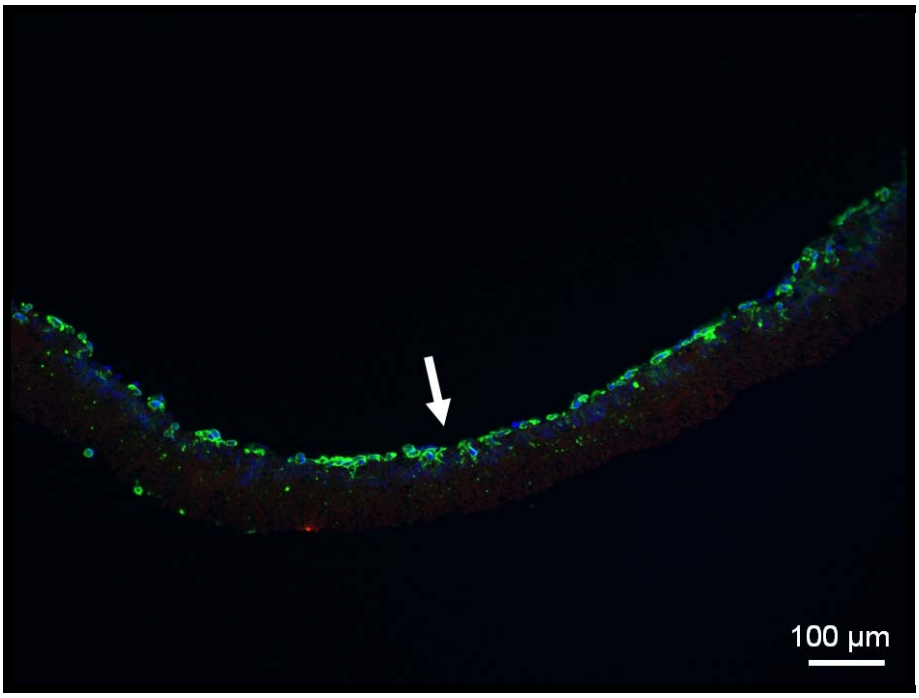

Figure E. 2 Representative results after 12 hours of static culture. Green = F-actin, blue = nuclei, red = ES scaffold. The arrow indicate the lumen of the scaffold.

After 24 hours the cell appeared completely spread on the luminal surface providing an endothelium-like layer (**Figure E. 3-A**). Samples cultured for 48 hours in static conditions exhibited a significant increase in cell number compared to the first 24 hours ($n = 3$, $p < 0.01$) (**Figure E. 4**). The luminal surface appeared covered with a confluent layer of cells (**Figure E. 3-B**). The constructs exposed to low shear stress had a significant decrease in cell number compared with both the 24 and 48 hours static culture groups ($n = 3$, $p < 0.01$) (**Figure E. 4**). The luminal surface presented several clusters of randomly aligned cells (**Figure E. 3-C**).

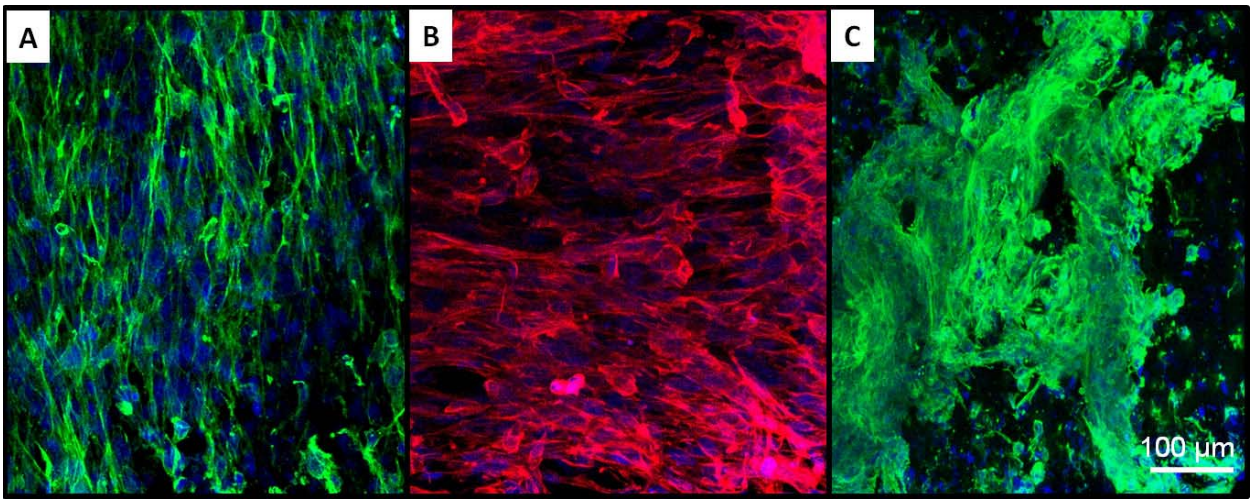

Figure E. 3 Representative results for the three different culture conditions. **A.** Static culture for 24 hours. Green = F-actin, blue = nuclei. **B.** Static culture for 48 hours. Red = F-actin, blue = nuclei. **C.** Exposure to shear stress for 24 hours. Green = F-actin, blue = nuclei.

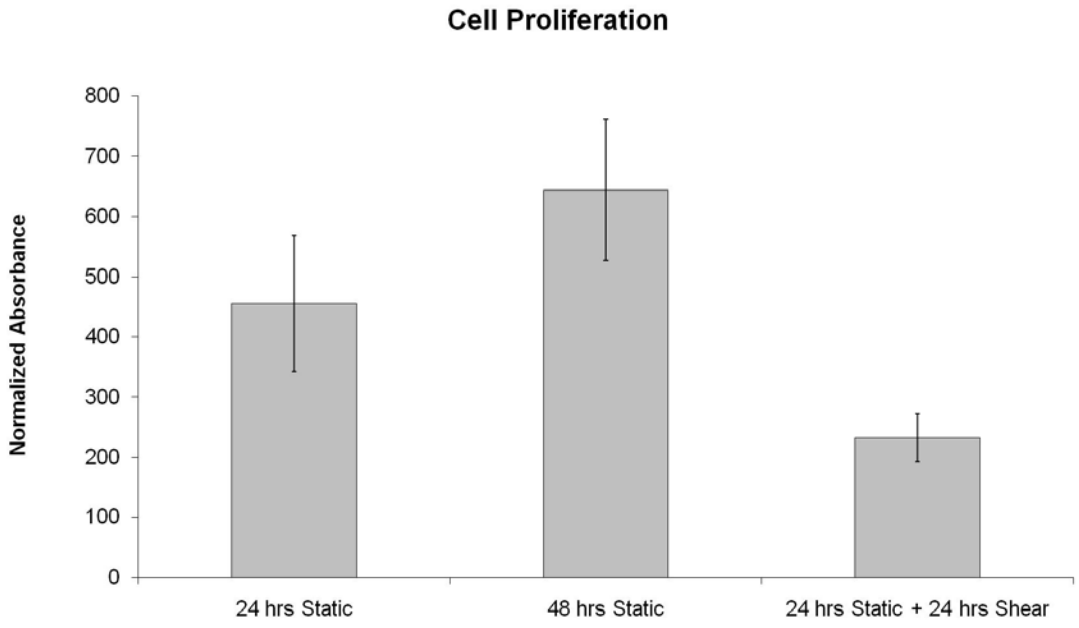

Figure E. 4 Quantification of cell proliferation.

In this preliminary study it was shown that MDSCs can be successfully seeded via the RVSD and statically cultured on the surface of an ES PEUU tubular scaffold to create a confluent endothelium. However, exposure to minimal levels of shear stress (1 dynes/cm^2) after only 24 hours of static culture from seeding was not well tolerated, leading to cluster formation, and cell loss.

APPENDIX F

APPENDIX F: PARALLAX ERROR

The calculations presented in this section are in support of the material presented in **Section 5.3.3**.

A parallax analysis was performed to correct the error introduced by measuring the distance between 2 points (*i.e.,* a random curl in the dye flow and the edge of the Perfuser plug for a defined frame (recall **Figure 5.15**)) in a 3D space by its projection on a 2D image. This method would be fully correct if the distance measured would lay on a plane parallel to the observer's plane; however, in our case the projection required a correction since the measured distance was lying on an oblique plane that was rotating with respect to the obsterver's plane.

Analyzing the plug of the Perfuser rotating clockwise toward the camera (**Figure F. 1**), is possible to identify, in a convenient way, three parameters: the inlet area of the Perfuser plug (magenta circle in Figure F. 1), the vector of the relative velocity between the dye and the plug (blue line in Figure F. 1), and the measured distance between a random point outside the Perfuser plug (*i.e.*, an arbitrary curl in the dye) and the right edge of the Perfuser plug inlet (green line in Figure F. 1). The movement of these three parameters is completely defined in the space since the geometric and kinematic values are known.

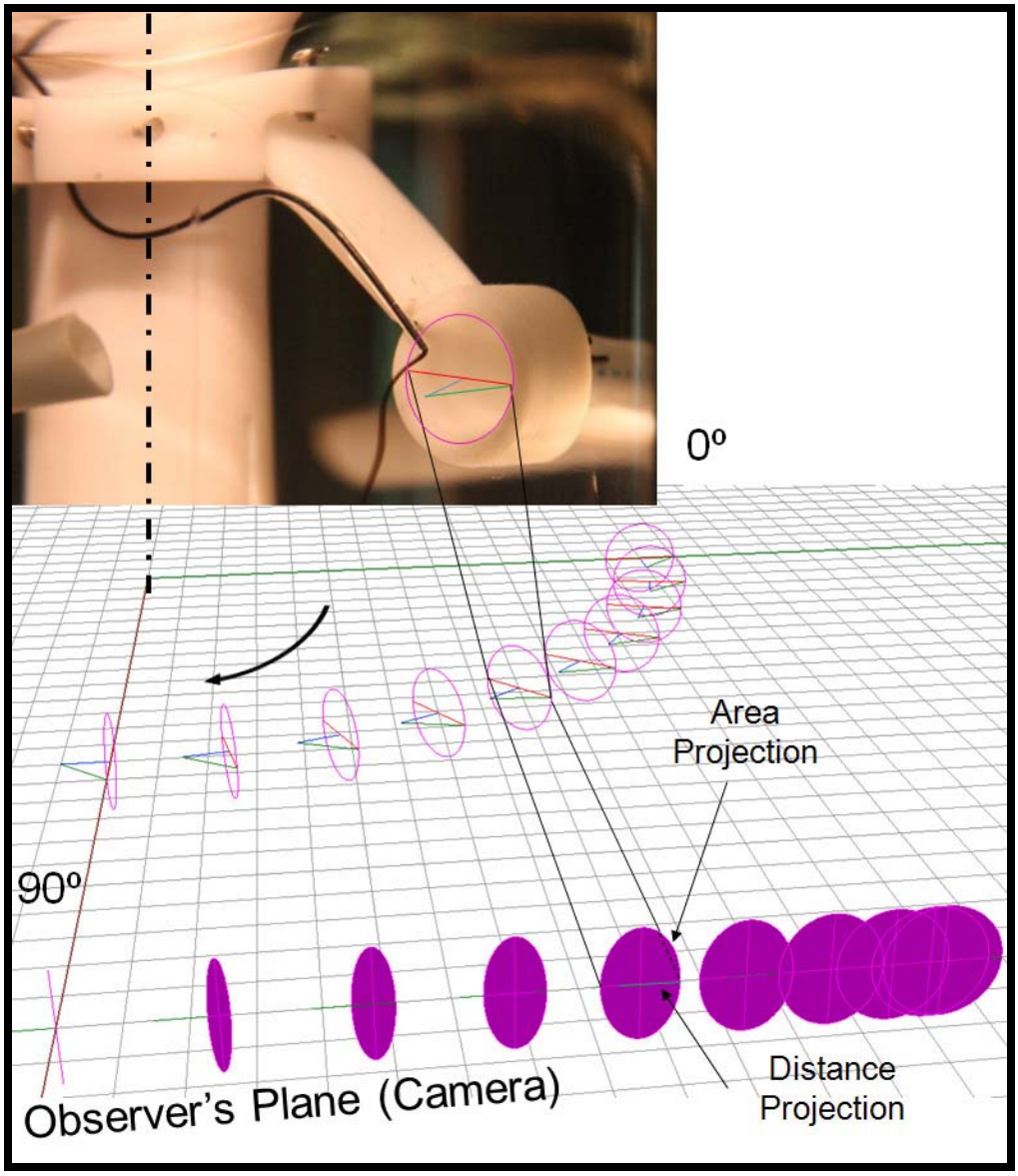

Figure F. 1 Schematic of the parallax calculations.

By some trigonometric calculations was possible to measure the projection of each of these parameters on the observer's plane (*i.e.*, the camera; Figure F. 1), and therefore establish a corrective factor to apply to the measured values from the images (*i.e.*, observer's plane) to retrieve the original values in the 3D space.

In particular the projections of the area and the velocity vector were simply obtained by multiplying the actual area by the cosine and the sine of the relative angle (α) between the observer's plane and the plug's inlet plane, respectively. The projection of the distance was instead, a little more complicated. To solve this, the projection of the distance (L') was decomposed in two components and calculated as a function of α as shown in **Figure F.** 2.

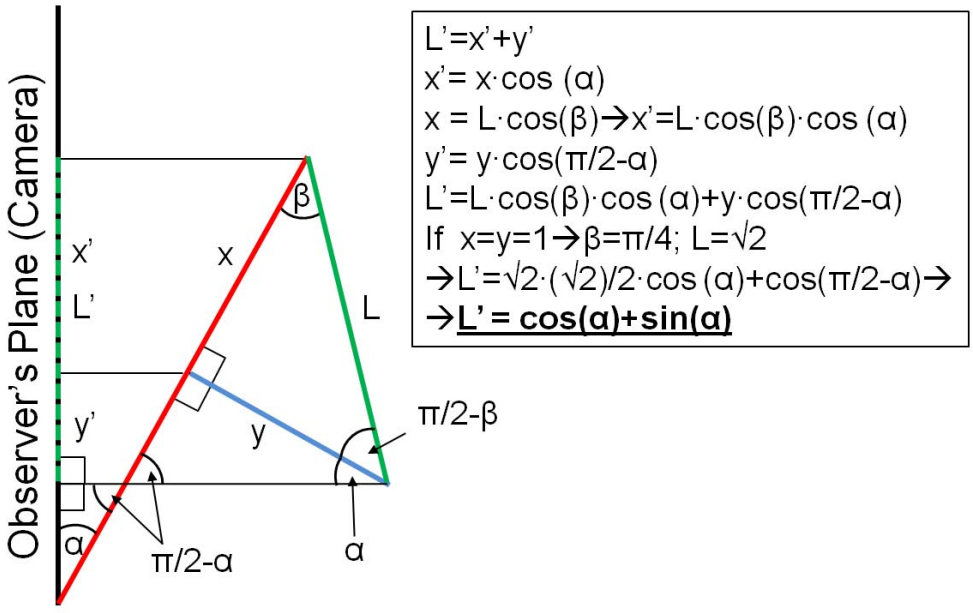

Figure F. 2 Schematic showing the calculation of the parallax. The plain green line indicate the real distance to measure (L), while the dashed green line represents the measure obtained via machine vision (L'). The red line represents the horizontal diameter of the Perfuser inlet area. The blue line indicates the velocity vector of the dye.

A summary of the corrective factors is shown in **Figure F. 3**.

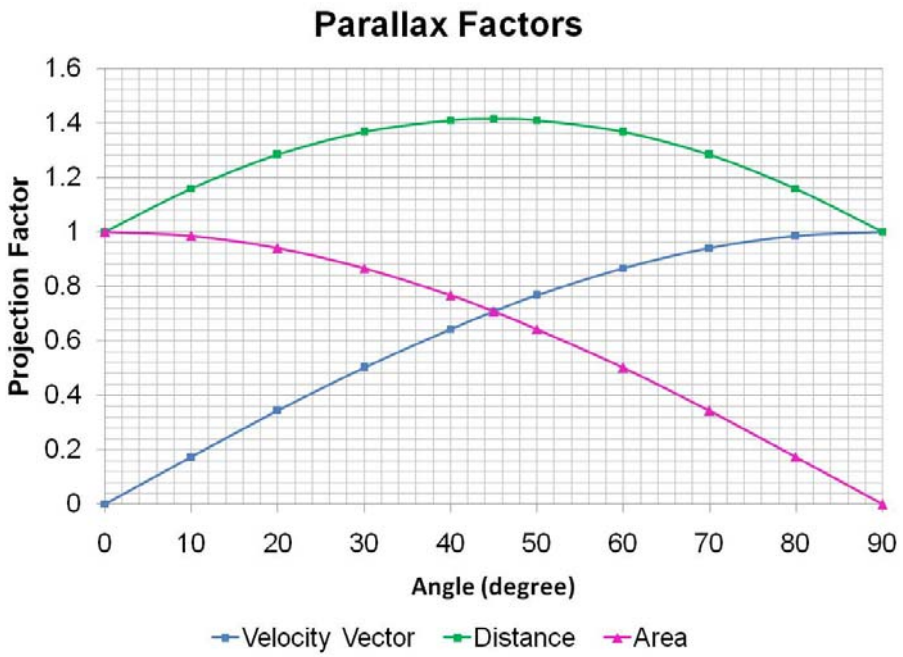

Figure F. 3 Parallax corrective factors. For simplicity, each parameter has been considered having a unitary measure in the 3D space.

Once the relationship between corrective factor and relative angle was obtained, the current angle was calculated by the simply dividing the measured distance (*i.e.*, the projected distance, L') by its relative correction factor to retrieve the real distance value (L).

APPENDIX G

APPENDIX G: PILOT STUDY FOR AUTOLOGOUS LARGE ANIMAL MODEL

The large animal model study described in **Chapter 7** was preceded by a pilot study (using the same animal model and endpoints described in **Section 7.1**) to test the feasibility of the proposed approach, and to troubleshoot a number of potential issues. This pilot study was characterized by the same basic protocols as the official study but resulted in the variation of several parameters to address a number of issues encountered during the course of the study. Furthermore, the pilot study did not entail the use of the Perfuser bioreactor (recall **Section 5.3**), which was replaced by a simple culture in spinner flask, as described for the small animal study in **Chapter 6**.

A total of 9 animals (n = 7 females and n = 2 males) were used for the three experimental groups described in **Section 7.1**. In particular n = 6 animals were used to test the experimental group pG-1, n = 2 animals were used for pG-2, and one animal was used for pG-3. All animal from the first two groups received a contralateral carotid sham interposition, while the two animals from pG-3 did not have any paired control.

Table G-1 summarizes the animal belonging to each experimental group and the number of available cells after the 2 weeks period for cell isolation and expansion.

Table G-1 Summary of the seeding procedures in the pilot study. The star indicates an animal that died days after the muscle biopsy procedure for unrelated causes.

Pig ID	Experimental Group	Seeding Date	Available Cell Number ($x10^6$)
P120-07	pG-1	05/02/07	6.6
P121-07	pG-1	05/02/07	4.65
P314-07	pG-2	10/08/07	90
P315-07	pG-1	10/09/07	44
P316-07	pG-3	10/14/07	16
P317-07	pG-1	10/14/07	28.5
P389-07	pG-1	12/11/07	30
P390-07*	pG-1	n/a	25
P391-07	pG-3	12/13/07	27.25

The first two animals of these studies (P120-07 and P121-07) served the important purpose of troubleshooting two main issues: the protocol for autologous cell isolations, and the scaffold characteristics (*i.e.*, *ID,* and thickness). These studies were originally conceived using only the PP6 fraction (MDSCs). However, the low cell yield ($6.6x10^6$ and $4.7x10^6$ cells, respectively) obtained after a two week period appeared immediately not adequate to match the expected $30x10^6$ cells. Therefore, at this point a decision was made to create a pooled population of cells as explained in **Section 7.3.1** for the future isolations.

Furthermore, the initial scaffold conceived for the large animal study was an ES-TIPS scaffold with an *ID* of 6.3 mm and a thickness of the ES layer of ~ 100 μm. These geometrical characteristics resulted in two issues once implanted *in vivo*: a size mismatch, and some mechanical inadequacies, which led to TEVG dilation after *in vivo* remodeling. Therefore, based on the actual size of the pig carotid arteries harvested, it was decided to reduce the *ID* of the ES-TIPS scaffold to 4.7 mm. This required a modification of the molds used for the TIPS layer (recall **Figure 4.1**), as well as a reduction in size for the Diffuser and the tees of the S-RVSD

(recall **Figure 3.4**). Moreover, the external ES layer thickness was increased to 250 μm by extending the ES time to 1 hour.

Both animals had very similar overall results. In particular, after seeding and dynamic culture in spinner flask both scaffolds exhibited a low number of cells (**Figure G.** 1**-A**). Upon implantation it was noticeable a significant mismatch in size between the *IDs* of the TEVG and the native carotid (**Figure G.** 1**-B**). After 1 month *in vivo*, a thick capsule formation surrounded the TEVG, which appeared dilated (**Figure G.** 1**-C**). No signs of acute inflammatory response or infections were detected. Fluoroscopy showed patency in both constructs with some stenosis at both anastomoses (more pronounced in the proximal anastomosis), and confirmed the scaffold dilation (**Figure G.** 1**-D**). Gross pathology showed a clear intimal hyperplasia formation, significantly more pronounced at the anastomosis levels, confirming the fluoroscopy findings (**Figure G.** 1**-E**). One animal had a pseudo-aneurysm which caused some blood infiltration in the central portion of the scaffold between the TIPS layer and the neointimal tissue formation leading to formation of an intramural thrombus. In some area of the remodeled scaffold was visible delamination between the two scaffold layers (**Figure G.** 1**-D**).

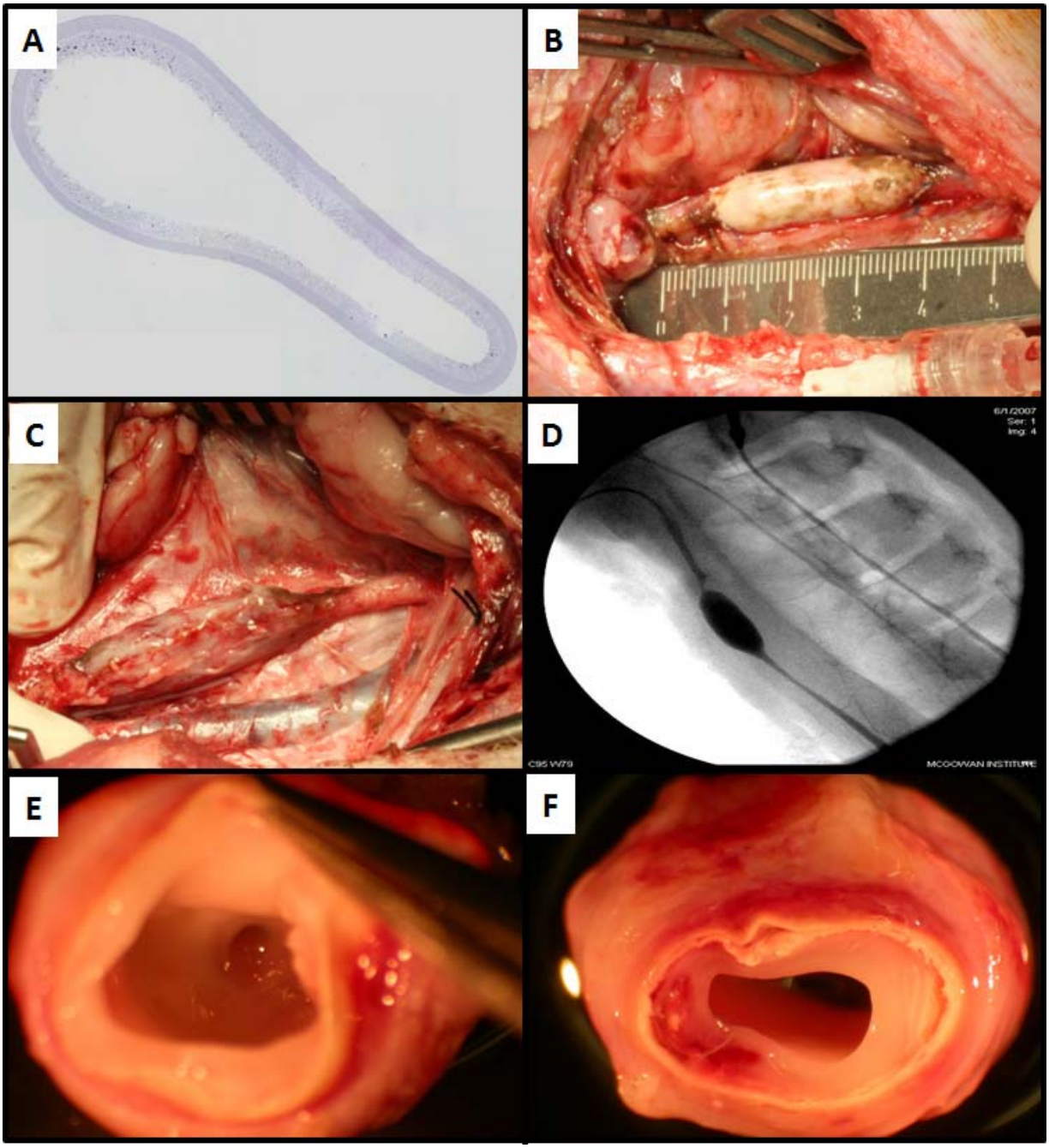

Figure G. 1 Representative results of the first two pigs of the pig pilot study. **A.** Pre-implantation histology. **B.** Surgical view immediately after completion of both anastomoses. **C.** Surgical view during necropsy. **D.** Fluoroscopy. **E.** Gross pathology findings at the proximal anastomosis level. **F.** Gross pathology finding in the central region of the scaffold.

Histological analysis confirmed the formation of intimal hyperplasia, which was more pronounced at the anastomotic levels (**Figure G.** 2**-A**) than in the central portion of the scaffolds (**Figure G.** 2**-B**). The neo-tissue formation was characterized by the presence of a highly cellularized, organized collagenous layer, highly cellularized. The ES-TIPS PEUU scaffolds appeared significantly degraded and/or remodeled, and presented some delaminations between the two layers, confirming the findings of the gross pathological assessment. SEM of the luminal of the TEVG demonstrated the presence of a significant restriction when transitioning between the native carotid and the TEVG (**Figure G.** 2**-C**). The TEVGs had a confluent layer of endothelial-like cells more pronounced at the peri-anastomotic levels (**Figure G.** 2**-D**) than in the central portion of the TEVG, in which the cell coverage was present, but with a lower density (**Figure G.** 2**-E)**. Finally, the TEVG and portions of native porcine carotid were mechanically tested for uniaxial tensile properties via the ring test (recall **Section 4.2.5.2**). The results confirmed the elevated scaffold degradation detected histologically by showing macroscopical difference in strength between the native vessels and the TEVGs (**Figure G.** 2**-F**).

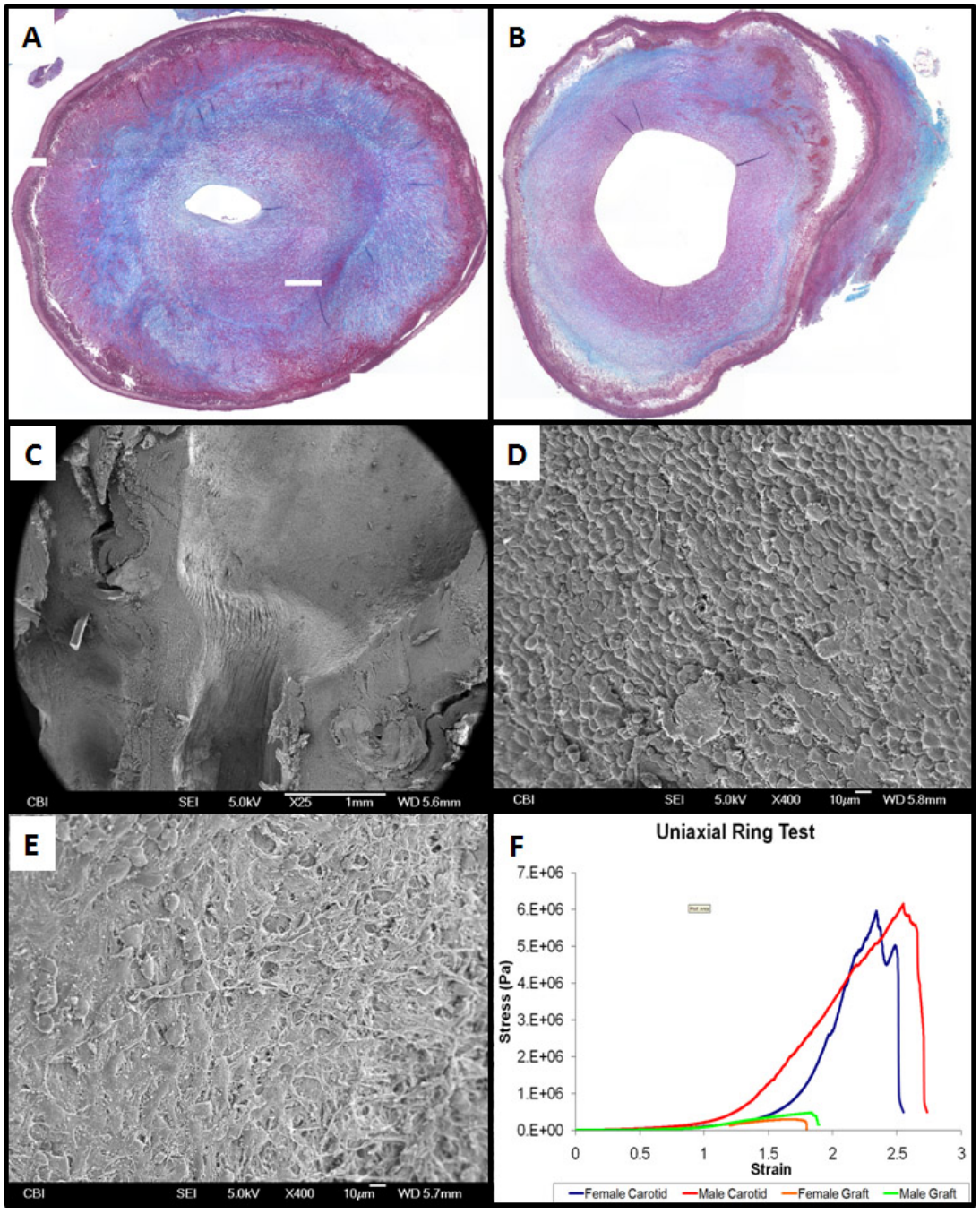

Figure G. 2 Representative results of the first two pigs of the pig pilot study. **A.** Masson's trichrome of the peri-anastomotic site. **B.** Masson's trichrome of the central site of the TEVG. **C.** Low magnification SEM focusing at the proximal anastomosis level. **D.** Higher magnification of the SEM at the anastomotic levels. **E.** Higher magnification of the SEM in the central portions of the TEVG. **F.** Uniaxial ring test.

All the remaining animals were implanted with the ID-4.7 ES-TIPS PEUU fabricated as described in **Section 4.2,** seeded with autologous SACs (see **Section 7.3**) previously transfected with the LacZ promoter as described in **Section 5.2.2**.

One of the following 4 pG-1 animals was euthanized a few days after muscle biopsy procedure for causes unrelated to this study (*i.e.*, suspected vertebral dislocation while moving in the cage). The remaining 3 pigs completed the 1 month survival period without complications. The patency rate of this group of animals was 67% (2/3). The results of the two patent vessels were similar to each other. In particular, the pre-implantation histology was consistently better than the first two animals but still not dense as expected (**Figure G.** 3**-A**). The new diameter appeared to have a good size matching with the native carotid (**Figure G.** 3**-B**). After one month *in vivo* the patent constructs were not surrounded by the same a thick collagenous layer seen with the first two animals (**Figure G.** 3**-C**). No signs of acute inflammatory response or infections were detected. Fluoroscopy showed no signs dilations and the presence of stenosis at anastomotic sites (**Figure G. 3-D**). The scaffold had a glistening, whitish neo-intimal formation, and some stenosis at the anastomoses; the scaffold appeared delaminated in some areas (**Figure G.** 3**-E/F**).

Masson's trichrome confirmed the presence of a thick neo-intimal tissue with variable thicknesses and the delamination of the scaffold. The TIPS layer appeared well remodeled with the presence of collagen, while the ES layer did not show sign of biological infiltration or significant remodeling **Figure G.** 4**-A/B**. The lumen of the scaffold was lined with a confluent layer of endothelial-like cells at the proximal a distal portions **Figure G.** 4**-C**, while the central portion of the TEVG was still covered with cells but not at the same level of confluency **Figure**

G. 4**-D**. The obstructed TEVG was characterized by the presence of an organized thrombus developed throughout the entire length of the TEVG **Figure G.** 4**-E/F**.

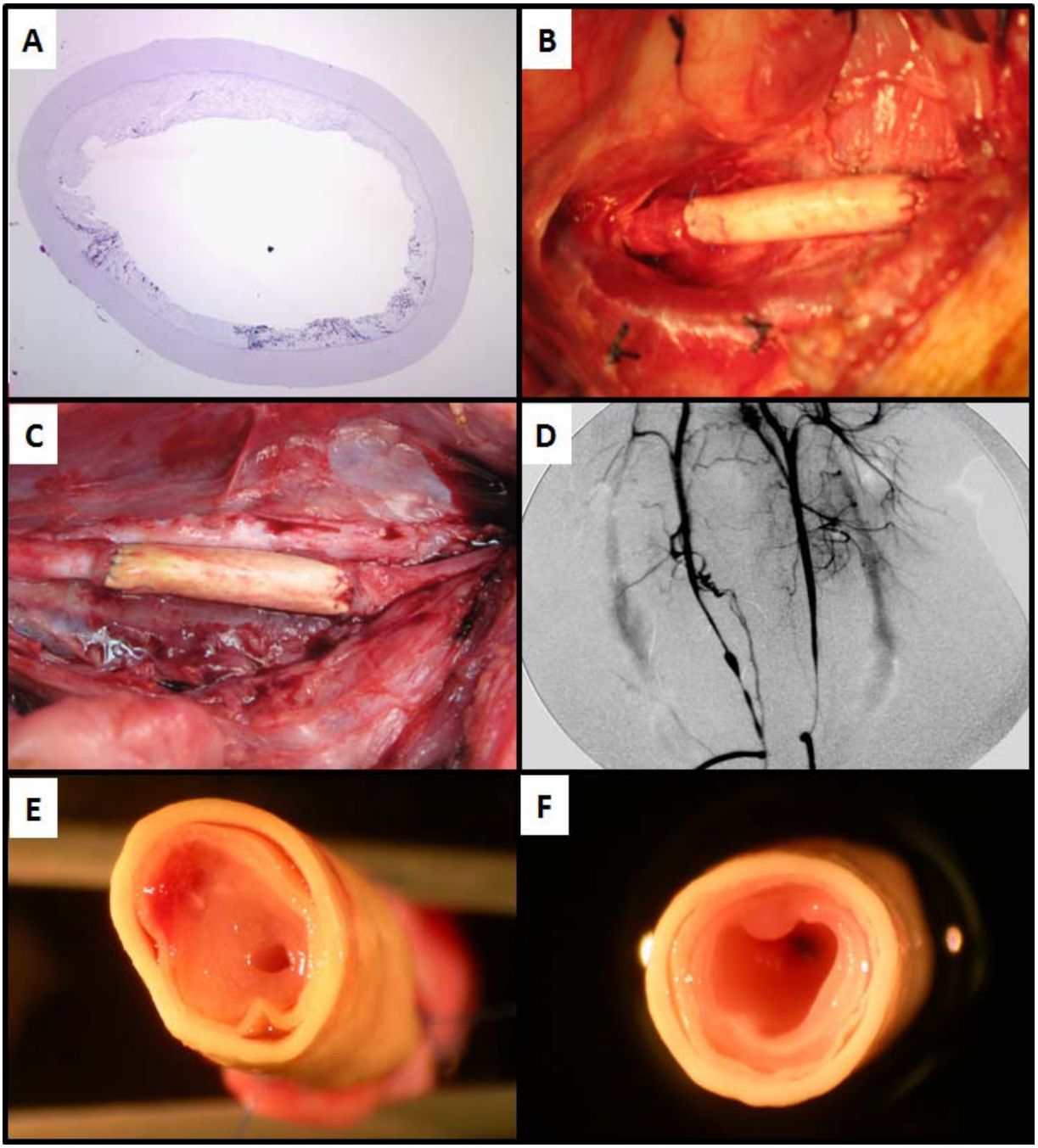

Figure G. 3 Representative results of the 67% patent constructs of pG-1 following the initial two animals experiments. **A.** Pre-implantation histology. **B.** Surgical view immediately after completion of both anastomoses. **C.** Surgical view during necropsy. **D.** Fluoroscopy. **E.** Gross pathology findings at the proximal anastomosis level of the patent constructs. **F.** Gross pathology finding in the central region of a patent TEVG.

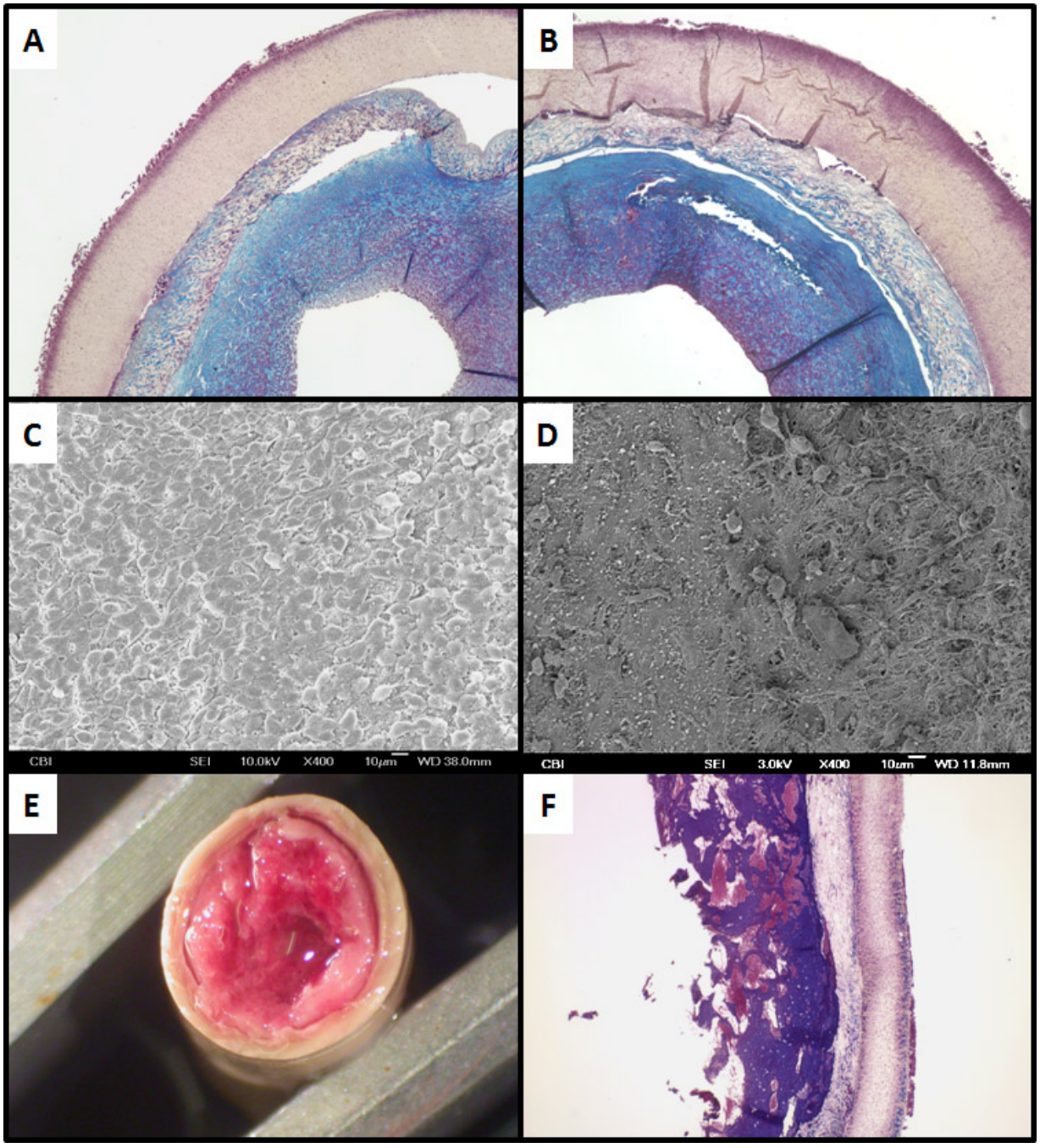

Figure G. 4 Representative results of the additional three pigs from pG-1. **A.** Masson's trichrome of the peri-anastomotic site. **B.** Masson's trichrome of the central site of the TEVG. **C.** SEM at the proximal anastomosis. **D.** SEM in the central portion of the TEVG. **E.** The obstructed TEVG had an organized thrombus throughout its entire length. **F.** Masson's trichrome of the obstructed TEVG.

The only TEVG implanted for three months had an acceptable pre-implantation cellularity **Figure G.** 5**-A**, during necropsy the TEVG showed encapsulation with native tissue (**Figure G.** 5**-B**), and did not show any sign of dilation or infection. The TEVG was obstructed by intimal hyperplasia/organized thrombus formation as seen in **Figure G.** 5**-C**. Masson's trichrome showed the presence of a remodeled TIPS layer surrounded by a thick ES layer poorply infiltrated with biological matrix (**Figure G.** 5**-D**).

After 1 month *in vivo* the pig was sedated with acepromazine, 0.15 mg/kg, and ketamine, 15.0 mg/kg (both intramuscular) and echo-color Doppler was performed to assess patency. The TEVG appeared completely patent at 1 month (**Figure G.** 6).

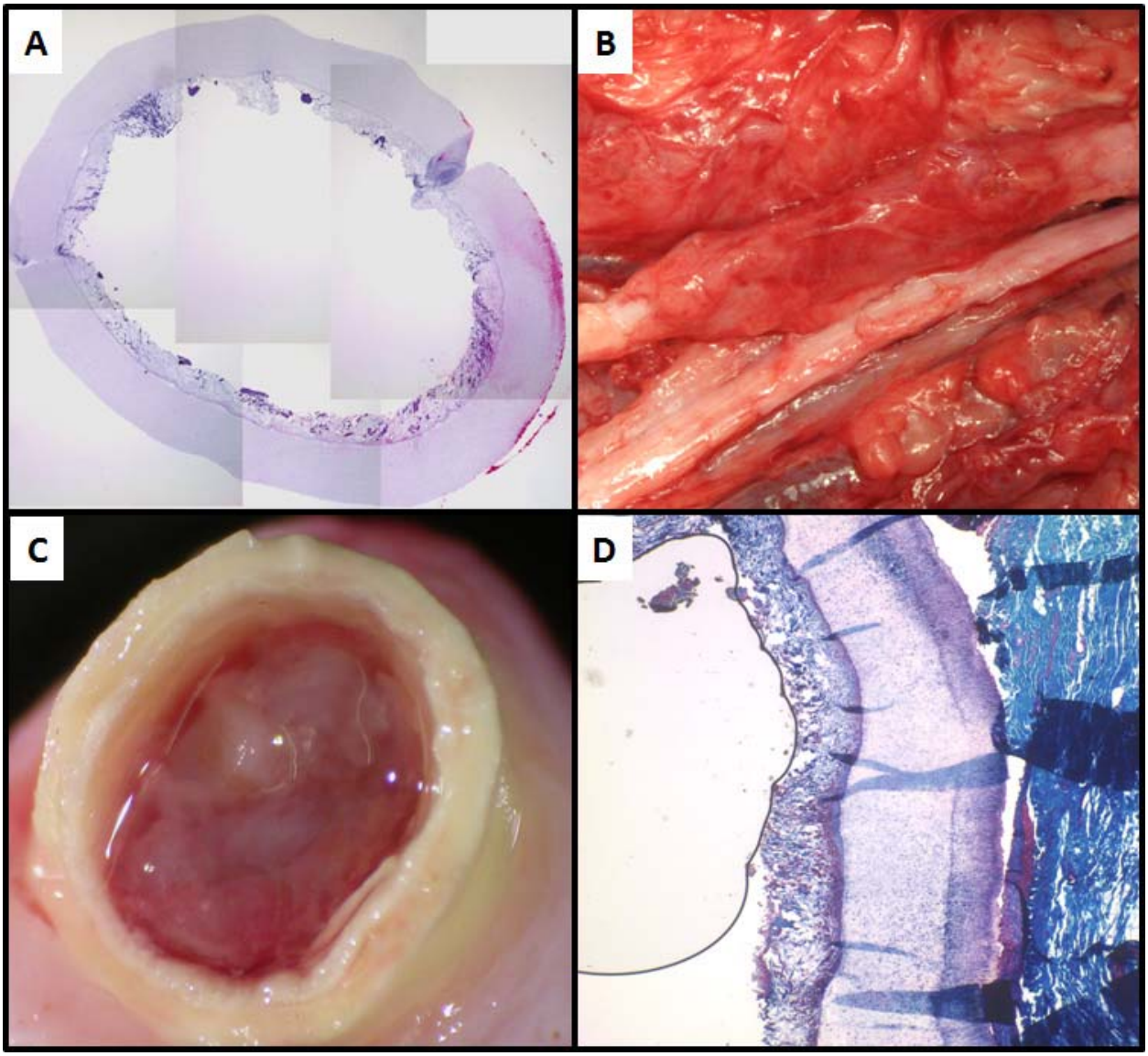

Figure G. 5 Results for the pG-2 pig. **A.** Pre-implantation histology. **B.** Surgical view during necropsy. **C.** Gross pathology. **D.** Masson's trichrome.

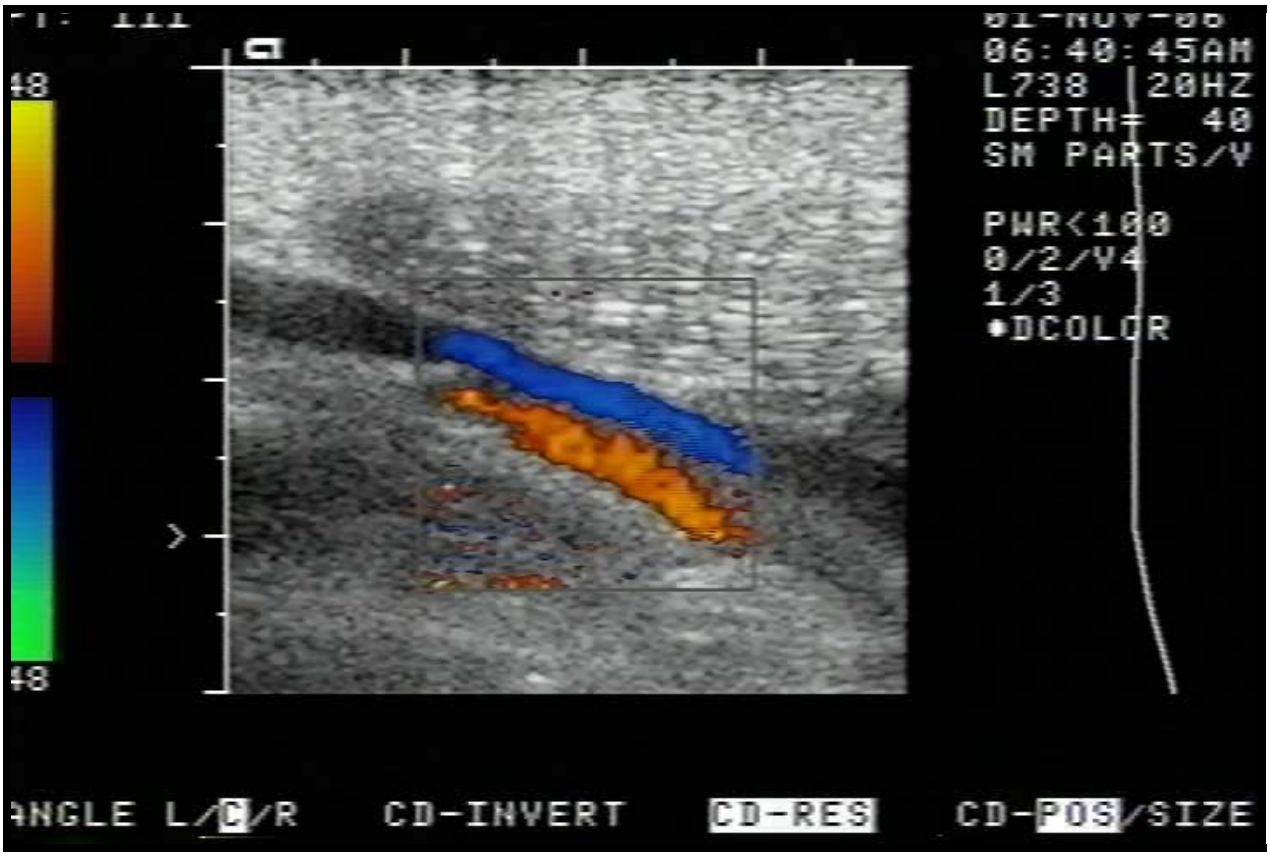

Figure G. 6 Echo-Doppler performed after one month on the pG-2 pig. The complete patency of the TEVG (red signal) is clearly detectable. The blue signal represents the IJV.

The two pG-3 animals showed the most promising results among all the pigs performed. In particular, immediately after necrospsy it was found that both AVG grafts were encapsulated with a thick collagenous sheath, suggesting scaffold dilation (**Figure G.** 7**-B**). Fluoroscopy revealed that both scaffolds were patent with some stenosis at the distal (venous) anastomosis. Moreover, both scaffolds did not show any sign of dilations in contradiction with the external appearance of the TEVGs during necropsy (**Figure G.** 7**-C**). While examining the remodeled TEVGs for gross pathology analysis, a hematoma was found enclosed between the scaffold and the external capsule surrounding both scaffolds (**Figure G.** 7**-D/E**). The scaffold showed a

lumen with the usual luminal neo-tissue formation (**Figure G.** 7**-F**), with a more pronounced thickness in proximity to the anastomoses, as seen for the other groups.

Histological assessment (Masson's trichome) showed a substantially remodeled TEVG throughout the entire length of the TEVG (**Figure G.** 8). Immunohistochemical assessment demonstrated the presence of smooth muscle and endothelial markers co-localized with LacZ+ cells suggesting a role of the seeded SACs in the remodeling toward an arterial like tissue (**Figure G.** 9).

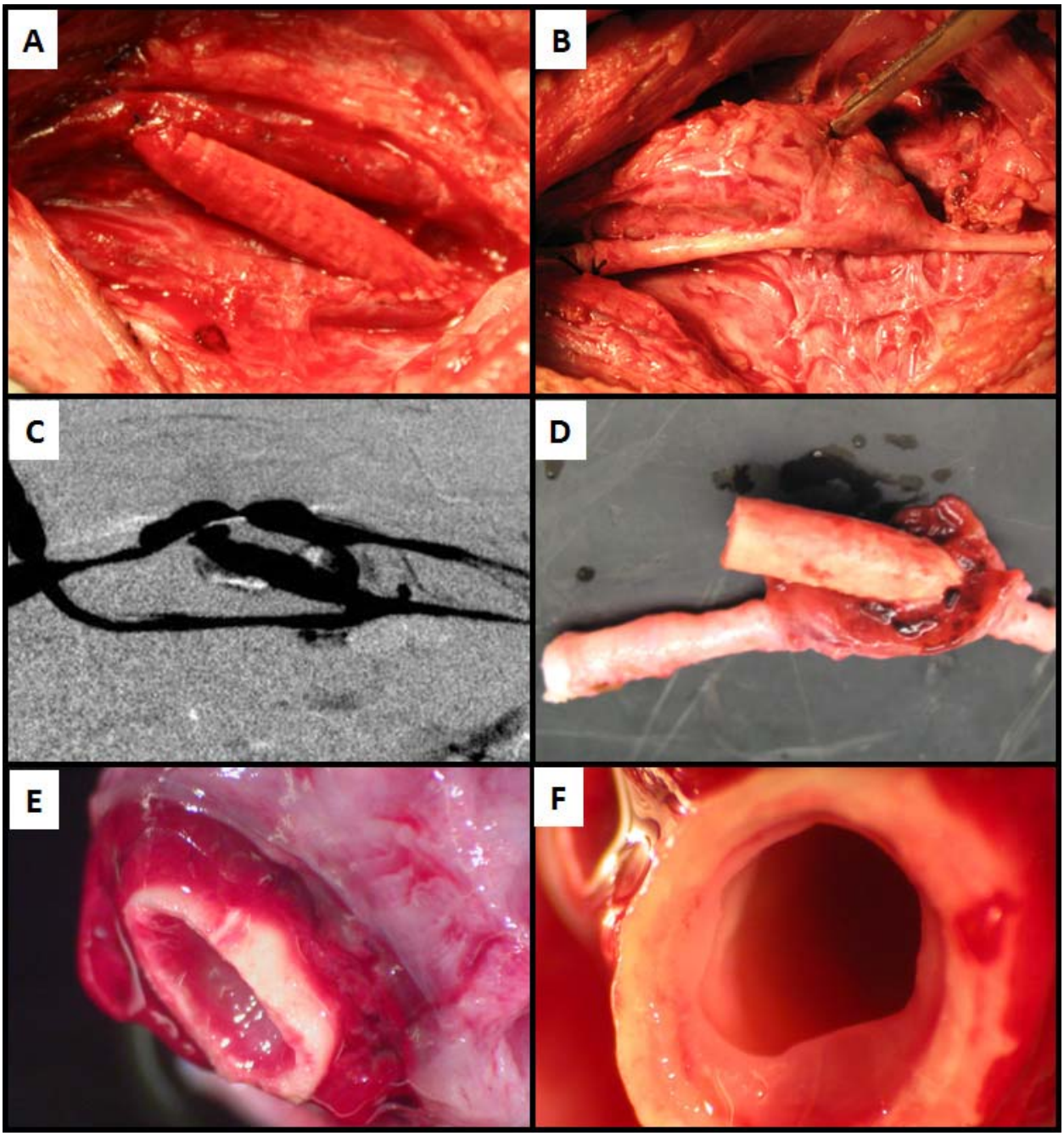

Figure G. 7 Representative results for both patent constructs of pG-3. **A.** Pre-implantation histology. **B.** Surgical view immediately after completion of both anastomoses. **C.** Surgical view during necropsy. **D.** Fluoroscopy. **E.** Gross pathology findings at the proximal anastomosis level of the patent constructs. **F.** Gross pathology finding in the central region of a patent TEVG.

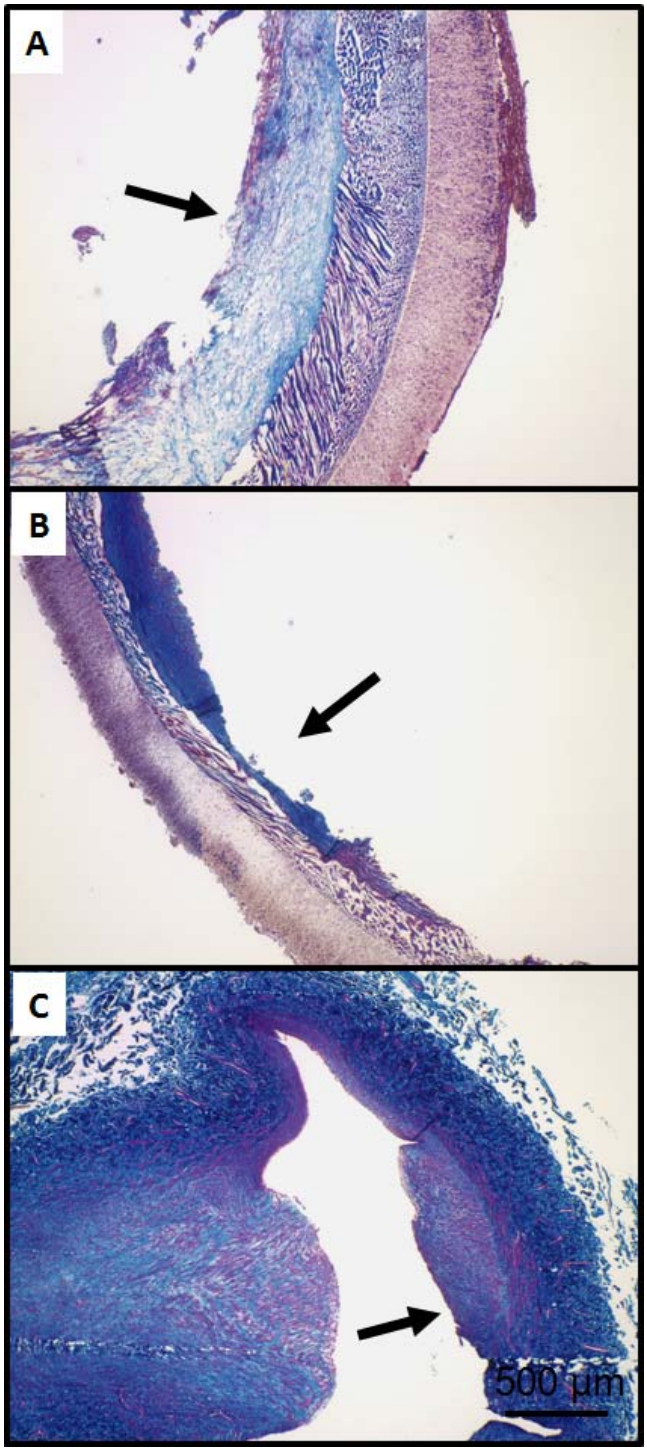

Figure G. 8 Representative Masson's trichrome images of pG-3. **A.** Proximal location (arterial). **B.** Central location. **C.** Distal location (venous). The arrows indicate the lumen of the graft.

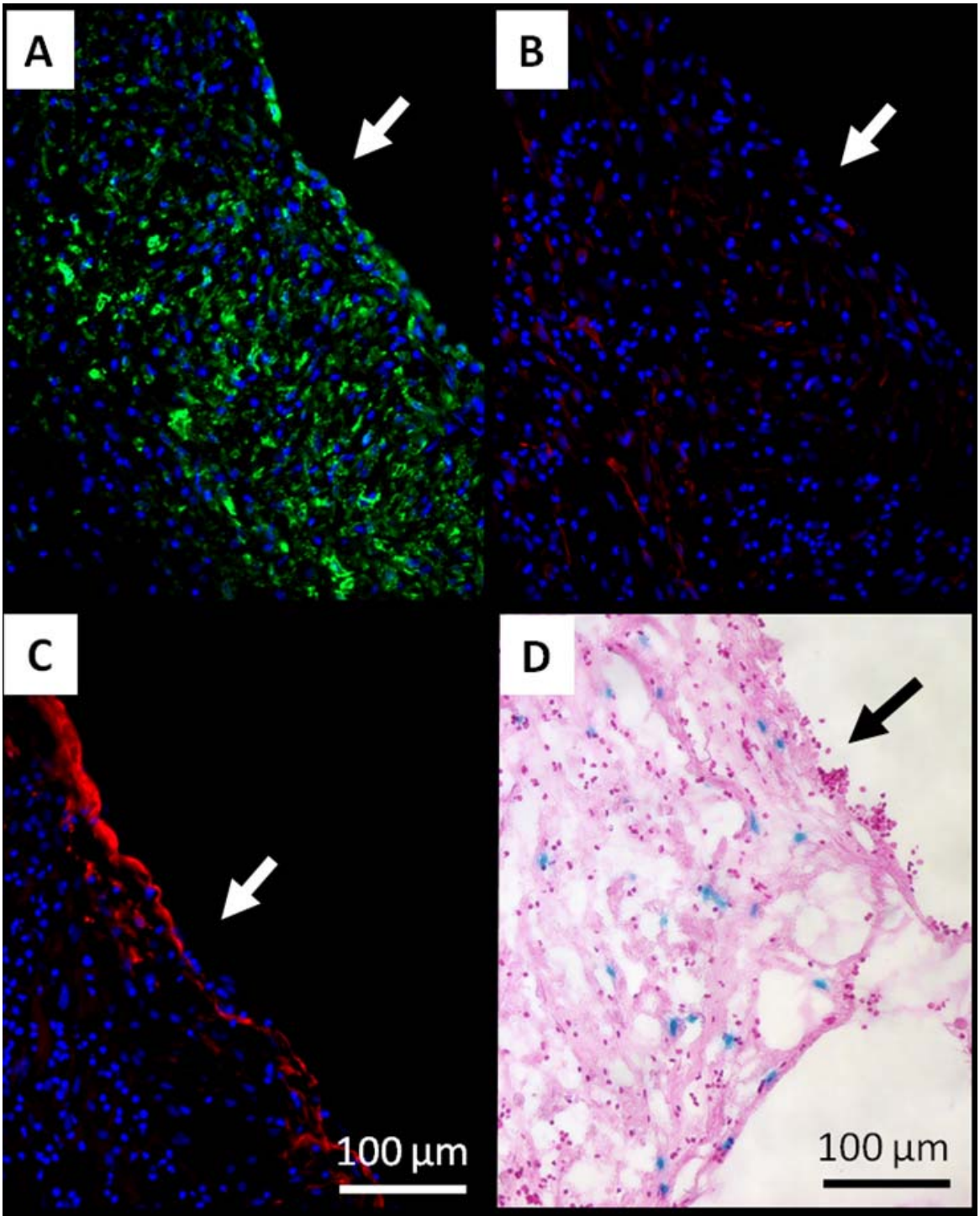

Figure G. 9 Representative results for the pG-3 animals after 1 month *in vivo*. **A.** α-SMA staining. Green = α-SMA; blue = nuclei. **B.** Calponin staining . Red = Calponin; blue = nuclei. **C.** vWF staining. Red = vWF; blue = nuclei. **D.** XGal Staining. Blue = LacZ+ cells; purple = nuclei.

APPENDIX H

APPENDIX H: RVSD PATENT APPLICATION

US 20060075963A1

(19) **United States**

(12) **Patent Application Publication** (10) **Pub. No.: US 2006/0075963 A1**

Nieponice et al. (43) **Pub. Date: Apr. 13, 2006**

(54) **VACUUM ROTATIONAL SEEDING AND LOADING DEVICE AND METHOD FOR SAME**

(76) Inventors: **Alejandro Nieponice**, Pittsburgh, PA (US); **David A. Vorp**, Pittsburgh, PA (US); **Lorenzo Soletti**, Pittsburgh, PA (US)

Correspondence Address:
BAKER & BOTTS
30 ROCKEFELLER PLAZA
NEW YORK, NY 10112

(21) Appl. No.: **11/243,818**

(22) Filed: **Oct. 5, 2005**

Related U.S. Application Data

(60) Provisional application No. 60/616,057, filed on Oct. 5, 2004. Provisional application No. 60/649,255, filed on Feb. 2, 2005.

Publication Classification

(51) **Int. Cl.**
B05C 3/00 (2006.01)
B05D 3/00 (2006.01)

(52) **U.S. Cl.** **118/417**; 427/2.14

(57) **ABSTRACT**

An apparatus for seeding material in a scaffold member capable of entrapping such seeding material therein is provided. The apparatus may include a chamber having an interior and capable of maintaining a negative pressure and capable of enclosing the scaffold member therein, and a support member for rotating the scaffold member disposed within the interior of the chamber and for introducing the seeding material into the chamber. At least a portion of rotating the scaffold member occurs simultaneously with applying the negative pressure condition to the scaffold member. The seeding material may be passed from the interior of the scaffold member to the exterior of the scaffold member in response to the application of negative pressure such that at least of portion of the seeding material is entrapped in the scaffold member.

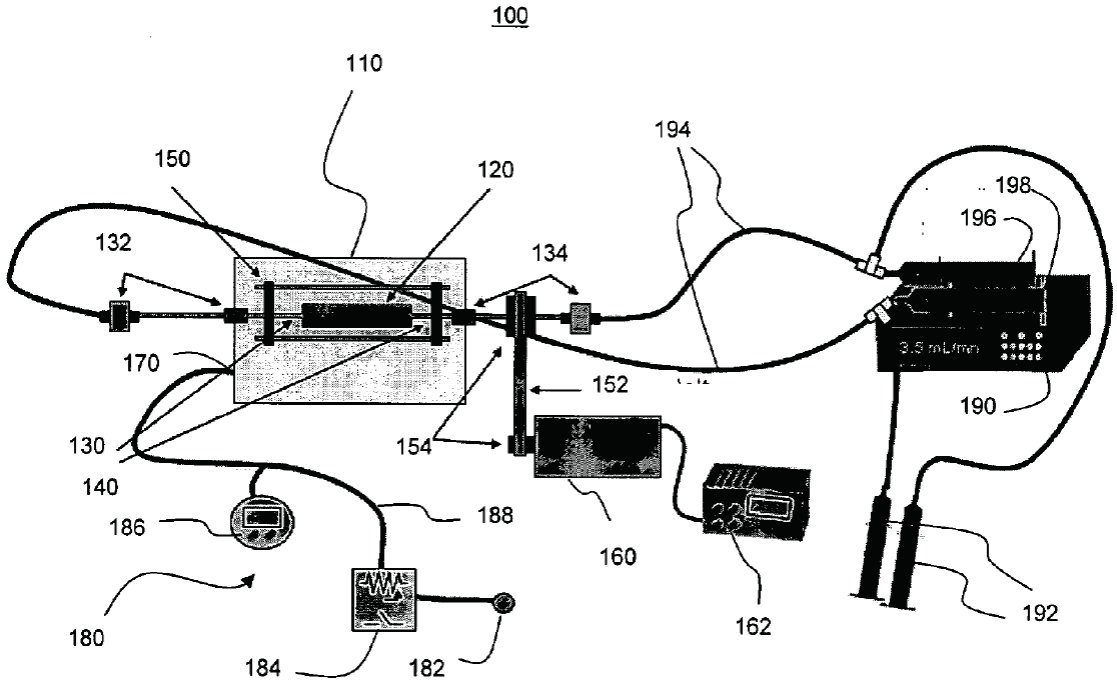

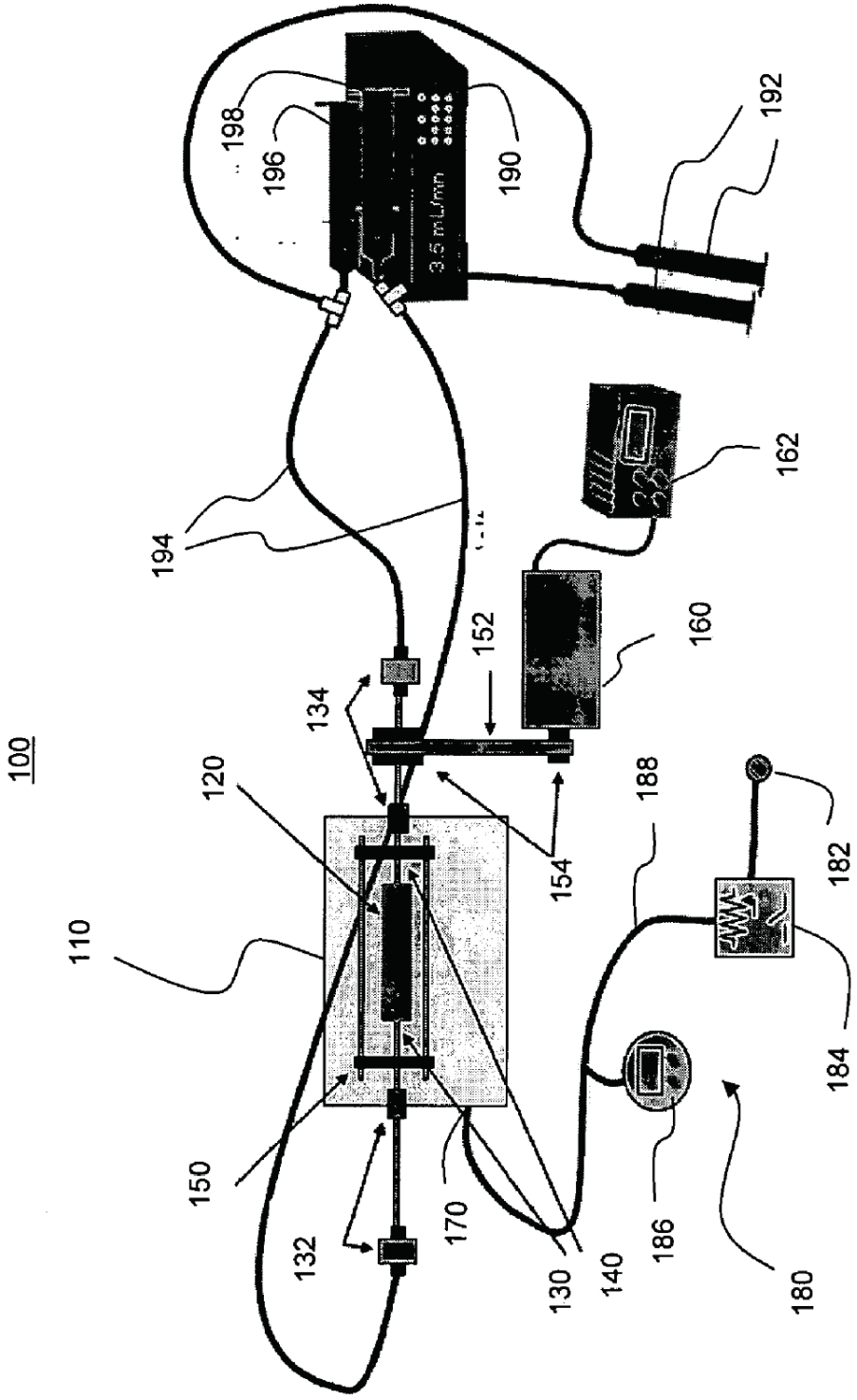
100
110
120
130
132
134
140
150
152
154
160
162
170
180
182
184
186
188
190
192
194
196
198

FIG. 1

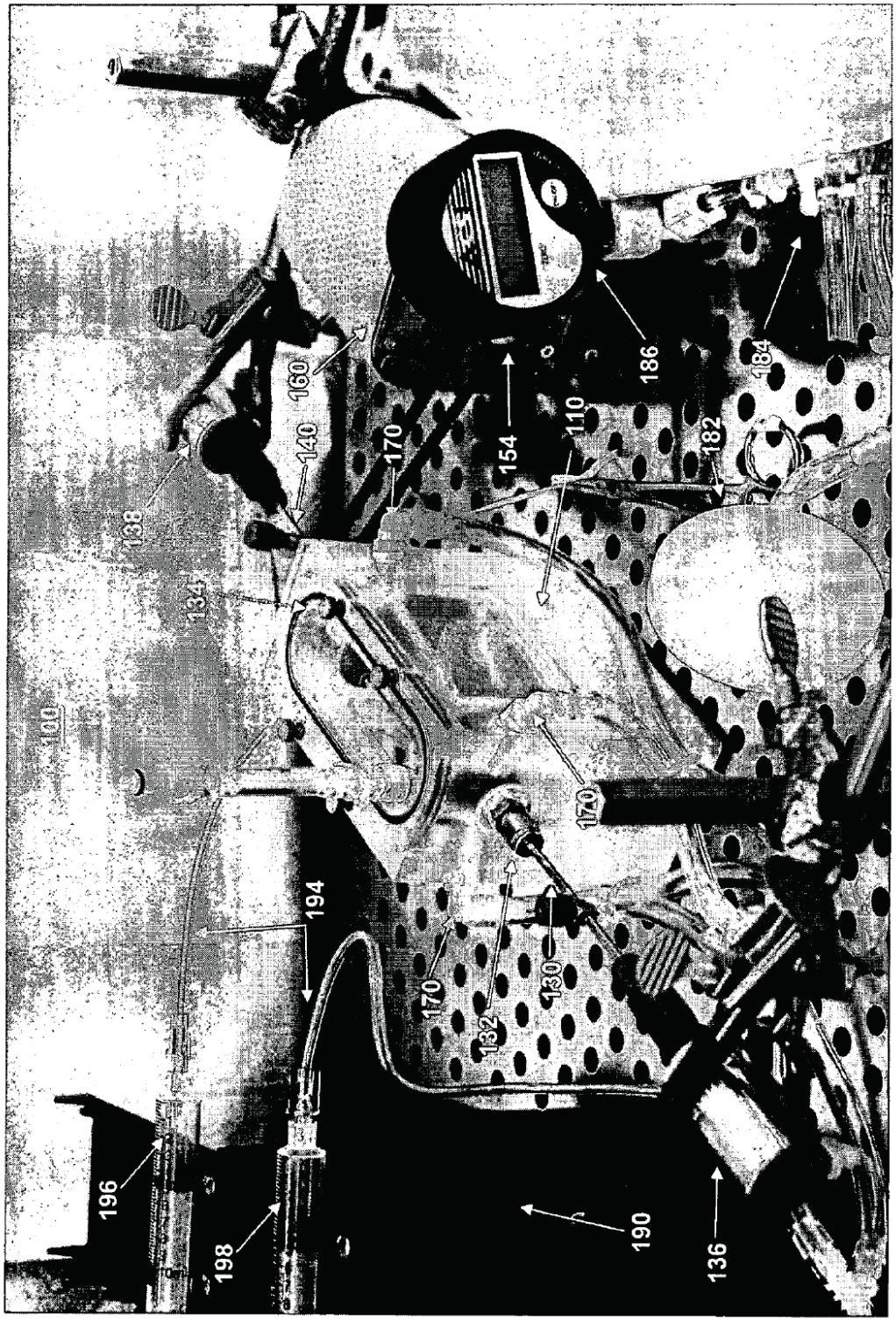
160
186
184
140
170
154
110
182
138
134
100
170
194
170
132
130
196
198
190
136

FIG. 2

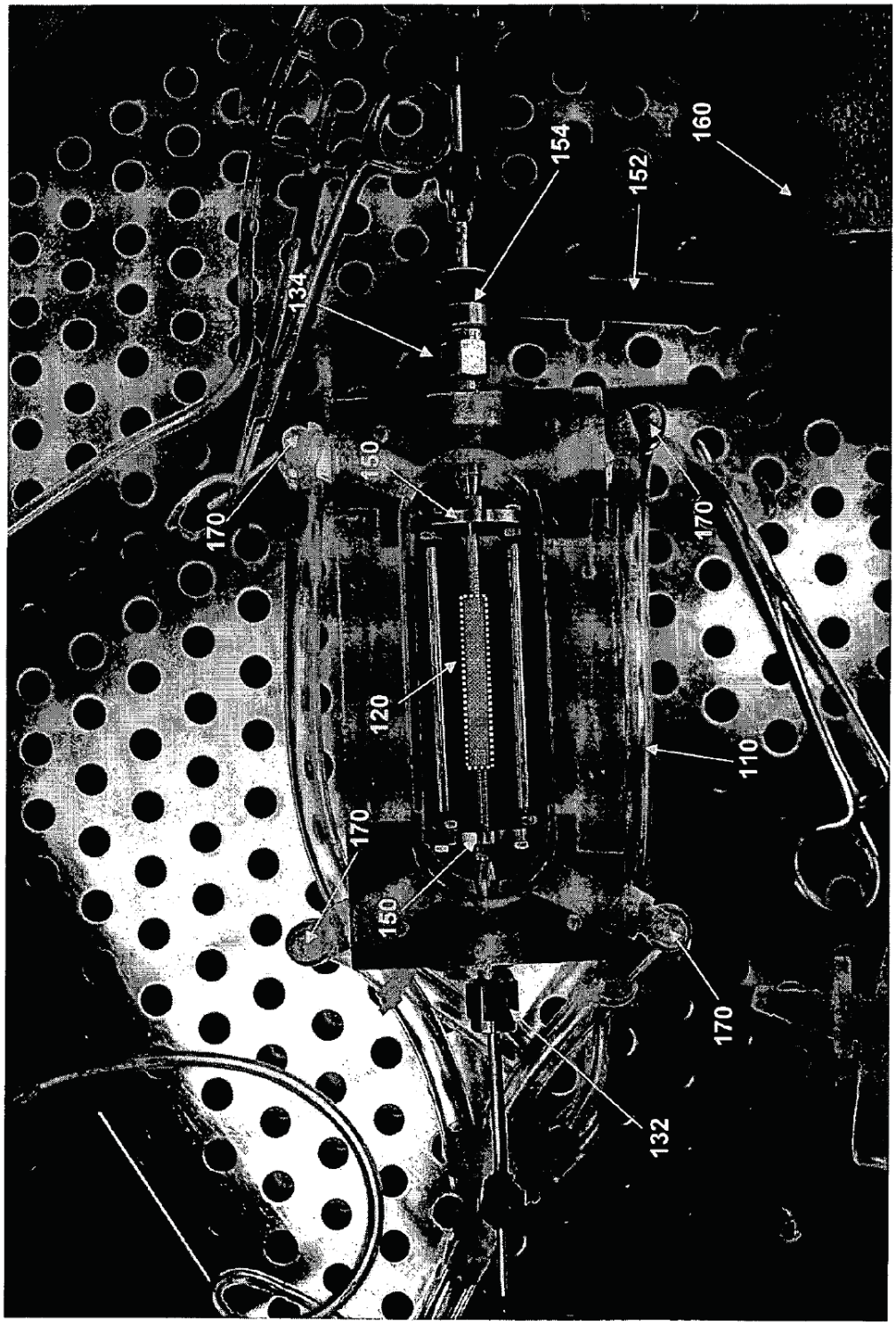

FIG. 3

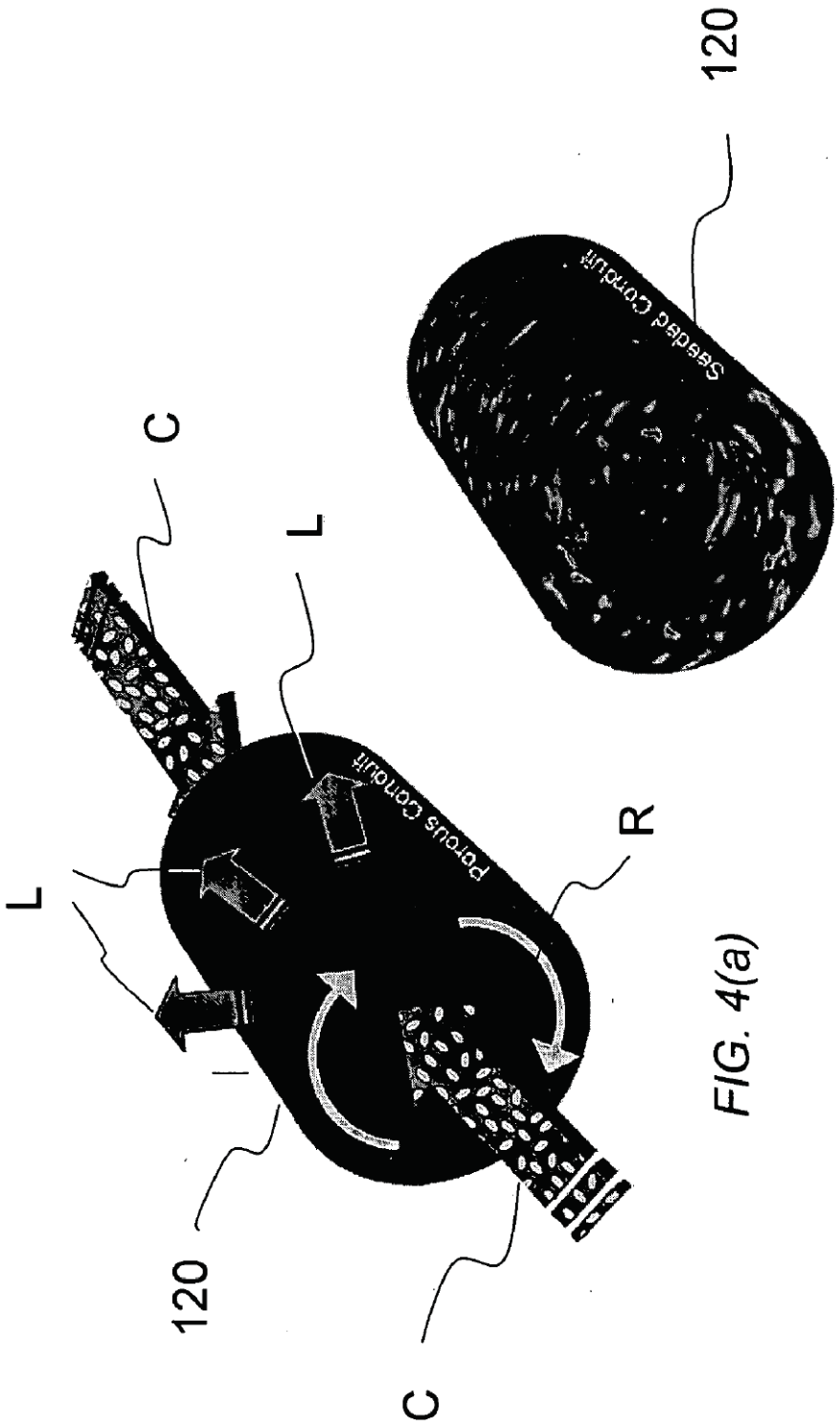

FIG. 4(b)

FIG. 4(a)

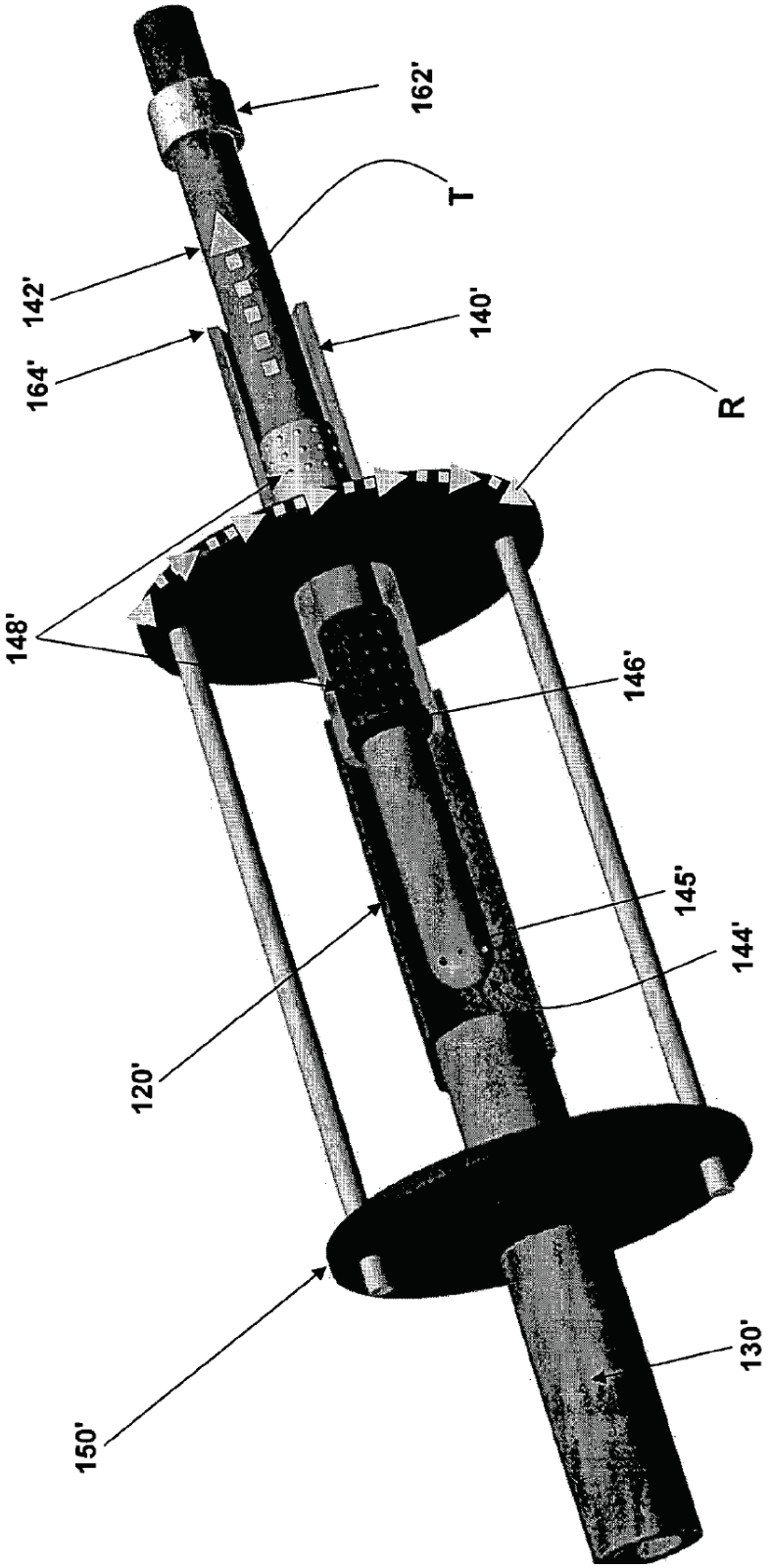

FIG. 5

FIG.6(a)

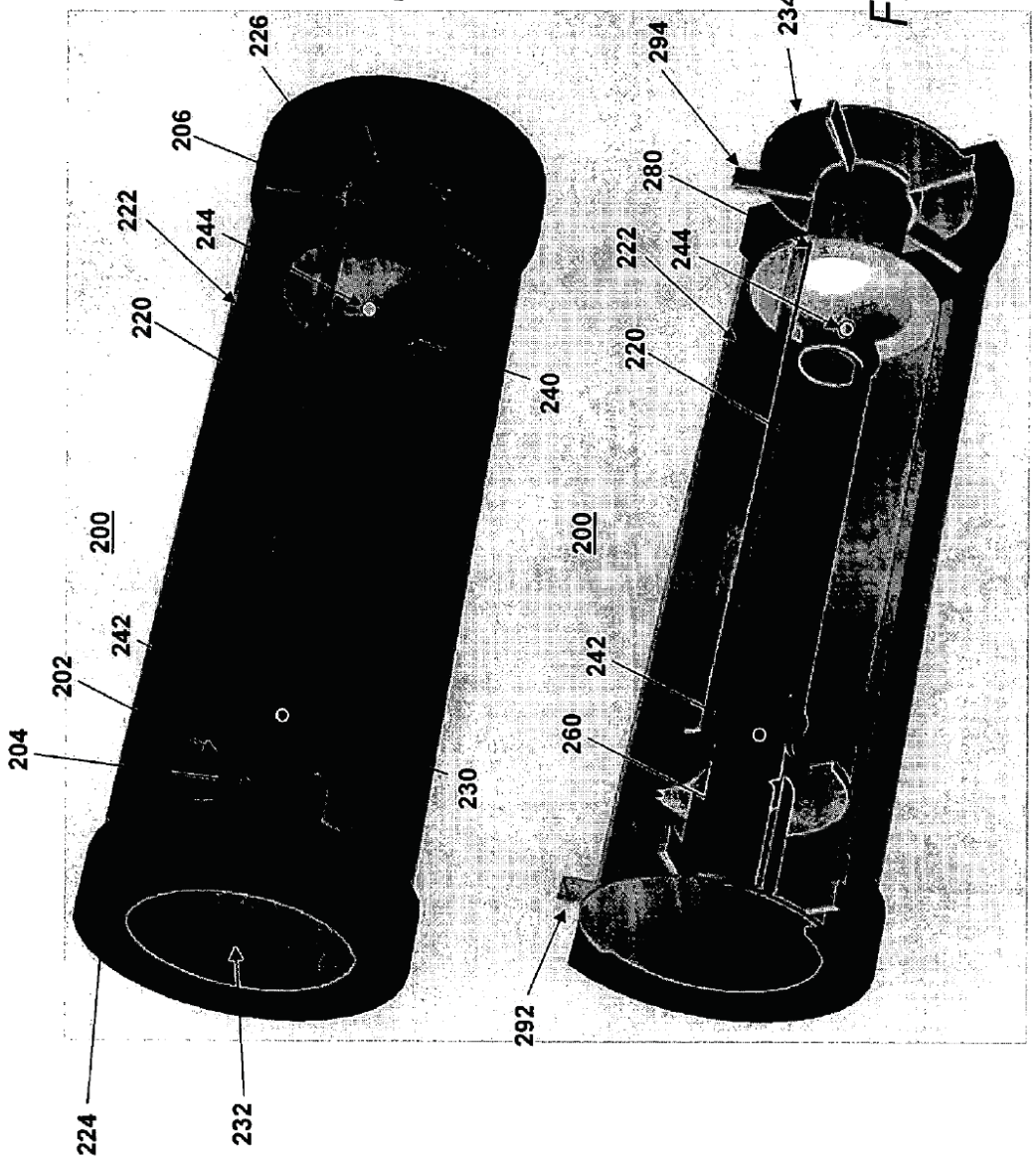
226
206
222
244
220
240
200
242
202
204
230
224
232

FIG.6(b)

234
294
280
222
244
220
200
242
260
292

FIG. 8

FIG. 7

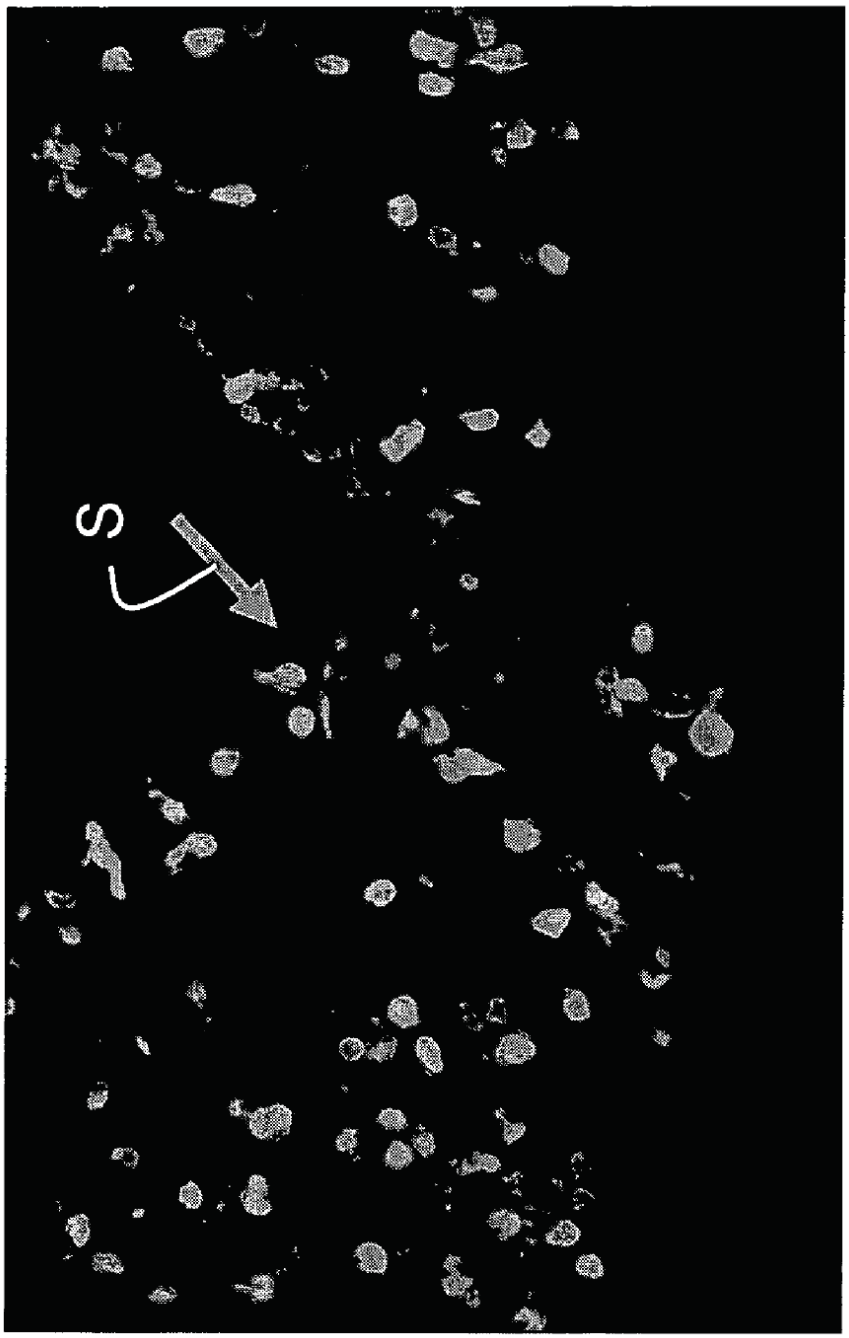

FIG. 9

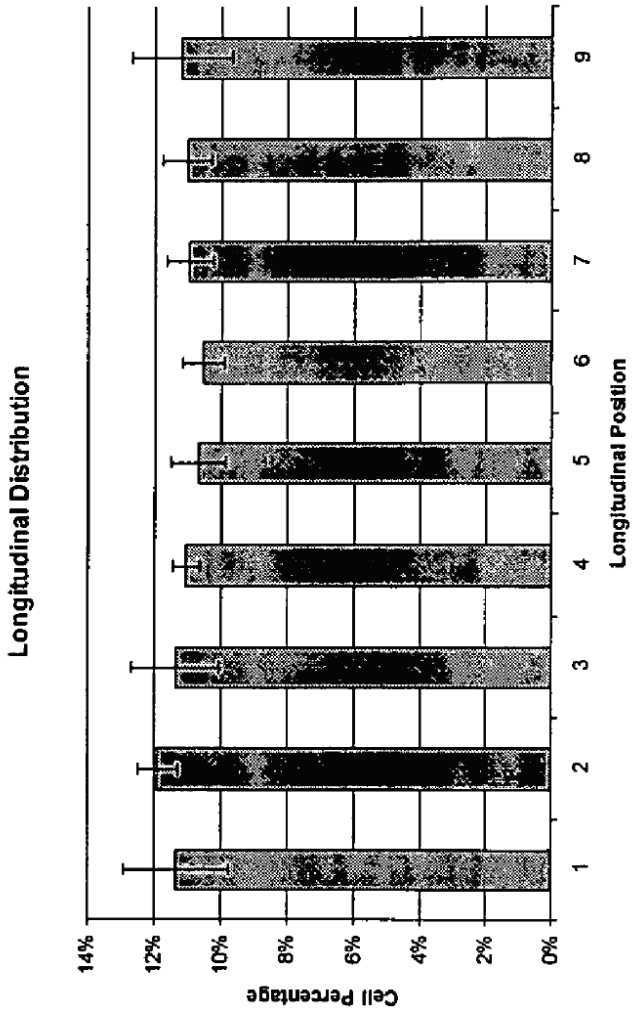
Longitudinal Distribution
Cell Percentage
14%
12%
10%
8%
6%
4%
2%
0%
1
2
3
4
5
6
7
8
9
Longitudinal Position

FIG. 10

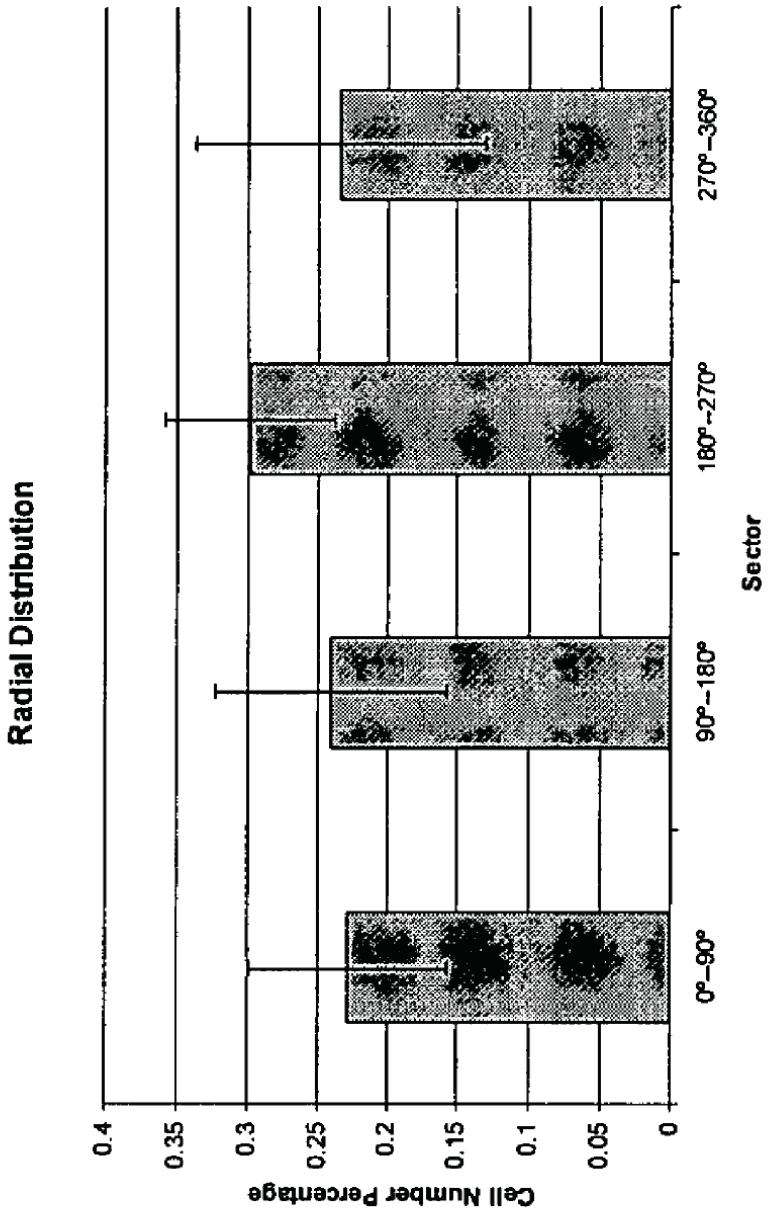
Radial Distribution
Cell Number Percentage
0.4
0.35
0.3
0.25
0.2
0.15
0.1
0.05
0
0°–90°
90°–180°
180°–270°
270°–360°
Sector

FIG. 11

FIG. 12

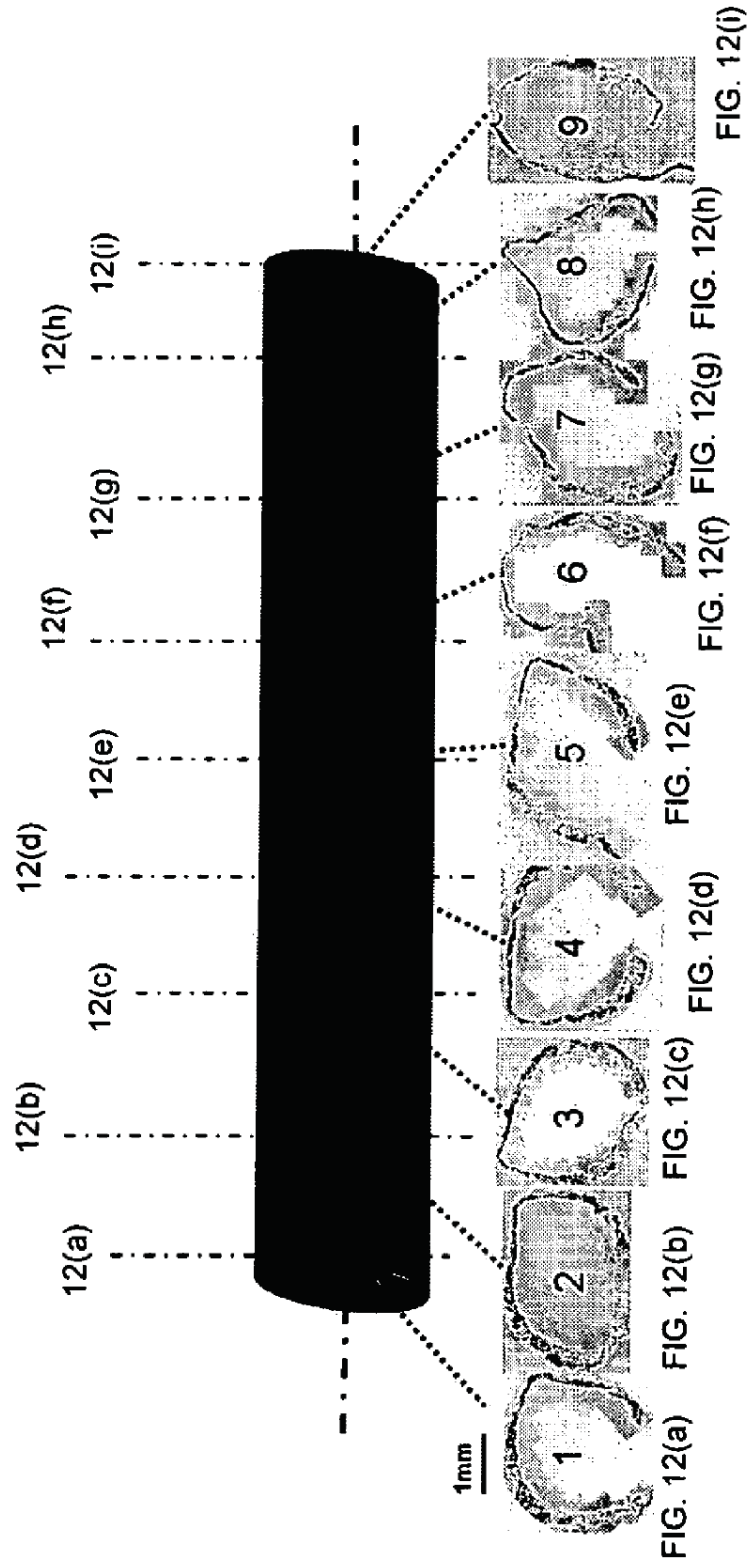
12(a)
12(b)
12(c)
12(d)
12(e)
12(f)
12(g)
12(h)
12(i)
1mm
1
2
3
4
5
6
7
8
9
FIG. 12(a)
FIG. 12(b)
FIG. 12(c)
FIG. 12(d)
FIG. 12(e)
FIG. 12(f)
FIG. 12(g)
FIG. 12(h)
FIG. 12(i)

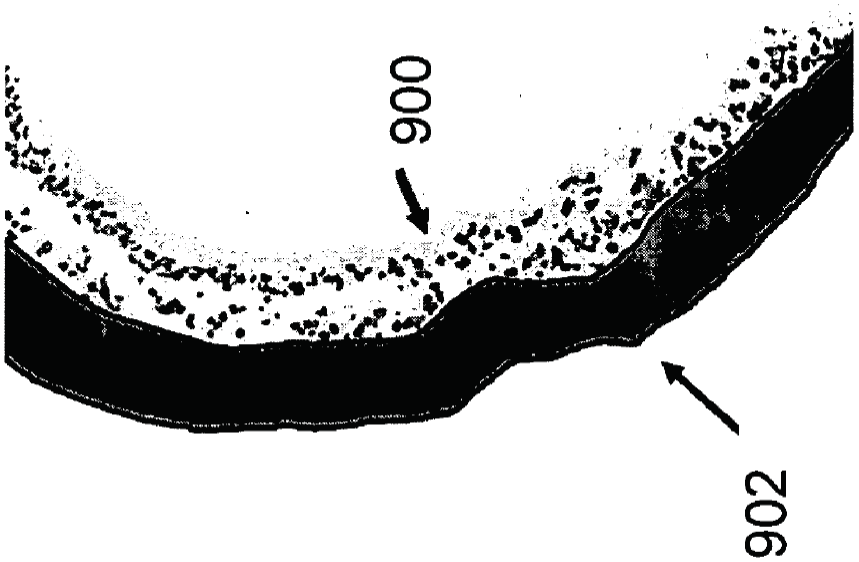

FIG. 13

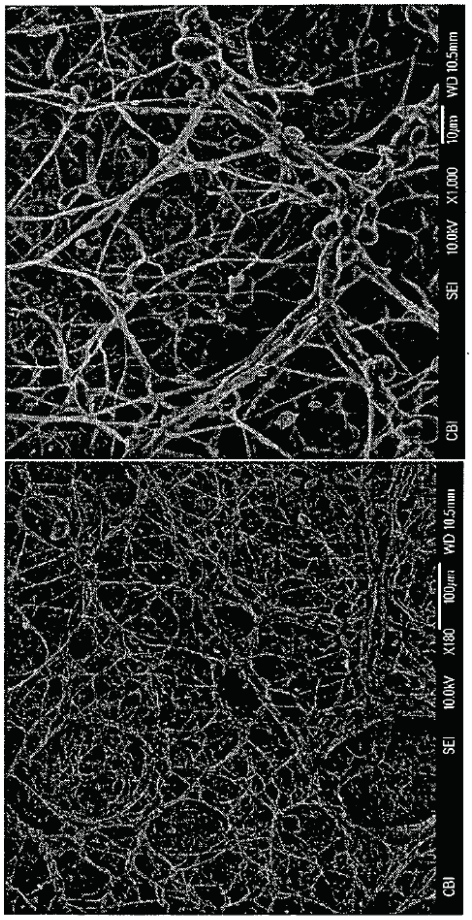

FIG. 14(a)

FIG. 14(b)

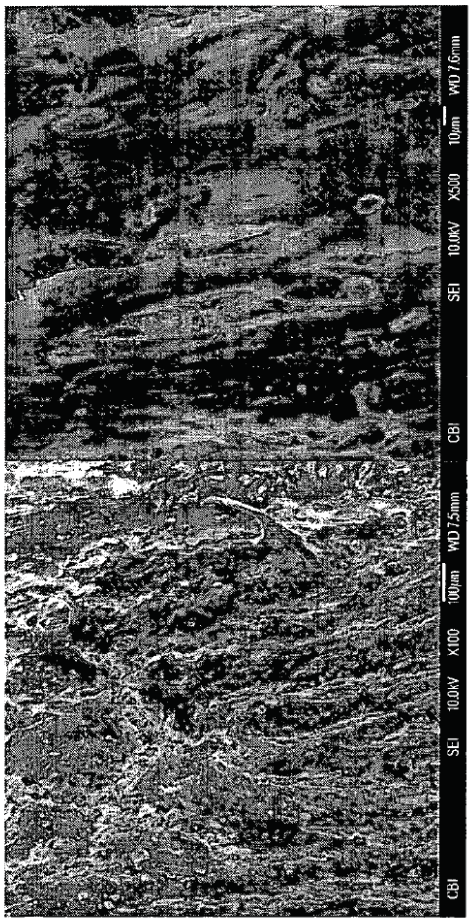

FIG. 15(a)

FIG. 15(b)

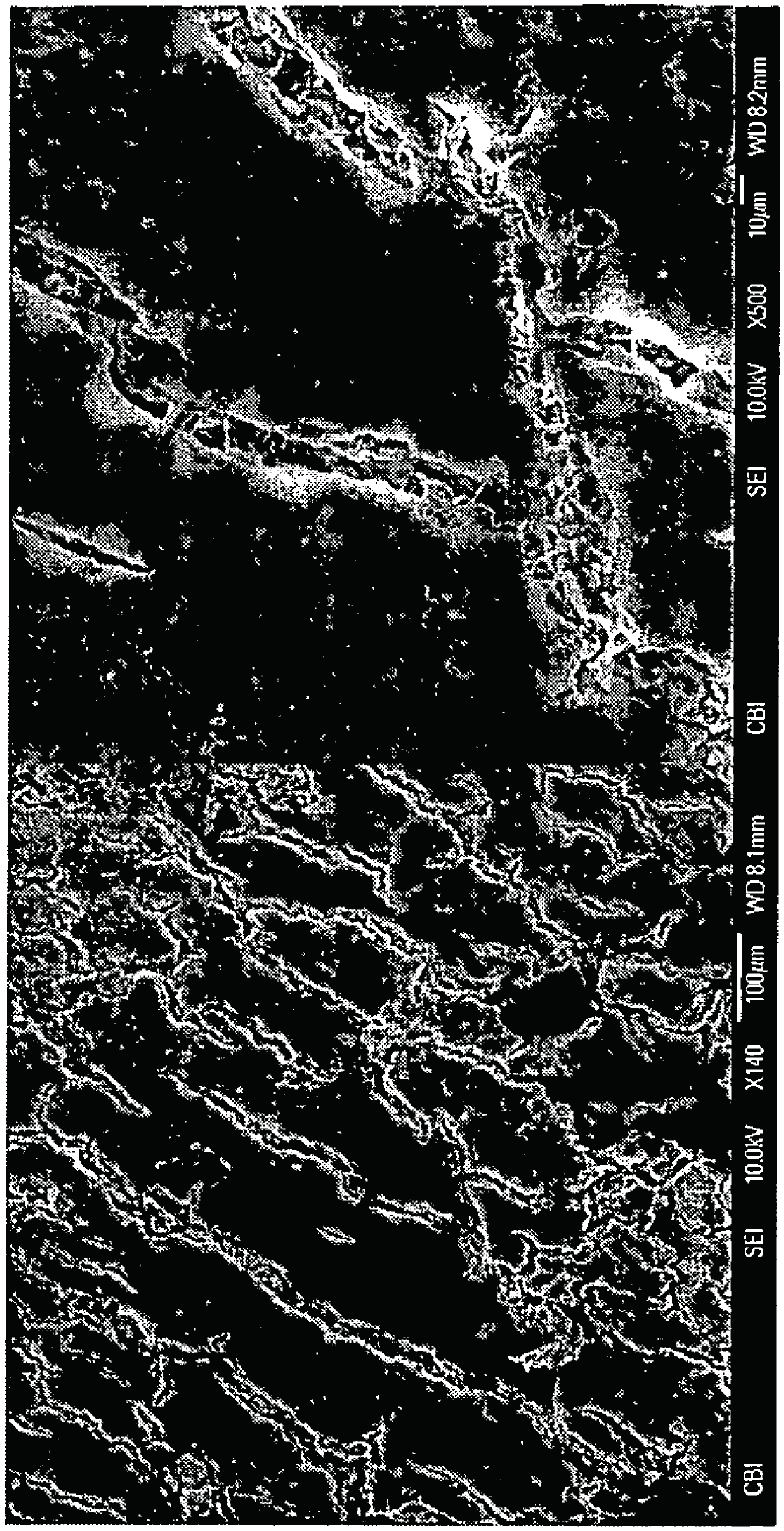

FIG. 16(a)

FIG. 16(b)

VACUUM ROTATIONAL SEEDING AND LOADING DEVICE AND METHOD FOR SAME

CLAIM FOR PRIORITY TO RELATED APPLICATIONS

[0001] This application claims the benefit of U.S. Provisional Patent Application Ser. No. 60/616,057, filed on Oct. 5, 2004, entitled "Vacuum Rotational Seeding and Loading Device and Method for Same," and U.S. Provisional Patent Application Ser. No. 60/649,255, filed on Feb. 2, 2005, entitled "Vacuum Rotational Seeding and Loading Device and Method for Same," both of which are hereby incorporated by reference in their entirety herein.

STATEMENT OF GOVERNMENT RIGHT

[0002] The work leading to this invention was supported in part by the U.S. Government under NIH Grant R10 HL069368-01A1. The U.S. Government has certain rights in the invention.

BACKGROUND

[0003] 1. Field of the Invention

[0004] The present invention relates generally to seeding and loading devices and methods, and particularly to vacuum seeding and loading devices and methods for vacuum seeding using such devices.

[0005] 2. Background of the Related Art

[0006] A very high demand exists for tissue and organ donations among patients affected by degenerative diseases or traumatic injuries. For example, in 2003 over 86,000 people were on waiting lists to receive tissue and organ transplantation in the United States, compared with 13,000 actual donors. (Organ Procurement and Transplantation Network. OPTN/SRTR Annual Report, 2004.) This discrepancy between recipients and donors over the years has stimulated the evolution of new disciplines such as regenerative medicine. The field of regenerative medicine offers hope to these patients by drawing upon advances in stem cell biology, developmental biology, and tissue engineering to provide tissue substitutes to the enormous number of patients in need of such tissues or organs. Tissue engineering has brought together scaffold structures and cells to create functional tissues.

[0007] Cell seeding constitutes a critical step in those tissue engineering approaches that incorporate cells into or onto scaffolds prior to culture or implantation. Surface seeding typically refers to lining cells on a luminal surface. Bulk seeding typically refers to the delivery of cells throughout the depth or thickness of the scaffold. Most of the current seeding techniques involve the use of a device to seed cells on surfaces. These devices take advantage of different driving forces such as sedimentation, rotation, electric field, or vacuum. The use of a seeding device may be challenging since mechanical forces are often involved in seeding procedures and can be responsible for force-mediated membrane lysis or triggering of apoptotic pathways.

[0008] Bulk seeding is typically a more difficult task to accomplish especially in a controllable manner. The complex micro-architectures of the scaffolds often hamper the passive incorporation of cells throughout the thickness of the material. Dripping cell suspension on the matrix for impregnating the scaffold is a typical technique for bulk incorporation of cells into scaffolds. This technique is not intrinsically able to warrant a high level of quality control on the final engineered tissue due to the manual nature of the procedure.

[0009] In addition to the limitations of known techniques, such as cell injury and non-uniform cell distribution, it typically requires a long culture duration (several weeks) to achieve full-thickness cellular content. Accordingly, a need exists for a seeding technique that would minimize cell injury, and provide uniform cell distribution, high seeding efficiency, reduced seeding time, reproducibility, and user independence.

SUMMARY OF THE PRESENT INVENTION

[0010] It is an object of the current invention is to overcome the aforementioned limitations to the state of the art seeding techniques.

[0011] It is another object of the current invention to provide a cell or particle seeding technique and apparatus for use with tubular scaffolds or synthetic tubular grafts.

[0012] In accordance with one embodiment of the present invention, an apparatus is provided for seeding material in a scaffold member capable of entrapping such seeding material therein. The apparatus may include a chamber having an interior and capable of maintaining a negative pressure environment and capable of enclosing a scaffold member therein, and a support member for rotating the scaffold member disposed within the interior of the chamber and for introducing the seeding material into the chamber. In some embodiments, an external infusion pump is provided to control internal delivery of a cell or particle suspension.

[0013] In some embodiments, the support member comprises a hollow shaft. The scaffold member may define an interior portion in communication with the interior portion of the support member, such that the seeding material is introduced into the interior of the scaffold member via the support member.

[0014] A method of the seeding material in a scaffold structure is also provided, which includes applying a negative pressure condition to a scaffold member positioned within a chamber, introducing seeding material in the scaffold member, and rotating the scaffold member, wherein at least a portion of rotating the scaffold member occurs simultaneously with the application of the negative pressure condition.

[0015] In some embodiments, the scaffold member has a tubular structure defining an interior, such that the seeding material is introduced into the interior of the scaffold member. The seeding material may be passed from the interior of the scaffold member to the exterior of the scaffold member in response to the application of negative pressure and a controlled infused flow such that at least of portion of the seeding material is entrapped in the scaffold member. In some embodiments, entrapping the seeding material includes entrapping the seeding material adjacent the interior surface of the scaffold member. In some embodiments, entrapping the seeding material includes entrapping the seeding material throughout the thickness of the scaffold member.

[0016] The contemporaneous application of a negative pressure condition, controlled infusion, and rotation of the scaffolding provides at least the following noteworthy advantages. First, it permits vacuum seeding for a tubular structure. Vacuum seeding as opposed to culture seeding is beneficial in terms of time and efficiency. This also permits bulk seeding as opposed to only surface seeding which provides for more rapid and spatially uniform distribution of cells. Second, it allows for synergistic rotation throughout the seeding to negate gravitational effects. Thus the end product is more likely to have an even distribution as opposed to an unbalanced distribution. Third, it permits the varying of vacuum strength and rotation speed. This may allow, after seeding, for dynamic culture options in the same chamber and can obviate the need for transferring the construct to a different bioreactor. Fourth, it allows the use of vacuum and centrifugal effect as driving forces for cell convection.

[0017] One aspect of the present invention may have particular relevance to bulk seeding, as it can allow the construct to be seeded in minutes with the desired amount of cells needing only the culture time that each cell type requires to adapt to the scaffold.

[0018] Another aspect of the present invention may also have particular relevance to surface seeding (e.g., endothelialization), as it can allow surface seeding of the luminal side of any tubular structure. For example, existing synthetic vascular grafts that can benefit from endothelialization to increase patency rates can be seeded with this device in a cost-effective manner.

[0019] Another aspect of the present invention may also have particular relevance to scaffold coating or loading with growth factors, drugs, microspheres, etc. Depending on the composition of each tubular scaffold, some may need further coatings with biological compounds to provide cells a more amenable environment to grow (e.g., fibronectin). Moreover, the biological action of the cells on the scaffold can sometimes be further stimulated with a variety of growth factors loaded in the polymer. This vacuum chamber allows any particulate (e.g., micro spheres) to be loaded into or coated onto tubular structures.

[0020] Another aspect of the present invention may also have particular relevance to rotating culture for tubular scaffolds, or tubular constructs. Tissue engineered tubular grafts (TETGs) often require dynamic culture to allow even distribution of nutrients to mural cells during development, especially when the thickness of the scaffold is enough to alter the diffusion of nutrients. Though different devices exist to perform this kind of culture, this chamber offers an alternative approach with its rotating capability. The TETG can be immersed in a bath of media with an equivalent perfusate while being rotated at the desired speed.

BRIEF DESCRIPTION OF THE DRAWINGS

[0021] For a more complete understanding of the present invention, and the advantages thereof, reference may be made to the following written description of exemplary embodiments, taken in conjunction with the accompanying drawings.

[0022] **FIG. 1** is a schematic of the interacting components of a seeding device in accordance with an exemplary embodiment of the present invention.

[0023] **FIG. 2** is a perspective view of a portion of the seeding device of **FIG. 1** in accordance with an exemplary embodiment of the present invention.

[0024] **FIG. 3** is a perspective view of a portion of the seeding device of **FIG. 1** in accordance with an exemplary embodiment of the present invention.

[0025] **FIG. 4**(*a*) is a schematic depiction of the introduction of the seeding material in the scaffold device in accordance with an exemplary embodiment of the present invention.

[0026] **FIG. 4**(*b*) is a schematic depiction of the seeded scaffold device in accordance with an exemplary embodiment of the present invention.

[0027] **FIG. 5** is perspective view of a cartridge suitable for use in a chamber of a seeding device in accordance with another exemplary embodiment of the present invention.

[0028] **FIG. 6**(*a*) is perspective view of a cartridge suitable for use in a chamber of a seeding device in accordance with a further exemplary embodiment of the present invention.

[0029] **FIG. 6**(*b*) is perspective view in partial section of a cartridge illustrated in **FIG. 6**(*a*) in accordance with a further exemplary embodiment of the present invention.

[0030] **FIG. 7** is a sectional view illustrating the nuclei distribution of a vacuum seeded tube in accordance with an exemplary embodiment of the present invention.

[0031] **FIG. 8** is a sectional view illustrating the nuclei distribution of a native rat aorta.

[0032] **FIG. 9** is a sectional view illustrating the cell distribution of a vacuum seeded tube in accordance with an exemplary embodiment of the present invention.

[0033] **FIG. 10** is a graph illustrating the cell distribution (averages and standard deviations) of the percentages of cells present in longitudinal segments of seeded scaffolds in accordance with an exemplary embodiment of the present invention.

[0034] **FIG. 11** is a graph illustrating the cell distribution (averages and standard deviations) of the percentages of cells present in circumferential segments of seeded scaffolds in accordance with an exemplary embodiment of the present invention.

[0035] **FIG. 12** is a schematic depiction of a seeded scaffold in accordance with an exemplary embodiment of the present invention.

[0036] FIGS. **12**(*a*)-**12**(*i*) are sectional views taken along lines **12***a*-**12***i*, respectively, of the seeded scaffold of **FIG. 12** in accordance with an exemplary embodiment of the present invention

[0037] **FIG. 13** is a sectional view of a surface seeded scaffold in accordance with an the present invention.

[0038] FIGS. **14**(*a*)-(*b*) illustrate sectional views by scanning electron microscopy (SEM) of an unseeded control polymer.

[0039] FIGS. **15**(*a*)-(*b*) illustrate sectional views by SEM of a surface seeded scaffold after 12 hours of culture in accordance with an exemplary embodiment of the present invention.

[0040] FIGS. **16**(*a*)-(*b*) illustrate sectional views by SEM of another surface seeded scaffold after 12 hours of culture in accordance with an exemplary embodiment of the present invention.

[0041] Throughout the figures, the same reference numerals and characters, unless otherwise stated, are used to denote like features, elements, components or portions of the illustrated embodiments. Moreover, while the present invention will now be described in detail with reference to the figures, it is done so in connection with the illustrative embodiments. It is intended that changes and modifications can be made to the described embodiments without departing from the true scope and spirit of the subject invention as defined by the appended claims.

DETAILED DESCRIPTION OF THE INVENTION

[0042] This invention will be further understood in view of the following detailed description of exemplary embodiments.

[0043] **FIGS. 1-3** depict a seeding device according to an exemplary embodiment of the present invention. The device **100** may include a chamber **110** capable of maintaining a reduced pressure environment, e.g., a "vacuum." In an exemplary embodiment, chamber **110** is airtight and machined from a solid block of acrylic. The chamber **110** may be capable of holding a porous tubular structure to be seeded, such as scaffold **120**, by use of two support tubes, such as tees **130**, **140**, which may be coaxially mounted in the chamber **110** and spaced apart according to the dimensions of the scaffold **120**. In the exemplary embodiments, scaffolds **120** are mounted onto the tees **130**, **140** via two tygon tubing tips secured with 2-0 silk sutures. It is understood that other means of attachment of the scaffolds **120** to the tees **130**, **140** may be employed, e.g., clamps, wires, adhesives, connectors, etc. In the exemplary embodiment, tees **130**, **140** are fabricated from stainless steel and have an outer diameter of about 3 mm, an inner diameter of about 2 mm, and a length of about 20 cm. Two pneumatically sealed rotating joints **132**, **134** allow for the rotation of the tees **130**, **140** through the wall of the chamber **110** without pressure loss.

[0044] In the exemplary embodiment, the tees **130**, **140** are coaxially mounted in the chamber **110** with a torque transmission device **150**, such as a concentric assembly of rods, which transmits rotation from one tee to the other, allowing the tees to rotate in a synchronized fashion. The torque may be applied to one of the tees through a belt driven mechanism including, e.g., a timing belt **152** and pulleys **154**, and powered by an electrical motor **160**. Console **162** includes a level control to allow the user to control the speed of rotation of the tees **130**, **140**. The rotation speed range useful for effective seeding is about 60 rpm to about 1000 rpm, although it is understood that other speeds are useful for the seeding process. Thus, the rotation of the scaffolds **120** may occur by the mechanical attachment of the scaffolds **120** to the rotating tees **130**, **140**, as described herein above.

[0045] A negative pressure (e.g., less than atmospheric pressure) environment may be applied within the chamber **110** by way of one or more evenly distributed ports or nozzles **170**. The pressure may be in the range of about −20 to −300 mm Hg. In an exemplary embodiment, four nozzles are used. The nozzles **170** inside the chamber **110** are connected to a vacuum circuit, such as pneumatic resistive circuit **180**, which in turn is connected to a vacuum port **182**. The pneumatic resistive circuit **180** is capable of maintaining a constant and controllable negative relative pressure inside the chamber **110** throughout the seeding process using a flow regulator **184** and a vacuum gauge, such as digital vacuum gauge **186** (An exemplary digital vacuum gauge is manufactured by ACSI, Irvine, Calif.). The nozzles **170** inside the chamber **110** may be connected to the lab vacuum line **188** by a 0.2 μm PTFE air filter **182** (An exemplary air filter is manufactured by Acro® 50, Pall Corporation, East Hills, N.Y.) illustrated in **FIG. 2**, placed in parallel to the air circuit **180**. The air circuit **180** may be kept sterile using the air filter which also may provide external resistance required to achieve the necessary flow.

[0046] The tees **130**, **140** are each connected to a precision syringe pump **190** (An exemplary syringe pump is manufactured by Harvard Apparatus Inc., Holliston, Mass.) outside the chamber **110**, by tubing, such as polyvinyl chloride (PVC) tubing **194**. As illustrated in **FIG. 2**, the tubes are connected to the tees **130**, **140** by means of rotating joints **136**, **138** that allow for the passage of the seeding suspension material from the tubing **194** to the tees **130**, **140** while the tubing is in rotation. Syringe pump **190** has a flow control for modulating the flow rate of the seeding material into the scaffold member **120**.

[0047] Scaffolds **120** may be manufactured from any type of porous tubular material. In an exemplary embodiment, for example, poly(ester urethane)urea (PEUU) may be used. According to one exemplary embodiment, scaffold **120** has a porosity of about 90% and a pore size range of about 10-200 μm, and may be prepared by thermally induced phase separation (TIPS) to a length of 2 cm, inner diameter 3.3 mm, and thickness 200-300 μm. (A TIPS technique is described in Guan J, Fujimoto K L, Sacks M S, and Wagner W R, "Preparation and characterization of highly porous, biodegradable polyurethane scaffolds for soft tissue applications,"*Biomaterials* 2005;26(18):3961-71, which is incorporated by reference in its entirety herein.) According to another exemplary embodiment, scaffold **120** has a porosity of about 90% and a pore size of about 10 μm, and may be fabricated by electrospinning PEUU onto a rotating 3.5 mm stainless steel mandrel to a length of 2 cm, and a thickness of 200 μm. (A useful technique for fabricating the scaffold is described in Stankus J J G J, and Wagner W R, "Fabrication of Biodegradable, Elastomeric Scaffolds with Sub-Micron Morphologies," In press 2004, which is incorporated by reference in its entirety herein.)

[0048] The loading process may be achieved with two axially coupled loading syringes **196**, **198** attached on each end of the tees **130**, **140** through a standard Luer® connection. Once the reduced pressure condition is applied inside the chamber **110**, the plungers of loading syringes **196**, **198** may be drawn by the infusion vacuum force with a flow rate proportional to the driving force. The tubing is connected through Luer® connectors. The seeding process may be performed within about 20 seconds to about 5 minutes depending on the volume of the seeding suspension, and the physical characteristics of the scaffold **120**. Priming and flushing syringes **192** may also be provided. The plungers of

loading syringes **196**, **198** may also be used to modulate the flow rate of the seeding material into the scaffold member **120**.

[**0049**] The seeding device **100** utilizes the synergistic actions of reduced pressure applied inside the chamber **110** and the flow generated by the syringe pump **190** to induce a transmural flow through the polymer material of the scaffold **120**. The interior portion of the scaffold member **120** is in communication with the interior portion of the tees **130**, **140**. The infused flow, e.g., cell material suspended in a medium, passes through the interior of the tees **130**, **140** to the scaffold **120**. **FIG. 4**(*a*) illustrates the infused flow entering the interior of the scaffold **120** as indicated by arrows C. During this phase, the particulate (e.g., cells, microspheres) infused by the syringe **196**, **198** become entrapped within the pores of the polymer material of the scaffold **120** while the liquid phase of the cell suspension exudes through (as indicated by arrow L). The tubular scaffold **120** rotates during the seeding (as indicated by arrow R) in order to increase the uniformity of seeding along its circumferential direction. **FIG. 4**(*b*) illustrates a seeded scaffold **120**. It is understood that the application of negative pressure, the infusion of the seeding suspension, and the rotation of the scaffold occur independently. However, the application the negative pressure and the rotation of the scaffold occur simultaneously for at least a portion of the process described herein.

[**0050**] The particulate material which is intended to be entrapped in the scaffold is generally referred to herein as the seeding material, which may include any appropriate cell material suspended in a medium. According to an exemplary embodiment, murine muscle-derived stem cells (MDSC) obtained from an established pre-plating technique may be cultured and seeded in Dulbecco Modified Eagle Medium (DMEM) (Sigma) supplemented with 1% Penicillin/Streptomycin (Gibco, Invitrogen Corporation, Carlsbad, Calif.), 10% Fetal Calf Serum (Atlanta Biologicals, Norcross, Ga.), and 10% Horse Serum (Gibco, Invitrogen Corporation). (A pre-plating technique is described in Qu-Petersen, Z., et al., "Identification of a novel population of muscle stem cells in mice: potential for muscle regeneration,"*The Journal of Cell Biology*, 2002. 157(5): p. 851-64, which is incorporated by reference in its entirety herein.) In another exemplary embodiment, isolated rat bone marrow derived progenitor cells (rBMPC) may be cultured and seeded in DMEM (Sigma) supplemented with 10% bovine serum (Gibco, Invitrogen Corporation) and 1% Penicillin/ Streptomycin (Gibco, Invitrogen Corporation). (A technique for isolating the bone marrow is described in Dexter, T. M. and L. G. Lajtha, "Proliferation of haemopoietic stem cells in vitro, "*British Journal of Haematology*, 1974. 28(4): p. 525-30, which is incorporated by reference in its entirety herein.) In a further exemplary embodiment, bovine aortic endothelial cells (bAEC) (Cambrex Corporation, East Rutherford, N.J.) were cultured and seeded in EGM-MV media (Cambrex). The seeding material may include any cell type, microspheres, microparticles, liposomes, adhesion proteins, growth factors, or drugs.

[**0051**] The device **100** may allow effective seeding without generating injurious mechanical conditions for the cells by maintaining low shear stresses acting on the cells during seeding. A calculation of the shear stresses was performed by use of the computational fluid dynamic (CFD) software Fluent (version 6.2, Fluent Inc., Lebanon N.H.). For this purpose, a $4.5 \cdot 10^5$ wedges volume mesh was created (Gambit 2.2, Fluent Inc., Lebanon, N.H.) with boundary layers on the luminal surface of the model. The model consisted of a composite tube modelled as porous media in the larger central portion corresponding to the scaffold **120** and as rigid tubes in the two peripheral portions corresponding to the tees **130**, **140**. The permeability of the polymer was calculated empirically via Darcy law by measuring the pressure loss (e.g., model TJE, Honeywell Sensotec, Columbus, Ohio) per unit surface area of the polymer for a measured exudation rate of saline. The density of the fluid was proportionally calculated for a 10% serum (1025 kg/m^3) solution in culture media (1008 kg/m^3) and determined to be 1010 kg/m^3. The dynamic viscosity of the cell suspension was measured with a capillary viscometer (e.g., Cannon-Manning, Cannon Instruments Company, State College, Pa.), and a rheologic curve was generated with a digital cone and plate rheometer (e.g., DV-III, Brookfield Engineering Labs, Middleboro, Mass.) in order to demonstrate the Newtonian properties of the fluid under shear rate ranges obtained with the device.

[**0052**] The CFD simulation was performed in steady state. The solver was segregated with implicit formulation and SIMPLE pressure-velocity coupling. A spatially uniform velocity was assigned to the two inlets with 10 diameters of flow extension to allow for flow profile development. The rotation of the tees **130**, **140** was simulated as a moving mesh. Convergence was taken as residual values $\leqq 10^{-4}$ and confirmed with stability of two surface monitors (average absolute pressure on outlet surface and average velocity on an interior surface). The outlet was modelled with a constant pressure equal to the vacuum pressure inside the chamber **110**. The wall shear stress (WSS) on the luminal surface of the model was determined by the software while the WSS acting on the scaffold pores was estimated analytically. In brief, the conservation of momentum in laminar flow conditions was considered for cylindrical pore and modified with the Hagen-Poiseuille equation for the pressure drop, as further described in R Byron Bird WES and Edwin N. Lightfoot, *Transport Phenomena,* (2nd ed: John Wiley & Sons, Inc.; 2002). The average velocity in the pore was set by considering the measured total flow rate entering the scaffold divided by the effective open area of the luminal surface of the scaffold (effective open area=porosity·internal luminal cylindrical area) with the assumption of even distribution of the inlet flow rate in the porous luminal surface of the scaffold. The resulting equation for wall shear stress is

$$\tau_{rz,\max} = \frac{\bar{v}_z \cdot 4 \cdot \mu \cdot}{R} \qquad [1]$$

where $\bar{v}_z$ is the average velocity in the pore, μ the dynamic viscosity, and R the radius. The radius used in the equation was 10 μm consistent with the smallest pores of the porous polymer.

[**0053**] **FIG. 5** illustrates a further embodiment of a cell delivery mechanism **100'** suitable for use in the chamber **110** for seeding longer scaffolds (>5 cm). Cell delivery mechanism is substantially identical to the mechanism described hereinabove, with the differences noted below. For example,

the internal structure of tee **140'** may be modified. A smaller coaxial internal tee **142'** may be inserted into the tee **140'**. The internal tee **142'** may terminate with a head **144'** radially drilled with a number of apertures, e.g., nozzles **145'**. The coaxial tees **142'** is free to move within the interior of the scaffold **120'**. In particular, coaxial tee **142'** may move axially with respect to the tee **140'** (as indicated by arrow T) with substantially reduced friction due to the presence of the linear bearings **148'**. The support member **162'** may connect the internal tee **142'** to a motor driven linear positioner controlled by a console (not shown) that moves the tee **142'** along the axial direction (as indicated by arrow T) without allowing rotation of the tee **142'**. The linear bearings **148'** may allow for the rotation of the tee **140'** around the tee **142'**. While the tee **140'** is put in rotation by the motor **160** (as indicated by arrow R), the tee **142'** may slide axially inside, driven by the linear positioner. In proximity of the scaffold **120'**, the two coaxial tees **140'**, **142'** may be sealed by a teflon seal **146'** that avoids pressure losses and seeding suspension spillings between the two coaxial tees **140'**, **142'** during mutual movements. The tee **140'** may cross the wall of the chamber **110** by means of the sealed joint **134** (not shown in **FIG. 5**). Externally to the chamber **110** in proximity of the joint **134**, the tee **140'** may be connected to the pulley **154**, and moved with the timing belt **152** by the motor **160**. The tee **140'** ends externally to the pulley **154**. The internal tee **142'** may be connected by tubing **194** to the syringe **196**. The head **144'** may be initially positioned to the level corresponding to an end of the scaffold **120**, in proximity with the opposite tee **130'**. The tees **130'**, **140'** may be put in rotation, the vacuum applied into the chamber, and the infusion pump **190** started to release the seeding suspension though the nozzles **145'** of the head **144'**. The seeding suspension begin to exude through the scaffold **120'** in proximity to the current level of the head **144.'** The head **144'** may be moved along the length of the scaffold (for example, in the direction of arrow T), with a velocity, for example, ranging from about 0.015 to about 0.15 cm/sec by means of the motor driven linear positioner. The exudation of seeding suspension moves accordingly with the internal tee **142'**, allowing for a uniform sseding along the length of the scaffold **120'**.

[0054] FIGS. **6**(*a*)-**6**(*b*) depict a disposable sterile cartridge **200** suitable for use in the chamber **10** of a seeding device according to another exemplary embodiment of the present invention. In contrast to the device illustrated in **FIGS. 1-3**, scaffold **120'** is rotated by a magnetic attachment to the support members, e.g., tees **130'**, **140'**. Cartridge **200** includes a porous scaffold **220**, which is substantially as described above regarding scaffold **120**, mounted on a removable cylindrical rotating internal main body **202**. The main body **202** may be composed of two peripheral cylindrical hollow spaces **204**, **206**, a built in torque transmission **280**, and two tees **230**, **240**. The hollow spaces **204**, **206** bear inside two collapsible bags made of PVC **260** (one shown in **FIG. 6**(*b*) and another collapsible bags is positioned adjacent the other end portion of the device) having a paraboloidal shape. The open circular edges of the collapsible bags are internally sealed with the tees **230**, **240** in proximity to the point where the scaffold **220** is mounted. The external walls of these two hollow spaces hold a disk of magnetic material used for communication of an external torque (not visible in the figures). A transparent polycarbonate tube, threaded at its ends, forms the external surface of the disposable cartridge **222**. Two caps **224**, **226** each include a 0.22 μm PTFE filter **232**, **234** that communicates the negative pressure from the chamber **110** to the interior of the cartridge **200**, maintaining the sterility into the cartridge, and a rotational support structure **292**, **294** that allow, when the cartridge is mounted, the rotation of the internal body **202** in respect to the external sheath **222** and the two caps **224**, **226**. The rotating body is removed from the sheath **222** by unscrewing one cap **224**. The cell suspension is introduced with a syringe into the interior of the rotating body **202**, which include the internal spaces of the collapsible bags **260**, and the internal space of the scaffold **220**, by means of the priming port **242** and the venting port **244** that allows for removal of air while filling with cell suspension. The loaded main body **202** is repositioned into the sheath **222** and the cap **224** repositioned as well. The main body **202** is put in rotation with external rotating magnets present in the chamber **110** that communicate the torque by means of the magnetic disks attached to the body **202**. The vacuum inside the modified chamber **110** is applied and communicated to the interior of the cartridge by means of the filters **232**, **234**. The transmural flow generated by the application of an external vacuum into the modified chamber **110** allows the liquid material to exude through the scaffold **220**. During the exudation of the liquid phase of the cell suspension through the scaffold, the collapsible bags **260** retract into the scaffold until they touch each other in the center of the scaffold completing the seeding procedure.

EXAMPLES

Bulk Seeding Experiments

[0055] Qualitative evaluation of the seeding was performed by seeding two 2 cm TIPS tubular scaffolds with 10.106 BMPC suspended in 10 mL of culture media (flow rate=3.4 mL/min, rotation speed=120 rpm, vacuum=−127 mmHg). Nuclear and cytoskeletal stains were visualized by epifluorescent microscopy of cross sections taken after two hours of static culture. Quantitative evaluation was performed by calculating the seeding efficiency of seeded scaffolds and also via two specifically designed experiments. The seeding efficiency (percent of the total number of cells incorporated) was calculated by determining the cell count in the seeding solution before and after seeding using a hemocytometer.

[0056] The first designated experiment for quantitative evaluation of the seeding performances involved six 2 cm long TIPS tubular scaffolds seeded with $15 \cdot 10^6$ MDSC. The cells were suspended in 20 mL of culture media and infused to the scaffold under identical conditions (flow rate=8 mL/min, rotation speed=350 rpm, vacuum=−127 mmHg, duration of seeding=1 minute). After seeding, each construct was kept for two hours in static culture and subsequently cut into nine serial equi-sized rings. Each ring underwent metabolic-based cell count (MTT) in order to detect the cell number in each ring and therefore in each longitudinal location for seeded construct. Comparisons of the average and standard deviation of the measures allowed assessment of the reproducibility of the longitudinal distribution of cells in the constructs seeded with the device.

[0057] The second experiment was designed to assess the cell distribution along the circumferential direction. For this, a 2 cm long construct was seeded, cultured, and cut using the same conditions, parameters, and cells as the first experi-

ment. However, the construct was cut along the longitudinal direction to keep track of the relative circumferential position among different sections. For each of the nine longitudinal segments, three 15 μm-thick sections were cut and stained with nuclear stain. Each stained section was digitally photographed reconstructing from 16 serial fields of view at 200× magnification. Subsequently, each reconstructed section image was cropped in four cardinal sectors according to the curve-abscissa on the centreline of the section. Each cardinal sector of each section underwent image-based quantification of the cell number with an intensity threshold filter (Scion Image 4.0, Scion Corporation). The cell number in each sector was measured dividing the total area occupied by the nuclei divided by the average area occupied by one nucleus.

[0058] For a qualitative assessment, a representative seeded section (**FIG. 7**) was compared with a native rat aorta treated with the same nuclear stain (**FIG. 8**). The native vessel and seeded construct had similar cell distribution throughout the thickness of the polymer within minutes of seeding procedure. As illustrated in **FIG. 9**, the cells incorporated into the constructs maintained the spheroidal shape two hours after seeding as evidenced by F-actin stain. Arrow S indicates the luminal surface of the scaffold. (200× magnification) The cells started to spread in the pores after 1 day (data not shown).

[0059] The first bulk seeding experiment showed a high level of longitudinal uniformity represented by the comparison of the normalized average cell number percentage for each of the nine longitudinal segments within each of the six seeded scaffolds. The Krustal Wallis test produced a p-value of 0.99 indicating no significant differences in the longitudinal distribution within each of the six scaffolds (**FIG. 10**). The reproducibility represented by the comparison of the cell number seeded in each location among six different scaffolds produced a p-value of 0.24 (**FIG. 10**). **FIG. 10** illustrates the percentage of the total cell number seeded in each construct calculated summing the MTT absorbances for each of the six scaffolds. The second experiment showed non-significant differences among the total cell number in the four circumferential sectors along the seeded construct (p=0.25 **FIGS. 11 and 12**). FIGS. **12**(*a*)-(*i*) illustrates the nuclear content in each of the nine longitudinal segments of the scaffold used for circumferential cell distribution assessment. (The image was inverted to represent the nuclei in black with a higher contrast.) The standard deviations observed in the circumferential cell distribution may be related to the heterogeneous thickness of the polymer around the circumferential dimension, as frequently observed in the microscope sections, allowing thicker sectors to bear more cells and thinner sectors to bear a lower amount of cells upon saturation of the available space. This dataset could not been normalized by thickness because the polymer was not visible in the microscope pictures taken under UV light. The observed variations in thickness are probably due to the manual nature of the polymer processing technique and should be dramatically reduced upon use of automated processes.

Endothelialization Experiments

[0060] The endothelialization capability of the device was tested with two experiments in which a small pore 2 cm long electrospun tubular construct was seeded with rBMPC or bAEC. The reduced pore size of the polymer prevented the passage of cells through the thickness of the tubular scaffold but did not prevent the passage of the liquid phase therethrough. The scaffolds were both seeded with 8 million cells suspended in 20 mL of culture media using the same seeding parameters used for the bulk seeding experiments; the duration of the seeding was one minute. A ring of the first construct was cut 1 hour after seeding, fixed, and stained with nuclear stain while the remainder of the first and second construct were kept for 12 hours in static culture conditions to allow the cells to spread on the surface. They were subsequently fixed and processed for electron microscopy.

[0061] The specimens were fixed in 4% paraformaldehyde for 1 hour and subsequently kept overnight in 30% sucrose solution. After PBS wash, the specimens were embedded in tissue freezing medium (TBS, Triangle Biomedical Sciences, Durham, N.C.) and sectioned with a Cryostat (Cryotome, ThermoShandon, Pittsburgh, Pa.). The sections prepared for cytoskeletal markers were permeabilized in Triton-X-100 solution (Fisher Scientific, Fair Lawn, N.J.) for 15 minutes and F-actin filaments were stained with 1:250 dilution of phalloidin conjugated to fluorescein-5-isothiocyanate (FITC) (Molecular Probes, Eugene, Oreg.) for an hour. The sections were counterstained with the nuclear stain DAPI (bisbenzimide, Sigma) for one minute. The sections were observed via epifluorescence microscopy using an Eclipse E800 (Nikon Instech Co., Ltd., Kanagawa, Japan) with UV filter for the DAPI stain and with FITC filter for the phalloidin stain.

[0062] Each specimen was placed in 200 μL of media supplemented with 20 μL of MTT solution [3-(4,5-dimethylthiazol-2-yl)-2,5-diphenyltetrazolium bromide] (Sigma) into a single well of a 96 multiwell plate immediately after culture. The specimens were kept for 4 hours at 37° C. Samples were then immersed in 2.5% isopropanol/HCl solution and kept for 24 hours at 4° C. The adsorbance was read at 570 nm with a microplate reader (model 680, Bio-Rad, Hercules, Calif.) and normalized to the dry weight of each ring and the total cell number in each construct. The cell number was obtained with a previously derived standard curve for the cell type of interest.

[0063] After 12 hours of static culture, the specimens were fixed in 2.5% glutaraldehyde for one hour, washed in PBS and re-fixed in 1% OsO_4 for another hour. After multiple washes in PBS the specimens were dehydrated with ethanol gradient (from 30% to 100%), and subsequently processed with critical point drying (Emscope CPD 750, Emscope Lab., Ashford, UK) with 4 cycles of liquid CO_2 soaking and venting at 10° C. before reaching the critical point for CO_2 at 31.1° C. at 1100 psi. After complete dehydration the specimens were gold sputter coated (Sputter Coater 108 auto, Cressington Scientific Instruments Inc., Cranberry Twp., Pa.) with a 3 nm thick layer of gold. The luminal surfaces in different location of the seeded scaffolds were observed with field emission scanning electron microscopy (JSM-6330F, JEOL ltd. Tokyo, Japan).

[0064] The construct seeded with BMPCs showed, immediately after seeding (1 hour), an accumulation and passive adhesion of all cellular components on the luminal surface **900**, they were homogeneously distributed in both the circumferential and the longitudinal direction of the construct. **FIG. 13** illustrates the accumulation of BMPCs (nuclei) in

the luminar surface **900** of the electrospun PEUU scaffold **902** one hour after seeding procedure. The picture was inverted for increasing the contrast and modified for localizing the polymer which is invisible under UV light. The thickness is 15 μm and the magnification 200×. After 12 hours of culture, SEM showed a luminal surface completely lined with spread cells that formed a continuous layer upon the fibers of the electrospun polymer (FIGS. **15**(*a*) and **15**(*b*)). The construct seeded with bAECs showed a similar lining of ECs on the luminal surface of the construct (FIGS. **16**(*a*) and **16**(*b*)). A control polymer without seeding is illustrated in FIGS. **14**(*a*) and **14**(*b*).

Performance of the Device

[**0065**] The device was able to maintain a defined and constant level of vacuum over the operational cycle and to infuse a defined flow rate of seeding suspension across the porous matrix of the scaffold while rotating with a defined angular velocity. The permeability was $2.6 \cdot 10^{-13}$ m^2 while the dynamic viscosity performed at 21° C. (consistent with the seeding temperature), was 1.03 cP. The CFD model simulation reached a prompt convergence with stability of the two surface monitors. The wall shear stress distribution on the luminal surface of the model was negligible (i.e. <1 dyne/cm^2). According to the analytical expression used, the WSS in the representative smallest pore was 5.4 dyne/cm^2. It was observed that the seeding efficiency was dependent on the pore size of the polymer and on the flow rate used during the seeding procedure. In particular, it increased with smaller pores and lower flow rates, and it ranged from 65% to 90% in the tested scaffolds. The viability two hours after seeding was near 100% of the initial effective cell number incorporated into the scaffold according to the MTT assay and previously obtained calibration curve.

[**0066**] While there have been described what are believed to be the preferred embodiments of the present invention, those skilled in the art will recognize that other and further changes and modifications may be made thereto without departing from the spirit of the invention, and it is intended to claim all such changes and modifications as fall within the true scope of the invention. For example, it is understood that the invention has applicability in, e.g., vascular, urological, neurological, and musculo-skeletal contexts. In addition, the tubular shape of the scaffold used for the seeding does not limit the range of applicability since the cylindrical shape may be slit open in order to produce a flat sheet. Other shapes of scaffolding may also be employed, such as conical, toroidal, or prismatic shapes.

We claim:

1. An apparatus for seeding material in a porous scaffold member capable of entrapping seeding material therein, comprising:

a chamber having an interior and capable of maintaining a negative pressure and capable of enclosing a scaffold member therein; and

a support member for rotating the scaffold member disposed within the interior of the chamber and for introducing the seeding material into the chamber.

2. The device as recited in claim 1, wherein the support member comprises a hollow configuration.

3. The apparatus as recited in claim 2, wherein the scaffold member defines an interior portion and wherein the interior portion of the scaffold member is in communication with an interior portion of the support member, and wherein the seeding material is introduced into the interior of the scaffold member via the support member.

4. The apparatus as recited in claim 3, wherein the support member defines at least one aperture for introducing the seeding material into the interior of the scaffold member.

5. The apparatus as recited in claim 3, wherein the support member comprises a portion defining at least one aperture.

6. The apparatus as recited in claim 5, wherein the portion defining at least one aperture is adapted for movement within the interior of the scaffold member.

7. The apparatus as recited in claim 6, wherein the portion defining at least one aperture is adapted for axial movement within the interior of the scaffold member.

8. The apparatus as recited in claim 1, further comprising an expandable bag positioned within the support member.

9. The apparatus as recited in claim 1, wherein the scaffold member is rotated by mechanical attachment to the support member.

10. The apparatus as recited in claim 1, wherein the scaffold member is rotated by magnetic attachment to the support member.

11. The apparatus as recited in claim 1, wherein the chamber provides a pressure of about −20 to about −300 mm Hg.

12. The apparatus as recited in claim 1, wherein the chamber comprises acrylic.

13. The apparatus as recited in claim 1, further comprises a level controller for modulating the rotation speed of the support member.

14. The apparatus as recited in claim 1, further comprising a flow regulator for modulating the pressure level within the chamber.

15. The apparatus as recited in claim 1, further comprising a flow regulator for modulating the flow rate of seeding material into the chamber.

16. A method for seeding material in a scaffold member comprising:

applying a negative pressure condition to a scaffold member positioned within a chamber;

introducing seeding material in the scaffold member; and

rotating the scaffold member, wherein at least a portion of rotating the scaffold member occurs simultaneously with applying the negative pressure condition to the scaffold member.

17. The method of claim 16, wherein introducing seeding material in the scaffold member comprises introducing seeding material with a controlled flow rate.

18. The method of claim 16, wherein the scaffold member has a tubular structure defining an interior and wherein introducing seeding material in the scaffold member comprises introducing seeding material into the interior of the scaffold member via the support member.

19. The method of claim 18, wherein introducing seeding material in the scaffold member comprises passing at least a portion of the seeding material from the interior of the scaffold member to an exterior of the scaffold member.

20. The method of claim 19, wherein passing at least a portion of the seeding material from the interior of the scaffold member to an exterior of the scaffold member comprising passing at least a portion of the seeding material from the interior of the scaffold member to an exterior of the

scaffold member in response to the negative pressure in the chamber and the flow of the seeding material.

21. The method of claim 18, wherein introducing seeding material in the scaffold member comprises introducing the seeding material into the interior of the scaffold member via at least one aperture in the support member.

22. The method of claim 21, wherein the support member comprises a portion defining at least one aperture, and wherein introducing seeding material in the scaffold member comprises moving the portion of the support member defining the aperture within the interior portion of the scaffold member.

23. The method of claim 22, wherein introducing seeding material in the scaffold member comprises axially moving the portion of the support member defining the aperture within the interior portion of the scaffold member.

24. The method of claim 16, wherein introducing seeding material in the scaffold member comprises entrapping at least a portion of the seeding material in the scaffold member.

25. The method of claim 24, wherein the scaffold member comprises an interior surface and wherein entrapping at least a portion of the seeding material in the scaffold member comprises entrapping the seeding material adjacent the interior surface of the scaffold member.

26. The method of claim 24, wherein the scaffold member defines a thickness and wherein entrapping at least a portion of the seeding material in the scaffold member comprises entrapping the seeding material throughout the thickness of the scaffold member.

27. The method of claim 16, further comprising modulating the pressure within the chamber.

28. The method of claim 16, further comprising modulating the rotational speed of the support member.

29. The method of claim 16, further comprising modulating the flow rate of the seeding material.

* * * * *

BIBLIOGRAPHY

1. Rosamond W, Flegal K, Furie K, Go A, Greenlund K, Haase N, et al. Heart disease and stroke statistics--2008 update: a report from the American Heart Association Statistics Committee and Stroke Statistics Subcommittee. Circulation. 2008 Jan 29;117(4):e25-146.

2. Allender S, Scarborough P, Peto V, Rayner M, Leal J, Luengo-Fernandez R, et al. European cardiovascular disease statistics: European Heart Network; 2008 Contract No.: Document Number|.

3. Nowygrod R, Egorova N, Greco G, Anderson P, Gelijns A, Moskowitz A, et al. Trends, complications, and mortality in peripheral vascular surgery. J Vasc Surg. 2006 Feb;43(2):205-16.

4. U.S. Renal Data System, USRDS 2007 annual data report: Atlas of chronic kidney disease and end-stage renal disease in the United States. Bethesda, MD.: National Institutes of Health, National Institute of Diabetes and Digestive and Kidney Diseases; 2007 Contract No.: Document Number|.

5. Basaran O, Karakayali H, Emiroglu R, Belli S, Haberal M. Complications and long-term follow-up of 4416 vascular access procedures. Transplant Proc. 2003 Nov;35(7):2578-9.

6. Zhang WJ, Liu W, Cui L, Cao Y. Tissue engineering of blood vessel. J Cell Mol Med. 2007 Sep-Oct;11(5):945-57.

7. Weintraub WS, Jones EL, Craver JM, Guyton RA. Frequency of repeat coronary bypass or coronary angioplasty after coronary artery bypass surgery using saphenous venous grafts. Am J Cardiol. 1994 Jan;73(2):103-12.

8. Xue L, Greisler HP. Biomaterials in the development and future of vascular grafts. J Vasc Surg. 2003 Feb;37(2):472-80.

9. Hsu CY, Vittinghoff E, Lin F, Shlipak MG. The incidence of end-stage renal disease is increasing faster than the prevalence of chronic renal insufficiency. Ann Intern Med. 2004 Jul 20;141(2):95-101.

10. McClellan WM. Epidemic end-stage renal disease in the United States. Artif Organs. 1994 Jun;18(6):413-5.

11. Kohler TR, Kirkman TR. Dialysis access failure: A sheep model of rapid stenosis. J Vasc Surg. 1999 Oct;30(4):744-51.

12. Fox CJ, Gillespie DL, O'Donnell SD, Rasmussen TE, Goff JM, Johnson CA, et al. Contemporary management of wartime vascular trauma. J Vasc Surg. 2005 Apr;41(4):638-44.

13. Clouse WD, Rasmussen TE, Perlstein J, Sutherland MJ, Peck MA, Eliason JL, et al. Upper extremity vascular injury: a current in-theater wartime report from Operation Iraqi Freedom. Ann Vasc Surg. 2006 Jul;20(4):429-34.

14. Huynh TT, Pham M, Griffin LW, Villa MA, Przybyla JA, Torres RH, et al. Management of distal femoral and popliteal arterial injuries: an update. Am J Surg. 2006 Dec;192(6):773-8.

15. Levick JR. An Introduction to Cardiovascular Physiology. 2nd ed. Oxford, UK: Butterworth-Heinemann Ltd; 1995.

16. The Basic Science of Vascular Disease. Sidawy AN, Sumpio BE, DePalma RG, editors. New York: Futura Publishing Compant, Inc.; 1997.

17. Nichols WW, O'Rourke MF. McDonald's Bloof Flow in Arteries. 3rd ed.: Lea & Febiger; 1990.

18. Correia ML, Haynes WG. Arterial compliance and endothelial function. Curr Diab Rep. 2007 Aug;7(4):269-75.

19. Stewart SF, Lyman DJ. Effects of a vascular graft/natural artery compliance mismatch on pulsatile flow. Journal of Biomechanics. 1992 Mar;25(3):297-310.

20. Sottiurai VS. Distal Anastomotic Intimal Hyperplasia: Histocytomorphology, Pathophysiology, Etiology, and Prevention. International Journal of Angiology. 1999;8(1):1-10.

21. Viola J, Lal B, Oren. G. The emergence of tissue engineering as a research field. The National Science Foundation; 2003 [updated 2003; cited]; Available from: http://www.nsf.gov/pubs/2004/nsf0450/start.htm.

22. Vacanti JP, Morse MA, Saltzman WM, Domb AJ, Perez-Atayde A, Langer R. Selective cell transplantation using bioabsorbable artificial polymers as matrices. J Pediatr Surg. 1988 Jan;23(1 Pt 2):3-9.

23. Bell E, Ivarsson B, Merrill C. Production of a tissue-like structure by contraction of collagen lattices by human fibroblasts of different proliferative potential in vitro. Proc Natl Acad Sci U S A. 1979 Mar;76(3):1274-8.

24. Nerem RM. Cellular engineering. Ann Biomed Eng. 1991;19(5):529-45.

25. Stock UA, Vacanti JP. Tissue engineering: current state and prospects. Annu Rev Med. 2001;52:443-51.

26. Zilla P, Greisler HP, editors. Tissue Engineering of Vascular Prosthetic Grafts. Austin: R.G. Landes; 1999.

27. Greisler HP, Cziperle DJ, Kim DU, Garfield JD, Petsikas D, Murchan PM, et al. Enhanced endothelialization of expanded polytetrafluoroethylene grafts by fibroblast growth factor type 1 pretreatment. Surgery. 1992 Aug;112(2):244-54; discussion 54-5.

28. Biomaterials Science. An Introduction to Materials in Medicine. Ratner BD, Hoffman AS, Schoen FJ, Lemons JE, editors. London, UK: Academic Press; 1996.

29. Weinberg CB, Bell E. A blood vessel model constructed from collagen and cultured vascular cells. Science. 1986 Jan;231(4736):397-400.

30. L'Heureux N, Germain L, Labbe R, Auger FA. *In vitro* construction of a human blood vessel from cultured vascular cells: a morphologic study. Journal of Vascular Surgery. 1993 Mar;17(3):499-509.

31. L'Heureux N, Paquet S, Labbe R, Germain L, Auger FA. A completely biological tissue-engineered human blood vessel. Faseb J. 1998 Jan;12(1):47-56.

32. L'Heureux N, Dusserre N, Konig G, Victor B, Keire P, Wight TN, et al. Human tissue-engineered blood vessels for adult arterial revascularization. Nat Med. 2006 Mar;12(3):361-5.

33. Campbell JH, Efendy JL, Campbell GR. Novel vascular graft grown within recipient's own peritoneal cavity. Circ Res. 1999 Dec 3-17;85(12):1173-8.

34. Ziegler T, Nerem RM. Tissue engineering a blood vessel: regulation of vascular biology by mechanical stresses. J Cell Biochem. 1994 Oct;56(2):204-9.

35. Nerem RM. Role of mechanics in vascular tissue engineering. Biorheology. 2003;40(1-3):281-7.

36. Niklason LE, Langer RS. Advances in tissue engineering of blood vessels and other tissues. Transpl Immunol. 1997 Dec;5(4):303-6.

37. Niklason LE, Gao J, Abbott WM, Hirschi KK, Houser S, Marini R, et al. Functional arteries grown in vitro. Science. 1999 Apr 16;284(5413):489-93.

38. Shin'oka T, Matsumura G, Hibino N, Naito Y, Watanabe M, Konuma T, et al. Midterm clinical result of tissue-engineered vascular autografts seeded with autologous bone marrow cells. J Thorac Cardiovasc Surg. 2005 Jun;129(6):1330-8.

39. Shin'oka T, Imai Y, Ikada Y. Transplantation of a tissue-engineered pulmonary artery. New England Journal of Medicine. 2001 Feb 15;344(7):532-3.

40. Nerem RM, Seliktar D. Vascular tissue engineering. Annu Rev Biomed Eng. 2001;3:225-43.

41. Hutmacher DW. Scaffold design and fabrication technologies for engineering tissues--state of the art and future perspectives. J Biomater Sci Polym Ed. 2001;12(1):107-24.

42. Deschamps AA, Grijpma DW, Feijen J. Phase separation and physical properties of PEO-containing poly(ether ester amide)s. J Biomater Sci Polym Ed. 2002;13(12):1337-52.

43. Yang S, Leong KF, Du Z, Chua CK. The design of scaffolds for use in tissue engineering. Part I. Traditional factors. Tissue Eng. 2001 Dec;7(6):679-89.

44. Berry CC, Campbell G, Spadiccino A, Robertson M, Curtis AS. The influence of microscale topography on fibroblast attachment and motility. Biomaterials. 2004 Nov;25(26):5781-8.

45. Naito Y, Imai Y, Shin'oka T, Kashiwagi J, Aoki M, Watanabe M, et al. Successful clinical application of tissue-engineered graft for extracardiac Fontan operation. J Thorac Cardiovasc Surg. 2003 Feb;125(2):419-20.

46. Niklason LE, Abbott W, Gao J, Klagges B, Hirschi KK, Ulubayram K, et al. Morphologic and mechanical characteristics of engineered bovine arteries. Journal of Vascular Surgery. 2001 Mar;33(3):628-38.

47. Shinoka T, Ma PX, Shum-Tim D, Breuer CK, Cusick RA, Zund G, et al. Tissue-engineered heart valves. Autologous valve leaflet replacement study in a lamb model. Circulation. 1996 Nov 1;94(9 Suppl):II164-8.

48. Santavirta S, Konttinen YT, Saito T, Gronblad M, Partio E, Kemppinen P, et al. Immune response to polyglycolic acid implants. J Bone Joint Surg Br. 1990 Jul;72(4):597-600.

49. Sung HJ, Meredith C, Johnson C, Galis ZS. The effect of scaffold degradation rate on three-dimensional cell growth and angiogenesis. Biomaterials. 2004 Nov;25(26):5735-42.

50. Shum-Tim D, Stock U, Hrkach J, Shinoka T, Lien J, Moses MA, et al. Tissue engineering of autologous aorta using a new biodegradable polymer. Ann Thorac Surg. 1999 Dec;68(6):2298-304; discussion 305.

51. Guan J, Sacks MS, Beckman EJ, Wagner WR. Synthesis, characterization, and cytocompatibility of elastomeric, biodegradable poly(ester-urethane)ureas based on poly(caprolactone) and putrescine. J Biomed Mater Res. 2002 Sep 5;61(3):493-503.

52. Guan J, Sacks MS, Beckman EJ, Wagner WR. Biodegradable poly(ether ester urethane)urea elastomers based on poly(ether ester) triblock copolymers and putrescine: synthesis, characterization and cytocompatibility. Biomaterials. 2004 Jan;25(1):85-96.

53. Guan J, Fujimoto KL, Sacks MS, Wagner WR. Preparation and characterization of highly porous, biodegradable polyurethane scaffolds for soft tissue applications. Biomaterials. 2005 Jun;26(18):3961-71.

54. Nieponice A, Soletti L, Guan J, Deasy BM, Huard J, Wagner WR, et al. Development of a tissue-engineered vascular graft combining a biodegradable scaffold, muscle-derived stem cells and a rotational vacuum seeding technique. Biomaterials. 2008 Mar;29(7):825-33.

55. Soletti L, Nieponice A, Guan J, Stankus JJ, Wagner WR, Vorp DA. A seeding device for tissue engineered tubular structures. Biomaterials. 2006 Oct;27(28):4863-70.

56. Courtney T, Sacks MS, Stankus J, Guan J, Wagner WR. Design and analysis of tissue engineering scaffolds that mimic soft tissue mechanical anisotropy. Biomaterials. 2006 Jul;27(19):3631-8.

57. Stankus JJ, Guan J, Wagner WR. Fabrication of biodegradable elastomeric scaffolds with sub-micron morphologies. J Biomed Mater Res A. 2004 Sep 15;70(4):603-14.

58. Stankus JJ, Soletti L, Fujimoto K, Hong Y, Vorp DA, Wagner WR. Fabrication of cell microintegrated blood vessel constructs through electrohydrodynamic atomization. Biomaterials. 2007 Jun;28(17):2738-46.

59. Berglund JD, Nerem RM, Sambanis A. Incorporation of intact elastin scaffolds in tissue-engineered collagen-based vascular grafts. Tissue Eng. 2004 Sep-Oct;10(9-10):1526-35.

60. Grassl ED, Oegema TR, Tranquillo RT. Fibrin as an alternative biopolymer to type-I collagen for the fabrication of a media equivalent. Journal of Biomedical Materials Research. 2002 Jun;60(4):607-12.

61. Remuzzi A, Mantero S, Colombo M, Morigi M, Binda E, Camozzi D, et al. Vascular smooth muscle cells on hyaluronic acid: culture and mechanical characterization of an engineered vascular construct. Tissue Eng. 2004 May-Jun;10(5-6):699-710.

62. Seliktar D, Black RA, Vito RP, Nerem RM. Dynamic mechanical conditioning of collagen-gel blood vessel constructs induces remodeling *in vitro*. Annals of Biomedical Engineering. 2000 Apr;28(4):351-62.

63. Roeder R, Wolfe J, Lianakis N, Hinson T, Geddes LA, Obermiller J. Compliance, elastic modulus, and burst pressure of small-intestine submucosa (SIS), small-diameter vascular grafts. J Biomed Mater Res. 1999 Oct;47(1):65-70.

64. McFetridge PS, Daniel JW, Bodamyali T, Horrocks M, Chaudhuri JB. Preparation of porcine carotid arteries for vascular tissue engineering applications. J Biomed Mater Res A. 2004 Aug 1;70(2):224-34.

65. Orban JM, Wilson LB, Kofroth JA, El-Kurdi MS, Maul TM, Vorp DA. Crosslinking of collagen gels by transglutaminase. Journal of Biomedical Materials Research. 2004;68A(4):756-62.

66. Seliktar D, Nerem RM, Galis ZS. Mechanical strain-stimulated remodeling of tissue-engineered blood vessel constructs. Tissue Eng. 2003 Aug;9(4):657-66.

67. Cummings CL, Gawlitta D, Nerem RM, Stegemann JP. Properties of engineered vascular constructs made from collagen, fibrin, and collagen-fibrin mixtures. Biomaterials. 2004 Aug;25(17):3699-706.

68. Boland ED, Matthews JA, Pawlowski KJ, Simpson DG, Wnek GE, Bowlin GL. Electrospinning collagen and elastin: preliminary vascular tissue engineering. Front Biosci. 2004 May 1;9:1422-32.

69. Lepidi S, Abatangelo G, Vindigni V, Deriu GP, Zavan B, Tonello C, et al. In vivo regeneration of small-diameter (2 mm) arteries using a polymer scaffold. FASEB J. 2006 Jan;20(1):103-5.

70. Badylak SF. Xenogeneic extracellular matrix as a scaffold for tissue reconstruction. Transpl Immunol. 2004;12(3-4):367-77.

71. Badylak SF, Lantz GC, Coffey A, Geddes LA. Small intestinal submucosa as a large diameter vascular graft in the dog. J Surg Res. 1989;47(1):74-80.

72. Atala A. Tissue engineering and regenerative medicine: concepts for clinical application. Rejuvenation Res. 2004;7(1):15-31.

73. Cho SW, Lim SH, Kim IK, Hong YS, Kim SS, Yoo KJ, et al. Small-diameter blood vessels engineered with bone marrow-derived cells. Ann Surg. 2005 Mar;241(3):506-15.

74. Schaner PJ, Martin ND, Tulenko TN, Shapiro IM, Tarola NA, Leichter RF, et al. Decellularized vein as a potential scaffold for vascular tissue engineering. J Vasc Surg. 2004 Jul;40(1):146-53.

75. Nieponice A, Maul TM, Soletti L, Vorp DA. Vascular Tissue Engineering. In: Bowlin GL, Wnek G, editors. Encyclopedia of Biomaterials and Biomedical Engineering: Informa Healthcare; 2006.

76. Hubbell JA. Bioactive biomaterials. Curr Opin Biotechnol. 1999 Apr;10(2):123-9.

77. Palecek SP, Loftus JC, Ginsberg MH, Lauffenburger DA, Horwitz AF. Integrin-ligand binding properties govern cell migration speed through cell-substratum adhesiveness. Nature. 1997 Feb 6;385(6616):537-40.

78. Seliktar D, Zisch AH, Lutolf MP, Wrana JL, Hubbell JA. MMP-2 sensitive, VEGF-bearing bioactive hydrogels for promotion of vascular healing. J Biomed Mater Res A. 2004 Mar 15;68(4):704-16.

79. Boura C, Menu P, Payan E, Picart C, Voegel JC, Muller S, et al. Endothelial cells grown on thin polyelectrolyte mutlilayered films: an evaluation of a new versatile surface modification. Biomaterials. 2003 Sep;24(20):3521-30.

80. Steffens GC, Yao C, Prevel P, Markowicz M, Schenck P, Noah EM, et al. Modulation of angiogenic potential of collagen matrices by covalent incorporation of heparin and loading with vascular endothelial growth factor. Tissue Eng. 2004 Sep-Oct;10(9-10):1502-9.

81. Lee M, Kim SW. Polyethylene glycol-conjugated copolymers for plasmid DNA delivery. Pharm Res. 2005 Jan;22(1):1-10.

82. Collins K, Mitchell JR. Telomerase in the human organism. Oncogene. 2002 Jan;21(4):564-79.

83. Klinger RY, Blum JL, Hearn B, Lebow B, Niklason LE. Relevance and safety of telomerase for human tissue engineering. Proc Natl Acad Sci U S A. 2006 Feb 21;103(8):2500-5.

84. McKee JA, Banik SS, Boyer MJ, Hamad NM, Lawson JH, Niklason LE, et al. Human arteries engineered *in vitro*. EMBO Rep. 2003 Jun;4(6):633-8.

85. Remy-Zolghadri M, Laganiere J, Oligny JF, Germain L, Auger FA. Endothelium properties of a tissue engineered blood vessel for small diameter vascular reconstruction. Journal of Vascular Surgery. 2004 Mar;39(3):613-20.

86. Crisostomo PR, Wang Y, Markel TA, Wang M, Lahm T, Meldrum DR. Human Mesenchymal Stem Cells Stimulated by Tnf, Lps, or Hypoxia Produce Growth Factors by an Nfkb but Not Jnk Dependent Mechanism. Am J Physiol Cell Physiol. 2008 Jan 30.

87. Togel F, Westenfelder C. Adult bone marrow-derived stem cells for organ regeneration and repair. Dev Dyn. 2007 Dec;236(12):3321-31.

88. Saini A, Stewart CE. Adult stem cells: the therapeutic potential of skeletal muscle. Curr Stem Cell Res Ther. 2006 May;1(2):157-71.

89. Gimble J, Guilak F. Adipose-derived adult stem cells: isolation, characterization, and differentiation potential. Cytotherapy. 2003;5(5):362-9.

90. Wilson A, Oser GM, Jaworski M, Blanco-Bose WE, Laurenti E, Adolphe C, et al. Dormant and self-renewing hematopoietic stem cells and their niches. Ann N Y Acad Sci. 2007 Jun;1106:64-75.

91. Chamberlain G, Fox J, Ashton B, Middleton J. Concise review: mesenchymal stem cells: their phenotype, differentiation capacity, immunological features, and potential for homing. Stem Cells. 2007 Nov;25(11):2739-49.

92. Hristov M, Erl W, Weber PC. Endothelial progenitor cells: mobilization, differentiation, and homing. Arterioscler Thromb Vasc Biol. 2003 Jul;23(7):1185-9.

93. Pittenger MF, Mackay AM, Beck SC, Jaiswal RK, Douglas R, Mosca JD, et al. Multilineage potential of adult human mesenchymal stem cells. Science. 1999 Apr;284(5411):143-7.

94. O'Cearbhaill ED, Punchard MA, Murphy M, Barry FP, McHugh PE, Barron V. Response of mesenchymal stem cells to the biomechanical environment of the endothelium on a flexible tubular silicone substrate. Biomaterials. 2008 Apr;29(11):1610-9.

95. Finkenzeller G, Torio-Padron N, Momeni A, Mehlhorn AT, Stark GB. In vitro angiogenesis properties of endothelial progenitor cells: a promising tool for vascularization of ex vivo engineered tissues. Tissue Eng. 2007 Jul;13(7):1413-20.

96. Matsumura G, Miyagawa-Tomita S, Shin-oka T, Ikada Y, Kurosawa H. First evidence that bone marrow cells contribute to the construction of tissue-engineered vascular autografts *in vivo*. Circulation. 2003 Oct;108(14):1729-34.

97. Fraser JK, Wulur I, Alfonso Z, Hedrick MH. Fat tissue: an underappreciated source of stem cells for biotechnology. Trends Biotechnol. 2006 Apr;24(4):150-4.

98. DiMuzio P, Tulenko T. Tissue engineering applications to vascular bypass graft development: the use of adipose-derived stem cells. J Vasc Surg. 2007 Jun;45 Suppl A:A99-103.

99. Qu-Petersen Z, Deasy B, Jankowski R, Ikezawa M, Cummins J, Pruchnic R, et al. Identification of a novel population of muscle stem cells in mice: potential for muscle regeneration. J Cell Biol. 2002 May 27;157(5):851-64.

100. Lee JY, Qu Petersen Z, Cao B, Kimura S, Jankowski R, Cummins J, et al. Clonal isolation of muscle-derived cells capable of enhancing muscle regeneration and bone healing. The Journal of Cell Biology. 2000 Sep;150(5):1085-100.

101. Deasy BM, Huard J. Gene therapy and tissue engineering based on muscle-derived stem cells. Curr Opin Mol Ther. 2002 Aug;4(4):382-9.

102. McCloskey KE, Gilroy ME, Nerem RM. Use of embryonic stem cell-derived endothelial cells as a cell source to generate vessel structures in vitro. Tissue Eng. 2005 Mar-Apr;11(3-4):497-505.

103. Levenberg S, Golub JS, Amit M, Itskovitz-Eldor J, Langer R. Endothelial cells derived from human embryonic stem cells. Proc Natl Acad Sci U S A. 2002 Apr 2;99(7):4391-6.

104. Ferreira LS, Gerecht S, Shieh HF, Watson N, Rupnick MA, Dallabrida SM, et al. Vascular progenitor cells isolated from human embryonic stem cells give rise to endothelial and smooth muscle like cells and form vascular networks in vivo. Circ Res. 2007 Aug 3;101(3):286-94.

105. Langer R. Tissue engineering. Mol Ther. 2000 Jan;1(1):12-5.

106. Shirota T, He H, Yasui H, Matsuda T. Human endothelial progenitor cell-seeded hybrid graft: proliferative and antithrombogenic potentials in vitro and fabrication processing. Tissue Eng. 2003 Feb;9(1):127-36.

107. Ito A, Ino K, Hayashida M, Kobayashi T, Matsunuma H, Kagami H, et al. Novel methodology for fabrication of tissue-engineered tubular constructs using magnetite nanoparticles and magnetic force. Tissue Eng. 2005 Sep-Oct;11(9-10):1553-61.

108. Bowlin GL, Rittgers SE. Electrostatic endothelial cell transplantation within small-diameter (<6 mm) vascular prostheses: a prototype apparatus and procedure. Cell Transplant. 1997 Nov-Dec;6(6):631-7.

109. Mazzucotelli JP, Roudiere JL, Bernex F, Bertrand P, Leandri J, Loisance D. A new device for endothelial cell seeding of a small-caliber vascular prosthesis. Artif Organs. 1993 Sep;17(9):787-90.

110. van Wachem PB, Stronck JW, Koers-Zuideveld R, Dijk F, Wildevuur CR. Vacuum cell seeding: a new method for the fast application of an evenly distributed cell layer on porous vascular grafts. Biomaterials. 1990 Oct;11(8):602-6.

111. Li Y, Ma T, Kniss DA, Lasky LC, Yang ST. Effects of filtration seeding on cell density, spatial distribution, and proliferation in nonwoven fibrous matrices. Biotechnol Prog. 2001 Sep-Oct;17(5):935-44.

112. Li H, Friend JR, Yeo LY. A scaffold cell seeding method driven by surface acoustic waves. Biomaterials. 2007 Oct;28(28):4098-104.

113. Dardik A, Chen L, Frattini J, Asada H, Aziz F, Kudo FA, et al. Differential effects of orbital and laminar shear stress on endothelial cells. J Vasc Surg. 2005 May;41(5):869-80.

114. Carter J, Hristova K, Harasaki H, Smith WA. Short exposure time sensitivity of white cells to shear stress. Asaio J. 2003 Nov-Dec;49(6):687-91.

115. Matsumura G, Hibino N, Ikada Y, Kurosawa H, Shin'oka T. Successful application of tissue engineered vascular autografts: clinical experience. Biomaterials. 2003 Jun;24(13):2303-8.

116. Hoerstrup SP, Zund G, Sodian R, Schnell AM, Grunenfelder J, Turina MI. Tissue engineering of small caliber vascular grafts. Eur J Cardiothorac Surg. 2001 Jul;20(1):164-9.

117. Stankus JJ, Guan J, Fujimoto K, Wagner WR. Microintegrating smooth muscle cells into a biodegradable, elastomeric fiber matrix. Biomaterials. 2006 Feb;27(5):735-44.

118. Varghese D, Deshpande M, Xu T, Kesari P, Ohri S, Boland T. Advances in tissue engineering: cell printing. J Thorac Cardiovasc Surg. 2005 Feb;129(2):470-2.

119. Chang CH, Liu HC, Lin CC, Chou CH, Lin FH. Gelatin-chondroitin-hyaluronan tri-copolymer scaffold for cartilage tissue engineering. Biomaterials. 2003 Nov;24(26):4853-8.

120. Duray PH, Hatfill SJ, Pellis NR. Tissue culture in microgravity. Sci Med (Phila). 1997 May-Jun;4(3):46-55.

121. R Byron Bird WES, Edwin N. Lightfoot. Transport Phenomena. 2nd ed.: John Wiley & Sons, Inc.; 2002.

122. Jeong SI, Kim SH, Kim YH, Jung Y, Kwon JH, Kim BS, et al. Manufacture of elastic biodegradable PLCL scaffolds for mechano-active vascular tissue engineering. J Biomater Sci Polym Ed. 2004;15(5):645-60.

123. Solan A, Mitchell S, Moses M, Niklason L. Effect of pulse rate on collagen deposition in the tissue-engineered blood vessel. Tissue Engineering. 2003 Aug;9(4):579-86.

124. Stiles CD, Capone GT, Scher CD, Antoniades HN, Van-Wyk JJ, Pledger WJ. Dual control of cell growth by somatomedins and platelet-derived growth factor. Proc Natl Acad Sci U S A. 1979 Mar;76(3):1279-83.

125. Nomi M, Atala A, Coppi PD, Soker S. Principals of neovascularization for tissue engineering. Molecular Aspects of Medicine. 2002 2002/12;23(6):463-83.

126. Pepper MS. Transforming growth factor-beta: vasculogenesis, angiogenesis, and vessel wall integrity. Cytokine Growth Factor Rev. 1997 Mar;8(1):21-43.

127. Stegemann JP, Nerem RM. Phenotype modulation in vascular tissue engineering using biochemical and mechanical stimulation. Annals of Biomedical Engineering. 2003 Apr;31(4):391-402.

128. Stegemann JP, Hong H, Nerem RM. Mechanical, biochemical, and extracellular matrix effects on vascular smooth muscle cell phenotype. J Appl Physiol. 2005 June 1, 2005;98(6):2321-7.

129. Kinner B, Zaleskas JM, Spector M. Regulation of smooth muscle actin expression and contraction in adult human mesenchymal stem cells. Experimental Cell Research. 2002 Aug;278(1):72-83.

130. Gehling UM, Ergun S, Schumacher U, Wagener C, Pantel K, Otte M, et al. *In vitro* differentiation of endothelial cells from AC133-positive progenitor cells. Blood. 2000 May;95(10):3106-12.

131. Lyman DJ, Stewart SF, Murray-Wijelath J, Wijelath E. Role of fluid dynamics on the healing of an in vivo tissue engineered vascular graft. J Biomed Mater Res B Appl Biomater. 2006 May;77(2):389-400.

132. Hiles MC, Badylak SF, Lantz GC, Kokini K, Geddes LA, Morff RJ. Mechanical properties of xenogeneic small-intestinal submucosa when used as an aortic graft in the dog. Journal of Biomedical Materials Research. 1995 Jul;29(7):883-91.

133. Badylak SF, Kochupura PV, Cohen IS, Doronin SV, Saltman AE, Gilbert TW, et al. The use of extracellular matrix as an inductive scaffold for the partial replacement of functional myocardium. Cell Transplant. 2006;15 Suppl 1:S29-40.

134. Lantz GC, Badylak SF, Coffey AC, Geddes LA, Sandusky GE. Small intestinal submucosa as a superior vena cava graft in the dog. J Surg Res. 1992;53(2):175-81.

135. Lantz GC, Badylak SF, Coffey AC, Geddes LA, Blevins WE. Small intestinal submucosa as a small-diameter arterial graft in the dog. J Invest Surg. 1990;3(3):217-27.

136. Hoerstrup SP, Cummings Mrcs I, Lachat M, Schoen FJ, Jenni R, Leschka S, et al. Functional growth in tissue-engineered living, vascular grafts: follow-up at 100 weeks in a large animal model. Circulation. 2006 Jul 4;114(1 Suppl):I159-66.

137. Hollister SJ. Porous scaffold design for tissue engineering. Nat Mater. 2005 Jul;4(7):518-24.

138. Hashi CK, Zhu Y, Yang GY, Young WL, Hsiao BS, Wang K, et al. Antithrombogenic property of bone marrow mesenchymal stem cells in nanofibrous vascular grafts. Proc Natl Acad Sci U S A. 2007 Jul 17;104(29):11915-20.

139. Isolated CAB Procedures Data Summary STS Spring 2007 Report: Duke Clinical Research Institute; 2007 Contract No.: Document Number|.

140. L'Heureux N, McAllister TN, de la Fuente LM. Tissue-engineered blood vessel for adult arterial revascularization. N Engl J Med. 2007 Oct 4;357(14):1451-3.

141. Griffon DJ, Sedighi MR, Sendemir-Urkmez A, Stewart AA, Jamison R. Evaluation of vacuum and dynamic cell seeding of polyglycolic acid and chitosan scaffolds for cartilage engineering. Am J Vet Res. 2005 Apr;66(4):599-605.

142. Solchaga LA, Tognana E, Penick K, Baskaran H, Goldberg VM, Caplan AI, et al. A rapid seeding technique for the assembly of large cell/scaffold composite constructs. Tissue Eng. 2006 Jul;12(7):1851-63.

143. Dexter TM, Lajtha LG. Proliferation of haemopoietic stem cells *in vitro*. Br J Haematol. 1974 Dec;28(4):525-30.

144. Fluent I. Fluent 6.2 Documentation. [cited]; Available from: http://www.engres.odu.edu/Applications/fluent6.2/help/index.htm.

145. Bajura RA, Jones EH. Flow distribution manifolds. Journal of Fluids Engineering. 1976 Dec;98:654-65.

146. Fumero R, Porro G, Beretta M, Remuzzi A. Sulla distribuzione uniforme di portata in scambiatori di massa e di calore, applicazione a un ossigenatore a membrana. Meccanica Italiana. 1980;146(12).

147. Gharaibeh B, Lu A, Tebbets J, Zheng B, Feduska J, Crisan M, et al. Isolation of a slowly adhering cell fraction containing stem cells from murine skeletal muscle by the preplate technique. Nature protocols. 2008;3(8).

148. Chung J, Li JK. Hemodynamic simulation of vascular prosthesis altering pulse wave propagation. Conf Proc IEEE Eng Med Biol Soc. 2004;5:3678-80.

149. Grassl ED, Oegema TR, Tranquillo RT. A fibrin-based arterial media equivalent. J Biomed Mater Res A. 2003 Sep 1;66(3):550-61.

150. Gumpenberger T, Heitz J, Bauerle D, Kahr H, Graz I, Romanin C, et al. Adhesion and proliferation of human endothelial cells on photochemically modified polytetrafluoroethylene. Biomaterials. 2003 Dec;24(28):5139-44.

151. Rashid ST, Salacinski HJ, Fuller BJ, Hamilton G, Seifalian AM. Engineering of bypass conduits to improve patency. Cell Prolif. 2004 Oct;37(5):351-66.

152. Zhu Y, Gao C, He T, Shen J. Endothelium regeneration on luminal surface of polyurethane vascular scaffold modified with diamine and covalently grafted with gelatin. Biomaterials. 2004 Feb;25(3):423-30.

153. Simon P, Kasimir MT, Seebacher G, Weigel G, Ullrich R, Salzer-Muhar U, et al. Early failure of the tissue engineered porcine heart valve SYNERGRAFT in pediatric patients. Eur J Cardiothorac Surg. 2003 Jun;23(6):1002-6; discussion 6.

154. Hubbell JA. Biomaterials in tissue engineering. Biotechnology (N Y). 1995 Jun;13(6):565-76.

155. Xu C, Inai R, Kotaki M, Ramakrishna S. Electrospun nanofiber fabrication as synthetic extracellular matrix and its potential for vascular tissue engineering. Tissue Eng. 2004 Jul-Aug;10(7-8):1160-8.

156. Sarkar S, Lee GY, Wong JY, Desai TA. Development and characterization of a porous micro-patterned scaffold for vascular tissue engineering applications. Biomaterials. 2006 Sep;27(27):4775-82.

157. Guan J, Wagner WR. Synthesis, characterization and cytocompatibility of polyurethaneurea elastomers with designed elastase sensitivity. Biomacromolecules. 2005 Sep-Oct;6(5):2833-42.

158. Engelmayr GC, Jr., Sacks MS. A structural model for the flexural mechanics of nonwoven tissue engineering scaffolds. J Biomech Eng. 2006 Aug;128(4):610-22.

159. Hayashi K, Takamizawa K, Saito T, Kira K, Hiramatsu K, Kondo K. Elastic properties and strength of a novel small-diameter, compliant polyurethane vascular graft. J Biomed Mater Res. 1989 Aug;23(A2 Suppl):229-44.

160. Severyn DA, Muluk SC, Vorp DA. The influence of hemodynamics and wall biomechanics on the thrombogenicity of vein segments perfused in vitro. J Surg Res. 2004 Sep;121(1):31-7.

161. Fujimoto KL, Guan J, Oshima H, Sakai T, Wagner WR. In vivo evaluation of a porous, elastic, biodegradable patch for reconstructive cardiac procedures. Ann Thorac Surg. 2007 Feb;83(2):648-54.

162. Fujimoto KL, Tobita K, Merryman WD, Guan J, Momoi N, Stolz DB, et al. An elastic, biodegradable cardiac patch induces contractile smooth muscle and improves cardiac remodeling and function in subacute myocardial infarction. J Am Coll Cardiol. 2007 Jun 12;49(23):2292-300.

163. Tajaddini A, Kilpatrick DL, Schoenhagen P, Tuzcu EM, Lieber M, Vince DG. Impact of age and hyperglycemia on the mechanical behavior of intact human coronary arteries: an ex vivo intravascular ultrasound study. Am J Physiol Heart Circ Physiol. 2005 Jan;288(1):H250-5.

164. Sell SA, McClure MJ, Barnes CP, Knapp DC, Walpoth BH, Simpson DG, et al. Electrospun polydioxanone-elastin blends: potential for bioresorbable vascular grafts. Biomedical Materials. 2006;1(1):72-80.

165. Butler DL, Goldstein SA, Guilak F. Functional tissue engineering: the role of biomechanics. J Biomech Eng. 2000 Dec;122(6):570-5.

166. Deasy BM, Li Y, Huard J. Tissue engineering with muscle-derived stem cells. Curr Opin Biotechnol. 2004 Oct;15(5):419-23.

167. Deasy BM, Jankowski RJ, Huard J. Muscle-derived stem cells: characterization and potential for cell-mediated therapy. Blood Cells Mol Dis. 2001 Sep-Oct;27(5):924-33.

168. Ciapetti G, Cenni E, Pratelli L, Pizzoferrato A. In vitro evaluation of cell/biomaterial interaction by MTT assay. Biomaterials. 1993;14(5):359-64.

169. Deasy BM, Gharaibeh BM, Pollett JB, Jones MM, Lucas MA, Kanda Y, et al. Long-term self-renewal of postnatal muscle-derived stem cells. Mol Biol Cell. 2005 Jul;16(7):3323-33.

170. Jankowski RJ, Huard J. Establishing reliable criteria for isolating myogenic cell fractions with stem cell properties and enhanced regenerative capacity. Blood Cells Mol Dis. 2004 Jan-Feb;32(1):24-33.

171. Healy L, May G, Gale K, Grosveld F, Greaves M, Enver T. The stem cell antigen CD34 functions as a regulator of hemopoietic cell adhesion. Proc Natl Acad Sci U S A. 1995 Dec 19;92(26):12240-4.

172. Hu Y, Bock G, Wick G, Xu Q. Activation of PDGF receptor alpha in vascular smooth muscle cells by mechanical stress. The FASEB Journal. 1998 Sep;12(12):1135-42.

173. Jankowski RJ, Deasy BM, Huard J. Muscle-derived stem cells. Gene Ther. 2002 May;9(10):642-7.

174. Hwang JH, Yuk SH, Lee JH, Lyoo WS, Ghil SH, Lee SS, et al. Isolation of muscle derived stem cells from rat and its smooth muscle differentiation [corrected]. Mol Cells. 2004 Feb 29;17(1):57-61.

175. Arriero M, Brodsky SV, Gealekman O, Lucas PA, Goligorsky MS. Adult skeletal muscle stem cells differentiate into endothelial lineage and ameliorate renal dysfunction after acute ischemia. Am J Physiol Renal Physiol. 2004 Oct;287(4):F621-7.

176. Beauchamp JR, Heslop L, Yu DS, Tajbakhsh S, Kelly RG, Wernig A, et al. Expression of CD34 and Myf5 defines the majority of quiescent adult skeletal muscle satellite cells. J Cell Biol. 2000 Dec 11;151(6):1221-34.

177. Vorp D, Maul T, Nieponice A. Molecular aspects of vascular tissue engineering. Frontiers in Bioscience. 2005 January 2005;10:768-89.

178. Hamilton D, Maul T, Vorp D. Characterization of the Response of Bone Marrow Derived Progenitor Cells to Cyclic Strain: Implications for Vascular Tissue Engineering Applications. Tissue Engineering. 2004;10(3/4):361-70.

179. Shieh SJ, Vacanti JP. State-of-the-art tissue engineering: from tissue engineering to organ building. Surgery. 2005 Jan;137(1):1-7.

180. Barron V, Lyons E, Stenson-Cox C, McHugh PE, Pandit A. Bioreactors for cardiovascular cell and tissue growth: a review. Ann Biomed Eng. 2003 Oct;31(9):1017-30.

181. Vascular Disease: Molecular Biology and Gene Therapy Protocols. Baker AH, editor. Bristol, UK: Humana Press; 1999.

182. Nottelet B, Pektok E, Mandracchia D, Tille JC, Walpoth B, Gurny R, et al. Factorial design optimization and in vivo feasibility of poly(epsilon-caprolactone)-micro- and nanofiber-based small diameter vascular grafts. J Biomed Mater Res A. 2008 May 8.

183. Jeschke MG, Hermanutz V, Wolf SE, Koveker GB. Polyurethane vascular prostheses decreases neointimal formation compared with expanded polytetrafluoroethylene. J Vasc Surg. 1999 Jan;29(1):168-76.

184. Ribbe EB, Holmin T, Lowenhielm PC. Microvascular polytetrafluoroethylene (Gore-Tex) grafts in the infrarenal rat aorta. Microsurgery. 1987;8(2):48-53.

185. Blidisel A, Jiga L, Nistor A, Dornean V, Hoinoiu B, Ionac M. Video-assisted versus conventional microsurgical training: a comparative study in the rat model. Microsurgery. 2007;27(5):446-50.

186. Riggio E, Parafioriti A, Tomic O, Podrecca S, Nava M, Colombetti A. Experimental study of a sleeve microanastomotic technique. Ann Plast Surg. 1999 Dec;43(6):625-31.

187. PhysioGenix I. [Website]; 2006 [updated 2006; cited]; Available from: http://ratresources.com/models.html.

188. Russell JC, Proctor SD. Small animal models of cardiovascular disease: tools for the study of the roles of metabolic syndrome, dyslipidemia, and atherosclerosis. Cardiovasc Pathol. 2006 Nov-Dec;15(6):318-30.

189. Biology of the domestic pig. Pond WG, Mersmann HS, editors.; 2001.

190. Zavan B, Vindigni V, Lepidi S, Iacopetti I, Avruscio G, Abatangelo G, et al. Neoarteries grown in vivo using a tissue-engineered hyaluronan-based scaffold. FASEB J. 2008 Apr 2.

191. Zhu C, Ying D, Mi J, Li L, Zeng W, Hou C, et al. Development of anti-atherosclerotic tissue-engineered blood vessel by A20-regulated endothelial progenitor cells seeding decellularized vascular matrix. Biomaterials. 2008 Jun;29(17):2628-36.

192. Torikai K, Ichikawa H, Hirakawa K, Matsumiya G, Kuratani T, Iwai S, et al. A self-renewing, tissue-engineered vascular graft for arterial reconstruction. J Thorac Cardiovasc Surg. 2008 Jul;136(1):37-45, e1.

193. Kapadia MR, Aalami OO, Najjar SF, Jiang Q, Murar J, Lyle B, et al. A reproducible porcine ePTFE arterial bypass model for neointimal hyperplasia. J Surg Res. 2008 Aug;148(2):230-7.

194. Wong G, Li JM, Hendricks G, Eslami MH, Rohrer MJ, Cutler BS. Inhibition of experimental neointimal hyperplasia by recombinant human thrombomodulin coated ePTFE stent grafts. J Vasc Surg. 2008 Mar;47(3):608-15.

195. Schmitz-Rixen T, Storck M, Erasmi H, Schmiegelow P, Horsch S. Vascular anastomoses with absorbable suture material: an experimental study. Ann Vasc Surg. 1991 May;5(3):257-64.

196. Cortez AJ, Paulson WD, Schwab SJ. Vascular access as a determinant of adequacy of dialysis. Semin Nephrol. 2005 Mar;25(2):96-101.

197. Phinney DG, Prockop DJ. Concise review: mesenchymal stem/multipotent stromal cells: the state of transdifferentiation and modes of tissue repair--current views. Stem Cells. 2007 Nov;25(11):2896-902.

198. Kataoka N, Ujita S, Sato M. Effect of flow direction on the morphological responses of cultured bovine aortic endothelial cells. Med Biol Eng Comput. 1998 Jan;36(1):122-8.

199. Loth F, Fischer PF, Arslan N, Bertram CD, Lee SE, Royston TJ, et al. Transitional flow at the venous anastomosis of an arteriovenous graft: potential activation of the ERK1/2 mechanotransduction pathway. J Biomech Eng. 2003 Feb;125(1):49-61.

200. Baig K, Fields RC, Gaca J, Hanish S, Milton LG, Koch WJ, et al. A porcine model of intimal-medial hyperplasia in polytetrafluoroethylene arteriovenous grafts. J Vasc Access. 2003 Jul-Sep;4(3):111-7.

201. Popov AF, Dorge H, Hinz J, Schmitto JD, Stojanovic T, Seipelt R, et al. Accelerated intimal hyperplasia in aortocoronary internal mammary vein grafts in minipigs. J Cardiothorac Surg. 2008;3:20.

202. Wei H, Soletti L, Hong Y, Crisan M, Peault B, Wagner WR, et al., editors. In-vitro assessment of a human pericytes-seeded tissue engineered vascular graft. TERMIS NA; 2008; San Diego.

203. Kalra S, Duggal S, Valdez G, Smalligan RD. Review of acute coronary syndrome diagnosis and management. Postgrad Med. 2008 Apr;120(1):18-27.

204. Dormandy JA, Rutherford RB. Management of peripheral arterial disease (PAD). TASC Working Group. TransAtlantic Inter-Society Consensus (TASC). J Vasc Surg. 2000 Jan;31(1 Pt 2):S1-S296.

205. El-Kurdi MS, Hong Y, Stankus JJ, Soletti L, Wagner WR, Vorp DA. Transient elastic support for vein grafts using a constricting microfibrillar polymer wrap. Biomaterials. 2008 Aug;29(22):3213-20.

206. Balducci E, Azzarello G, Valenti MT, Capuzzo GM, Pappagallo GL, Pilotti I, et al. The impact of progenitor enrichment, serum, and cytokines on the *ex vivo* expansion of mobilized peripheral blood stem cells: a controlled trial. Stem Cells. 2003;21(1):33-40.

207. Makino S, Fukuda K, Miyoshi S, Konishi F, Kodama H, Pan J, et al. Cardiomyocytes can be generated from marrow stromal cells in vitro. J Clin Invest. 1999 Mar;103(5):697-705.

208. Toma C, Pittenger MF, Cahill KS, Byrne BJ, Kessler PD. Human mesenchymal stem cells differentiate to a cardiomyocyte phenotype in the adult murine heart. Circulation. 2002 Jan 1;105(1):93-8.

209. Haider H, Ashraf M. Bone marrow cell transplantation in clinical perspective. J Mol Cell Cardiol. 2005 Feb;38(2):225-35.